&EPA

Modeling of Simulated Photochemical Smog with Kinetic Mechanisms

Volume 1. Interim Report

RESEARCH REPORTING SERIES

Research reports of the Office of Research and Development, U S Environmental Protection Agency, have been grouped into nine series. These nine broad categories were established to facilitate further development and application of environmental technology. Elimination of traditional grouping was consciously planned to foster technology transfer and a maximum interface in related fields. The nine series are:

1. Environmental Health Effects Research
2. Environmental Protection Technology
3. Ecological Research
4. Environmental Monitoring
5. Socioeconomic Environmental Studies
6. Scientific and Technical Assessment Reports (STAR)
7. Interagency Energy-Environment Research and Development
8. "Special" Reports
9. Miscellaneous Reports

This report has been assigned to the ECOLOGICAL RESEARCH series. This series describes research on the effects of pollution on humans, plant and animal species, and materials. Problems are assessed for their long- and short-term influences. Investigations include formation, transport, and pathway studies to determine the fate of pollutants and their effects. This work provides the technical basis for setting standards to minimize undesirable changes in living organisms in the aquatic, terrestrial, and atmospheric environments.

MODELING OF SIMULATED PHOTOCHEMICAL SMOG WITH KINETIC MECHANISMS
VOLUME 1. INTERIM REPORT

by

G. Z. Whitten
H. Hogo
M. J. Meldgin
J. P. Killus
P. J. Bekowies

Systems Applications, Incorporated
950 Northgate Drive
San Rafael, California 94903

Project Officer

DISCLAIMER

This report has been reviewed by the Environmental Sciences Research Laboratory, U.S. Environmental Protection Agency, and approved for publication. Approval does not signify that the contents necessarily reflect the views and policies of the U.S. Environmental Protection Agency, nor does mention of trade names or commercial products constitute endorsement or recommendation for use.

ABSTRACT

Computer modeling of smog chamber data is discussed in three parts. First, a series of detailed chemical mechanisms were developed to describe the photochemical formation of ozone from nitrogen oxides and the following compounds (alone and in various combinations): formaldehyde, acetaldehyde, ethylene, propylene, butane, 1-butene, trans-2-butene, and 2,3-dimethylbutane. The aldehyde mechanisms were verified independently using data from experiments containing only nitrogen oxides and the appropriate aldehyde. The hydrocarbon mechanisms were then developed by adding the chemical reactions detailing the photooxidation steps of the particular hydrocarbon to the aldehyde mechanisms. Second, a generalized kinetic scheme intended for use in models simulating the formation of ozone in urban atmospheres was refined. The generalized mechanism includes a condensed version of the explicit mechanisms developed in the first part plus a semi-empirical scheme to describe the oxidation of aromatic hydrocarbons. Third, the effects of smog chambers on ozone formation were examined. For this part of the study, similar experiments using nitrogen oxides and propylene in eight different smog chambers were simulated. The main chamber effects identified thus far are apparently due to nitrogen oxides degassing from the walls during experiments and differences between chambers in the spectral distribution of ultraviolet irradiation.

This volume contains all textual material; Volume 2 (Appendix) contains graphs of measured and simulated pollutant concentrations for many smog chamber experiments. This two-volume report was submitted to the U.S. Environmental Protection Agency in fulfillment of Contract No. 68-02-2428 by Systems Applications, Incorporated. This report covers the period 23 August 1976 to 23 August 1978, and work was completed as of 18 August 1978.

CONTENTS

FIGURES

TABLES

ABBREVIATIONS

ALD2	Acetaldehyde	O3	Ozone
ALD3	Propionaldehyde	OLE	Olefins
ALD4	Butyraldehyde	PAN	Peroxyacetyl nitrate
AONE	Acetone	PAR	Paraffins
ARO	Aromatics	PPN	Peroxypropionyl nitrate
BLA	Blacklamp irradiation	PROP	Propylene
BUT	n-Butane	SCN3	Sec-butyl nitrate
BUT1	1-Butene	SPN3	Isopropyl nitrate
BUT2	Trans-2-butene	SUN	Sunlamp irradiation
CO	Carbon monoxide	SUNLAMP	Sunlamp irradiation
C2N3	Ethyl nitrate	UCR	University of California at Riverside
C4N3	n-Butyl nitrate		
C6N3	2,3-Dimethylbutyl nitrate	UNCB	University of North Carolina ("blue" side of chamber)
DBUT	2,3-Dimethylbutane		
EC	Evacuable chamber (at UCR)	UNCR	University of North Carolina ("red" side of chamber)
ETH	Ethylene		
FORM	Formaldehyde		
HCHO	Formaldehyde		
H2O2	Hydrogen peroxide		
MEK	Methylethylketone		
MEN3	Methyl nitrate		
NO	Nitrogen oxide		
NOX	Oxides of nitrogen ($NO + NO_2$)		
NO2	Nitrogen dioxide		

SECTION 1

INTRODUCTION

This report describes the first two years of a three-year study, spon-
sored by the Environmental Protection Agency (EPA), to model the formation
and evolution of photochemical oxidants. The study has three parts:

> Development and refinement of chemical kinetic mechanisms*
  for simulating smog chamber experiments that were initiated
  with a few simple hydrocarbon species and NO_x. This effort
  is intended to develop greater understanding of the forma-
  tion of photochemical oxidants, to point out specific chemical
  reactions most in need of further study, and to support the
  second part of this study.

> Refinement of a mechanism for describing the chemical aspects
  of photochemical oxidant formation in the atmosphere. This
  mechanism is to be incorporated in large air quality simula-
  tion models used for predicting spatial and temporal pollutant
  distributions in the atmosphere. Consequently, the mechanism
  must be able to treat complex mixtures of hydrocarbons yet
  have modest computing requirements.

> Analysis of the effects of the physical and chemical character-
  istics of smog chambers on smog formation and evolution.
  Knowledge of these chamber effects is valuable for validating
  kinetic mechanisms with smog chamber data and for applying
  mechanisms in atmospheric studies.

The technical approach in the first part of this study was based on
simulating smog chamber experiments with explicit kinetic mechanisms. An
explicit mechanism for a given chemical system individually treats each.

---

* A chemical kinetic mechanism is a set of chemical reactions and rate
  constants. From a kinetic mechanism one can derive a set of coupled
  differential equations, which, when integrated using a computer, yield
  concentration/time profiles for the chemical species in the mechanism.

1

species and reaction thought to be important in that system. Published data on reactions and rate constants were used as much as possible in constructing those mechanisms, but, because of gaps in the data, all mechanisms contained hypothetical reactions or estimated rate constants. Simulation results were compared with smog chamber data to evaluate the hypotheses and estimates and, thus, to develop a deeper understanding of the formation of photochemical oxidants.

In constructing mechanisms we followed the concept of a hierarchy of chemical species. Each species can be assigned to a hierarchical level on the basis of the number of photochemical-oxidant-forming systems in which it occurs. NO, NO_2, CO, ozone, and some other inorganic species, for example, occur in every photochemical-oxidant-forming system, and they are thus assigned to the lowest level. Formaldehyde, which occurs in every system except the CO/NO_x system, occupies a higher level in the hierarchy. Acetaldehyde occurs in most systems, but not in formaldehyde/NO_x or CO/NO_x, and so it is at a still higher level. The above description of the hierarchical concept may be slightly ambiguous, but it has the immediate benefit of suggesting an order for development of explicit kinetic mechanisms. After constructing and evaluating a mechanism for CO, one can develop a formaldehyde mechanism by adding a few reactions and rate constants to the CO mechanism, and the same procedure can be used for acetaldehyde. In validating each successive mechanism, one can focus attention on the added reactions and rate constants because the other reactions and rate constants have already been validated. Following this procedure reduces the probability that a complex mechanism, such as that for propylene, contains errors that compensate each other in simulations of a set of smog chamber experiments.

We constructed explicit mechanisms for formaldehyde, acetaldehyde, ethylene, and five larger hydrocarbons using data from experiments in the evacuable smog chamber (EC) at the University of California at Riverside (UCR) and other sources for validation. These mechanisms produced simulations that generally agreed well with measurements and pointed out several

2

areas for further research. The hierarchical concept has proved very useful, though its application was limited somewhat by the paucity of data on formaldehyde and acetaldehyde smog chamber experiments.

The explicit mechanism work also provided a framework for the second part of this study, refinement of the Carbon-Bond Mechanism (CBM). Developed in an earlier SAI study for the EPA (Whitten and Hogo, 1977), the CBM is a generalized mechanism--it treats generalized species rather than individual compounds, primarily for the purpose of reducing computing requirements. Many generalized mechanisms treat chemically similar molecules in groups, but the CBM treats chemically similar carbon atoms in groups, regardless of the compounds in which they occur. Our approach to refining the CBM involved condensing the essential features of the revised or newly developed explicit mechanisms from the first part of this study. Because no adequate mechanism exists for aromatic hydrocarbons, we included some empirical reactions. The revised CBM was validated using smog chamber data and was incorporated in the current SAI Airshed Model, which is now being used to model air quality in Los Angeles, Sacramento, and St. Louis.

For the study of chamber effects we used the explicit propylene mechanism to simulate data from propylene/NO_x experiments performed in eight smog chambers. We also analyzed the relative speeds of reaction and diffusion to the chamber walls to determine which are rate limiting for various species. The simulation results and that analysis were used to evaluate the effects of different wall materials, light sources, surface/volume ratios, and other characteristics. At this point in the study, differences in the spectral distribution of irradiation between chambers appear to account for most of the observed differences in photochemical oxidant formation.

The organization of this report follows the three-part structure of the study. The conclusions and recommendations from the first two years of this three-year study are summarized in Section 2. Section 3 discusses in general terms the development of chemical kinetic mechanisms using computer modeling. Because all mechanisms include the reactions of NO_x, HO_x, and O_x,

a separate section (4) is devoted to discussions of recent research on
those reactions and their rate constants. Section 5 presents in detail
the work on explicit kinetic mechanisms, starting with formaldehyde and
ending with hydrocarbon mixes. The studies of and refinements in the
Carbon-Bond Mechanism are presented in Section 6. Section 7 concludes
this volume with a description of the chamber effects study. Because
the simulation results are voluminous, they are contained in a separate data
volume, though some are also presented in this volume to clarify or sup-
port points in the text. In all graphs of simulation results, the symbols
represent pollutant measurements during smog chamber experiments, and the
lines represent simulated pollutant concentrations.

SECTION 2

SUMMARY OF RESULTS, CONCLUSIONS, AND RECOMMENDATIONS

In this section we present general conclusions from this study and
summarize the results of explicit mechanism refinement, Carbon-Bond Mech-
anism refinement, and the study of chamber effects. We then discuss the
work planned for the coming year and our recommendations for future labor-
atory and modeling studies.

In computer modeling studies such as the present effort, many
ideas are tried, and large quantities of computer output are produced.
In the descriptions of what was done to produce the current closest
agreement between simulations and observational data, the implicit
conclusion is that the steps taken were both unique and necessary.
However, experience has shown that equally close agreement is possible
from several combinations of adjustments to physical conditions and
mechanisms. Hence, the conclusions presented here must be qualified
with the caveat that the results are subject to change in accordance
with new data and further modeling efforts.

GENERAL CONCLUSIONS

We have made significant progress in developing mechanisms during the
past two years. Simulations of smog chamber experiments at the University
of California at Riverside (UCR) with explicit mechanisms in this study pro-
duced average differences between simulated and measured maximum one-hour-
average ozone and NO_2 concentrations of roughly 13 percent and 15 percent,
with average standard deviations of 20 and 13 percent. In most cases, the
accuracy of the predictions was comparable to the reproducibility of the
smog chamber experiments. Nevertheless, several problems remain.

In the majority of cases, consumption of the initial hydrocarbon was
simulated closely (our first criterion for a simulation), but the maximum

5

one-hour-average NO_2 and O_3 concentrations were overpredicted by approximately 5 to 20 percent. Thus, our predictions for NO_2 and O_3 show a slight positive bias. In experiments for which the hydrocarbon decay was predicted accurately, the measured net rate of conversion of NO to NO_2 was high at first, but lower after the NO/NO_2 crossover (the time at which [NO] = [NO_2]). The net conversion rates in the simulations could be adjusted to match the high initial rates in the experiments because the assumed initial [HONO] usually determined the initial rate. After the NO/NO_2 crossover, however, the simulated conversion rates did not always drop enough, and so the maximum simulated concentrations of both NO_2 and O_3 tended to occur earlier and to be greater than the corresponding measurements. The differences between simulations and measurements were small in many cases, but for some experiments, such as EC-151, they were large. Varying uncertain parameters in the mechanisms within reasonable limits usually improved the fit between the simulations and measurements of the early conversion rate but degraded the fit for the later conversion rate, or vice-versa. Because the net rates of formation of NO_2 and O_3 are related to the concentrations of radicals, one possible explanation is that some radical sink active in the smog chamber experiments after the NO/NO_2 crossover is not treated adequately in the mechanisms.

REFINEMENT OF EXPLICIT MECHANISMS

All simulations were obtained using the mechanisms described in Sections 5 and 6 under the reported physical conditions for each experiment. The only arbitrary and individual adjustments were the following:

> A small initial concentration of HONO was assumed in each simulation to help reproduce the measured rate of consumption of the initial hydrocarbon(s) early in each experiment. The amount of HONO assumed was almost always less than the equilibrium concentration calculated for the initial NO and NO_2 concentrations using the equation (Durbin, Hecht, and Whitten, 1975):

$$[HONO]_{eq} \simeq 0.18\{[NO][NO_2]\}^{1/2} \quad .$$

Typically, the assumed initial HONO concentration was about 0.33 $[HONO]_{eq}$ (see Figure 6 of Section 4).

> In some simulations, small adjustments were made in the intensity of irradiation at wavelengths that cause photolysis. Like the adjustments of the initial HONO concentration, these adjustments helped to simulate accurately the measured consumption of the initial hydrocarbon(s). The adjustments were within the range of reported intensity variations. The main justification for the adjustments is that they ensured that hydrocarbon decay products were being used in the mechanisms at the observed rates (see Figure 5 of Section 4).

> In a few simulations, the initial HC or NO_x concentration was changed slightly from the measured value. These changes were made to improve the overall agreement between the simulated and measured precursor concentrations. The adjustments were within the uncertainty of measurement of the reported initial concentrations. Furthermore, each concentration measurement is merely one data point in a series, and the closest overall agreement between simulated and measured concentrations of HC and NO_x provides the best foundation for examining how well a mechanism describes the formation of smog in a particular simulation.

> In some UCR experiments for which the reported initial NO_x concentration was zero, PAN was detected. The presence of PAN, which contains nitrogen, indicates the presence of NO_x at some time during the experiment. To simulate these experiments we had to assume limited degassing of NO_x from the chamber walls. The assumed input of NO_x was so small that including it in simulations of smog chamber experiments with nonzero initial NO_x concentrations had no discernable effects. In fact, there seemed to be an unexplained loss of NO_x in many UCR experiments, which may be the result of trapping of NO_x on the walls of the chamber.

We used the above methods to adjust the simulated hydrocarbon consumption rate to fit the measurements so that the simulation results would reflect the generation of secondary products in the chamber from the decay products of the primary precursors. Future research on absorption cross sections and quantum yields of carbonyls or improvements in the measurements of spectral intensity or carbonyl concentrations may show that the adjustments used in this report are in error. Other sources of radicals and possibly radical sinks may be discovered that our current mechanisms do not properly describe. In any case, the present approach can be considered as using carbonyl compounds as surrogates for the compounds produced during an experiment that in turn generate radicals. In this approach, the rate of production of radicals varies during the simulations. This variation produces different simulations than does a constant rate of radical production, as occurs in simulations in which radicals are assumed to be supplied by the walls of the chamber.

The assumption that radicals are supplied by the photolysis of products formed from the decay of the precursors is directly applicable to atmospheric modeling. The range of photolysis rate constants used to simulate UCR experiments provides an indication of the sensitivity of radical production and subsequent ozone formation to light intensity. The average value of 0.003 for the ratio of the aldehyde photolysis rate constant to the NO_2 photolysis rate constant that we used in simulations of UCR experiments is essentially the same value we used in simulations of experiments in the outdoor smog chamber at the University of North Carolina (UNC) (see Figure 5 of Section 4). Thus, the solar simulator used at UCR produces a spectrum that is consistent with the actual solar spectrum in terms of the aldehyde photolysis required in our mechanisms.

Three chambers were used to test the explicit formaldehyde mechanism: a small (160 liter) Teflon bag, the UCR chamber, and the UNC chamber. The bag experiments used relatively high (12 ppm) concentrations, and the predictions of the mechanism did not agree qualitatively with the observed NO_x

and ozone curves until the chemistry of peroxynitric acid (PNA) was added. Experiments in the other two chambers could be simulated adequately using the explicit formaldehyde mechanism with or without PNA chemistry because the pollutant concentrations were so low that, even if PNA was formed, it was formed in negligible concentrations.

Experimental problems complicated our studies with the formaldehyde mechanism. At UCR, the known amounts of formaldehyde added to the smog chamber did not agree with the measured initial concentrations, and in two experiments that were ostensibly started with no NO_x, NO_2 and other nitrogenous compounds were measured. For simulating these experiments it was necessary to assume that NO_x was degassing from the walls. At UNC, the formaldehyde experiment was contaminated by some ethylene from the nitric acid detector. Thus, our explicit formaldehyde mechanism requires further testing with "problem-free" data. Yet, the present simulations plus the simulations of experiments in which formaldehyde was purposely added (UCR Runs EC-45 and EC-257) support the present formaldehyde mechanism.

For the acetaldehyde/NO_x system and all other systems involving PAN chemistry, it was necessary to use the lowest reported values for the ratio of the rate constants for the reactions of NO and NO_2 with peroxyacetyl radicals. In agreement with the results of modeling work by Carter et al. (1978), we found that using an even lower ratio improved the agreement between our simulations and the measurements for both PAN and ozone. The disparity between the low ratio that produces accurate simulations and the higher ratio reported from laboratory measurement suggests some inaccuracy in the treatment of PAN chemistry in mechanisms.

The ethylene mechanism was constructed to be similar to a previous mechanism for propylene (Whitten and Hogo, 1977). At UCR, ethylene

experiments were performed in two groups. One group contained essentially twice the initial concentrations of precursors of the other, yet those experiments tended to have roughly the same or even somewhat lower maximum ozone concentrations. Simulations with the ethylene mechanism do not show this "reverse" effect, but the increase in the simulated maximum ozone concentration due to doubling of the initial precursor concentrations is small. The ozone isopleth diagram in Section 5 (Figure 15) demonstrates the slight ozone increase that results from doubling the precursors. We cannot tell now whether the ethylene mechanism tends to overpredict or underpredict ozone concentrations because it overpredicts for the low concentration experiments and underpredicts for the high concentration experiments. Thus, more experiments that produce low ozone levels (less than 0.7 ppm) need to be performed and modeled.

For propylene, closer agreement between simulations and measurements was obtained after we introduced into the mechanism a moderately rapid reaction between ozone and a peroxy radical that apparently forms following the reaction of hydroxyl radicals and propylene in air. Otherwise, the mechanism was essentially the same as that for ethylene, except for the higher rate constants and extra carbon atoms.

In the n-butane smog chamber experiments at UCR, we assumed:

> Values for the percentages of occurrence (or "splits")
  of various reaction pathways for alkoxyl radicals.
> A rather high quantum yield for production of radicals
  from methylethylketone (MEK) photolysis.

The assumed pathway splits were necessary to simulate the measured concentrations of MEK, acetaldehyde, and butyraldehyde. The high quantum yield for MEK photolysis was necessary to supply sufficient radicals in the simulations. Since other species whose concentrations are not measured, such as hydroxy-substituted aldehydes, may actually be supplying the required radicals, MEK may be a surrogate source of radicals.

Our simulations of n-butane/NO_x systems support the work of Darnall et al. (1976a) in that nitrate formation from the reactions of alkylperoxy radicals with NO had to be included in the mechanism. These reactions were necessary to simulate the roughly constant peak concentrations of ethyl and longer nitrates (relative to initial HC) despite variations in the initial butane/NO_x ratio. Production of alkyl nitrates from the reactions of alkoxyl radicals with NO_2, which were the only pathways for nitrate formation in an earlier mechanism (Whitten and Hogo, 1977), depends strongly on the hydrocarbon/NO_x ratio.

The mechanism developed for 1-butene is similar to the propylene mechanism, except that the main initial aldehyde produced is propion-aldehyde rather than acetaldehyde. The simulations with the 1-butene and propylene mechanisms exhibit similar agreement with the respective experimental data. As in the propylene mechanism, a low ratio for the rate constants of the reactions of NO and NO_2 with the peroxypropionyl radical seems to be necessary for accurate simulations. Unlike the propylene case, however, no data on the value of that ratio are available at present.

The trans-2-butene molecule decays rapidly to produce two molecules of acetaldehyde. Hence, its chemistry in smog-forming systems is similar to that of acetaldehyde, except for a brief period after the beginning of the experiment. As might be expected, the simulations with the trans-2-butene and acetaldehyde mechanisms exhibit similar agreement with measurements.

The only alkane other than butane for which we have data from UCR is 2,3-dimethylbutane. In terms of reaction with hydroxyl radical, this molecule should be much more reactive than butane. In the overall chem-istry leading to ozone production, however, 2,3-dimethylbutane appears to be less reactive than butane on a per-carbon-atom basis. The main reasons for this low reactivity are the formation of alkyl nitrates, which decreases

11

the rate of ozone production because it is a radical sink, and the production of compounds that do not photolyze readily. Nitrate formation from the reactions of alkylperoxy radicals with NO was included in the explicit 2,3-dimethylbutane mechanism, as it was in the butane mechanism, but the rate constants used in the 2,3-dimethylbutane mechanism are all estimated and thus require experimental confirmation. Nitrate formation reactions consume radicals, and so when incorporating them into the mechanism it was necessary to increase the production of radicals. The main source of radicals in the 2,3-dimethylbutane mechanism is acetone photolysis. As is the case for other mechanisms, acetone may partly be a surrogate for other compounds that are the actual sources of radicals. One line of evidence suggests that acetone is a major radical source. PAN is formed from peroxyacetyl radicals, which are generated by the photolysis of acetone or the hydroxyl attack on acetaldehyde. The high PAN concentrations and low acetaldehyde concentrations in the experiments suggest that acetone is the more important source of peroxyacetyl radicals. In general, the simulations with the 2,3-dimethylbutane mechanism indicate that more mechanism development work is necessary to simulate the high nitrate production without removing the radicals necessary to sustain chemical reactions in the simulations.

For simulating smog chamber experiments involving mixtures of hydrocarbons, no new reactions entailing interactions of carbon-containing species were necessary; the combination of the appropriate explicit kinetic mechanisms produced simulations that agreed reasonably well with measurements. For the special case of mixtures containing large amounts of acetaldehyde in the presence of propylene, the combination of the present mechanisms did not produce predictions that agreed with observations. The rates of consumption of propylene and acetaldehyde cannot be simultaneously simulated for EC-217 (propylene plus acetaldehyde) or EC-149 (propylene plus trans-2-butene). In the latter experiment, the trans-2-butene rapidly decayed to acetaldehyde. Further mechanism development for both acetaldehyde and propylene is in progress.

12

REFINEMENT OF GENERALIZED MECHANISM

From our studies of the generalized Carbon-Bond Mechanism (CBM) during the past-two years, we have drawn the following conclusions:

> Simulations in which initial hydrocarbon species were treated individually, rather than in groups, closely agreed with simulations using fully explicit mechanisms. These tests show that the secondary chemistry, such as reactions of alkylperoxy radicals and aldehydes, can be treated in condensed form at a small sacrifice in accuracy, thus saving considerable computing costs compared with the fully explicit treatment. To a large extent, this result was expected: The reactions of many secondary species in the explicit mechanisms, such as alkylperoxy radicals, are given the same rate constants because experimental values are not available and theory cannot adequately distinguish among the variety of alkyl structures. (These tests were performed using earlier versions of both the explicit and CBM mechanisms and will be repeated in the coming year with the revised mechanisms. The latter now contain special reactions, such as those for nitrate formation from alkylperoxy radicals, that depend on molecular structure.)

> Treating ethylene separately from other olefins is very important because of the wide difference in reactivity.

> Several types of averaging methods were considered for use in calculating rate constants for generalized species in the Carbon-Bond Mechanism. The weighted averages considered were the arithmetic, geometric, and harmonic means and a root-mean-square. In tests to date, the last method is the best. Thus, users of the CBM should compute weighted root-mean-square rate constants for reactions of the initial

mixture of hydrocarbons (if the individual rate constants
are known).

> Aromatics were treated separately from ethylene (unlike
earlier versions of the CBM). Instead of condensing pre-
sent versions of explicit chemistry, we developed a new
semi-empirical mechanism to simulate smog chamber data and
be consistent with the explicit chemistry.

> The CBM had to be changed in many ways to make it consistent
with the current explicit chemistry for olefins, paraffins,
and PAN. The revised version of the CBM was used to simu-
late many of the same experiments simulated with the explicit
mechanisms. In addition, a special set of 11 experiments
using three different mixtures of seven hydrocarbons was used
to evaluate the revised CBM. The three mixtures had differ-
ent reactivities due to different proportions of olefins,
paraffins, and aromatics. The results of this validation
exercise indicate that the revised CBM should be useful
for atmospheric modeling.

STUDY OF CHAMBER EFFECTS

Our conclusions from the study of chamber effects suggest an overall
verification of current smog chemistry. The same mechanism was found to
produce reasonable simulations of similar experiments performed in a var-
iety of smog chambers when important chamber-specific parameters (primar-
ily the light intensity and spectra) were taken into account. The specific
conclusions at this point are:

> The rate of disappearance of ozone by reaction with the
chamber walls can be calculated approximately given the
chamber's surface-to-volume ratio, mixing time, and
wall material.

> Assuming immediate reaction at the wall, the losses of
HONO and ozone affect the outcome of typical simulations

of UCR experiments significantly more than losses of other species, such as radicals.

> Uncertainties in measurements of pollutant concentrations and light intensities confound the search for wall effects.

> Some experiments in the Lockheed chamber with the spectrum attenuated at short wavelength could not be modeled accurately with our propylene mechanism, which suggests that a source of radicals in the Lockheed chamber is not treated in that mechanism. One possible radical source is ozone-olefin reactions.

> In some chambers, NO_x is apparently adsorbed by the walls during experiments in which the concentration of NO_x is high and desorbed during those in which NO_x is low.

> For some experiments at unusually high or low temperatures, adjustments in temperature-dependent rate constants alone were not sufficient to produce good fits between simulations and measurements. We found that changing the carbonyl photolysis rate constants greatly improved the fits, but the possibility of wall effects in those experiments remains.

RECOMMENDATIONS

In this section, we offer specific recommendations that focus on using modeling to highlight needs for future studies. In many cases, the discussions in the rest of this report explain the reasons for these recommendations more extensively. The recommendations are divided into three categories: laboratory measurements of reaction products and rate constants, smog chamber experiments, and analytical techniques. In addition to these specific recommendations, we wish to emphasize the need for both continued research to reduce the uncertainties in reaction rate constants and product distributions for individual reactions associated with and under experimental conditions relevant to smog chemistry and for continued chamber and modeling studies and analytical improvements to provide carbon and nitrogen mass balances for smog chamber experiments.

15

The specific recommendations regarding smog chamber experiments to be used with modeling studies are:

> Performance of a series of experiments using individual hydrocarbons from homologous series. Present extensions of explicit mechanisms, such as using similar reactions in mechanisms for ethylene, propylene, and 1-butene, are encouraging but limited. In the paraffin series, only butane and 2,3-dimethylbutane have been carefully studied. Such molecules as pentane, hexane, and others found in the atmosphere should be studied so that the schemes used in generalized mechanisms to generate average rate constants can be evaluated.

> Performance of experiments using molecules with various ring structures so that explicit mechanisms for them can be developed. Cyclohexane and cyclohexene are observed in the atmosphere, as are the various ring structures of natural hydrocarbons such as α-pinene. However, the details of the smog chemistry of such compounds are not known well enough to justify using generalized mechanisms to evaluate the importance of those compounds in photo-chemical oxidant formation in the atmosphere.

> Formulation of a new procedure for establishing the reactivity of individual compounds based on the influence that a single compound has on the overall reactivity of standard hydrocarbon mix. A suggested procedure is to establish a standard set of conditions for a standard hydrocarbon mix, such as specific concentrations of propylene and butane, and then to perform smog chamber runs with the standard mix and with 50 percent of the carbon atom concentration of the standard mix replaced by the compound being tested. Such a procedure should be useful for estimating (1) the potential influence of the test compound on ozone formation and (2) the fate of the test compound in urban atmospheres. The latter

information is necessary for modeling the chemistry in many industrial plumes.

The-recommendations concerning laboratory experiments of specific reactions are:

> Study of the reactions and rate constants of alkylperoxy radicals at typical atmospheric concentrations. The reactions of alkylperoxy radicals with NO, NO_2, O_3, and other radicals (particularly HO_2) are most appropriate for study. In addition to the rate of reaction with NO, the pathway to nitrate formation needs to be determined as a function of the structure of the alkyl group.

> Determination of the fate of the addition products when hydroxyl radicals react with olefins under atmospheric conditions. In particular, the peroxy radical that apparently forms when oxygen reacts with the addition product may react with ozone; this possibility warrants consideration.

> Study of the photolysis of ketones and aldehydes under typical atmospheric conditions to determine possible radical products. Modern kinetic mechanisms generally rely on the photolysis of carbonyl compounds (which are intermediate products in the atmospheric oxidation of hydrocarbons) to supply the majority of the radicals necessary to sustain the overall smog formation process in simulations.

> Further study of the decay routes of propylene and acetaldehyde. Using the currently recommended rate constants for hydroxyl attack, the mechanisms in this report do not simulate the observed rates of consumption of these two compounds simultaneously. We are now investigating whether any combination of acetaldehyde photolysis rate constants and-rate constants for reactions of hydroxyl

17

radical with acetaldehyde and propylene can produce simu-
lations in good agreement with measurements. However,
simultaneous observation of the reactions of these two
compounds in laboratory experiments with various reactive
species will be necessary to evaluate the modeling results.

Our main recommendation for improved measurements is:

> Determination of light spectra directly applicable to $O(^1D)$
generation and aldehyde photolysis. Although standard proce-
dures have been in use for some time to characterize light
intensity directly applicable to NO_2 photolysis, specific
procedures for these other species are needed. In the pre-
sent modeling study, the decay profile of hydrocarbon
(propylene) and the NO and NO_2 time profiles appeared to
be independent of NO_2 photolysis but strongly dependent on
aldehyde photolysis. The ozone time profile was strongly
dependent on both. In our studies, we often attempted to
increase the supply of radicals derived from $O(^1D)$ atoms.
However, the time profiles for many species (including ozone)
did not then conform to the shape of observed profiles.
Hence, a standard procedure for measuring the production of
$O(^1D)$ from ozone photolysis for a given smog chamber situa-
tion is needed to assimilate this reactive species into the
kinetic mechanisms correctly.

SECTION 3

BACKGROUND AND APPROACH

The computer modeling approach to the development of kinetic mechanisms was first used at SAI in 1972 under EPA Contract 68-02-0580. Efforts under that five-year contract were reviewed from a historical perspective by Whitten and Hogo (1977). Much of that work was directed toward the development of explicit mechanisms for propylene and butane, because most smog chamber experiments up to that time were carried out with those species as initial hydrocarbons. Two other early studies also emphasized the chemistry of propylene and butane (Niki, Daby, and Weinstock, 1972; Demerjian, Kerr, and Calvert, 1974). SAI's efforts, however, also had an underlying goal of developing generalized smog mechanisms suitable for use in photo-chemical air quality simulation models. The present study thus represents a continuation of previous efforts at SAI.

Three generalized smog mechanisms were developed in whole or in part at SAI for use in air quality modeling: the Hecht and Seinfeld (1972) mechanism (HS), the Hecht, Seinfeld, and Dodge (1974) mechanism (HSD), and the Carbon-Bond Mechanism (CBM) (Whitten and Hogo, 1977). The character of these mechanisms has progressed from a highly parameterized representation, based on a limited set of smog chamber data, to essentially a condensation of explicit mechanisms for propylene and butane that have been validated using a large data base. The HS mechanism was used in the original SAI Airshed Model (Reynolds et al., 1974). The HSD mechanism was used in several modeling studies at SAI and also in the Lawrence Livermore Laboratory's LIRAQ, a two-dimensional grid-type air quality model (MacCracken and Sauter, 1975). The CBM has been used by SAI in two major air quality modeling studies, one of the Denver area (Anderson et al., 1977) and the other of Los Angeles (Tesche and Burton, 1978). The latest version of the CBM, presented in Section 6, has been incorporated in SAI's current Airshed Model and is being used to model air quality in Los Angeles, Sacramento, and St. Louis.

Progression in the development of generalized mechanisms has been paralleled by improvements in experimental data:

> Individual reactions identified by computer modeling as being important in smog formation have been carefully studied in independent laboratories employing state-of-the-art experimental methods. Thus, the uncertainties in product distributions and rate constants have diminished considerably over the past few years.

> Efforts to assess all available information on individual chemical reactions have produced carefully evaluated sets of reactions and rate constants. These evaluations have greatly reduced the apparent ranges of uncertainty in various reactions, rate constants, and products, thus making computer modeling techniques more usable for testing hypotheses about photochemical oxidant formation.

> More smog chamber experiments have been performed, and the number of species used as initial hydrocarbons has increased. The data currently available at SAI include detailed concentration/ time profiles for several species in each of about 140 experiments in 10 different smog chambers.

These improvements have had the beneficial effects of both reducing the number of empirical parameters in kinetic mechanisms and opening up a new approach for mechanism validation. Below we describe computer modeling in general terms and then present our approach for validating kinetic mechanisms.

THE PROCESS OF COMPUTER MODELING

To simulate a smog chamber experiment, one must have data from the smog chamber experiment, a kinetic mechanism, and a computer program that simulates gas-phase chemistry by integrating the differential equations developed

20

from the chemical mechanism. The data and the mechanism have inherent uncertainties.* Some smog chamber measurements are accurate only to within ±50 percent. In addition, smog chamber data are never complete because it is not currently possible to measure the concentrations of all species present in a smog chamber experiment. In experiments initiated with toluene and NO_x, for example, toluene decays to produce a host of complex organic molecules, many of which have not even been identified, much less routinely measured.

Kinetic mechanisms also have inherent uncertainties, the most obvious being the uncertainties in laboratory measurements of rate constants. Another source of uncertainty is the reaction pathway: In some cases the rate constant for the reaction between two species is known, but the products of that reaction are not. In other cases a reaction can produce either of two sets of products, but the fraction of reactions leading to either set is not known. In many cases rate constants or pathways are determined under laboratory conditions far removed from atmospheric conditions. Extrapolation to atmospheric pressure, temperature, and concentrations of O_2 and water vapor may lead to error. Another type of uncertainty is associated with "wall effects." Smog chambers have much lower surface-to-volume ratios than most laboratory reaction vessels, and so wall effects that are unimportant in smog chambers may perturb laboratory measurements.

A principal goal in computer modeling of smog chemistry is to develop a set of reactions and rate constants that provides the closest possible agreement between simulations and measurements for a series of experiments. This development is carried out by:

---

* Computer programs for simulating gas-phase chemistry incorporate numerical integration methods that have nonzero error tolerances, but the uncertainty due to numerical integration is negligible compared with the sources of uncertainty mentioned above. SAI used the CHEMK computer program (Whitten and Meyer, 1975) for simulating gas-phase chemistry.

> Using measurements or estimates of all important reactions,
  products, and rate constants known or expected to occur
  in the system of interest, within their limits of uncertainty,
  to formulate a kinetic mechanism.
> Estimating the physical conditions appropriate for the experi-
  ments performed (e.g., the initial HONO concentrations, the
  temperature during each experiment, and other parameters).
> Simulating the smog chamber experiments using a computer.
> Modifying or adding reactions, products, and rate constants
  until satisfactory agreement between simulations and measure-
  ments is achieved.

APPROACH FOR MECHANISM VALIDATION

During this study we developed an approach for validating a series of
kinetic mechanisms that is intended to minimize the possibility of fortui-
tous agreement between simulations and measurements. A valid kinetic
mechanism, unlike a mere curve-fitting exercise, should give reasonable
predictions when used in applications such as atmospheric modeling that
are outside the range of conditions and smog chamber experiments for which
it was developed. Our approach is based on the following principles:

> The first measurements that must be reproduced with accept-
  able accuracy are those related to the consumption of the
  initial hydrocarbon(s). A mechanism for propylene/NO_x
  systems, for example, should describe the disappearance
  of propylene and the reactions of intermediate species
  that eventually lead to the formation of ozone. Good
  agreement between measured and simulated ozone concen-
  trations, coupled with poor agreement for propylene,
  is indicative of compensating errors in the kinetic mech-
  anism. Errors that compensate one another under the con-
  ditions of a particular smog chamber experiment are not
  likely to do so for other experiments or atmospheric
  applications.

> In simulating a series of experiments in the same smog
  chamber, chamber-dependent effects must be treated con-
  sistently. If ozone is assumed to react with the walls
  of the chamber, for example, the same rate constant for
  that reaction should be used in all simulations of exper-
  iments in that chamber unless some characteristic of the
  chamber has been changed. If a light source is assumed to
  emit progressively lower amounts of short-wavelength radia-
  tion over a period of several months, the photolysis rate
  constants for the series of experiments must diminish in
  accordance with the order of performance of the experiments.
  Arbitrary adjustments for such effects must be avoided.
> The smog chamber walls should not be assumed to be major
  sources or sinks of radicals or other chemical species.
  Our research thus far suggests, though it does not prove,
  that the walls are at most minor sources or sinks of radicals.
  Dependence on wall reactions to supply or consume
  radicals in order to produce more accurate simulations
  tends to mask inadequacies in kinetic mechanisms and to
  confound their application to atmospheric problems.

Besides the above principles, we have applied another principle of
mechanism validation, one that is based on the concept of a hierarchy of
chemical species in photochemical oxidant formation. This concept is
discussed in the next section.

THE CONCEPT OF A HIERARCHY OF SPECIES

Much of the work on explicit mechanisms in this study has been guided
by the concept of a hierarchy of chemical species in photochemical oxidant
formation. As mentioned in Section 1, each species involved in oxidant
formation can be assigned to a hierarchical level on the basis of the
number of HC/NO_x systems in which it occurs, with the most ubiquitous
species occupying the lowest level. As an example consider the reactions

of butane and acetaldehyde. Acetaldehyde is formed in significant quantities during photochemical oxidation of butane/NO_x systems, and the reactions of acetaldehyde must therefore be included in an explicit mechanism for butane. The reverse is not true: Little or no butane is formed in the photochemical oxidation of acetaldehyde/NO_x systems. As a consequence, butane reactions need not be included in an explicit mechanism for acetaldehyde. Thus, butane is assigned to a higher hierarchical level than acetaldehyde. The hierarchical levels used in our study are shown schematically in Figure 1.

The value of the hierarchical concept is the principle it suggests for validating explicit mechanisms for a series of hydrocarbons. In brief, one should validate mechanisms for species at the lowest level first. For example, one can begin by validating the explicit formaldehyde mechanisms, using data from formaldehdye/NO_x smog chamber experiments. An explicit acetaldehyde mechanism can then be constructed by adding a few reactions and rate constants to the explicit formaldehyde mechanism. In validating the acetaldehyde mechanism (using data from acetaldehyde/NO_x experiments), only the additions need be examined--the reactions and rate constants from the validated explicit formaldehyde mechanism should not be modified in any way. Mechanisms for the hydrocarbons can be constructed by adding the appropriate reactions and rate constants to mechanisms for these aldehydes.

Validating mechanisms in the stepwise order suggested by the hierarchical levels clarifies the sources of uncertainty in simulations and reduces the probability that a complex mechanism for a large hydrocarbon contains conpensating errors. In a series of mechanisms validated in this way, if the formaldehyde mechanism provides simulations that agree well with measurements but the acetaldehyde mechanism does not, the portions of the acetaldehyde mechanism that might be the cause should be obvious.

24
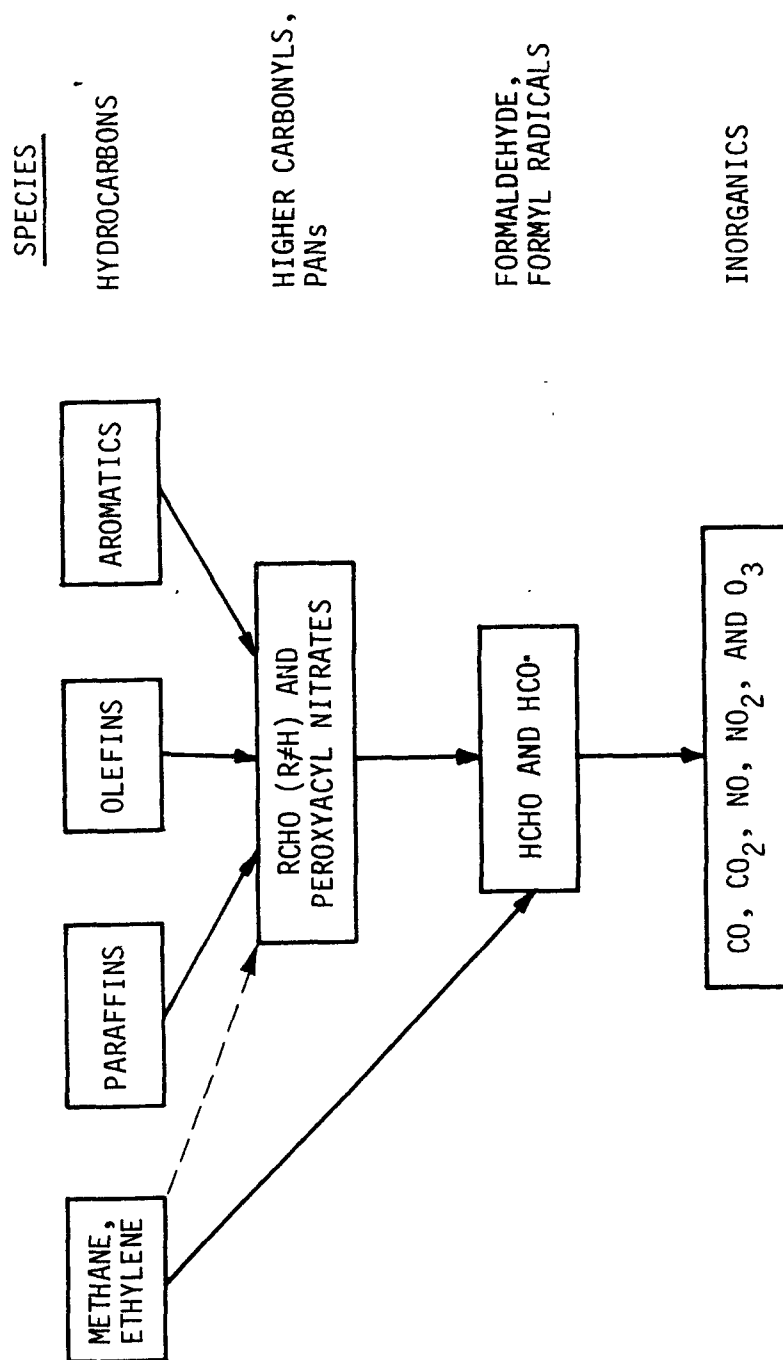
Figure 1. Schematic diagram of hierarchical levels of species in photochemical smog

SECTION 4

TREATMENT OF INORGANIC REACTIONS

One of the most important needs in developing kinetic mechanisms is accurate rate constant measurements. The inorganic chemistry in hydrocarbon/NO_x kinetic mechanisms includes reactions for which both the rate constants and the detailed reaction pathways are not well known. In this section we discuss recent observations about these reactions that have led us to modify their reaction rate constants and reaction pathways.

PHOTOLYSIS REACTIONS

As in previous work, for simulating smog chamber experiments at the University of California at Riverside, we used the NO_2 photolysis rate constant, k_1, exactly as reported. Wu and Niki (1975) reported that the uncertainty in the measured NO_2 decay rate, k_d, which is used to derive k_1, is as great as ± 30 percent, depending on the timing of the measurements. During this past year, we found much better fits between simulated and measured concentrations could be obtained by varying k_1 within that uncertainty range. Therefore, for smog chambers other than UCR, we varied k_1 within that range.

In previous simulations of UCR smog chamber data (Durbin, Hecht, and Whitten, 1975; Whitten and Hogo, 1977), we determined photolysis rate constants for O_3, HONO, H_2O_2, and the aldehydes by multiplying the ratios of those rate constants to the NO_2 photolysis rate constant times the measured NO_2 photolysis rate constant (usually described as the ratio to k_1). For any measured light spectrum, we were able to generate a set of ratios of photolysis rate constants that could be related to the measured NO_2 photolysis rate constant.

Although data from the later UCR runs include measured light intensities for each run, the uncertainties associated with those measurements

need to be quantified. Since aldehyde photolysis is of major importance in photochemical smog mechanisms (Whitten and Dodge, 1976; Whitten and Hogo, 1977), the light intensity measurements must be very accurate in the region in which aldehydes photolyze. Figure 2 shows the photolysis cross sections of HONO, acetaldehyde, O_3, and NO_2. Note that O_3 and acetaldehyde photolyze in the region from 280 nm to 340 nm. Because of the method used by UCR to report measured intensities at various wavelengths (namely, as ratios relative to the intensity at 370 nm normalized to 0.75), the intensities in the range from 280 to 330 nm are highly uncertain. Figure 3 shows the relative intensities in the range from 300 nm to 330 nm reported by UCR for experiments up to Run EC-253. The "old simulator" is the solar simulator used by UCR beginning with experiment EC-20. The scatter between reported values is greatest at 300 nm and decreases at higher wavelengths. A factor of almost 8 separates the lowest and highest intensities reported at 300 nm, compared with a factor of roughly 2 between the lowest and highest intensities at 330 nm. Figure 4 presents an exploded view of the intensities reported at 320 nm, which is near the peak of the acetaldehyde photolysis range.

Owing to the large uncertainties in measured light intensities in the 280 to 330 nm range, we varied the aldehyde photolysis rate constants to give better predictions in the simulations of the UCR experiments. Recent work by Moortgat et al. (1978) provided us with new quantum yields for formaldehyde photolysis. Through calculations using quantum yields from Moortgat et al. (1978) and a spectral distribution typical of the UCR solar simulator, we found that the rate constant for photolysis of formaldehyde leading to radicals was, within experimental error, equal to the rate constant for photolysis of formaldehyde leading to nonradical products. For convenience, we define the numerical value of this rate constant by the symbol "FORM→ Products" [note that the total formaldehyde photolysis rate constant is thus 2 x (FORM→Products)]. If the quantum yield for photolysis of acetaldehyde leading to radicals is assumed to be 1.0, the calculated photolysis rate constant turns out to be equal to FORM→Products. Through trial and
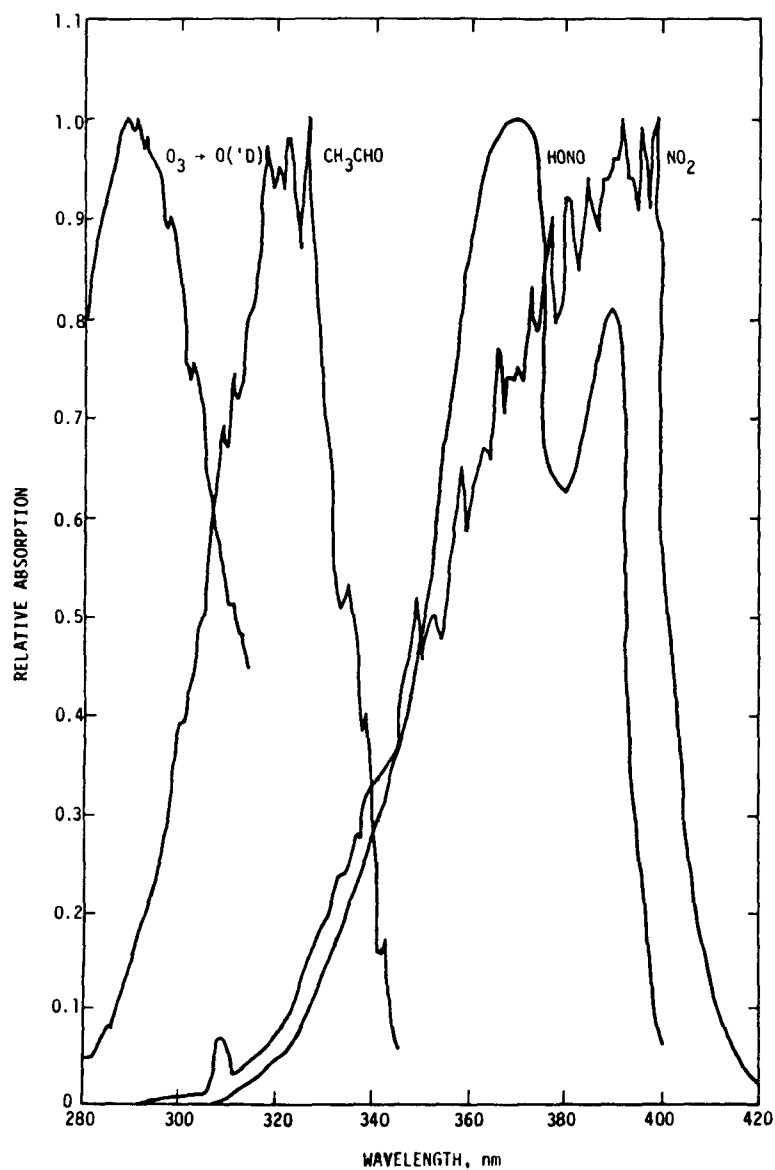
Figure 2. Absorption cross sections for photolysis of O_3, acetaldehyde, HONO, and NO_2
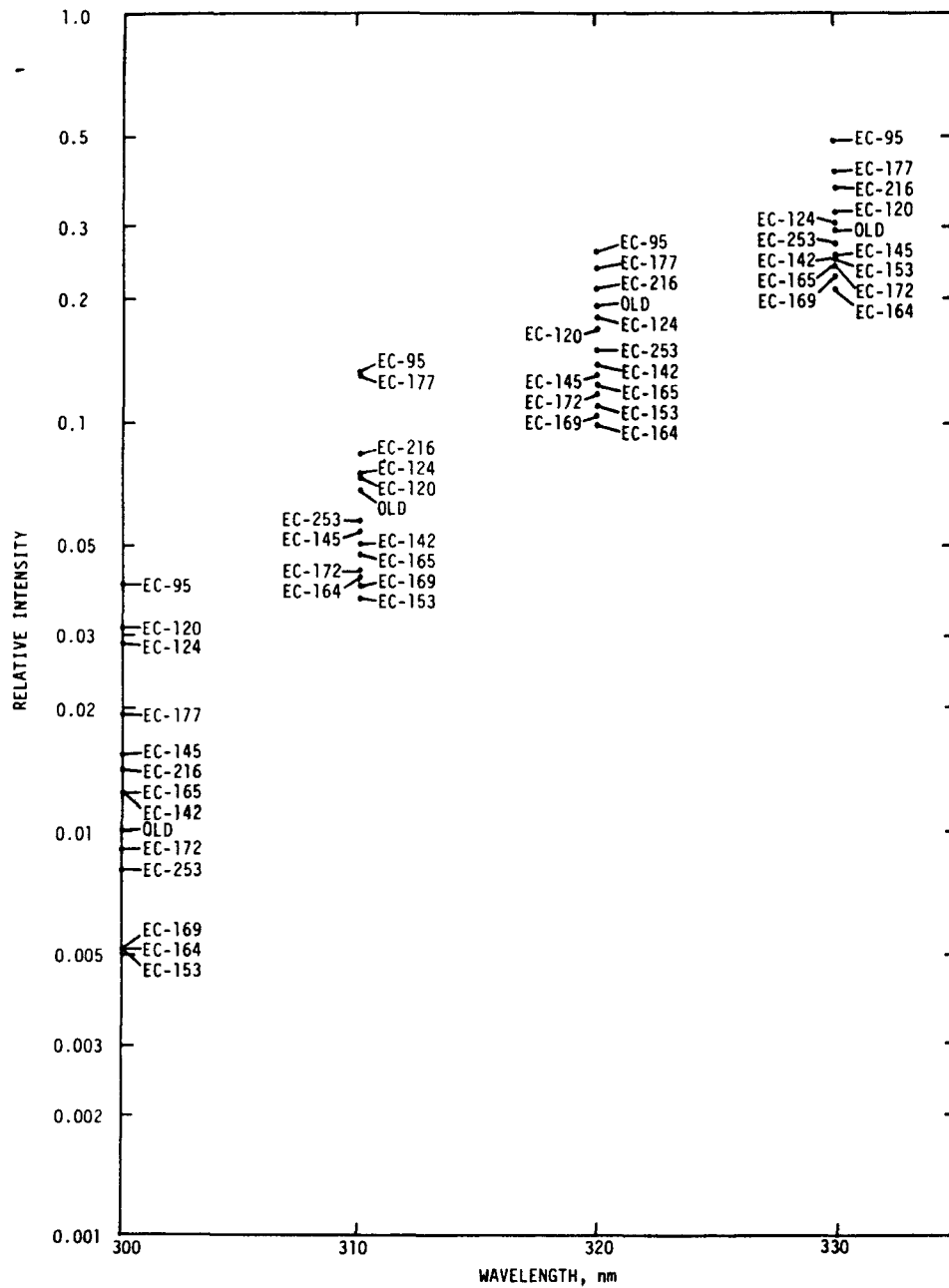
Figure 3. Relative light intensities in the range from 300 to 330 nm for different experiments at UCR. "Old" refers to the original solar simulation, which was used in early UCR runs.
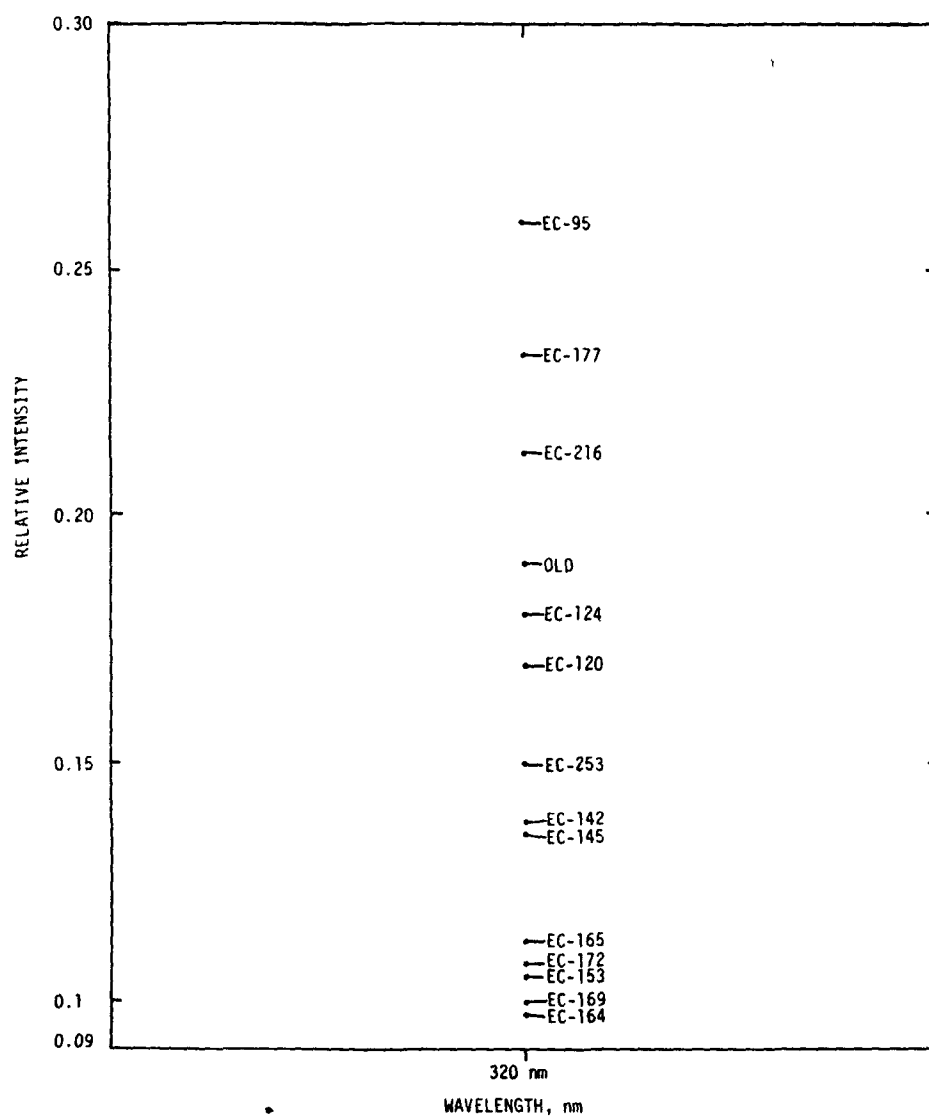
Figure 4.   Relative light intensities at 320 nm for
             different experiments at UCR

error, however, we found that a quantum yield of 0.5 (corresponding to a photolysis rate constant of 0.5 FORM→Products) provided the best fit to the available data. For all aliphatic aldehydes except formaldehyde, in all UCR simulations, we assumed photolysis rate constants for radical production of 0.5 FORM→Products. For ketones and difunctional aldehydes (such as hydroxyaldehydes), we assumed photolysis rate constants of FORM→Products. Thus, photolysis rate constants for nearly all carbonyl species, in all simulations of UCR experiments, were equal to FORM→Products multiplied by either 1.0 or 0.5.

We varied the numerical value of FORM→Products within a small range to optimize the fits between simulations and measurements. Note that intensities at 320 nm (the peak wavelength for aldehyde photolysis) are reported by UCR not in terms of absolute intensity, but in terms of intensity relative to 0.75 of the intensity at 370 nm. The intensities at 320 nm reported by UCR had a slightly greater variability (in terms of standard deviation) than did our choices of FORM→Products. To show this, we plot in Figure 5 (1) the product of FORM→Products divided by the NO_2 photolysis rate constant
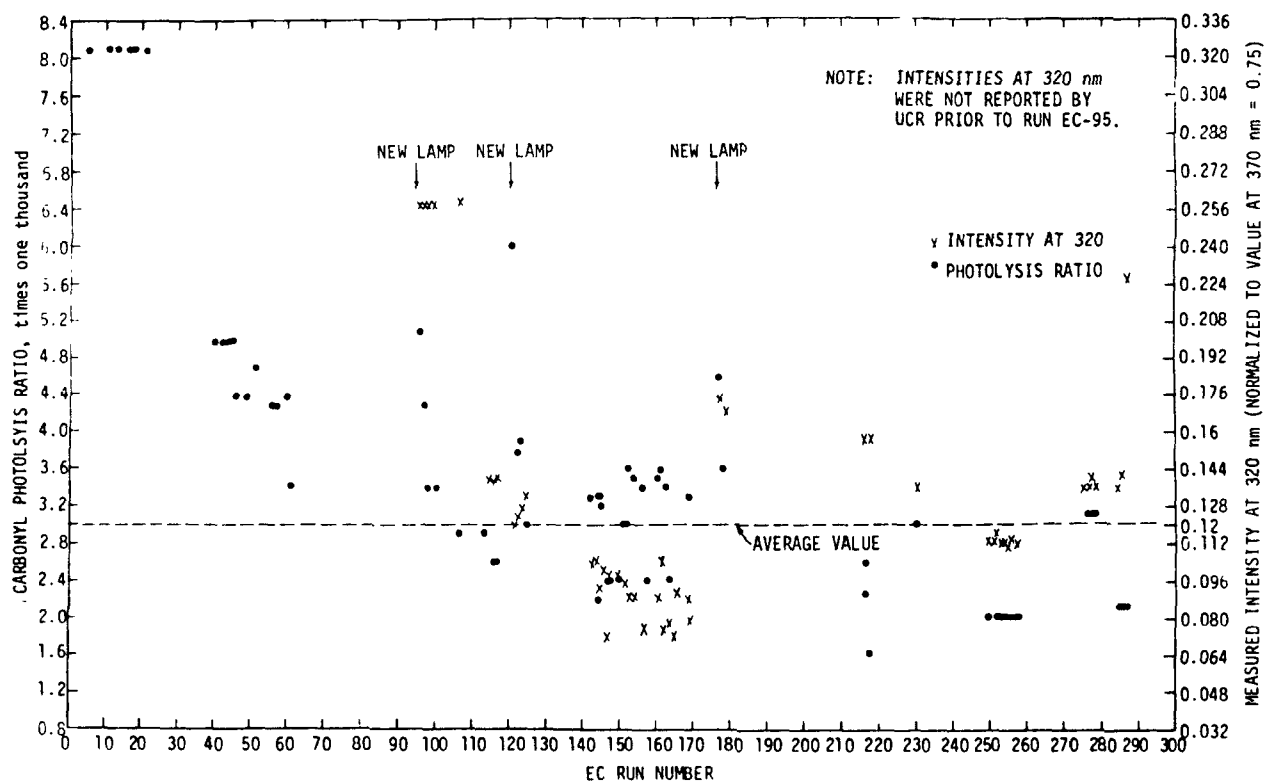
Figure 5. Comparison of carbonyl photolysis ratios used in the UCR simulations and reported intensities at 320 nm.

used in each simulation (termed the "carbonyl photolysis ratio") and, on the other vertical axis, (2) the reported intensity at 320 nm relative to 0.75 times the intensity at 370 nm. In Figure 5 the vertical axes were chosen such that the averages of (1) and (2) for runs EC-95 through EC-287 are on the same horizontal line, and the scale divisions were chosen so that scale divisions on the left and right vertical axes are equal to the same percentage differences in (1) and (2). This choice permits visual examination of the spread of values. The standard deviation of (1) is 29 percent, and of (2), 31 percent, over all UCR experiments from UCR EC-95 through EC-287.

CHEMISTRY OF HONO

Nitrous acid (HONO) can be an important initial radical source in simulating a smog chamber experiment performed with a constant radiation flux (Whitten and Hogo, 1977). Figure 6 shows the initial HONO values used in our simulations. Cox and Derwent (1976) reported HONO absorption cross sections higher than those reported by Graham (private communication, 1975), which had been used by Whitten and Hogo (1977). The higher absorption cross sections mean a higher initial rate of radical production. The rate of formation of HONO from OH$\cdot$ and NO was reported to be faster than previously estimated (Cox, Derwent, and Holt, 1976). Finally, gas-phase formation by the nonradical reaction $NO + NO_2 + H_2O \rightarrow 2HONO$ was reported to be much slower than thought previously (Kaiser and Wu, 1977). Modifying our kinetic mechanisms in accordance with these three developments has two implications: Nonradical HONO formation in the gas phase is not significant; and HONO is now a noncritical species.

Noncritical status means that HONO is present at a very low steady-state concentration during most of a simulation. The low concentration guarantees that no significant amount of radicals or NO_x is tied up in HONO. Neither its formation rate nor its photolysis rate is critical to the outcome of a smog chamber simulation as long as the formation and

destruction rates are fast. Note that HONO may not be in a steady state during the first few minutes of a smog chamber experiment with constant light: HONO formation in the dark may occur slowly, but the rate of HONO destruction by photolysis is zero until the light is turned on.

AVERAGE (INITIAL $[HONO]/[HONO]_{eq}$) = 0.36
STANDARD DEVIATION = ±0.26

(y-axis) INITIAL $[HONO]/[HONO]_{eq}$

(x-axis) UCR EXPERIMENT EC-Number
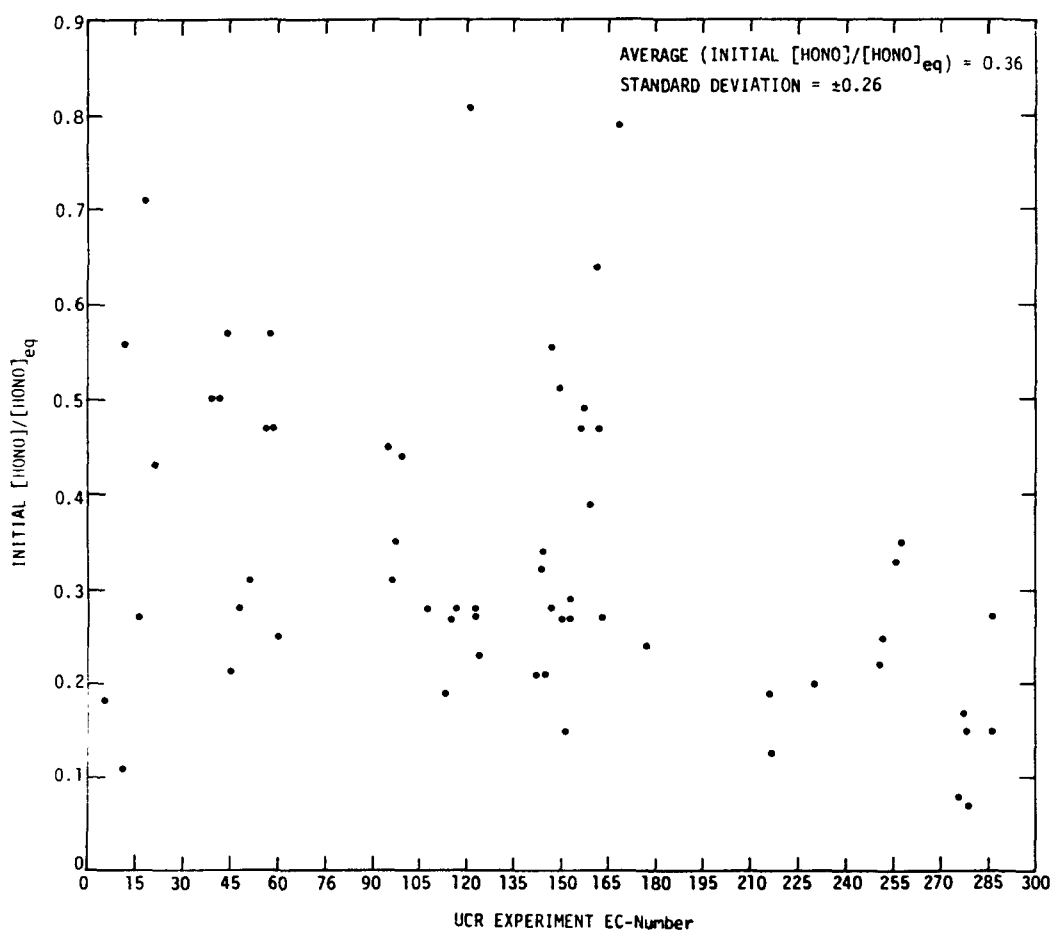
Figure 6. Initial HONO concentrations (expressed as fractions of equilibrium concentrations) assumed for simulations of UCR experiments

In other words, eliminating HONO chemistry from a mechanism should cause very little difference in simulations of smog chamber experiments with slowly increasing irradiation. To demonstrate this, we simulated an experiment in the outdoor chamber at the University of North Carolina, where the slow increase in light intensity suppresses the initial radical problem seen in experiments with constant light. Figures 7 and 8 show the measured NO, NO_2, O_3, and propylene concentrations and those calculated with and without HONO in the explicit kinetic mechanism for propylene.* Simulation of this UNC experiment required a small initial concentration of HONO to provide initial radicals. Simulation of the UNC experiment without HONO chemistry also required a small initial source of radicals, which we provided by introducing a species "RX" which decays to produce OH· radicals at a rate equal to the HONO photolysis rate.

PHOTOLYSIS OF O_3

The photolysis of ozone that leads to the production of $O(^1D)$ is caused mainly by 280 to 310 nm UV. There is still some uncertainty in the quantum yields for the production of $O(^1D)$ (Philen, Watson, and Davis, 1977). During our work on chamber effects and the 2,3-dimethylbutane/NO_x system, we found that the input of radicals from the $O(^1D)-H_2O$ reaction might be important. Detailed discussions of this potential radical source are presented in Section 6 on chamber effects and Section 5 on 2,3-dimethylbutane chemistry.

Our major conclusion concerning $O(^1D)$ production is that accurate quantum yields for the production of $O(^1D)$ from the photolysis of ozone are needed, or possibly an NO titration from the N_2O reaction with $O(^1D)$ in a smog chamber using an accurate NO detector (Stedman, 1977) could be used. Recent work by Kajimoto and Cvetanovic (1976) has shown that $O(^1D)$ production from ozone may be temperature-dependent. The effect of temperature is to spread the range of UV that photolyzes O_3 to produce $O(^1D)$ from 280 to 310 nm to 280 to 317 nm or 280 to 320 nm.

---

* As noted earlier, in all figures in this report symbols represent measured concentrations and lines represent simulated concentrations.
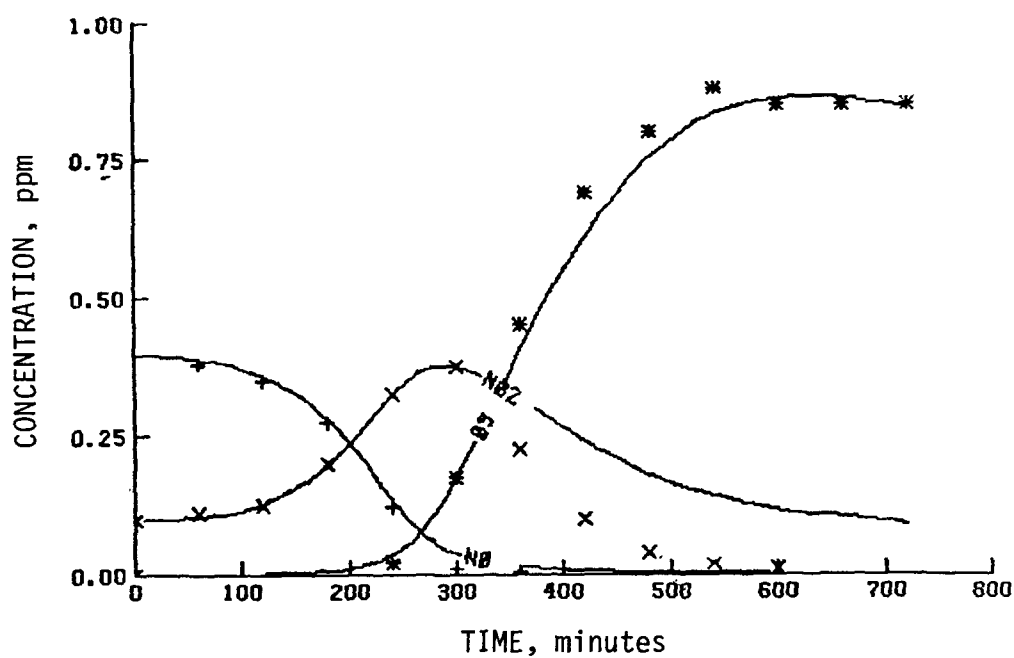
(a) NO_2, NO, and O_3
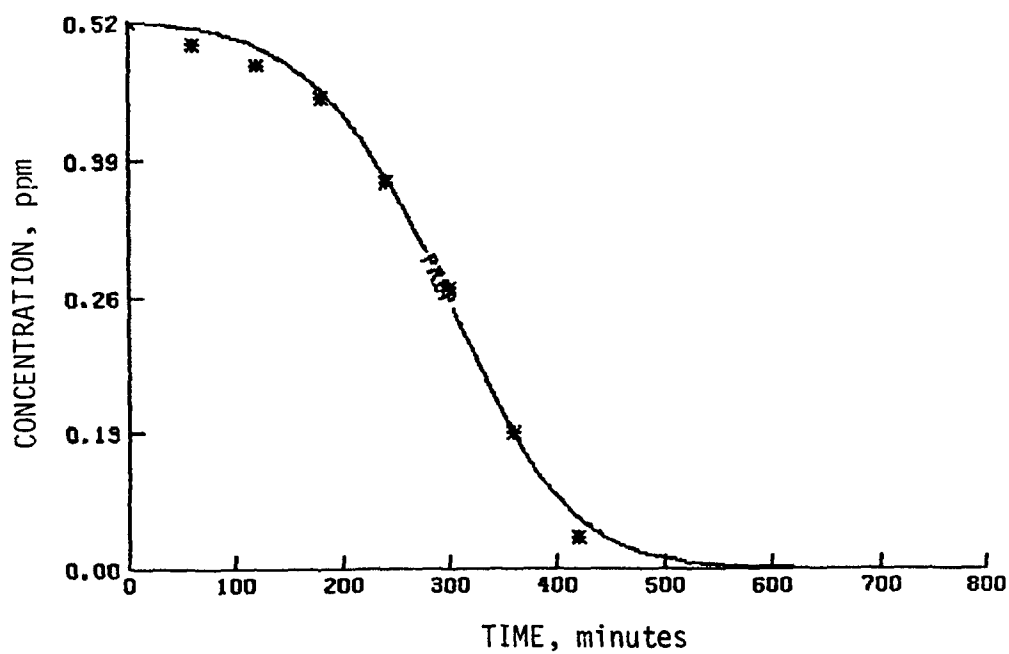
(b) Propylene

Figure 7. UNC propylene/NO_x measurements (8 August 1977) and
explicit propylene mechanism predictions with HONO
chemistry included (initial HONO concentration
of 3 ppb)

35
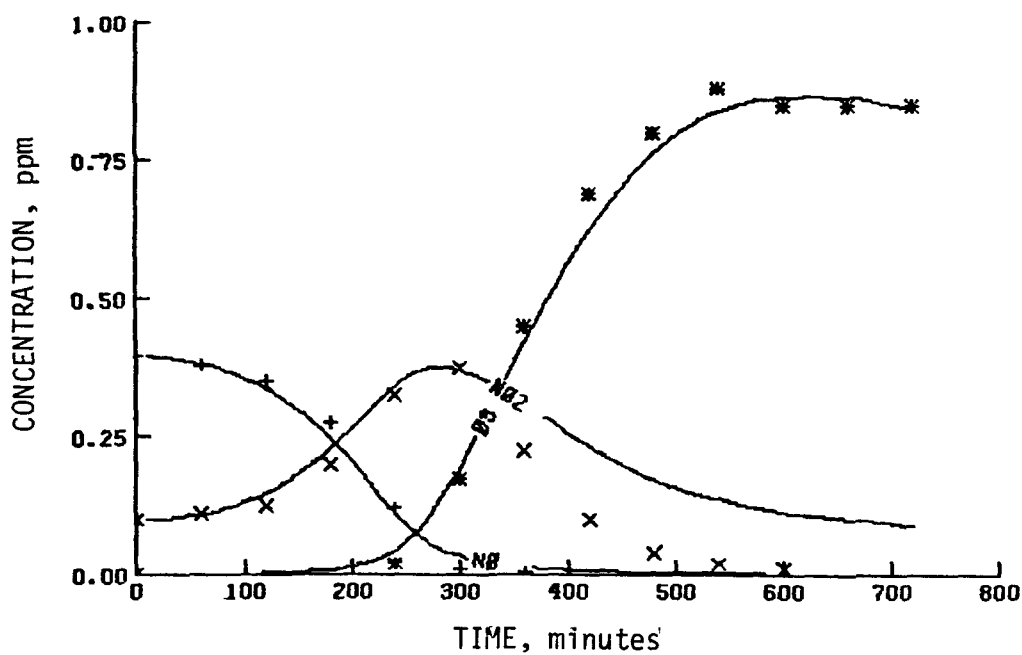
(a) NO_2, NO, and O_3
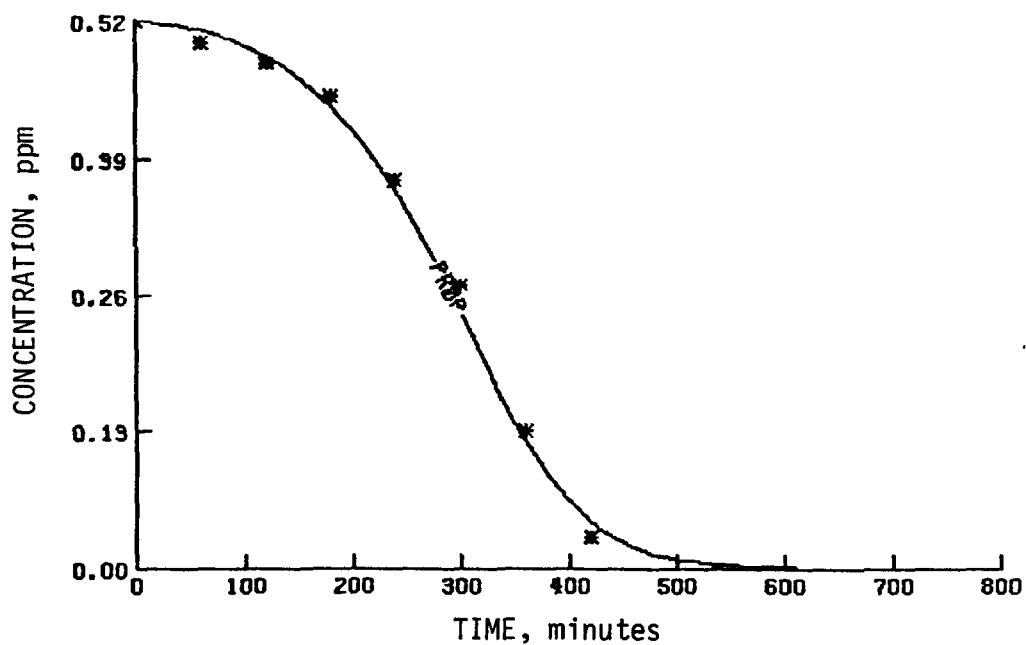
(b) Propylene

Figure 8.   UNC propylene/NO_x measurements (8 August 1977) and explicit propylene mechanism predictions without HONO chemistry (an initial concentration of 1.5 ppb of radical source "RX" was included)

PHOTOLYSIS OF HYDROGEN PEROXIDE

The absorption cross sections for the photolysis of hydrogen peroxide (H_2O_2) were measured by Lin, Rohatgi, and DeMore (1978). The new values are approximately 40 percent lower than the values used by Whitten and Hogo (1977). We incorporated the new absorption cross sections into the calculation of the hydrogen peroxide photolysis rate constant.

REACTIONS OF OH· WITH NO AND WITH NO_2

The reaction of nitrogen dioxide (NO_2) with hydroxyl radical (OH·) is a sink of both radicals and NO_x:

$$OH· + NO_2 \rightarrow HONO_2 \quad . \tag{1}$$
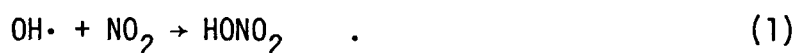
As discussed above, the reaction of OH· with nitric oxide (NO),

$$OH· + NO \xrightarrow{M} HONO \quad , \tag{2}$$

is of little importance during a smog chamber experiment because HONO photolyzes, at a time constant of about 5 minutes, to regenerate OH· and NO. Recent evaluations by Hampson and Garvin (1978) have shown that the rate constants for these two reactions are faster than previously reported values of 9×10^3 and 9.2×10^3 $ppm^{-1}min^{-1}$, respectively. The values now used in our kinetic mechanisms for the rate constants of NO + OH· and NO_2 + OH· are 1.4×10^4 and 1.4×10^4 $ppm^{-1}min^{-1}$, respectively.

REACTION OF N_2O_5 WITH H_2O

One of the major wall reactions we have considered in past studies is that of dinitrogen pentoxide (N_2O_5) with H_2O:

$$N_2O_5 + H_2O \rightarrow 2HONO_2 \tag{3}$$

This reaction has been studied extensively, but the contributions of the heterogeneous and homogeneous pathways are still uncertain. In previous simulations of the University of California at Riverside smog chamber data, we used a value of 5×10^{-6} $ppm^{-1}min^{-1}$ as the rate constant for this reaction. Jeffries, Fox, and Kamens (1975) used a value of 5.6×10^{-7} $ppm^{-1}min^{-1}$ for the $N_2O_5 + H_2O$ reaction to simulate experiments in the outdoor smog chamber at the University of North Carolina. Carter et al. (1978) reported that earlier UCR experiments (before EC-116) required a higher $N_2O_5 + H_2O$ rate. Some of our simulations of more recent UCR experiments suggest that this rate constant may be lower than the value of 5×10^{-6} $ppm^{-1}min^{-1}$. Therefore, for UCR experiments before EC-121, we used a value of 1.5×10^{-5} $ppm^{-1}min^{-1}$ [which is the upper limit reported by Morris and Niki (1975)]. For more recent UCR experiments, we are using a value of 5×10^{-6} $ppm^{-1}min^{-1}$ in the computer simulations until more conclusive results are reached.

REACTION OF $HO_2^{\cdot}$ WITH NO_2

One of the interesting results in smog chemistry is the observation of the intermediate species $HOONO_2$ (peroxynitric acid or PNA) from the reaction of hydroperoxyl radicals $(HO_2^{\cdot})$ with NO_2. This species has been observed by Niki et al. (1977) and Levine et al. (1977). The fate of peroxynitric acid is a matter of controversy. Apparently, PNA can decompose to re-form $HO_2^{\cdot}$ and NO_2 or decompose on surfaces to form HONO and O_2. Niki et al. (1977), however, did not detect any HONO in their experiments on $HOONO_2$:

$$HO_2^{\cdot} + NO_2 \overset{M}{\underset{\rightleftharpoons}{}} HOONO_2 \quad , \tag{4}$$

$$PNA \rightarrow HONO + O_2 \quad . \tag{5}$$
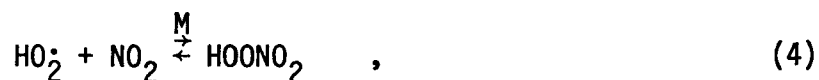
Jeffries (1976) hypothesized that the decomposition of peroxynitric acid is analogous to that of peroxyacyl nitrates and with a similar (high) activation energy for decomposition. Howard (1977) measured the pressure-dependent

rate constant for the PNA formation reaction to be approximately 7200 ppm^{-1} $ppm^{-1}min^{-1}$ and estimated that the reaction to form HONO and O_2 has a rate constant of less than 4 $ppm^{-1}min^{-1}$. Graham, Winer, and Pitts (1978) reported the $HOONO_2$ decomposition rate constant as 5.8 min^{-1} at 298K. This is the limiting first-order high-pressure rate constant. The activation energy for the decomposition of $HOONO_2$ was reported to be 19.9 kcal mol^{-1}. Baldwin and Golden (1978) also investigated $HOONO_2$ formation and decomposition. From thermochemical estimates, they reported the PNA formation rate to be approximately 7750 $ppm^{-1}min^{-1}$ and the activation energy for the decomposition reaction to be 23 kcal mol^{-1}. Since the rapid formation and decomposition of PNA leads to a steady-state relationship, which can be eliminated from current mechanisms, we chose for the time being to not include PNA formation or decomposition in our kinetic mechanisms.

REACTIONS OF $O(^1D)$

Two reactions of $O(^1D)$ are included in the inorganic reactions in our kinetic mechanisms: $O(^1D)$ + M and $O(^1D)$ + H_2O. The rate constants for these reactions have been updated to the values recommended by Hampson and Garvin (1978). The rate constant for $O(^1D)$ + M is 3.22 x 10^4 exp(98.6/T) $ppm^{-1}min^{-1}$. The rate constant for $O(^1D)$ + H_2O is 3.4 x 10^5 $ppm^{-1}min^{-1}$.

REACTIONS OF $HO_2^{\cdot}$ WITH NO AND WITH $HO_2^{\cdot}$

The series of reactions involving hydroperoxy radicals ($HO_2^{\cdot}$) was recently studied by Howard and Evenson (1977). For $HO_2^{\cdot}$ + NO, they reported a rate constant of 1.2 x 10^4 $ppm^{-1}min^{-1}$, which is a factor of 6 higher than the value estimated by Cox and Derwent (1975). We used the increase in the $HO_2^{\cdot}$ + NO reaction rate constant to justify increasing our estimated rate constants of all reactions involving $HO_2^{\cdot}$, since most of the rate constants of reactions with $HO_2^{\cdot}$ have been measured relative to a base reaction. As an example, for the $HO_2^{\cdot}$ + $HO_2^{\cdot}$ reaction we are tentatively using a value of 1.5 x 10^4 $ppm^{-1}min^{-1}$.

REACTIONS OF OZONE WITH OH· AND WITH HO_2

Rate constants for the reactions of ozone with OH· and HO_2 have been updated to the values recommended by Hampson and Garvin (1978). Both reactions have an activation energy of ~1000K. The rate constant at 298K for O_3 + OH· reaction is 77.2 $ppm^{-1}min^{-1}$, and the rate constant at 298K for O_3 + HO_2 is 1.5 $ppm^{-1}min^{-1}$. Based on the higher HO_2 + NO rate constant reported by Howard and Evenson (1977), we raised the O_3 + HO_2 rate constant to 5 $ppm^{-1}min^{-1}$. As noted above, rate constants for reactions involving HO_2 are still very uncertain because most rate constants are measured relative to the rate constant of a reference reaction.

DARK DECAY OF OZONE

The ozone dark decay rate was reevaluated for the UCR chamber on 6-7 July 1976. UCR found an ozone half-life of 16 hours, which gives an ozone dark decay constant of 7.2 x 10^{-4} min^{-1}. Determinations of the ozone dark decay in June 1973 gave values of 1 x 10^{-3} min^{-1}. Another determination on 18 May 1976 gave a rate of 9.7 x 10^{-4} min^{-1}. Due to the uncertainties involved in any specific value, we assumed a value of 1 x 10^{-3} min^{-1} for the ozone dark decay rate in all simulations of UCR experiments. For simulations of experiments in other chambers we developed a theoretical method for estimating the ozone dark decay (see Section 7).

REACTIONS OF NO_3 WITH NO AND WITH NO_2

Graham and Johnston (1978) studied systems involving the nitrate radical (NO_3) and reported rate constants for the reactions of NO_3 with NO and NO_2 that are different than those recommended by Hampson and Garvin (1975). We are currently using the rate constants of 2.8 x 10^4 $ppm^{-1}min^{-1}$ for NO_3 + NO and 3800 $ppm^{-1}min^{-1}$ for NO_3 + NO_2 reported by Graham and Johnston (1978).

REACTION OF CO WITH OH·

The reaction rate constant for CO + OH· has been reported to be higher than the value of 206 $ppm^{-1}min^{-1}$ recommended by Hampson and Garvin (1975). Cox, Derwent, and Holt (1976) reported a rate constant of 400 $ppm^{-1}min^{-1}$ and Sie, Simonaitis, and Heicklen (1976) reported a high pressure limit value of 524 $ppm^{-1}min^{-1}$. We are currently using a value of 440 $ppm^{-1}min^{-1}$, as reported by Chan et al. (1977).

THE INORGANIC REACTIONS IN THE EXPLICIT MECHANISMS

The 25 inorganic reactions common to all explicit kinetic mechanisms discussed in this report are presented in Table 1.

TABLE 1. INORGANIC REACTIONS AND RATE CONSTANTS IN THE EXPLICIT MECHANISMS

Reaction	Rate constant at 298K $(ppm^{-1}min^{-1})$	Activation energy (K)
$NO_2 + h\nu \rightarrow NO + O(^3P)$	Experimental*	--
$O(^3P) + O_2 + M \rightarrow O_3 + M$	$2.08 \times 10^{-5+}$	--
$O(^3P) + NO_2 \rightarrow NO + O_2$	1.34×10^4	--
$O_3 + NO \rightarrow NO_2 + O_2$	2.39×10^1	1450
$O(^1D) + M \rightarrow O + M$	4.45×10^4	-97.3
$O(^1D) + H_2O \rightarrow 2OH·$	3.4×10^5	--
$O_3 + OH· \rightarrow HO_2· + O_2$	7.72×10^1	1000
$O_3 + HO_2· \rightarrow OH· + 2O_2$	5.3	1525
$O_3 + NO_2 \rightarrow NO_3 + O_2$	4.75×10^{-2}	2450
$O_3 + h\nu \rightarrow O(1D) + O_2$	Experimental*	--
$O_3 + h\nu \rightarrow O(^3P) + O_2$	Experimental*	--

41

TABLE 1 (Concluded)

Reaction	Rate constant at 298k $(ppm^{-1}min^{-1})$	Activation energy (K)
$2HONO \rightarrow NO + NO_2 + H_2O$	1.5×10^{-5}	--
$HONO + h\nu \rightarrow OH\cdot + NO$	Experimental*	--
$NO_2 + OH\cdot + M \rightarrow HONO_2 + M$	1.4×10^4	--
$NO + OH\cdot \rightarrow HONO$	1.4×10^4	--
$CO + OH\cdot \xrightarrow{O_2} HO_2^{\cdot} + CO_2$	4.4×10^2	--
$HO_2^{\cdot} + NO \rightarrow OH\cdot + NO_2$	1.2×10^4	--
$2HO_2^{\cdot} \rightarrow H_2O_2 + O_2$	1.5×10^4	--
$H_2O_2 + h\nu \rightarrow 2OH\cdot$	Experimental*	--
$O_3 \rightarrow wall$	1×10^{-3}	--
$NO_3 + NO \rightarrow 2NO_2$	2.8×10^4	--
$NO_3 + NO_2 \rightarrow N_2O_5$	3.8×10^3	--
$N_2O_5 (+M) \rightarrow NO_3 + NO_2 (+M)$	$1.22 \times 10^{1*}$	10600
$NO + NO_2 + H_2O \rightarrow 2HONO$	$1.6 \times 10^{-11+}$	--
$N_2O_5 + H_2O \rightarrow 2HONO_2$	$5 \times 10^{-6\$}$	--

*Rate constant in min^{-1}.

+Rate constant in $ppm^{-2}min^{-1}$.

$ In simulations of runs before UCR EC-121 $k = 1.5 \times 10^{-5}$ $ppm^{-1}min^{-1}$ was used.

SECTION 5

DEVELOPMENT AND APPLICATION OF THE EXPLICIT MECHANISMS

During the past two years, we shifted the focus of our studies on explicit mechanisms from propylene and butane to other compounds. While continuing to revise the explicit mechanisms for propylene and butane as new information became available, we began more fundamental studies of formaldehyde chemistry and acetaldehyde chemistry (the latter includes PAN chemistry). We also expanded upon or extrapolated from the basic pathways of oxidation of propylene and butane to obtain oxidation pathways for other molecules, including ethylene, 1-butene, trans-2-butene, and 2,3-dimethylbutane. The rationale behind much of our work on explicit kinetic mechanisms was the concept of hierarchical levels of chemical species in smog, as discussed in Section 3.

In the subsections that follow, we discuss explicit mechanisms in the order suggested by the hierarchy of species. Only sample results are shown in this volume--all of the simulated and measured pollutant concentrations for all smog chamber experiments studied are presented graphically in Volume II.

FORMALDEHYDE

As hydrocarbons are oxidized in photochemical smog, they generally produce formaldehyde at some point. Therefore, the atmospheric chemistry of formaldehyde is common to almost all smog chamber experiments and mechanisms dealing with ozone formation in the troposphere. In fact, NO and formaldehyde are the minimum precursors required for urban ozone formation. [CO and NO would be the minimum precursors appropriate for tropospheric ozone since $O(^1D)$ radicals rather than radicals from aldehydes would be important in that case.]

43

There appear to be three primary reactions of formaldehyde in photo-chemical smog: photolysis (two reactions) and reaction with OH· :

$$HCHO + h\nu \rightarrow H\cdot + HCO\cdot \qquad , \qquad (6)$$

$$HCHO + h\nu \rightarrow H_2 + CO \qquad , \qquad (7)$$

$$HCHO + OH\cdot \rightarrow H_2O + HCO\cdot \qquad . \qquad (8)$$
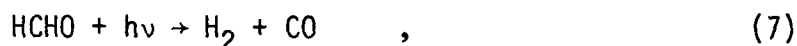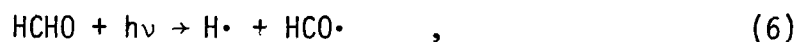
Note that formaldehyde photolysis can produce both radical and nonradical products. The former is a major source of radicals important to smog chemistry:

$$H\cdot + O_2 + M \rightarrow HO_2^\cdot + M \qquad , \qquad (9)$$

$$HCO\cdot + O_2 \rightarrow HO_2^\cdot + CO \qquad . \qquad (10)$$

In air at atmospheric pressure, Reactions (9) and (10) are very fast, and so Reactions (6) and (8) are normally written as:

$$HCHO + h\nu \xrightarrow{2O_2} 2HO_2^\cdot + CO \qquad , \qquad (11)$$

$$HCHO + OH\cdot \xrightarrow{O_2} H_2O + HO_2^\cdot + CO \qquad \cdot \qquad (12)$$
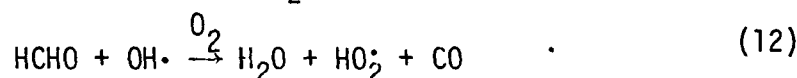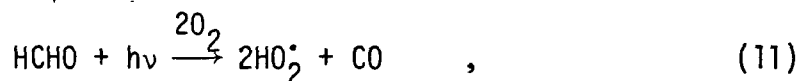
Although the absorption cross section of formaldehyde in the ultra-violet region is fairly well defined, the split between different photolysis pathways under atmospheric conditions is somewhat uncertain. The total formaldehyde photolysis rate (relative to the NO_2 photolysis rate) and the ratio of radical to nonradical photolysis products must be known or estimated for simulations with the explicit kinetic mechanisms in this report. Moortgat et al. (1978) recently measured the quantum yield for the photolysis of formaldehyde [Reactions (6) and (7)]. Their results imply that the radical and nonradical pathways occur at approximately equal rates for typical atmospheric conditions. We are currently using the results of Moortgat et al. in the computer simulations. Unfortunately, the total formaldehyde photolysis rate is not determined experimentally at UCR, unlike the NO_2

44

photolysis rate, even though an accurate value of that rate is just as important for simulating smog formation as an accurate NO_2 photolysis rate (Whitten and Hogo, 1977).

The abstraction of a hydrogen atom from formaldehyde by OH· [Reaction (12)] has been the subject of various investigations (Morris and Niki, 1971a; Wilson, 1972). The rate constant of 1.4×10^4 $ppm^{-1}min^{-1}$ recently reported by Atkinson and Pitts (1978) was used in all mechanisms discussed in this report.

Data on formaldehyde experiments were available to us from three sources:

> Bufalini, Gay, and Brubaker (1972) reported some experiments in small (160 liter) Teflon bags exposed to blacklights or fluorescent sunlamps. In these experiments, relatively high initial concentrations of formaldehyde (about 12 ppm) were used.

> UCR performed four experiments with initial concentrations of both formaldehyde and NO_x of less than 0.6 ppm.

> UNC supplied us with data for one run in its outdoor smog chamber initiated with about 1 ppm of formaldehyde and about 0.5 ppm of NO_x.

These experiments were simulated with the explicit formaldehyde mechanism, which consists of the inorganic reactions listed in Table 1 and the formaldehyde reactions in Table 2. The initial conditions and photolysis rate constants used in the simulations are listed in Table 3.

Experiments Reported by Bufalini, Gay, and Brubaker

For each experiment reported by Bufalini, Gay, and Brubaker (1972), the ratio of the photolysis rate constant of formaldehyde to that of NO_2 was calculated using the method reported by Durbin, Hecht, and Whitten (1975). That method utilizes the manufacturer's reported light spectra

45

TABLE 2. REACTIONS OF FORMALDEHYDE AND ACETALDEHYDE*

Reaction	Rate constant $(ppm^{-1}min^{-1})$
$HCHO + h\nu \rightarrow H_2 + CO$	Experimental[†]
$HCHO + h\nu \xrightarrow{2O_2} 2HO_2^{\cdot} + CO$	Experimental[†]
$HCHO + OH^{\cdot} \xrightarrow{O_2} HO_2^{\cdot} + CO + H_2O$	1.4×10^4
$CH_3CHO + h\nu \xrightarrow{2O_2} CH_3O_2^{\cdot} + HO_2^{\cdot} + CO$	Experimental[†]
$CH_3CHO + OH^{\cdot} \xrightarrow{O_2} CH_3C(O)O_2^{\cdot} + H_2O$	2.4×10^4
$CH_3C(O)O_2^{\cdot} + NO \xrightarrow{O_2} CH_3O_2^{\cdot} + NO_2 + CO_2$	3.8×10^3
$CH_3O_2^{\cdot} + NO \rightarrow CH_3O^{\cdot} + NO_2$	1.2×10^4
$CH_3O^{\cdot} + O_2 \rightarrow HCHO + HO_2^{\cdot}$	1.2
$CH_3C(O)O_2^{\cdot} + HO_2^{\cdot} \rightarrow CH_3C(O)O_2H + O_2$	4×10^3
$CH_3O_2^{\cdot} + HO_2^{\cdot} \rightarrow CH_3O_2H + O_2$	4×10^3
$CH_3C(O)O_2^{\cdot} + NO_2 \rightarrow CH_3C(O)O_2NO_2$	2×10^3
$CH_3C(O)O_2NO_2 \rightarrow CH_3C(O)O_2^{\cdot} + NO_2$	$2.8 \times 10^{-2\,[†§]}$
$CH_3O^{\cdot} + NO_2 \rightarrow CH_3ONO_2$	1.5×10^4
$CH_3O^{\cdot} + NO_2 \rightarrow HCHO + HONO$	4.4×10^3
$CH_3O_2^{\cdot} + O_3 \rightarrow CH_3O^{\cdot} + 2O_2$	4×10^1

* The first three reactions in this table and the inorganic reactions listed earlier constitute the explicit formaldehyde mechanism. The reactions in this table and the inorganic reactions listed earlier constitute the explicit acetaldehyde mechanism.

† Rate constant in min^{-1}.

§ Activation energy is 12,500K; rate constant is given at 298K.

46

TABLE 3. INITIAL CONDITIONS AND PHOTOLYSIS RATE CONSTANTS FOR THE FORMALDEHYDE/NO_x SMOG CHAMBER EXPERIMENTS

Run number	Light source	Initial concentration (ppm)				Photolysis rate constant ($\times 10^4$ min^{-1})						
		HCHO	NO	NO_2	HONO	$NO_2 \rightarrow NO+O$*	$O_3 \rightarrow O(^1D)$	$O_3 \rightarrow O(^3P)$	HONO$\rightarrow$NO+OH·	$H_2O_2 \rightarrow 2OH$·	HCHO$\rightarrow H_2$+CO	HCHO$\rightarrow 2HO_2$·+CO
1	Blacklamps	12.9	0	0	0	0.2	45.0	12.0	900	23.0	10.0	10.0
2	Blacklamps	12.7	0	1.01	0	0.2	45.0	12.0	900	23.0	10.0	10.0
3	Sunlamps	12.5	0	0	0	0.084	538	72.4	260	17.6	34.0	33.0
4	Sunlamps	12.0	0	1.20	0	0.084	538	72.4	260	17.6	34.0	33.0
EC-250	Xenon arc	0.50	0.008	0.0	0.0005	0.3	6.9	90	830	3.5	6	6
EC-251	Xenon arc	0.55	0.08	0.033	0.002	0.3	6.9	90	830	3.5	6	6
EC-252	Xenon arc	0.56	0.392	0.103	0.009	0.3	6.9	90	830	3.5	6	6
EC-255	Xenon arc	0.51	0.006	0.00	0.0004	0.3	6.9	90	830	3.5	6	6

* Rate constant in min^{-1}.

and reported cross sections and quantum yields for NO_2 and formaldehyde. Bufalini, Gay, and Brubaker (1972) reported NO_2 photolysis rate constants of 0.32 min^{-1} for blacklights and 0.14 min^{-1} for sunlamps using the method recommended by Tuesday (1961). Wu and Niki (1975), however, reported that such measurements can be in error by ±30 percent. We used values at the low end of the range for the NO_2 photolysis constants to simulate the experiments reported by Bufalini, Gay, and Brubaker. The simulation results did follow the measured formaldehyde disappearance fairly closely, but the predicted ozone concentrations early in the simulations were too high (see Figure 9).

A second set of simulations was performed using the explicit formaldehyde mechanism and the following reactions:

$$HO_2^{\cdot} + NO_2 \rightarrow HOONO_2 \ , \quad k = 7800 \ ppm^{-1}min^{-1} \qquad , \qquad (13)$$

$$HOONO_2 \rightarrow HO_2^{\cdot} + NO_2 \ , \quad k = 5 \ min^{-1} \qquad . \qquad (14)$$
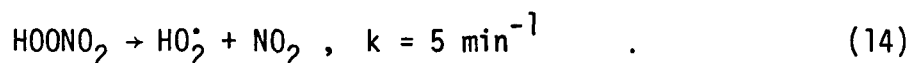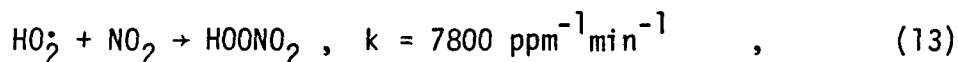
The formation of peroxynitric acid ($HOONO_2$ or PNA) is likely to be more significant in the Bufalini, Gay, and Brubaker experiments than in the UCR experiments discussed later because of the higher concentrations in the former experiments. Figure 10 shows the results of a simulation with Reactions (13) and (14) included in the mechanism; including PNA chemistry slowed down both the simulated rate of disappearance of formaldehyde and the simulated ozone formation rate.

All other simulations in this report were performed with mechanisms that did not include PNA chemistry because experience indicated that it is unnecessary unless high concentrations of hydrocarbons and NO_x are used and the rate of ozone formation is very large.

UCR Experiments

The UCR smog chamber with formaldehyde included small concentrations of butane as indicators of the radical concentrations. These experiments
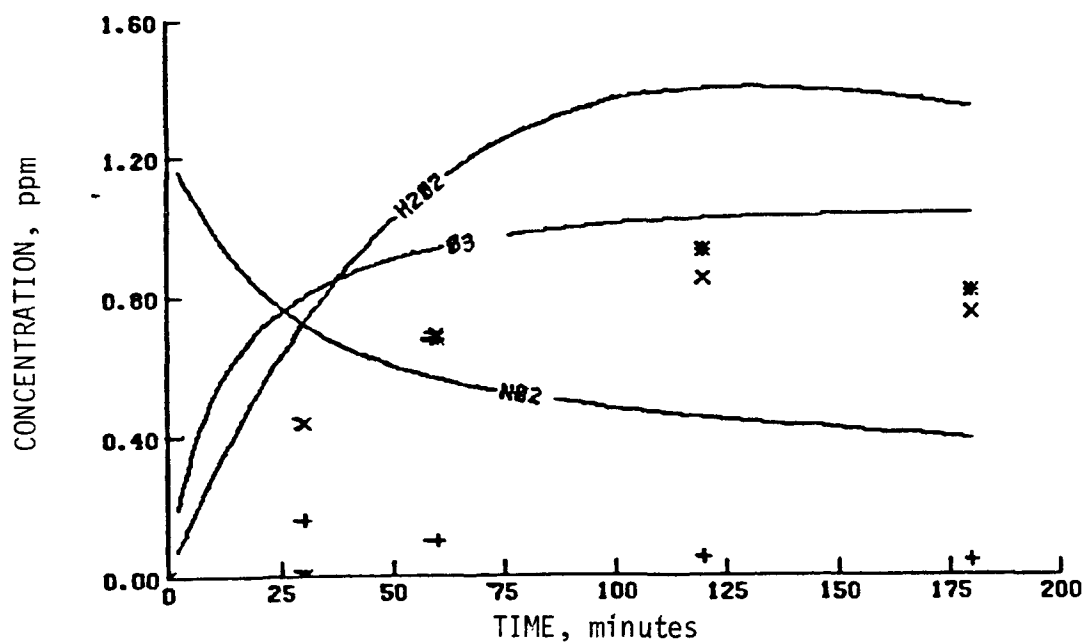
(a) H_2O_2, NO_2 and O_3
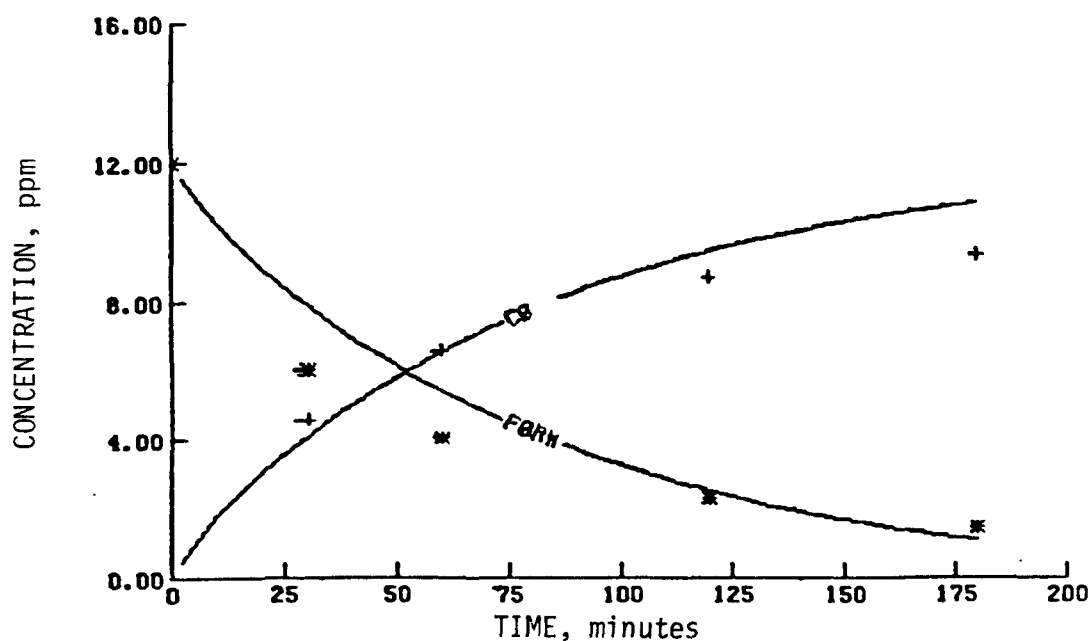
(b) CO and formaldehyde

Figure 9. Pollutant concentrations measured in an experiment by Bufalini, Gay, and Brubaker (1972) and simulation results--PNA chemistry not included

49
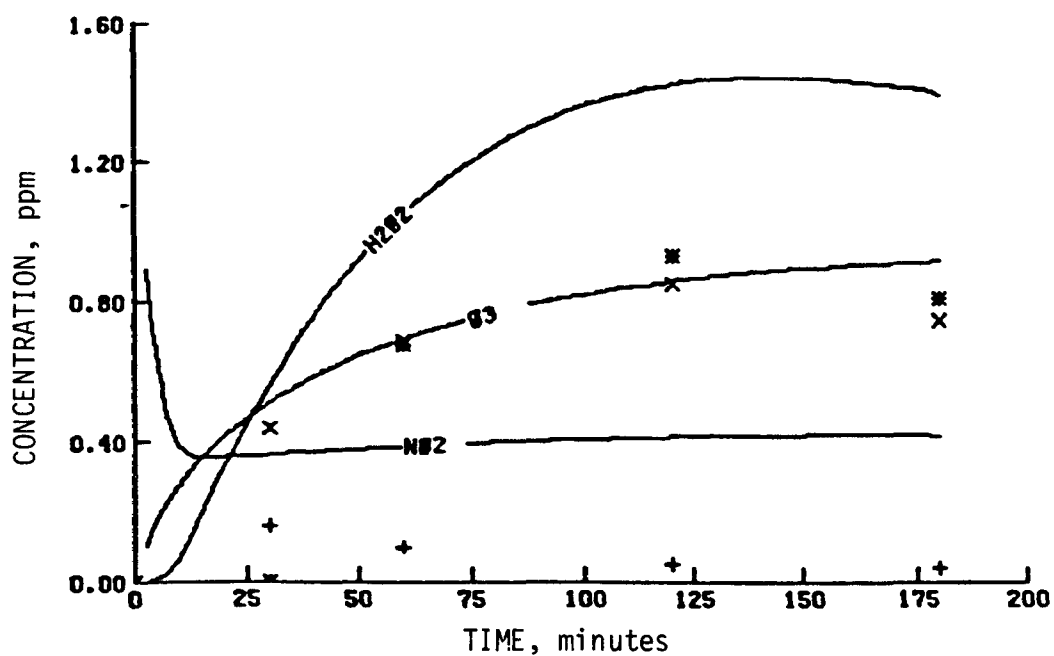
(a) H_2O_2, NO_2, and O_3
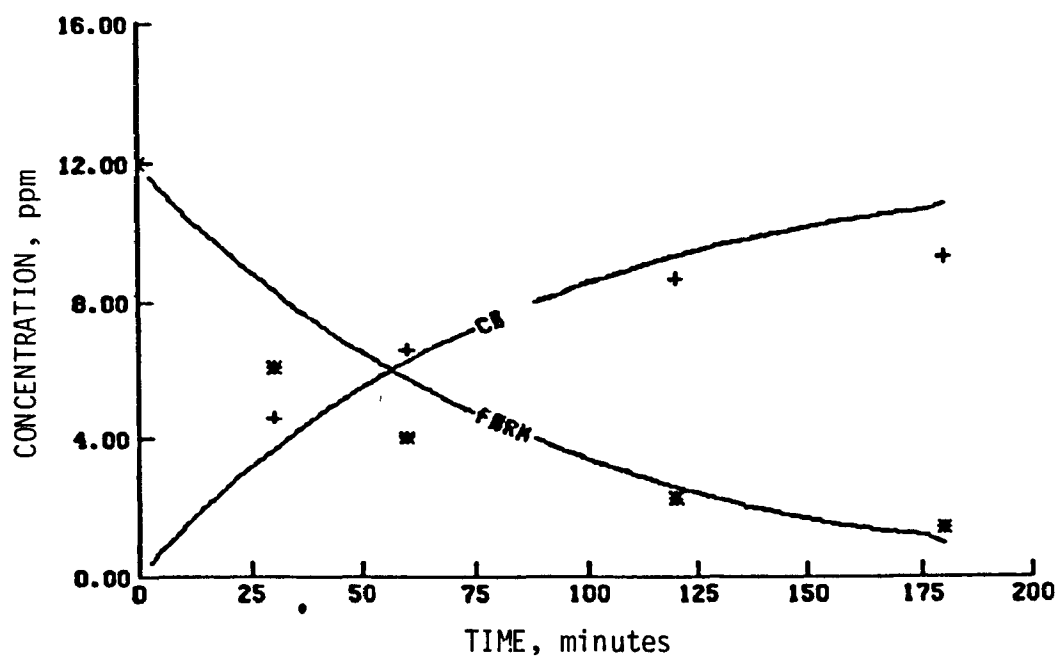
(b) CO and formaldehyde

Figure 10.   Pollutant concentrations measured in an experiment
by Bufalini, Gay, and Brubaker (1972) and simulation
results--PNA chemistry included

50

were simulated with the formaldehyde mechanism plus the reaction

$$CH_3CH_2CH_2CH_3 + OH\cdot \rightarrow Products \qquad . \qquad (15)$$
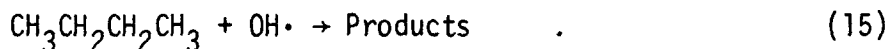
The products of Reaction (15) were not treated in the formaldehyde mechanism because the butane concentration was so low that more than 99 percent of the OH· produced reacted with other species. The butane decay curve thus provided a convenient monitor of the OH· concentration. Attempting to simulate the concentrations of butane, formaldehyde, and NO_2 constitutes a stringent test of the mechanism. The simulation results and measurements for Run EC-251 are shown in Figure 11 for illustration purposes; all results are included in the appendix (Volume II). A comparison of simulated and and measured data appears in Table 4(a).

Two of the four UCR experiments (EC-250 and EC-255) were ostensibly free of NO_x, though trace concentrations of NO_x near the analytical detection limits were reported by UCR. We were able to simulate the ozone measurements by assuming that NO degassed from the chamber walls at a rate of 4.2 ppb hr^{-1}, which leads to an influx of 25 ppb in six hours. Such an NO_x concentration is near UCR's reported values, and tests showed that adding that concentration to simulations of experiments with measurable initial NO_x concentrations (e.g., EC-251) had negligible effects.

In all four UCR formaldehyde experiments, the measured initial formaldehyde concentration was lower than the concentration calculated from dividing the amount of formaldehyde put into the chamber by the volume of the chamber. On our simulations, we used the calculated rather than the measured values. The simulated formaldehyde concentration/time profiles have the same slope as the measured ones, but they differ in magnitude by the same factor as the difference between the measured and calculated initial formaldehyde concentrations. The latter difference is being investigated at UCR. Hopefully, the cause will be found to be a simple calibration error, since the reactions in formaldehyde mechanisms are important in almost all kinetic mechanisms for ozone formation. Studies with formaldehyde at the UNC

(a) O_3
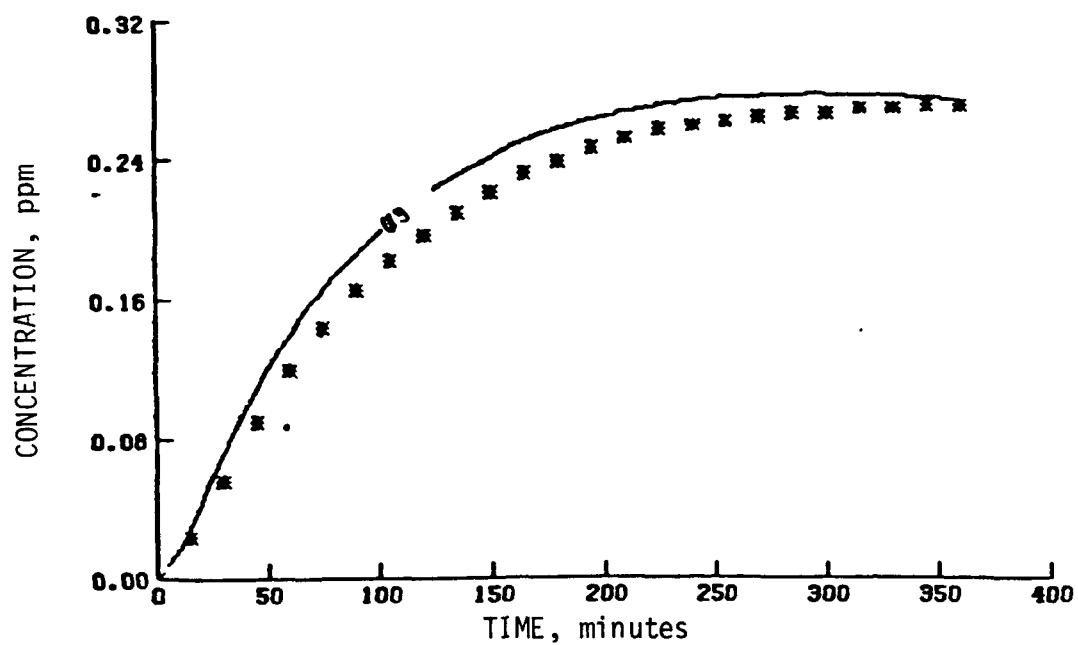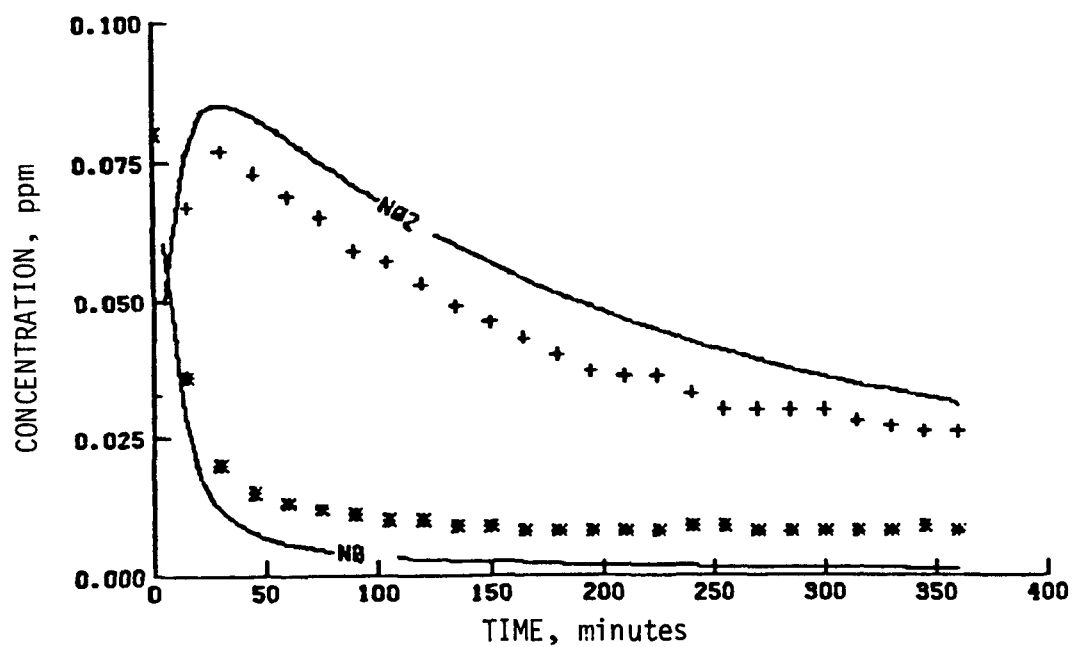
(b) NO_2 and NO

Figure 11. UCR formaldehyde experiment EC-251:
measurements and simulation results

52
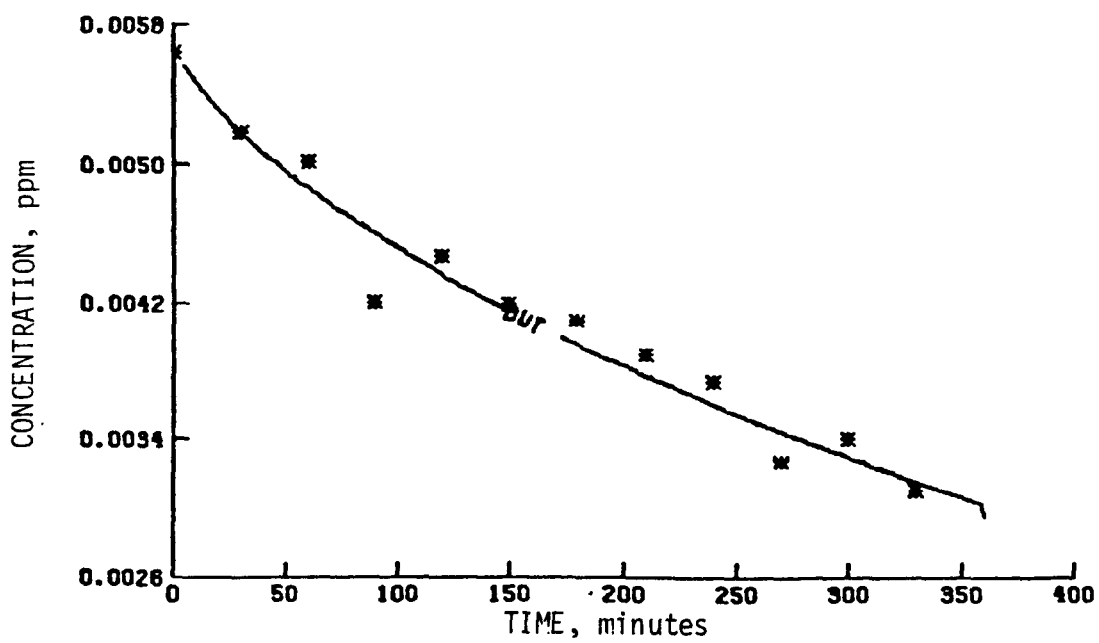
(c) Formaldehyde

(d) Butane

Figure 11 (Concluded)

TABLE 4. UCR ALDEHYDE EXPERIMENTS--SIMULATIONS AND MEASUREMENTS

(a) Formaldehyde

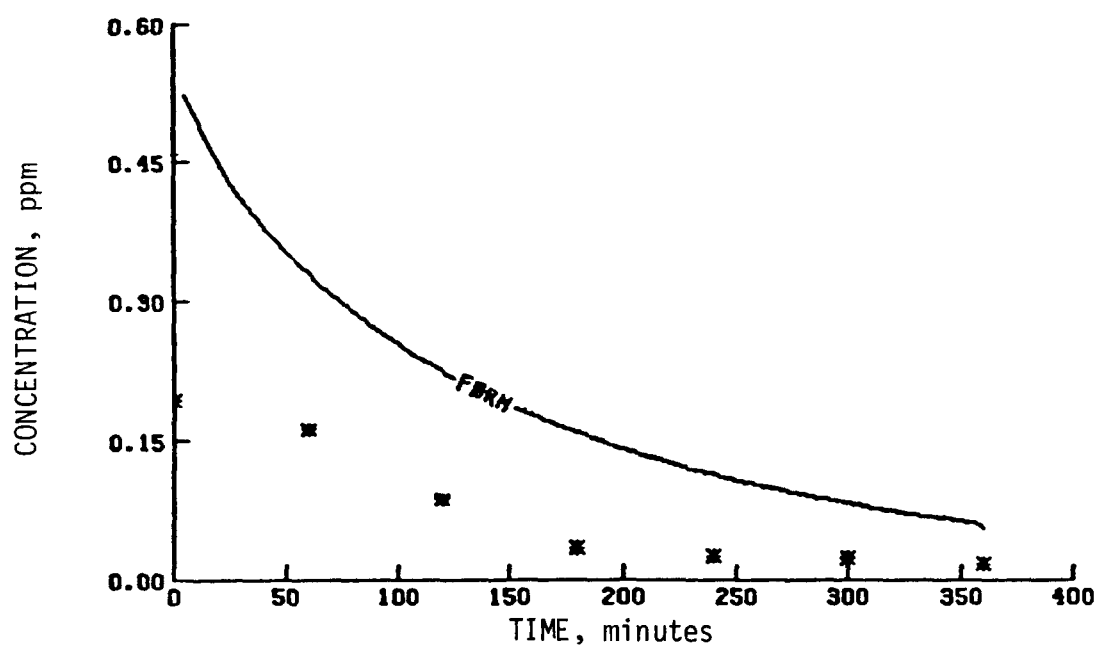| Exp. no.	Initial [NOx] (ppm)	Initial NO2/NOx ratio	Initial HC/NOx ratio (ppmC/ppm)	Maximum [O3] (ppm)* Sim.	Meas.	Difference in O3 maxima (percent)†	Time to maximum [O3] (minutes)§ Sim.	Meas.	Difference in times to O3 maxima (percent)†	Maximum [NO2] (ppm) Sim.	Meas.	Difference in NO2 maxima (percent)†	Time to maximum [NO2] (minutes)§ Sim.	Meas.	Difference in times to NO2 maxima (percent)†
EC-250	0.008	0.0	62.5	0.20	0.21	-5	>360	>360	--	0.014	0.021	-33	>360	>360	--
EC-251	0.11	0.29	4.9	0.274	0.27	2	220	220	0	0.084	0.077	9	30	30	0
EC-252	0.495	0.21	1.1	0.027	0.019	42	>360	>360	--	0.243	0.24	1	100	100	0
EC-255	0.006	0.0	85.0	0.19	0.19	0	>360	>360	--	0.013	0.017	-22	>360	>360	--

O3 maxima: average difference = 10 percent; standard deviation = ±22 percent.
NO2 maxima: average difference = -11 percent; standard deviation = ±20 percent.
* Maximum one-hour-average concentration.
† [(Simulated Value - Measured Value) : Measured Value] x 100.
§ Time from beginning of irradiation to beginning of the period during which the maximum one-hour-average concentration occurred.

(b) Acetaldehyde

Exp. no.	Initial [NOx] (ppm)	Initial NO2/NOx ratio	Initial HC/NOx ratio (ppmC/ppm)	Maximum [O3] (ppm)* Sim.	Meas.	Difference in O3 maxima (percent)†	Time to maximum [O3] (minutes)§ Sim.	Meas.	Difference in times to O3 maxima (percent)†	Maximum [NO2] (ppm) Sim.	Meas.	Difference in NO2 maxima (percent)†	Time to maximum [NO2] (minutes)§ Sim.	Meas.	Difference in times to NO2 maxima (percent)†
EC-253	0.0	0.0	--	0.12	0.12	0	>360	>360	--	0.009	0.009	0	>360	>360	--
EC-254	0.11	0.24	9.1	0.28	0.24	17	>360	>360	--	0.082	0.064	28	60	60	0

O3 maxima: average difference = 9 percent; standard deviation = ±12 percent.
NO2 maxima: average difference = 14 percent; standard deviation = ±20 percent.
* Maximum one-hour-average concentration.
† [(Simulated Value - Measured Value) : Measured Value] x 100.
§ Time from beginning of irradiation to beginning of the period during which the maximum one-hour-average concentration occurred.

facility have shown a temperature-dependent adhesion of formaldehyde to the chamber walls (Jeffries, private communication, 1978). No adhesion was observed at UCR, however, at typical operating temperatures around 303K.

In simulating the formaldehyde experiment at the UNC outdoor smog chamber, we encountered a different problem. We first simulated the diurnal light changes and matched the measured disappearance of formaldehyde by choosing a formaldehyde-to-NO_2 photolysis ratio of about 0.005. The ozone concentration ceased to rise after the formaldehyde had disappeared, however. We then assumed that a small background concentration of some other hydrocarbon was present. To keep the mechanisms simple, we assumed that the hydrocarbon was ethylene, at an initial concentration of 0.1 ppm. We later found that some ethylene (0.1 ppm being a reasonable estimate) was indeed present as a result of the method being used to monitor HNO_3 (Jeffries, private communication, 1978). The results of this simulation are shown in Figure 12.

In conclusion, the formaldehyde mechanisms can generate reasonable simulations, but the data available for validation are limited, and some special assumptions were required in simulating each data set. We hope that more data will become available in the near future. Since carbon monoxide concentration around 10 ppm should begin to perturb experiments such as that performed at UNC, similar formaldehyde/NO_x experiments with and without added CO would provide valuable data for studying the relative rate constants for the reactions of OH· with formaldehyde, NO_2, and CO. The use of trace concentrations of butane in formaldehyde experiments would also assist the modeling by providing some indication of the OH· concentrations.

ACETALDEHYDE

As suggested by the hierarchical levels discussed earlier, an explicit kinetic mechanism for acetaldehyde can be generated by adding acetaldehyde chemistry to the formaldehyde and inorganic chemical reactions. As with formaldehyde, acetaldehyde apparently reacts by two major pathways, photolysis and reaction with OH·:

.
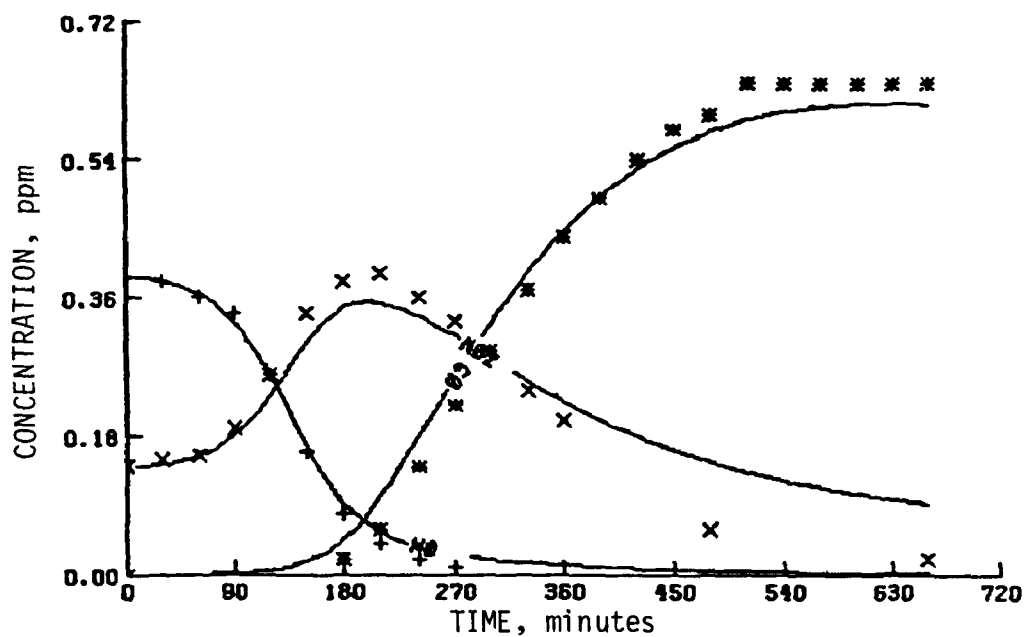
(a) NO_2, NO, and O_3
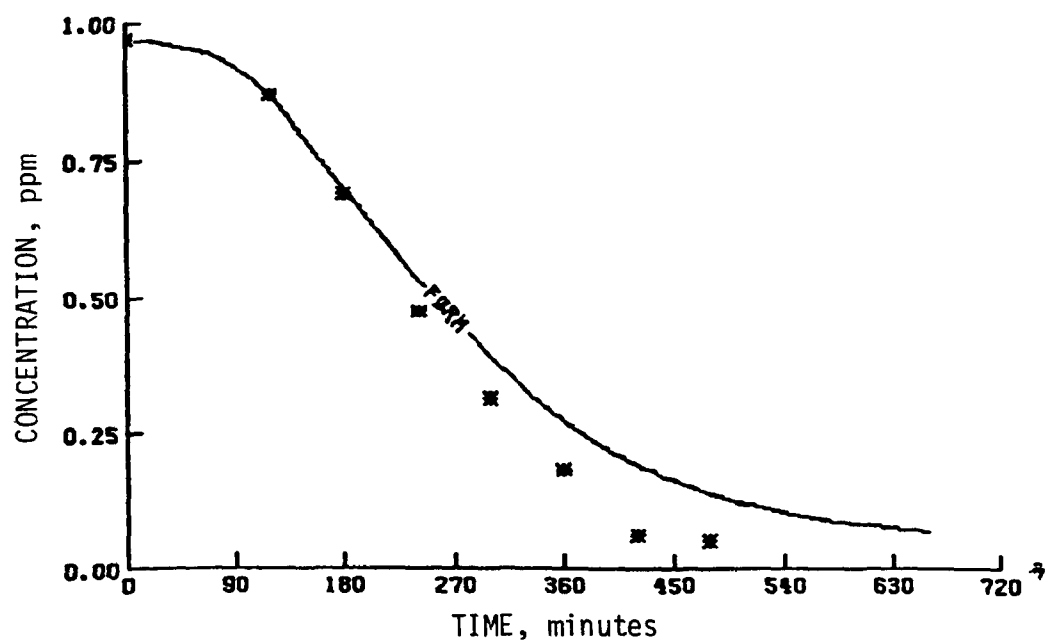
(b) Formaldehyde

Figure 12.   UNC formaldehyde experiment (18 July 1977):
measurements and simulation results

56

$$CH_3CHO + h\nu \rightarrow CH_3^\bullet + HCO^\bullet \quad , \tag{16}$$

$$CH_3CHO + OH^\bullet \rightarrow CH_3C(O)^\bullet + H_2O \quad . \tag{17}$$
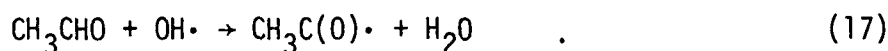
Photolysis of acetaldehyde to yield molecular, nonradical products, analogous to the formaldehyde reaction $HCHO + h\nu \rightarrow H_2 + CO$, does not seem to occur extensively (Calvert and Pitts, 1966). The radicals produced in Reactions (16) and (17) are rapidly converted in air as follows:

$$CH_3 + O_2 \rightarrow CH_3O_2 \quad , \tag{18}$$

$$HCO^\bullet + O_2 \rightarrow HO_2^\bullet + CO \quad , \tag{19}$$

$$CH_3C(O)^\bullet + O_2 \rightarrow CH_3C(O)O_2^\bullet \quad . \tag{20}$$
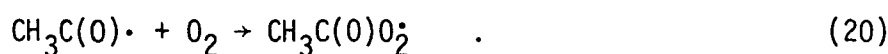
Reactions (16) and (17) are thus usually written as:

$$CH_3CHO + h\nu \xrightarrow{2O_2} CH_3O_2^\bullet + HO_2^\bullet + CO \quad , \tag{21}$$

$$CH_3CHO + OH^\bullet \xrightarrow{O_2} CH_3C(O)O_2^\bullet + H_2O \quad . \tag{22}$$
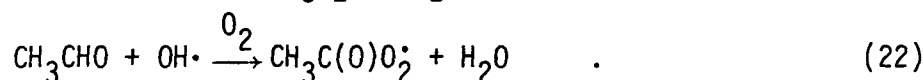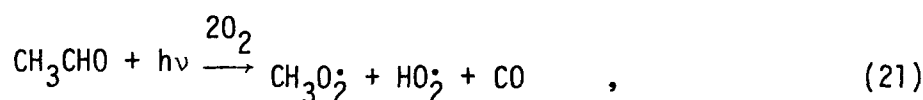
Acetaldehyde chemistry introduces the chemistry of alkylperoxy radicals ($RO_2^\bullet$) via the methylperoxy radical and the chemistry of peroxyacyl nitrates [$RC(O)O_2NO_2$] via the formation of peroxyacetyl nitrate [$CH_3C(O)O_2NO_2$, or PAN] from acetylperoxy radical:

$$CH_3C(O)O_2^\bullet + NO \xrightarrow{O_2} CH_3O_2^\bullet + NO_2 + CO_2 \quad , \tag{23}$$

$$CH_3C(O)O_2^\bullet + NO_2 \rightleftarrows CH_3C(O)O_2NO_2 \quad , \tag{24}$$

$$CH_3O_2^\bullet + NO \rightarrow CH_3O^\bullet + NO_2 \quad , \tag{25}$$

$$CH_3O^\bullet + O_2 \rightarrow HCHO + HO_2^\bullet \quad , \tag{26}$$

$$2CH_3O_2^\bullet \rightarrow 2CH_3O^\bullet + O_2 \quad , \tag{27}$$

$$CH_3O_2 + HO_2^\bullet \rightarrow CH_3O_2H + O_2 \quad , \tag{28}$$

$$CH_3O_2^\bullet + O_3 \rightarrow CH_3O^\bullet + 2O_2 \quad , \tag{29}$$

$$CH_3O^\bullet + NO_2 \rightarrow CH_3ONO_2 \quad , \tag{30}$$

$$CH_3O^\bullet + NO_2 \rightarrow HCHO + HONO \quad . \tag{31}$$
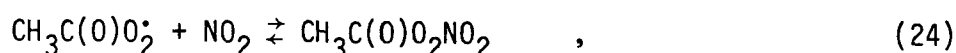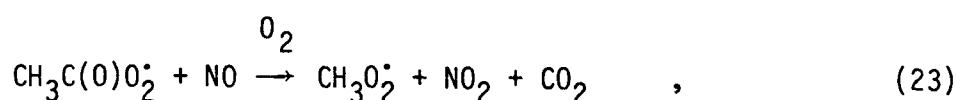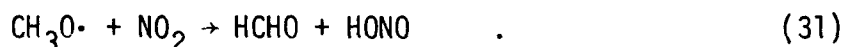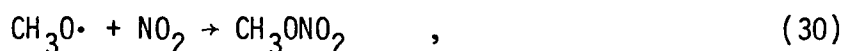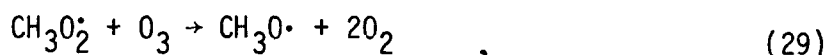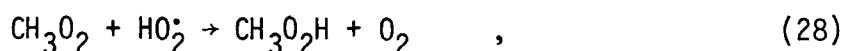
PAN formation was recently studied by two independent groups (Hendry and Kenley, 1977; Cox and Roffey, 1977). Cox and Roffey (1977) reported a value of 0.54 for the ratio of $k_{(CH_3C(O)O_2^\bullet + NO_2)}/k_{(CH_3C(O)O_2^\bullet + NO)}$, whereas Hendry and Kenley (1977) reported a value of 0.29 for the same ratio.

For the rate constant of the reaction of $CH_3C(O)O_2^\bullet$ with NO, Cox and Roffey (1977) reported a value of 3800 $ppm^{-1}min^{-1}$. Hendry and Kenley (1977) reported a value of 4900 $ppm^{-1}min^{-1}$ based on the above ratio and the PAN formation rate. Our simulations of the UCR experiments involving PAN chemicals appear to fit the data the best for values near 1.0 for the ratio $k_{(CH_3C(O)O_2^\bullet + NO_2)}/k_{(CH_3C(O)O_2^\bullet + NO)}$. The modeling study by Carter et al. (1978) also seems to suggest a ratio near 1.0. Until the matter can be resolved, however, we will use the highest experimentally determined value (0.54), as did Carter et al. (1978).

The methylperoxy radical $(CH_3O_2^\bullet)$ produced in Reaction (23) most certainly reacts with NO to give NO_2. The rate constant for the latter reaction seems uncertain at present in light of the recent evaluation of the similar reaction of the hydroperoxy radical with NO (Howard and Evenson, 1977). As in earlier modeling studies at SAI, we used identical rate constants for the reactions of $CH_3O_2^\bullet$ and $HO_2^\bullet$ with NO--in this study, we used 1.2×10^4 $ppm^{-1}min^{-1}$. Since the steady-state $CH_3O_2^\bullet$ concentration is controlled largely by the reaction of $CH_3O_2^\bullet$ with NO, the importance of other reactions of $CH_3O_2^\bullet$, such as Reactions (27) and (28), must remain uncertain until experimental verification of the rate constant for Reaction (25) is obtained.

The chemistry of the methoxyl radical $(CH_3O^\bullet)$ is apparently determined by the competition among Reactions (26), (30), and (31). Using

the same reaction rate constants for Reactions (30) and (31) as did Whitten and Hogo (1977), we found that a rate constant of 1.2 $ppm^{-1}min^{-1}$ for Reaction (26) gave the best overall agreement with the methyl nitrate concentration measurements for UCR acetaldehyde experiments and for all other UCR experiments as well. Our choice of rate constant for Reaction (26) is somewhat larger than the value of 0.95 $ppm^{-1}min^{-1}$ reported by Barker, Benson, and Golden (1977), which was extrapolated from high temperature experiments.

Reactions (27) and (28) are important only at high radical concentrations, because their rates depend on the square of the peroxy radical concentration. The products of these two reactions are uncertain, but the rate constant of Reaction (27) is apparently low (Whitbeck et al., 1976). The rate constant for Reaction (28) is not known; so in the explicit mechanisms in this report we used the geometric mean of the rate constants for Reaction (27) and the reaction

$$2HO_2^{\bullet} \rightarrow H_2O_2 + O_2 \qquad . \qquad\qquad (32)$$
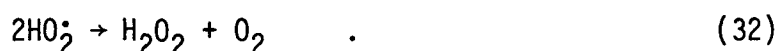
The rate constant for the reaction of $CH_3O_2^{\bullet}$ with ozone (Reaction 29) was estimated by Walter, Bufalini, and Gay (1977) to be between 10 and 22 $ppm^{-1}min^{-1}$, based primarily on the rate constant 2.3 $ppm^{-1}min^{-1}$ for the reaction of $HO_2^{\bullet}$ with ozone. Since we chose a value of 5.3 $ppm^{-1}min^{-1}$ for the latter rate constant, we used a value of 40 $ppm^{-1}min^{-1}$ for the rate constant of Reaction (29).

We used the explicit acetaldehyde mechanism shown in Table 2 to simulate two acetaldehyde/NO_x experiments performed in the evacuable chamber at the University of California at Riverside. The initial conditions in those experiments and the calculated photolysis rate constants are listed in Table 5. Simulated and measured values are compared in Table 4(b). A third UCR acetaldehyde experiment (EC-164) was not included because the temperature data for that run indicate that the temperature control system was not functioning properly.

The results of the simulation of EC-254 are shown in Figure 13. As was done for the formaldehyde experiments, small amounts of n-butane were

TABLE 5. INITIAL CONDITIONS AND PHOTOLYSIS RATE CONSTANTS FOR THE ACETALDEHYDE/NO_x SMOG CHAMBER EXPERIMENTS

Run number	Initial concentration (ppm)				Photolysis rate constant ($\times 10^4$ min^{-1})					
	Acetaldehyde	NO	NO_2	HONO	$NO_2 \rightarrow NO+O$*	$O_3 \rightarrow O(^1D)$	$O_3 \rightarrow O(^3P)$	HONO→NO+OH·	$H_2O_2 \rightarrow 2OH$·	FORM→Products
EC-253	0.56	0.0	0.0	0.0	0.30	6.9	90	830	3.5	6
EC-254	0.52	0.085	0.027	0.0	0.30	6.9	90	830	3.5	6

* Rate constant in min^{-1}.

† The relationship between FORM→Products and carbonyl photolysis rate constants is discussed in Section 4.

TABLE 5. INITIAL CONDITIONS AND PHOTOLYSIS RATE CONSTANTS FOR THE ACETALDEHYDE/NO_x SMOG CHAMBER EXPERIMENTS

Run number	Initial concentration (ppm)				Photolysis rate constant ($\times 10^4$ min^{-1})					
	Acetaldehyde	NO	NO_2	HONO	$NO_2 \rightarrow NO+O$*	$O_3 \rightarrow O(^1D)$	$O_3 \rightarrow O(^3P)$	HONO→NO+OH·	$H_2O_2 \rightarrow 2OH$·	FORM→Products
EC-253	0.56	0.0	0.0	0.0	0.30	6.9	90	830	3.5	6
EC-254	0.52	0.085	0.027	0.0	0.30	6.9	90	830	3.5	6

* Rate constant in min^{-1}.

† The relationship between FORM→Products and carbonyl photolysis rate constants is discussed in Section 4.

(a) Acetaldehyde and O_3
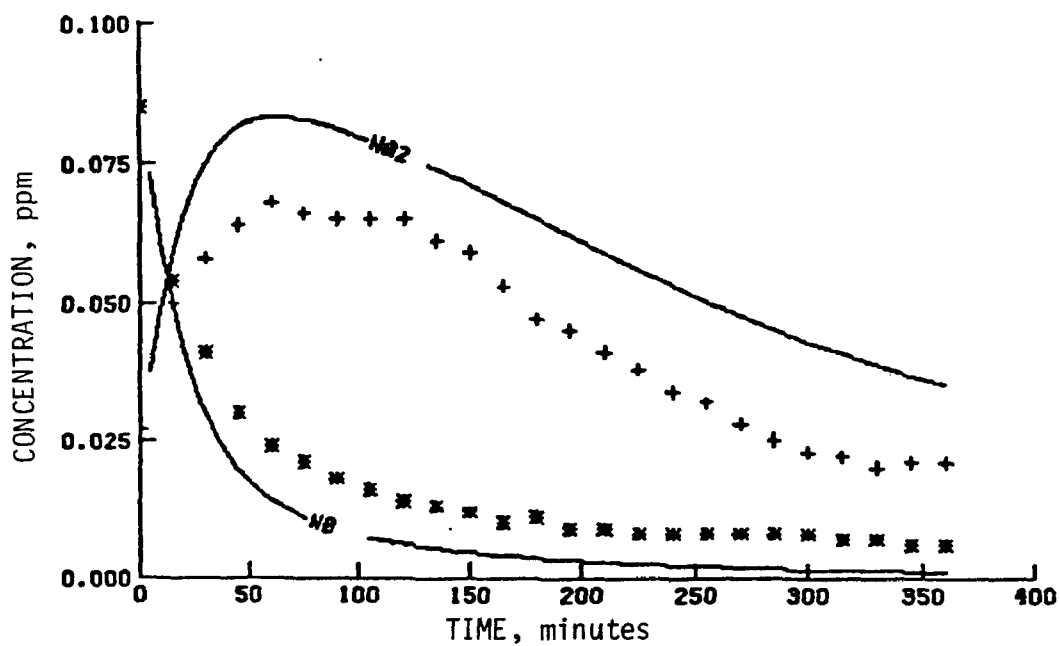
(b) NO_2 and NO

Figure 13. UCR acetaldehyde experiment EC-254:
measurements and simulation results
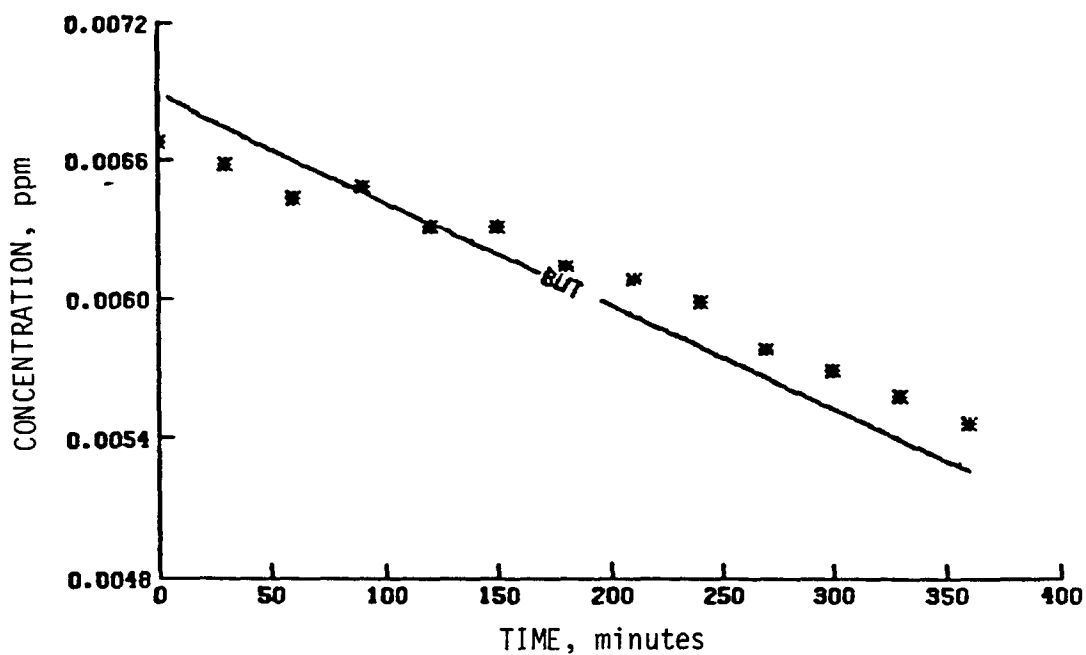
(c) n-Butane
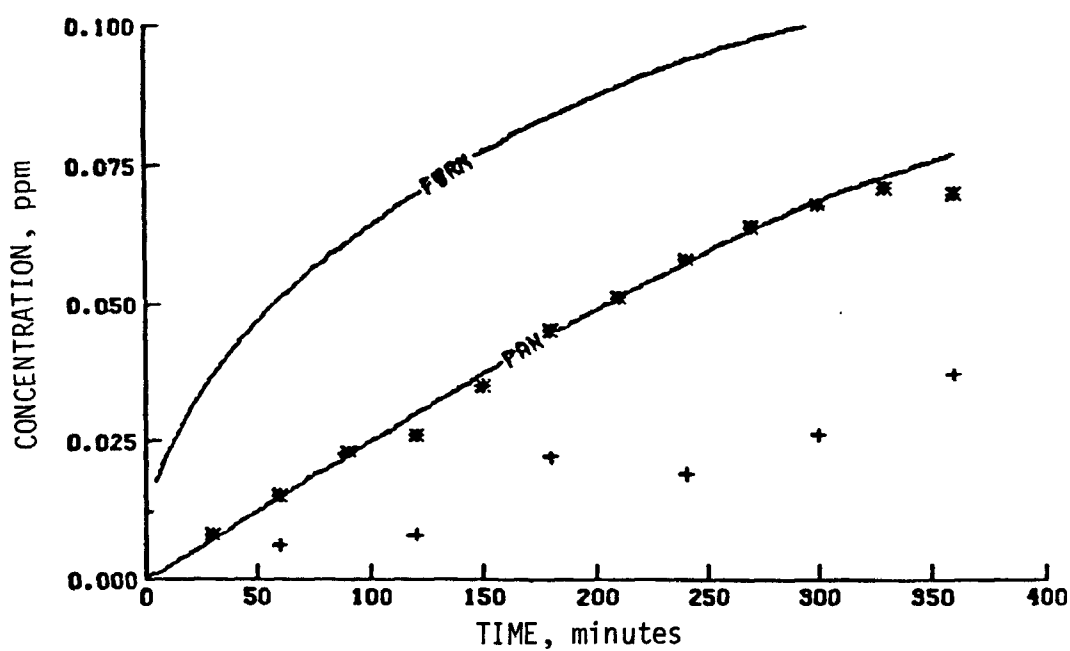
(d) Formaldehyde and PAN

Figure 13 (Continued)

62
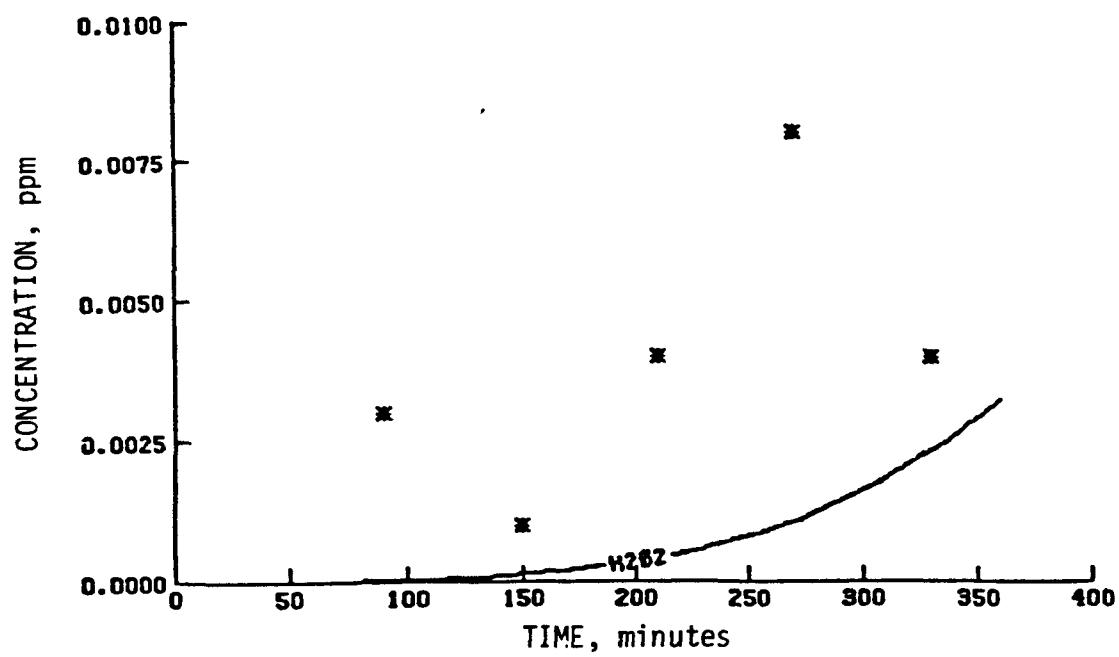
(e) H_2O_2

Figure 13 (Concluded)

added to act as monitors of the concentration of OH· in the smog chamber. (Assuming that n-butane reacts primarily with OH·, the disappearance of butane can be correlated with the production of OH·). The simulations follow the observed n-butane disappearance very well, which suggests that the explicit mechanism generates the correct amount of OH·.

In UCR Run EC-253 the measured O_3 concentration was greater than the calculated steady-state concentration by a factor of 7:

$$\left[O_3\right]_{ss} \simeq \frac{k_1[NO_2]}{k_3[NO]} = \frac{0.3[NO_2]}{25.2[NO]} = \left(\frac{0.3}{25.2}\right)\left(\frac{0.013}{0.008}\right) = 0.019 \text{ ppm} \qquad . \qquad (33)$$

(In EC-253 the measured concentrations of NO and NO_2 were nearly constant throughout the experiment.) If the steady-state approximation is to hold, some source of NO_x is needed in this low-NO_x experiment. We introduced NO into the simulations of EC-253 and EC-254 at a rate of 7×10^{-5} ppm min^{-1} and thereby obtained a better simulation of O_3 in EC-253 with little change in simulated O_3 generation in EC-254, which contained added NO_x.

ETHYLENE

Two new olefin/NO_x systems were investigated at UCR during the past year: ethylene/NO_x (six experiments) and trans-2-butene/NO_x (three experiments). So far, these two systems represent the slowest- and fastest-reacting olefins studied at UCR. The rate constants for the ethylene + OH· reaction and the trans-2-butene + OH· reaction are 3.5 times lower and 2.8 times greater than the propylene + OH· rate constant. The mechanisms developed for these two olefin/NO_x systems are basically extensions of previously developed propylene/NO_x mechanisms. We discuss ethylene chemistry below and trans-2-butene chemistry following the subsection on propylene.

Ethylene + O(^{3}P) Reaction

The reaction of ethylene with O(^{3}P) atoms has been studied by Davis et al. (1972), who reported a rate constant of 1200 ppm^{-1}min^{-1}, which is

1.6 times greater than the value reported by Atkinson and Cvetanovic (1971) and Niki, Daby, and Weinstock (1969). Westenberg and de Haas (1969) reported a rate constant of 1100 $ppm^{-1}min^{-1}$ for this reaction. In the explicit ethylene mechanism, we are currently using the Davis et al. value of 1200 $ppm^{-1}min^{-1}$.

The products of the ethylene + $O(^3P)$ reaction under atmospheric conditions seem uncertain since most studies of the products have been conducted at low pressure. For the present, we are using two basic pathways with a 50 percent split:

$$CH_2=CH_2 + O(^3P) \xrightarrow{2O_2} CH_3O_2^{\cdot} + HO_2^{\cdot} + CO$$

$$\longrightarrow CH_2\overset{O}{\underset{}{\diagdown}}CH_2 \ ^*$$

$$CH_2\overset{O}{\underset{}{\diagdown}}CH_2 \ ^* \xrightarrow{M} CH_3CHO \qquad .$$
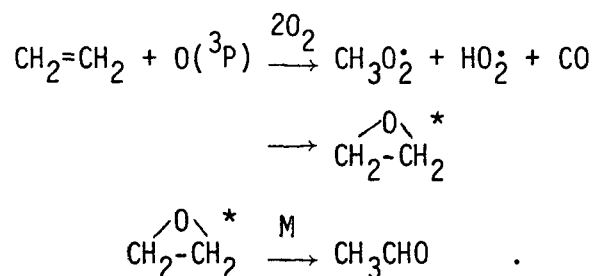
Ethylene oxide and acetaldehyde were observed by UCR as minor products in the ethylene/NO_x experiments. During the coming year, we hope to elucidate the formation mechanism for these two compounds more clearly. For now, the choice of rate constants produced simulated acetaldehyde concentrations within the apparent "scatter" of the UCR data. Through more careful analysis, we may be able to develop a mechanism for acetaldehyde production from the ethylene chemistry that could eliminate some of the apparent "scatter."

Ethylene + OH· Reaction

Analogous to the propylene + OH· reaction, ethylene and OH· react to form a hydroxyalkylperoxy radical:

$$CH_2=CH_2 + OH\cdot \xrightarrow{O_2} CH_2(O_2^{\cdot})CH_2OH \qquad .$$
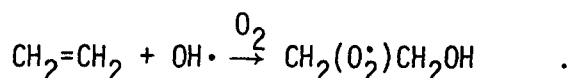
$CH_2(O_2^{\cdot})CH_2OH$ apparently reacts with NO and perhaps O_3 as follows:

$$CH_2(O_2^{\cdot})CH_2OH + NO \rightarrow NO_2 + CH_2(O\cdot)CH_2OH \qquad ,$$

$$CH_2(O_2^{\cdot})CH_2OH + O_3 \rightarrow CH_2(O\cdot)CH_2OH + 2O_2 \qquad ,$$

$$CH_2(O\cdot)CH_2OH \rightarrow HCHO + \cdot CH_2OH \qquad ,$$

$$\cdot CH_2OH \xrightarrow{O_2} HCHO + HO_2^{\cdot} \qquad .$$
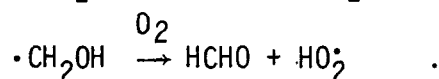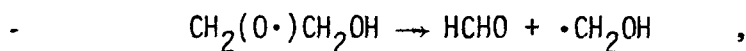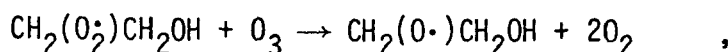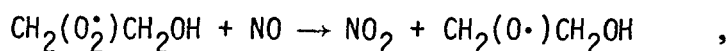
These reactions lead mainly to the formation of formaldehyde. Indeed, UCR observed high formaldehyde concentrations (a peak of approximately 0.9 ppm of formaldehyde from an initial ethylene concentration of 2 ppm). The rate constant of the ethylene + OH· reaction has been studied by several groups (Davis et al., 1975; Pastrana and Carr, 1975; Davis, 1976; Howard, 1976; Meagher and Heicklen, 1976). The more recent measurements of the rate constant are higher than the earlier ones. Davis (1976) estimated a value of $7.9 \times 10^3 \text{ ppm}^{-1}\text{min}^{-1}$, yet Lloyd et al. (1976) reported an average value of $1.2 \times 10^4 \text{ ppm}^{-1}\text{min}^{-1}$. We are currently using the average value of Lloyd et al. in the explicit ethylene mechanism.

Ethylene + O3 Reaction

The ethylene + O_3 reaction has recently been reviewed by Niki (1978). Its initial products appear to be formaldehyde and a reactive intermediate sometimes referred to as a Criegee intermediate:

$$CH_2=CH_2 + O_3 \rightarrow HCHO + CH_2O_2 \qquad .$$
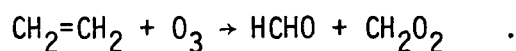
Herron and Huie (1977) have elucidated the unimolecular pathways for the Criegee intermediate:

$$CH_2O_2 \rightarrow H_2\overset{\frown}{C}OO \xrightarrow{67\%} H_2O + CO$$

$$\xrightarrow{18\%} H_2 + CO_2$$

$$\xrightarrow{9\%} 2H + CO_2$$

$$\xrightarrow{6\%} HCOOH \qquad .$$

66
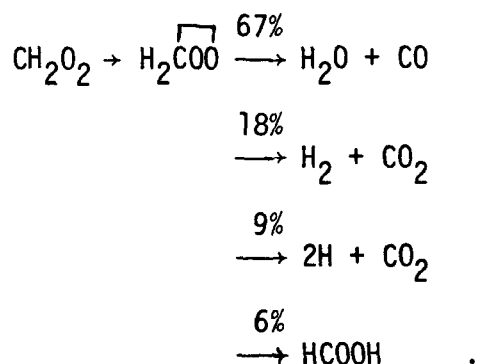
However, the intermediate apparently can react with NO, NO_2, and alde-
hydes:

$$CH_2O_2 + NO \rightarrow NO_2 + HCHO \quad ,$$

$$CH_2O_2 + NO_2 \rightarrow NO_3 + HCHO \quad ,$$

$$CH_2O_2 + Aldehyde \rightarrow Ozonide \quad .$$
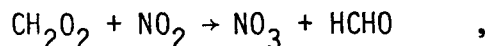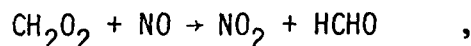
Moreover, the relative rates of these reactions are not yet available.
For the present, we have used rates similar to those employed by Carter
et al. (1978). We set the sum of the unimolecular pathways equal to
1000 min^{-1}; for the reaction with NO, we used the rate constant equal to
the HO_2 reaction constant at 12,000 $ppm^{-1}min^{-1}$; for the reaction with NO_2,
we used the rate constant equal to the HO_2 reaction constant at 7700
$ppm^{-1}min^{-1}$, and for the reaction with aldehydes, we used a rate constant
of 2000 $ppm^{-1}min^{-1}$ to be consistent with observations of ozonides from
aldehydes (Niki, 1978). During the coming year, we hope to develop more
information on the relative rates for this reactive intermediate. However,
the overall simulation results are not strongly dependent on these para-
meters.
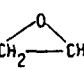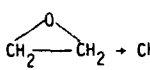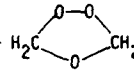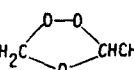
For the rate constant of O_3 with ethylene, we are currently using an
intermediate value of 0.0024 $ppm^{-1}min^{-1}$ from the range reviewed by Niki
(1978) of 0.0018 to 0.0045 $ppm^{-1}min^{-1}$.

Simulations with the Ethylene Mechanism

Tables 6, 7, and 8 list the explicit mechanism for ethylene chemistry,
the conditions used to model six experiments, and the results of comparing
some observed and simulated values. A sample computer output for UCR
Run EC-143 is shown in Figure 14.

The present UCR data set presents a difficult problem for the predic-
tions of the mechanism. In particular, the second data set from UCR for

TABLE 6. REACTIONS OF ETHYLENE*

Reaction	Rate constant $(ppm^{-1}min^{-1})$
$CH_2=CH_2 + O \xrightarrow{2O_2} CH_3O_2^{\cdot} + HO_2^{\cdot} + CO$	6×10^2
$CH_2=CH_2 + O \rightarrow CH_2 \overset{O}{-\!\!-\!\!-} CH_2$	6×10^2
$CH_2 \overset{O}{-\!\!-\!\!-} CH_2 \rightarrow CH_3CHO$	$1 \times 10^{-1\dagger}$
$CH_2=CH_2 + OH \cdot \xrightarrow{O_2} HOCH_2CH_2O_2^{\cdot}$	1.2×10^4
$CH_2=CH_2 + NO_3 \rightarrow NO_2 + Product$	1.1
$CH_2=CH_2 + O_3 \rightarrow HCHO + CH_2O_2^{\cdot}$	2.4×10^{-3}
$CH_2O_2^{\cdot} + HCHO \rightarrow H_2C \overset{O-O}{\underset{O}{\diagup \diagdown}} CH_2$	2×10^3
$CH_2O_2^{\cdot} + CH_3CHO \rightarrow H_2C \overset{O-O}{\underset{O}{\diagup \diagdown}} CHCH_3$	2×10^3
$CH_2O_2^{\cdot} + NO \rightarrow NO_2 + HCHO$	1.2×10^4
$CH_2O_2^{\cdot} + NO_2 \rightarrow NO_3 + HCHO$	8×10^3
$CH_2O_2^{\cdot} \rightarrow CO + H_2 + O_2$	$6.7 \times 10^{2\,+}$
$CH_2O_2^{\cdot} \rightarrow CO_2 + H_2$	$1.8 \times 10^{2\,+}$
$CH_2O_2^{\cdot} \rightarrow 2HO_2^{\cdot} + CO_2$	$9 \times 10^{1\,+}$
$CH_2O_2^{\cdot} \rightarrow HC(O)OH$	$6 \times 10^{1\,+}$
$HOCH_2CH_2O_2^{\cdot} + NO \rightarrow NO_2 + HOCH_2CH_2O \cdot$	1.2×10^4
$HOCH_2CH_2O \cdot \xrightarrow{O_2} 2HCHO + HO_2^{\cdot}$	$3 \times 10^{5\dagger}$
$HOCH_2CH_2O_2^{\cdot} + HO_2^{\cdot} \rightarrow HOCH_2CH_2O_2H + O_2$	4×10^3
$2HOCH_2CH_2O_2^{\cdot} \rightarrow 2HOCH_2CH_2O \cdot + O_2$	5.0×10^2
$HOCH_2CH_2O_2^{\cdot} + O_3 \rightarrow HOCH_2CH_2O \cdot + 2O_2$	5.0

* The inorganic, formaldehyde, and acetaldehyde reactions listed earlier must be added to construct the explicit ethylene mechanism.

+ Rate constant in min^{-1}.

68

TABLE 7. INITIAL CONDITIONS AND PHOTOLYSIS RATE CONSTANTS FOR THE ETHYLENE/NO$_x$ SMOG CHAMBER EXPERIMENTS

Run number	Initial concentration (ppm)				Photolysis rate constant ($\times 10^4$ min^{-1})					
	Ethylene	NO	NO$_2$	HONO	NO$_2 \to$NO+O*	O$_3 \to$O(^{1}D)	O$_3 \to$O(^{3}P)	HONO$\to$NO+OH·	H$_2$O$_2 \to$2OH·	FORM$\to$Products†
EC-142	0.92	0.322	0.158	0.010	0.33	10	107	990	4	11
EC-143	1.95	0.39	0.11	0.012	0.33	10	107	990	4	11
EC-156	1.95	0.376	0.124	0.018	0.32	5	104	600	5	11
EC-285	1.9	0.791	0.215	0.02	0.39	5	120	1100	5	8
EC-286	3.758	0.708	0.237	0.02	0.39	5	120	1100	5	8
EC-287	3.995	0.404	0.124	0.008	0.39	5	120	1100	5	8

* Rate constant in min^{-1}.

† The relationship between FORM→Products and carbonyl photolysis rate constants is discussed in Section 4.

TABLE 8. UCR ETHYLENE EXPERIMENTS--SIMULATIONS AND MEASUREMENTS

Exp. no.	Initial [NO$_x$] (ppm)	Initial NO$_2$/NO$_x$ ratio	Initial HC/NO$_x$ ratio (ppmC/ppm)	Maximum [O$_3$] (ppm)*		Difference in O$_3$ maxima (percent)†	Time to maximum [O$_3$] (minutes)§		Difference in times to O$_3$ maxima (percent)†	Maximum [NO$_2$] (ppm)§		Difference in NO$_2$ maxima (percent)†	Time to maximum [NO$_2$] (minutes)§		Difference in times to NO$_2$ maxima (percent)†
				Sim.	Meas.		Sim.	Meas.		Sim.	Meas.		Sim.	Meas.	
EC-142	0.48	0.33	3.8	0.77	0.77	0	~330	~330	0	0.36	0.30	20	120	100	20
EC-143	0.50	0.22	7.8	0.96	1.07	-10	170	170	0	0.41	0.38	8	65	60	8
EC-156	0.50	0.25	7.8	0.92	1.03	-11	170	150	13	0.41	0.36	14	60	50	20
EC-285	1.0	0.21	3.8	0.75	0.75	0	>360	>360	--	0.71	0.70	1	190	150	27
EC-286	0.95	0.25	7.95	1.30	1.06	23	170	160	6	0.80	0.75	7	70	60	17
EC-287	0.53	0.24	15.1	1.09	0.92	18	120	100	20	0.47	0.45	4	45	45	0

O$_3$ maxima: average difference = 3 percent, standard deviation = ±14 percent.

NO$_2$ maxima: average difference = 9 percent, standard deviation = ±7 percent.

* Maximum one-hour-average concentration.

† [(Simulated Value - Measured Value) / Measured Value] x 100.

§ Time from beginning of irradiation to beginning of the period during which the maximum one-hour-average concentration occurred.

(a) O_3
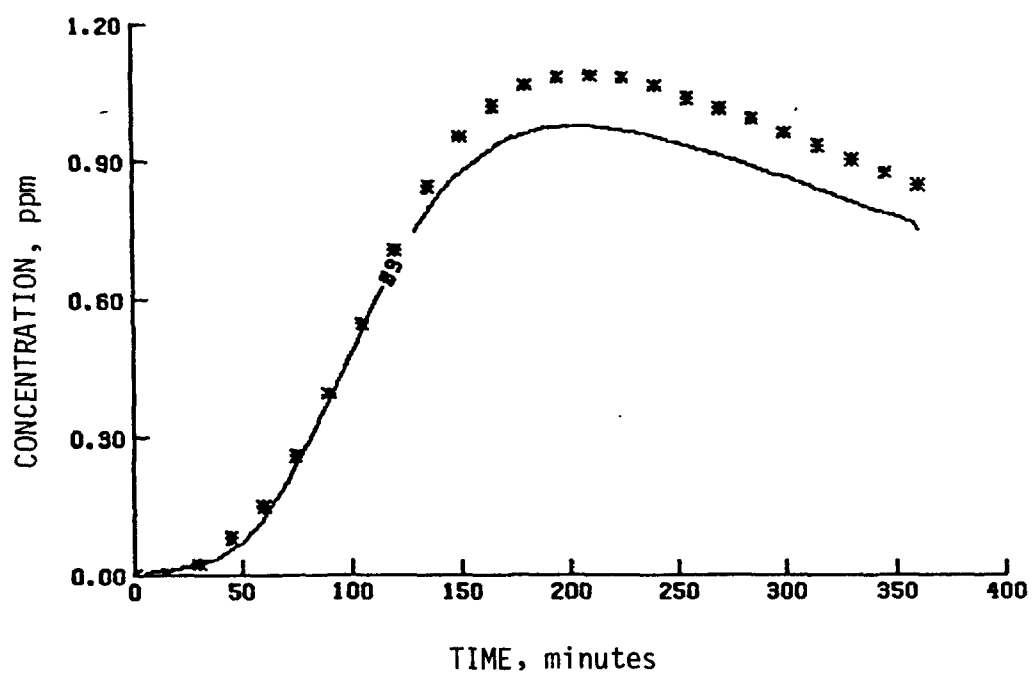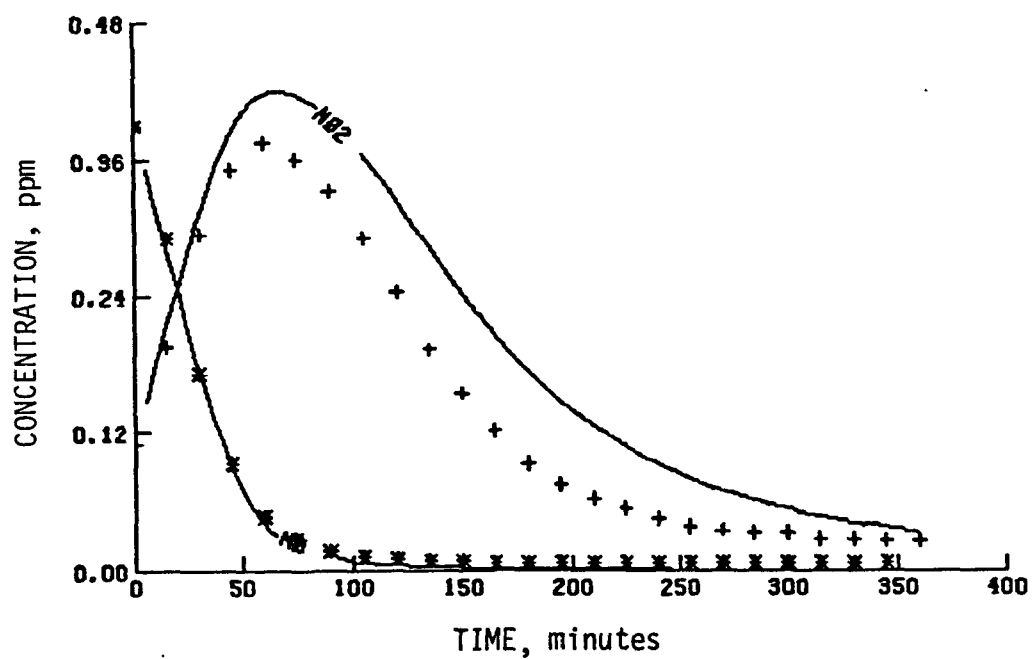
(b) NO_2 and NO

Figure 14. Simulation results for a UCR ethylene experiment (EC-143)
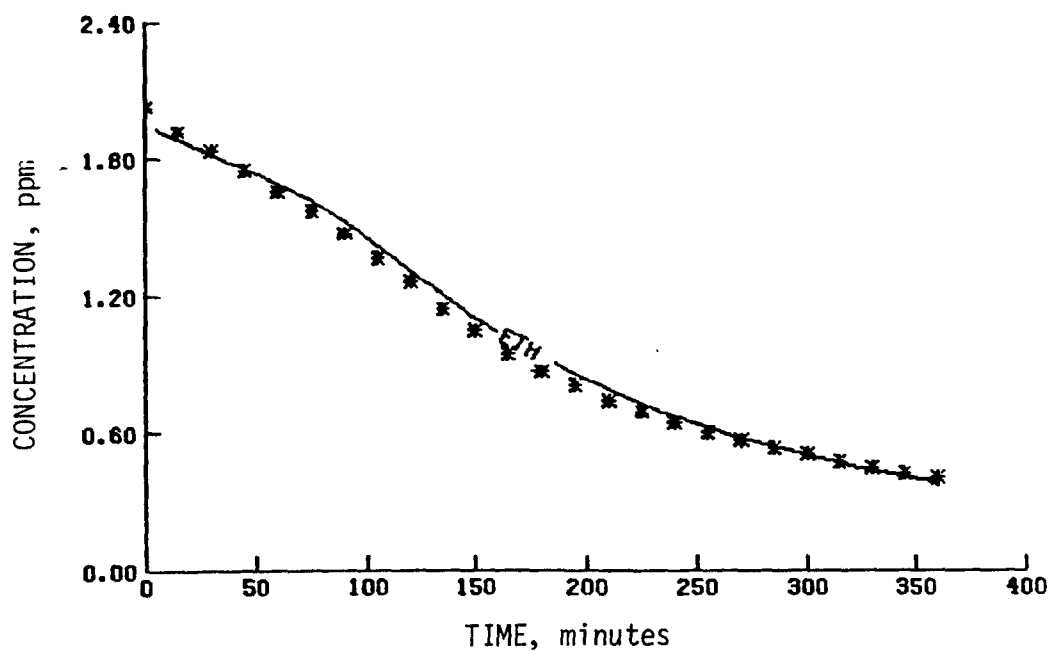
(c) Ethylene
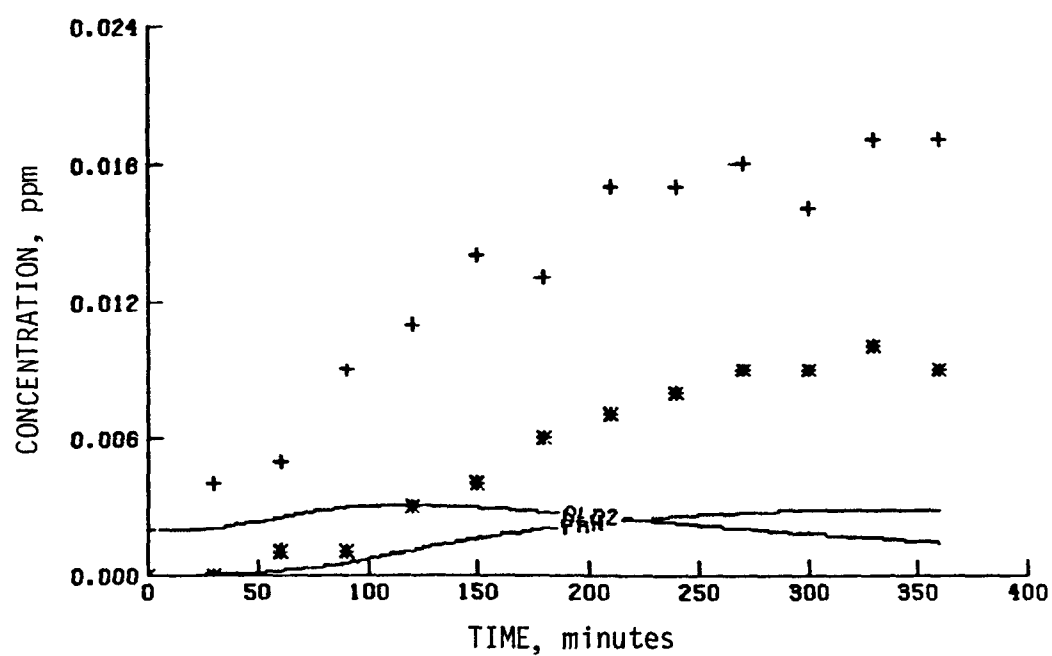
(d) Acetaldehyde and PAN

Figure 14 (Continued)

71
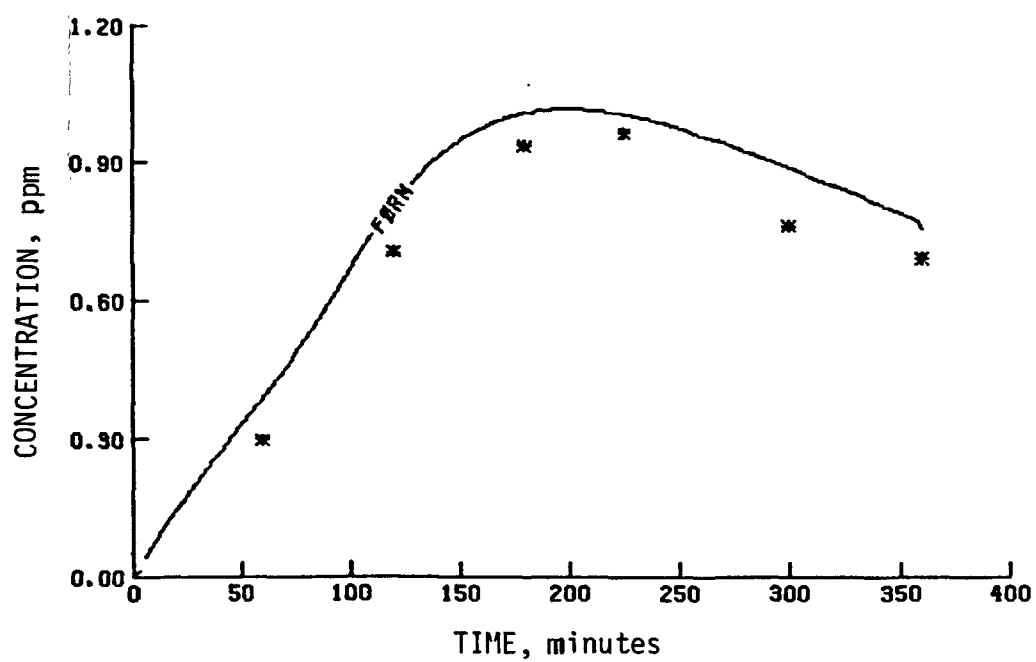
(e) Formaldehyde

Figure 14   (Concluded)

three experiments was generated using twice the concentrations of the first set of three experiments. However, the resultant ozone maxima were somewhat lower in the second set even though the NO_2 photolysis rates were higher. When the precursor concentrations are doubled, our present mechanism tends to produce somewhat more ozone. Figure 15 shows an isopleth diagram of simulated maximum one-hour ozone levels using our present ethylene mechanism and the lighting conditions appropriate to the first series of UCR experiments (EC-142, EC-143, and EC-156). The initial concentrations for all six UCR experiments are shown. In this figure, the rapid change in possible ozone maxima in the high-NO_x and low-ethylene concentration region stems from the arbitrary six-hour cutoff for the simulation time. However, as is clear from the diagram, ozone production increases very slowly with increased concentration in the region where the UCR experiments were performed. Thus, more experiments using lower concentrations will be necessary to verify the present mechanism.

PROPYLENE AND BUTANE

In a previous report (Whitten and Hogo, 1977), we discussed explicit propylene and butane mechanisms that produced reasonable computer simulations of a factorially designed series of experiments performed at UCR. As discussed in Section 3, changes in the inorganic, aldehyde, or PAN chemistry can have effects on simulations with the propylene and butane mechanisms. These changes must be evaluated. Changes in the chemistry at the lower hierarchical levels (see Figure 1) that produce a deterioration in the fit between simulations with the propylene or butane mechanism and the corresponding UCR measurements imply that some aspect of the propylene or butane chemistry is in error.

Some important changes in the chemistry of the lowest level (inorganic) species were made in the past two years as a result of recent research (see Section 4 for a discussion). These changes must be compensated for by additional changes within the propylene and butane mechanisms if agreement between the simulations and the UCR data are to be retained.
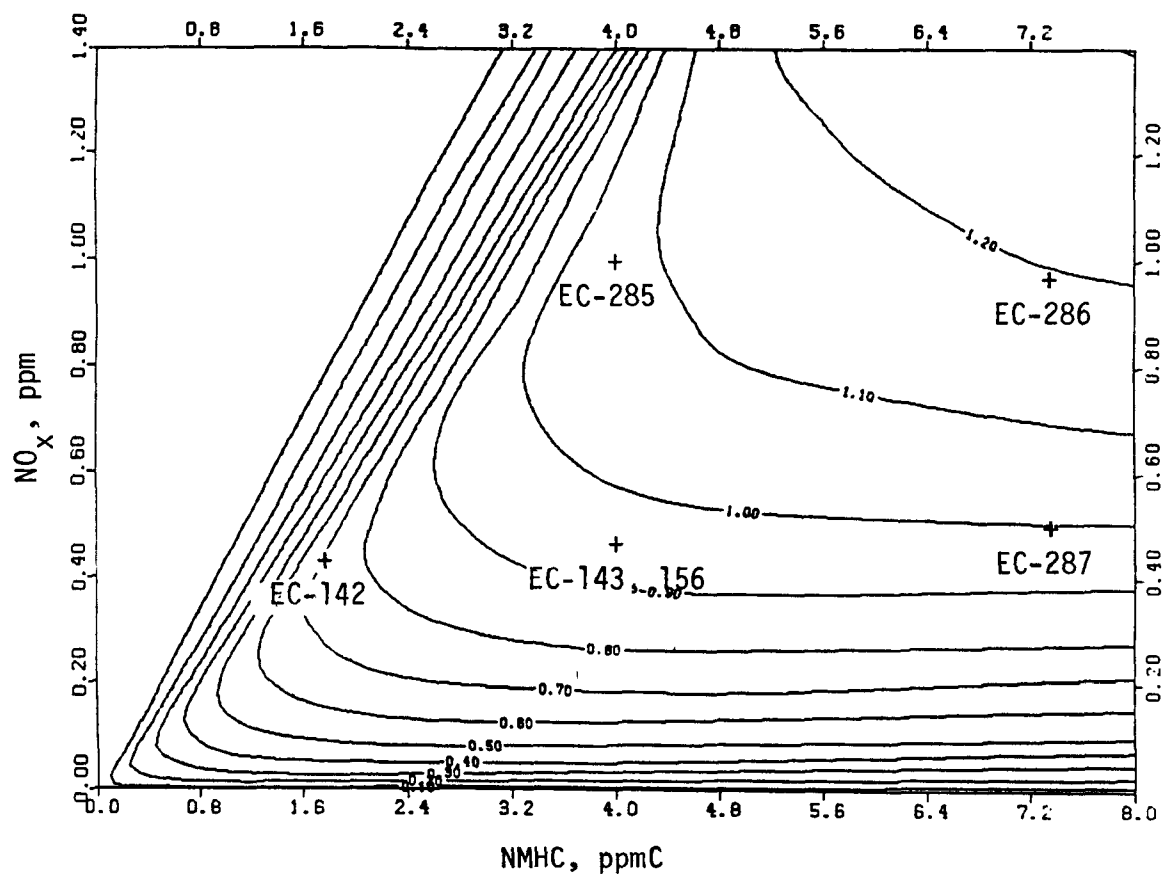
Figure 15.   Isopleth diagram of simulated maximum one-hour-average
ozone concentrations using the ethylene mechanism

To compensate for these changes, we examined three parts of the propylene/butane chemistry:

> Radical production from ozone-olefin reactions
> Peroxy radical reactions with ozone
> Alkoxyl radical chemistry in the butane mechanism.

We also updated some rate constants and made other minor changes in the propylene and butane mechanisms. This work is described in the following subsections.

Ozone-Olefin Reactions

The propylene mechanism concerning this reaction was changed to be similar to the ethylene mechamism discussed earlier. However, in the propylene case two initial pathways are possible:

$$CH_3CH=CH_2 + O_3 \rightarrow CH_3CHO + CH_2O_2$$
$$\rightarrow HCHO + CH_3CHO_2 \quad .$$
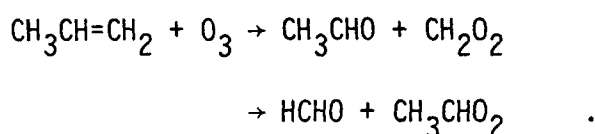
The reaction has been studied by Dodge and Arnts (1978), and we have used both their mechanism for the methyl-Criegee intermediate and their assumption of a 50 percent split from the initial ozone attack. As with the ethylene mechanism, we used similar rate constants for the reactions of the methyl-Criegee intermediate with NO, NO_2, and aldehydes. However, the present scheme will be evaluated more extensively in the coming year as more laboratory data on the relative reactivity of these Criegee-intermediate species become available.

Peroxy Radical Reactions with Ozone

Although we discussed the methylperoxy and hydroperoxy reactions with ozone earlier in connection with the acetaldehyde mechanism, the special peroxy radical that apparently forms after the hydroxyl addition to propylene has never been reported in the literature as reacting with ozone:

$$CH_3CH=CH_2 + OH\cdot \xrightarrow{O_2} CH_3\overset{\overset{\displaystyle O_2^{\cdot}}{|}}{C}HCH_2OH \quad (RAO_2) \quad ,$$

$$RAO_2 + O_3 \rightarrow CH_3CHO + HCHO + HO_2^{\cdot} + O_2 \quad .$$
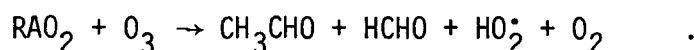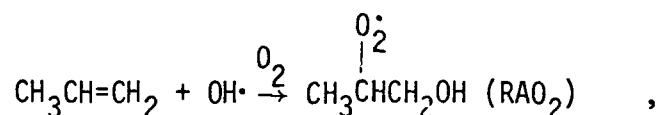
The RAO_2 radical actually has two versions: one as shown and the other from hydroxyl attack at the central carbon atom. However, the products from reaction with either ozone or NO are probably indistinguishable; so we did not consider the alternate route. Our basic reason for including this possible reaction scheme with ozone is that the simulations without it tend to have too many NO-to-NO_2 conversions after the onset of significant ozone formation. Thus, the present scheme may prove to be incorrect, b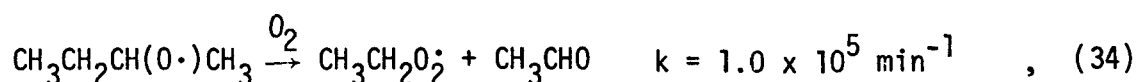ut some other scheme producing similar overall behavior seems necessary. In a typical propylene simulation, more conversions of NO to NO_2 per molecule of propylene reacted are required to simulate the NO decay and NO_2 production than the amount needed later in the simulation when NO_2 has decayed and ozone is rapidly forming. During the coming year, we will study the time-dependent NO-to-NO_2 conversion yield per hydrocarbon reacted for propylene and other molecules. Such information can be generated from both the simulations and the data, and the information should clearly highlight discrepancies between the observational data and various propylene mechanisms.

Alkoxyl Radical Chemistry

The alkoxyl radical (RO·) chemistry in our mechanisms was discussed in detail by Whitten and Hogo (1977). In the propylene and butane mechanisms, only alkoxyl radicals with four carbon atoms or less are important. The following reactions for the primary alkoxyl radicals are used in these mechanisms:

$$CH_3CH_2CH(O\cdot)CH_3 \xrightarrow{O_2} CH_3CH_2O_2^{\cdot} + CH_3CHO \qquad k = 1.0 \times 10^5 \ min^{-1} \quad , \quad (34)$$

$$CH_3CH_2CH(O\cdot)CH_3 + O_2 \rightarrow CH_3CH_2C(O)CH_3 + HO_2^\cdot \qquad k = 1.43 \; ppm^{-1}min^{-1} \qquad , \quad (35)$$

$$CH_3CH_2CH_2CH_2O\cdot \xrightarrow{O_2} HOCH_2CH_2CH_2CH_2O_2^\cdot \qquad k = 2 \times 10^6 \; min^{-1} \qquad , \quad (36)$$

$$CH_3CH_2CH_2CH_2O\cdot + O_2 \rightarrow CH_3CH_2CH_2CHO + HO_2^\cdot \qquad k = 3.3 \; ppm^{-1}min^{-1} \qquad , \quad (37)$$

$$CH_3CH_2CH_2O\cdot + O_2 \rightarrow CH_3CH_2CHO + HO_2^\cdot \qquad k = 3.3 \; ppm^{-1}min^{-1} \qquad , \quad (38)$$

$$CH_3CH_2O\cdot + O_2 \rightarrow CH_3CHO + HO_2^\cdot \qquad k = 3.3 \; ppm^{-1}min^{-1} \qquad , \quad (39)$$

$$CH_3O\cdot + O_2 \rightarrow HCHO + HO_2^\cdot \qquad k = 1.2 \; ppm^{-1}min^{-1} \qquad . \quad (40)$$
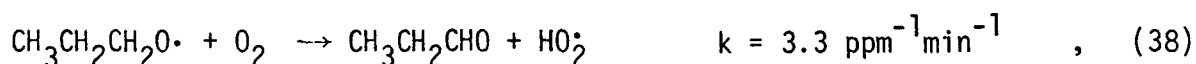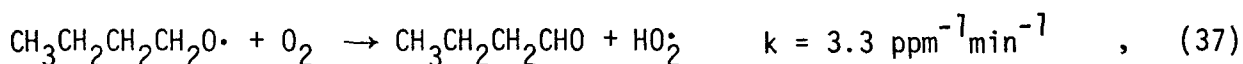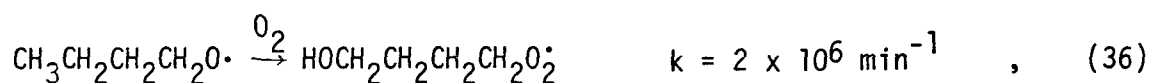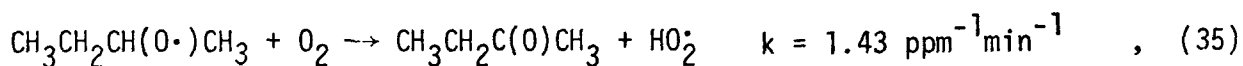
The rate constants given above are somewhat different from those recommended by Barker et al. (1977), as shown by the following tabulation:

Reaction	Recommended rate constant by Barker et al. (1977)	Uncertainty factor	Factor used in current mechanism
34	$2.9 \times 10^5 \; min^{-1}$	8	1/3
35	$0.32 \; ppm^{-1}min^{-1}$	16	4.5
36	$3.7 \times 10^7 \; min^{-1}$	60	1/18.5
37	$6.2 \times 10^{-1} \; ppm^{-1}min^{-1}$	16	5.3
38	$6.2 \times 10^{-1} \; ppm^{-1}min^{-1}$	16	5.3
39	$6.2 \times 10^{-1} \; ppm^{-1}min^{-1}$	16	5.3
40	$9.5 \times 10^{-1} \; ppm^{-1}min^{-1}$	16	1.3

The values we have used resulted in simulations consistent with UCR measurements of methylethylketone, n-butyraldehyde and various nitrates.

The chemistry of the alkoxyl radicals plays an important role in hydrocarbon oxidation in the propylene and butane mechanisms. Besides decomposition and reaction with molecular oxygen, alkoxyl radicals may react with NO and NO_2 to form alkyl nitrites and alkyl nitrates, which are temporary and permanent sinks of alkoxyl radicals. In simulations of propylene and butane smog chamber experiments, alkyl nitrates are a minor sink of NO_x.

The reactions of RO· with NO and NO_2 in our mechanisms discussed by Whitten and Hogo (1977) have not been changed.

Rate constants for the propylene + HO· and butane + HO· reactions--

In their review of previous studies of the reactions of alkanes and alkenes with hydroxyl radicals (OH·), Lloyd et al. (1976) reported average values of the rate constants for the propylene + OH· and butane + OH· reactions based on previous studies. For the propylene + OH· rate constant, the reported value was 4.2×10^4 $ppm^{-1}min^{-1}$, close to that used by Whitten and Hogo (1977). For the butane + OH· rate constant, the reported value was 4.2×10^3 $ppm^{-1}min^{-1}$, approximately 25 percent higher than the value used by Whitten and Hogo (1977). We incorporated these average values into our explicit mechanisms instead of choosing a rate constant measured in any one study.

Reactions of alkylperoxy radicals with NO and NO_2--In all modern kinetic mechanisms for smog formation, the reactions of alkylperoxy radicals ($RO_2^·$) with NO are the major cause of conversion of NO to NO_2, which is required to form ozone. Since Howard and Evenson (1977) recently measured a high value for the rate constant of the $HO_2^·$ + NO reaction, we raised the rate constants of all $RO_2^·$ + NO reactions in our mechanisms to be equal to the measured value. The overall effect of this change has been to shorten the induction period for ozone formation.

Besides the $RO_2^·$ + NO reactions, $RO_2^·$ may react with NO_2 to form an alkylperoxy nitrate. This reaction is analogous to the reaction of $HO_2^·$ and NO_2 to produce peroxynitric acid (HO_2NO_2 or PNA). Recent estimates of PNA formation and destruction rates are high, suggesting that this species is in a steady state (see Section 4 for further discussion). Barker and Golden (1977) reported that the rates of formation and destruction of alkylperoxy nitrates should be comparable to the formation and destruction rates of PNA. Consequently, neither PNA nor alkylperoxy nitrates are included in the kinetic mechanisms.

However, pathways to alkylnitrate formation from the $RO_2^{\cdot}$ + NO reactions have been added to our mechanisms as for alkyl groups larger than methyl (Darnell et al., 1976a). The UCR data show that the formation of larger nitrates does not depend strongly on the HC/NO_x ratio as one would predict from the RO· + NO_2 pathway. But the $RO_2^{\cdot}$ + NO pathway tends to be independent of the HC/NO_x ratio because the concentration of $RO_2^{\cdot}$ is regullated by the NO concentration since the major reaction of $RO_2^{\cdot}$ is with NO. The RO·˙ radicals usually react unimolecularly or with O_2 rather than with NO_2. Darnell et al.(1976a) reported that only C_4 and larger groups form significant amounts of alkyl nitrates via the $RO_2^{\cdot}$ + NO reaction. C_2 and C_3 groups may form alkyl nitrates via the $RO_2^{\cdot}$ + NO reaction, but we assumed that alkyl nitrates account for less than 1 percent of products of $RO_2^{\cdot}$ + NO reactions. Either pathway to nitrate formation can be an important sink for both radicals and NO_x; thus, simulations consistent with the observed nitrate data are necessary for mechanism development.

Sinks of alkylperoxy radicals--A major sink of alkylperoxy radicals may be their reaction with hydroperoxy radicals to form organic peroxides:

$$RO_2^{\cdot} + HO_2^{\cdot} \rightarrow ROOH + O_2 \qquad . \qquad (41)$$

The rate constant for Reaction (41) was formerly based on the rate constant of 4×10^3 $ppm^{-1}min^{-1}$ for the $HO_2^{\cdot} + HO_2^{\cdot}$ reaction and the ratios of the rate constants for various $HO_2^{\cdot}$ reactions recommended by Hampson and Garvin (1978). Using the same ratios of rate constants with Howard and Evenson's (1977) measurement of the $HO_2^{\cdot}$ + NO rate constant, we have estimated values of 1.5×10^4 $ppm^{-1}min^{-1}$ and 4.0×10^3 $ppm^{-1}min^{-1}$ for $HO_2^{\cdot} + HO_2^{\cdot}$ and $RO_2^{\cdot} + HO_2^{\cdot}$, respectively. These values are used in the mechanisms at present, but they are tentative and may be changed in light of new measurements.

Simulation Results for Propylene/NO_x Systems

Much of the work on the propylene mechanism was performed with early UCR runs and was discussed by Whitten and Hogo (1977). However, updating the rate constants in the kinetic mechanism (as discussed above) produced

TABLE 9. REACTIONS OF PROPYLENE*

Reaction	Rate constant $(ppm^{-1}min^{-1})$
$CH_3CH=CH_2 + O \xrightarrow{2O_2} CH_3O_2^{\cdot} + CH_3C(O)O_2^{\cdot}$	2.7×10^3
$CH_3CH=CH_2 + O \rightarrow CH_3\overset{O}{\overbrace{CH-\!\!\!-\!\!\!-CH_2}}$	2.7×10^3
$CH_3\overset{O}{\overbrace{CH-\!\!\!-\!\!\!-CH_2}} \rightarrow CH_3CH_2CHO$	3×10^{-1}
$CH_3CH=CH_2 + OH\cdot \xrightarrow{O_2} CH_3CH(O_2^{\cdot})CH_2OH$	4.2×10^4
$CH_3CH=CH_2 + NO_3 \rightarrow NO_2 + Products$	7.82
$CH_3CH=CH_2 + O_3 \rightarrow HCHO + CH_3CHO_2^{\cdot}$	7.5×10^{-3}
$CH_3CH=CH_2 + O_3 \rightarrow CH_3CHO + CH_2O_2^{\cdot}$	7.5×10^{-3}
$CH_2O_2^{\cdot} + HCHO \rightarrow H_2C\overset{O-\!O}{\underset{O}{\diagdown\diagup}}CH_2$	2×10^3
$CH_2O_2^{\cdot} + CH_3CHO \rightarrow H_2C\overset{O-\!O}{\underset{O}{\diagdown\diagup}}CHCH_3$	2×10^3
$CH_2O_2^{\cdot} + NO \rightarrow NO_2 + HCHO$	1.2×10^4
$CH_2O_2^{\cdot} + NO_2 \rightarrow NO_3 + HCHO$	8×10^3
$CH_2O_2^{\cdot} \rightarrow CO + H_2 + O_2$	$6.7 \times 10^{2\dagger}$
$CH_2O_2^{\cdot} \rightarrow CO_2 + H_2$	$1.8 \times 10^{2\dagger}$
$CH_2O_2^{\cdot} \rightarrow 2HO_2^{\cdot} + CO_2$	$9 \times 10^{1\dagger}$
$CH_2O_2^{\cdot} \rightarrow HC(O)OH$	$6 \times 10^{1\dagger}$
$CH_3CHO_2^{\cdot} + HCHO \rightarrow CH_3CH\overset{O-\!O}{\underset{O}{\diagdown\diagup}}CH_2$	2×10^3
$CH_3CHO_2^{\cdot} + CH_3CHO \rightarrow CH_3CH\overset{O-\!O}{\underset{O}{\diagdown\diagup}}CHCH_3$	2×10^3
$CH_3CHO_2^{\cdot} + NO \rightarrow NO_2 + CH_3CHO$	1.2×10^4
$CH_3CHO_2^{\cdot} + NO_2 \rightarrow NO_3 + CH_3CHO$	8×10^3

(continued)

80

TABLE 9 (Concluded)

Reaction	Rate constant $(ppm^{-1}min^{-1})$
$CH_3CHO_2^- \rightarrow CO_2 + CH_4$	$1.5 \times 10^{2\dagger}$
$CH_3CHO_2^- \xrightarrow{O_2} CH_3O_2^- + CO + OH\cdot$	$3.4 \times 10^{2\dagger}$
$CH_3CHO_2^- \xrightarrow{2O_2} CH_3O_2^- + CO_2 + HO_2^-$	$4.25 \times 10^{2\dagger}$
$CH_3CHO_2^- \xrightarrow{O_2} CH_3O\cdot + CO + HO_2^-$	$8.5 \times 10^{1\dagger}$
$CH_3CH_2CHO + h\nu \xrightarrow{2O_2} CH_3CH_2O_2^- + HO_2^- + CO$	Experimental†
$CH_3CH_2CHO + OH\cdot \xrightarrow{O_2} CH_3CH_2C(O)O_2^- + H_2O$	2.4×10^4
$CH_3CH_2C(O)O_2^- + NO \xrightarrow{O_2} NO_2 + CH_3CH_2O_2^- + CO_2$	3.8×10^3
$CH_3CH(O_2^-)CH_2OH + NO \rightarrow NO_2 + CH_3CH(O\cdot)CH_2OH$	1.2×10^4
$CH_3CH_2O_2^- + NO \rightarrow NO_2 + CH_3CH_2O\cdot$	1.2×10^4
$CH_3CH_2O_2^- + NO \rightarrow CH_3CH_2ONO_2$	1×10^2
$CH_3CH(O\cdot)CH_2OH \xrightarrow{O_2} CH_3CHO + HCHO + HO_2^-$	$3 \times 10^{5\dagger}$
$CH_3CH_2O\cdot + O_2 \rightarrow CH_3CHO + HO_2^-$	3.3
$CH_3CH_2C(O)O_2^- + HO_2^- \rightarrow CH_3CH_2C(O)O_2H + O_2$	4×10^3
$CH_3CH(O_2^-)CH_2OH + HO_2^- \rightarrow CH_3CH(O_2H)CH_2OH + O_2$	4×10^3
$CH_3CH_2O_2^- + HO_2^- \rightarrow CH_3CH_2O_2H + O_2$	4×10^3
$CH_3CH_2C(O)O_2^- + NO_2 \rightarrow CH_3CH_2C(O)O_2NO_2$	2×10^3
$CH_3CH_2C(O)O_2NO_2 \rightarrow NO_2 + CH_3CH_2C(O)O_2^-$	$2.8 \times 10^{-2\dagger\S}$
$CH_3CH_2O\cdot + NO_2 \rightarrow CH_3CH_2ONO_2$	1.5×10^4
$CH_3CH_2O\cdot + NO_2 \rightarrow CH_3CHO + HNO_2$	2.9×10^3
$CH_3CH(O_2^-)CH_2OH + CH_3CH(O_2^-)CH_2OH \rightarrow CH_3CH(O\cdot)CH_2OH + CH_3CH(O\cdot)CH_2OH + O_2$	5.0×10^2
$CH_3CH(O_2^-)CH_2OH + O_3 \rightarrow CH_3CH(O\cdot)CH_2OH + 2O_2$	2×10^2

* The inorganic, formaldehyde, and acetaldehyde reactions listed earlier must be added to construct the explicit propylene mechanism.

† Rate constant in min^{-1}.

§ Activation energy is 12,500K; rate constant is given at 298K.

81

simulation results different from those documented by Whitten and Hogo (1977). The current explicit propylene mechanism is presented in Table 9. A factorial block of initial concentrations for the propylene/NO_x experiments at UCR is shown in Figure 16. The initial conditions for each propylene experiment are presented in Table 10, and the simulation results are shown in Figures 17 through 32 for the most recent series of propylene experiments (EC-256, EC-257, EC-276, EC-277, EC-278, and EC-279); all of the simulations are shown in the appendix. Table 11 presents some quantitative information on the agreement between the simulated NO_2 and O_3 results and the UCR data.
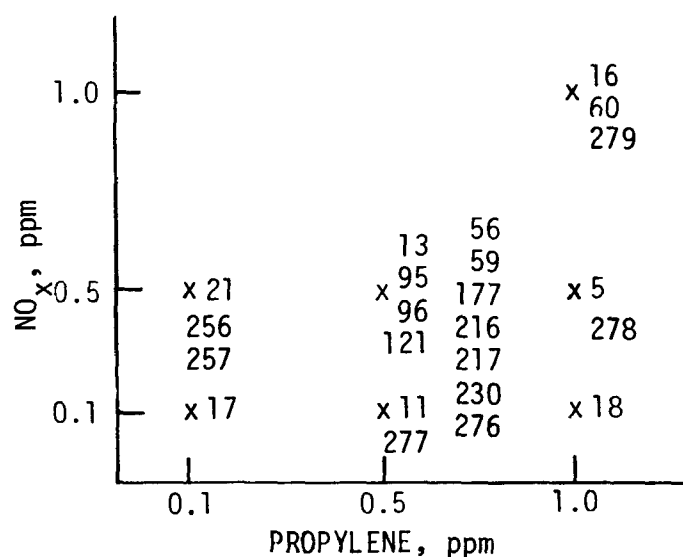

Figure 16. Factorial block of initial concentrations in UCR propylene/NO_x experiments. Numbers correspond to UCR run numbers.

The current propylene mechanism produced simulations of ozone concentrations as close to observational data as did the propylene mechanism of Whitten and Hogo (1977). Excluding EC-55 and EC-56, the average difference in simulated and observed ozone one-hour maxima was 3.8 percent in their study. In the present mechanism, the inorganic, formaldehyde, and acetaldehyde chemistry used agrees with recently published information, and the formaldehyde and acetaldehyde mechanisms also give reasonable simulations of independent smog chamber experiments without propylene. Unpublished simulations using the old Whitten and Hogo (1977) aldehyde chemistry tend to underpredict ozone generation compared with the smog chamber experiments using the aldehydes. Likewise, a mere updating of their old mechanism produces simulated ozone concentrations grossly exceeding the observed values. Hence, although the present propylene mechanism may not produce simulations as close to observations as did the earlier Whitten and Hogo (1977) mechanism, the new mechanism should have fewer errors.

Simulation Results for the Butane/NO_x Systems

The reactions which are special to the butane system are listed in Table 12. Figure 33 illustrates the factorial block of concentrations used in the smog chamber experiments. The initial conditions and photolysis constants used in the butane simulations are listed in Table 13, and the simulation results for NO_2 and O_3 are presented in Table 14. Sample simulation results are shown for EC-162 and EC-178 in Figures 34 and 35.

The following general observations about the modeling of the butane experiments can be made:

> PAN formation stems from the photolysis of MEK as the major peroxyacetyl radical source rather than the hydroxyl radical attack on acetaldehyde.

TABLE 10. INITIAL CONDITIONS AND PHOTOLYSIS RATE CONSTANTS FOR THE PROPYLENE/NO_x SMOG CHAMBER EXPERIMENTS

| Run number	Initial concentration (ppm)				Photolysis rate constant (x 10^4 min^{-1})					
	Propylene	NO	NO_2	HONO	$NO_2 \to NO+O^*$	$O_3 \to O(^1D)$	$O_3 \to O(^3P)$	$HONO \to NO+OH\cdot$	$H_2O_2 \to 2OH\cdot$	$FORM \to Products^+$
EC-5	0.97	0.551	0.047	0.005	0.223	10	78.1	620	5.0	18
EC-11	0.447	0.115	0.02	0.001	0.223	10	78.1	620	5.0	18
EC-13	0.48	0.45	0.14	0.025	0.223	10	78.1	620	5.0	18
EC-16	1.036	1.122	0.156	0.02	0.223	10	78.1	620	5.0	18
EC-17	0.103	0.106	0.014	0.005	0.223	10	78.1	620	5.0	18
EC-18	0.972	0.106	0.014	0.0001	0.223	10	78.1	620	5.0	18
EC-21	0.104	0.558	0.066	0.015	0.223	10	78.1	620	5.0	18
EC-5127	0.5	0.53	0.06	0.01	0.213	12.8	70	600	4.0	10
EC-55	0.545	0.48	0.121	0.02	0.209	12.8	70	600	4.0	9
EC-56	0.531	0.311	0.283	0.03	0.208	12.8	70	600	4.0	9
EC-59	0.52	0.124	0.46	0.020	0.204	1.22	58.1	600	2.5	9
EC-60	1.082	1.105	0.145	0.018	0.204	1.22	58.1	600	2.5	7
EC-95	0.48	0.365	0.092	0.015	0.351	27	270	920	5.5	18
EC-96	0.48	0.349	0.09	0.010	0.351	27	270	920	5.5	15
EC-121	0.483	0.41	0.101	0.03	0.3	39	300	700	4.0	18
EC-177	0.45	0.364	0.099	0.008	0.33	14	105	608	5.0	15
EC-216	0.46	0.412	0.104	0.007	0.43	35.3	135	1280	6.0	11
EC-217§	0.085	0.21	0.238	0.005	0.43	35.3	135	1280	6.0	7
EC-230	0.546	0.392	0.128	0.008	0.3	13.0	92	870	4.0	9
EC-256**	0.109	0.52	0.042	0.009	0.3	6.9	90	830	3.6	6
EC-257	0.112	0.53	0.032	0.008	0.3	6.9	90	830	3.6	6
EC-276	0.510	0.41	0.106	0.003	0.35	9.9	108	1000	5.0	11
EC-277	0.564	0.098	0.010	0.001	0.35	9.9	108	1000	5.0	11
EC-278	1.016	0.366	0.128	0.006	0.35	9.9	108	1000	5.0	11
EC-279	1.10	0.73	C.244	0.005	0.35	9.9	108	1000	5.0	11

* Rate constant in min^{-1}.

+ The relationship between FORM→Products and carbonyl photolysis rate constants is discussed in Section 4.

§ 0.146 ppm of acetaldehyde added.

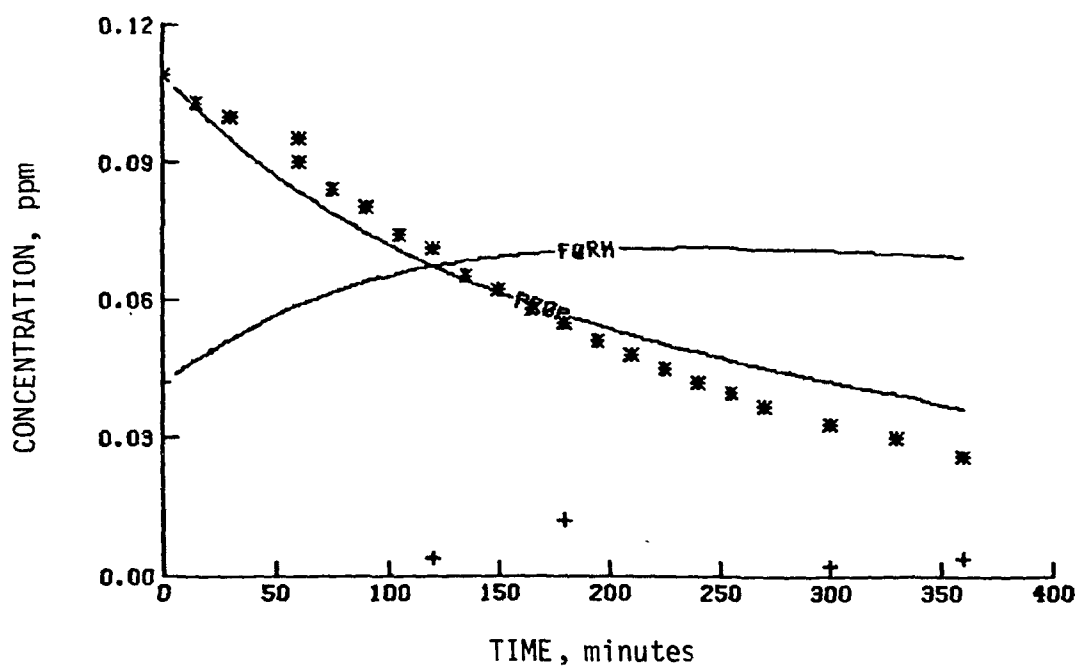** 0.371 ppm of formaldehyde added.

(a) O_3
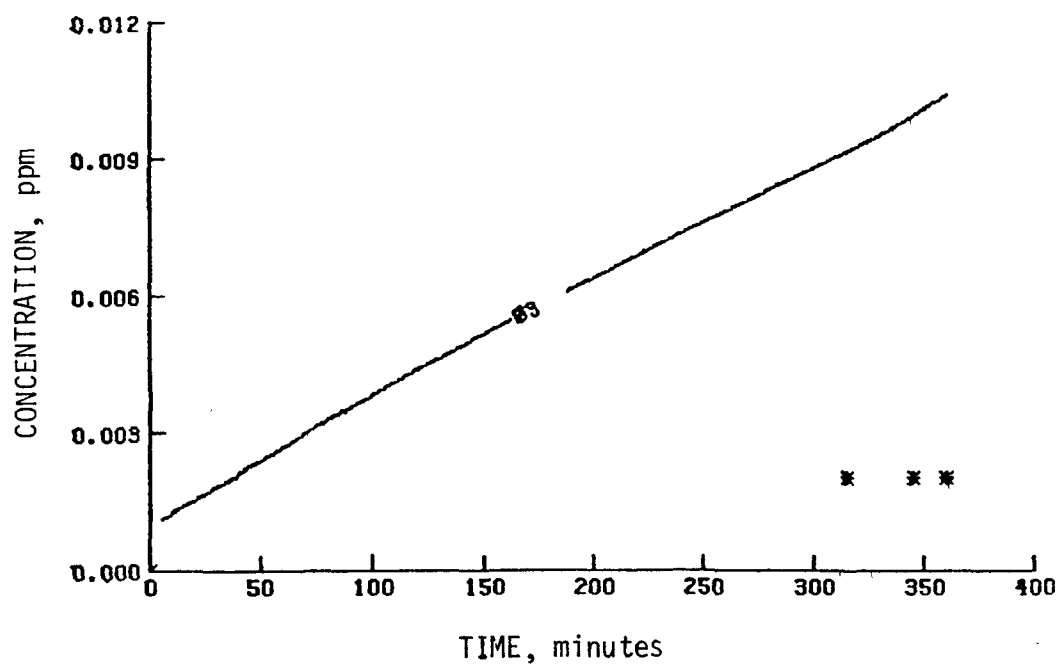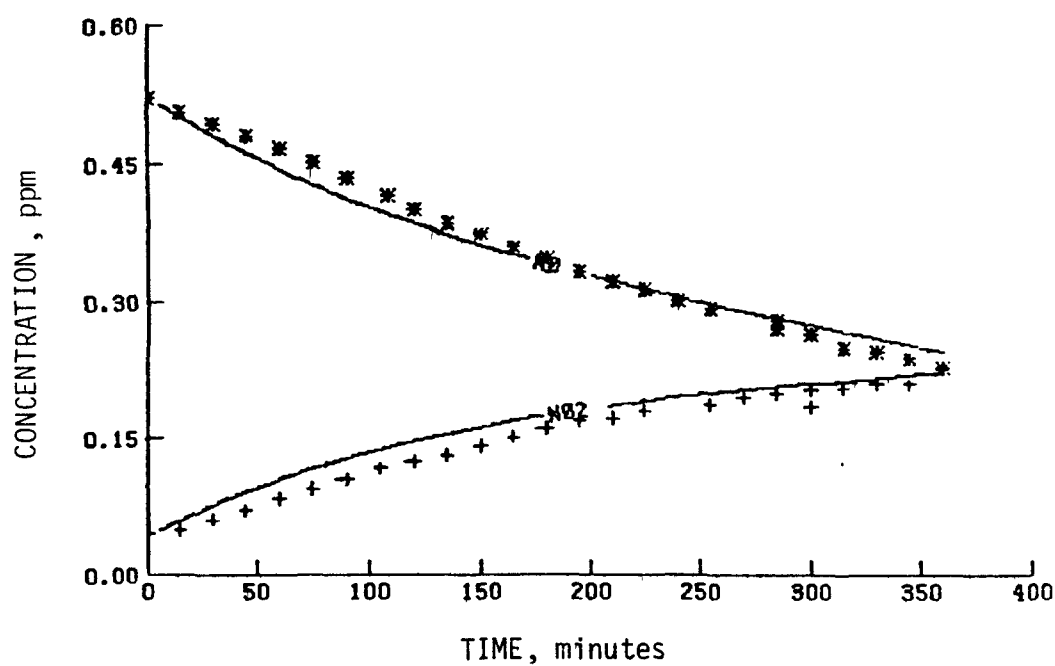
(b) NO_2 and NO

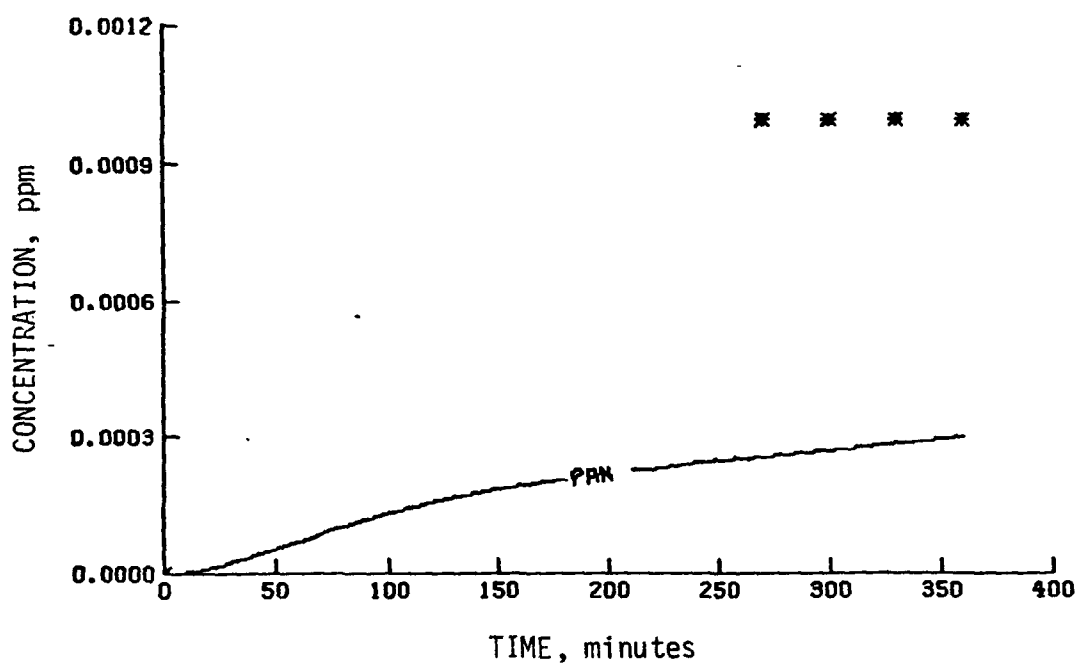Figure 17.   Simulation results of a UCR propylene experiment (EC-256)
for O_3, NO_2, and NO

85

(a) Formaldehyde and propylene

(b) PAN

Figure 18. Simulation results of a UCR propylene experiment (EC-256) for formaldehyde, propylene, and PAN

(a) Acetaldehyde

(b) Propionaldehyde

Figure 19. Simulation results of a UCR propylene experiment (EC-256)
for acetaldehyde and propionaldehyde

(a) O_3
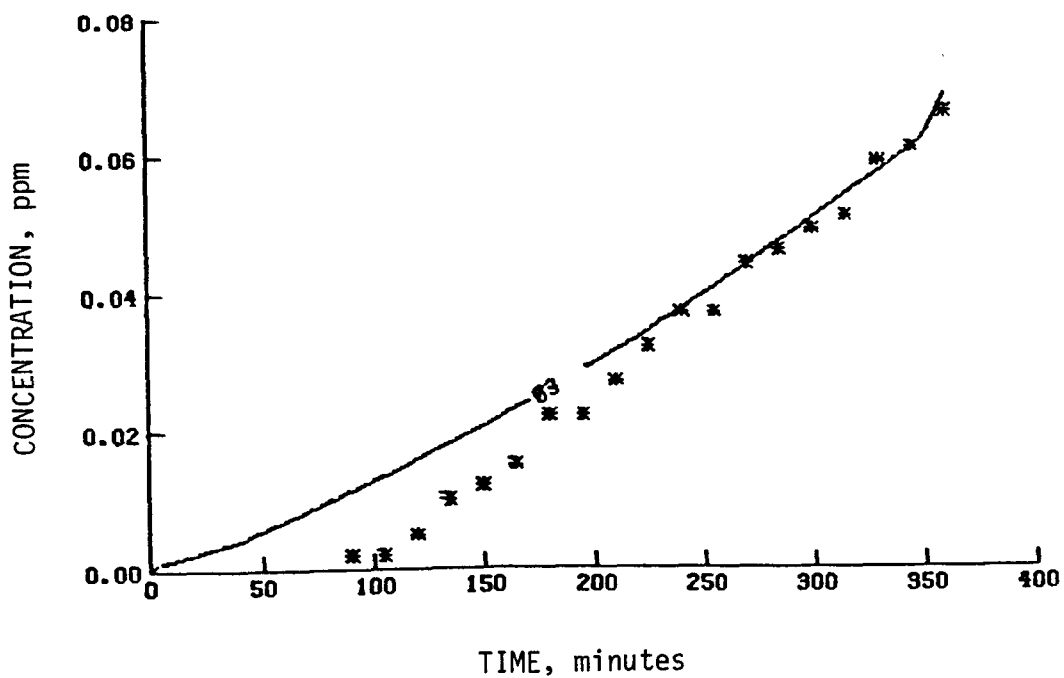
(b) NO_2 and NO

Figure 20.   Simulation results of a UCR propylene experiment (EC-257) for O_3, NO_2, and NO

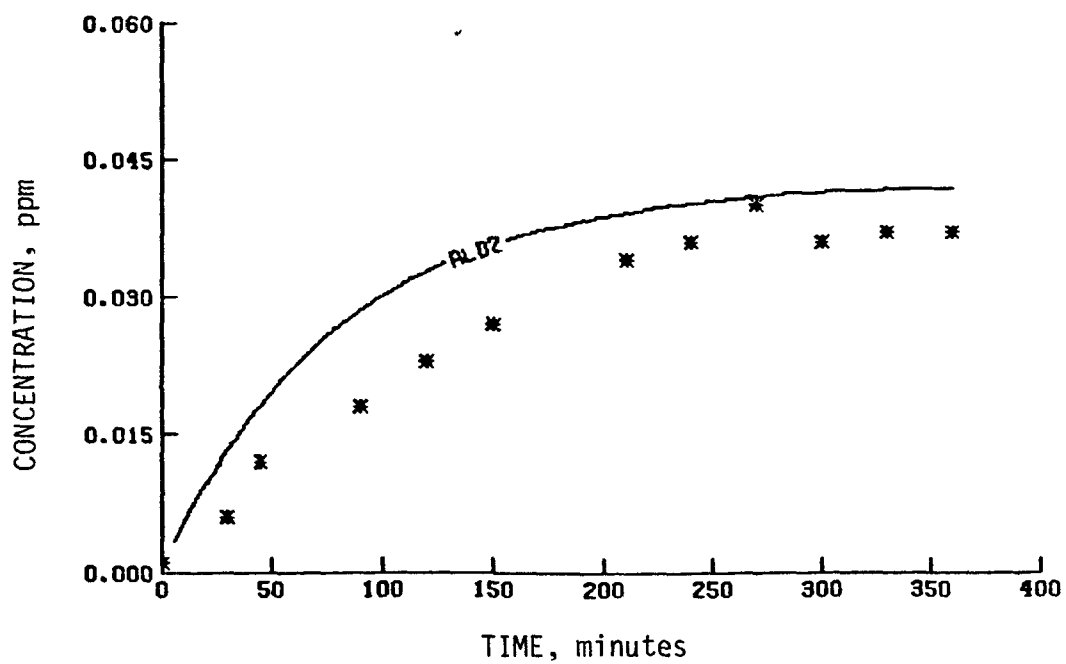Figure 21. Simulation results of a UCR propylene experiment (EC-257) for propylene and formaldehyde
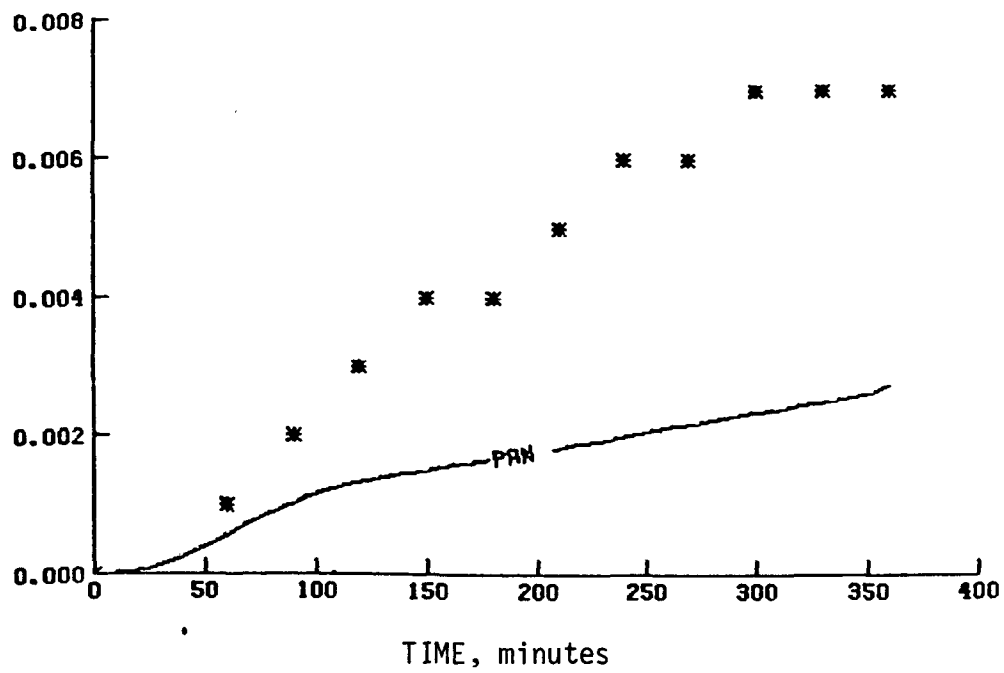
(a) PAN
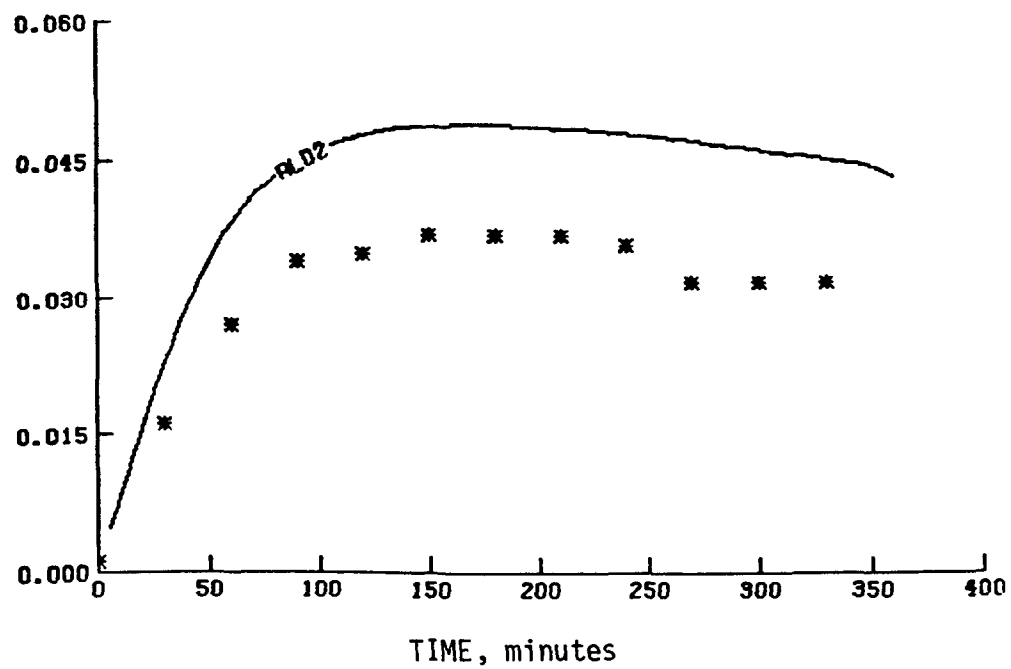
(b) Acetaldehyde

Figure 22. Simulation results of a UCR propylene experiment (EC-257) for PAN and acetaldehyde

90
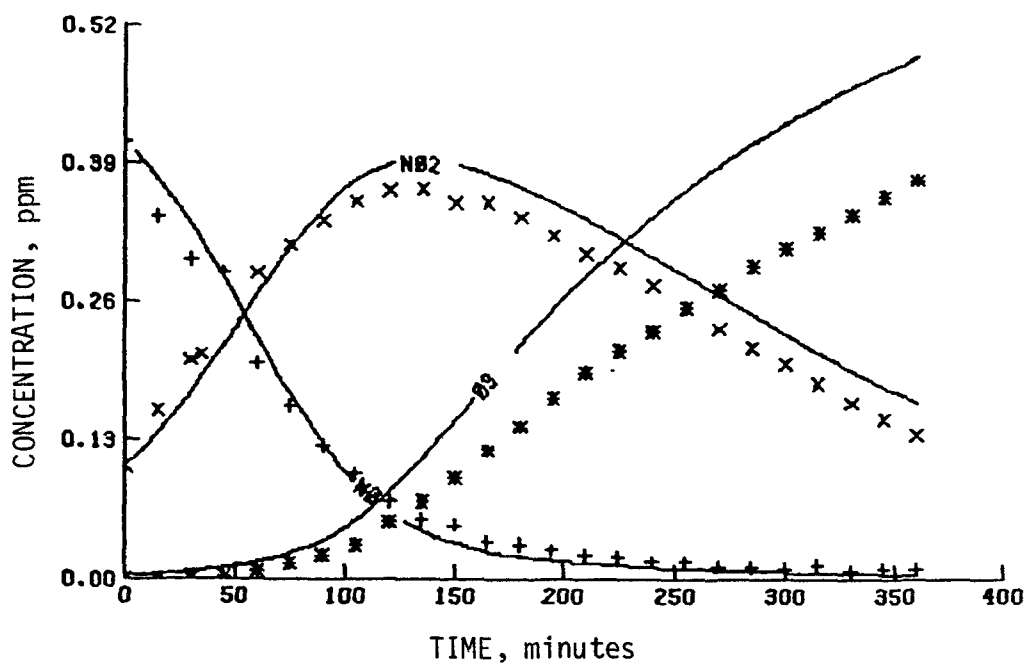
(a) NO_2, NO, and O_3
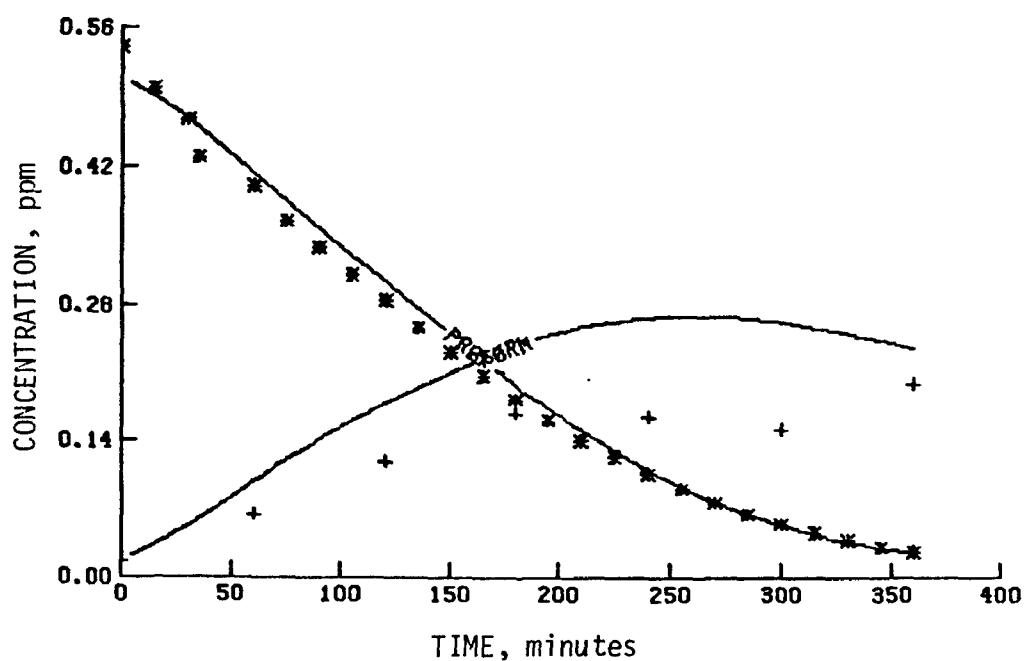
(b) Formaldehyde and propylene

Figure 23. Simulation results of a UCR propylene experiment (EC-276) for O_3, NO_2, NO, formaldehyde, and propylene

91
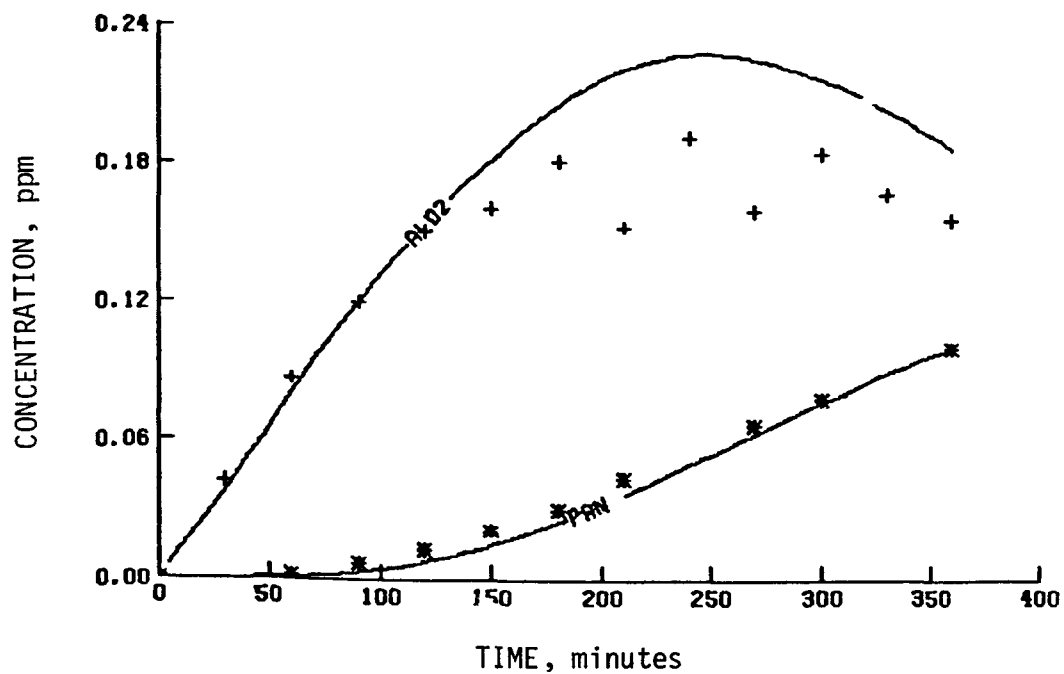
(a) Acetaldehyde and PAN

(b) Methyl nitrate and propionaldehyde

Figure 24.   Simulation results of a UCR propylene experiment (EC-276)
for acetaldehyde, PAN, methyl nitrate, and propionaldehyde

(a) O_3

(b) NO_2 and NO

Figure 25. Simulation results of a UCR propylene experiment (EC-277)
for O_3, NO_2, and NO
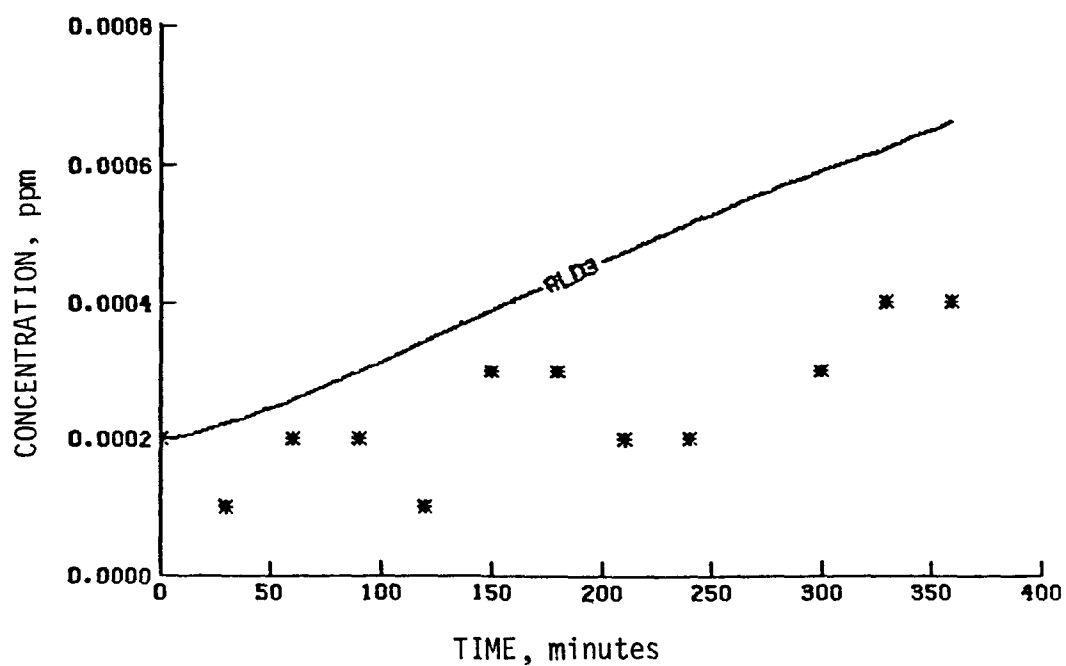
93

(a) Formaldehyde and propylene

(b) Acetaldehyde and PAN

Figure 26. Simulation results from a UCR propylene experiment (EC-277) for formaldehyde, propylene, acetaldehyde, and PAN

94

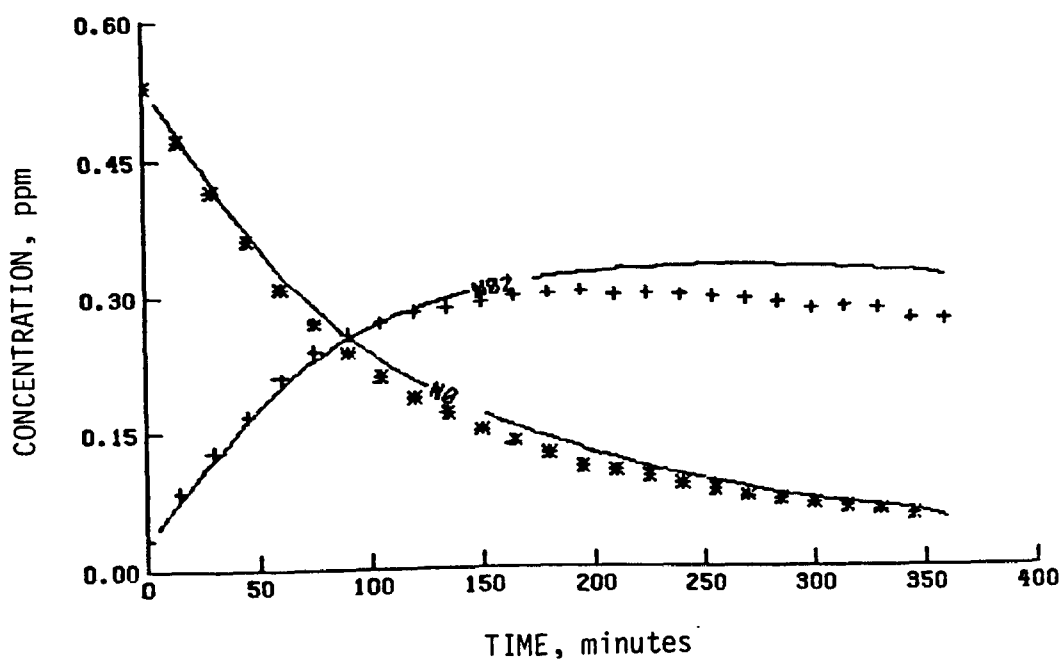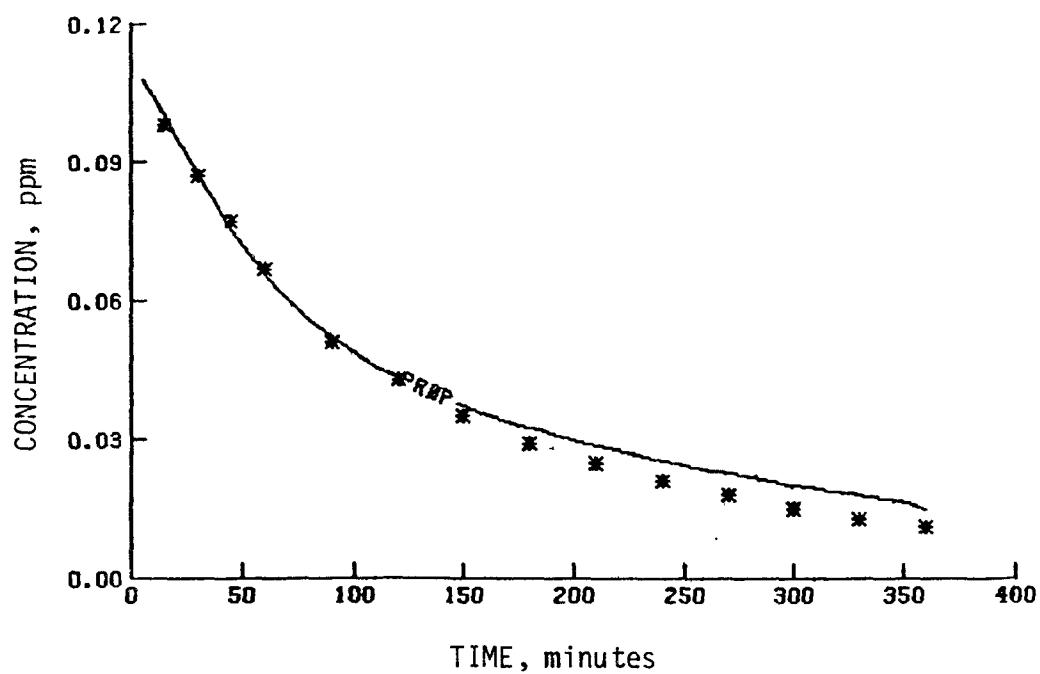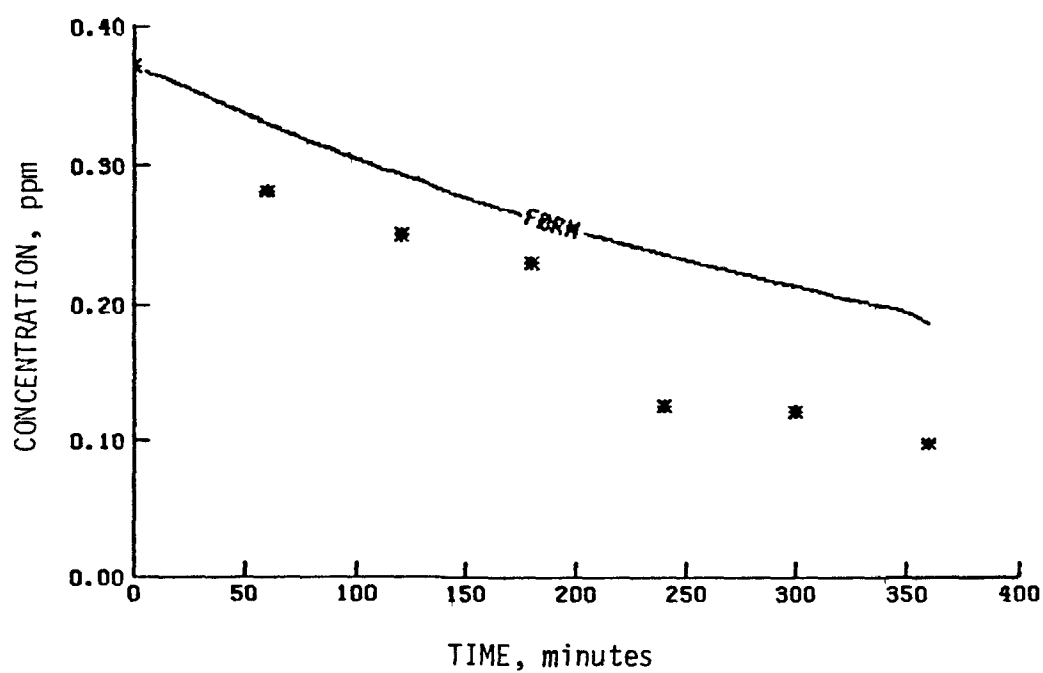Figure 27. Simulation results of a UCR propylene experiment (EC-277) for propionaldehyde
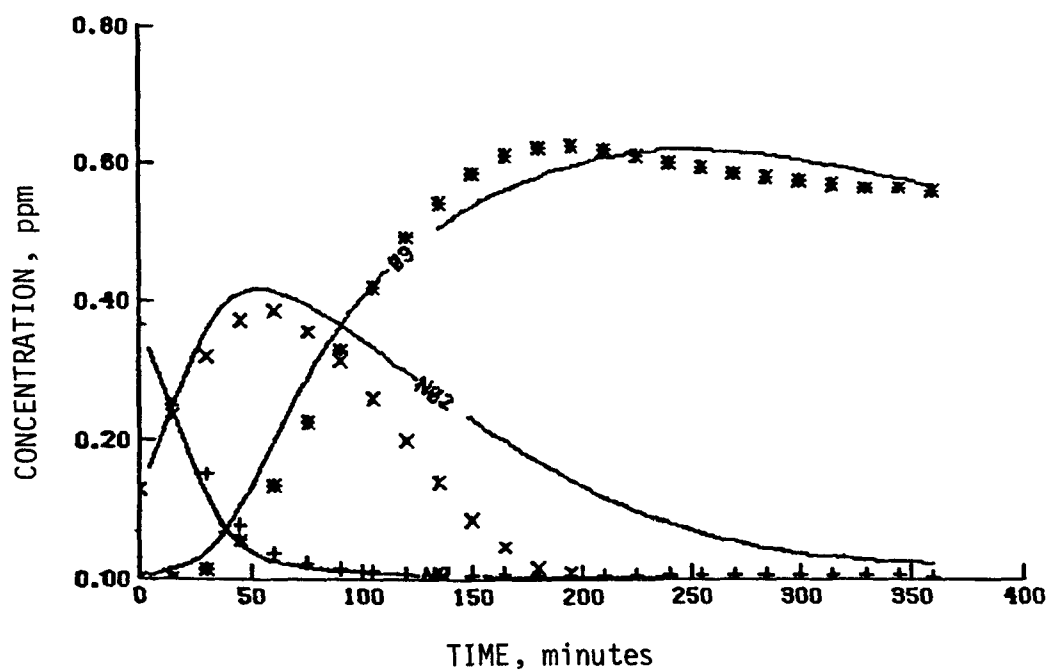
(a) NO_2, NO, and O_3
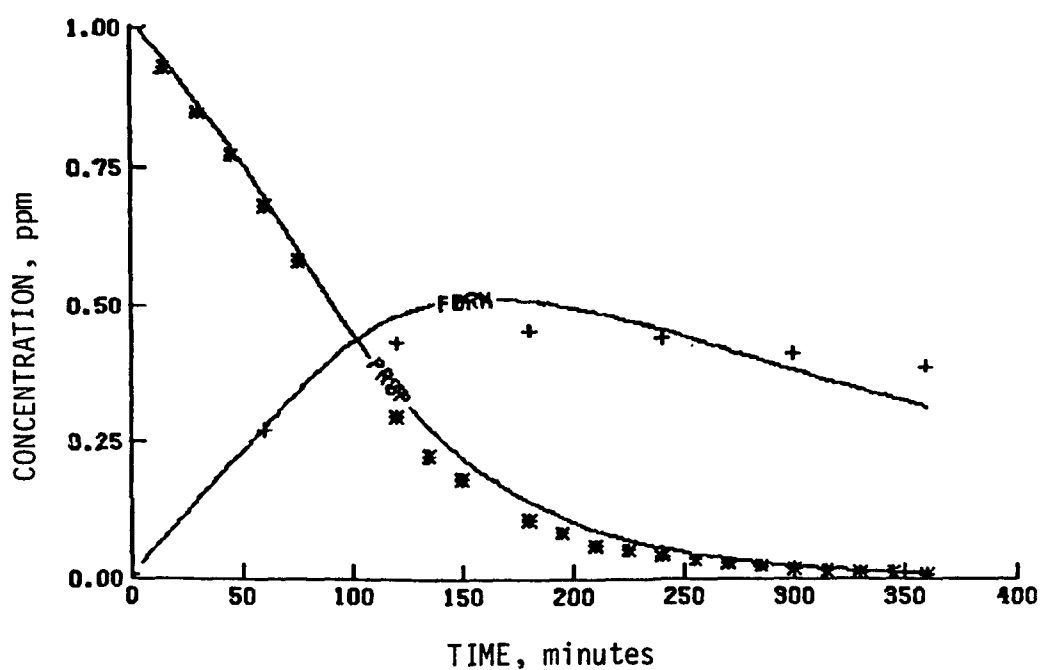
(b) Formaldehyde and propylene

Figure 28. Simulation results of a UCR propylene experiment (EC-278) for NO_2, NO, O_3, formaldehyde, and propylene

(a) Acetaldehyde and PAN

(b) Methyl nitrate and propionaldehyde

Figure 29.   Simulation results of a UCR propylene experiment (EC-278)
for acetaldehyde, PAN, methyl nitrate, and propionaldehyde

97
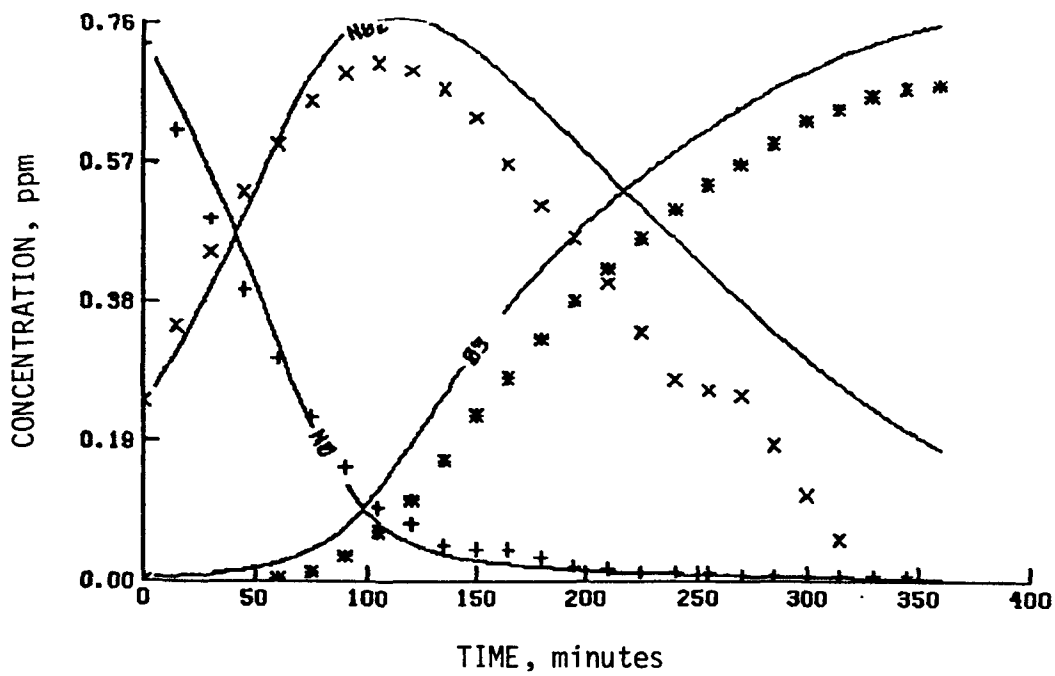
(a) NO_2, NO, and O_3
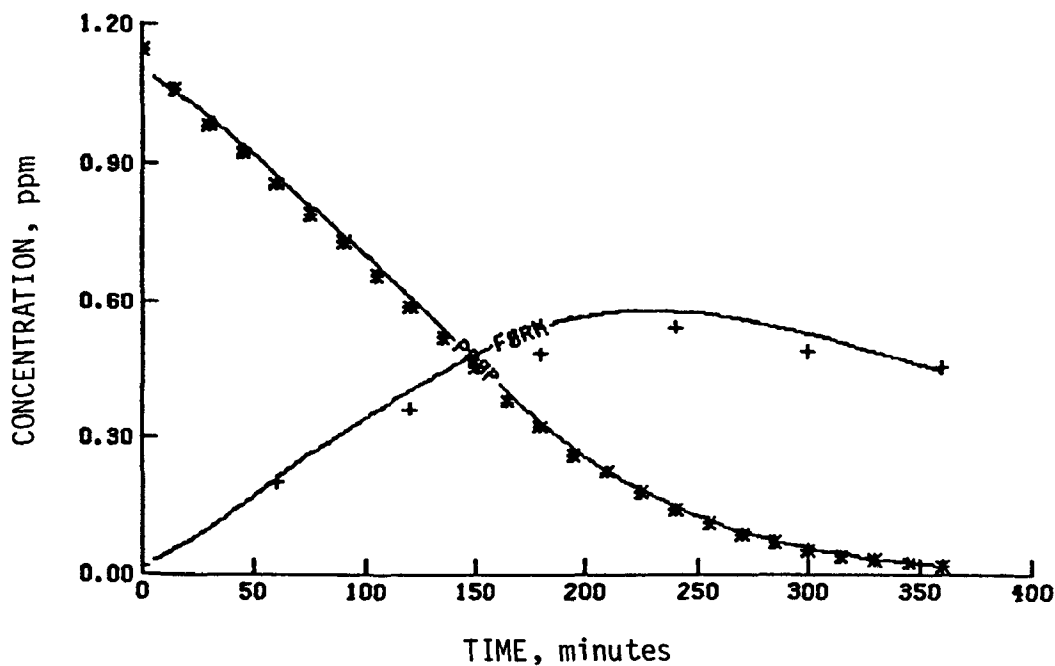
(b) Formaldehyde and propylene

Figure 30. Simulation results of a UCR propylene experiment (EC-279)
for NO_2, NO, O_3, formaldehyde, and propylene
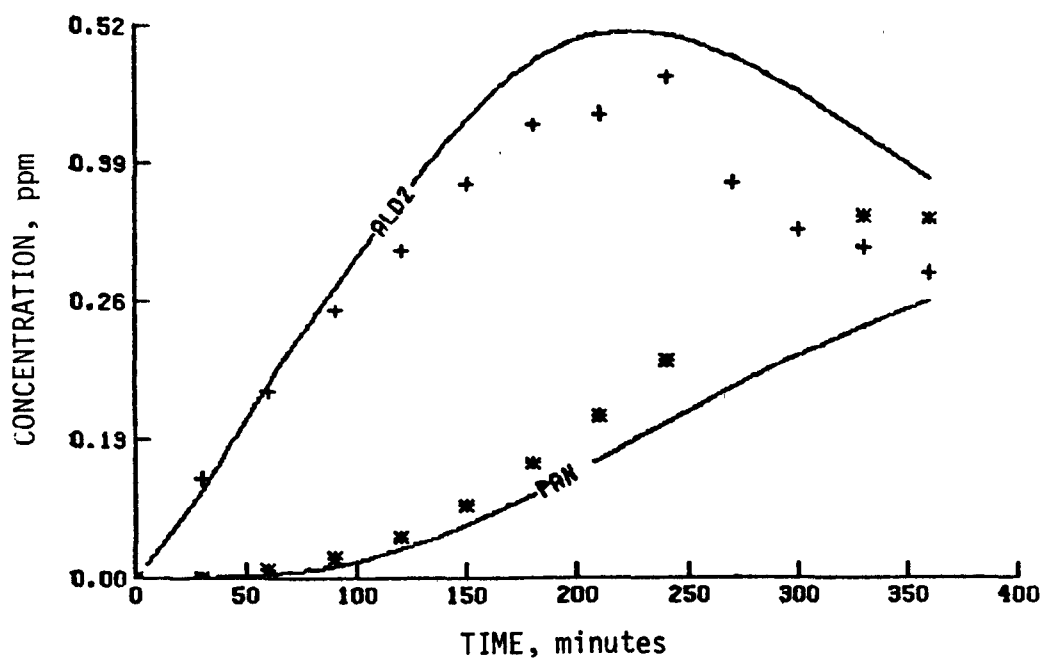
(a) Acetaldehyde and PAN
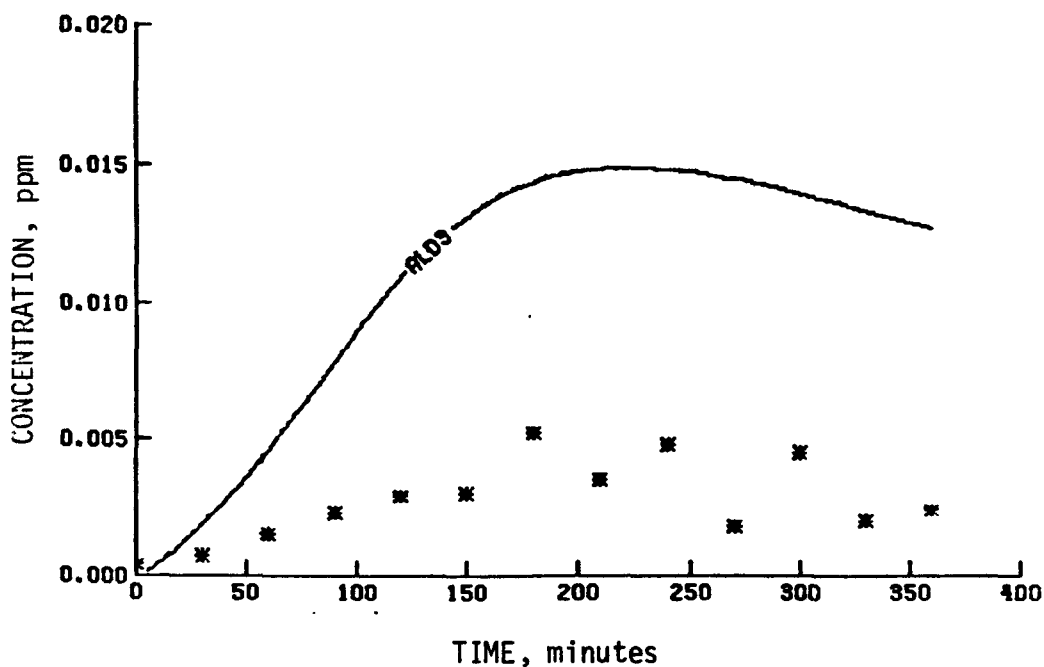
(b) Propionaldehyde

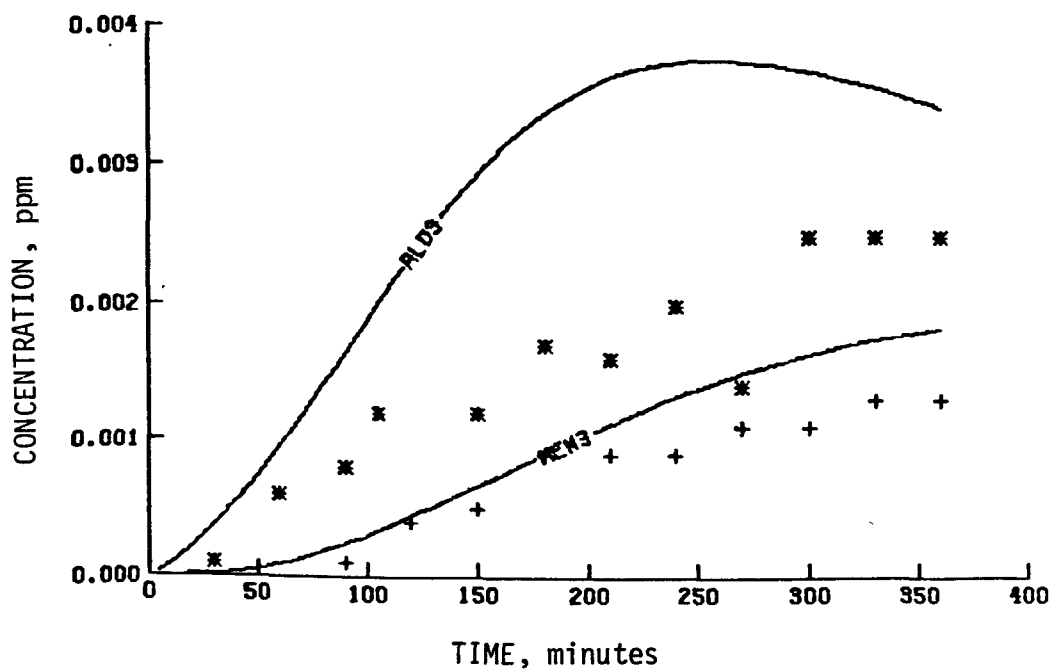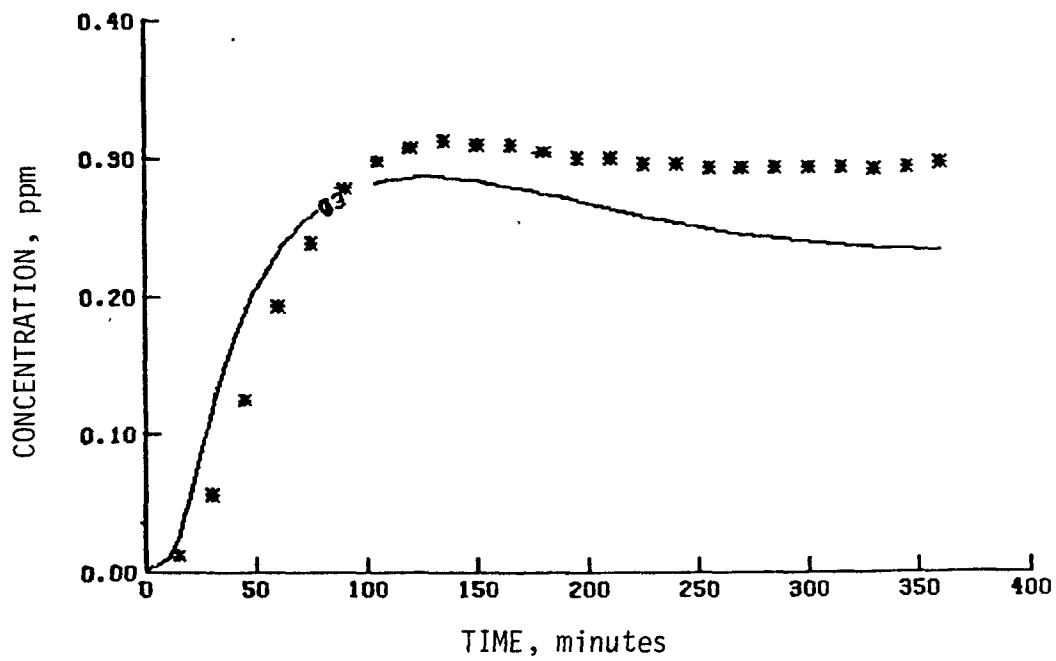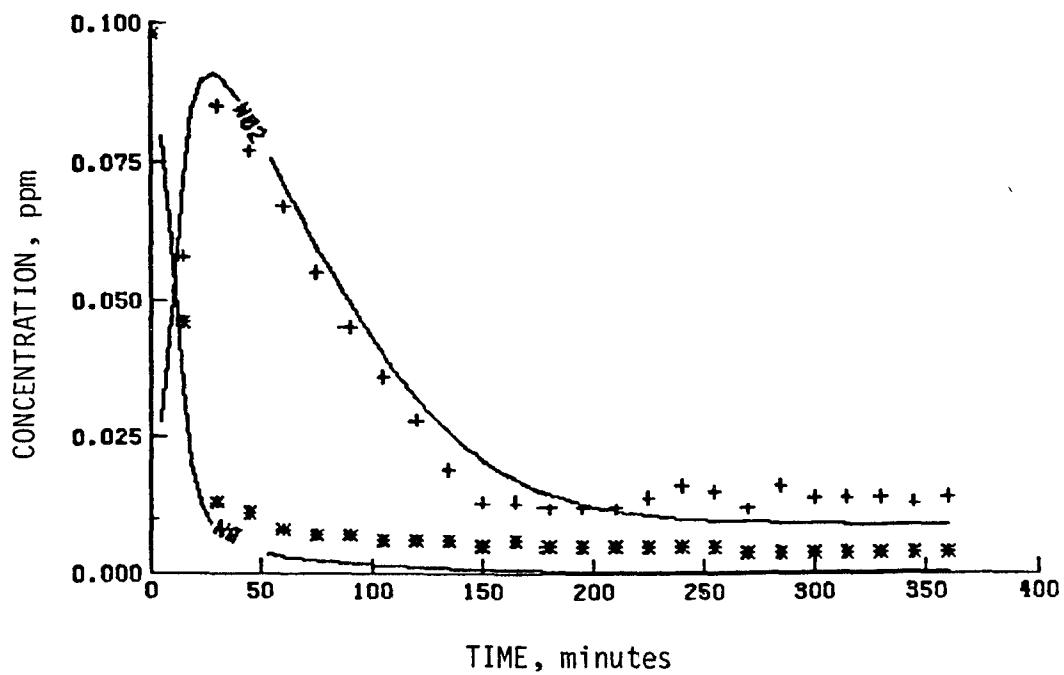Figure 31. Simulation results of a UCR propylene experiment (EC-279) for acetaldehyde, PAN, and propionaldehyde

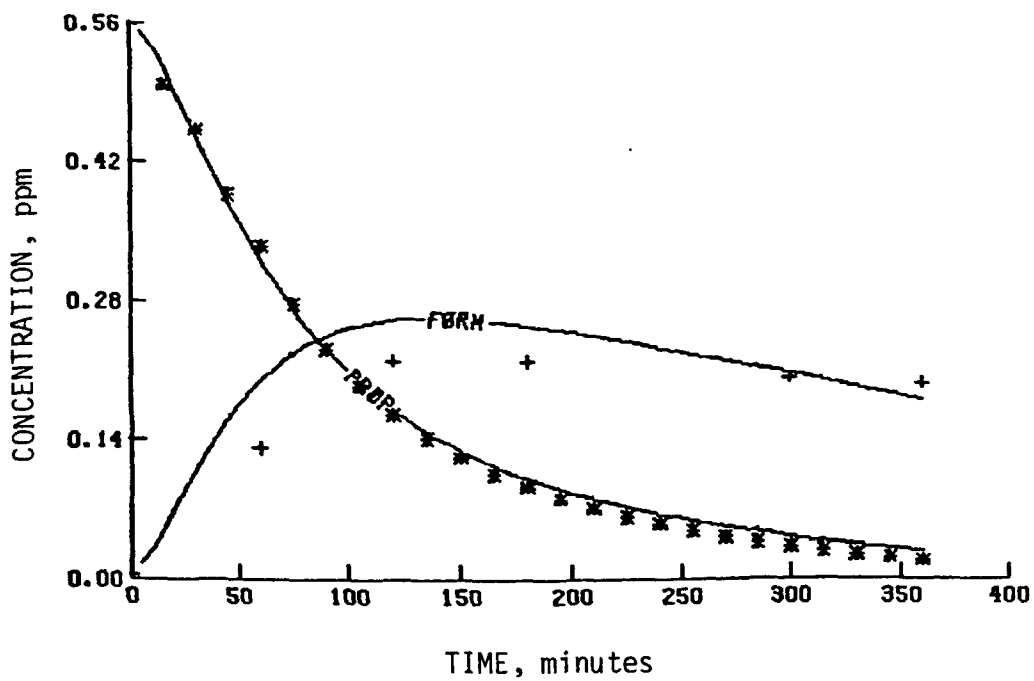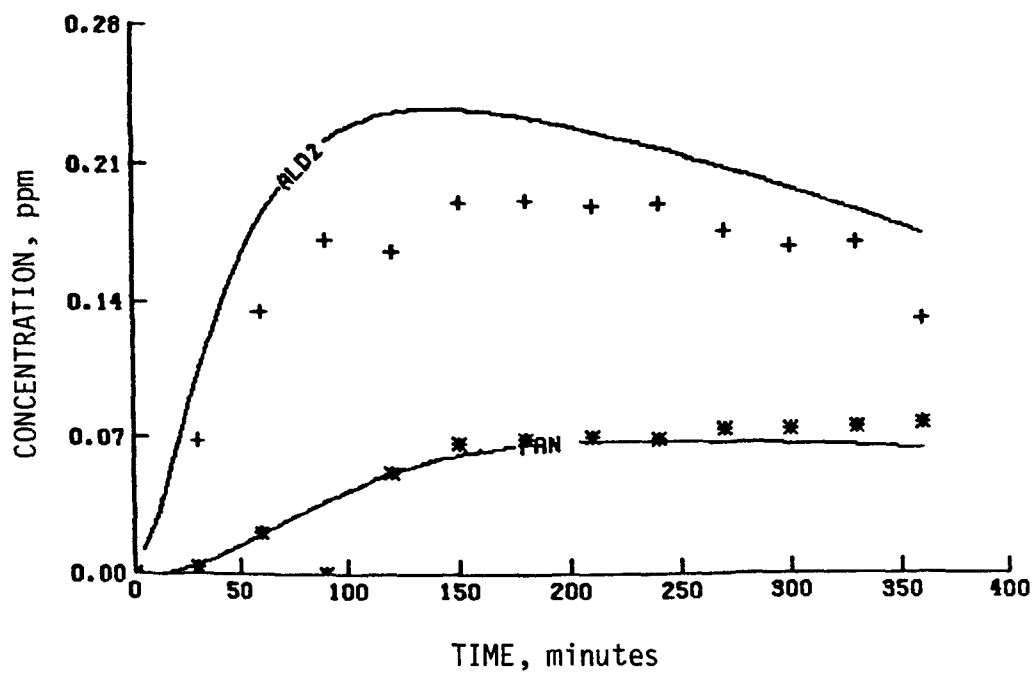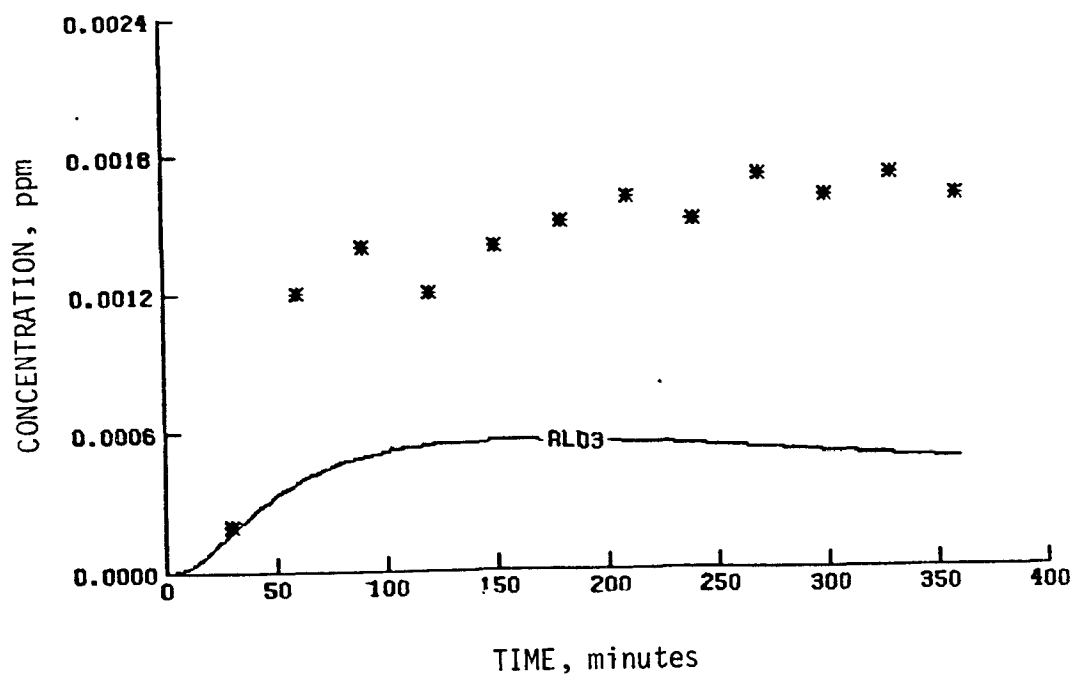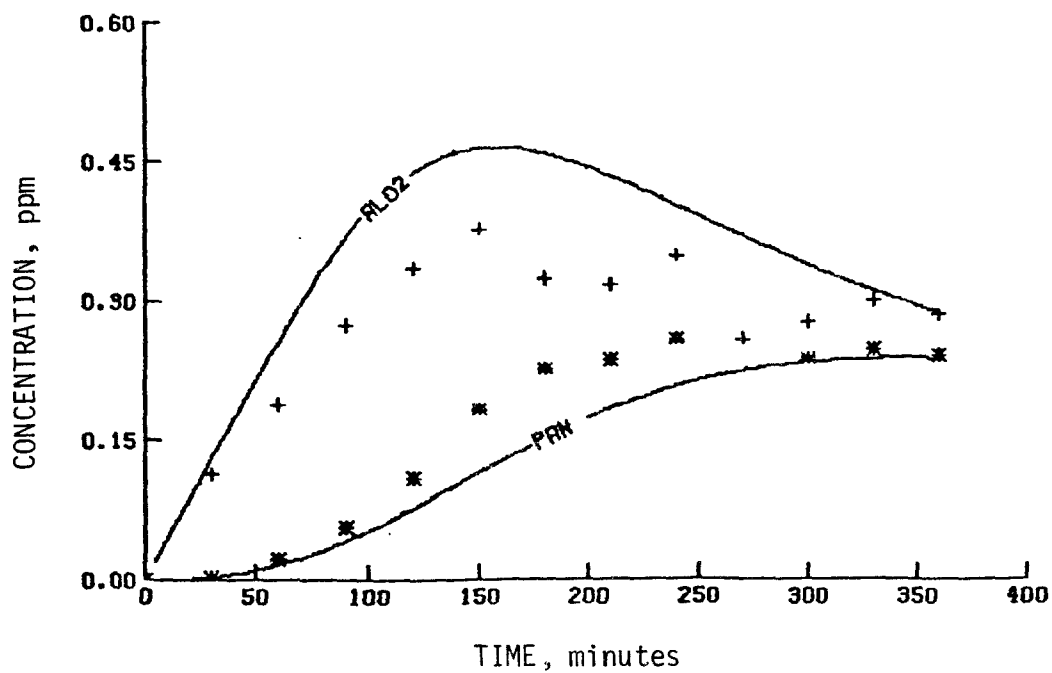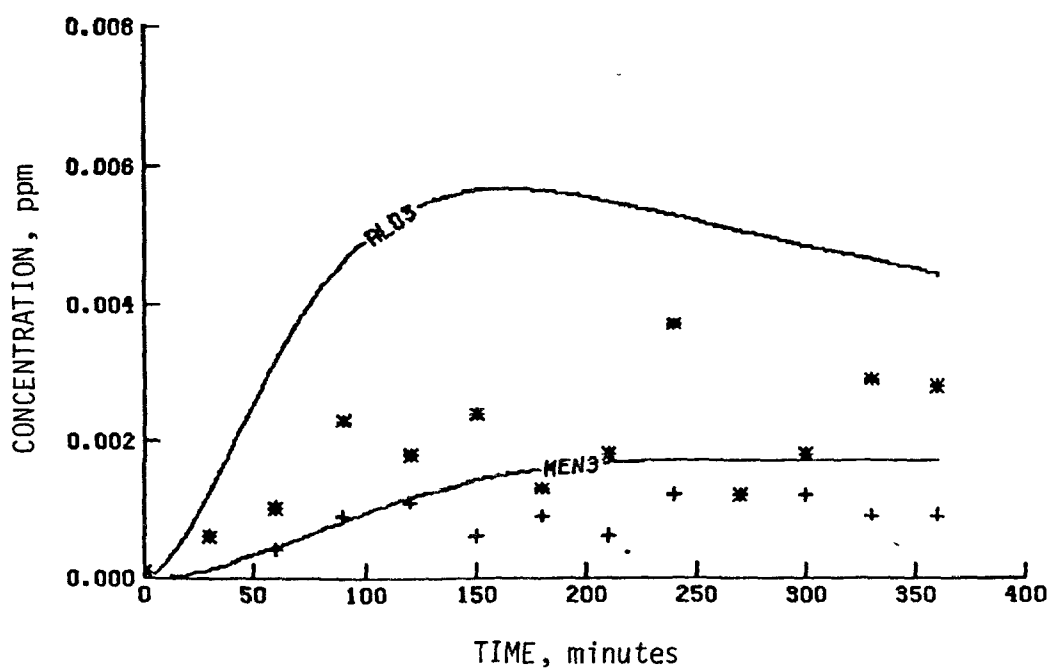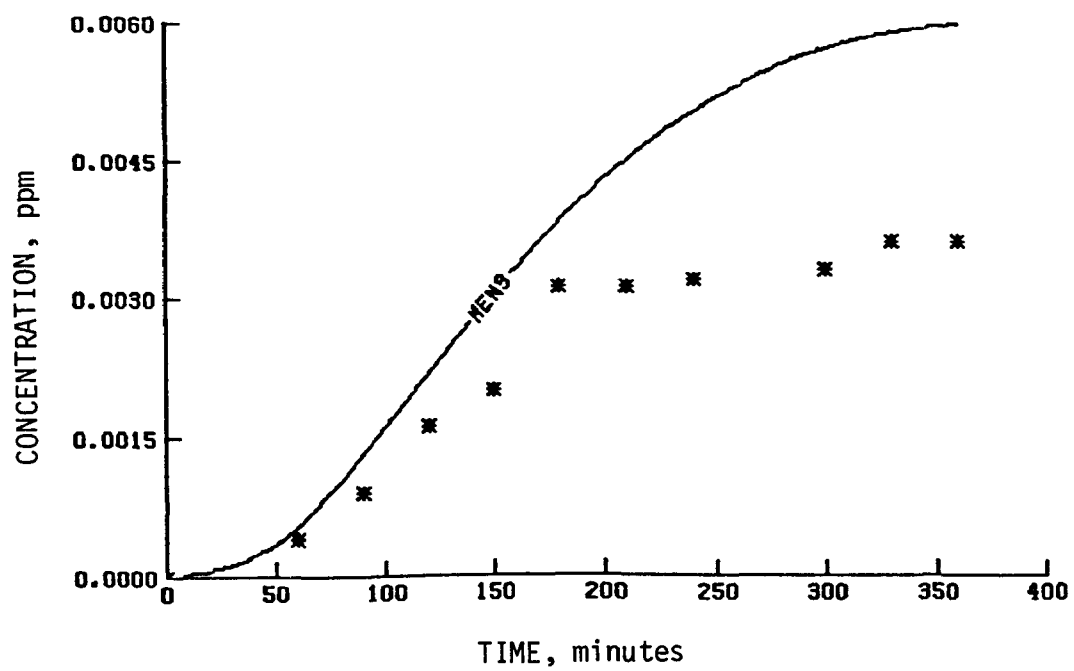Figure 32.   Simulation results of a UCR propylene experiment (EC-279) for methyl nitrate

TABLE 11. UCR PROPYLENE EXPERIMENTS--SIMULATIONS AND MEASUREMENTS

Exp. no.	Initial [NOx] (ppm)	Initial NO2/NOx ratio	Initial HC/NOx ratio (ppmC/ppm)	Maximum [O3] (ppm)* Sim.	Meas.	Difference in O3 maxima (percent)†	Time to maximum [O3] (minutes)§ Sim.	Meas.	Difference in times to O3 maxima (percent)†	Maximum [NO2] (ppm) Sim.	Meas.	Difference in NO2 maxima (percent)†	Time to maximum [NO2] (minutes)§ Sim.	Meas.	Difference in times to NO2 maxima (percent)†
5	0.557	0.084	5.2	0.47	0.45	4	150	130	15	0.47	0.40	18	70	60	17
11	0.135	0.15	9.9	0.26	0.22	18	110	90	22	0.11	0.11	0	40	30	33
13	0.59	0.24	2.4	0.45	0.36	25	270	230	17	0.47	0.43	9	70	60	17
16	1.28	0.12	2.4	0.57	0.45	27	300	300	0	0.97	0.95	2	110	105	5
17	0.12	0.12	2.6	0.21	0.14	50	320	180	78	0.089	0.085	5	90	60	50
18	0.12	0.12	24.3	0.22	0.18	22	60	60	0	0.11	0.09	22	30	30	0
21	0.62	0.11	0.5	0.011	0.006	83	>360	>360	--	0.28	0.27	4	~330	~330	0
5127**	0.59	0.10	2.5	0.31	0.26	19	>360	>360	--	0.44	0.39	13	160	150	7
55	0.60	0.20	2.7	0.35	0.29	21	>360	>360	--	0.48	0.42	14	120	105	14
56	0.59	0.48	2.7	0.38	0.29	31	>360	>360	--	0.49	0.44	11	85	75	13
59	0.58	0.79	2.7	0.37	0.32	16	>360	>360	--	0.50	0.49	2	30	30	0
60	1.25	0.12	2.6	0.31	0.20	55	>360	>360	--	0.94	0.84	12	195	195	0
95	0.457	0.20	2.9	0.50	0.42	19	210	210	0	0.37	0.32	16	70	50	40
96	0.44	0.20	3.3	0.45	0.41	10	210	260	-19	0.34	0.30	13	60	60	0
121	0.51	0.20	2.8	0.51	0.49	4	260	260	0	0.41	0.34	21	70	50	40
177	0.46	0.20	3.0	0.54	0.54	0	320	340	6	0.36	0.31	16	80	75	7
216	0.52	0.20	2.8	0.58	0.55	5	360	360	3	0.39	0.37	5	80	70	14
217††	0.45	0.53	1.3	0.26	0.14	86	>720	>720	--	0.29	0.27	7	100	50	50
230	0.52	0.25	3.2	0.46	0.32	44	>360	>360	--	0.40	0.35	14	120	120	0

(continued)

TABLE 11 (Concluded)

Exp. no.	Initial [NO$_x$] (ppm)	Initial NO$_2$/NO$_x$ ratio	Initial HC/NO$_x$ ratio (ppmC/ppm)	Maximum [O$_3$] (ppm)*		Difference in O$_3$ maxima (percent)†	Time to maximum [O$_3$] (minutes)§		Difference in times to O$_3$ maxima (percent)†	Maximum [NO$_2$] (ppm)		Difference in NO$_2$ maxima (percent)†	Time to maximum [NO$_2$] (minutes)§		Difference in times to NO$_2$ maxima (percent)†
				Sim.	Meas.		Sim.	Meas.		Sim.	Meas.		Sim.	Meas.	
256	0.56	0.08	0.58	0.0096	0.002	380	>360	>360	--	0.21	0.20	5	>360	>360	--
257§§	0.56	0.06	1.3	0.054	0.054	0	>360	>360	--	0.33	0.30	10	150	150	0
276	0.52	0.20	3.0	0.46	0.33	39	>360	>360	--	0.39	0.36	8	130	125	4
277	0.11	0.09	15.7	0.29	0.30	-3	80	100	20	0.089	0.036	4	30	30	0
278	0.49	0.26	6.2	0.60	0.60	0	190	150	27	0.41	0.39	5	65	70	7
279	0.97	0.25	3.4	0.75	0.65	15	330	330	0	0.76	0.71	7	110	105	5

O$_3$ maxima: average difference = 25 percent (excluding EC-256); standard deviation = ±24 percent (excluding EC-256).

NO$_2$ maxima: average difference = 10 percent (excluding EC-256); standard deviation = ±6 percent (excluding EC-256).

* Maximum one-hour-average concentration.

† [(Simulated Value - Measured Value)/ Measured Value] x 100.

§ Time from beginning of irradiation to beginning of the period during which the maximum one-hour-average concentration occurred.

** Run based on averages of data from EC-51, EC-52, and EC-57.

†† Acetaldehyde/propylene experiment: initial acetaldehyde concentration = 0.165 ppm; initial propylene concentration = 0.085 ppm.

§§ Formaldehyde/propylene experiment: initial formaldehyde concentration = 0.371 ppm; initial propylene concentration = 0.112 ppm.

TABLE 12.   REACTIONS OF BUTANE*

Reaction	Rate constant $(ppm^{-1}min^{-1})$
$CH_3CH_2CH_2CH_3 + O \xrightarrow{O_2} CH_3CH_2CH(O_2^{\cdot})CH_3 + OH\cdot$	6.4×10^1
$CH_3CH_2CH_2CH_3 + OH\cdot \xrightarrow{O_2} CH_3CH_2CH_2CH_2O_2^{\cdot} + H_2O$	6.0×10^2
$CH_3CH_2CH_2CH_3 + OH\cdot \xrightarrow{O_2} CH_3CH_2CH(O_2^{\cdot})CH_3 + H_2O$	3.6×10^3
$HOCH_2CH_2CH_2C(O)O_2^{\cdot} + NO \xrightarrow{O_2} NO_2 + HOCH_2CH_2CH_2O_2^{\cdot} + CO_2$	3.8×10^3
$HOCH_2CH_2C(O)O_2^{\cdot} + NO \xrightarrow{O_2} NO_2 + HOCH_2CH_2O_2^{\cdot} + CO_2$	3.8×10^3
$CH_3CH_2CH_2C(O)O_2^{\cdot} + NO \xrightarrow{O_2} CH_3CH_2CH_2O_2^{\cdot} + NO_2 + CO_2$	3.8×10^3
$CH_3CH_2C(O)O_2^{\cdot} + NO \xrightarrow{O_2} CH_3CH_2O_2^{\cdot} + NO_2 + CO_2$	3.8×10^3
$HOCH_2CH_2CH_2CH_2O_2^{\cdot} + NO \xrightarrow{O_2} NO_2 + HO_2^{\cdot} + HOCH_2CH_2CH_2CHO$	1.2×10^4
$CH_3CH(O_2^{\cdot})C(O)CH_3 + NO \xrightarrow{O_2} NO_2 + HO_2^{\cdot} + CH_3C(O)C(O)CH_3$	$.1.2 \times 10^4$
$CH_3CH_2CH(O_2^{\cdot})CH_3 + NO \rightarrow NO_2 + CH_3CH_2CH(O\cdot)CH_3$	1.1×10^4
$CH_3CH_2CH(O_2^{\cdot})CH_3 + NO \rightarrow CH_3CH_2CH(ONO_2)CH_3$	1×10^3
$CH_3CH_2CH_2CH_2O_2^{\cdot} + NO \rightarrow NO_2 + CH_3CH_2CH_2CH_2O\cdot$	1.1×10^4
$CH_3CH_2CH_2CH_2O_2^{\cdot} + NO \rightarrow CH_3CH_2CH_2CH_2ONO_2^{\cdot}$	1×10^3
$HOCH_2CH_2CH_2O_2^{\cdot} + NO \xrightarrow{O_2} NO_2 + HO_2^{\cdot} + HOCH_2CH_2CHO$	1.2×10^4
$HOCH_2CH_2O_2^{\cdot} + NO \xrightarrow{O_2} NO_2 + HO_2^{\cdot} + HOCH_2CHO$	1.2×10^4
$CH_3CH_2CH_2O_2^{\cdot} + NO \rightarrow NO_2 + CH_3CH_2CH_2O\cdot$	1.2×10^4
$CH_3CH_2CH_2O_2^{\cdot} + NO \rightarrow CH_3CH_2CH_2ONO_2$	1×10^2
$CH_3CH_2O_2^{\cdot} + NO \rightarrow NO_2 + CH_3CH_2O\cdot$	1.2×10^4
$CH_3CH_2O_2^{\cdot} + NO \rightarrow CH_3CH_2ONO_2$	1×10^2

(continued)

103

TABLE 12 (Continued)

Reaction	Rate constant $(ppm^{-1}min^{-1})$
$CH_3CH_2CH(O\cdot)CH_3 \xrightarrow{O_2} CH_3CH_2O_2^{\cdot} + CH_3CHO$	$1 \times 10^{5\dagger}$
$CH_3CH_2CH_2CH_2O\cdot \xrightarrow{O_2} HOCH_2CH_2CH_2CH_2O_2^{\cdot}$	$2 \times 10^{6\dagger}$
$CH_3CH_2CH(O\cdot)CH_3 + O_2 \rightarrow CH_3CH_2C(O)CH_3 + HO_2^{\cdot}$	1.43
$CH_3CH_2CH_2CH_2O\cdot + O_2 \rightarrow CH_3CH_2CH_2CHO + HO_2^{\cdot}$	3.3
$CH_3CH_2CH_2O\cdot + O_2 \rightarrow CH_3CH_2CHO + HO_2^{\cdot}$	3.3
$CH_3CH_2O\cdot + O_2 \rightarrow CH_3CHO + HO_2^{\cdot}$	3.3
$CH_3CH_2CHO + h\nu \xrightarrow{2O_2} CH_3CH_2O_2^{\cdot} + HO_2^{\cdot} + CO$	Experimental†
$CH_3CH_2CH_2CHO + h\nu \xrightarrow{2O_2} CH_3CH_2CH_2O_2^{\cdot} + HO_2^{\cdot} + CO$	Experimental†
$CH_3CH_2CH_2CHO + h\nu \rightarrow CH_3CHO + C_2H_4$	Experimental†
$CH_3CH_2C(O)CH_3 + h\nu \xrightarrow{2O_2} CH_3C(O)O_2^{\cdot} + CH_3CH_2O_2^{\cdot}$	Experimental†
$HOCH_2CHO + h\nu \xrightarrow{2O_2} HCHO + 2HO_2^{\cdot} + CO$	$1 \times 10^{-3\dagger}$
$HOCH_2CH_2CHO + h\nu \xrightarrow{2O_2} HOCH_2CH_2O_2^{\cdot} + HO_2^{\cdot} + CO$	$1 \times 10^{-3\dagger}$
$HOCH_2CH_2CH_2CHO + h\nu \xrightarrow{2O_2} HOCH_2CH_2CH_2O_2^{\cdot} + HO_2^{\cdot} + CO$	Experimental†
$CH_3C(O)C(O)CH_3 + h\nu \xrightarrow{2O_2} 2CH_3C(O)O_2^{\cdot}$	2×10^{-3}
$CH_3CH_2CHO + OH\cdot \xrightarrow{O_2} CH_3CH_2C(O)O_2^{\cdot} + H_2O$	2.4×10^4
$CH_3CH_2CH_2CHO + OH\cdot \xrightarrow{O_2} CH_3CH_2CH_2C(O)O_2^{\cdot} + H_2O$	2.4×10^4
$CH_3CH_2C(O)CH_3 + OH\cdot \xrightarrow{O_2} CH_3CH(O_2^{\cdot})C(O)CH_3 + H_2O$	4.9×10^3
$HOCH_2CH_2CH_2CHO + OH\cdot \xrightarrow{O_2} HOCH_2CH_2CH_2C(O)O_2^{\cdot} + H_2O$	2.2×10^4
$HOCH_2CH_2CHO + OH\cdot \xrightarrow{O_2} HOCH_2CH_2C(O)O_2^{\cdot} + H_2O$	2.2×10^4

TABLE 12 (Concluded)

Reaction	Rate constant $(ppm^{-1}min^{-1})$
$HOCH_2CHO + OH\cdot \xrightarrow{O_2} HCHO + HO_2^- + CO + H_2O$	2.2×10^4
$HOCH_2CH_2CH_2C(O)O_2^- + HO_2^- \rightarrow HOCH_2CH_2CH_2C(O)O_2H + O_2$	4×10^3
$HOCH_2CH_2C(O)O_2^- + HO_2^- \rightarrow HOCH_2CH_2C(O)O_2H + O_2$	4×10^3
$CH_3CH_2CH_2C(O)O_2^- + HO_2^- \rightarrow CH_3CH_2CH_2C(O)O_2H + O_2$	4×10^3
$CH_3CH_2C(O)O_2^- + HO_2^- \rightarrow CH_3CH_2C(O)O_2H + O_2$	4×10^3
$HOCH_2CH_2CH_2CH_2O_2^- + HO_2^- \rightarrow HOCH_2CH_2CH_2CH_2O_2H + O_2$	4×10^3
$CH_3CH(O_2^-)C(O)CH_3 + HO_2^- \rightarrow CH_3CH(O_2H)C(O)CH_3 + O_2$	4×10^3
$CH_3CH_2CH(O_2^-)CH_3 + HO_2^- \rightarrow CH_3CH_2CH(CH_3)O_2H + O_2$	4×10^3
$CH_3CH_2CH_2CH_2O_2^- + HO_2^- \rightarrow CH_3CH_2CH_2CH_2O_2H + O_2$	4×10^3
$CH_3CH_2CH_2O_2^- + HO_2^- \rightarrow CH_3CH_2CH_2O_2H + O_2$	4×10^3
$CH_3CH_2O_2^- + HO_2^- \rightarrow CH_3CH_2O_2H + O_2$	4×10^3
$CH_3CH_2CH_2C(O)O_2^- + NO_2 \rightarrow CH_3CH_2CH_2C(O)O_2NO_2$	2×10^3
$CH_3CH_2C(O)O_2^- + NO_2 \rightarrow CH_3CH_2C(O)O_2NO_2$	2×10^3
$CH_3CH_2C(O)O_2NO_2 \rightarrow NO_2 + CH_3CH_2C(O)O_2^-$	2.8×10^{-2}[†]
$CH_3CH_2CH_2C(O)O_2NO_2 \rightarrow NO_2 + CH_3CH_2CH_2C(O)O_2^-$	2.8×10^{-2}[†§]
$CH_3CH_2O\cdot + NO_2 \rightarrow CH_3CH_2ONO_2$	1.5×10^4
$CH_3CH_2O\cdot + NO_2 \rightarrow CH_3CHO + HONO$	2.9×10^3
$CH_3CH_2CH_2O\cdot + NO_2 \rightarrow CH_3CH_2CH_2ONO_2$	1.5×10^4
$CH_3CH_2CH_2O\cdot + NO_2 \rightarrow CH_3CH_2CHO + HONO$	2.9×10^3
$CH_3CH_2CH_2CH_2O\cdot + NO_2 \rightarrow CH_3CH_2CH_2CH_2ONO_2$	1.5×10^4
$CH_3CH_2CH_2CH_2O\cdot + NO_2 \rightarrow CH_3CH_2CH_2CHO + HONO$	2.9×10^3
$CH_3CH_2CH(O\cdot)CH_3 + NO_2 \rightarrow CH_3CH_2CH(ONO_2)CH_3$	1.5×10^4
$CH_3CH_2CH(O\cdot)CH_3 + NO_2 \rightarrow CH_3CH_2C(O)CH_3 + HONO$	2.9×10^3

* The inorganic, formaldehyde, and acetaldehyde reactions listed earlier must be added to construct the explicit butane mechanism.
† Rate constant in min^{-1}.
§ Activation energy is 12,500K; rate constant is given at 298K.
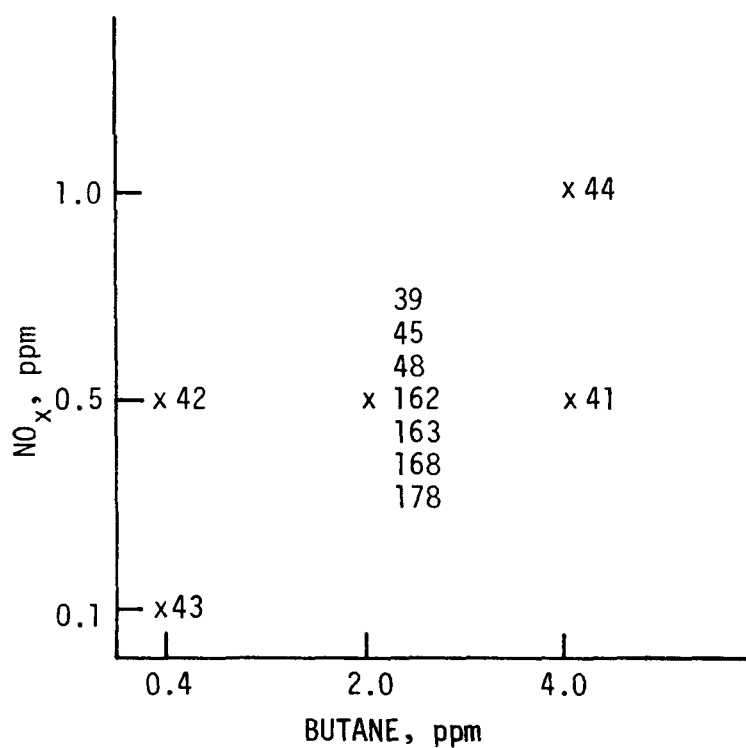
Figure **33.** Factorial block of initial concentrations in UCR butane/NO_x experiments. Numbers correspond to UCR run numbers.

TABLE 13. INITIAL CONDITIONS AND PHOTOLYSIS RATE CONSTANTS FOR THE BUTANE/NOx SMOG CHAMBER EXPERIMENTS

Run number	Initial concentration (ppm)				Photolysis rate constant ($\times 10^4$ min^{-1})					
	Butane	NO	NO$_2$	HONO	NO$_2 \rightarrow$NO+O*	O$_3 \rightarrow$O(^{1}D)	O$_3 \rightarrow$O(^{3}P)	HONO$\rightarrow$NO+OH·	H$_2$O$_2 \rightarrow$2OH·	FORM$\rightarrow$Products†
EC-39	2.2	0.547	0.06	0.016	0.24	10	82	700	4.4	12
EC-41	3.93	0.524	0.0684	0.017	0.24	1	82	700	4.4	12
EC-42	0.392	0.5424	0.0588	0.04	0.235	10	82	700	4.4	12
EC-43	0.38	0.126	0.013	0.01	0.233	10	82	700	4.4	12
EC-44	3.9	1.14	0.132	0.04	0.23	10	82	700	4.4	12
EC-45	1.94	0.55	0.062	0.007	0.227	14	81	700	4.0	10
EC-48	1.97	0.535	0.059	0.009	0.227	14	81	700	4.0	10
EC-162	1.99	0.383	0.122	0.018	0.35	20	113	650	4.5	12
EC-163	1.978	0.377	0.113	0.01	0.34	3	113	650	4.5	8
EC-168	1.95	0.327	0.166	0.033	0.33	12	105	620	4.0	11
EC-178	1.961	0.087	0.011	0.006	0.33	10	105	608	5.0	12

* Rate constant in min^{-1}.

† The relationship between FORM→Products and carbonyl photolysis rate constants is discussed in Section 4.

TABLE 14. UCR BUTANE EXPERIMENTS--SIMULATIONS AND MEASUREMENTS

Exp. no.	Initial [NOx] (ppm)	Initial NO2/NOx ratio	Initial HC/NOx ratio (ppmC/ppm)	Maximum [O3] (ppm)*		Difference in O3 maxima (percent)[†]	Time to maximum [O3] (minutes)[§]		Difference in times to O3 maxima (percent)[†]	Maximum [NO2] (ppm)		Difference in NO2 maxima (percent)[†]	Time to maximum [NO2] (minutes)[§]		Difference in times to NO2 maxima (percent)[†]
				Sim.	Meas.		Sim.	Meas.		Sim.	Meas.		Sim.	Meas.	
EC-39	0.61	0.10	14.5	0.05	0.055	-9	>360	>360	--	0.39	0.34	15	~330	250	32
EC-41	0.59	0.12	26.5	0.22	0.21	5	>360	>360	--	0.41	0.39	5	220	150	47
EC-42	0.60	0.10	2.6	0.005	0.004	25	>360	>360	--	0.17	0.21	-19	>360	>360	--
EC-43	0.14	0.09	10.9	0.07	0.11	-36	>360	>360	--	0.09	0.08	13	220	120	83
EC-44	1.30	0.10	12.3	0.03	0.011	173	>360	>360	--	0.75	0.67	12	~330	~330	0
EC-45**	0.61	0.10	13.0	0.13	0.12	8	>360	>360	--	0.40	0.38	5	260	200	30
EC-48††	0.59	0.10	14.0	0.19	0.15	27	>360	>360	--	0.41	0.36	14	220	150	47
EC-162	0.51	0.24	15.8	0.11	0.097	13	>360	>360	--	0.34	0.26	31	270	250	8
EC-163§§	0.49	0.23	17.6	0.36	0.37	3	>360	>360	--	0.36	0.28	29	120	70	71
EC-168△	0.49	0.34	15.8	0.66	0.66	0	630	630	0	0.36	0.30	20	80	50	60
EC-178	0.10	0.11	80.0	0.35	0.38	-8	320	360	-11	0.075	0.063	19	60	40	50

O_3 maxima: average difference = 3 percent; standard deviation = ±18 percent.
NO_2 maxima: average difference = 13 percent; standard deviation = ±14 percent.

* Maximum one-hour-average concentration.

† [(Simulated Value - Measured Value) / Measured Value] x 100.

§ Time from beginning of irradiation to beginning of the period during which the maximum one-hour-average concentration occurred.

** Formaldehyde/butane experiment: initial formaldehyde concentration = 0.14 ppm; initial butane concentration = 1.94 ppm.

†† Acetaldehyde/butane experiment: initial acetaldehyde concentration = 0.20 ppm; initial butane concentration = 1.97 ppm.

§§ Acetaldehyde/butane experiment: initial acetaldehyde concentration = 0.42 ppm; initial butane concentration = 1.95 ppm.

△ Formaldehyde/butane experiment: initial formaldehyde concentration = 0.101 ppm; initial butane concentration = 1.92 ppm.
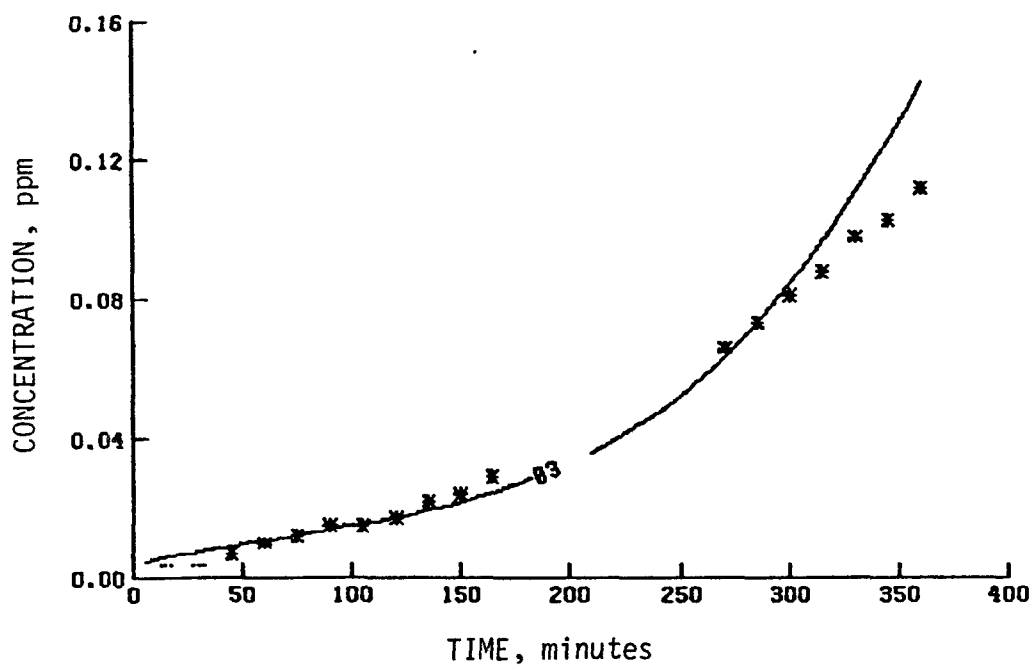
(a) O_3
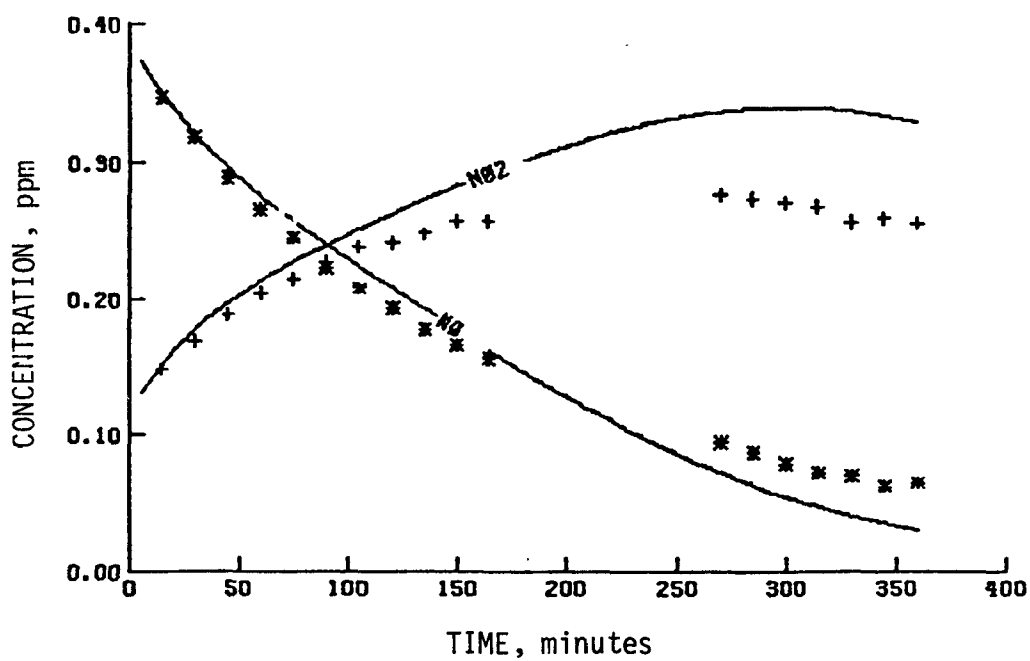
(b) NO and NO_2

Figure 34. Simulation results of a UCR butane experiment (EC-162)

109
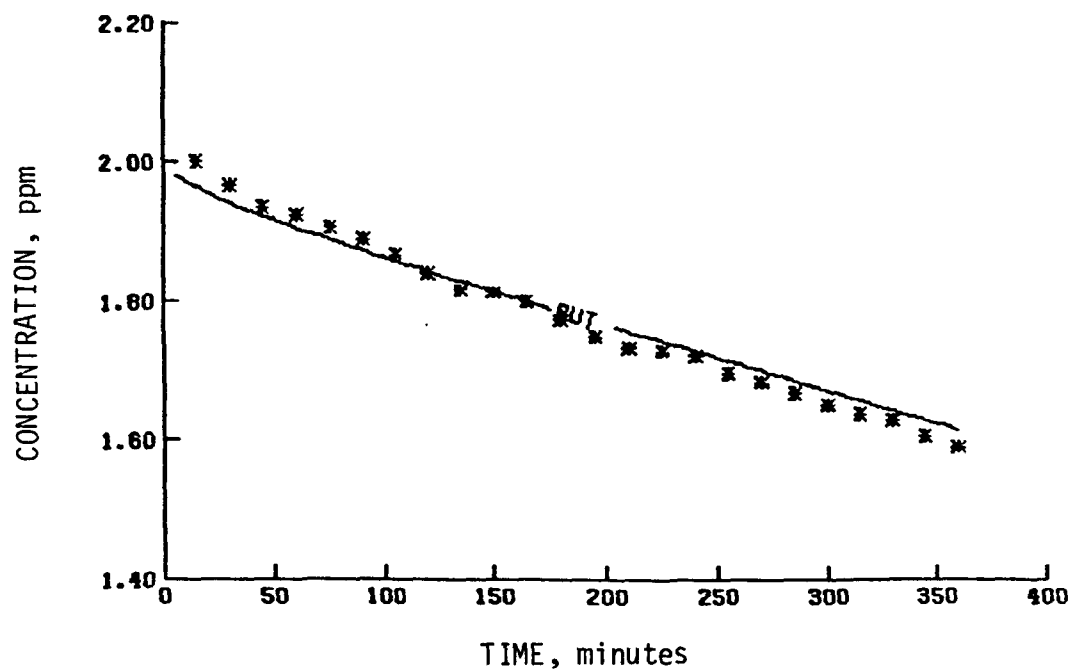
(c) Butane
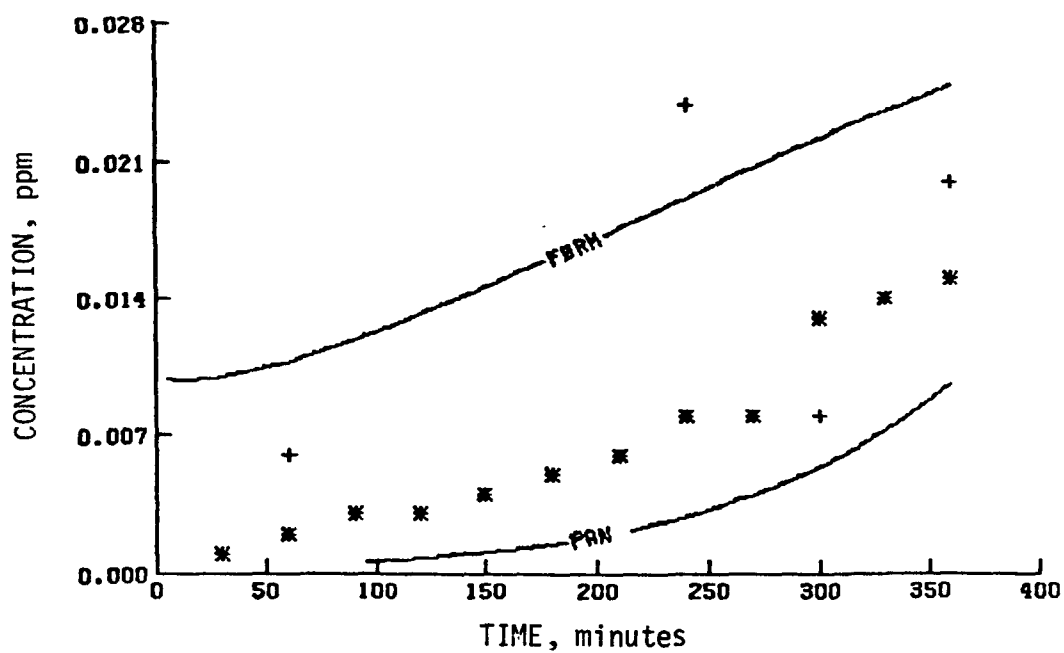
(d) Formaldehyde and PAN

Figure 34 (Continued)
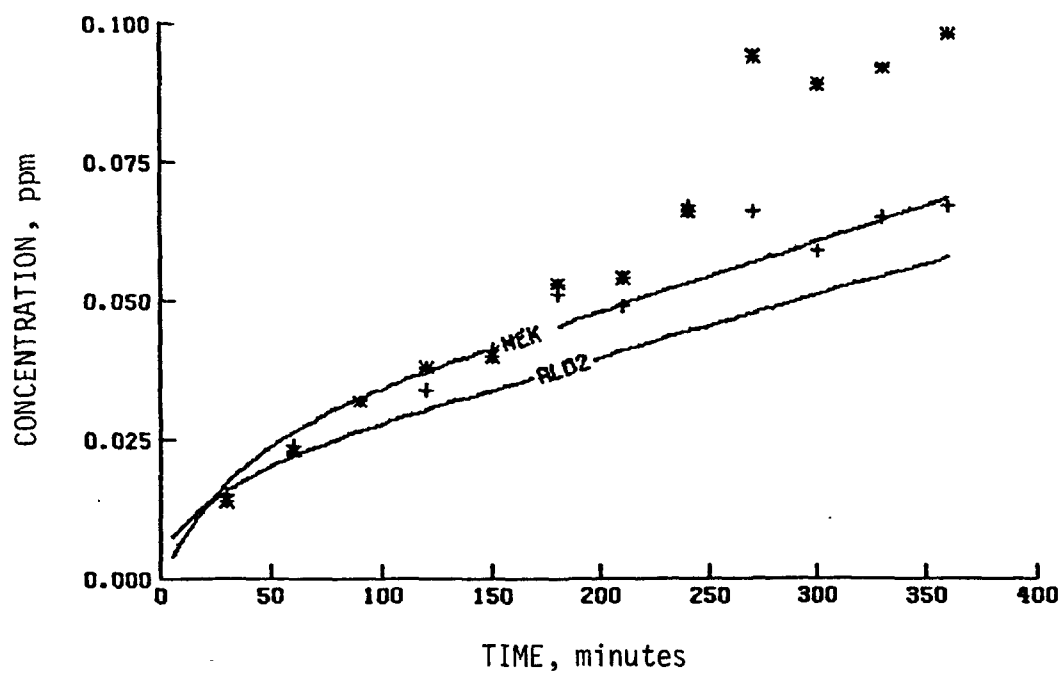
(e) MEK and acetaldehyde
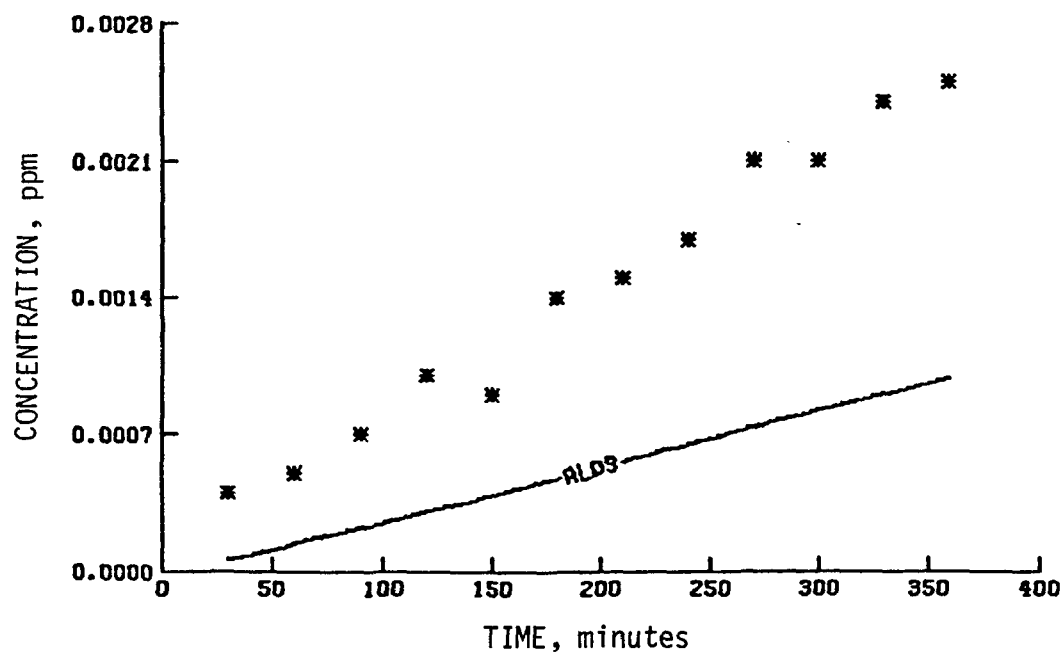
(f) Propionaldehyde

Figure 34 (Continued)

111
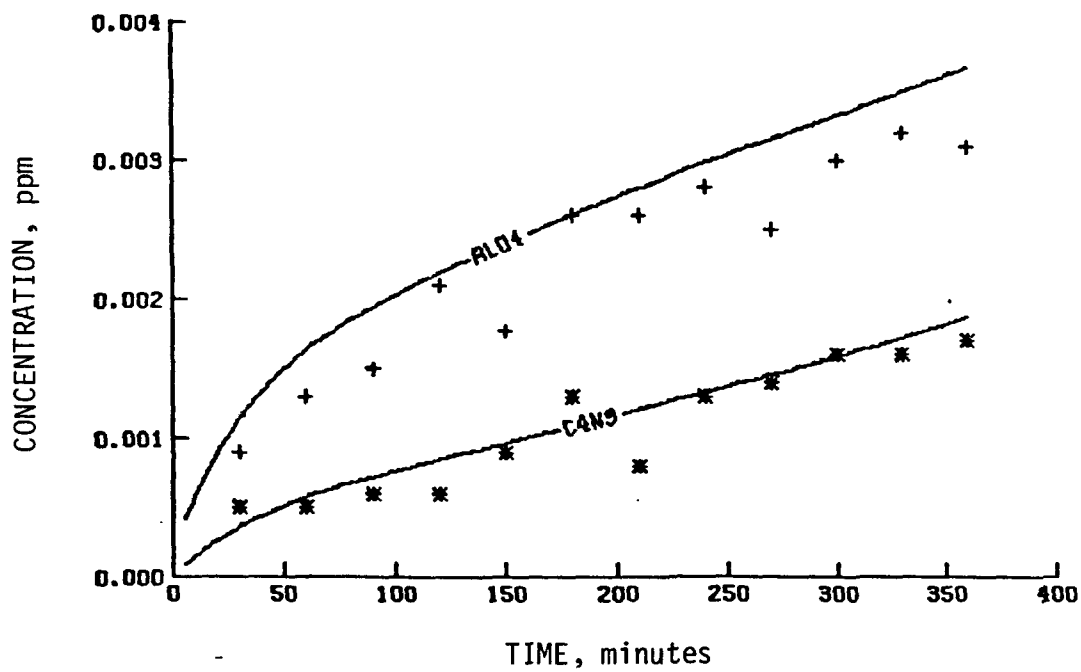
(g) Butyraldehyde and n-butyl nitrate
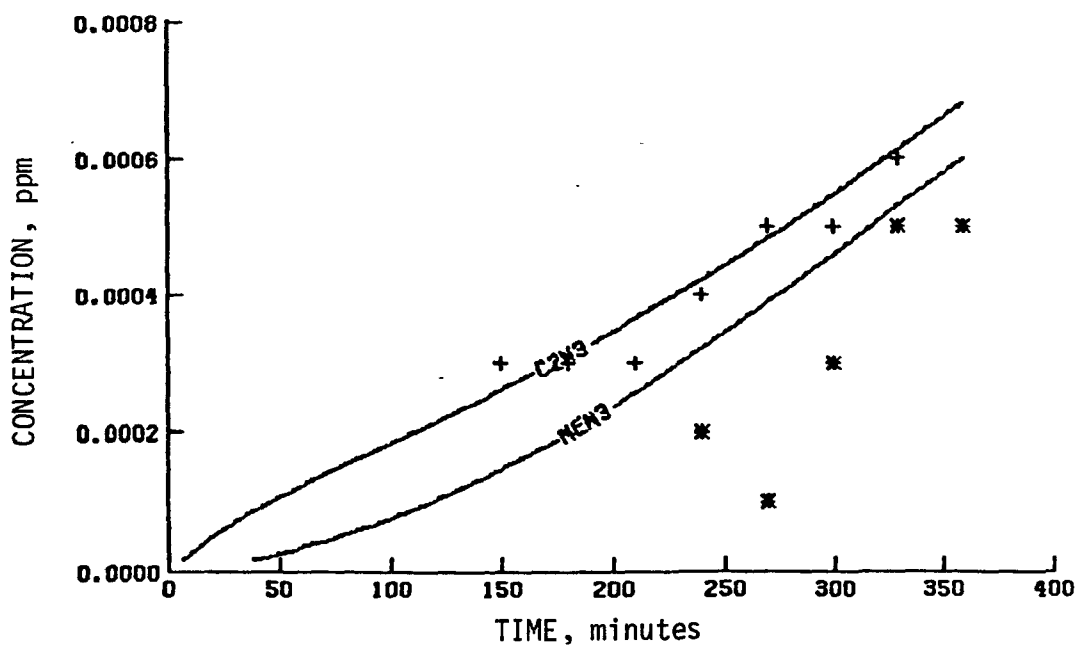
(h) Ethyl nitrate and methyl nitrate

Figure 34 (Continued)
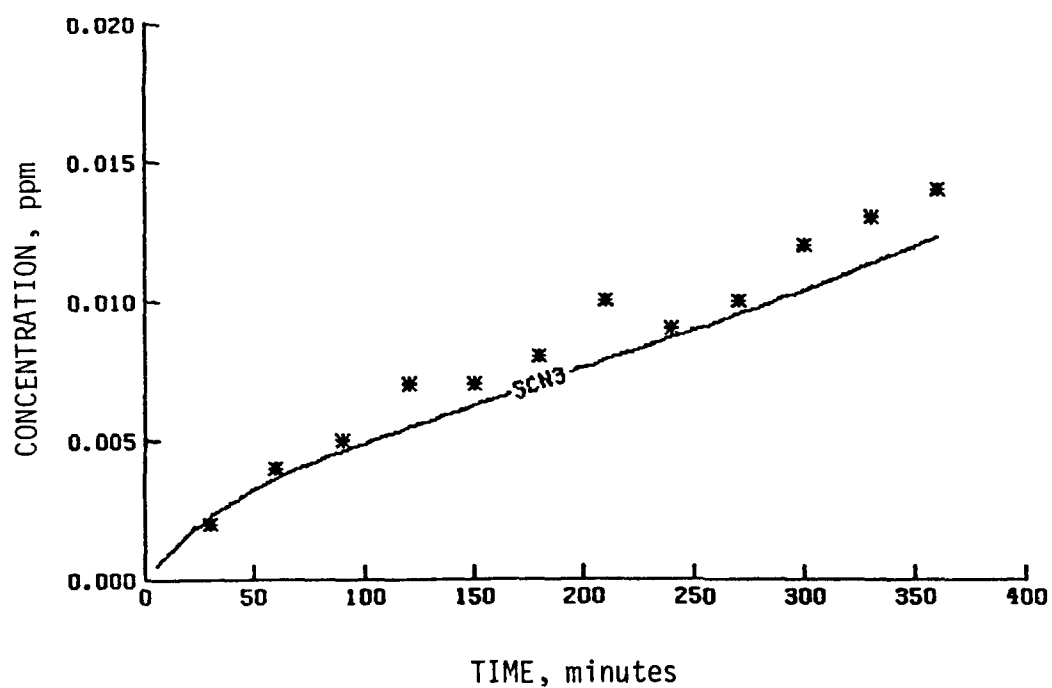
(i) Sec-butyl nitrate

Figure 34   (Concluded)

(a) O_3
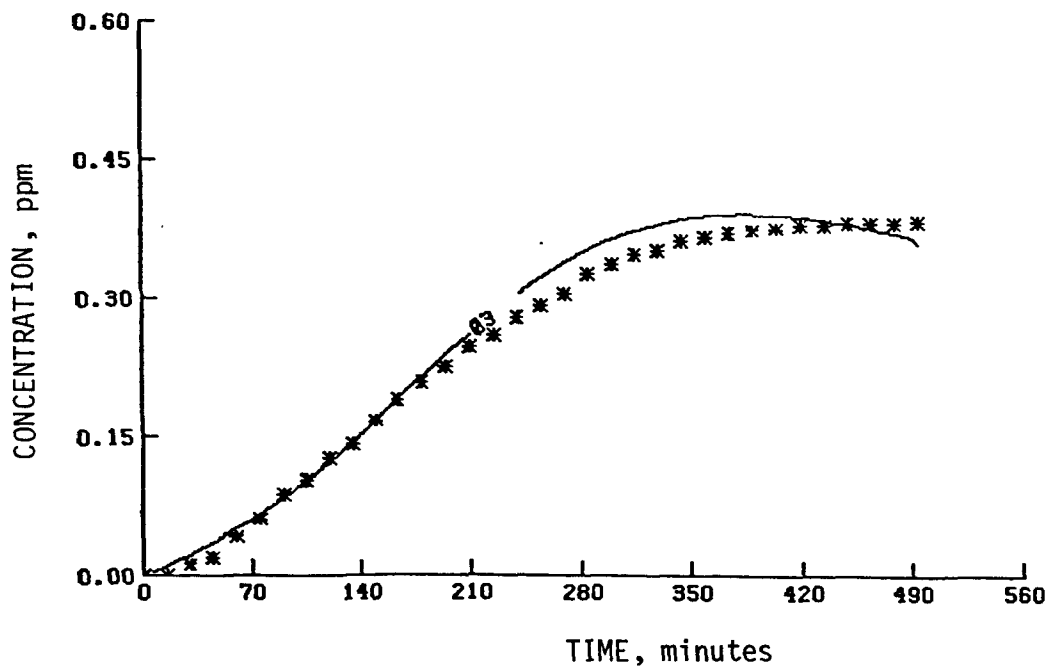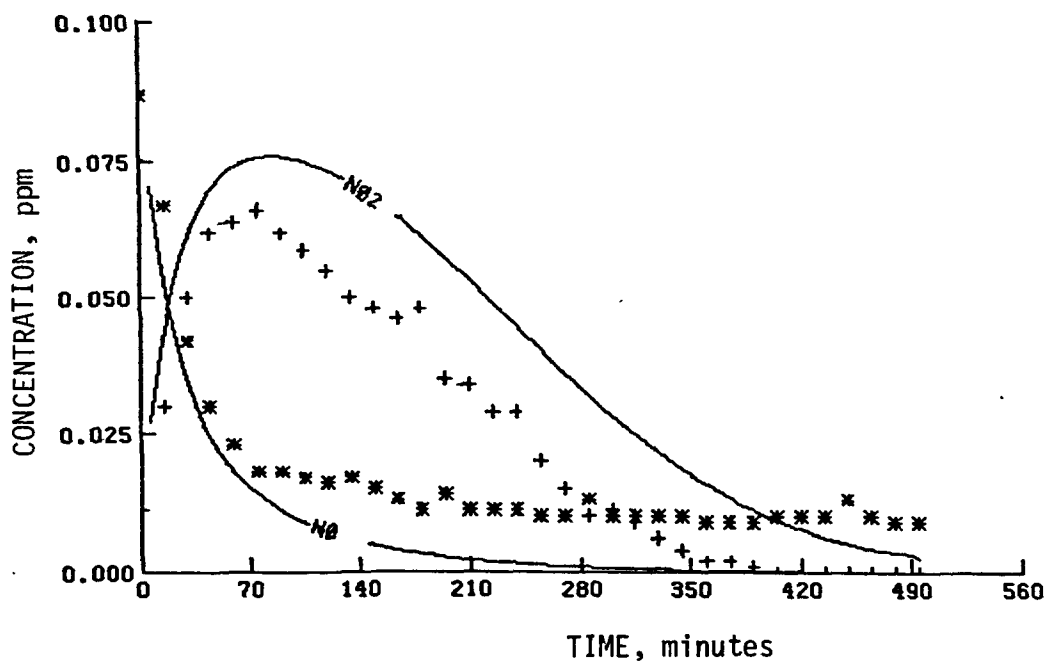
(b) NO_2 and NO

Figure 35. Simulation results of a UCR butane experiment (EC-178)

114
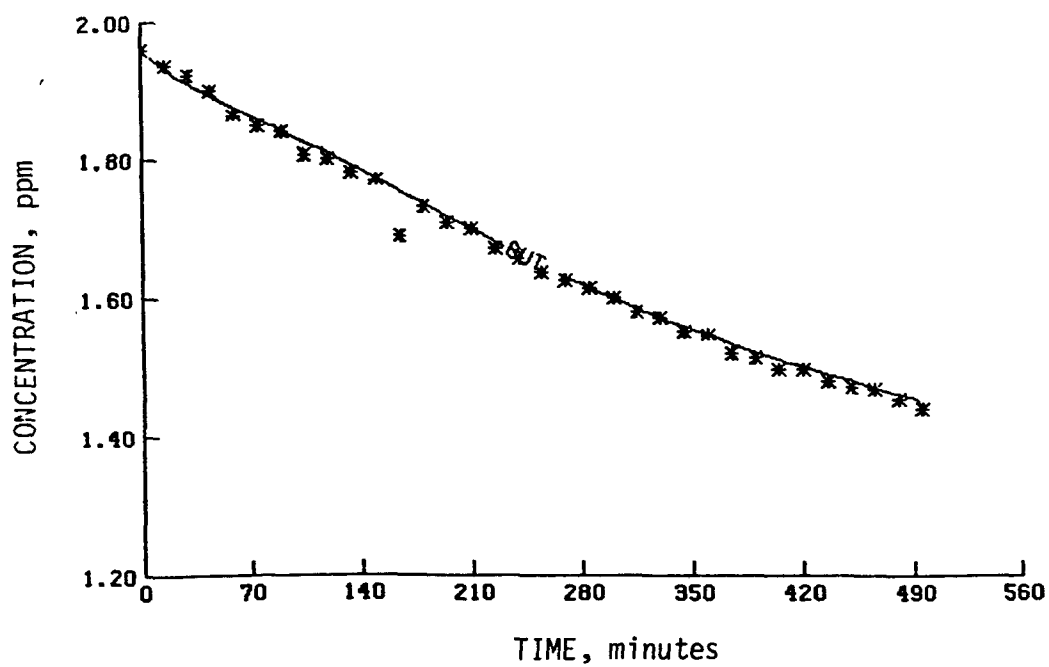
(c) Butane
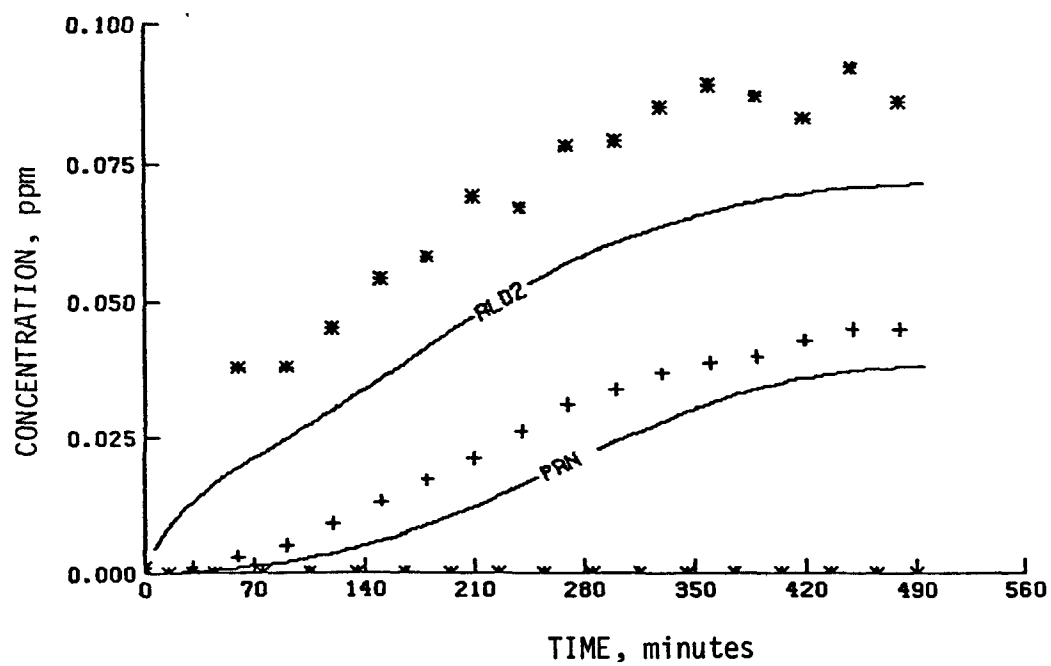
(d) Acetaldehyde and PAN

Figure 35 (Continued)
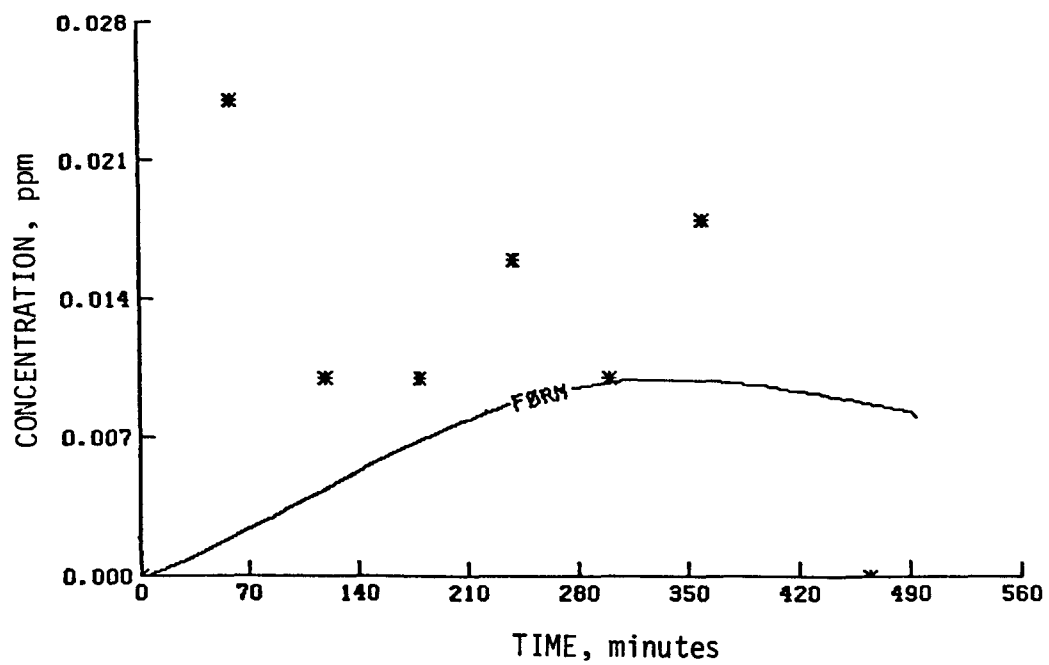
(e) Formaldehyde
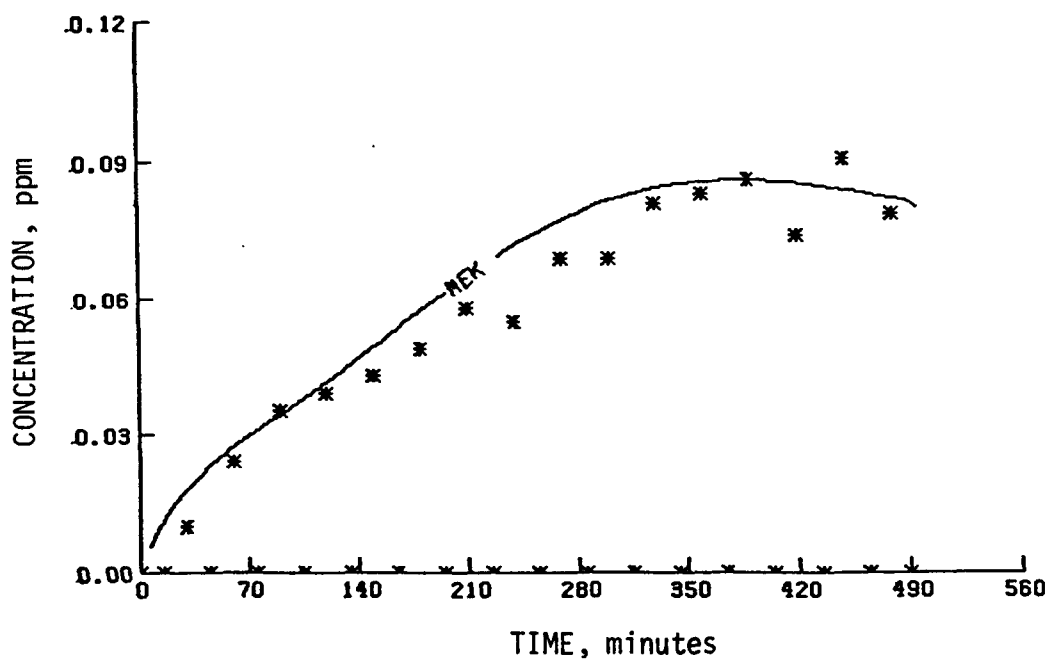
(f) MEK

Figure 35 (Continued)

116
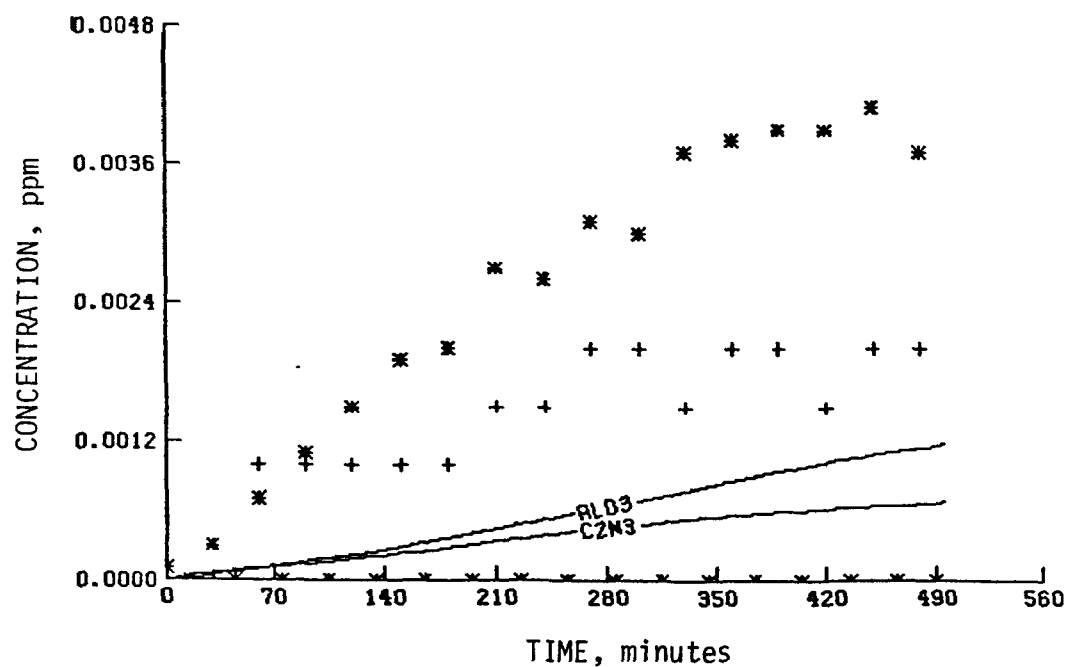
(g) Ethyl nitrate and propionaldehyde
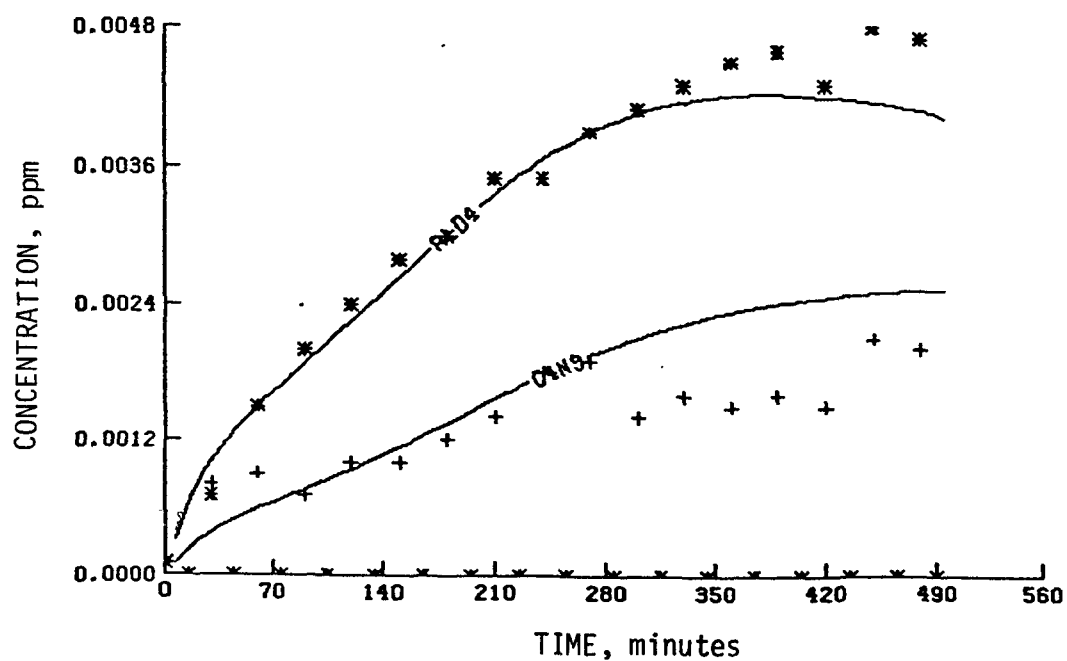
(h) N-butyl nitrate and butyraldehyde

Figure 35 (Continued)

117
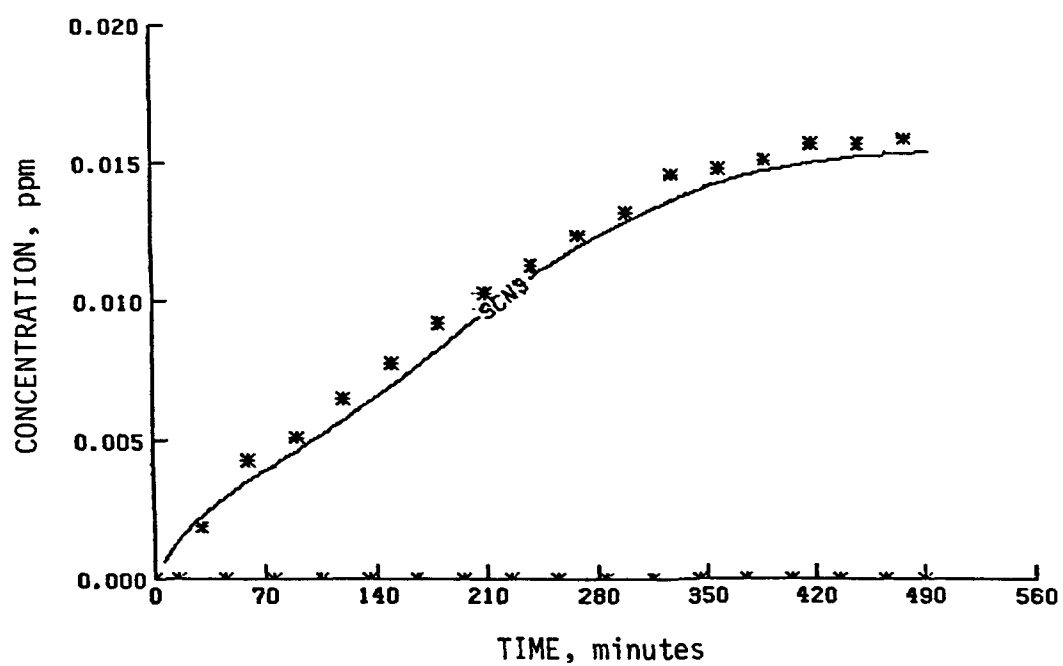
(i)   Sec-butyl nitrate

Figure 35   (Concluded)

118

> The main source of formaldehyde is the reaction of the peroxyacetyl radical with NO.

> The simulations are very sensitive to the assumed initial value of HONO.

1-BUTENE

A mechanism was constructed for this olefin based on the present propylene mechanism. All of the rate constants used are identical to the corresponding rate constants in the propylene system except the one for the hydroxyl radical reaction with 1-butene. For this reaction, a rather wide range of both absolute and relative values have been reported. Pastrana and Carr (1975) and Morris and Niki (1971b) reported rates that are two to three times as high as the propylene + OH· rate constant, whereas Davis (1976) reported values for 1-butene and propylene in the ratio of only 1.1. We used a ratio of about 1.7 based on simulations using the four olefins ethylene, propylene, 1-butene, and trans-2-butene. The absolute value used was 7×10^4 ppm^{-1}min^{-1}, which produced the best overall olefin decay for 1-butene in the presence of the other three.

The explicit 1-butene mechanism is given in Table 15. The initial conditions used in the three UCR experiments using only 1-butene/NO$_x$ ratio are presented in Table 16. The NO$_2$ and O$_3$ results are summarized in Table 17, and a sample simulation for EC-123 is shown in Figure 36. As is the case with PAN in other systems, the peroxypropionyl nitrate (PPN) results could be brought closer to the observed values by using a lower ratio of reactions rate constants for the competition for peroxy radicals NO and NO$_2$. Unfortunately, all of the UCR experiments did not reach a definite ozone maximum, and so our present verification of the 1-butene mechanism is not complete.

TRANS-2-BUTENE

As mentioned earlier, trans-2-butene is the fastest reacting olefin used thus far as a reactant in a UCR smog chamber. We constructed an explicit mechanism for trans-2-butene based on the propylene mechanism. Various reactions in the explicit trans-2-butene mechanism are discussed below.

TABLE 15. REACTIONS OF 1-BUTENE*

Reaction	Rate constant $(ppm^{-1}min^{-1})$
$CH_3CH_2CH=CH_2 + O \xrightarrow{2O_2} CH_2O_2^* + CH_3CH_2C(O)O_2^*$	2.7×10^3
$CH_3CH_2CH=CH_2 + O \rightarrow CH_3CH_2\overset{O}{\overbrace{CH-\!\!-\!\!CH_2}}$	2.7×10^3
$CH_3CH_2\overset{O}{\overbrace{CH-\!\!-\!\!CH_2}} \rightarrow CH_3CH_2CH_2CHO$	5×10^{-2}
$CH_3CH_2CH=CH_2 + OH\cdot \xrightarrow{O_2} CH_3CH_2CH(O_2^*)CH_2OH$	7×10^4
$CH_3CH_2CH=CH_2 + NO_3 \rightarrow NO_2 + \text{Stable Products}$	1.2×10^1
$CH_3CH_2CH=CH_2 + O_3 \rightarrow HCHO + CH_3CH_2CHO_2^*$	7.5×10^{-3}
$CH_3CH_2CH=CH_2 + O_3 \rightarrow CH_3CH_2CHO + CH_2O_2^*$	7.5×10^{-3}
$CH_2O_2^* + HCHO \rightarrow H_2C\overset{O-O}{\underset{O}{\diamond}}CH_2$	2×10^3
$CH_2O_2^* + CH_3CHO \rightarrow H_2C\overset{O-O}{\underset{O}{\diamond}}CHCH_3$	2×10^3
$CH_2O_2^* + NO \rightarrow NO_2 + HCHO$	1.2×10^4
$CH_2O_2^* + NO_2 \rightarrow NO_3 + HCHO$	8×10^3
$CH_2O_2^* \rightarrow CO + H_2 + O_2$	$6.7 \times 10^{2\dagger}$
$CH_2O_2^* \rightarrow CO_2 + H_2$	$1.8 \times 10^{2\dagger}$
$CH_2O_2^* \rightarrow 2HO_2^* + CO_2$	$9 \times 10^{1\dagger}$
$CH_2O_2^* \rightarrow HC(O)OH$	$6 \times 10^{1\dagger}$
$CH_3CH_2CHO_2^* + HCHO \rightarrow CH_3CH_2CH\overset{O-O}{\underset{O}{\diamond}}CH_2$	2×10^3
$CH_3CH_2CHO_2^* + CH_3CHO \rightarrow CH_3CH_2CH\overset{O-O}{\underset{O}{\diamond}}CHCH_3$	2×10^3
$CH_3CH_2CHO_2^* + NO \rightarrow NO_2 + CH_3CH_2CHO$	1.2×10^4
$CH_3CH_2CHO_2^* + NO_2 \rightarrow NO_3 + CH_3CH_2CHO$	8×10^3

(continued)

120

TABLE 15 (Continued)

Reaction	Rate constant $(ppm^{-1}min^{-1})$
$CH_3CH_2CHO_2^. \rightarrow CO_2 + CH_3CH_3$	$1.5 \times 10^{2+}$
$CH_3CH_2CHO_2^. \xrightarrow{O_2} CH_3CH_2O_2^. + CO + OH \cdot$	$3.4 \times 10^{2+}$
$CH_3CH_2CHO_2^. \xrightarrow{2O_2} CH_3CH_2O_2^. + CO_2 + HO_2^.$	$4.25 \times 10^{2+}$
$CH_3CH_2CHO_2^. \xrightarrow{O_2} CH_3CH_2O \cdot + CO + HO_2^.$	$8.5 \times 10^{1+}$
$CH_3CH_2CH_2C(O)O_2^. + NO \xrightarrow{O_2} CH_3CH_2CH_2O_2^. + NO_2 + CO_2$	3.8×10^3
$CH_3CH_2C(O)O_2^. + NO \xrightarrow{O_2} CH_3CH_2O_2^. + NO_2 + CO_2$	3.8×10^3
$CH_3CH_2CH(O_2^.)CH_2OH + NO \rightarrow CH_3CH_2CH(O \cdot)CH_2OH + NO_2$	1.2×10^4
$CH_3CH_2CH_2O_2^. + NO \rightarrow CH_3CH_2CH_2O \cdot + NO_2$	1.2×10^4
$CH_3CH_2CH_2O_2^. + NO \rightarrow CH_3CH_2CH_2ONO_2$	1×10^2
$CH_3CH_2O_2^. + NO \rightarrow CH_3CH_2O \cdot + NO_2$	1.2×10^4
$CH_3CH_2O_2^. + NO \rightarrow CH_3CH_2ONO_2$	1×10^2
$CH_3CH_2CH(O \cdot)CH_2OH \xrightarrow{O_2} CH_3CH_2CHO + HCHO + HO_2^.$	$3 \times 10^{5+}$
$CH_3CH_2CH_2O_2^. + O_2 \rightarrow CH_3CH_2CHO + HO_2^.$	3.3
$CH_3CH_2O_2^. + O_2 \rightarrow CH_3CHO + HO_2^.$	3.3
$CH_3CH_2CHO + h\nu \xrightarrow{2O_2} CH_3CH_2O_2^. + HO_2^. + CO$	$Experimental^+$
$CH_3CH_2CH_2CHO + h\nu \xrightarrow{2O_2} CH_3CH_2CH_2O_2^. + HO_2^. + CO$	$Experimental^+$
$CH_3CH_2CHO + OH \cdot \xrightarrow{O_2} CH_3CH_2C(O)O_2^. + H_2O$	2.4×10^4
$CH_3CH_2CH_2CHO + OH \cdot \xrightarrow{O_2} CH_3CH_2CH_2C(O)O_2^. + H_2O$	2.4×10^4
$CH_3CH_2CH_2C(O)O_2^. + HO_2^. \rightarrow CH_3CH_2CH C(O)OOH + O_2$	4×10^3
$CH_3CH_2C(O)O_2^. + HO_2^. \rightarrow CH_3CH_2C(O)OOH + O_2$	4×10^3
$CH_3CH_2CH_2O_2^. + HO_2^. \rightarrow CH_3CH_2CH_2OOH + O_2$	4×10^3

(continued)

TABLE 15 (Concluded)

Reaction	Rate constant $(ppm^{-1}min^{-1})$
$CH_3CH_2O_2^{\cdot} + HO_2^{\cdot} \rightarrow CH_3CH_2OOH + O_2$	4×10^3
$CH_3CH_2CH_2C(O)O_2^{\cdot} + NO_2 \rightarrow CH_3CH_2CH_2C(O)O_2NO_2$	2×10^3
$CH_3CH_2C(O)O_2^{\cdot} + NO_2 \rightarrow CH_3CH_2C(O)O_2NO_2$	2×10^3
$CH_3CH_2C(O)O_2NO_2 \rightarrow CH_3CH_2C(O)O_2^{\cdot} + NO_2$	$2.8 \times 10^{-2 \dagger\S}$
$CH_3CH_2CH_2C(O)O_2NO_2 \rightarrow CH_3CH_2CH_2C(O)O_2^{\cdot} + NO_2$	$2.8 \times 10^{-2 \dagger\S}$
$CH_3CH_2CH(O_2^{\cdot})CH_2OH + O_3 \rightarrow CH_3CH_2CH(O\cdot)CH_2OH + 2O_2$	2×10^2
$CH_3CH_2O\cdot + NO_2 \rightarrow CH_3CH_2ONO_2$	1.5×10^4
$CH_3CH_2O\cdot + NO_2 \rightarrow CH_3CHO + HONO$	2.9×10^3
$CH_3CH_2CH_2O\cdot + NO_2 \rightarrow CH_3CH_2CH_2ONO_2$	1.5×10^4
$CH_3CH_2CH_2O\cdot + NO_2 \rightarrow CH_3CH_2CHO + HONO$	2.9×10^3

* The inorganic, formaldehyde, and acetaldehyde reactions listed earlier must be added to construct the explicit 1-butene mechanism.

† Rate constant in min^{-1}.

§ Activation energy is 12,500K; rate constant is given at 298K.

TABLE 16. INITIAL CONDITIONS AND PHOTOLYSIS RATE CONSTANTS FOR THE 1-BUTENE/NO_x SMOG CHAMBER EXPERIMENTS

Run number	Initial concentration (ppm)				Photolysis rate constant ($\times 10^4$ min^{-1})					
	1-Butene	NO	NO_2	HONO	$NO_2 \rightarrow NO+O$*	$O_3 \rightarrow O(^1D)$	$O_3 \rightarrow O(^3P)$	$HONO \rightarrow NO+OH\cdot$	$H_2O_2 \rightarrow 2OH\cdot$	FORM→Products†
EC-122	0.217	0.398	0.080	0.009	0.29	10	93	700	4	11
EC-123	0.404	0.401	0.106	0.01	0.28	10	93	700	4	11
EC-124	0.420	0.608	0.385	0.02	0.27	34	82	700	4	8

* Rate constant in min^{-1}.

† The relationship between FORM→Products and carbonyl photolysis rate constants is discussed in Section 4.

TABLE 17. UCR 1-BUTENE EXPERIMENTS--SIMULATIONS AND MEASUREMENTS

Exp. no.	Initial [NO_x] (ppm)	Initial NO_2/NO_x ratio	Initial HC/NO_x ratio (ppmC/ppm)	Maximum [O_3] (ppm)*		Difference in O_3 maxima (percent)†	Time to maximum [O_3] (minutes)§		Difference in times to O_3 maxima (percent)†	Maximum [NO_2] (ppm)		Difference in NO_2 maxima (percent)†	Time to maximum [NO_2] (minutes)§		Difference in times to NO_2 maxima (percent)†
				Sim.	Meas.		Sim.	Meas.		Sim.	Meas.		Sim.	Meas.	
EC-122	0.48	0.17	1.8	0.22	0.21	5	>360	>360	--	0.34	0.28	21	140	110	27
EC-123	0.51	0.21	3.2	0.50	0.50	0	>360	~330	--	0.40	0.32	25	80	60	33
EC-124	0.99	0.39	1.7	0.27	0.23	17	>630	>630	--	0.67	0.53	26	240	190	26

O_3 maxima: average difference = 7 percent; standard deviation = ±9 percent.
NO_2 maxima: average difference = 24 percent; standard deviation = ±3 percent.

* Maximum one-hour-average concentration.

† [(Simulated Value - Measured Value) / Measured Value] x 100.

§ Time from beginning of irradiation to beginning of the period during which the maximum one-hour-average concentration occurred.

123
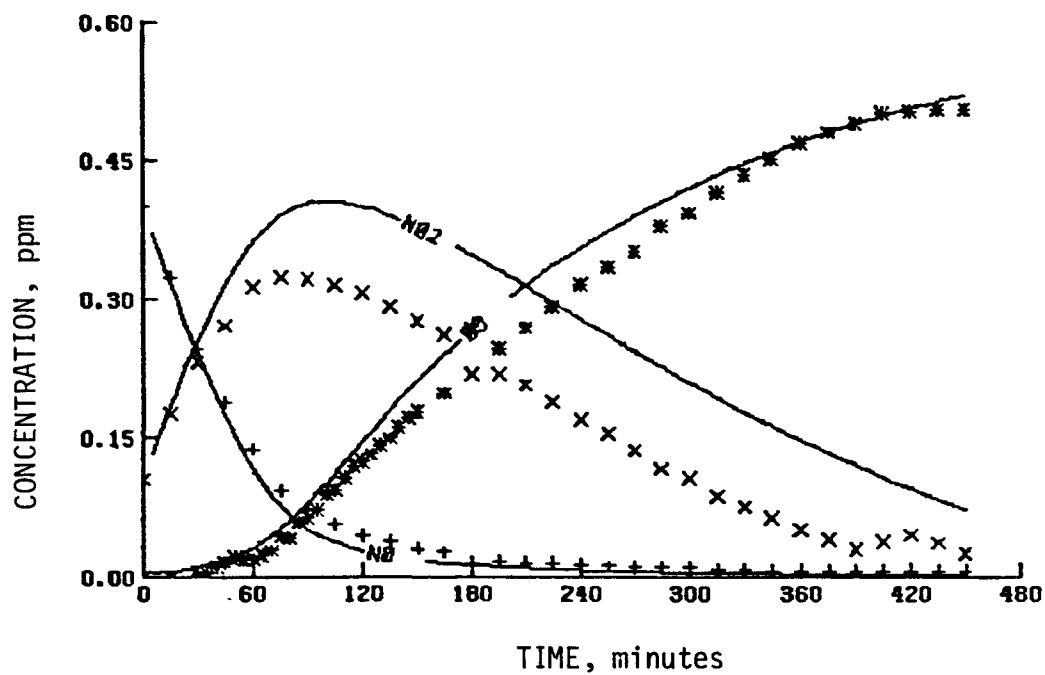
(a) NO_2, NO, and O_3 .
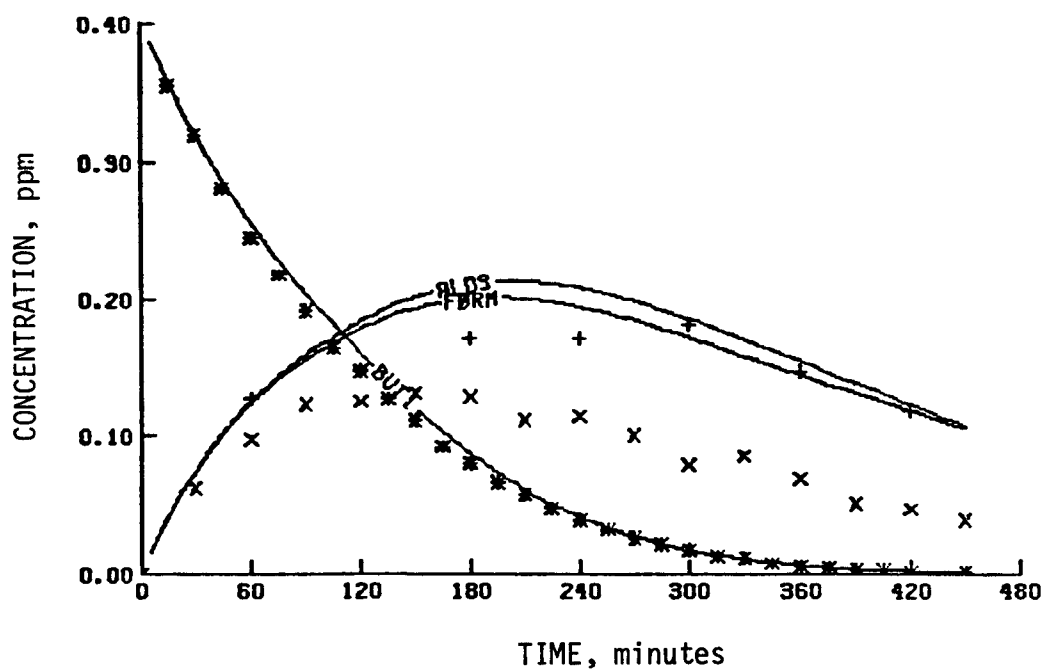
(b) 1-Butene, formaldehyde, and acetaldehyde

Figure 36. Simulation results of a UCR 1-butene experiment (EC-123)

124
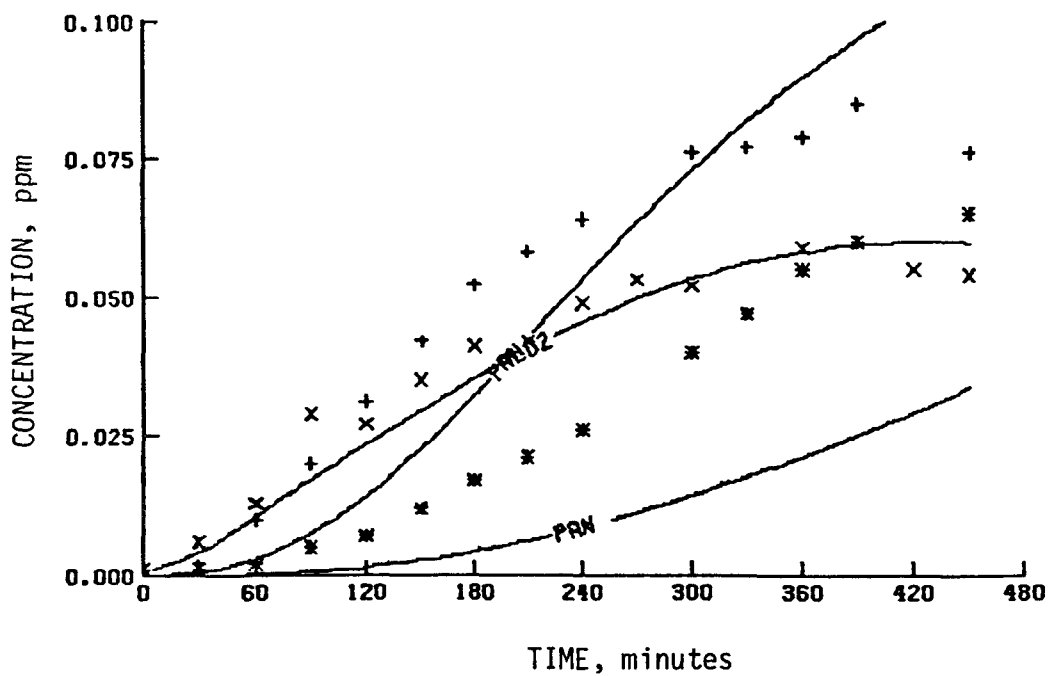
(c) Acetaldehyde, PPN, and PAN
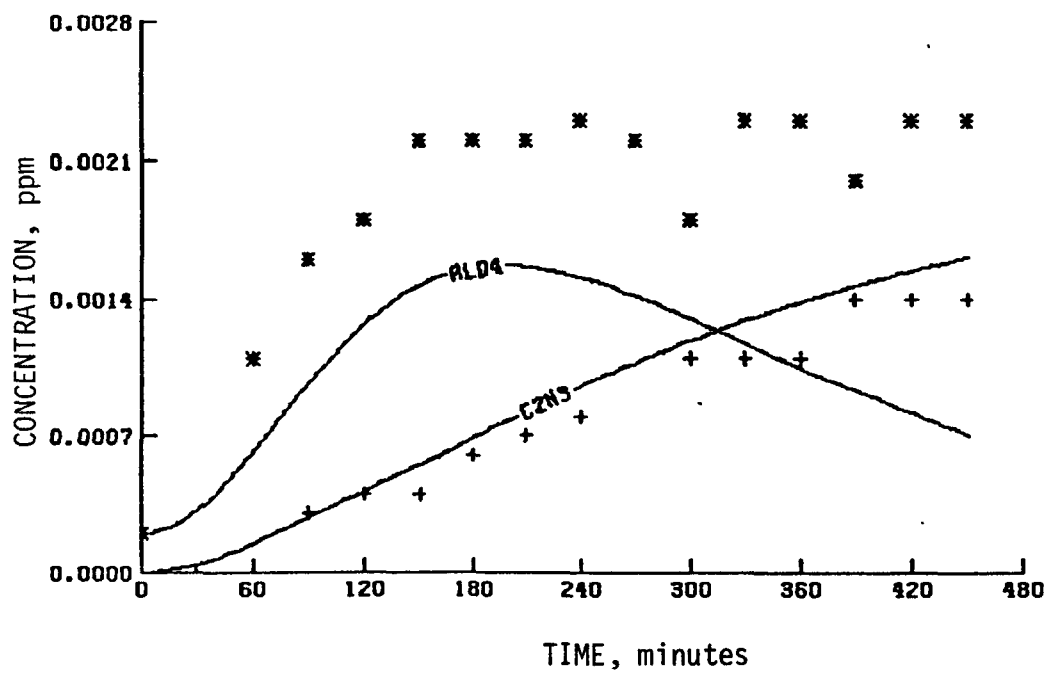
(d) Ethyl nitrate and butyraldehyde

Figure 36 (Concluded)

Trans-2-Butene + O(^{3}P) Reaction

Japar and Niki (1975) reported a rate constant of 2.7×10^4 ppm^{-1}min^{-1} for the trans-2-butene + O(^{3}P) reaction--almost five times greater than the propylene + O(^{3}P) rate constant. They proposed that the products of the reaction are acetylperoxy radicals and ethylperoxy radicals:

$$CH_3CH=CHCH_3 + O(^3P) \xrightarrow{2O_2} CH_3CH_2O_2^{\bullet} + CH_3C(O)O_2^{\bullet} \qquad . \qquad (42)$$
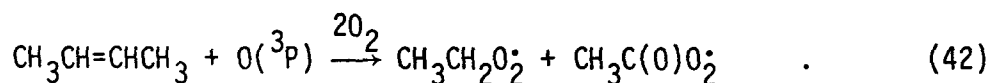
Trans-2-Butene + OH· Reaction

Wu, Japar, and Niki (1976) found that the reaction of trans-2-butene with OH· is 1.3 times faster than the reaction of cis-2-butene with OH·, whereas Morris and Niki (1971b) reported a relative rate of 1.2. With a relative rate of 1.3 and the rate constant for cis-2-butene + OH· reaction estimated by Lloyd et al. (1976), we estimated the rate constant for the trans-2-butene + OH· reaction to be 1.2×10^5 ppm^{-1}min^{-1}.

The product of this reaction is a hydroxyalkylperoxy radical, analogous with the propylene + OH· reaction:

$$CH_2CH=CHCH_3 + OH\cdot \xrightarrow{O_2} CH_3CH(OH)CH(O_2^{\bullet})CH_3 \qquad , \qquad (43)$$

$$CH_3CH(OH)CH(O_2^{\bullet})CH_3 + NO \rightarrow CH_3CH(OH)CH(O\cdot)CH_3 + NO_2 \qquad , \qquad (44)$$

$$CH_3CH(OH)CH(O\cdot)CH_3 \xrightarrow{O_2} CH_3CHO + CH_3CH(OH)O_2^{\bullet} \qquad , \qquad (45)$$

$$CH_3CH(OH)O_2^{\bullet} \rightarrow CH_3CHO + HO_2^{\bullet} \qquad . \qquad (46)$$
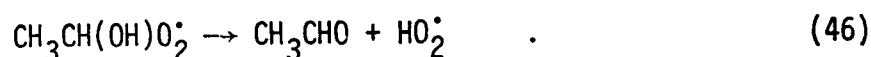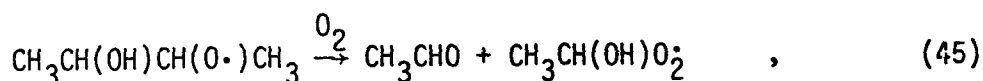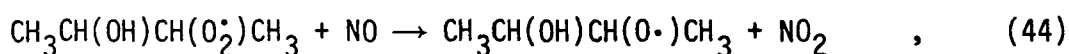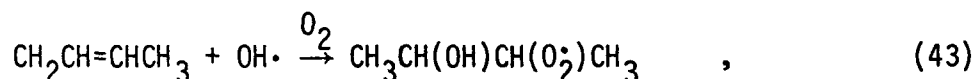
Trans-2-Butene + O$_3$ Reaction

The rate constant of the trans-2-butene + O$_3$ reaction is 20 times larger than that of the propylene + O$_3$ reaction. Japar, Wu, and Niki (1974)

reported a rate constant of 0.39 $ppm^{-1}min^{-1}$ for the trans-2-butene + O_3 reaction. Reaction pathways have been assumed to occur analogous with the propylene-O_3 reaction. For trans-2-butene, we used the following reactions:

$$CH_3CH=CHCH_3 + O_3 \rightarrow CH_3CHO + CH_3CHO_2^{\cdot} \qquad . \qquad (47)$$
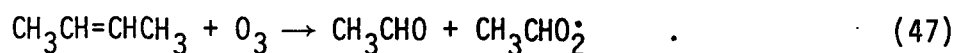
The Criegee intermediate ($CH_3CHO_2^{\cdot}$) reacts in the same manner as discussed in the section on the propylene-O_3 reaction.

Trans-2-Butene + $NO_3^{\cdot}$ Reaction

The rate constant for the reaction of trans-2-butene with nitrate radicals was measured by Japar and Niki (1975) to be 207 $ppm^{-1}min^{-1}$. Trans-2-butene is the first olefin studied at UCR that has a high rate constant for reaction with $NO_3^{\cdot}$, but its reaction with NO_3 is insignificant because it has typically all reacted with OH· before a significant concentration of $NO_3^{\cdot}$ appears.

Simulation Results for the Trans-2-Butene/NO_x Systems

Only three trans-2-butene/NO_x experiments were performed at UCR. Table 18 lists the reactions in the explicit trans-2-butene mechanism, and Table 19 shows the initial conditions and photolysis rate constants used in the simulation of each experiment. The percentage differences between measured and simulated maximum one-hour-averages NO_2 and O_3 concentrations for each experiment are shown in Table 20. Figure 37 shows the results of the computer simulations for EC-146.

2,3-DIMETHYLBUTANE

Besides n-butane, the only alkane investigated at UCR was 2,3-dimethylbutane. Reported rate constants for oxidation of 2,3-dimethylbutane by O atoms and OH radicals are approximately 2.5 to 3 times faster than the corresponding rate constants for n-butane. According to some reactivity scales, this alkane should therefore have a much higher reactivity than

TABLE 18. REACTIONS OF TRANS-2-BUTENE*

Reaction	Rate constant $(ppm^{-1}min^{-1})$
$CH_3CH=CHCH_3 + O \xrightarrow{2O_2} CH_3CH_2O_2^{\cdot} + CH_3C(O)O_2^{\cdot}$	1.4×10^4
$CH_3CH=CHCH_3 + O \rightarrow CH_3\overset{O}{\overset{\triangle}{CH}}{-\!\!-}CHCH_3$	1.4×10^4
$CH_3\overset{O}{\overset{\triangle}{CH}}{-\!\!-}CHCH_3 \rightarrow CH_3CH_2C(O)CH_3$	$5 \times 10^{-2\dagger}$
$CH_3CH=CHCH_3 + OH\cdot \xrightarrow{O_2} CH_3CH(O_2^{\cdot})CH(OH)CH_3$	1.2×10^5
$CH_3CH=CHCH_3 + O_3 \rightarrow CH_3CHO + CH_3CHO_2^{\cdot}$	3.9×10^{-1}
$CH_3CHO_2^{\cdot} + HCHO \rightarrow CH_3\overset{O{-}O}{\overset{\frown}{CH}}\underset{\underset{O}{\smile}}{CH_2}$	2×10^3
$CH_3CHO_2^{\cdot} + CH_3CHO \rightarrow CH_3\overset{O{-}O}{\overset{\frown}{CH}}\underset{\underset{O}{\smile}}{CHCH_3}$	2×10^3
$CH_3CHO_2^{\cdot} + NO \rightarrow NO_2 + CH_3CHO$	1.2×10^4
$CH_3CHO_2^{\cdot} + NO_2 \rightarrow NO_3 + CH_3CHO$	8×10^3
$CH_3CHO_2^{\cdot} \rightarrow CO_2 + CH_4$	$1.5 \times 10^{2\dagger}$
$CH_3CHO_2^{\cdot} \xrightarrow{O_2} CH_3O_2^{\cdot} + CO + OH\cdot$	$3.4 \times 10^{2\dagger}$
$CH_3CHO_2^{\cdot} \xrightarrow{2O_2} CH_3O_2^{\cdot} + CO_2 + HO_2^{\cdot}$	$4.25 \times 10^{2\dagger}$
$CH_3CHO_2^{\cdot} \xrightarrow{O_2} CH_3O\cdot + CO + HO_2^{\cdot}$	$8.5 \times 10^{1\dagger}$
$CH_3CH=CHCH_3 + NO_3^{\cdot} \rightarrow NO_2 + Stable\ Products$	2.07×10^2
$CH_3C(O_2^{\cdot})C(O)CH_3 + NO \rightarrow NO_2 + CH_3C(O)C(O)CH_3 + HO_2^{\cdot}$	1.2×10^4
$CH_3CH(O_2^{\cdot})CH(OH)CH_3 + NO \rightarrow NO_2 + CH_3CH(O\cdot)CH(OH)CH_3$	1.2×10^4
$CH_3CH_2O_2^{\cdot} + NO \rightarrow NO_2 + CH_3CH_2O\cdot$	1.2×10^4
$CH_3CH_2O_2^{\cdot} + NO \rightarrow CH_3CH_2ONO_2$	1×10^2
$CH_3CH(O\cdot)CH(OH)CH_3 \rightarrow 2CH_3CHO + HO_2^{\cdot}$	$3 \times 10^{5*}$
$CH_3CH_2O\cdot + O_2 \rightarrow CH_3CHO + HO_2^{\cdot}$	3.3

(continued)

128

TABLE 18 (Concluded)

Reaction	Rate constant $(ppm^{-1} min^{-1})$
$CH_3CH_2C(O)CH_3 + h\nu \xrightarrow{2O_2} CH_3CH_2O_2^\cdot + CH_3C(O)O_2^\cdot$	Experimental[+]
$CH_3C(O)C(O)CH_3 + h\nu \xrightarrow{2O_2} 2CH_3C(O)O_2^\cdot$	$1 \times 10^{-3*}$
$CH_3C(O)CH_2CH_3 + OH\cdot \rightarrow CH_3C(O)CH(O_2^\cdot)CH_3 + H_2O$	4.9×10^3
$CH_3C(O)CH(O_2^\cdot)CH_3 + HO_2^\cdot \rightarrow CH_3C(O)CH(O_2H)CH_3 + O_2$	4×10^3
$CH_3CH(OH)CH(O_2^\cdot)CH_3 + HO_2^\cdot \rightarrow CH_3CH(OH)CH(O_2H)CH_3 + O_2$	4×10^3
$CH_3CH_2O_2^\cdot + HO_2^\cdot \rightarrow CH_3CH_2O_2H + O_2$	4×10^3
$2CH_3CH(OH)CH(O_2^\cdot)CH_3 \rightarrow 2CH_3CH(OH)CH(O\cdot)CH_3 + O_2$	5×10^2
$CH_3CH_2O_2^\cdot + NO_2 \rightarrow CH_3CH_2ONO_2$	1.5×10^4
$CH_3CH_2O_2^\cdot + NO_2 \rightarrow CH_3CHO + HONO$	2.9×10^3
$CH_3CH(OH)CH(O_2^\cdot)CH_3 + O_3 \rightarrow CH_3CH(OH)CH(O\cdot)CH_3 + 2O_2$	2×10^2

* The inorganic, formaldehyde, and acetaldehyde reactions listed earlier must be added to construct the explicit trans-2-butene mechanism.

+ Rate constant in min^{-1}.

TABLE 19. INITIAL CONDITIONS AND PHOTOLYSIS RATE CONSTANTS FOR THE TRANS-2-BUTENE/NOx SMOG CHAMBER EXPERIMENTS

Run number	Initial concentration (ppm)				Photolysis rate constant ($\times 10^4$ min^{-1})					
	t-2-Butene	NO	NO$_2$	HONO	NO$_2 \cdot$NO+O*	O$_3 \rightarrow$O(^{1}D)	O$_3 \rightarrow$O(^{3}P)	HONO$\cdot$NO+OH$\cdot$	H$_2$O$_2 \cdot$2OH$\cdot$	FORM→Products†
EC-146	0.231	0.385	0.124	0.021	0.33	43.2	106	990	4.7	8.0
EC-147	0.38	0.782	0.20	0.02	0.34	44.5	109	990	4.8	8.0
EC-157	0.19	0.397	0.129	0.02	0.33	43.2	106	990	4.7	8.0

* Rate constant in min^{-1}.

† The relationship between FORM→Products and carbonyl photolysis rate constants is discussed in Section 4.

TABLE 20. UCR TRANS-2-BUTENE EXPERIMENTS—SIMULATIONS AND MEASUREMENTS

Exp. no.	Initial [NO$_x$] (ppm)	Initial NO$_2$/NO$_x$ ratio	Initial HC/NO$_x$ ratio (ppmC/ppm)	Maximum [O$_3$] (ppm)*		Difference in O$_3$ maxima (percent)†	Time to maximum [O$_3$] (minutes)§		Difference in times to O$_3$ maxima (percent)†	Maximum [NO$_2$] (ppm)		Difference in NO$_2$ maxima (percent)†	Time to maximum [NO$_2$] (minutes)§		Difference in times to NO$_2$ maxima (percent)†
				Sim.	Meas.		Sim.	Meas.		Sim.	Meas.		Sim.	Meas.	
EC-146	0.51	0.24	1.80	0.27	0.23	17	>360	>360	--	0.37	0.29	28	70	60	17
EC-147	0.53	0.25	1.45	0.20	0.13	54	>360	>360	--	0.68	0.53	28	90	50	80
EC-157	0.98	0.21	1.55	0.18	0.18	0	>360	>360	--	0.37	0.30	23	80	80	60

O$_3$ maxima: average difference = 24 percent; standard deviation = ±28 percent.

NO$_2$ maxima: average difference = 26 percent; standard deviation = ±3 percent.

* Maximum one-hour-average concentration.

† [(Simulated Value - Measured Value) / Measured Value] x 100.

§ Time from beginning of irradiation to beginning of the period during which the maximum one-hour-average concentration occurred.

130
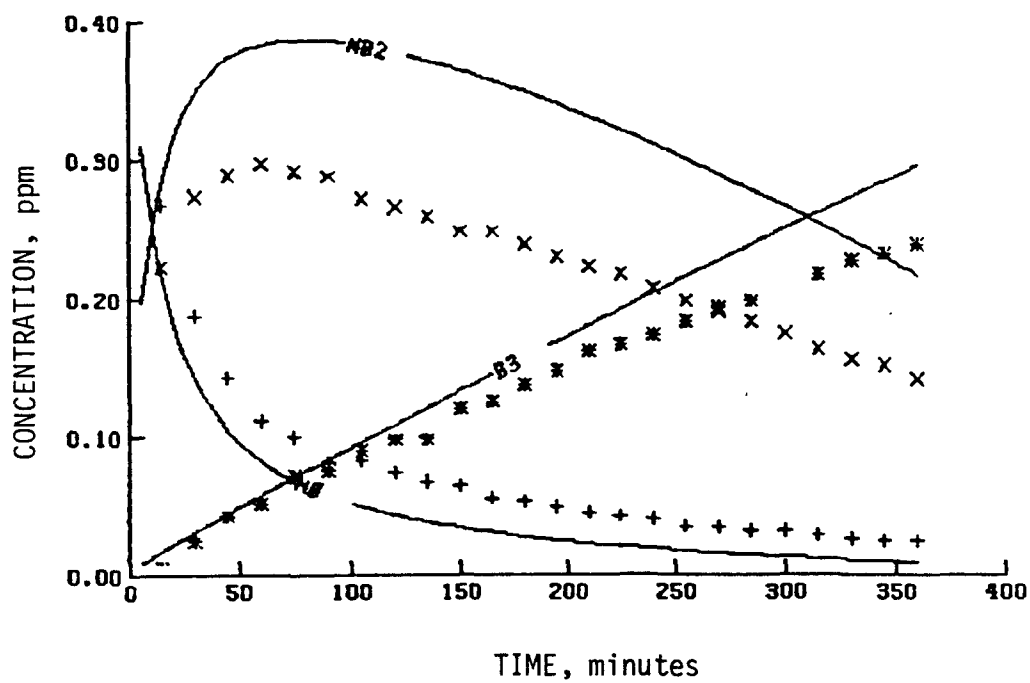
(a) NO_2, NO, and O_3
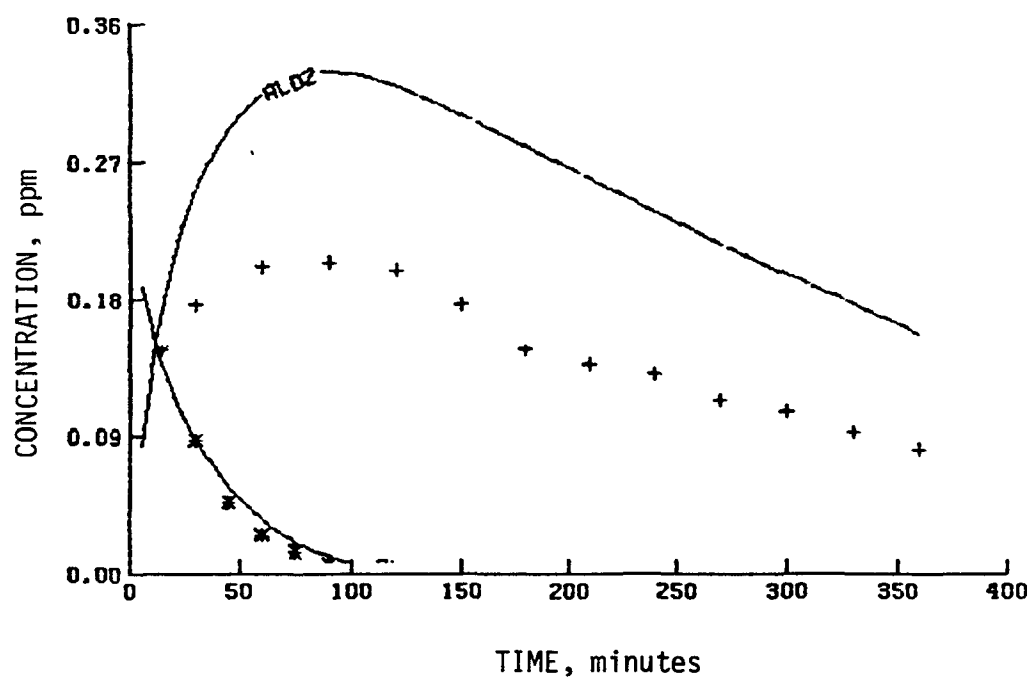
(b) Trans-2-butene and acetaldehyde

Figure 37. Simulation results of a UCR trans-2-butene experiment (EC-146)
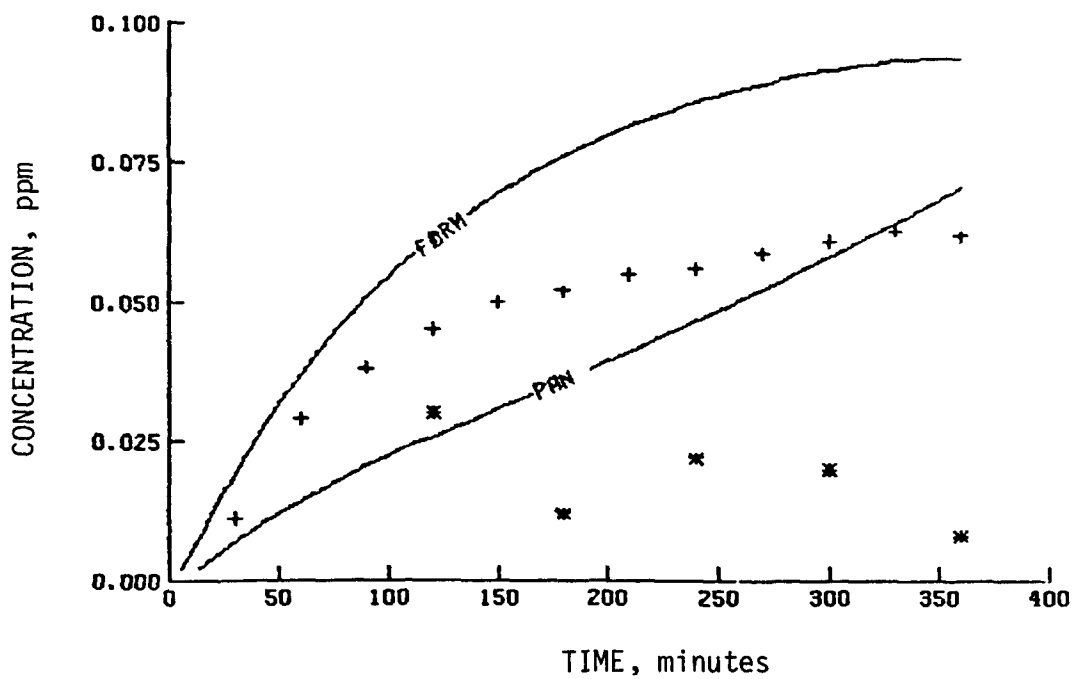
(c) PAN and formaldehyde
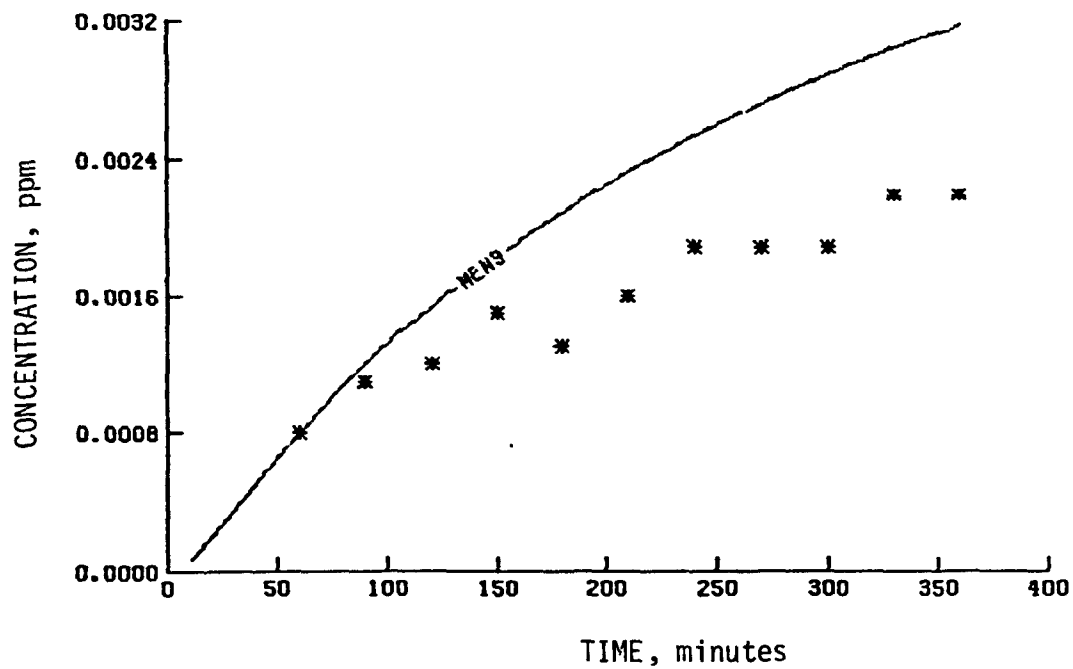
(d) Methyl nitrate

Figure 37 (Concluded)

132

n-butane (Darnall et al., 1976b). However, the UCR data show that on a per-molecule basis, 2,3-dimethylbutane produces approximately the same amount of ozone as does n-butane after a five-hour period. (For example, compare UCR Runs EC-165 and EC-178.) On a per-carbon-atom basis, this implies that 2,3-dimethylbutane has a lower reactivity than n-butane. The reasons for this lower reactivity for 2,3-dimethylbutane may stem from the same tertiary carbon atoms that suggest the high reactivity.

2,3-Dimethylbutane + O(^{3}P) Reaction

This reaction has been studied by Herron and Huie (1974), who reported a rate constant of 337 $ppm^{-1}min^{-1}$. The products of this reaction are postulated to be:

$$CH_3CH(CH_3)CH(CH_3)CH_3 + O(^3P) \xrightarrow{O_2} CH_3CH(CH_3)CH(CH_3)(O_2^{\cdot})CH_3 + OH\cdot \qquad . \quad (48)$$
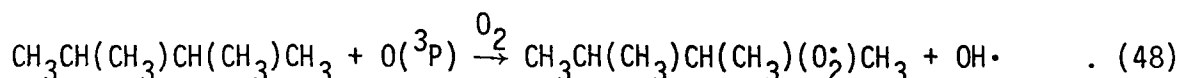
2,3-Dimethylbutane + OH· Reaction

Using Greiner's (1970) formula for the rate constants of alkane + OH· reactions,

$$k = [1.46 \exp(-820/T)N_p + 3.35 \exp(-430/T)N_s + 3.05 \exp(95/T)N_T]$$
$$\times 10^3 \ ppm^{-1}min^{-1}, \qquad\qquad (49)$$

we can estimate the rate constant for the 2,3-dimethylbutane + OH· reaction. Since there are 12 primary and 2 tertiary hydrogen atoms, the total rate constant is 9.7 x 10^3 $ppm^{-1}min^{-1}$, which is divided between reaction at a rate constant of 8.5 x 10^3 $ppm^{-1}min^{-1}$ at the tertiary hydrogens and 1.2 x 10^3 $ppm^{-1}min^{-1}$ at the primary hydrogens:

$$\qquad\qquad (50)$$

133

$$\text{(structure)} + OH\cdot \xrightarrow{O_2} \text{(structure)} + H_2O \qquad . \qquad (51)$$
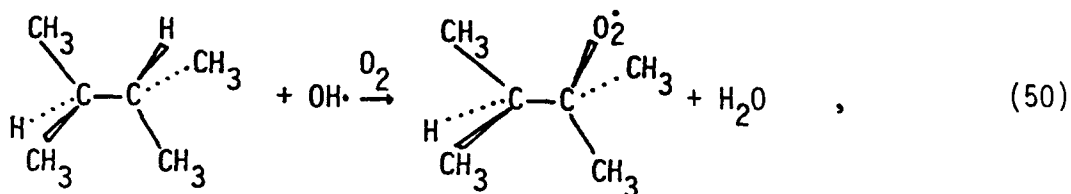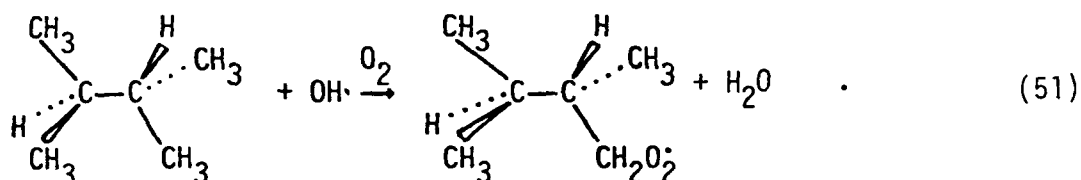
The tertiary alkylperoxy radical produced in Reaction (50) may convert NO to NO_2 and form a tertiary alkoxyl radical:

$$CH_3CH(CH_3)C(CH_3)(O_2^{\cdot})CH_3 + NO \rightarrow CH_3CH(CH_3)C(CH_3)(O\cdot)CH_3 + NO_2 \qquad . \quad (52)$$
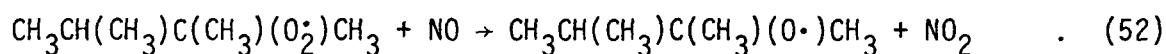
Initial simulations of UCR experiments with the rate constant of 9.7×10^3 $ppm^{-1}min^{-1}$ calculated from Greiner's formula showed a slower disappearance of 2,3-dimethylbutane than was observed, and so we raised the rate constant to 1.1×10^4 $ppm^{-1}min^{-1}$. This rate constant is based on a reevaluation of the rate constant for the n-butane + OH· reaction (discussed earlier) and a ratio of 2.5 for the rate constants of the 2,3-dimethylbutane + OH· and n-butane + OH· reactions calculated using Greiner's formula.

Alkoxyl and Alkylperoxy Radical Chemistry

The reactions of 2,3-dimethylbutane discussed thus far have been based on reactions analogous with those of n-butane. Because 2,3-dimethylbutane is larger and more branched than n-butane, it can undergo more internal rearrangements, and some of its reactions are not analogous to n-butane reactions. These reactions are discussed below.

Decomposition of the tertiary alkoxyl radical formed in Reaction (50) apparently would lead to acetone and an isopropyl radical (which would immediately react with molecular oxygen to form an isopropylperoxy radical):

$$CH_3CH(CH_3)CH(CH_3)(O\cdot)CH_3 \xrightarrow{O_2} CH_3CH(O_2^{\cdot})CH_3 + CH_3C(O)CH_3 \qquad . \quad (53)$$
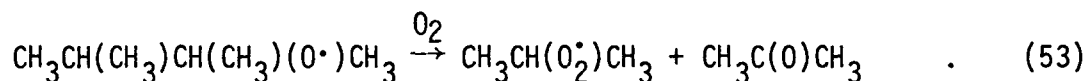
The isopropylperoxy radical will convert another NO to NO_2 and form the isopropoxyl radical. UCR reported acetone and isopropyl nitrate concentrations that would be expected from reactions of the isopropoxyl radical:

134

$$CH_3CH(O\cdot)CH_3 + O_2 \rightarrow CH_3C(O)CH_3 + HO_2^\bullet \qquad , \qquad (54)$$

$$CH_3CH(O\cdot)CH_3 + NO_2 \rightarrow CH_3CH(CH_3)ONO_2 \qquad . \qquad (55)$$
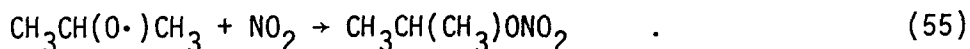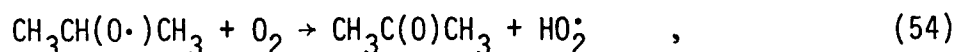
The primary alkylperoxy radical from Reaction (51) probably undergoes a series of reactions as follows:

$$CH_3CH(CH_3)CH(CH_3)CH_2O_2^\bullet + NO \rightarrow CH_3CH(CH_3)CH(CH_3)CH_2O\cdot + NO_2 \qquad , \qquad (56)$$

$$CH_3CH(CH_3)CH(CH_3)CH_2O\cdot + O_2 \rightarrow CH_3CH(CH_3)CH(CH_3)CHO + HO_2^\bullet \qquad , \qquad (57)$$

$$CH_3CH(CH_3)CH(CH_3)CH_2O\cdot \longrightarrow CH_3CH(CH_3)CH(CH_3)O_2^\bullet + HCHO \qquad , \qquad (58)$$

$$CH_3CH(CH_3)CH(CH_3)CH_2O\cdot + NO_2 \longrightarrow CH_3CH(CH_3)CH(CH_3)CH_2ONO_2 \qquad , \qquad (59)$$
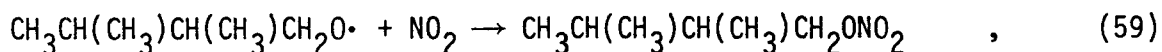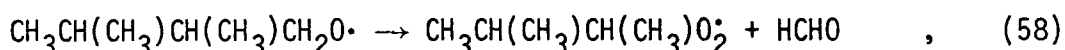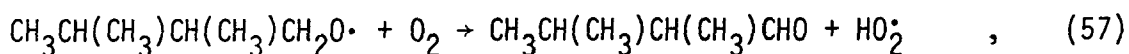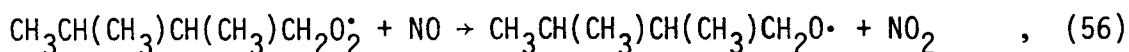
At this point, the differences from the chemistry in the n-butane explicit mechanism become striking. The fast reactions of primary alkoxyl radicals (RO·) have been postulated to be hydrogen abstraction by molecular oxygen to form aldehydes [(R-1)CHO] (Barker et al., 1977) and internal hydrogen migration to form hydroxyalkylperoxy radicals [(R-2)CH(OH)CH$_2$O$_2^\bullet$] (Carter et al., 1976). The reaction of primary alkoxyl radicals with NO$_2$ to form nitrates is apparently much slower than the above reactions. For secondary alkoxyl radicals, hydrogen abstraction by molecular oxygen is still possible (to form ketones), but internal hydrogen migration would be suppressed unless five- or six-membered ring intermediates are possible. Whitten and Hogo (1977) included the unimolecular decomposition of secondary butoxyl radicals in the n-butane mechanism to account for the concentrations of acetaldehyde observed in n-butane/NO$_x$ experiments at UCR. However, Barker et al. (1977) estimated that the unimolecular decomposition of secondary butoxyl radicals is much slower than their reaction with molecular oxygen.

The tertiary radicals formed from 2,3-dimethylbutane have no hydrogens to react with molecular oxygen, and five- or six-membered ring intermediates for internal hydrogen migration would be formed with difficulty. Hence, unimolecular decomposition and reaction with NO$_2$ to form nitrates seem to be

likely paths for reaction of the tertiary radicals in 2,3-dimethylbutane/ NO_x systems. The postulated slow reactivity of these tertiary alkoxyl radicals would lead to high steady-state concentrations, implying that the $RO\cdot + NO_2$ or $RO_2^\cdot + NO$ reactions to form the nitrate would be more important in the 2,3-dimethylbutane/NO_x system than in the n-butane/NO_x system.

Nitrate formation was indeed found to be more important in the 2,3-dimethylbutane experiments than in the n-butane experiments. Comparing the nitrate measurements in the 2,3-dimethylbutane experiments at UCR with those in the more recent n-butane experiments at UCR (EC-162, EC-163, EC-168, and EC-178), we found that approximately 16 percent of the total reacted hydrocarbon appeared as nitrates in the former experiments and only 8 to 9 percent in the latter. Since nitrate formation is a radical sink, the normal peroxy-oxyl cyclic series of radical transfer reactions is more limited when tertiary alkoxyl radicals are involved. This limitation reduced the number of NO to NO_2 conversions and, hence, the amount of O_3 formed per carbon atom in the 2,3-dimethylbutane/NO_x system relative to the n-butane/NO_x system.

Alkoxyl Radical Decomposition Reactions

Hendry et al. (1977) evaluated rate constants for the 2,3-dimethylbutoxyl radical decomposition. For the decomposition of tertiary dimethylbutoxyl radicals, Hendry et al. assumed a rate constant of 3.8×10^7 min^{-1}:

$$ CH_3C(O)CH_3 + CH_3CH(O_2^\cdot)CH_3 \quad . \tag{60} $$
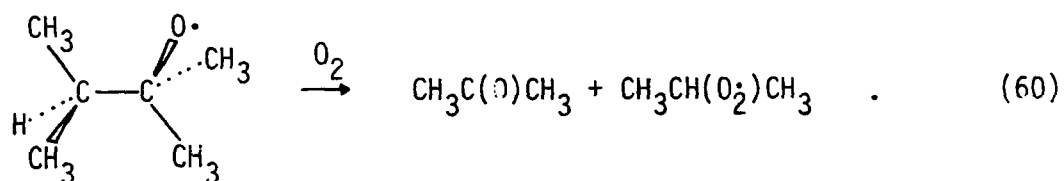
For the primary dimethylbutoxyl radical, decomposition was assumed to have a rate constant of 2.4×10^3 min^{-1}, and the isomerization of this radical was assumed to be at least as fast as the internal isomerization of the n-butoxyl radical:

136

$$CH_3CH(CH_3)CH(CH_3)CH_2O \cdot \rightarrow \begin{bmatrix} H \cdots O \\ H_2C \qquad CH_2 \\ CH — CH \\ CH_3 \qquad CH_3 \end{bmatrix} \xrightarrow{O_2} CH_3CH(CH_2O_2^\cdot)CH(CH_3)CH_2OH \quad .$$

$$(61)$$
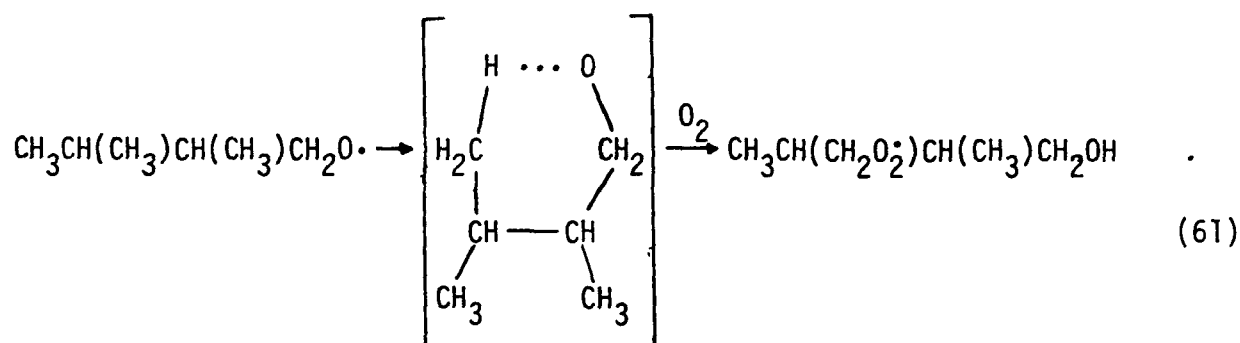
These two peroxyl radicals [2,3-dimethyl-2-peroxy butyl radical from Reaction (51) and 1-peroxy-2,3-dimethyl-4-hydroxy butyl radical from Reaction (61)] can undergo a series of reactions. For the latter, a series of reactions similar to those in the explicit butane mechanism is possible.

Hendry et al. (1977) estimated rate constants for isomerizations of alkoxyl radicals and found for the primary 2,3-dimethylbutoxyl radical an isomerization rate of 3.7×10^7 min^{-1}. The uncertainty in their estimates of isomerization rate constants may be as high as a factor of 60 (Barker et al., 1977). Initial simulations of 2,3-dimethylbutane/NO$_x$ systems with this value and published values for alkoxyl radical decomposition rates, reactions with molecular oxygen, and reactions with NO$_2$ produced organic nitrate concentrations lower than the observations. If the estimates of Hendry et al. are accepted, we must look for other reactions that produce (or will eventually lead to production of) nitrates in the alkane/NO$_x$ chemistry. Several groups have suggested the possibility of nitrate formation from reactions involving alkylperoxy radicals and NO or NO$_2$. Darnall et al. (1976a) postulated that alkoxyl radicals (with four or more carbon atoms) as discussed in the section on butane chemistry, will add to NO to form an excited complex:

$$RO_2^\cdot + NO \rightarrow [RO_2NO]^* \quad , \tag{62}$$

$$[RO_2NO]^* \rightleftarrows [RONO_2]^* \quad , \tag{63}$$

$$[RONO_2]^* \rightarrow RO \cdot + NO_2 \quad , \tag{64}$$

$$[RONO_2]^* \xrightarrow{M} RONO_2 \quad , \tag{65}$$
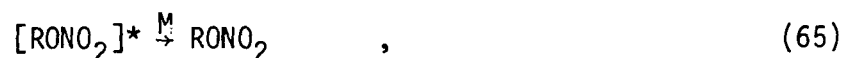
where (*) represents an excited state. Darnall et al. (1976a) estimated the ratio k_{65}/k_{64} to be 0.09 for butyl, 0.16 for pentyl, and 0.6 for hexyl systems. Simulations of 2,3-dimethylbutane experiments with these estimates showed a major decrease in chemical reactions and a major loss of NO_x. Simulations with lower ratios produced small amounts of nitrate and maintained the NO_x concentration. We have included the RO_2 + NO reaction pathway to form radicals in the 2,3-dimethylbutane simulations. Rate constants for the tertiary and primary 2,3-dimethylperoxybutyl radicals with NO have been assumed to be 1.5×10^3 $ppm^{-1}min^{-1}$. Another possible source of nitrate may be alkyperoxy + NO_2 reactions:

$$RO_2^{\cdot} + NO_2 \rightarrow RO_2NO_2 \quad , \qquad\qquad (66)$$

$$RO_2^{\cdot} + NO_2 \rightarrow (R-1)CHO + HONO_2 \quad . \qquad\qquad (67)$$
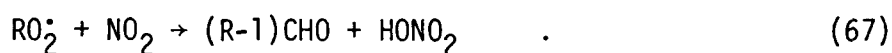
Simonaitis and Heicklen (1974) reported that the alkylperoxy nitrate in Reaction (66) accounts for 75 percent of the total reaction products. Spicer et al. (1973) postulated the formation of alkyl nitrates from the alkylperoxy nitrate:

$$RO_2NO_2 \rightarrow RONO_2 \quad . \qquad\qquad (68)$$

They based their conclusion on observations of alkyl nitrates in their experiments. Simonaitis and Heicklen are not definite on the production of nitrates from the alkylperoxy nitrate, but they recommend a value of 2.2 for the ratio of the rate constant of the reactions of $RO_2^{\cdot}$ with NO and with NO_2. Simulations with this ratio showed a major decrease in chemical reactivity and a major loss of NO_x, similar to the effects on simulations of adopting the estimates by Darnall et al. (1976a) mentioned earlier.

The production of nitrates from the $RO_2^{\cdot}$ + NO_2 reaction may be a minor or a reversible pathway. Since the $RO_2^{\cdot}$ + NO_2 reaction may be analogous to the $HO_2^{\cdot}$ + NO_2 reaction, the RO_2NO_2 may decompose to form $RO_2^{\cdot}$. Barker and Golden (1977) postulated that the abstraction reaction may be important:

$$\underset{\substack{\text{CH}_3 \\ \diagdown \\ \text{H} \cdots \text{C} \text{---} \text{C} \cdots \text{H} \\ \diagup \quad \diagdown \\ \text{CH}_3 \quad \text{CH}_3}}{\overset{\text{O}_2^{\cdot}}{}} + \text{NO}_2 \longrightarrow \text{CH}_3\text{CH}(\text{CH}_3)\dot{\text{C}}(\text{O})\text{CH}_3 + \text{HONO}_2 \quad . \tag{69}$$
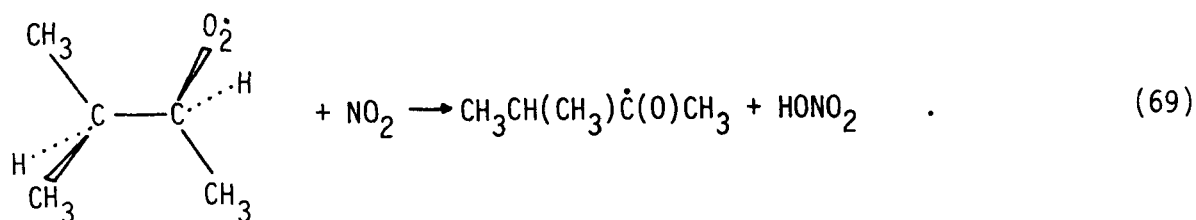
All of the possible reaction products of RO_2 with NO_2 will be examined in further detail before any of these reactions are incorporated into kinetic mechanisms.

Photolysis of Acetone

Acetone is known to photolyze in the UV region (Calvert and Pitts, 1966). At low pressures, the main process is:

$$\underset{\text{CH}_3\overset{\text{O}}{\overset{\|}{\text{C}}}\text{CH}_3}{} \xrightarrow{h\nu} \left[\underset{\text{CH}_3\overset{\text{O}}{\overset{\|}{\text{C}}}\cdot}{}\right]^* + \text{CH}_3^{\cdot} \quad . \tag{70}$$
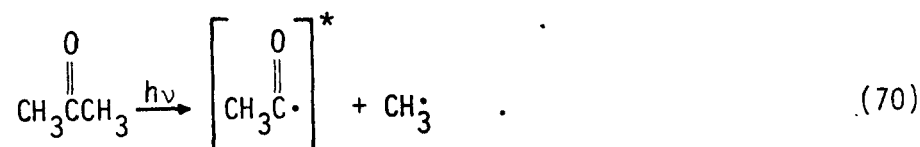
The excited acetyl radical may decompose to form $CH_3^{\cdot}$ and CO. Calvert and Pitts reported that at 313 nm only 7 percent decomposes, whereas at 254 nm 22 percent decomposes. Leighton (1961) reviewed the quantum yields of the photolysis of acetone and reported a value of 0.7 for the production of acetyl and methyl radicals; he also found that the quenching of excited acetone molecules is negligible.

Acetone was present at a low concentration in many early UCR smog chamber experiments because it was used to clean the chamber. In the 2,3-dimethylbutane experiments, acetone is apparently one of the major products of the initial oxidation. Therefore, its photolysis is important in this system. Indeed, UCR data show PAN in the 2,3-dimethylbutane experiments. Preliminary simulations show that PAN concentrations are underpredicted when the acetone photolysis reaction is left out of the mechanism.

139

Results for the 2,3-Dimethylbutane/NO$_x$ System

Three 2,3-dimethylbutane/NO$_x$ experiments were performed at UCR. The present 2,3-dimethylbutane kinetic mechanism is shown in Table 21. The initial conditions and photolysis rate constants used in the simulations of these experiments are presented in Table 22. Table 23 presents the simulated and measured maximum one-hour-average NO$_2$ and O$_3$ concentrations. Figures 38 through 40 show the results of the computer simulations of EC-169. The results of all computer simulations of the 2,3-dimethylbutane experiments are presented in Volume II.

To simulate the high yields of organic nitrates in the 2,3-dimethylbutane runs, we introduced the RO$_2$ + NO to form nitrates (at rate constants of 1.5 x 10^3 ppm^{-1}min^{-1} for the 2,3-dimethylbutyl peroxy radicals), which caused a decrease in the concentration of radicals in the simulations. This decrease led to a less reactive system. The predicted rate of disappearance of 2,3-dimethylbutane is slower than the measured rate in the middle of each simulation. If the observed organic nitrate concentrations are correct, we must look for sources of radicals from the major secondary products (namely, higher aldehydes and ketones) to sustain the disappearance rate of 2,3-dimethylbutane. Owing to the low reactivity in the simulations, the predicted O$_3$ induction period is longer while the time to ozone maximum was shorter than that in the observational data; yet the predicted maxima agree fairly well with the measured data (see Table 23). Although the predicted induction periods for all organic species are longer than the observed times, NO and NO$_2$ behavior tend to agree with the observed behavior. The absolute amounts of NO$_2$ in the simulations seem very suspicious, however.

MULTIPLE HYDROCARBONS

During the past year, UCR conducted smog chamber experiments with mixtures of several initial hydrocarbons. Experiments with multiolefin/NO$_x$ systems will aid in the development of generalized mechanisms in which olefins are treated as one (or more) generalized species. The formulation of generalized mechanisms is discussed in Section 6. In this subsection, our main

TABLE 21. REACTIONS OF 2,3-DIMETHYLBUTANE*

Reaction	Rate constant $(ppm^{-1}min^{-1})$
$(CH_3)_2CHCH(CH_3)_2 + O \xrightarrow{O_2} (CH_3)_2CHC(O_2^-)(CH_3)_2 + OH\cdot$	3.37×10^2
$(CH_3)_2CHCH(CH_3)_2 + OH\cdot \xrightarrow{O_2} (CH_3)_2CHC(O_2^-)(CH_3)_2 + H_2O$	9.8×10^3
$(CH_3)_2CHCH(CH_3)_2 + OH\cdot \xrightarrow{O_2} (CH_3)_2CHCH(CH_3)CH_2O_2^- + H_2O$	1.4×10^3
$CH_3C(O)(O_2^-)CHCH(CH_3)CH_2OH + NO \xrightarrow{O_2} NO_2 + CH_3CH(O_2^-)CH(CH_3)CH_2OH + CO_2$	3.8×10^3
$(CH_3)_2CHC(O_2^-)(CH_3)_2 + NO \rightarrow NO_2 + (CH_3)_2CHC(O\cdot)(CH_3)_2$	1.1×10^4
$(CH_3)_2CHC(O_2^-)(CH_3)_2 + NO \rightarrow (CH_3)_2CHC(ONO_2)(CH_3)_2$	1.5×10^3
$(CH_3)_2CHCH(CH_3)CH_2O_2^- + NO \rightarrow NO_2 + (CH_3)_2CHCH(CH_3)CH_2O\cdot$	1.1×10^4
$(CH_3)_2CHCH(CH_3)CH_2O_2^- + NO \rightarrow NO_2 + (CH_3)_2CHCH(CH_3)CH_2ONO_2$	1.5×10^3
$CH_3CH_2(O_2^-)CHCH(CH_3)CH_2OH + NO \rightarrow NO_2 + CH_3CH_2(O_2^-)CHCH(CH_3)CH_2OH$	1.2×10^4
$CH_3CH_2(O_2^-)CH(CH_3)CH_2OH + NO \rightarrow NO_2 + CH_3CH(O\cdot)CH(CH_3)CH_2OH$	1.2×10^4
$CH_3CH(O_2^-)CH_2OH + NO \rightarrow NO_2 + CH_3CH(O\cdot)CH_2OH$	1.2×10^4
$(CH_3)_2CHCH(O_2^-)CH_3 + NO \rightarrow NO_2 + (CH_3)_2CHCH(O\cdot)CH_3$	1.1×10^4
$(CH_3)_2CHCH(O_2^-)CH_3 + NO \rightarrow (CH_3)_2CHCH(ONO_2)CH_3$	6×10^2
$(CH_3)_2C(O_2^-)C(O)CH_3 + NO \rightarrow NO_2 + (CH_3)_2C(O\cdot)C(O)CH_3$	1.2×10^4
$CH_3C(O)C(O_2^-)(CH_3)CH_2OH + NO \rightarrow NO_2 + CH_3C(O)C(O\cdot)(CH_3)CH_2OH$	1.2×10^4
$CH_3C(O)CH(O_2^-)OH + NO \rightarrow NO_2 + CH_3C(O)CH(O\cdot)OH$	1.2×10^4
$(CH_3)_2CHCH(CH_3)C(O)O_2^- + NO \xrightarrow{O_2} NO_2 + (CH_3)_2CHCH(O_2^-)CH_3 + CO_2$	3.8×10^3
$(CH_3)_2CHO_2^- + NO \rightarrow NO_2 + (CH_3)_2CHO\cdot$	1.1×10^4
$(CH_3)_2CHO_2^- + NO \rightarrow (CH_3)_2CHONO_2$	3×10^2
$(CH_3)_2CHC(O\cdot)(CH_3)_2 \xrightarrow{O_2} CH_3C(O)CH_3 + (CH_3)_2CHO_2^-$	$3.8 \times 10^{7\,\dagger}$
$(CH_3)_2CHCH(CH_3)CH_2O\cdot \xrightarrow{O_2} CH_3CH_2(O_2^-)CHCH(CH_3)CH_2OH$	$1.7 \times 10^{8\,\dagger}$
$(CH_3)_2CHCH(CH_3)CH_2O\cdot \xrightarrow{O_2} HCHO + (CH_3)_2CHCH(O_2^-)CH_3$	$2.4 \times 10^{3\,\dagger}$

(continued)

141

TABLE 21 (Continued)

Reaction	Rate constant $(ppm^{-1}min^{-1})$
$CH_3CH_2(O\cdot)CHCH(CH_3)CH_2OH \xrightarrow{O_2} HCHO + CH_3CH(O_2^\cdot)CH(CH_3)CH_2OH$	$1.0 \times 10^{5*}$
$CH_3CH(O\cdot)CH(CH_3)CH_2OH \xrightarrow{O_2} CH_3CHO + CH_3CH(O_2^\cdot)CH_2OH$	$1.0 \times 10^{5\dagger}$
$(CH_3)_2CHCH(O\cdot)CH_3 \xrightarrow{O_2} CH_3CHO + (CH_3)_2CHO_2^\cdot$	$2.9 \times 10^{5\dagger}$
$(CH_3)_2C(O\cdot)C(O)CH_3 \xrightarrow{O_2} CH_3C(O)O_2^\cdot + CH_3C(O)CH_3$	$2.9 \times 10^{5\dagger}$
$CH_3C(O)C(O\cdot)(CH_3)CH_2OH \xrightarrow{O_2} CH_3C(O)O_2^\cdot + CH_3C(O)CH_2OH$	$2.9 \times 10^{5\dagger}$
$(CH_3)_2CHO\cdot \xrightarrow{O_2} CH_3CHO + CH_3O_2^\cdot$	1.6×10^2
$(CH_3)_2CHCH(CH_3)CH_2O\cdot + O_2 \rightarrow (CH_3)_2CHCH(CH_3)CHO + HO_2^\cdot$	8.57
$(CH_3)_2CHCH(CH_3)O\cdot + O_2 \rightarrow (CH_3)_2CHC(O)CH_3 + HO_2^\cdot$	3.2×10^{-1}
$CH_3CH_2(O\cdot)CHCH(CH_3)CH_2OH + O_2 \rightarrow CH_3C(O)CHCH(CH_3)CH_2OH + HO_2^\cdot$	7.1×10^{-2}
$CH_3CH(O\cdot)CH(CH_3)CH_2OH + O_2 \rightarrow CH_3C(O)CH(CH_3)CH_2OH + HO_2^\cdot$	7.1×10^{-2}
$CH_3CH(O\cdot)CH_2OH + O_2 \rightarrow CH_3C(O)CH_2OH + HO_2^\cdot$	3.2×10^{-1}
$CH_3C(O)CH(O\cdot)OH + O_2 \rightarrow CH_3C(O)C(O)OH + HO_2^\cdot$	3.33
$(CH_3)_2CHO\cdot + O_2 \rightarrow CH_3C(O)CH_3 + HO_2^\cdot$	4.8×10^{-1}
$(CH_3)_2CHCH(CH_3)CHO + h\nu \xrightarrow{2O_2} (CH_3)_2CHCH(O_2^\cdot)CH_3 + HO_2^\cdot + CO$	$Experimental^-$
$CH_3CH(O\cdot)CHCH(CH_3)CH_2OH + h\nu \xrightarrow{2O_2} CH_3CH(O_2^\cdot)CH(CH_3)CH_2OH + HO_2^\cdot + CO$	$Experimental^\dagger$
$CH_3C(O)CH(CH_3)CH_2OH + h\nu \xrightarrow{2O_2} CH_3C(O)O_2^\cdot + CH_3CH(O_2^\cdot)CH_2OH$	$Experimental^\dagger$
$CH_3C(O)CH_2OH + h\nu \xrightarrow{2O_2} CH_3C(O)O_2^\cdot + HCHO + HO_2^\cdot$	$Experimental^\dagger$
$(CH_3)_2CHC(O)CH_3 + h\nu \xrightarrow{2O_2} CH_3C(O)O_2^\cdot + (CH_3)_2CHO_2^\cdot$	$Experimental^\dagger$
$CH_3C(O)C(O)OH + h\nu \rightarrow CH_3CHO + CO_2$	$Experimental^\dagger$
$CH_3C(O)CH_3 + h\nu \xrightarrow{2O_2} CH_3O_2^\cdot + CH_3C(O)O_2^\cdot$	$Experimental^\dagger$

(continued)

142

TABLE 21 (Concluded)

Reaction	Rate constant $(ppm^{-1}min^{-1})$
$(CH_3)_2CHCH(CH_3)CHO + OH\cdot \xrightarrow{O_2} (CH_3)_2CHCH(CH_3)C(O)O_2^\cdot + H_2O$	2.4×10^4
$CH_3CH(O\cdot)CHCH(CH_3)CH_2OH + OH\cdot \xrightarrow{O_2} CH_3C(O)(O_2^\cdot)CHCH(CH_3)CH_2OH + H_2O$	6.0×10^3
$CH_3C(O)CH(CH_3)CH_2OH + OH\cdot \xrightarrow{O_2} CH_3C(O)C(O_2^\cdot)(CH_3)CH_2OH + H_2O$	6.0×10^3
$CH_3C(O)CH_2OH + OH\cdot \xrightarrow{O_2} CH_3C(O)CH(O_2^\cdot)OH + H_2O$	6.0×10^3
$(CH_3)_2CHC(O)CH_3 + OH\cdot \xrightarrow{O_2} (CH_3)_2C(O_2^\cdot)C(O)CH_3 + H_2O$	6.0×10^3
$\cdot O_2C(O)CH(CH_3)CH(CH_3)CH_2OH + HO_2^\cdot \rightarrow HOOC(O)CH(CH_3)CH(CH_3)CH_2OH + O_2$	4.0×10^3
$(CH_3)_2CHCH(CH_3)C(O)O_2^\cdot + HO_2^\cdot \rightarrow (CH_3)_2CHCH(CH_3)C(O)OOH + O_2$	4.0×10^3
$(CH_3)_2CHC(O_2^\cdot)(CH_3)_2 + HO_2^\cdot \rightarrow (CH_3)_2CHC(OOH)(CH_3)_2 + O_2$	1.0×10^3
$(CH_3)_2CHCH(CH_3)CH_2O_2^\cdot + HO_2^\cdot \rightarrow (CH_3)_2CHCH(CH_3)CH_2OOH + O_2$	1.0×10^3
$CH_3CH_2(O_2^\cdot)CHCH(CH_3)CH_2OH + HO_2^\cdot \rightarrow CH_3CH_2(OOH)CH(CH_3)CH_2OH + O_2$	4.0×10^3
$CH_3CH(O_2^\cdot)CH(CH_3)CH_2OH + HO_2^\cdot \rightarrow CH_3CH(OOH)CH(CH_3)CH_2OH + O_2$	4.0×10^3
$CH_3CH(O_2^\cdot)CH_2OH + HO_2^\cdot \rightarrow CH_3CH(OOH)CH_2OH + O_2$	4.0×10^3
$(CH_3)_2CHCH(O_2^\cdot)CH_3 + HO_2^\cdot \rightarrow (CH_3)_2CHCH(OOH)CH_3 + O_2$	4.0×10^3
$(CH_3)_2C(O_2^\cdot)C(O)CH_3 + HO_2^\cdot \rightarrow (CH_3)_2C(OOH)C(O)CH_3 + O_2$	4.0×10^3
$CH_3C(O)C(O_2^\cdot)(CH_3)CH_2OH + HO_2^\cdot \rightarrow CH_3C(O)C(OOH)(CH_3)CH_2OH + O_2$	4.0×10^3
$CH_3C(O)CH(O_2^\cdot)OH + HO_2^\cdot \rightarrow CH_3C(O)CH(OOH)OH + O_2$	4.0×10^3
$(CH_3)_2CHC(O\cdot)(CH_3)_2 + NO_2 \rightarrow (CH_3)_2CHC(CH_3)_2ONO_2$	1.5×10^4
$(CH_3)_2CHO\cdot + NO_2 \rightarrow (CH_3)_2CHONO_2$	1.5×10^4
$(CH_3)_2CHO\cdot + NO_2 \rightarrow CH_3C(O)CH_3 + HONO$	2.9×10^3
$(CH_3)_2CHCH(CH_3)CH_2O\cdot + NO_2 \rightarrow (CH_3)_2CHCH(CH_3)CH_2ONO_2$	1.5×10^4
$(CH_3)_2CHCH(CH_3)CH_2O\cdot + NO_2 \rightarrow (CH_3)_2CHCH(CH_3)CHO + HONO$	2.9×10^3

* The inorganic, formaldehyde, and acetaldehyde reactions listed earlier must be added to construct the 2,3-dimethylbutane mechanism.

+ Rate constant in min^{-1}.

143

TABLE 22. INITIAL CONDITIONS AND PHOTOLYSIS RATE CONSTANTS FOR THE 2,3-DIMETHYLBUTANE/NO_x SMOG CHAMBER EXPERIMENTS

Run number	Initial concentration (ppm)				Photolysis rate constant ($x\ 10^4\ min^{-1}$)						
	2,3-Dimethyl-butane	NO	NO_2	HONO	$NO_2 \to NO+O^*$	$O_3 \to O(^1D)$	$O_3 \to O(^3P)$	$HONO \to NO+OH^*$	$H_2O_2 \to 2OH^*$	$FORM \to Products^+$	Acetone$\to$Products
EC-165	1.863	0.088	0.011	0.003	0.33	10.0	97.7	917	3.8	12	4
EC-169	0.725	0.127	0.064	0.013	0.33	5.0	97.7	917	3.8	12	2
EC-171	0.586	0.086	0.013	0.003	0.33	10.0	97.7	917	3.8	12	4

* Rate constant in min^{-1}.

+ The relationship between FORM→Products and carbonyl photolysis rate constants is discussed in Section 4.

TABLE 23. UCR 2,3-DIMETHYLBUTANE EXPERIMENTS--SIMULATIONS AND MEASUREMENTS

Exp. no.	Initial [NO_x] (ppm)	Initial NO_2/NO_x ratio	Initial HC/NO_x ratio (ppmC/ppm)	Maximum [O_3] (ppm)*		Difference in O_3 maxima (percent)+	Time to maximum [O_3] (minutes)§		Difference in times to O_3 maxima (percent)+	Maximum [NO_2] (ppm)		Difference in NO_2 maxima (percent)+	Time to maximum [NO_2] (minutes)§		Difference in times to NO_2 maxima (percent)+
				Sim.	Meas.		Sim.	Meas.		Sim.	Meas.		Sim.	Meas.	
EC-165	0.099	0.11	112.9	0.51	0.48	6	270	350	-23	0.077	0.057	35	110	60	83
EC-169	0.191	0.34	22.8	0.54	0.49	10	500	590	-15	0.15	0.11	36	90	105	-14
EC-171	0.099	0.13	35.5	0.40	0.40	0	400	420	- 5	0.071	0.052	37	160	65	146

O_3 maxima: average difference = 10 percent; standard deviation = 22 percent.
NO_2 maxima: average difference = -11 percent; standard deviation = 20 percent.

* Maximum one-hour-average concentration.

+ [(Simulated Value - Measured Value) / Measured Value] x 100.

§ Time from beginning of irradiation to beginning of the period during which the maximum one-hour-average concentration occurred.

144

(a) O_3
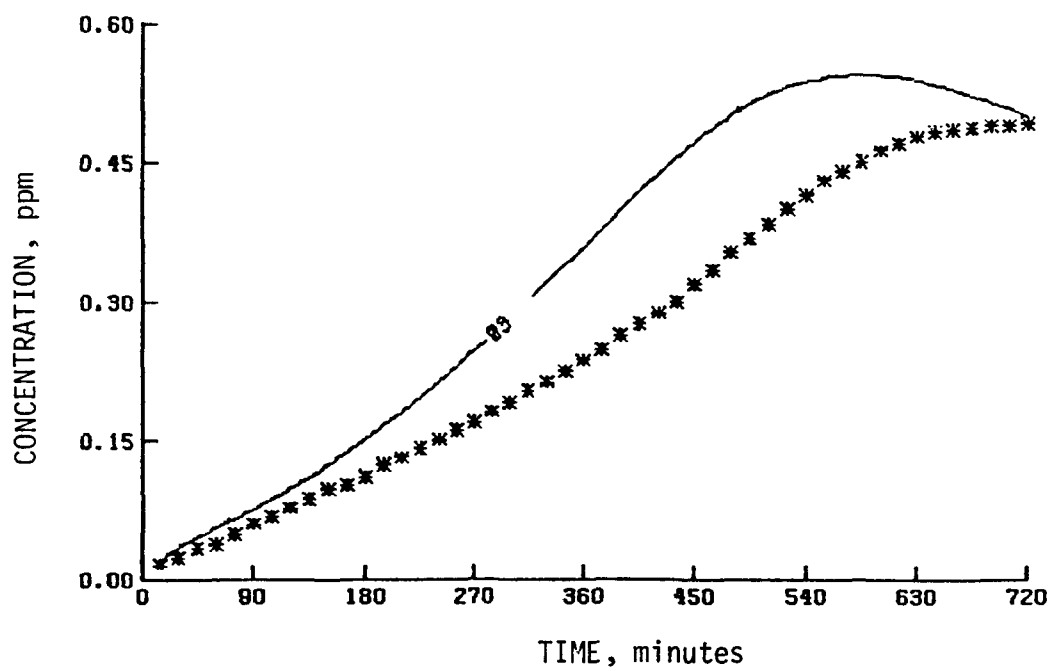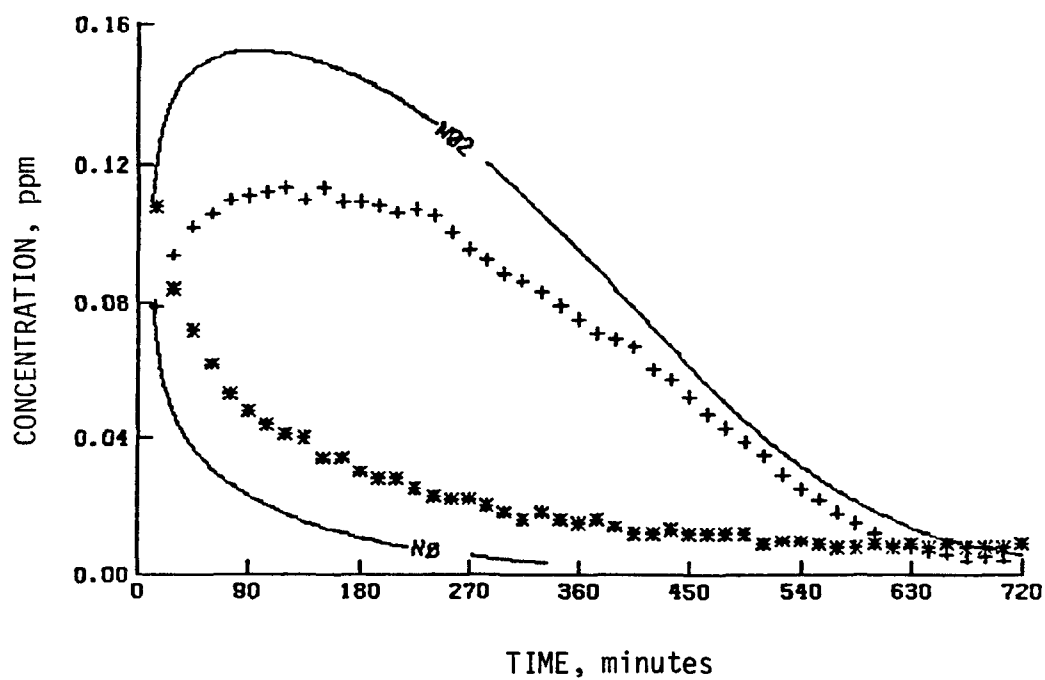
(b) NO_2 and NO

Figure 38. Simulation results of a UCR 2,3-dimethylbutane experiment (EC-169)

145
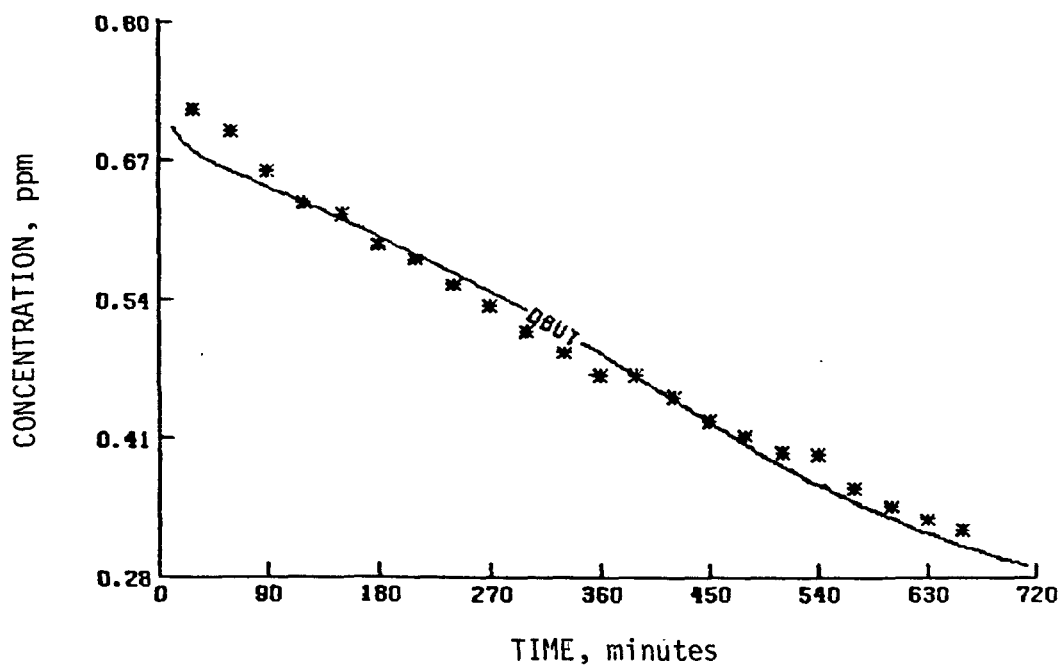
(a) 2,3-Dimethylbutane
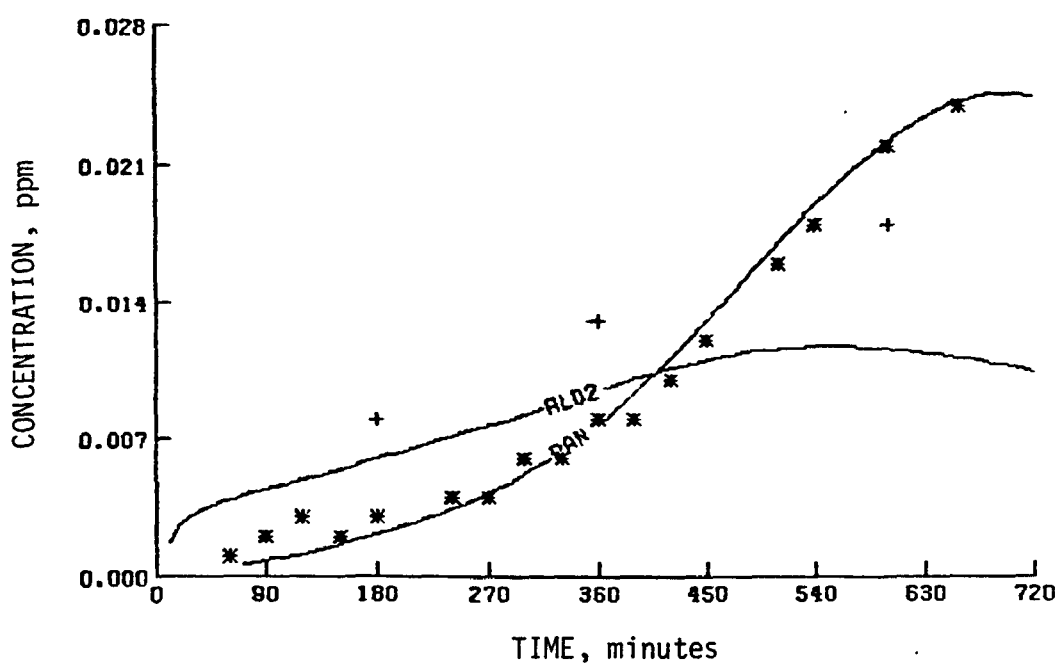
(b) Acetaldehyde and PAN

Figure 39. Simulation results of a UCR 2,3-dimethylbutane experiment (EC-169) for 2,3-dimethylbutane, acetaldehyde, and PAN
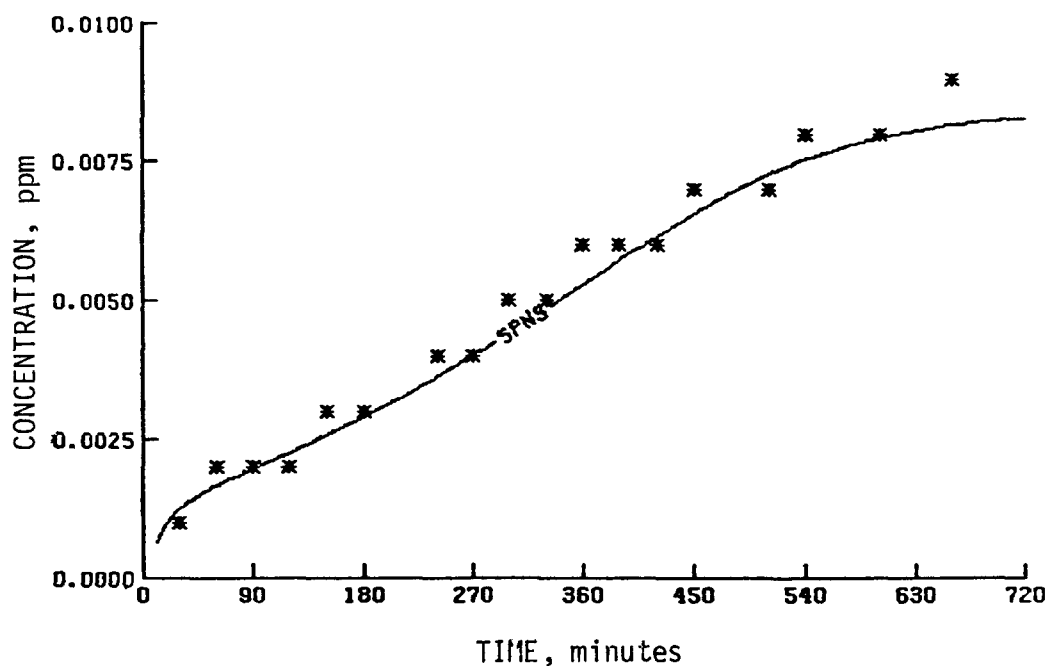
(a) Isopropyl nitrate
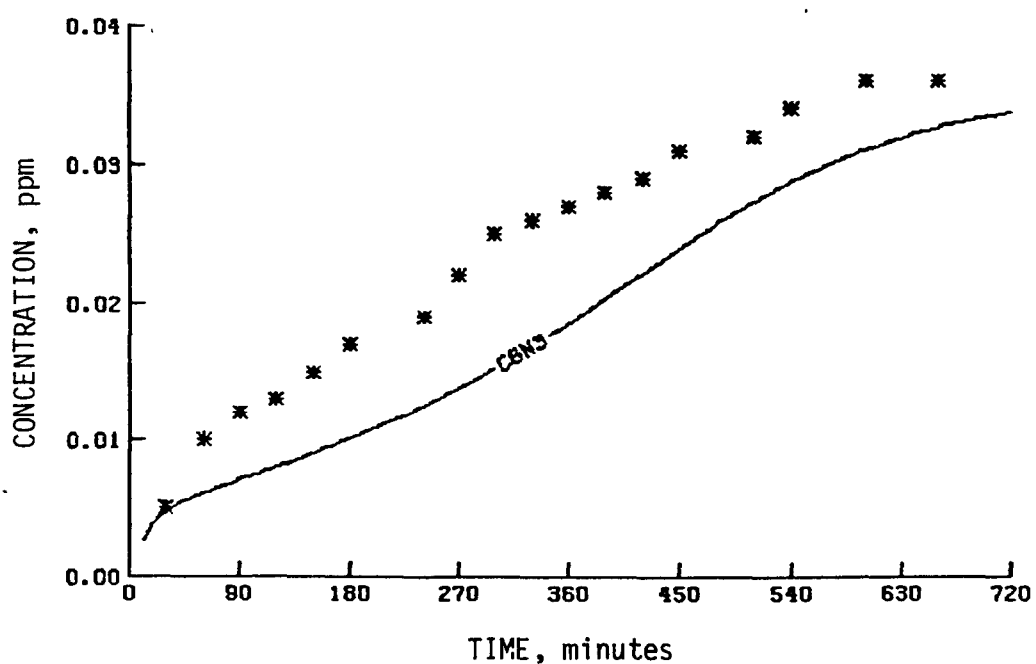
(b) 2,3-Dimethylbutyl nitrate

Figure 40. Simulation results of a UCR 2,3-dimethylbutane experiment (EC-169) for isopropyl nitrate and 2,3-dimethylbutyl nitrate

147

interest is the validation of the combinations of explicit mechanisms used to simulate the multiolefin/NO_x systems. UCR performed the following multiolefin experiments:

> Ethylene/propylene/NO_x (three experiments),
> Propylene/trans-2-butene/NO_x (one experiment),
> Ethylene/propylene/1-butene/trans-2-butene/NO_x (five experiments).

The simulations of these three multiolefin/NO_x systems are discussed in turn below:

Propylene/Butane Simulations

Before discussing the multiple olefin experiments, we discuss the simulations of the propylene/butane/NO_x experiments performed at UCR. Our investigation of these experiments began earlier and was documented by Whitten and Hogo (1977). During this study, we updated the rate constants of various reactions in the explicit propylene and butane mechanisms, as discussed earlier, and combined them to create the propylene/butane kinetic mechanism.

The initial conditions for the propylene/butane simulations are presented in Table 24 along with the photolysis rate constants used in the simulations. Simulated maximum one-hour-average NO_2 and O_3 concentrations are presented in Table 25. The results of the computer simulations are shown in Figures 41 through 47 for EC-113 and EC-114.

Ethylene/Propylene Simulations

Three experiments were performed at UCR using ethylene and propylene as initial hydrocarbons. The kinetic mechanism used to simulate the ethylene/propylene experiments is a combination of the explicit mechanisms for ethylene and propylene. The initial conditions and photolysis rate constants for the ethylene/propylene experiments are presented in Table 26,

TABLE 24. INITIAL CONDITIONS AND PHOTOLYSIS RATE CONSTANTS FOR THE PROPYLENE/BUTANE/NO$_x$ SMOG CHAMBER EXPERIMENTS

Run number	Initial concentration (ppm)					Photolysis rate constant ($\times 10^4$ min^{-1})					
	Propylene	Butane	NO	NO$_2$	HONO	NO$_2$·NO+O*	O$_3$·O(^{1}D)	O$_3$·O(^{3}P)	HONO·NO+OH·	H$_2$O$_2$·2OH·	FORM+Products[†]
EC-97	0.5	2.05	0.397	0.088	0.012	0.351	8	270	920	5.5	12
EC-99	0.4	2.0	0.407	0.09	0.015	0.351	8	270	920	5.5	12
EC-106	0.402	2.0	0.401	0.102	0.01	0.351	8	270	920	5.5	10
EC-113	0.43	2.08	0.91	0.021	0.0015	0.351	8	270	920	5.5	10
EC-114	0.758	3.67	0.794	0.205	0.025	0.351	8	270	920	5.5	10
EC-115	0.31	2.94	0.402	0.104	0.01	0.351	8	270	920	5.5	9
EC-116	0.824	4.0	0.391	0.104	0.01	0.351	8	270	920	5.5	9

* Rate constant in min^{-1}.

† The relationship between FORM+Products and carbonyl photolysis rate constants is discussed in Section 4.

TABLE 25. UCR PROPYLENE/BUTANE EXPERIMENTS--SIMULATIONS AND MEASUREMENTS

Exp. no.	Initial [NO$_x$] (ppm)	Initial NO$_2$/NO$_x$ ratio	Initial HC/NO$_x$ ratio (ppmC/ppm)	Maximum [O$_3$] (ppm)*		Difference in O$_3$ maxima (percent)†	Time to maximum [O$_3$] (minutes)§		Difference in times to O$_3$ maxima (percent)†	Maximum [NO$_2$] (ppm)		Difference in NO$_2$ maxima (percent)†	Time to maximum [NO$_2$] (minutes)§		Difference in times to NO$_2$ maxima (percent)†
				Sim.	Meas.		Sim.	Meas.		Sim.	Meas.		Sim.	Meas.	
EC-97	0.49	0.18	20	0.63	0.56	13	220	200	10	0.40	0.33	21	70	60	17
EC-99	0.50	0.18	19	0.63	0.54	17	250	250	0	0.40	0.34	18	80	70	14
EC-106	0.50	0.20	18	0.64	0.59	8	280	250	12	0.40	0.34	18	90	90	0
EC-113	0.11	0.19	85	0.37	0.34	9	120	100	20	0.09	0.08	13	40	30	33
EC-114	1.0	0.21	17	0.82	0.73	12	300	300	0	0.79	0.70	13	100	90	11
EC-115	0.51	0.21	13	0.69	0.59	17	340	340	0	0.37	0.36	3	110	90	22
EC-116	0.50	0.21	37	0.70	0.73	-4	170	150	13	0.41	0.36	14	60	60	0

O$_3$ maxima: average difference = 10 percent; standard deviation = ±7 percent.

NO$_2$ maxima: average difference = 14 percent; standard deviation = ±6 percent.

* Maximum one-hour-average concentration.

† [(Simulated Value - Measured Value) / Measured Value] x 100.

§ Time from beginning of irradiation to beginning of the period during which the maximum one-hour-average concentration occurred.
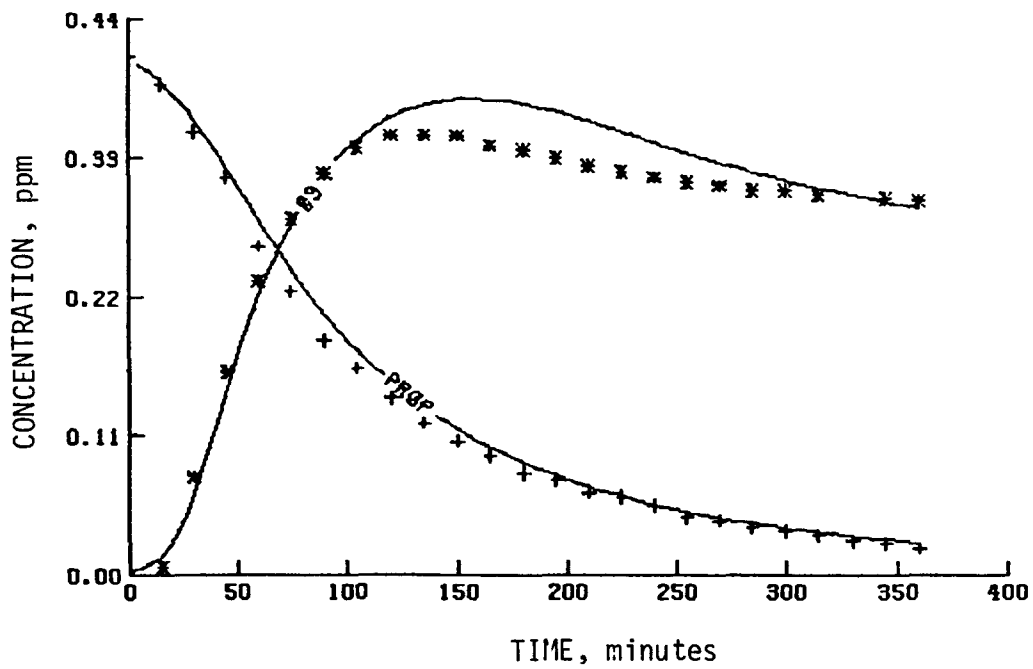
(a) Propylene and O_3
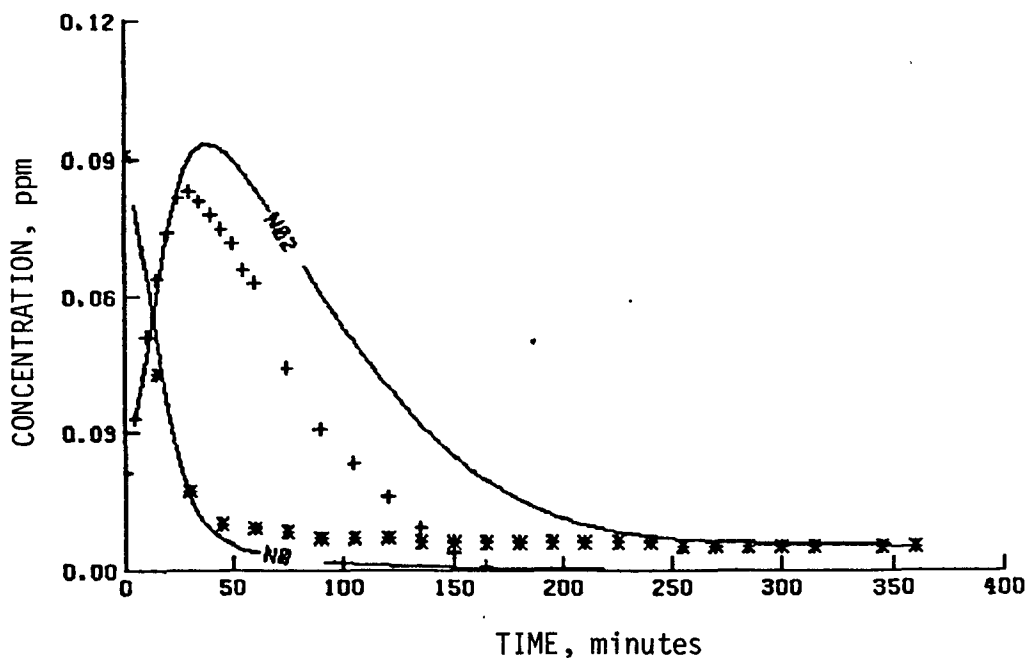
(b) NO_2 and NO

Figure 41. Simulation results of a UCR propylene/butane experiment (EC-113) for propylene, O_3, NO_2, and NO
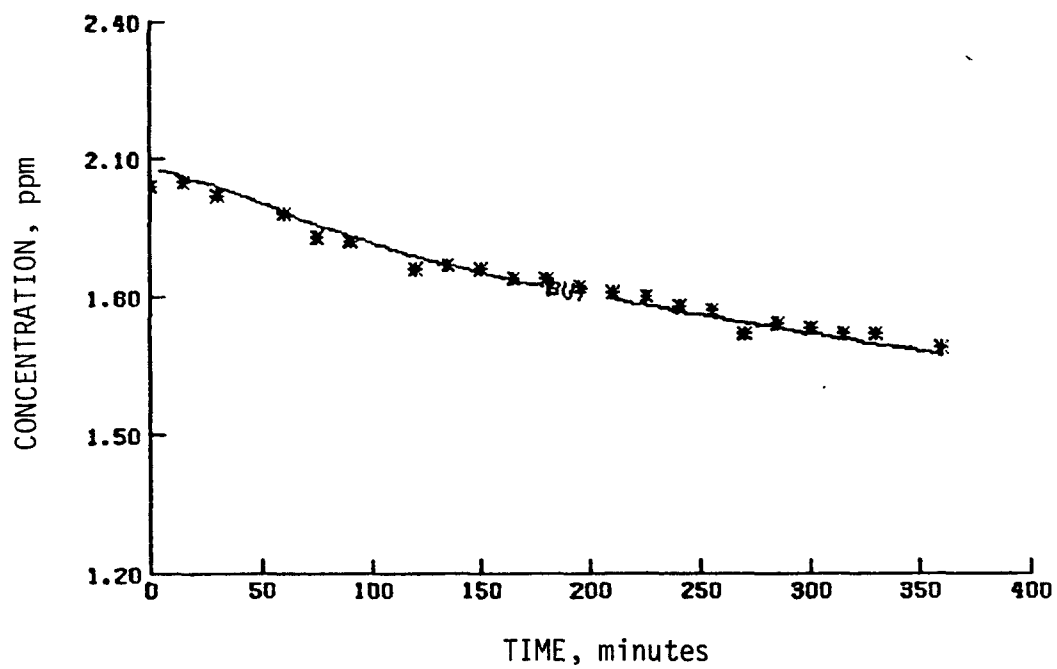
(a) Butane
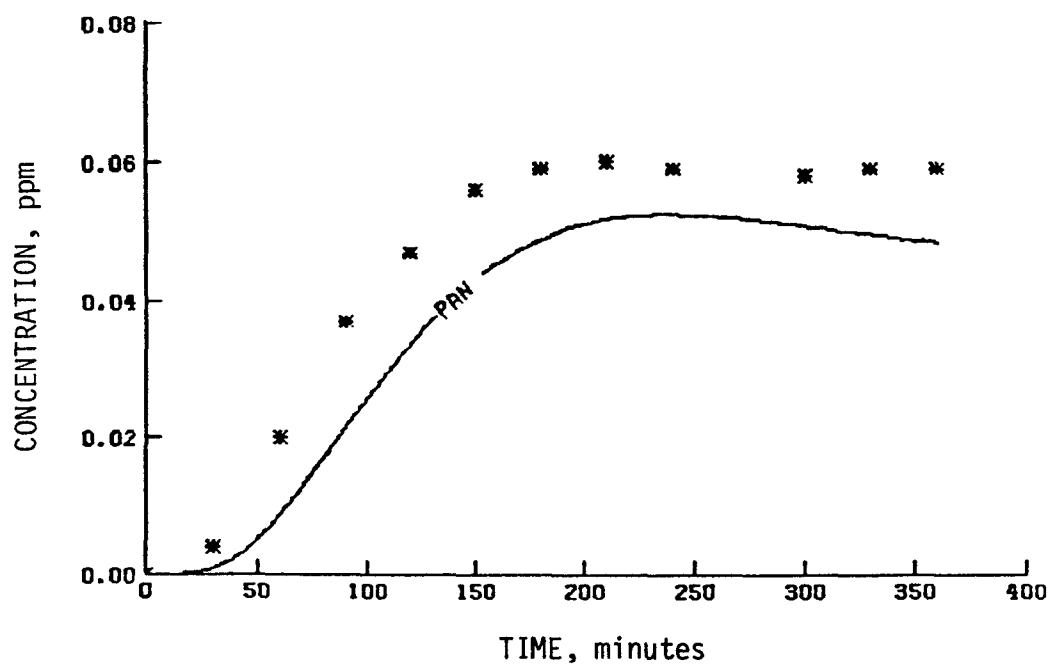
(b) PAN

Figure 42. Simulation results of a UCR propylene/butane experiment (EC-113) for butane and PAN

151
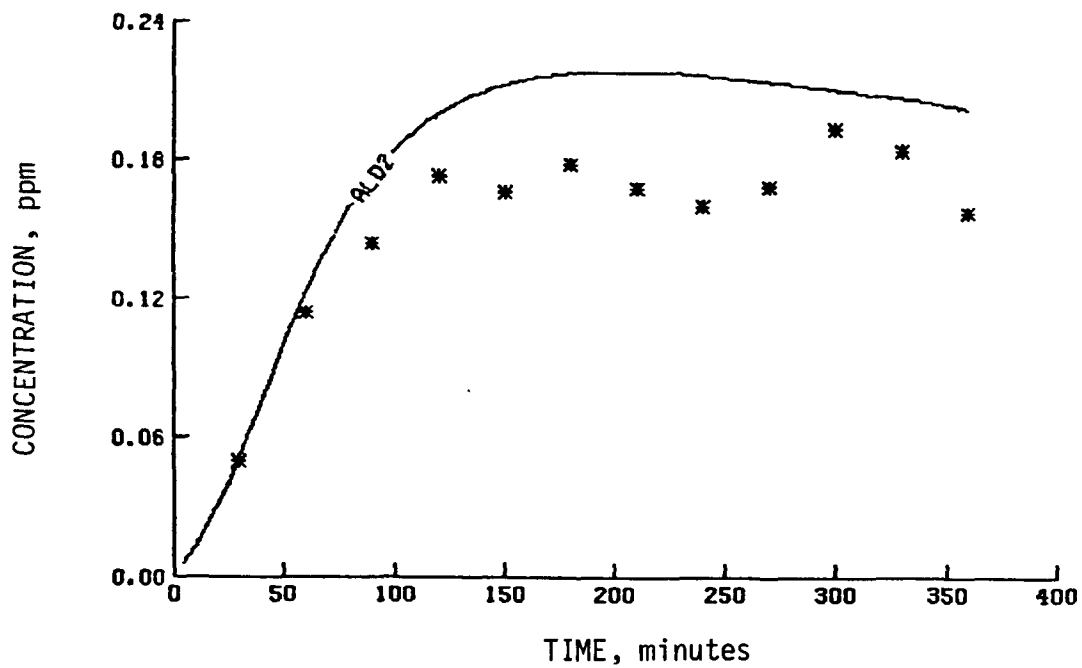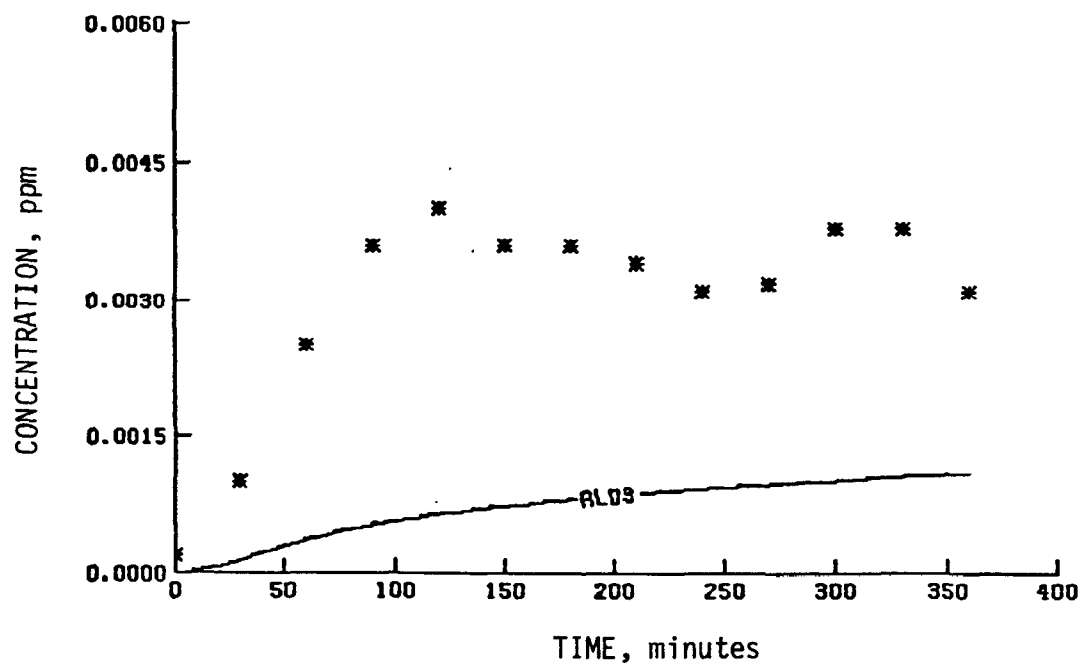
Figure 43. Simulation results of a UCR propylene/butane experiment (EC-113) for acetaldehyde and propionaldehyde
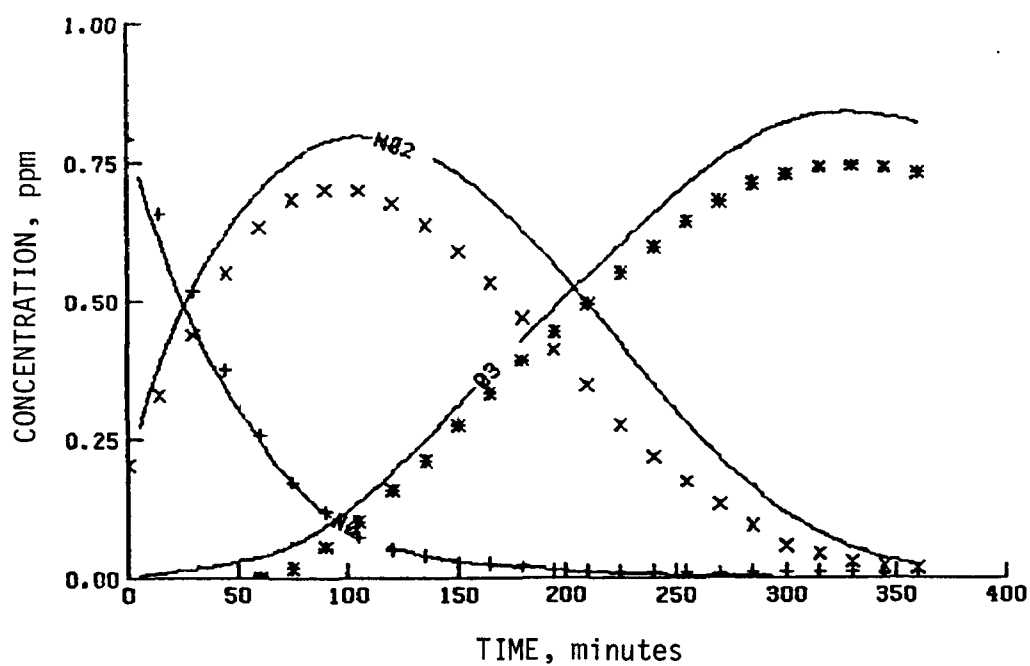
(a) NO_2, NO, and O_3
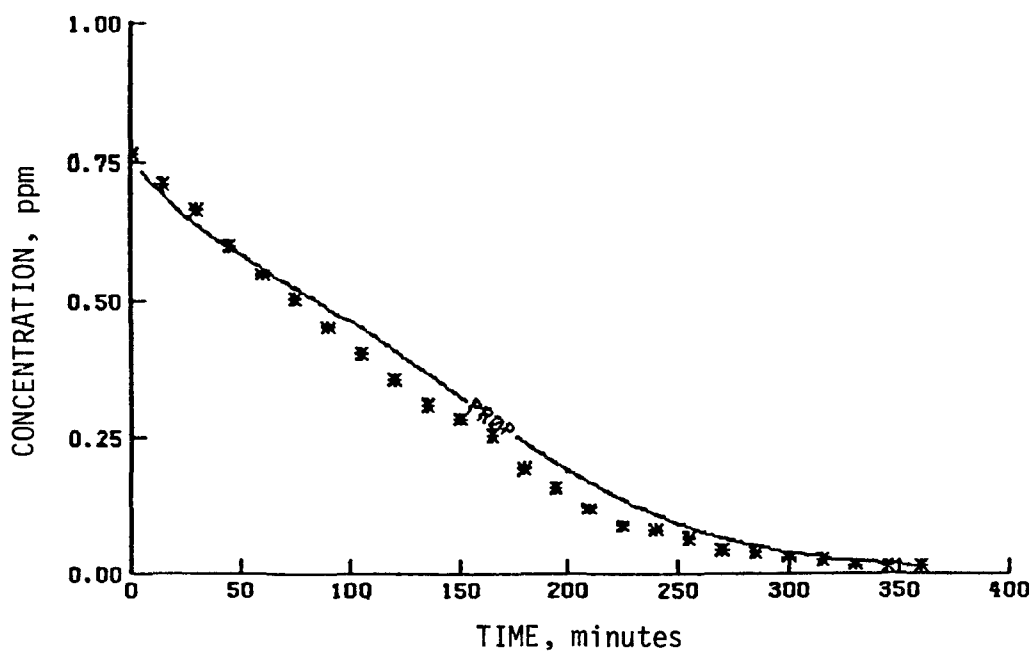
(b) Propylene

Figure 44.   Simulation results of a UCR propylene/butane experiment
(EC-119) for NO_2, NO, O_3, and propylene
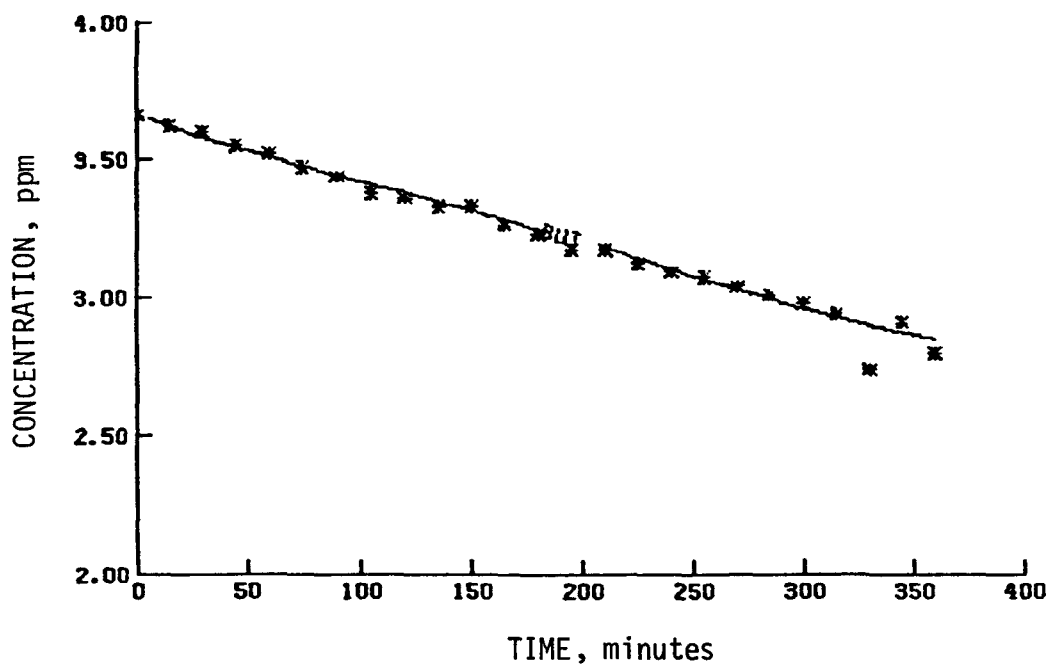
(a) Butane
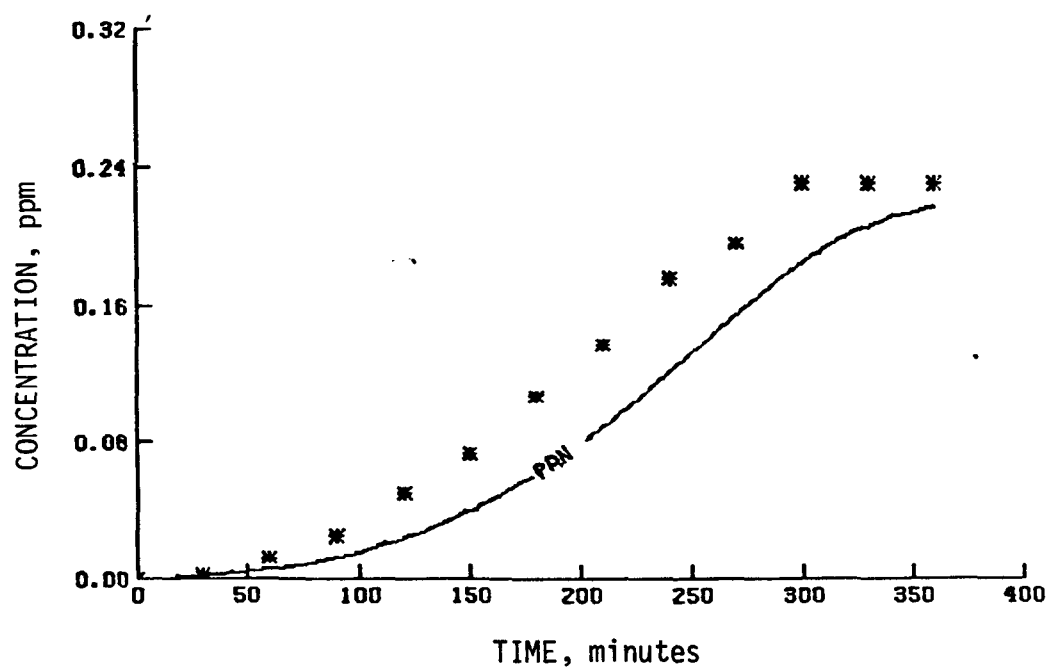
(b) PAN

Figure 45. Simulation results of a UCR propylene/butane experiment (EC-114) for butane and PAN

154
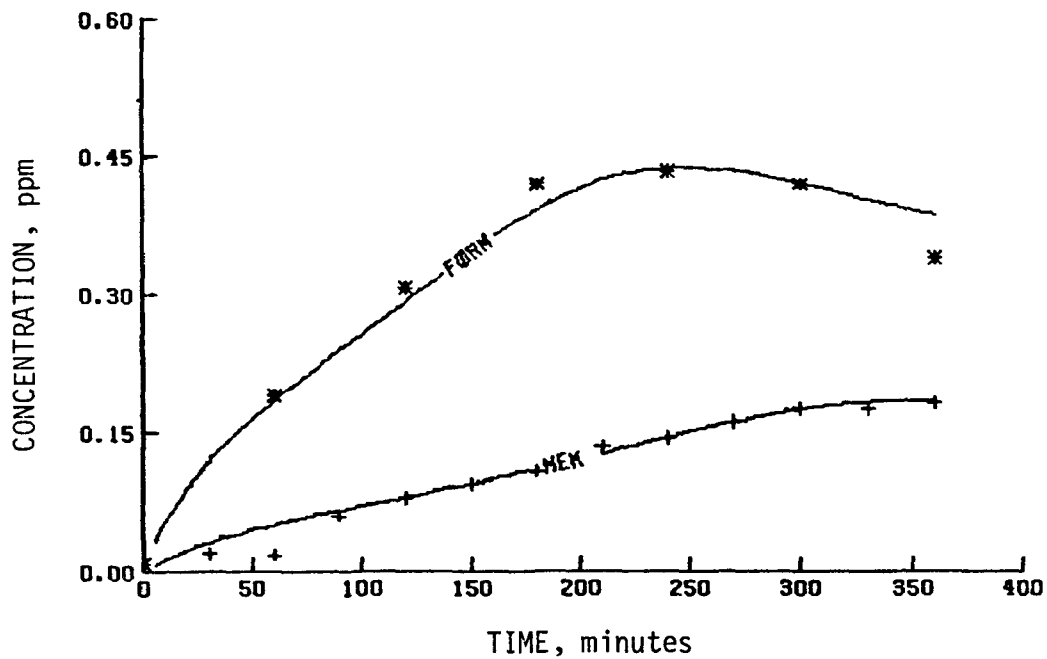
(a) MEK and formaldehyde
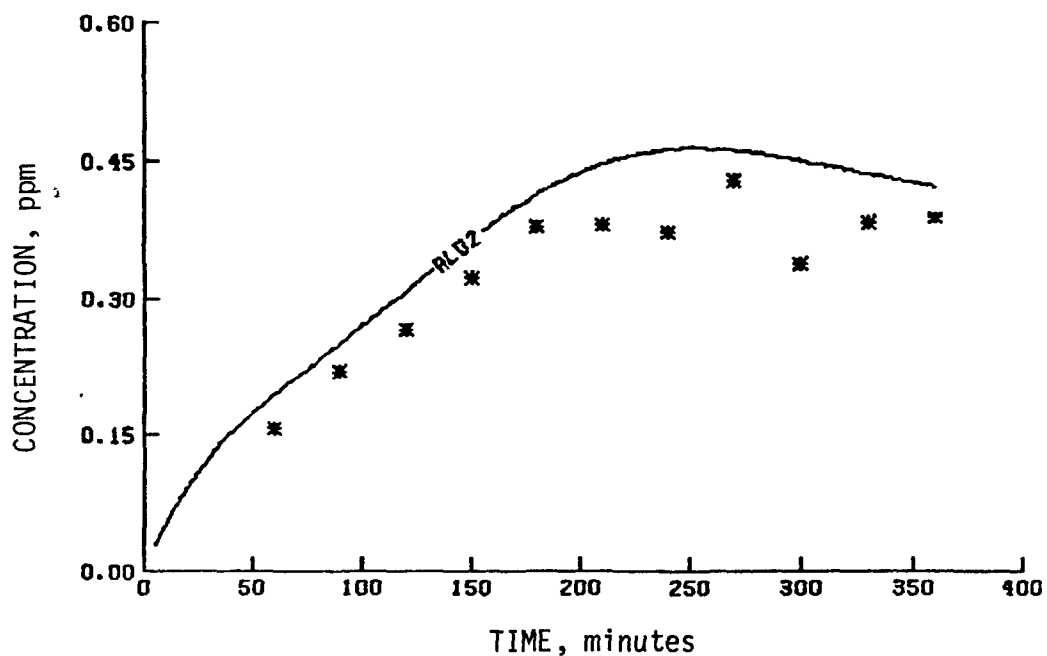
(b) Acetaldehyde

Figure 46.   Simulation results of a UCR propylene/butane experiment (EC-114)
for methylethylketone, formaldehyde, and acetaldehyde

155
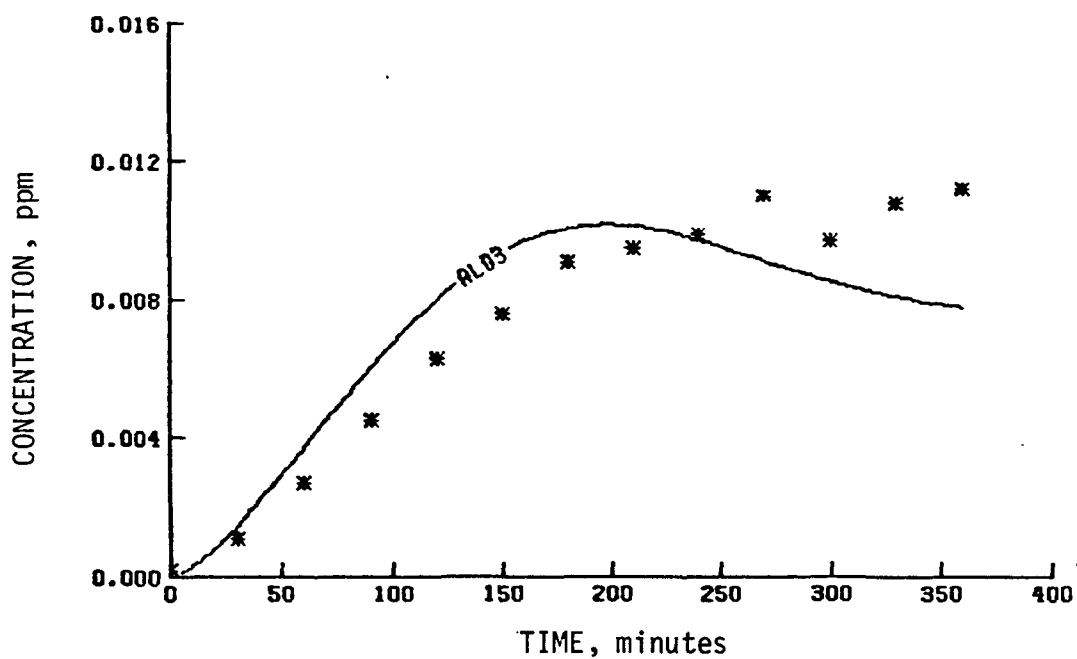
(a) Propionaldehyde
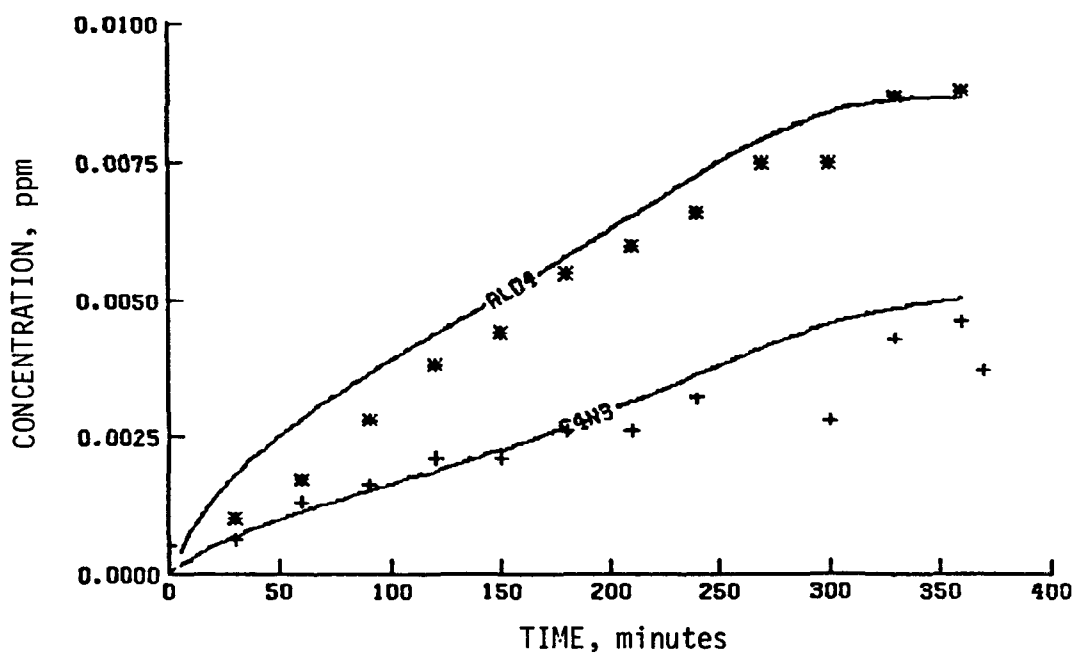
(b) n-Butyl nitrate and butyraldehyde

Figure 47. Simulation results of a UCR propylene/butane experiment (EC-114) for propionaldehyde, n-butyl nitrate, and butyraldehyde

TABLE 26. INITIAL CONDITIONS AND PHOTOLYSIS RATE CONSTANTS FOR THE ETHYLENE/PROPYLENE/NO_x SMOG CHAMBER EXPERIMENTS

Run number	Initial concentration (ppm)					Photolysis rate constant ($\times 10^4$ min^{-1})					
	Ethylene	Propylene	NO	NO_2	HONO	$NO_2 \rightarrow NO+O^*$	$O_3 \rightarrow O(^1D)$	$O_3 \rightarrow O(^3P)$	$HONO \rightarrow NO+OH^*$	$H_2O_2 \rightarrow 2OH^*$	$FORM \rightarrow Products$[+]
EC-144	2.027	0.221	0.398	0.111	0.013	0.33	2.5	97	900	3.6	11
EC-145	1.05	0.428	0.745	0.246	0.020	0.34	12.8	102	900	3.6	11
EC-160	1.014	0.39	0.752	0.241	0.03	0.34	12.8	.102	900	4.0	12

* Rate constant in min^{-1}.

+ The relationship between FORM$\rightarrow$Products and carbonyl photolysis rate constants is discussed in Section 4.

157

and the measured and simulated NO_2 and O_3 maxima are given in Table 27. A sample simulation result is shown in Figure 48 for EC-145.

The Propylene/Trans-2-Butene Simulation

Only one propylene/trans-2-butene experiment was performed at UCR. The initial conditions for this experiment and the photolysis rate constants for the computer simulations are presented in Table 28, and the measured and simulated O_3 in Table 29. The kinetic mechanism used in the computer simulation is a combination of the individual propylene and trans-2-butene mechanisms. Figure 49 shows the simulation results. Since the major product from trans-2-butene is acetaldehyde, the simulation becomes an acetaldehyde/propylene situation shortly after the start. The results are very similar in appearance to those for the simulation of the propylene experiment with added acetaldehyde (EC-217). The computer simulations show that radicals generated in the current mechanism can account for the consumption of either acetaldehyde or propylene in EC-217, but not both.

The competition for OH· radicals in simulations of EC-217 occurs mainly between three reactions:

$$CO + OH \cdot \xrightarrow{O_2} HO_2^{\cdot} + CO_2 \qquad k = 4.4 \times 10^2 \text{ ppm}^{-1}\text{min}^{-1} \qquad , \quad (71)$$

$$CH_3CH=CH_2 + OH \cdot \longrightarrow \text{Radical} \qquad k = 4.2 \times 10^4 \text{ ppm}^{-1}\text{min}^{-1} \qquad , \quad (72)$$

$$CH_3CHO + OH \cdot \xrightarrow{O_2} CH_3C(O)O_2^{\cdot} + H_2O \qquad k = 2.4 \times 10^4 \text{ ppm}^{-1}\text{min}^{-1} \qquad . \quad (73)$$
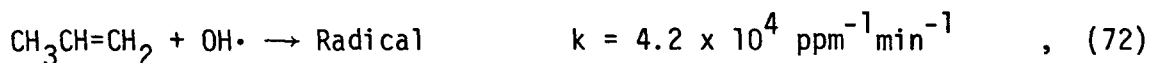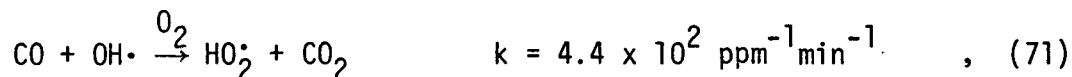
This competition implies several possible causes of the apparent lack of radicals. First, the propylene + OH· reaction may have a rate constant faster than the currently accepted value. Second, propylene may react with radicals other than OH·; for example, some RO· may react with propylene later in the simulation period. Third, the simulated propylene decay may be correct and the measurements wrong. Because of the low initial propylene concentration (0.08 ppm) in EC-217, the measurements of propylene may not

158

TABLE 27. UCR ETHYLENE/PROPYLENE EXPERIMENTS--SIMULATIONS AND MEASUREMENTS

Exp. no.	Initial [NOx] (ppm)	Initial NO2/NOx ratio	Initial HC/NOx ratio (ppmC/ppm)	Maximum [O3] (ppm)*		Difference in O3 maxima (percent)†	Time to maximum [O3] (minutes)§		Difference in times to O3 maxima (percent)†	Maximum [NO2] (ppm)		Difference in NO2 maxima (percent)†	Time to maximum [NO2] (minutes)§		Difference in times to NO2 maxima (percent)†
				Sim.	Meas.		Sim.	Meas.		Sim.	Meas.		Sim.	Meas.	
EC-144	0.51	0.22	9.3	0.90	1.05	-14	140	130	8	0.44	0.38	16	50	50	0
EC-145	0.99	0.25	3.3	0.86	0.66	30	>360	>360	--	0.75	0.63	19	120	100	20
EC-160	0.99	0.24	3.2	0.88	0.79	11	>360	>360	--	0.75	0.61	23	100	90	11

O_3 maxima: average difference = 9 percent; standard deviation = ±22 percent.
NO_2 maxima: average difference = 19 percent; standard deviation = ±4 percent.

* Maximum one-hour-average concentration.

† [(Simulated Value - Measured Value) / Measured Value] x 100.

§ Time from beginning of irradiation to beginning of the period during which the maximum one-hour-average concentration occurred.

TABLE 28. INITIAL CONDITIONS AND PHOTOLYSIS RATE CONSTANTS FOR THE PROPYLENE/TRANS-2-BUTENE SMOG CHAMBER EXPERIMENT

	Initial concentration (ppm)					Photolysis rate constant ($\times 10^4$ min^{-1})					
Run number	Propylene	t-2-Butene	NO	NO$_2$	HONO	NO$_2$→NO+O*	O$_3$→O(^{1}D)	O$_3$→O(^{3}P)	HONO→NO+OH·	H$_2$O$_2$→2OH·	FORM→Products[†]
EC-149	0.36	0.209	0.813	0.176	0.035	0.33	10.9	98.3	990	6.49	8

* Rate constant in min^{-1}.
† The relationship between FORM→Products and carbonyl photolysis rate constants is discussed in Section 4.

TABLE 29. UCR PROPYLENE/TRANS-2-BUTENE EXPERIMENT--SIMULATIONS AND MEASUREMENTS

Exp. no.	Initial [NO$_x$] (ppm)	Initial NO$_2$/NO$_x$ ratio	Initial HC/NO$_x$ ratio (ppmC/ppm)	Maximum [O$_3$] (ppm)* Sim.	Meas.	Difference in O$_3$ maxima (percent)[†]	Time to maximum [O$_3$] (minutes)§ Sim.	Meas.	Difference in times to O$_3$ maxima (percent)[†]	Maximum [NO$_2$] (ppm) Sim.	Meas.	Difference in NO$_2$ maxima (percent)[†]	Time to maximum [NO$_2$] (minutes)§ Sim.	Meas.	Difference in times to NO$_2$ maxima (percent)[†]
EC-149	0.99	0.18	1.94	0.27	0.25	9	>360	>360	--	0.73	0.58	26	130	70	66

* Maximum one-hour-average concentration.
† [(Simulated Value - Measured Value) / Measured Value] x 100.
§ Time from beginning of irradiation to beginning of the period during which the maximum one-hour-average concentration occurred.

160
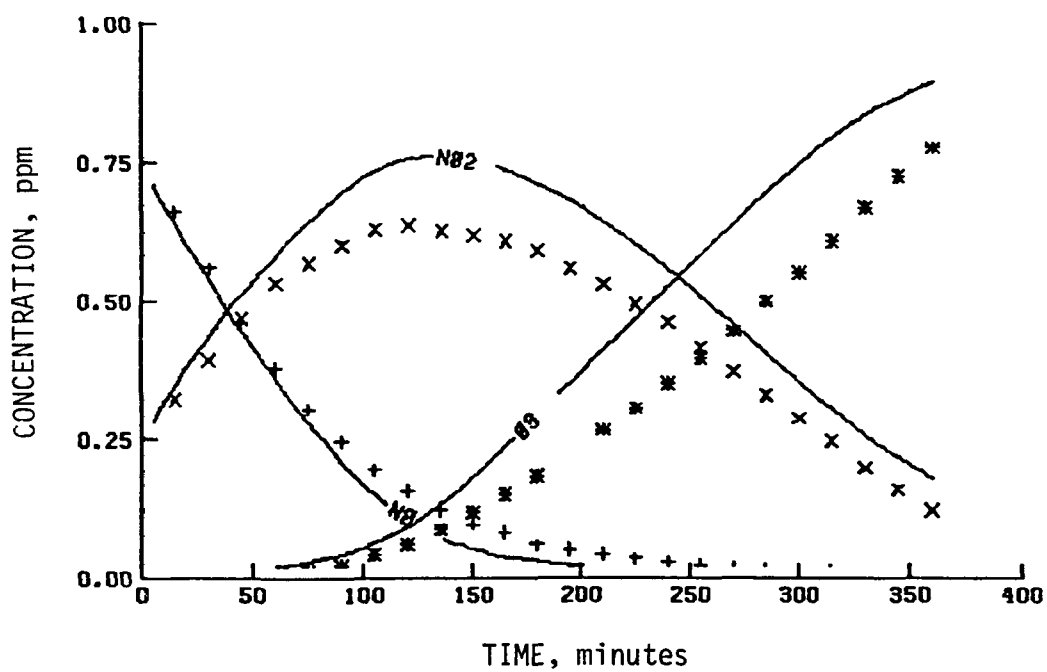
(a) NO_2, NO, and O_3
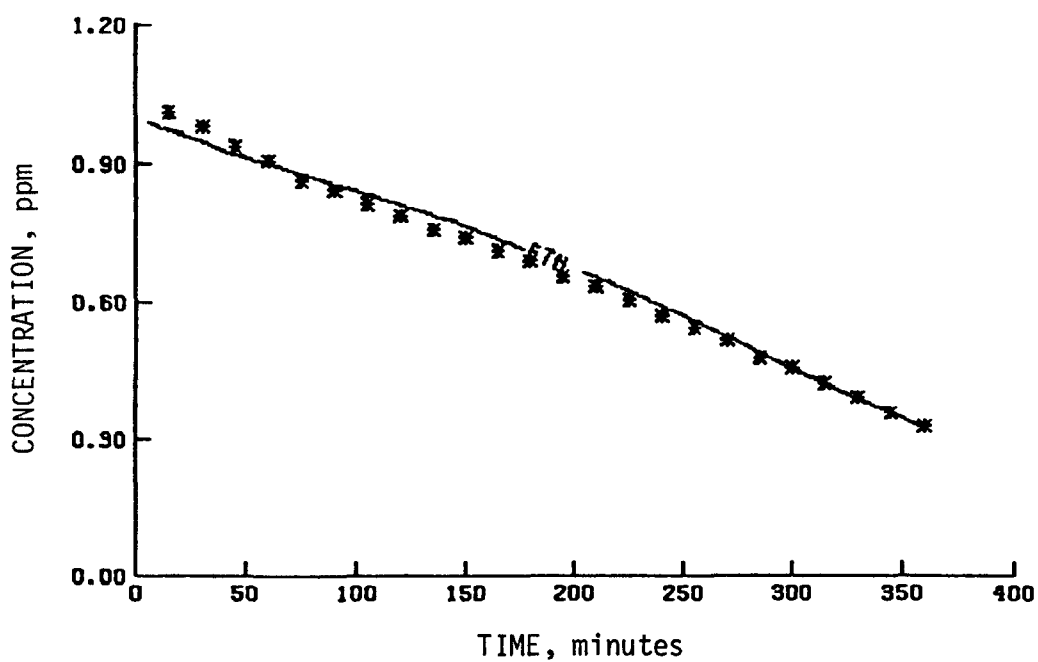
(b) Ethylene

Figure 48.   Simulation results of a UCR ethylene/propylene experiment
(EC-145)

161
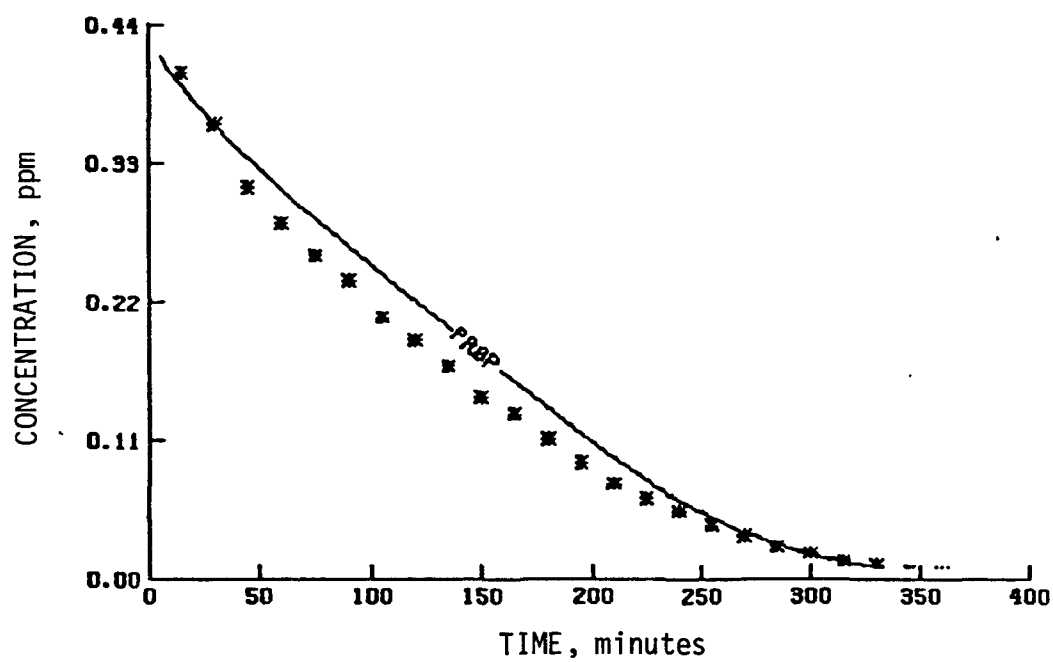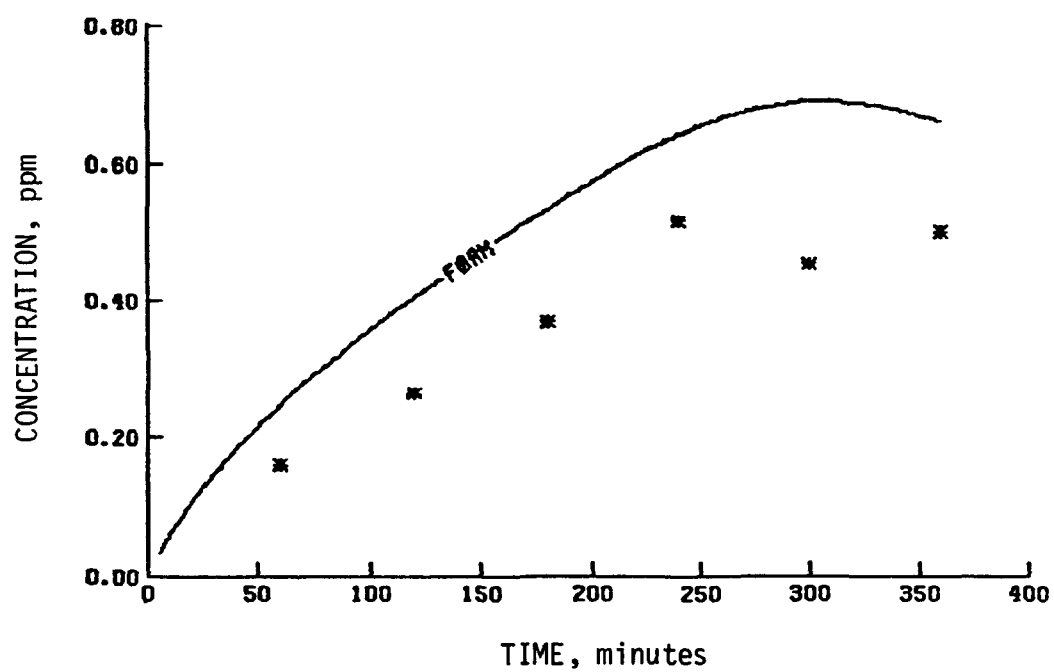
(c) Propylene

(d) Formaldehyde

Figure 48 (Continued)

162
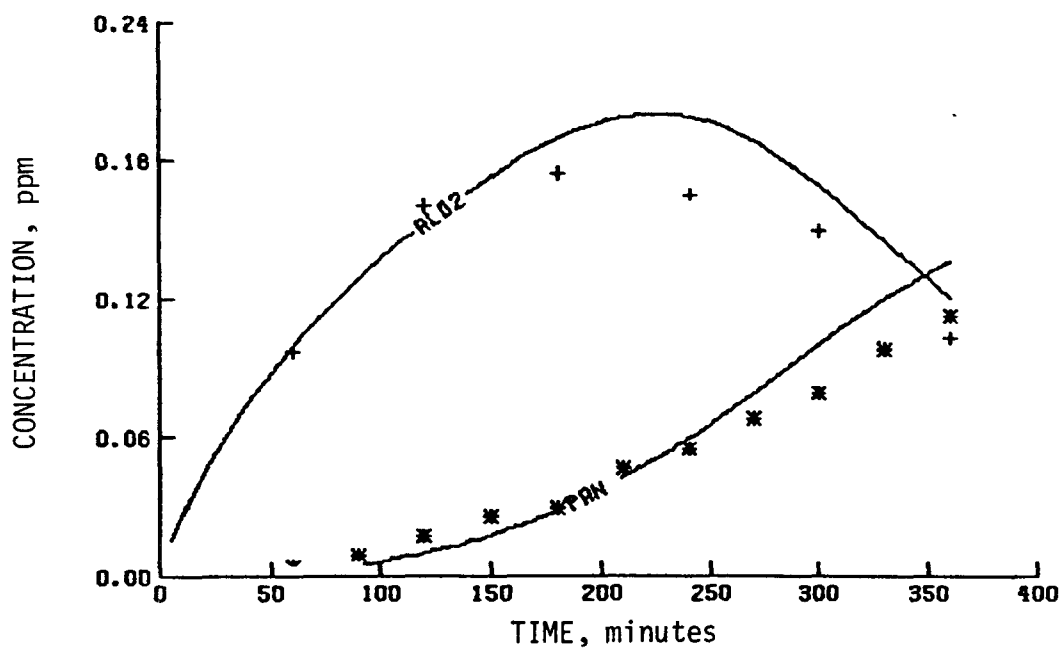
(e) Acetaldehyde and PAN
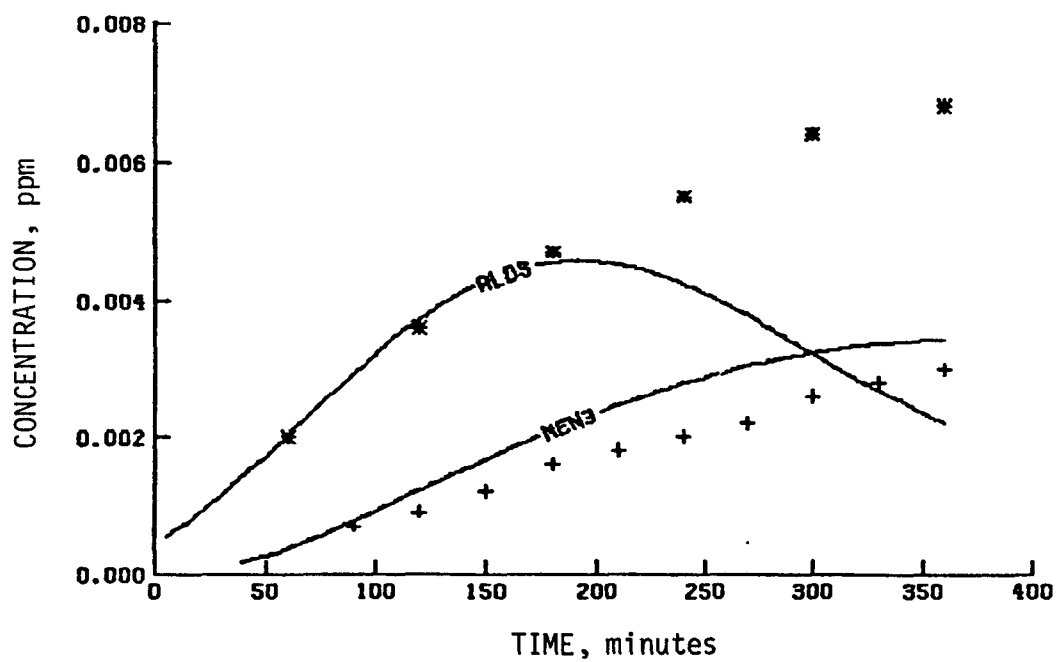
(f) Propionaldehyde and methyl nitrate

Figure 48 (Concluded)

163

(a) O_3
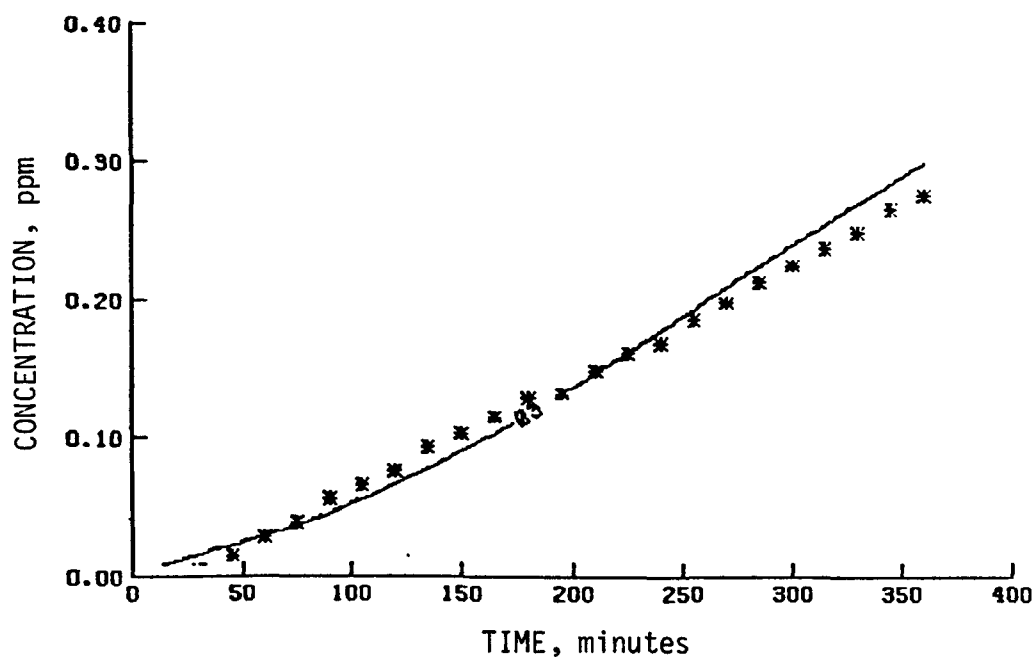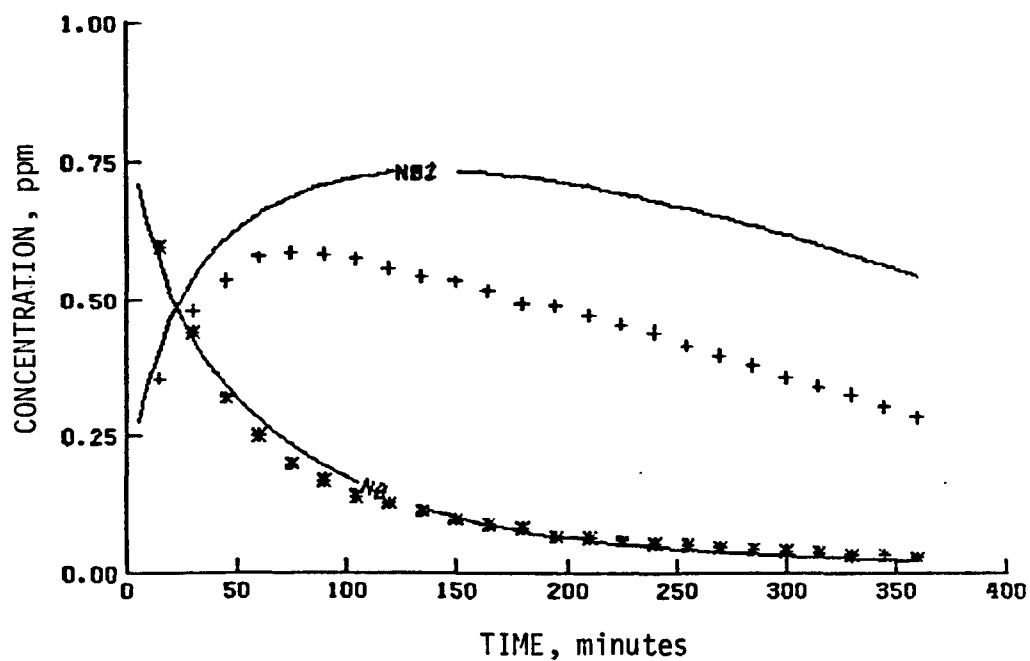
(b) NO_2 and NO

Figure 49. Simulation results of a UCR propylene/trans-2-butene
experiment (EC-149)

164
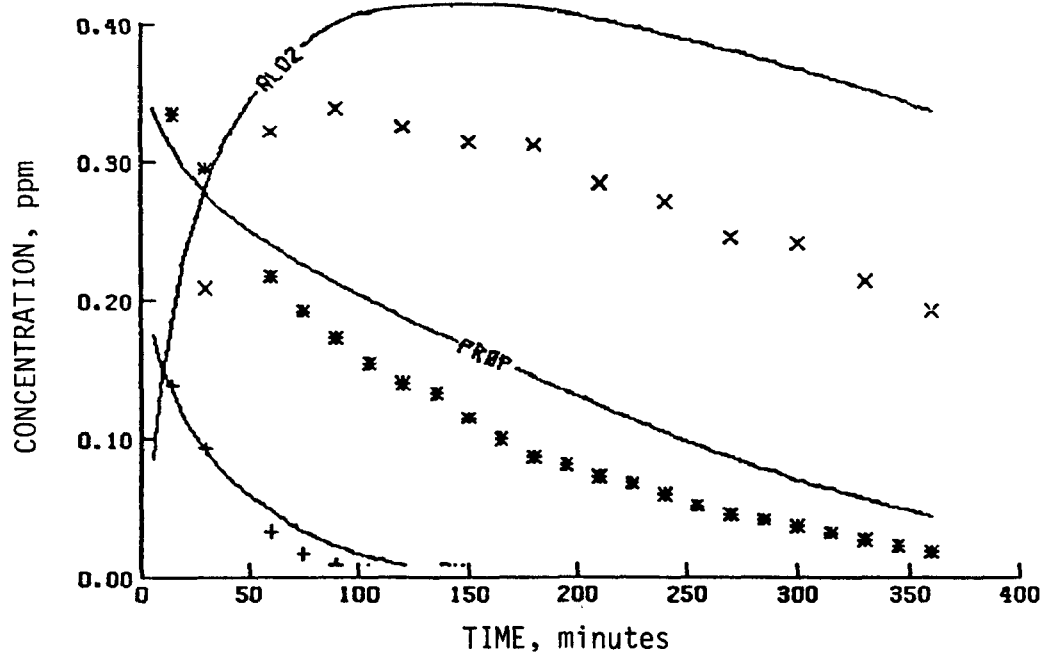
(c) Acetaldehyde, trans-2-butene, and propylene
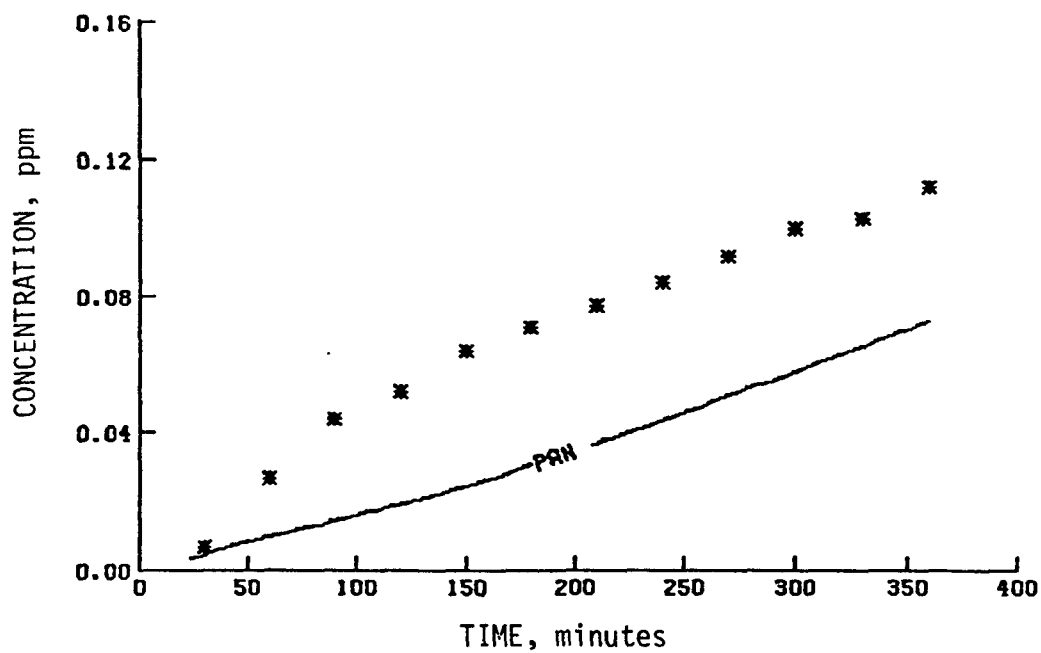
(d) PAN

Figure 49   (Continued)
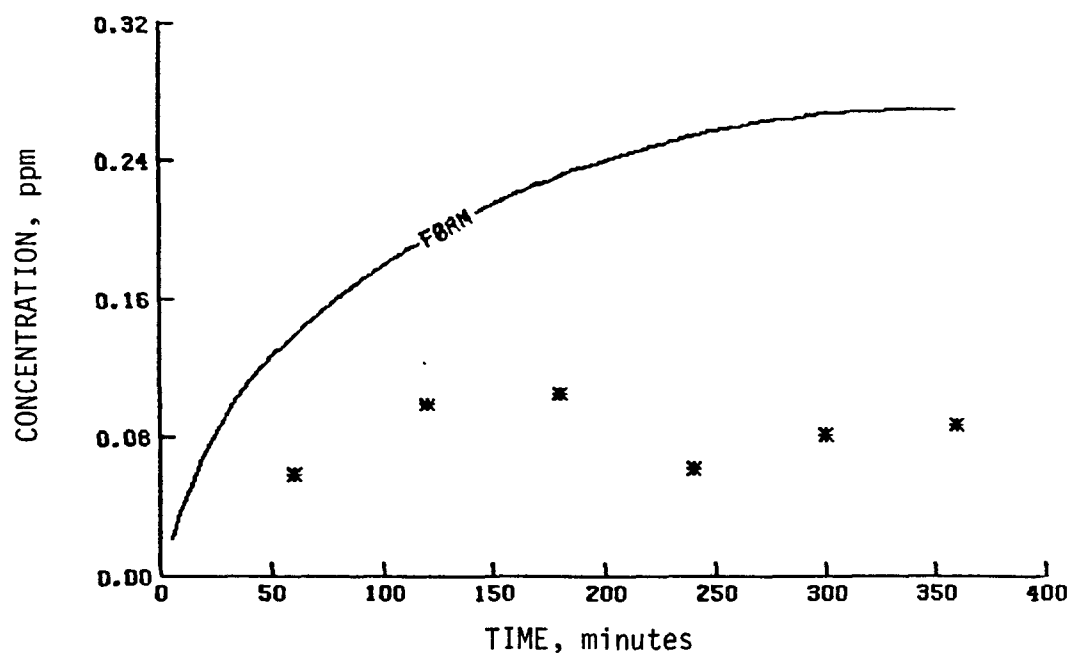
(e) Formaldehyde
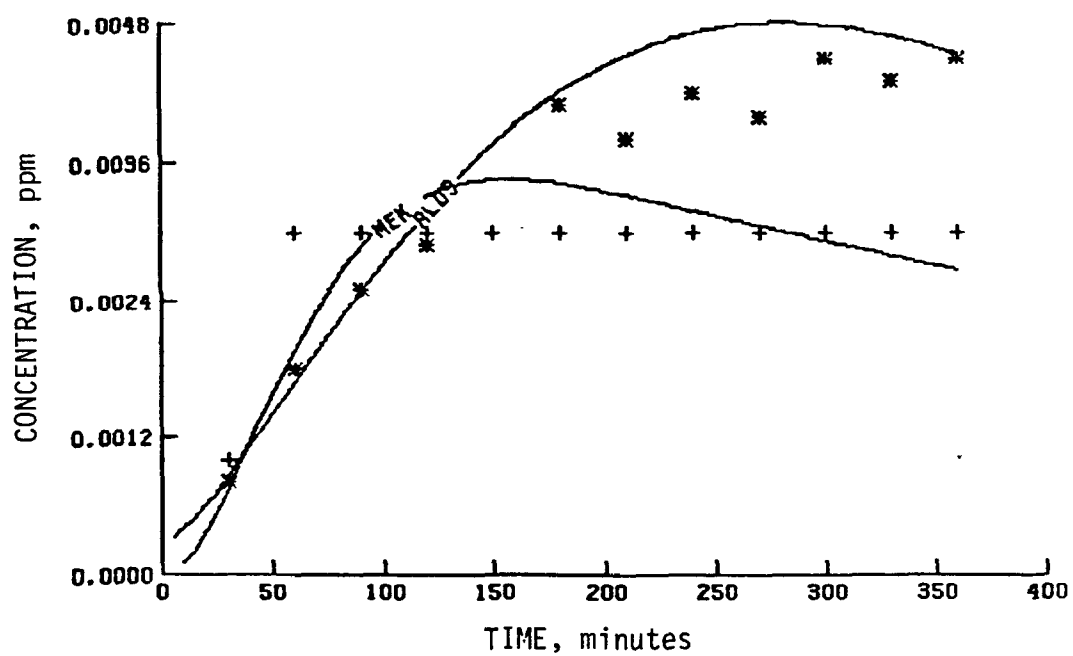
(f) MEK and propionaldehyde

Figure 49 (Continued)
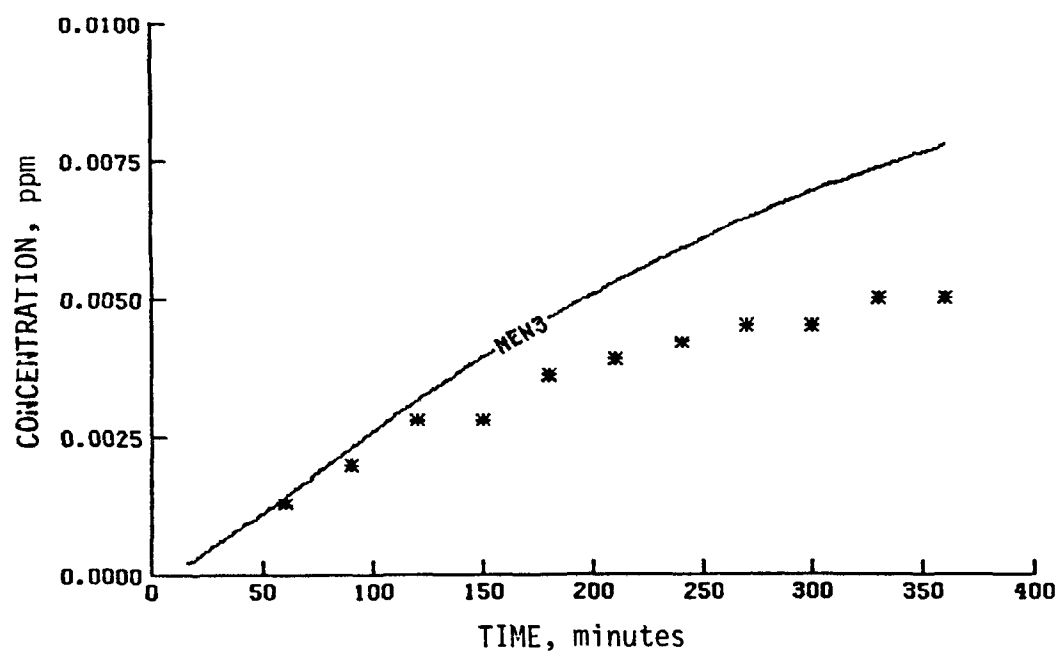
(g) Methyl nitrate

Figure 49 (Concluded)

be as accurate as measurements made in more typical runs (usually with propylene concentrations between 0.5 and 1.0 ppm). Fourth, the currently accepted value of Reaction (73) may be too fast, or the photolysis rate constant for acetaldehyde may be too low. The overall decay of acetaldehyde may be predicted correctly by adjusting the balance between the photolysis reactions and Reaction (73). If the photolysis reaction is faster and Reaction (73) is slower, we may still be able to follow the acetaldehyde decay and increase the radical concentration enough to simulate the propylene decay accurately. More detailed studies will be performed in the coming year to elucidate the possible effects of the causes discussed above.

Results of the Simulations of Multiolefin Systems

Five experiments were performed at UCR using different mixtures of the olefins ethylene, propylene, 1-butene, and trans-2-butene. The simulations of the ethylene/propylene and propylene/trans-2-butene experiments discussed earlier show that combining the individual explicit mechanisms is currently a sound method for simulating multiple hydrocarbon systems. The cumulation of the individual mechanisms leads to a four-olefin mechanism containing 140 reactions with 61 species. The initial conditions and photolysis rate constants used in the computer simulations are presented in Table 30. Simulated maximum one-hour-average NO_2 and O_3 concentrations are presented in Table 31. Figures 50 through 54 show the simulation results of the multiple-olefin systems.

The results of simulating EC-151 show a major overprediction of O_3 throughout the simulation [Figure 51(a)]. This run had an unusually high initial concentration of NO_x (2 ppm compared with 1 ppm in the other runs). In all of the simulations, the simulated O_3 induction period is slightly short, even though the time to $NO-NO_2$ crossover is simulated accurately. More work will be needed in the coming year to refine the predictions of the explicit multiolefin mechanism.

TABLE 30. INITIAL CONDITIONS AND PHOTOLYSIS RATE CONSTANTS FOR THE MULTIOLEFIN/NO$_x$ SMOG CHAMBER EXPERIMENTS

Run number	Initial concentration (ppm)							Photolysis rate constant ($\times 10^4$ min^{-1})					
	Ethylene	Propylene	1-Butene	t-2-Butene	NO	NO$_2$	HONO	NO$_2 \to$NO+O*	O$_3\to$O(^{1}D)	O$_3\to$O(^{3}P)	HONO$\to$NO+OH*	H$_2$O$_2\to$2OH*	FORM$\to$Products[†]
EC-150	1.00	0.224	0.100	0.093	0.774	0.222	0.02	0.33	10.9	98.3	900	6.49	10
EC-151	0.95	0.42	0.209	0.17	1.466	0.59	0.025	0.33	8	104	980	6.88	11
EC-152	1.015	0.116	0.222	0.102	0.398	0.104	0.010	0.35	8	104	900	6.88	12
EC-153	1.900	0.100	0.415	0.193	0.774	0.197	0.020	0.34	10.4	94	900	6.2	12
EC-161	0.908	0.099	0.189	0.088	0.386	0.123	0.025	0.33	10.9	98.3	900	6.49	12

* Rate constant in min^{-1}.

† The relationship between FORM$\to$Products and carbonyl photolysis rate constants is discussed in Section 4.

TABLE 31. UCR MULTIOLEFIN EXPERIMENTS--SIMULATIONS AND MEASUREMENTS

Exp. no.	Initial [NO$_x$] (ppm)	Initial NO$_2$/NO$_x$ ratio	Initial HC/NO$_x$ ratio (ppmC/ppm)	Maximum [O$_3$] (ppm)*		Difference in O$_3$ maxima (percent)†	Time to maximum [O$_3$] (minutes)§		Difference in times to O$_3$ maxima (percent)†	Maximum [NO$_2$] (ppm)		Difference in NO$_2$ maxima (percent)†	Time to maximum [NO$_2$] (minutes)§		Difference in times to NO$_2$ maxima (percent)†
				Sim.	Meas.		Sim.	Meas.		Sim.	Meas.		Sim.	Meas.	
EC-150	0.996	0.22	3.5	0.79	0.70	12	>360	>360	--	0.77	0.53	45	100	90	11
EC-151	2.1	0.29	2.3	0.38	0.11	245	>360	>360	--	1.40	1.11	26	170	120	42
EC-152	0.5	0.21	7.3	0.75	0.77	-3	180	180	0	0.42	0.36	17	50	50	0
EC-153	0.97	0.20	6.7	1.01	0.96	5	170	170	0	0.82	0.71	15	45	45	0
EC-161	0.51	0.24	6.3	0.73	0.82	-11	180	180	0	0.43	0.37	16	30	40	-25

O$_3$ maxima: average difference = 1 percent (excluding EC-151); standard deviation = ±10 percent (excluding EC-151).

NO$_2$ maxima: average difference = 24 percent (excluding EC-151); standard deviation = ±13 percent (excluding EC-151).

* Maximum one-hour-average concentration.

† [(Simulated Value - Measured Value) / Measured Value] × 100.

§ Time from beginning of irradiation to beginning of the period during which the maximum one-hour-average concentration occurred.

169
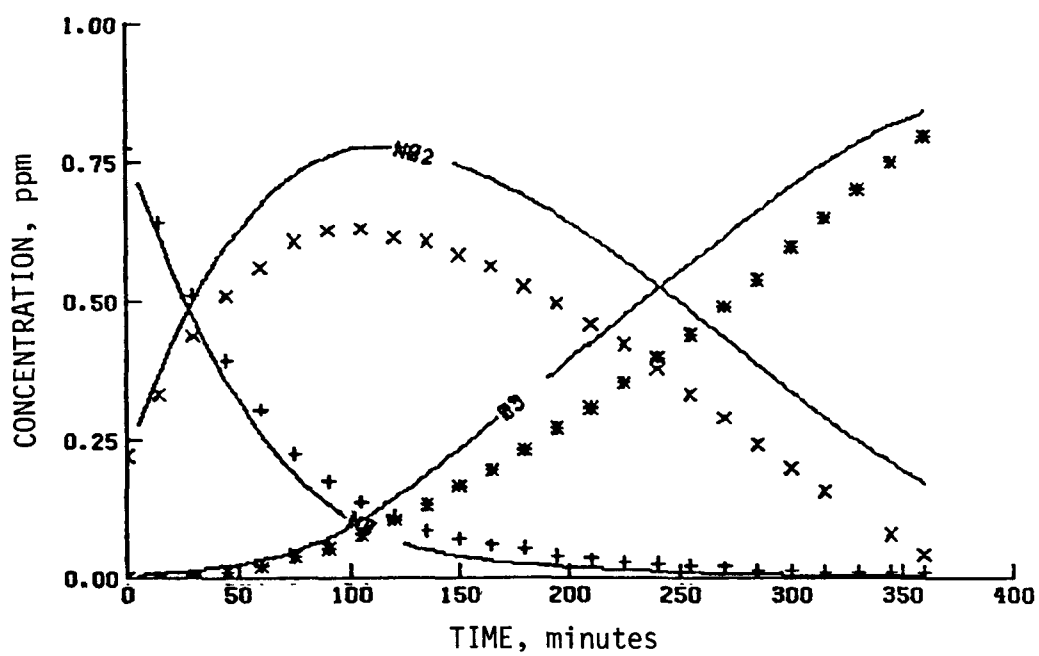
(a) NO_2, NO, and O_3
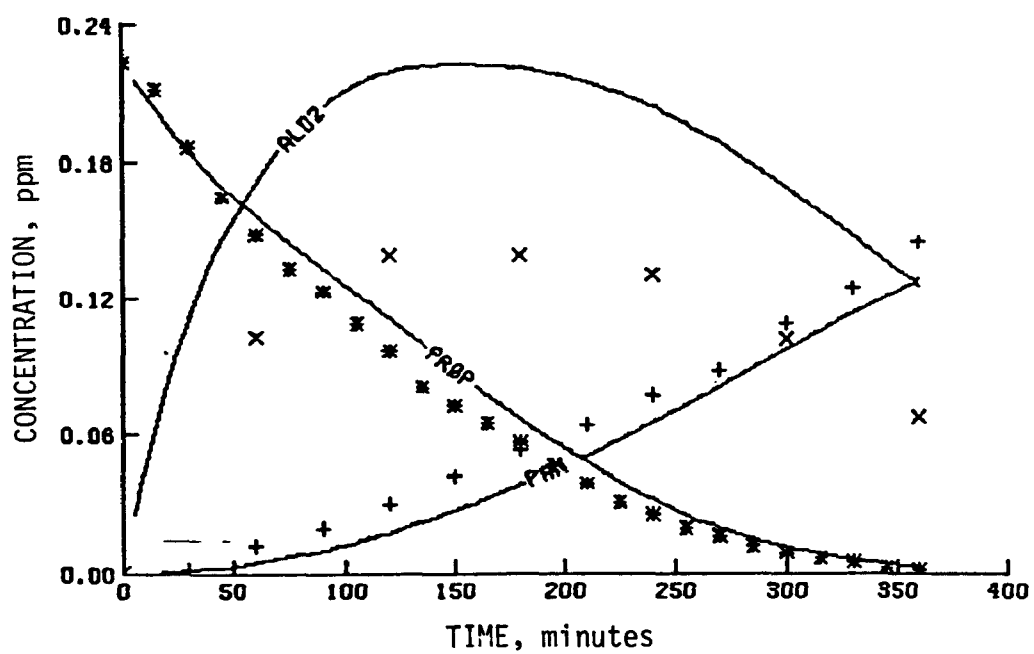
(b) Acetaldehyde, PAN, and propylene

Figure 50.   Simulation results of a UCR multiolefin experiment (EC-150)

170
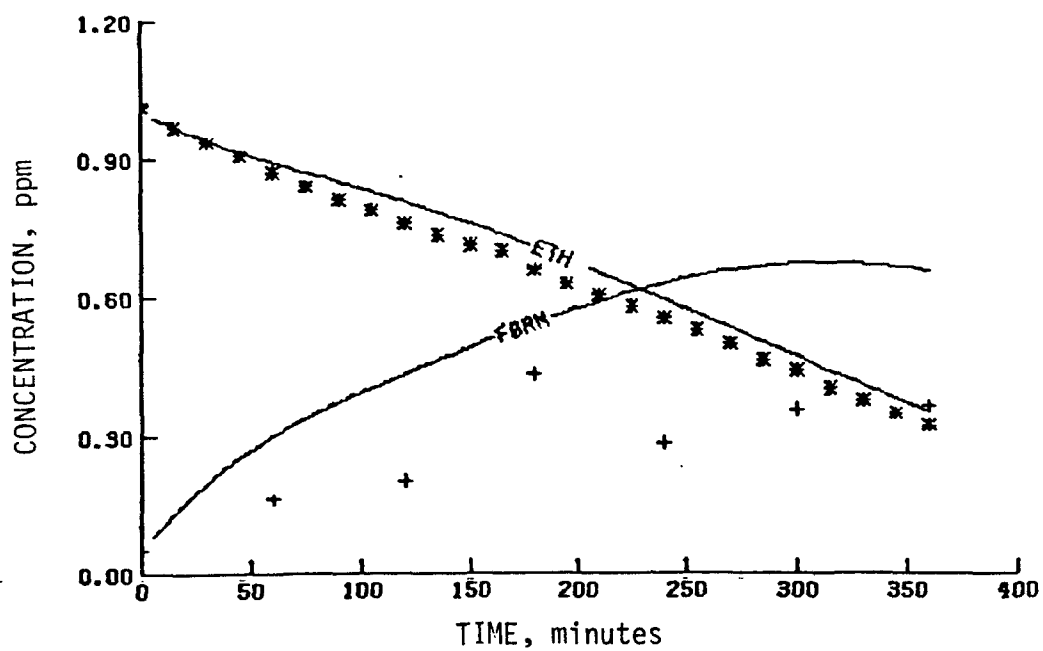
(c) Formaldehyde and ethylene
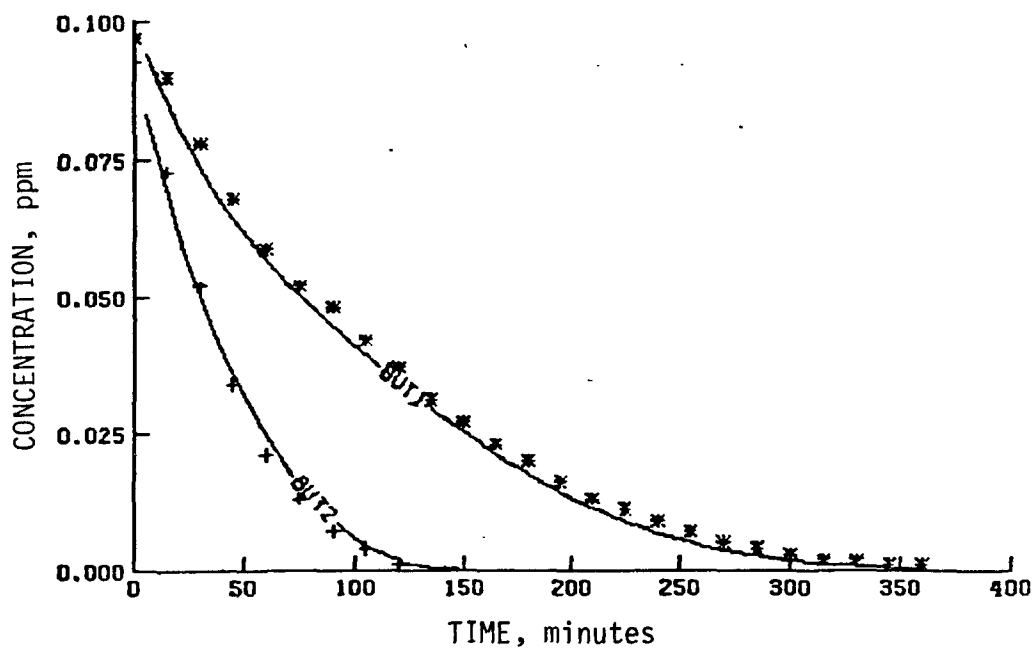
(d) Trans-2-butene and 1-butene

Figure 50 (Continued)

171
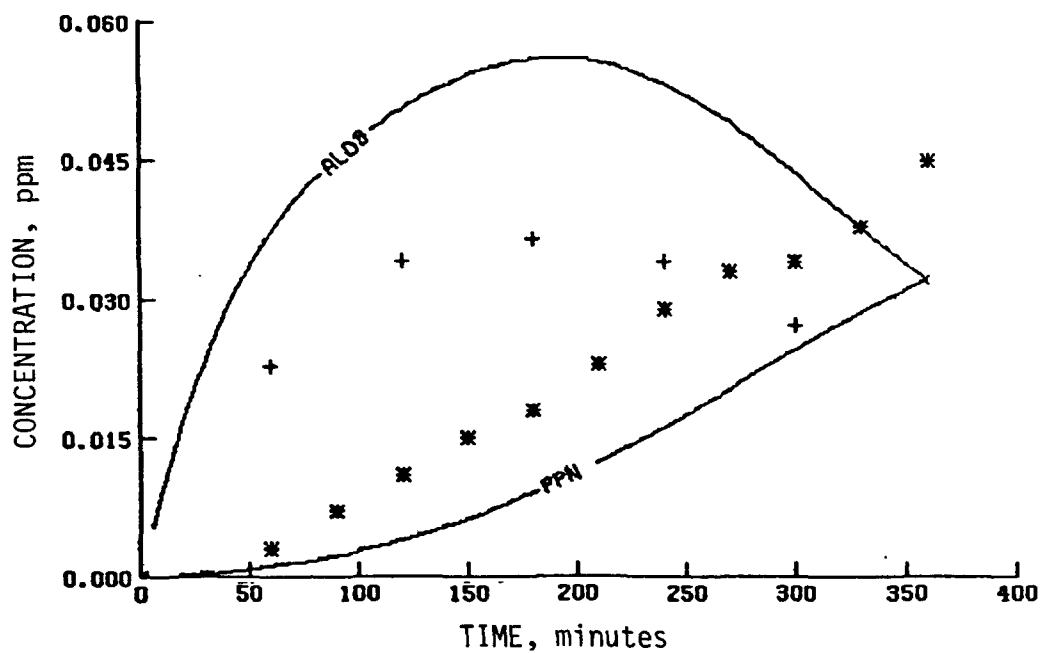
(e) Propionaldehyde and PPN
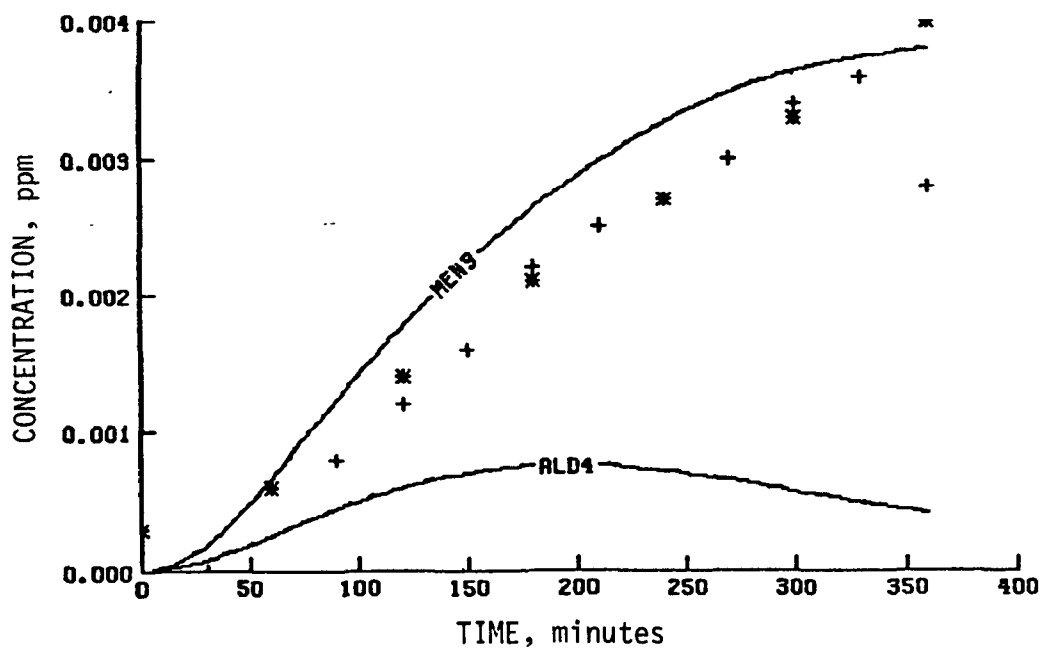
(f) Methyl nitrate and butyraldehyde

Figure 50 (Concluded)

(a) O_3

(b) Ethylene, NO_2 and NO
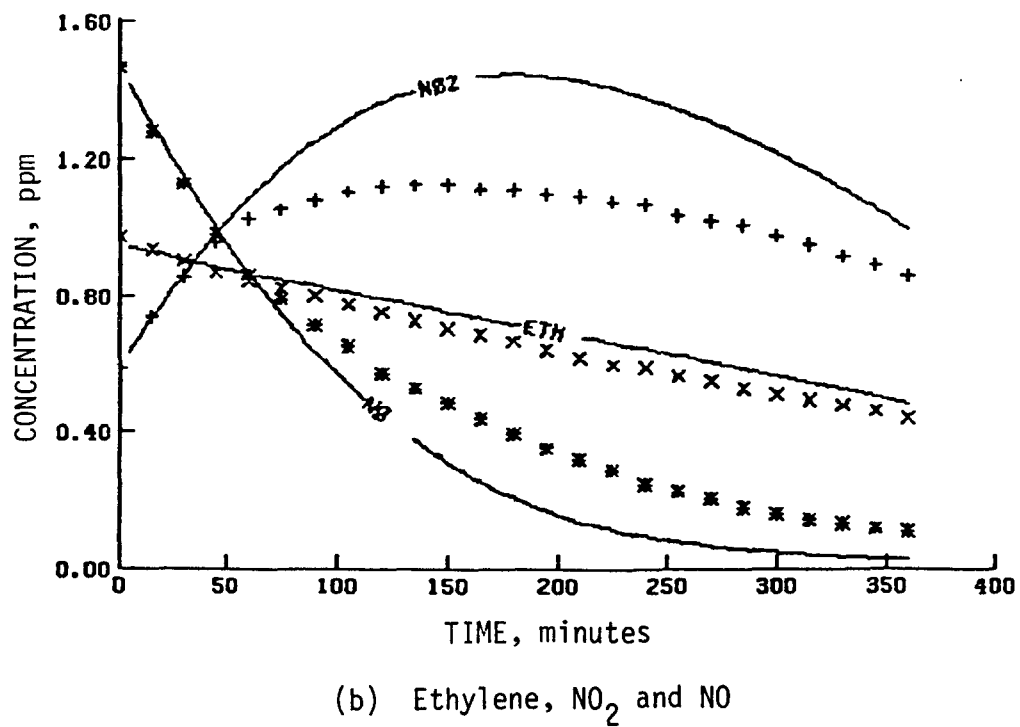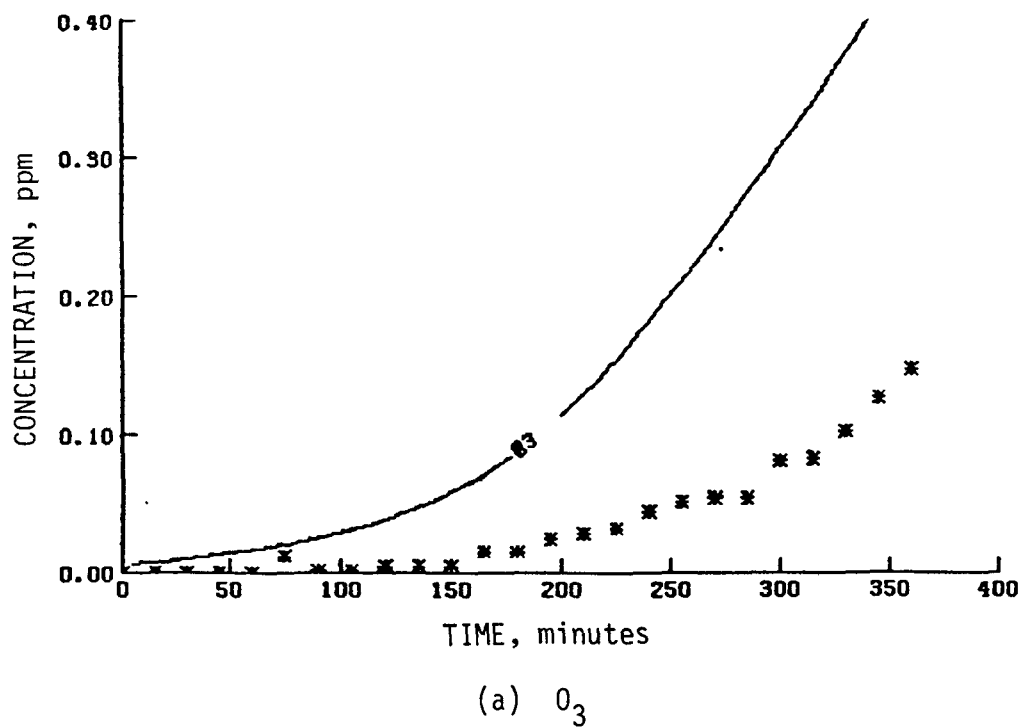
Figure 51. Simulation results of a UCR multiolefin experiment (EC-151)

173
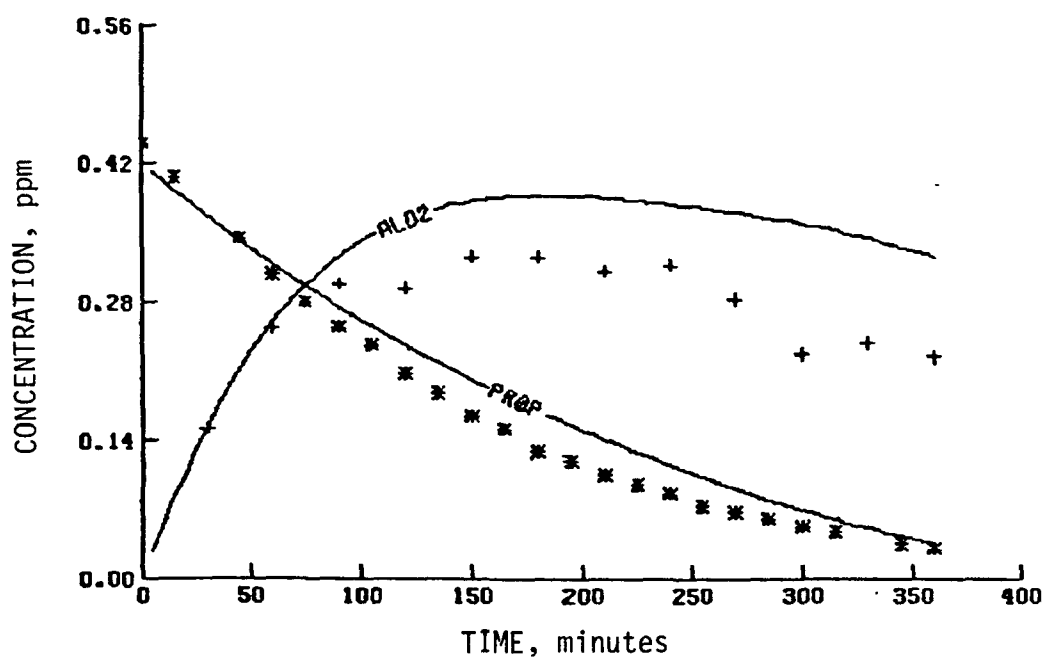
(c) Acetaldehyde and propylene
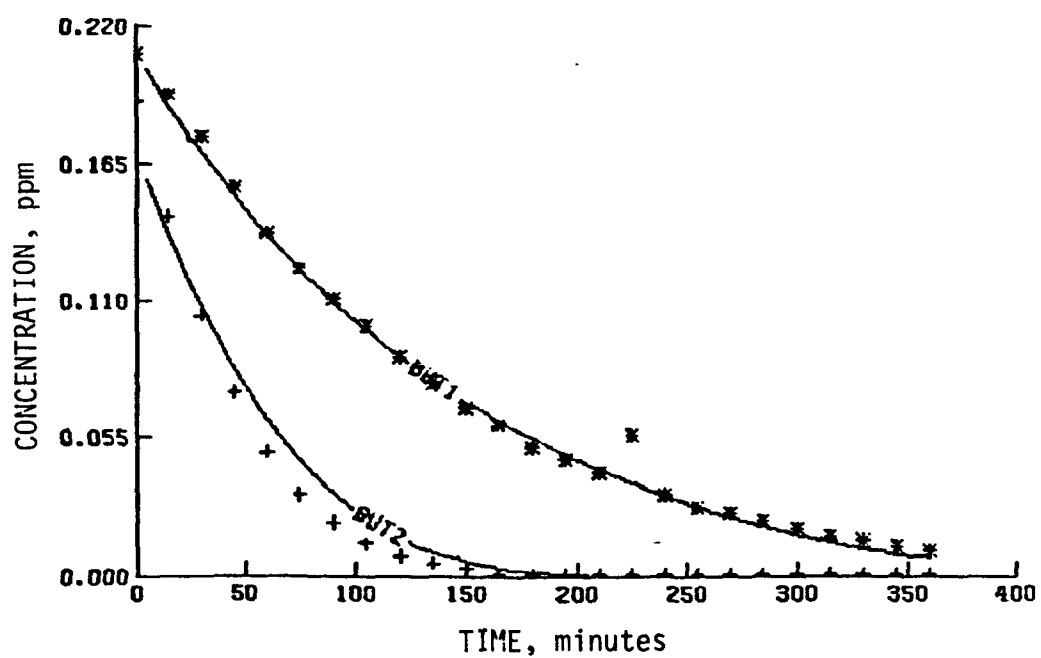
(d) Trans-2-butene and 1-butene

Figure 51 (Continued)

174
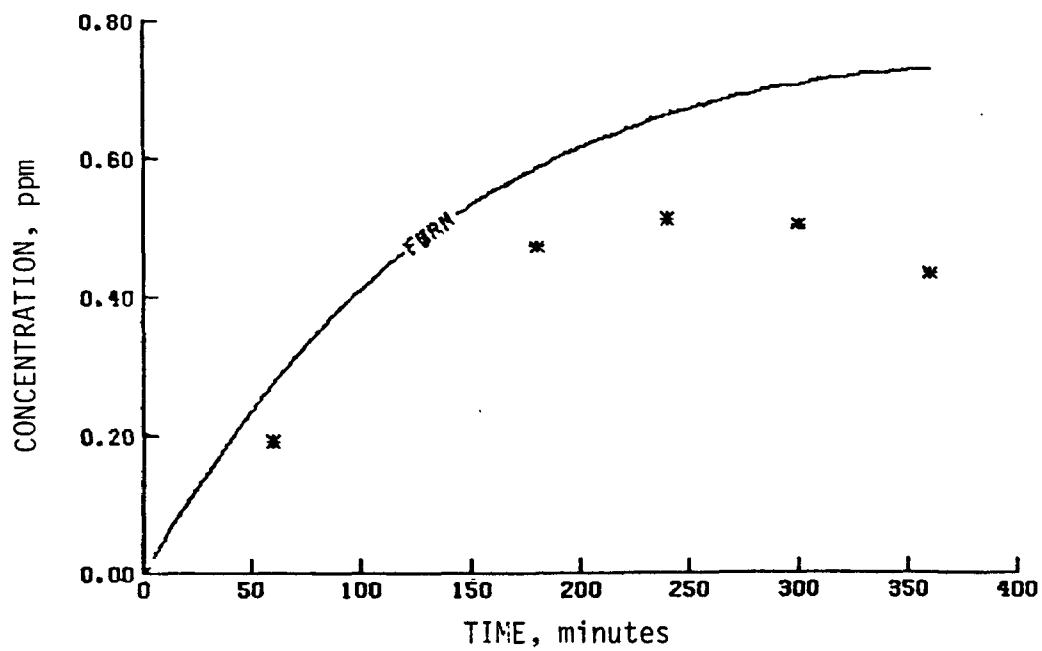
(e) Formaldehyde
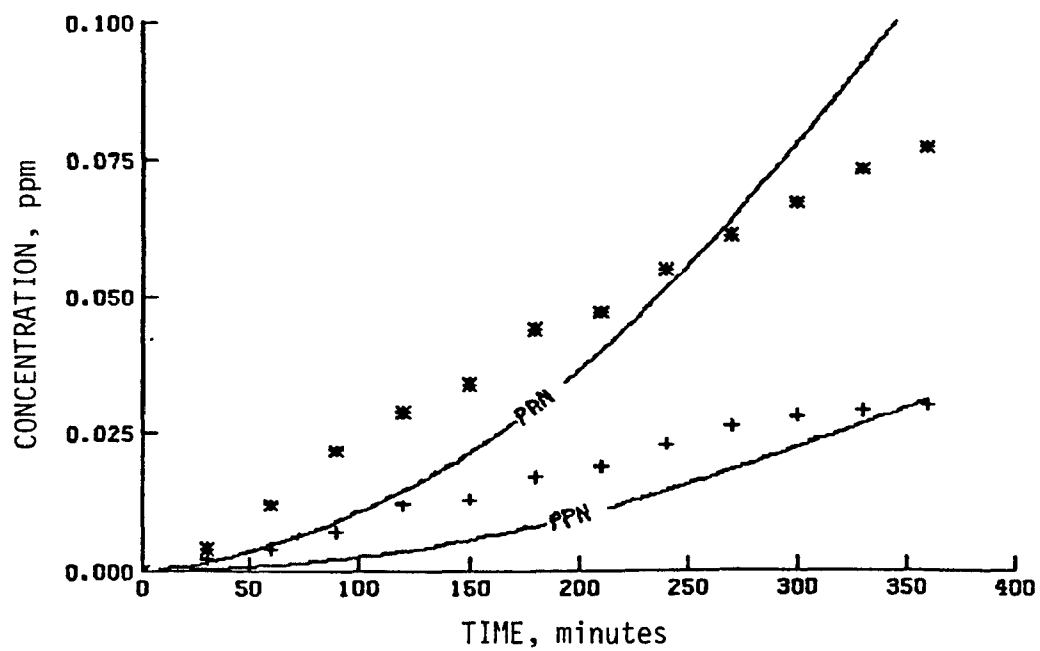
(f) PAN and PPN

Figure 51 (Continued)

175
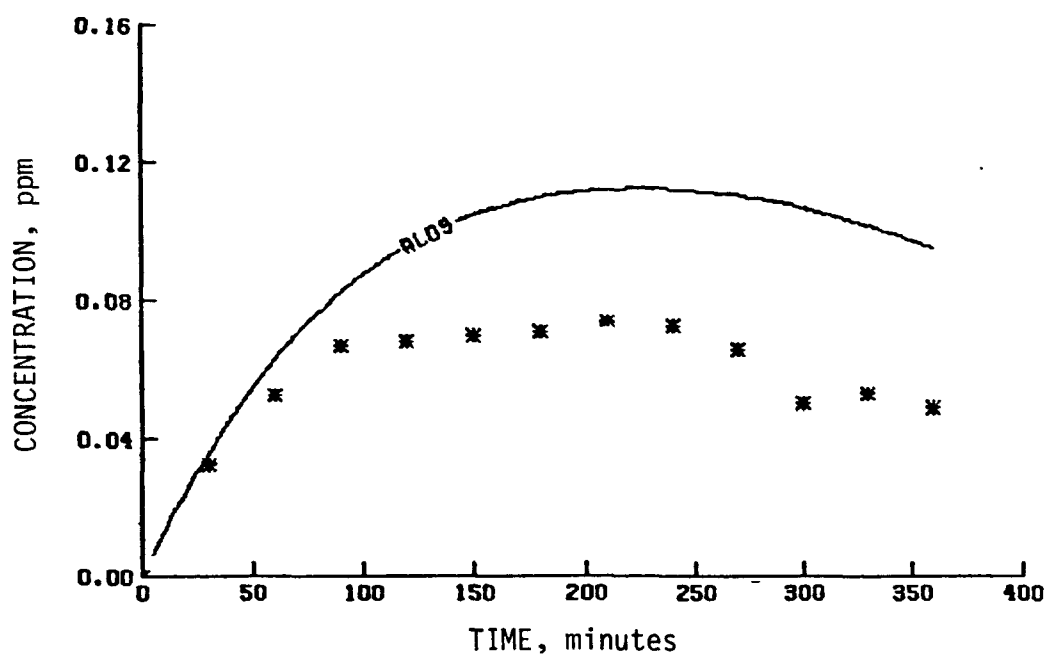
(g)   Propionaldehyde
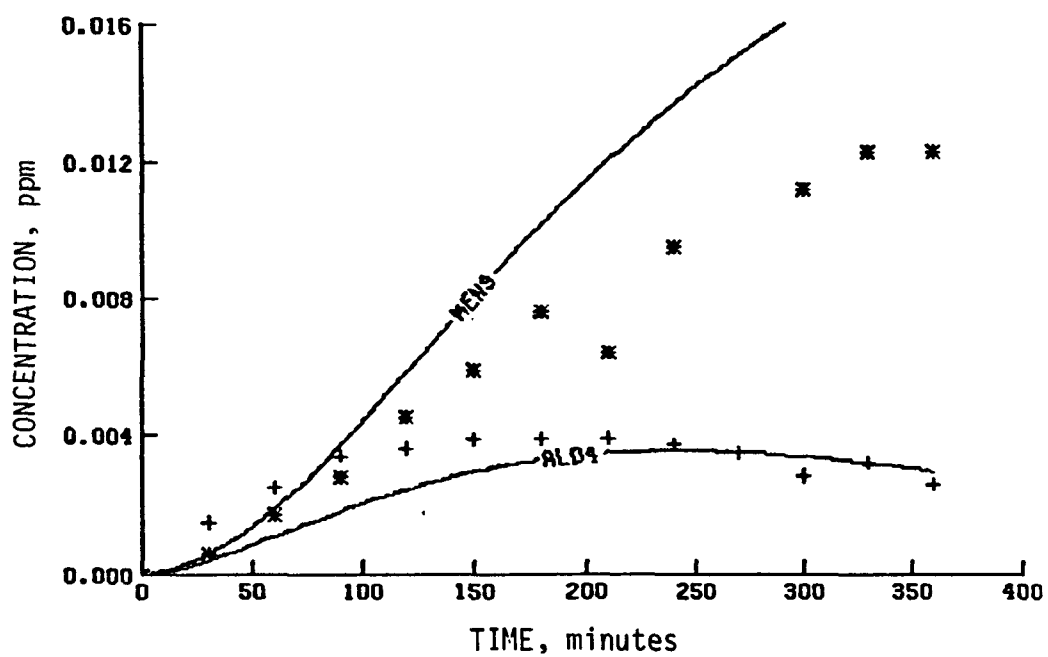
(h)   Butyraldehyde and methyl nitrate

Figure 51 (Concluded)

176

(a) O_3
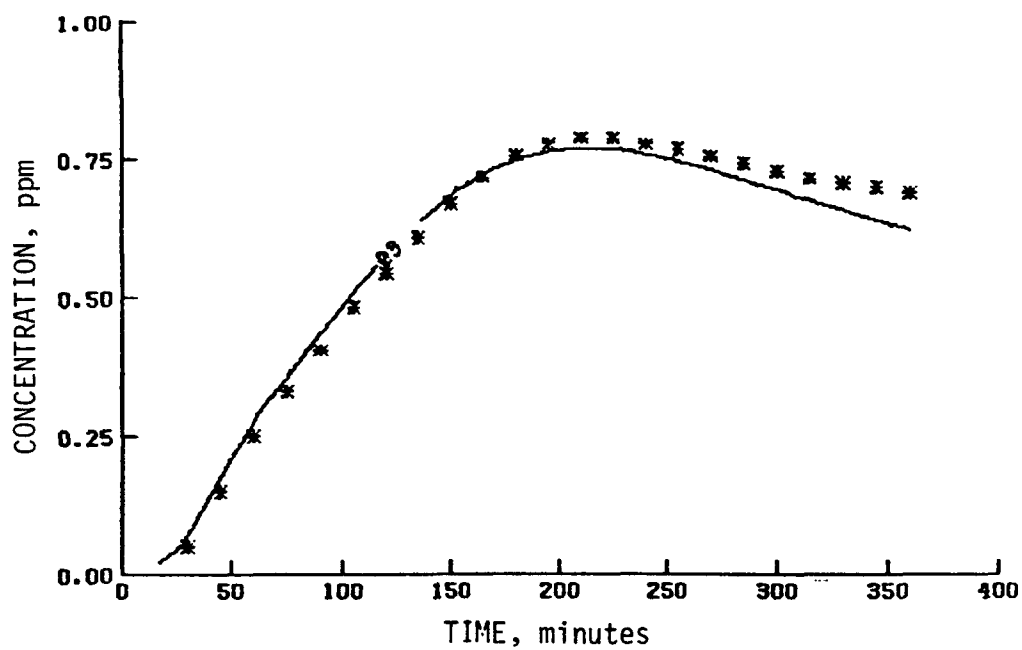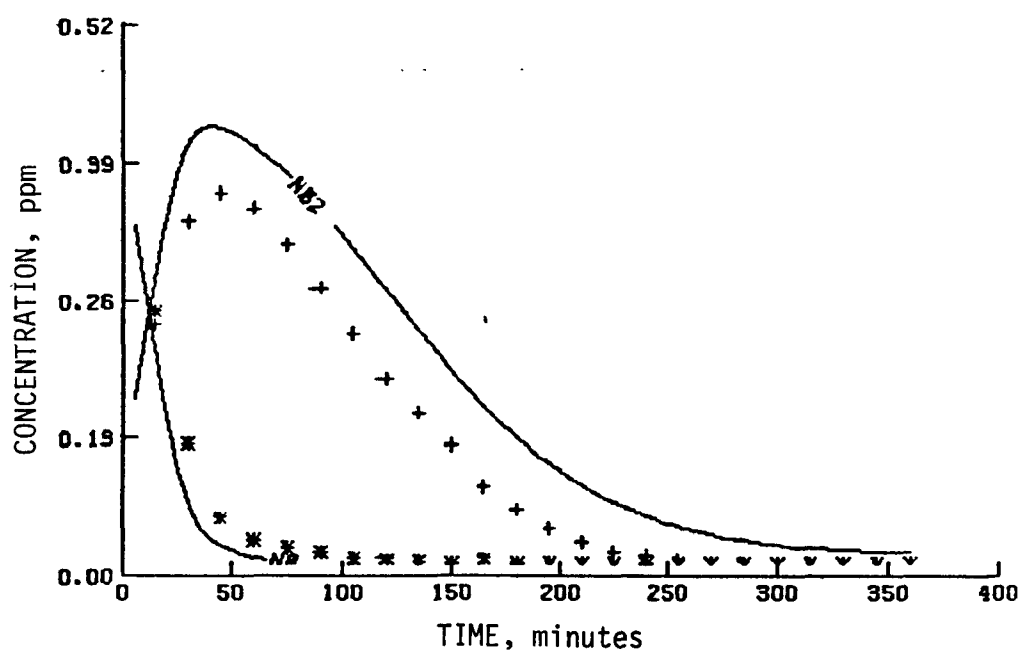
(b) NO_2 and NO

Figure 52.   Simulation results of a UCR multiolefin experiment (EC-152)

177
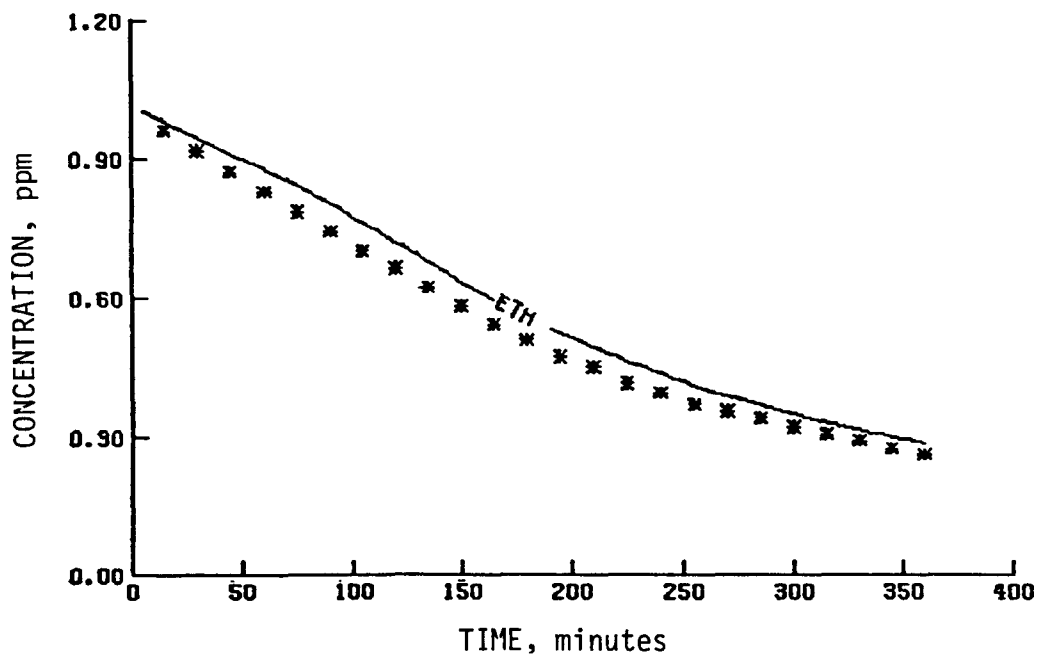
(c) Ethylene
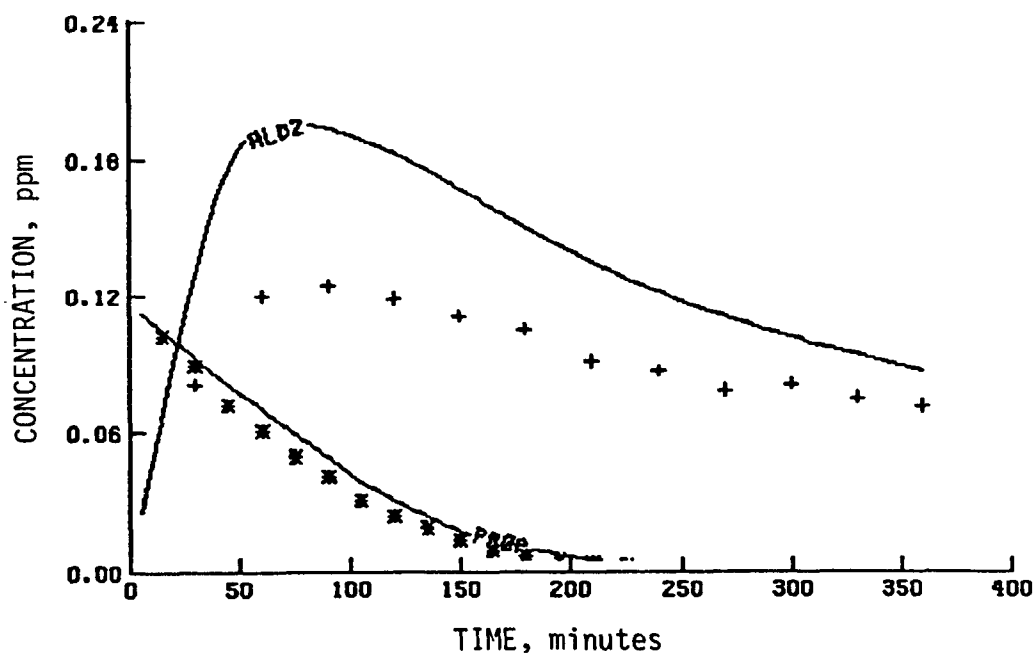
(d) Acetaldehyde and propylene

Figure 52 (Continued)

178
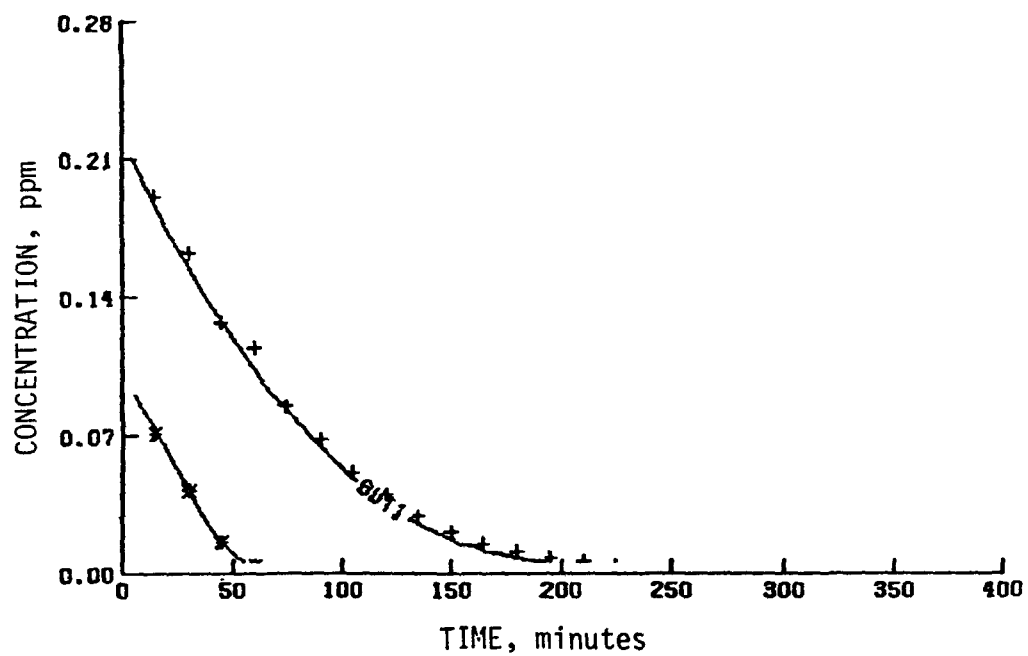
(e)   1-Butene and trans-2-butene
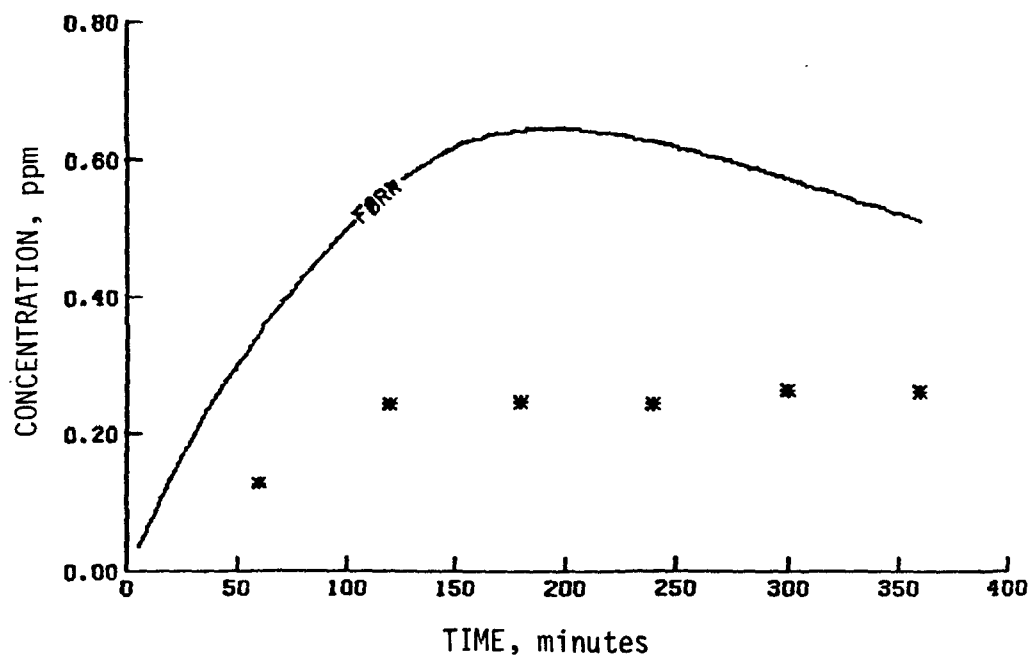
(f)   Formaldehyde

Figure 52   (Continued)

179
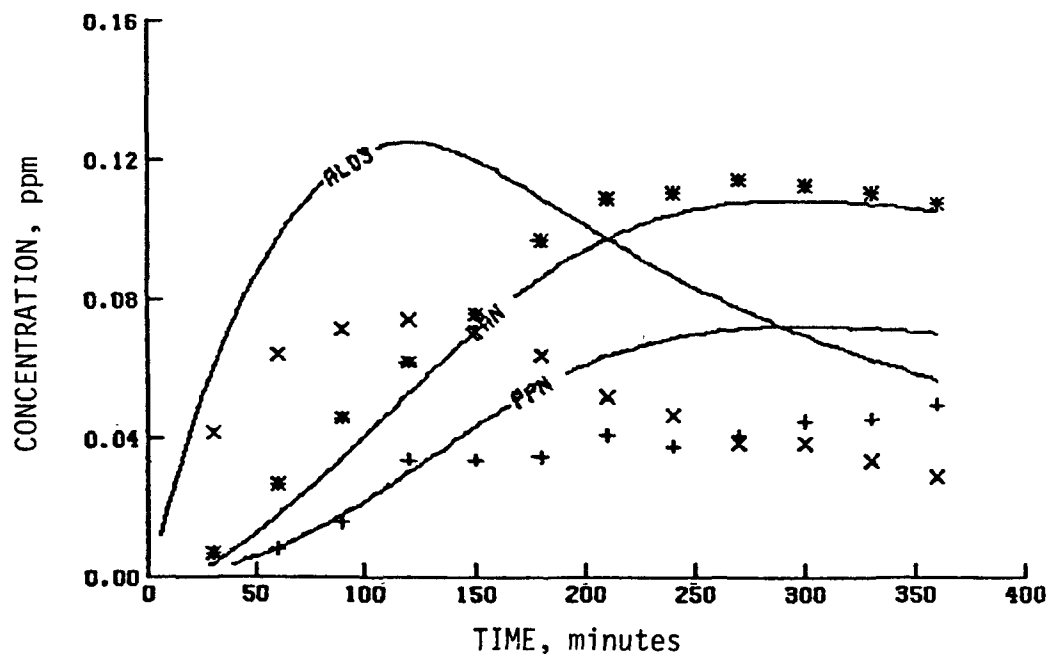
(g) Propionaldehyde, PPN, and PAN
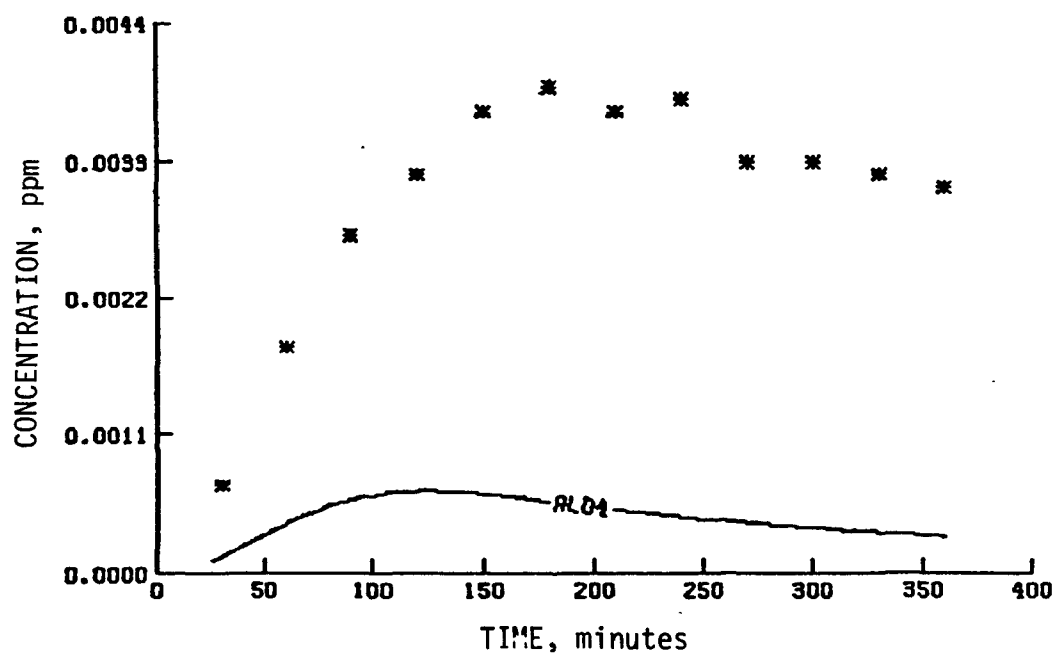
(h) Butyraldehyde

Figure 52 (Concluded)

(a) O_3
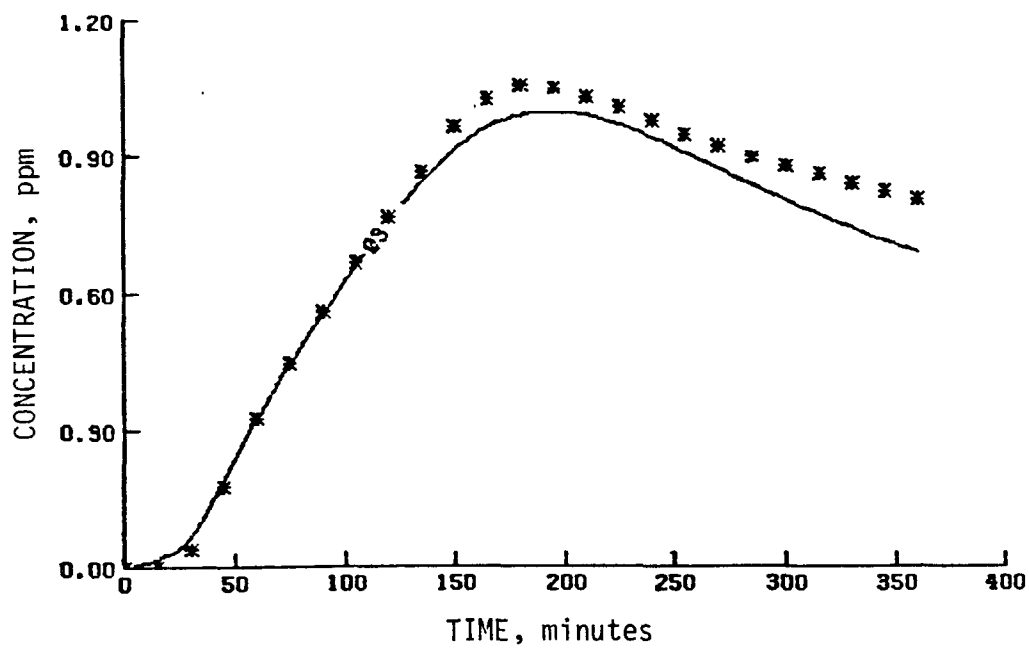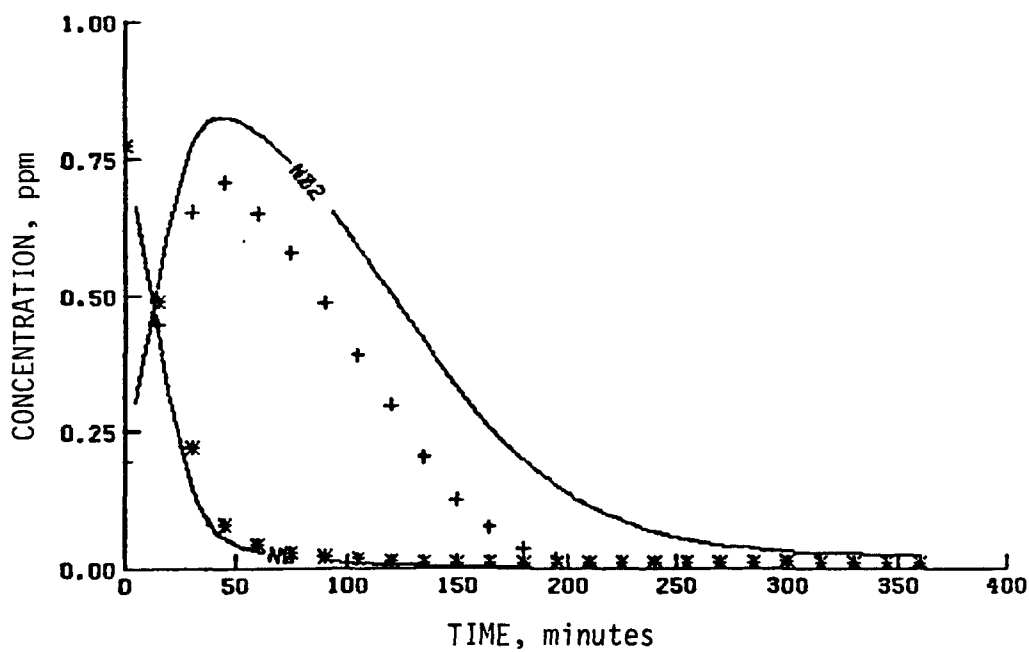
(b) NO_2 and NO

Figure 53. Simulation results of a UCR multiolefin experiment (EC-153)
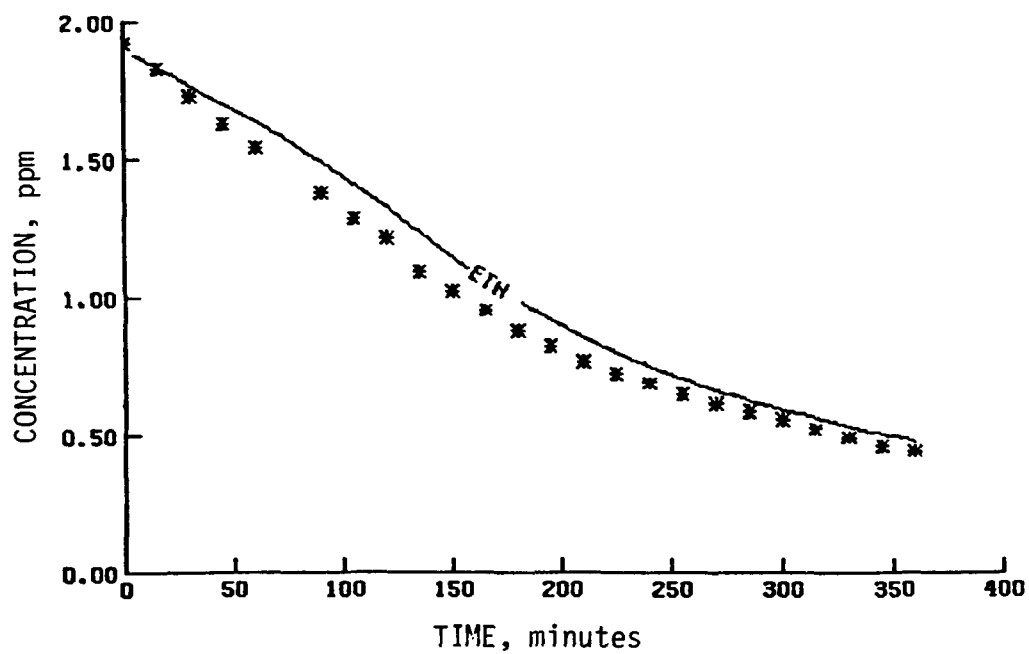
(c) Ethylene
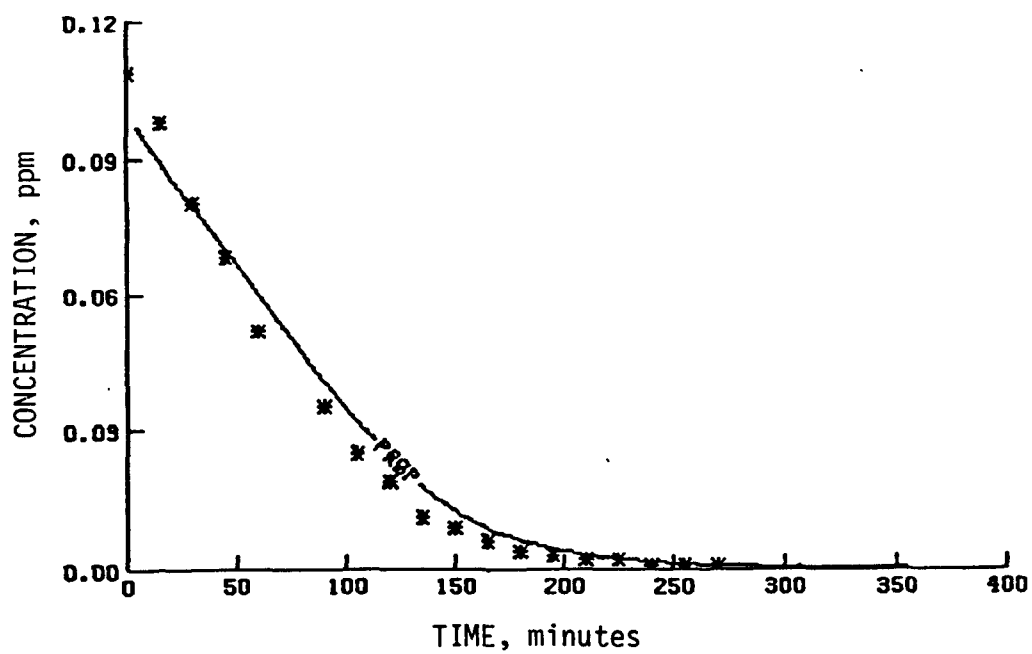
(d) Propylene

Figure 53 (Continued)
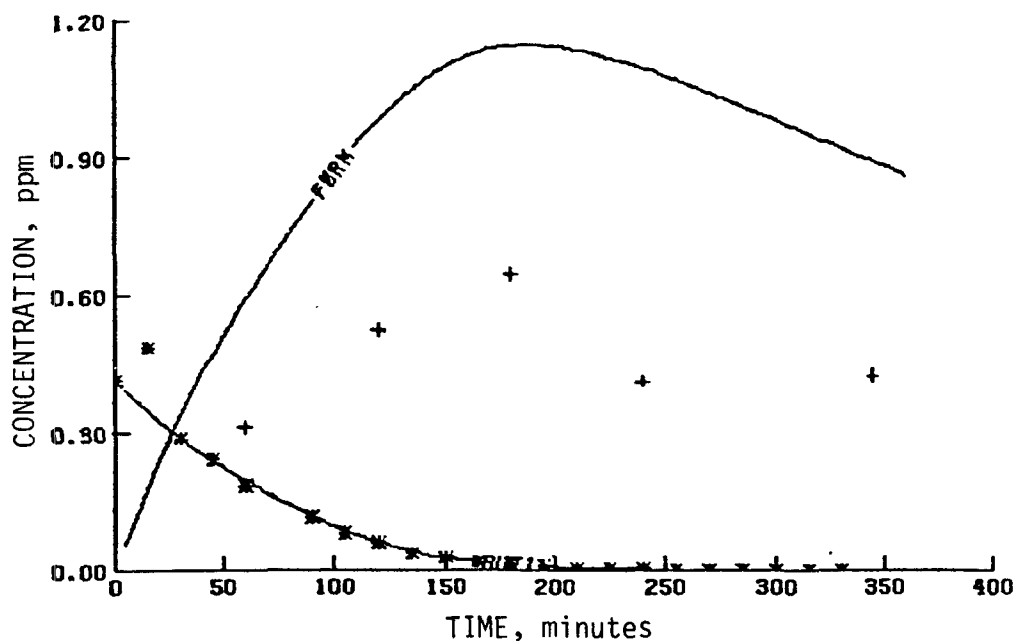
(e) Formaldehyde and 1-butene
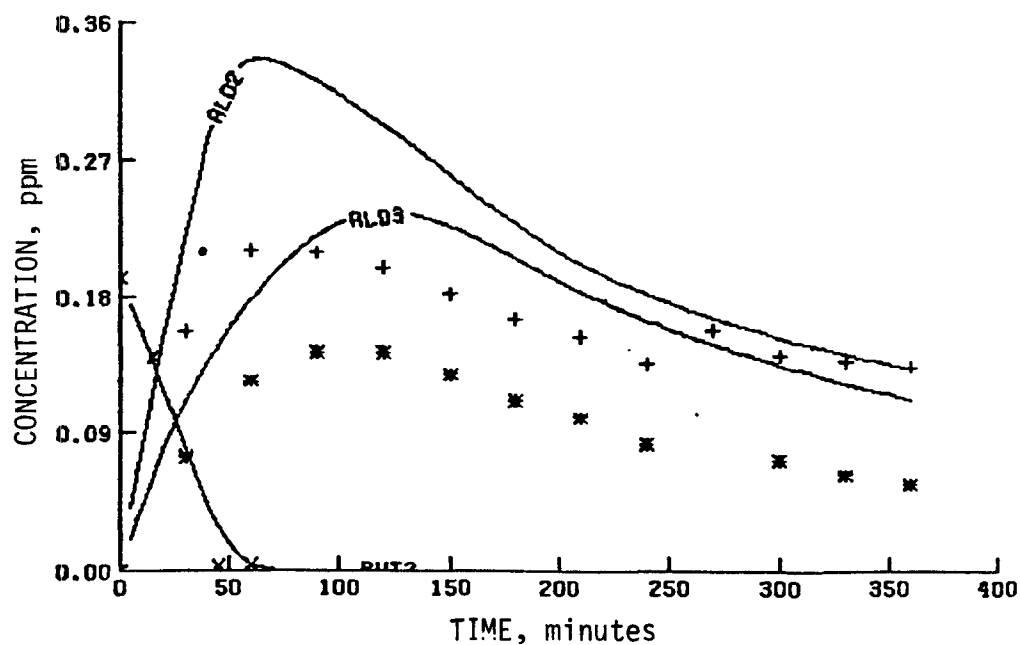
(f) Trans-2-butene, acetaldehyde, and propionaldehyde

Figure 53 (Continued)

183
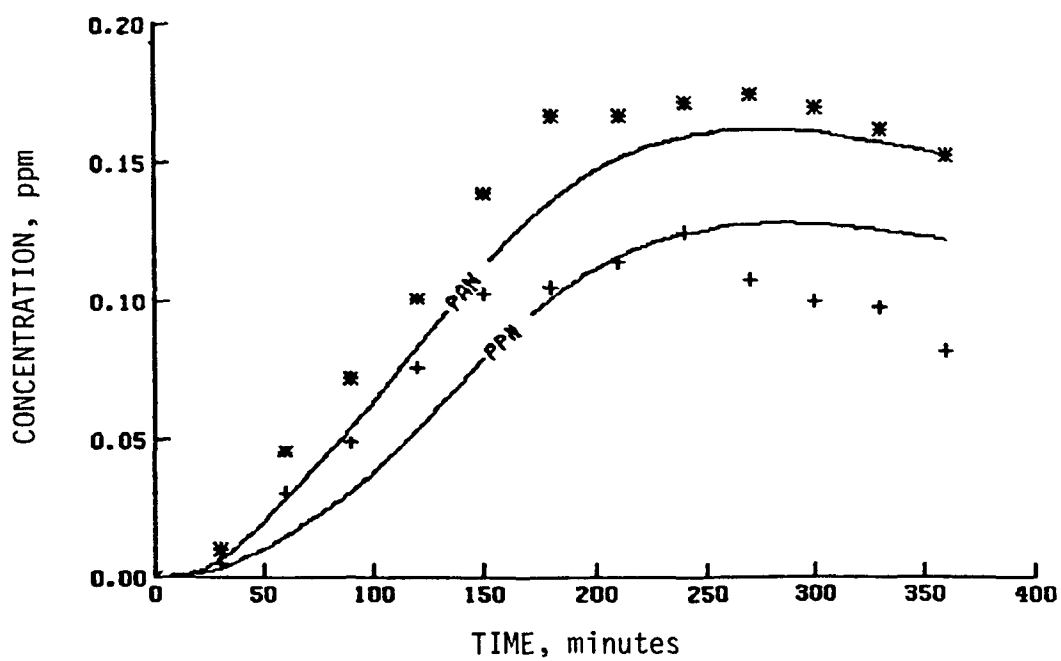
(g) PPN and PAN
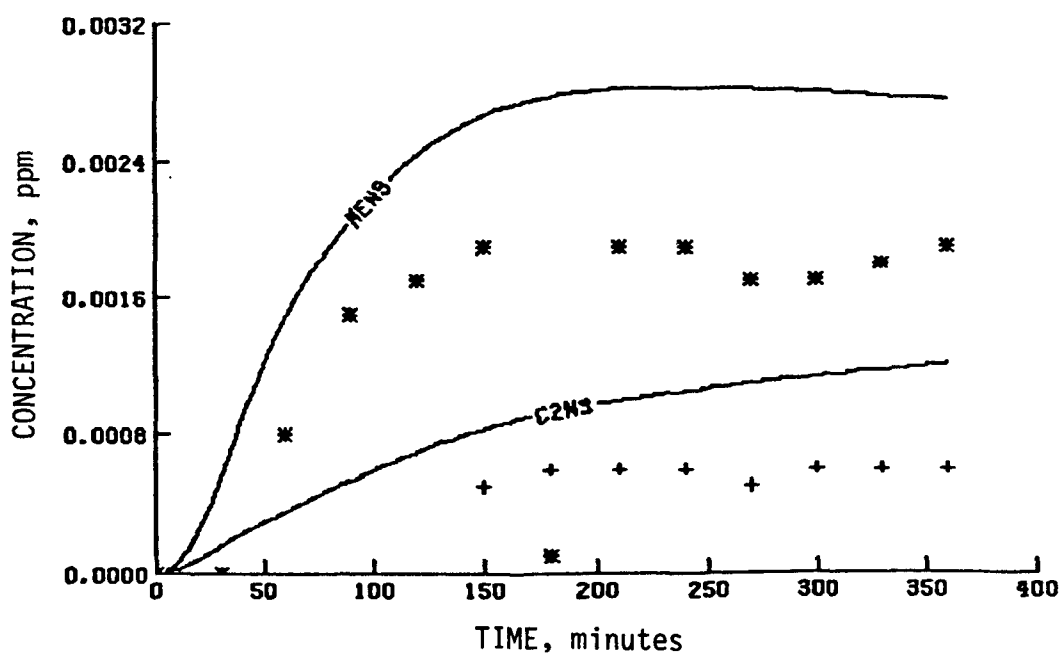
(h) Ethyl nitrate and methyl nitrate

Figure 53 (Concluded)
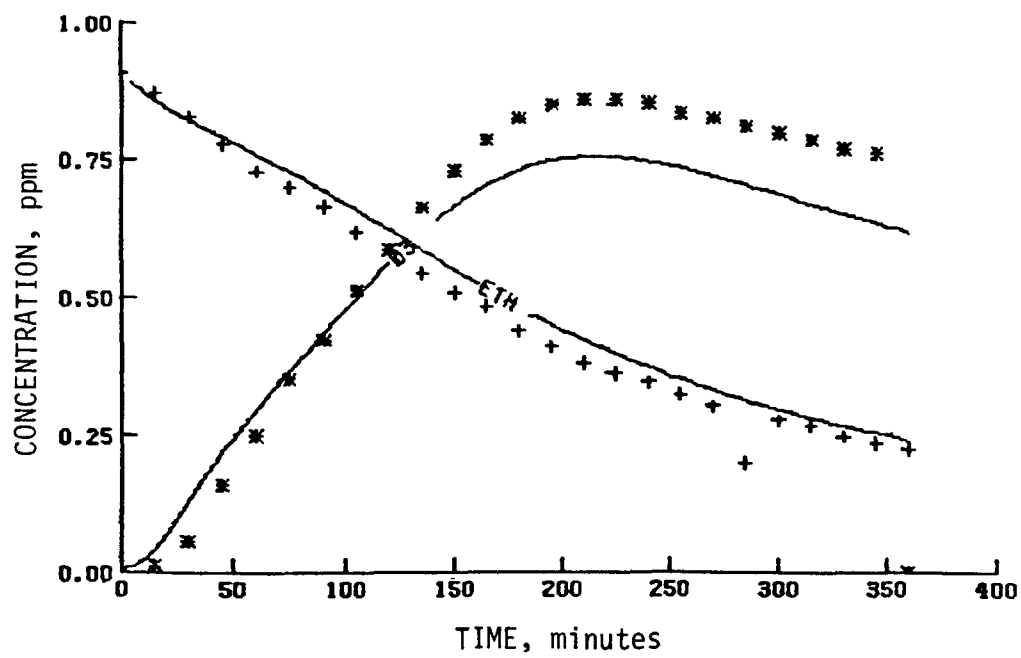
(a) Ethylene and O_3
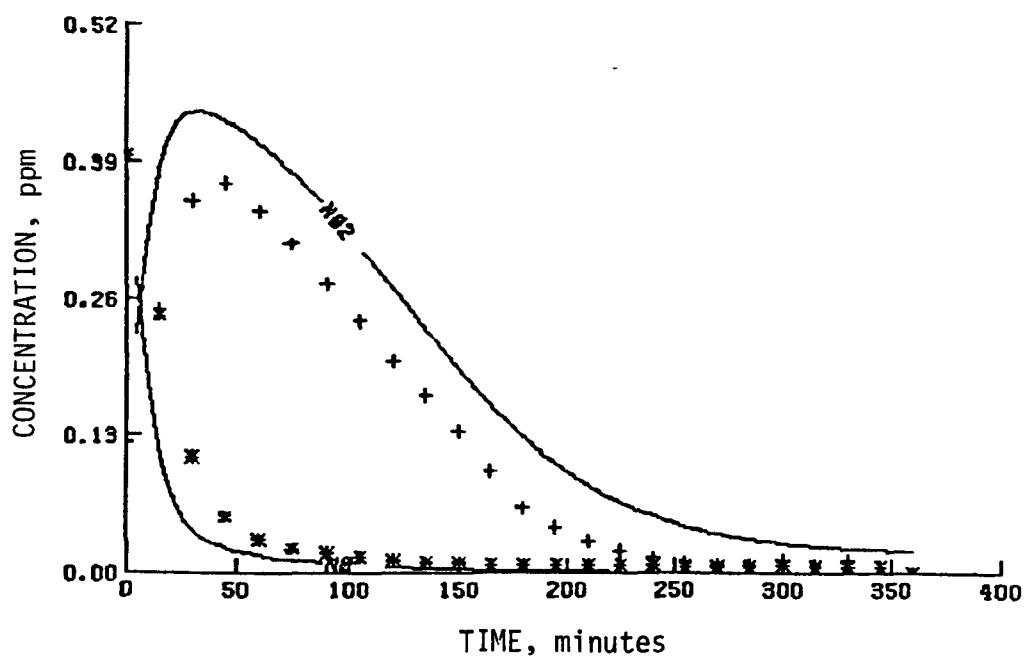
(b) NO_2 and NO

Figure 54. Simulation results of a UCR multiolefin experiment (EC-161)
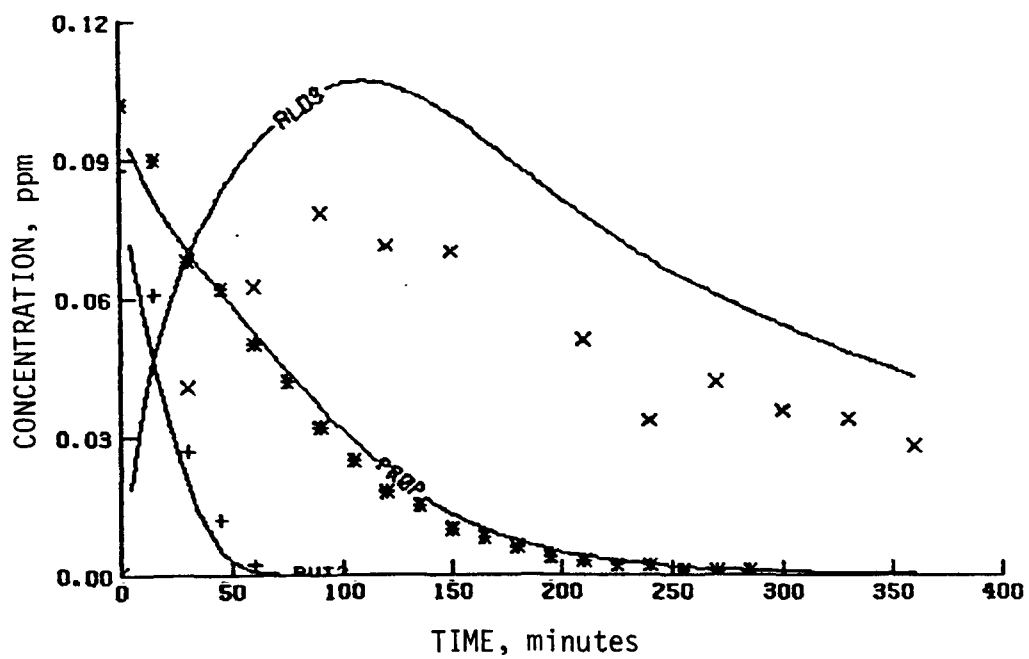
(c) Propionaldehyde, trans-2-butene, and propylene
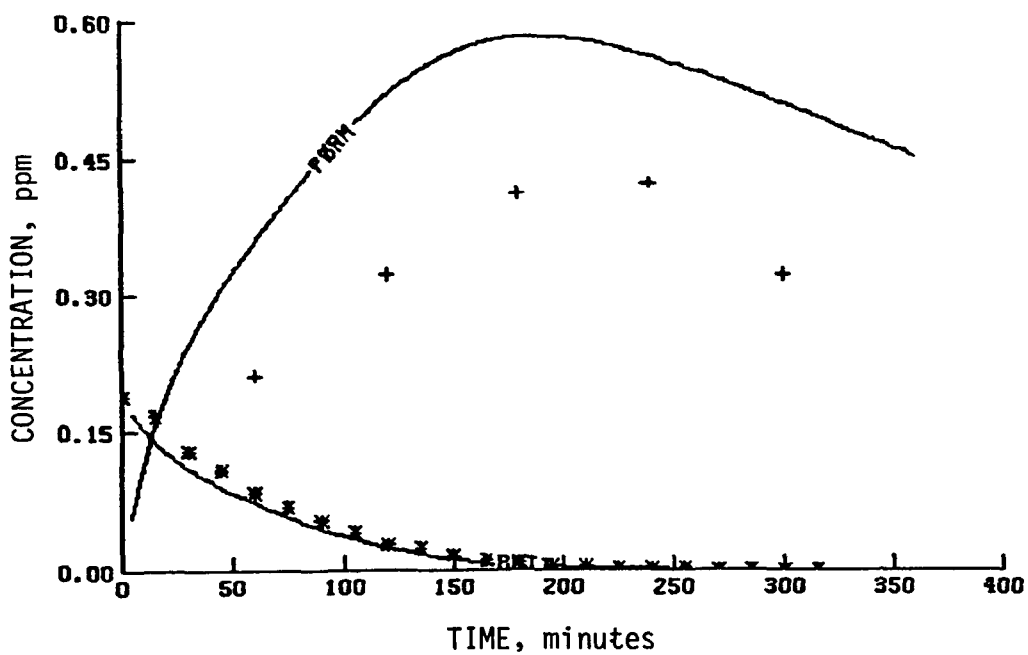
(d) Formaldehyde and 1-butene

Figure 54 (Continued)
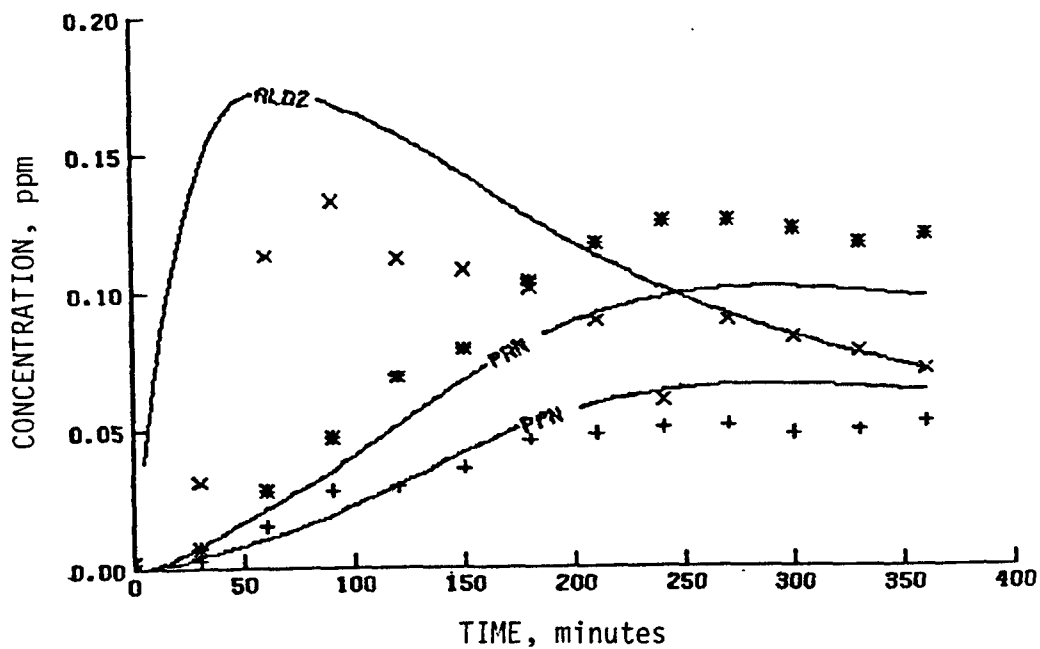
(e) Acetaldehyde, PPN, and PAN
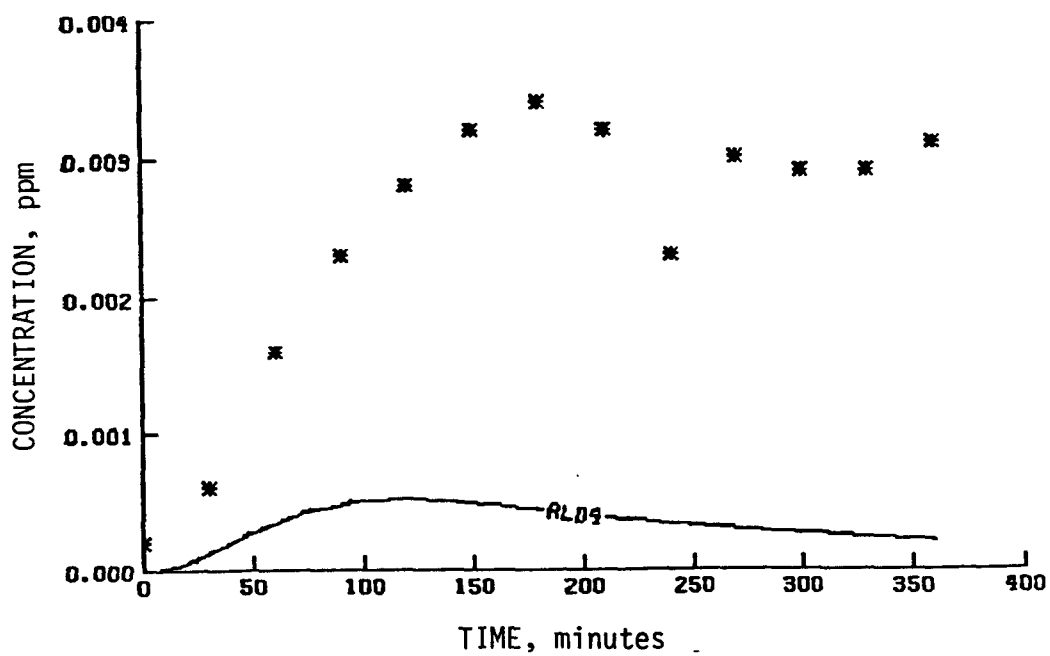
(f) Butyraldehyde

Figure 54 (Continued)
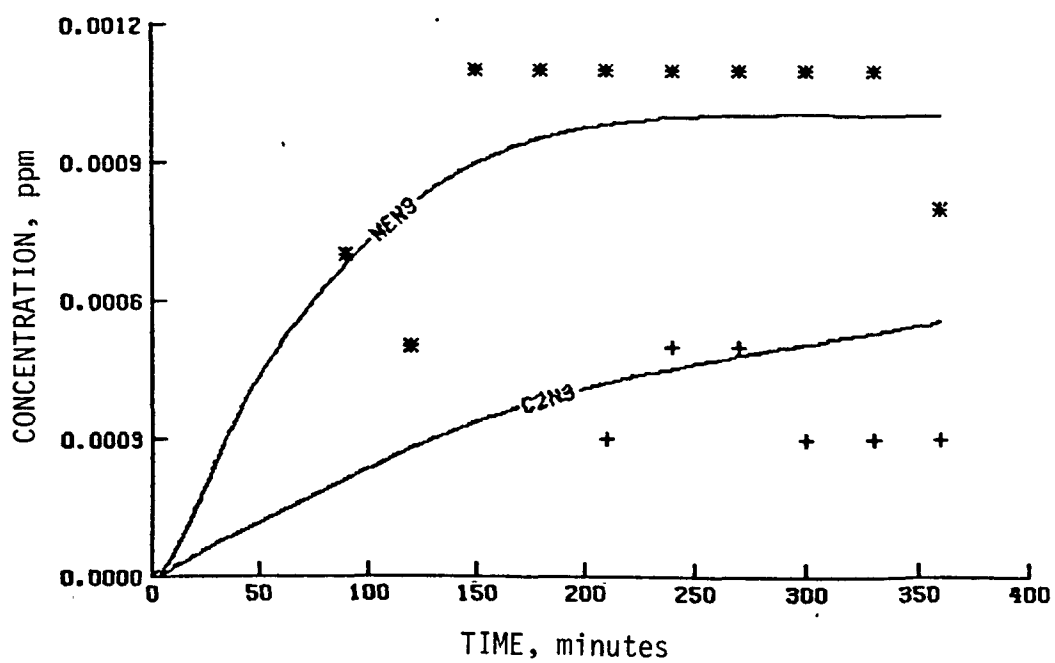
(g) Ethyl nitrate and methyl nitrate

Figure 54 (Concluded)

SECTION 6

THE CARBON-BOND MECHANISM

Modeling the smog chemistry of hydrocarbons by treating certain types of carbon bonds in hydrocarbon molecules and radicals as individual species was introduced by Whitten and Hogo (1977). Their Carbon-Bond Mechanism (CBM) was formulated to create a mechanism that:

> Has few or no empirical parameters that must be used to adjust it to produce simulations in agreement with smog chamber experiments.

> Is capable of accepting atmospheric hydrocarbon measurements in the forms usually provided (ppmC or as weight rather than moles of molecules), eliminating the need to estimate average molecular weights for paraffins, olefins, and other classes of species.

> Is compact enough to be used in conjunction with a regional model of air pollutant transport and dispersion for calculating pollutant concentrations as functions of space and time in urban areas.

> Is based on a generalization of explicit mechanisms rather than an empirical best fit of smog chamber data. Refinements in explicit mechanisms can then lead directly to similar refinements in such a generalized mechanism.

> Is applicable to the complex mixtures of hydrocarbons found in urban atmospheres.

The first four objectives in the above list have largely been accomplished: The original formulation of the CBM has only two empirical parameters that were chosen to fit smog chamber data: the rate constants that account for PAN formation and NO_3 behavior in aromatic oxidation. Using the CBM requires an estimate of the nonmethane hydrocarbon (NMHC) concentration and the percentages of various bond types in the NMHC, whereas some

189

previous generalized mechanisms require the total NMHC concentration, the percentages of various classes of molecules (such as olefins and aromatics) in the NMHC, and the average molecular weight of each class. The CBM is applicable to urban atmospheres as part of a regional air quality model, as exemplified by the study by Anderson et al. (1977). From their use of a regional model to study present and future pollutant concentrations in Denver, they concluded that: "The accuracy of the ozone concentrations predicted by the DAQM [Denver Air Quality Model] is on the order of the accuracy of the ozone monitoring instruments." (The new CBM will soon be used in regional air quality models for St. Louis, Missouri, and Los Angeles California). Finally, the new CBM is based on generalization of our explicit mechanism for four olefins and two paraffins plus a semi-empirical mechanism for aromatics. The last objective in the above list, the ability of the CBM to treat mixtures of hydrocarbons accurately, has been tested during this contract period.

In the following sections, we first present the original formulation of the Carbon-Bond Mechanism and describe our study to determine the accuracies of mechanisms at different degrees of condensation, including an explicit mechanism and the CBM. Second, we present the formulation of the new CBM, which is based on the explicit mechanisms discussed in Section 5.

THE ORIGINAL CARBON-BOND MECHANISM

The Carbon-Bond Mechanism as originally formulated is presented in Table 32. As discussed by Whitten and Hogo (1977), the CBM is largely an aggregation and generalization, or "condensation," of the chemical reactions used in explicit kinetic mechanisms. For example, all explicit mechanisms in this report include the reaction $OH\cdot + NO_2 \rightarrow HNO_3$ with the same rate constant, and so does the CBM. The CBM treats four types of carbon atoms as reactants:

> PAR (all single-bonded carbon atoms, including those in paraffins, alkyl groups attached to aromatics, and so on, but excluding methane and ethane).

190

TABLE 32.   THE ORIGINAL FORMULATION OF THE CARBON-BOND MECHANISM

Reaction	Rate constant $(ppm^{-1} min^{-1})$
$NO_2 + h\nu \rightarrow NO + O\cdot$	k_1^*
$O\cdot + O_2(+ M) \rightarrow O_3 (+ M)$	2.08×10^{-5}
$O_3 + NO \rightarrow NO_2 + O_2$	25.2
$O\cdot + NO_2 \rightarrow NO + O_2$	1.34×10^4
$O_3 + NO_2 \rightarrow NO_3 + O_2$	5×10^{-2}
$NO_3 + NO \rightarrow NO_2 + NO_2$	1.3×10^4
$NO_3 + NO_2 + H_2O \rightarrow 2HNO_3$	$1.66 \times 10^{-3\dagger}$
$NO + NO_2 + H_2O \rightarrow 2HNO_2$	$2.2 \times 10^{-9\dagger}$
$HNO_2 + h\nu \rightarrow NO + OH$	$k_{HNO_2}^*$
$NO_2 + OH\cdot \rightarrow HNO_3$	9×10^3
$NO + OH\cdot \rightarrow HNO_2$	9×10^3
$CO + OH\cdot \rightarrow CO_2 + HO_2$	2.06×10^2
$OLE + OH\cdot \xrightarrow{O_2} HCHO + CH_3O_2$	3.8×10^4
$PAR + OH\cdot \xrightarrow{O_2} CH_3O_2 + H_2O$	1.3×10^3
$ARO + OH\cdot \xrightarrow{O_2} HCHO + CH_3O_2$	8×10^3
$OLE + O\cdot \xrightarrow{2O_2} HC(O)O_2\cdot + CH_3O_2$	5.3×10^3
$PAR + O\cdot \xrightarrow{O_2} CH_3O_2\cdot + OH\cdot$	20
$ARO + O\cdot \xrightarrow{2O_2} HC(O)O_2 + CH_3O_2$	37
$OLE + O_3 \xrightarrow{O_2} HC(O)O_2 + HCHO + OH\cdot$	0.01

TABLE 32 (Concluded)

Reaction	Rate constant $(ppm^{-1} min^{-1})$
$ARO + O_3 \overset{O_2}{\rightarrow} HC(O)O_2 + HCHO + OH\cdot$	0.002
$OLE + O_3 \rightarrow ozonide$	0.005
$HCHO + h\nu \overset{2O_2}{\rightarrow} HC(O)O_2 + HO_2$	$k^*_{HCHO \rightarrow Radicals}$
$HCHO + h\nu \rightarrow CO + H_2$	$k^*_{HCHO \rightarrow CO}$
$HCHO + OH\cdot \overset{O_2}{\rightarrow} HC(O)O_2 + H_2O$	1×10^4
$HO_2 + NO \rightarrow OH\cdot + NO_2$	2×10^3
$CH_3O_2 + NO \rightarrow NO_2 + HCHO + HO_2$	2×10^3
$HC(O)O_2 + NO \rightarrow NO_2 + CO_2 + HO_2$	2×10^3
$H_2O_2 + h\nu \rightarrow OH\cdot + OH\cdot$	$k^*_{H_2O_2}$
$HO_2 + HO_2 \rightarrow H_2O_2 + O_2$	4×10^3
$CH_3O_2 + HO_2 \rightarrow H_3COOH + O_2$	4×10^3
$HC(O)O_2 + HO_2 \rightarrow HC(O)OOH + O_2$	1×10^4
$HC(O)O_2 + NO_2 \rightarrow PAN$	150
$PAN \rightarrow HC(O)O_2 + NO_2$	0.02
$ARO + NO_3 \rightarrow Products$	50
$HO_2 + NO_2 \rightarrow HNO_2$	20.

* Photolysis rate constants in units of min^{-1}.
† Units of $ppm^{-2}min^{-1}$.

Source: Whitten and Hogo (1977).

> OLE (all atoms in carbon-carbon double bonds, treated in
pairs of carbon atoms, except those in ethylene and
aromatic rings).

> ARO (all atoms in carbon-carbon double bonds in ethylene
and aromatic rings, treated in pairs).

> CAR (carbonyl carbon atoms, whether in aldehydes or ketones).

These four species were chosen to account for the types of carbon atoms
that are important in photochemical smog; carbon atoms in alkynes, amines,
alcohols, and other species appear to be unimportant because they are
emitted only in small quantities. In addition, explicit mechanisms and
smog chamber experiments involving those species are not readily available.

The CBM, as a condensation of explicit kinetic mechanisms, was
designed to reproduce as closely as possible the results of simulations
of smog chamber data using explicit mechanisms rather than the data them-
selves. Thus, there are two standards of performance for the CBM:

> How well it reproduces smog chamber data.

> How well it reproduces simulations of smog chamber data
using explicit mechanisms.

The importance of the former is obvious, the latter is important because
it is a measure of how well the CBM represents the state of knowledge of
smog chemistry expressed in explicit kinetic mechanisms. As discussed by
Whitten and Hogo (1977), the latter performance standard is more meaning-
ful, and a closer fit of smog chamber data by a CBM simulation than by
a simulation with the appropriate explicit mechanism is fortuitous.

The difference in these performance standards is shown by results
from Whitten and Hogo (1977). As measured by the difference between the
maximum one-hour-average O_3 concentration measured in a smog chamber
experiment and that calculated in the corresponding computer simulation,
the CBM fit the explicit mechanisms with a standard deviation of 10

percent and the UCR smog chamber data with a standard deviation of 27 percent. The explicit mechanisms themselves fit the UCR smog chamber data with a standard deviation of 20 percent. These figures suggest that more of the uncertainty in a CBM simulation of a smog chamber experiment was caused by deficiencies in knowledge of smog chemistry or inaccuracies in smog chamber data than by the approximations and assumptions on which the CBM is based.

Degree of Condensation in a Mechanism

This section describes some tests of how an increase in condensation in a kinetic mechanism affects its predictive accuracy. An approximation used in the CBM is the assumption that carbon atoms with similar bonding react alike and have similar rate constants. This approximation has been made to reduce (or condense) the number of chemical reactions treated in the CBM. Of course, the CBM is only one of many possible mechanisms based on that approximation. A mechanism less condensed than the CBM could be formulated by treating primary, secondary, and tertiary carbon atoms in paraffins separately. A more condensed mechanism could be formulated, for example, by treating olefins and aromatics together.

We used four mechanisms with different degrees of condensation to simulate a smog chamber experiment to study the way in which condensation affects accuracy. The smog chamber experiment studied (UCR EC-150) was begun with four olefins of widely different reactivities (ethylene, propylene, 1-butene, and trans-2-butene). This experiment was chosen because the reactions of the initial hydrocarbons can be treated at different degrees of condensation. The four mechanisms at different degrees of condensation used to simulate EC-150 are:

(1) An early explicit kinetic mechanism [the combination of explicit mechanisms for the four initial hydrocarbons taken from Whitten and Hogo (1977)].

194

(2) A modification of the CBM in which all initial
(unreacted) double bonds are treated explicitly and
all other species are treated using generalized
species (e.g., propylene is treated as one PAR and
one "propylene double bond"; an oxidized species such
as $CH_3CO_3^*$ is treated as one PAR and one HCO_3^*).

(3) The original formulation of the CBM (e.g., propylene
is treated as one PAR and one OLE; ethylene is treated
as ARO).

(4) The CBM with ethylene grouped with OLE rather than with
the less reactive ARO.

In this discussion, it is helpful to consider hydrocarbon oxidation in
smog in two phases: primary and secondary. In primary oxidation, the
original olefin is attacked by OH·, O, or O_3, producing mainly RO_2^*, RCO_3^*,
and RCHO. In secondary oxidation, those products react until CO or CO_2
is finally reached.

Mechanism 1 treats all important reactions in both primary and secondary
oxidation explicitly. Mechanism 2 treats the secondary oxidation reactions
through the generalized species used in the CBM. The treatment of the
primary oxidation reactions in Mechanism 2 is somewhat more detailed than in
Mechanism 1 because the latter ignores the possibility of attack by OH·
on the paraffinic portions of the olefins. This difference is unlikely
to be important for small olefins such as propylene because OH· apparently
attacks the double bond in the olefins of interest far more frequently than
it attacks the paraffinic portions. For longer aliphatic olefins, however,
the competition for OH· between the double and single bonds should be con-
sidered. We used Greiner's (1970) formula for calculating alkane-OH· rate
constants to estimate that the single bond attack becomes competitive for
olefins with ten or more carbon atoms. Mechanism 3, the original formula-
tion of the CBM, treats both the primary and secondary oxidation reactions
through generalized species. The initial olefins propylene, 1-butene, and

trans-2-butene are treated as OLE (with the appropriate number of PARs), and ethylene is treated as ARO. Mechanism 4, the most condensed of the four mechanisms studied, is similar to Mechanism 3 expect that ethylene is treated as OLE rather than ARO.

Before presenting the simulation results, we wish to point out that the simulations with Mechanism 1 were carried out early in the contract period and do not reflect the refinements discussed in Section 5. Figure 55 compares Mechanisms 1 and 2. Excellent agreement is seen; hence there is no loss of accuracy when secondary oxidation products are condensed. To test Mechanism 3, we have to calculate rate constants for olefin + OH· for the surrogate olefins. Four ways of doing this are: the arithmetic mean (k_{AM}), the geometric mean (k_{GM}), the harmonic mean (k_{HM}), and the root-mean-square-value (k_{RMS}):

$$k_{AM} = \frac{\sum_i w_i k_i}{\sum_i w_i} \quad , \tag{74}$$

$$\ell n \; k_{GM} = \frac{\sum_i w_i \; \ell n \; k_i}{\sum_i w_i} \quad , \tag{75}$$

$$k_{HM} = \frac{\sum_i w_i}{\sum_i w_i/k_i} \quad , \tag{76}$$

$$k_{RMS} = \left(\frac{\sum w_i k_i^2}{\sum w_i} \right)^{1/2} \quad , \tag{77}$$

196
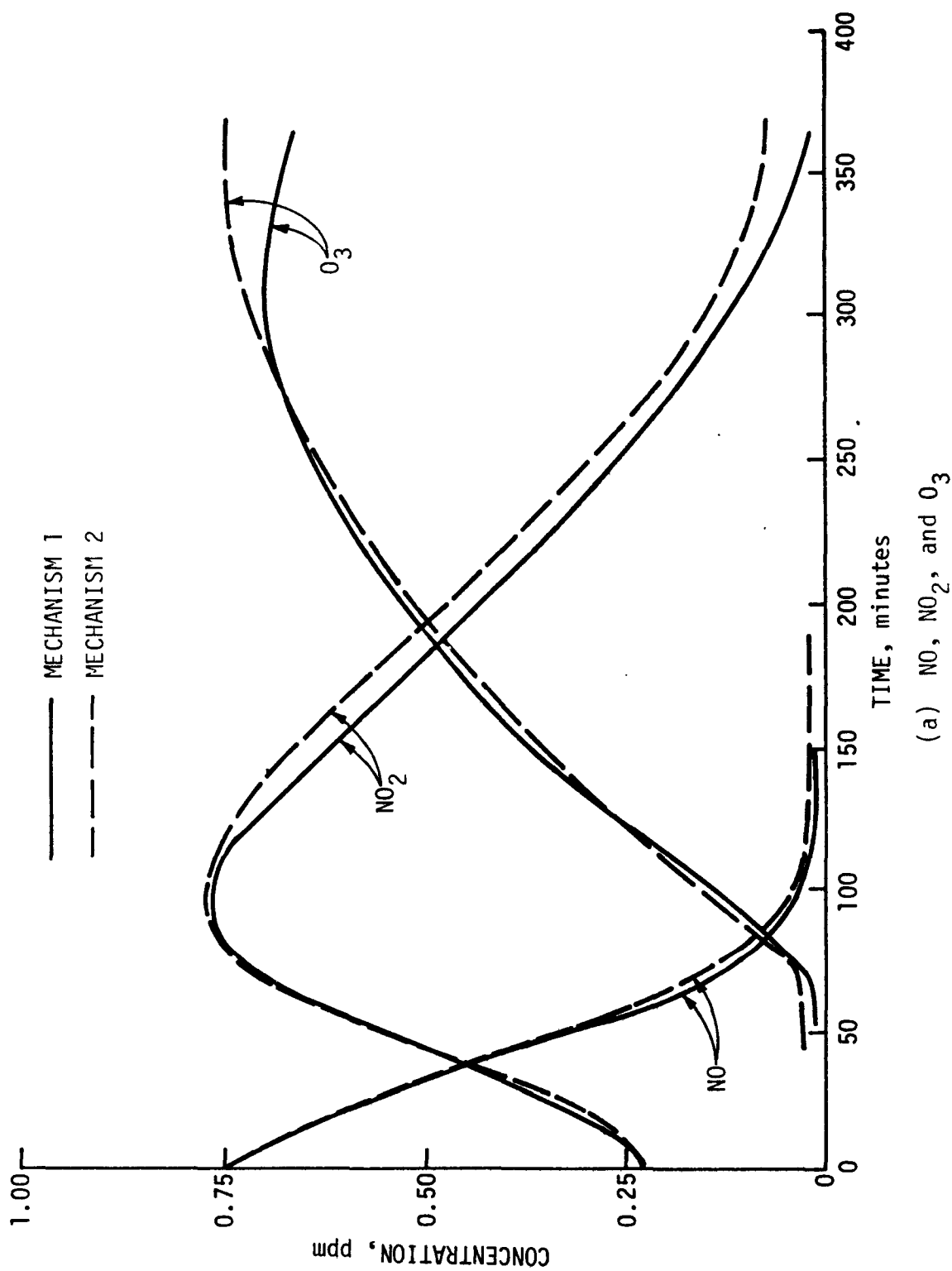
Figure 55. Concentrations of various pollutants in simulations of a multiolefin experiment (EC-150) using Mechanisms 1 and 2

(a) NO, NO_2, and O_3

(b) Ethylene

Figure 55   (Continued)

198

MECHANISM 1
MECHANISM 2

PROPYLENE

CONCENTRATION, ppm

TIME, minutes
(c) Propylene
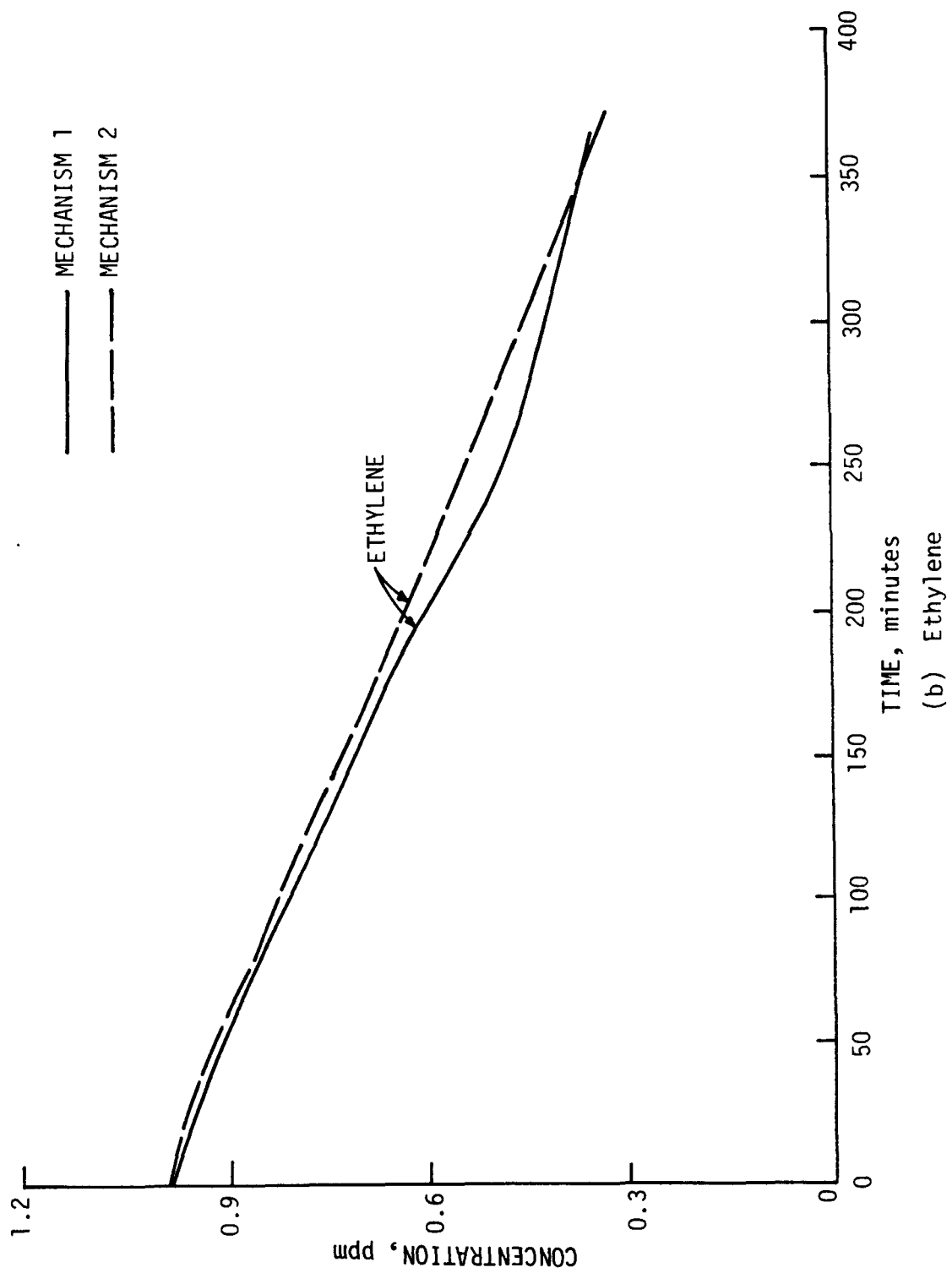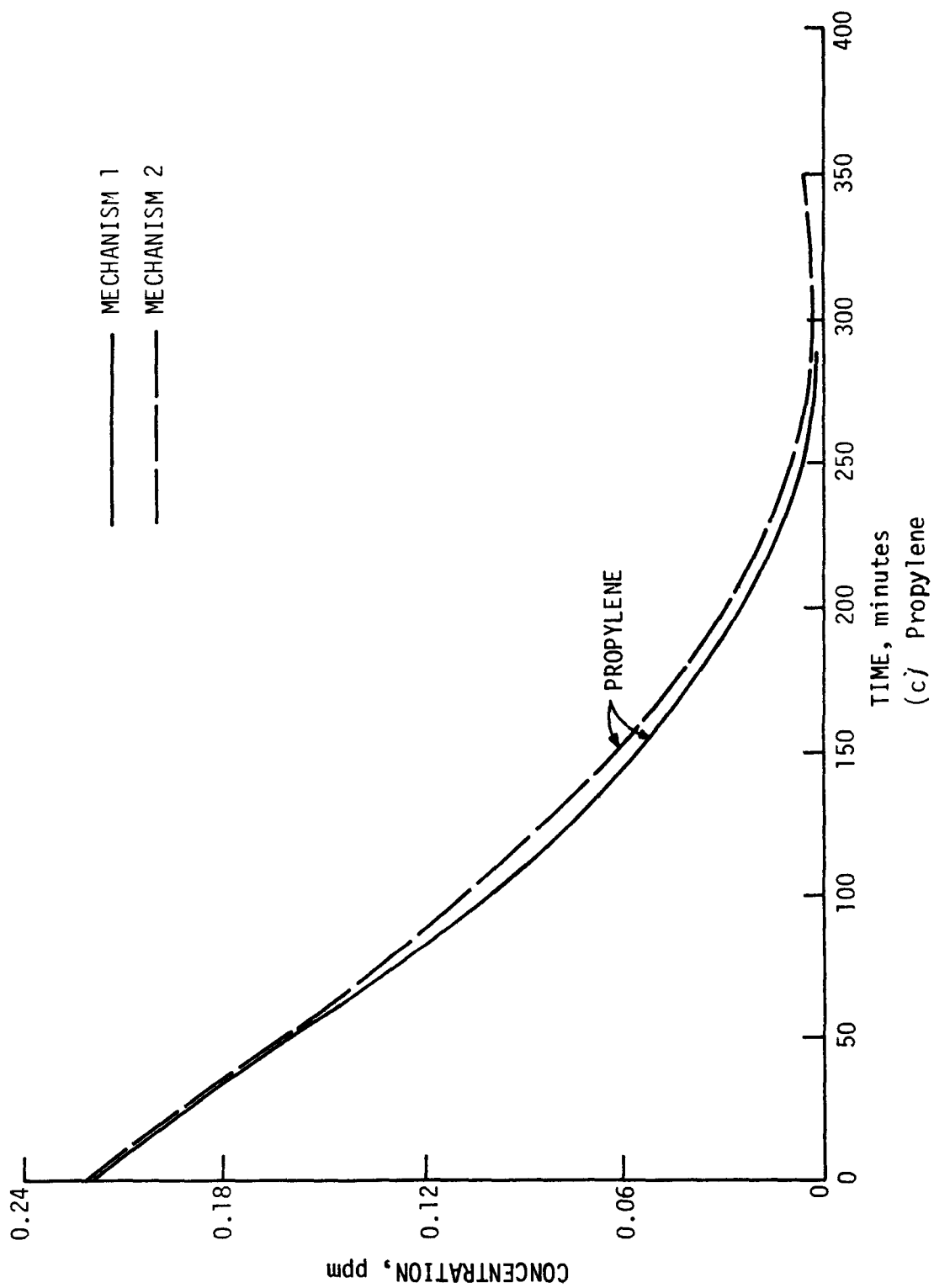
Figure 55 (Continued)
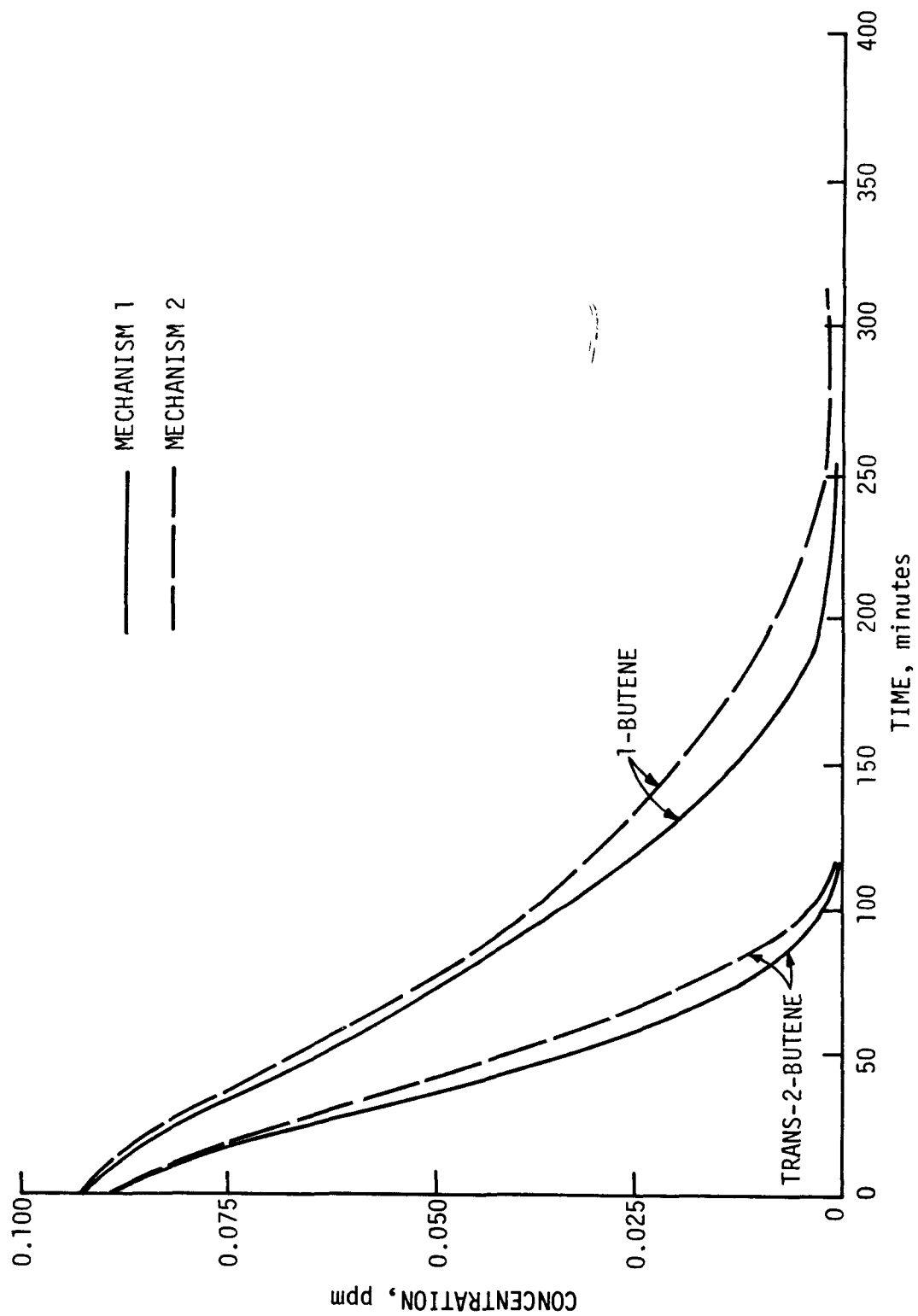
(d) 1-butene and trans-2-butene

Figure 55 (Concluded)

where w_i is the mole fraction of olefin i (relative to the total olefin concentration) and k_i is the rate constant for reaction of olefin i with OH·.

The results of the simulation of the multiolefin experiment with the four mechanisms are summarized in Table 33. The results of using Mechanism 3 are shown in Figure 56 for each of the four averaging methods just discussed. The results are compared to those of Mechanism 2, which we have already shown to be accurate. Note that the root-mean-square rate constant, k_{RMS}, works best.

Figure 57 compares Mechanism 4 to Mechanism 2. Acceptable agreement is obtained for NO when the arithmetic mean of olefin rate constants is used, but NO_2 and O_3 are poorly reproduced regardless of what averaging method is used. Since the simulation with Mechanism 3 agreed fairly closely with those from Mechanisms 1 and 2, the difference between those simulations and the simulation with Mechanism 4 arises from the loss in accuracy inherent in the condensation of the primary oxidation reactions.

TABLE 33.   RESULTS OF SIMULATING A MULTIOLEFIN EXPERIMENT WITH FOUR MECHANISMS

No.	Mechanism	No. of species	No. of reactions	Mechanism (N-1)
1	Full explicit	53	117	--
2	Explicit olefin reactions, condensed secondary oxidation	25	50	Excellent
3	Carbon-Bond Mechanism--olefins treated in two groups, condensed secondary oxidation	21	40	Good
4	CBM, except olefins treated in one group	20	35	Poor
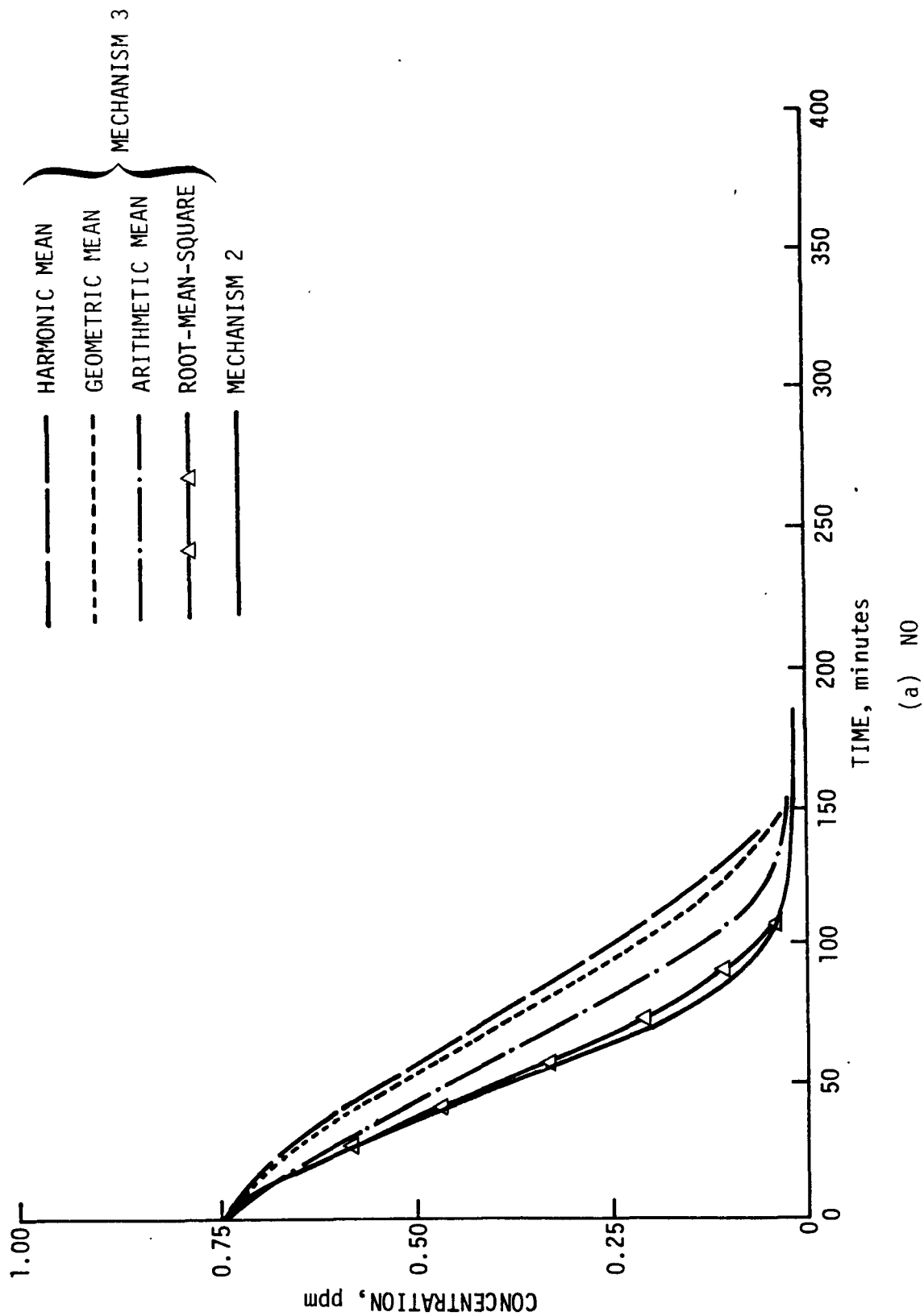
Figure 56. Concentrations of various pollutants in simulations of a multiolefin experiment (EC-150) using Mechanisms 2 and 3

TIME, minutes
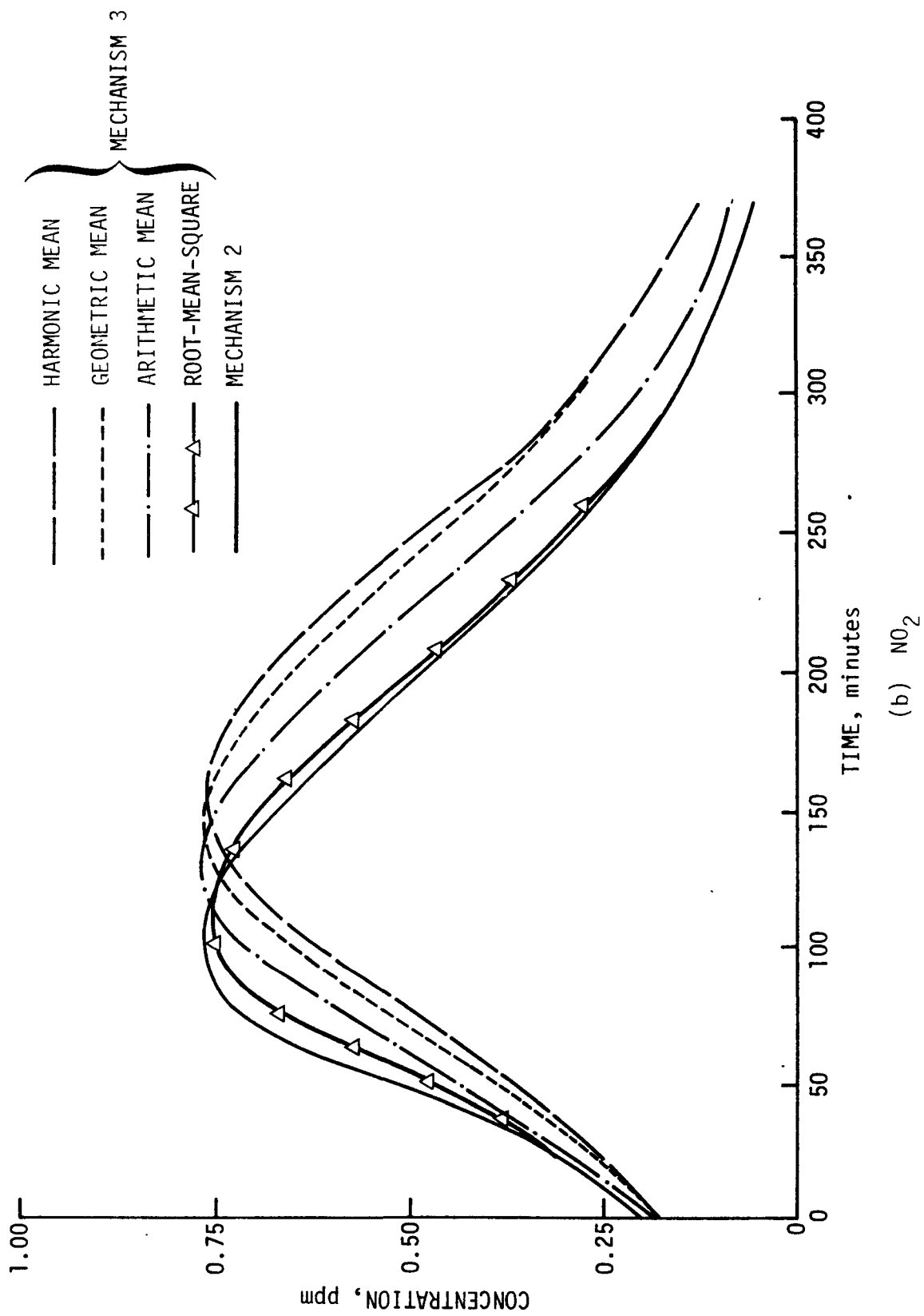
(b) NO$_2$

Figure 56 (Continued)

203
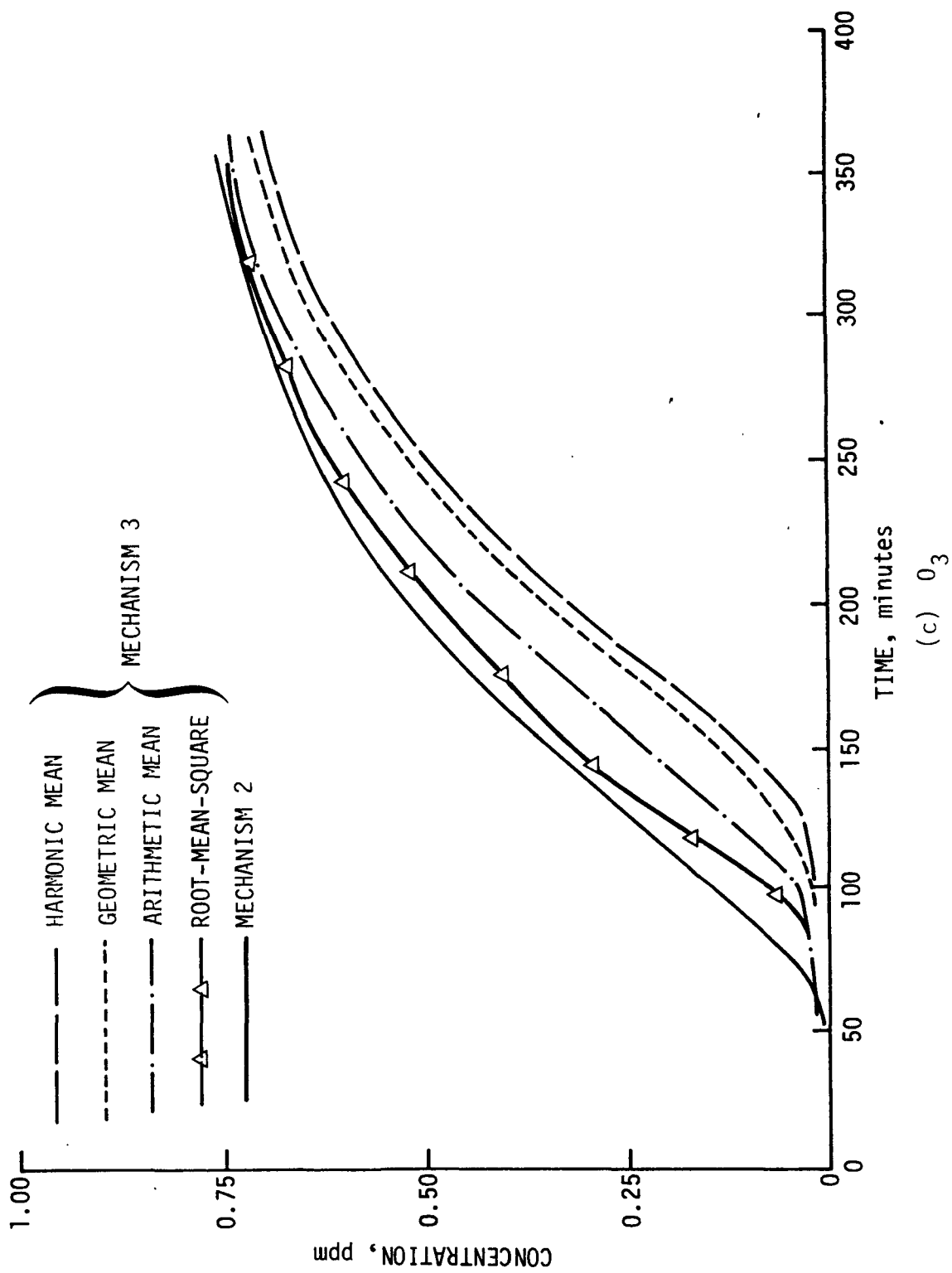
Figure 56 (Concluded)

(c) O_3
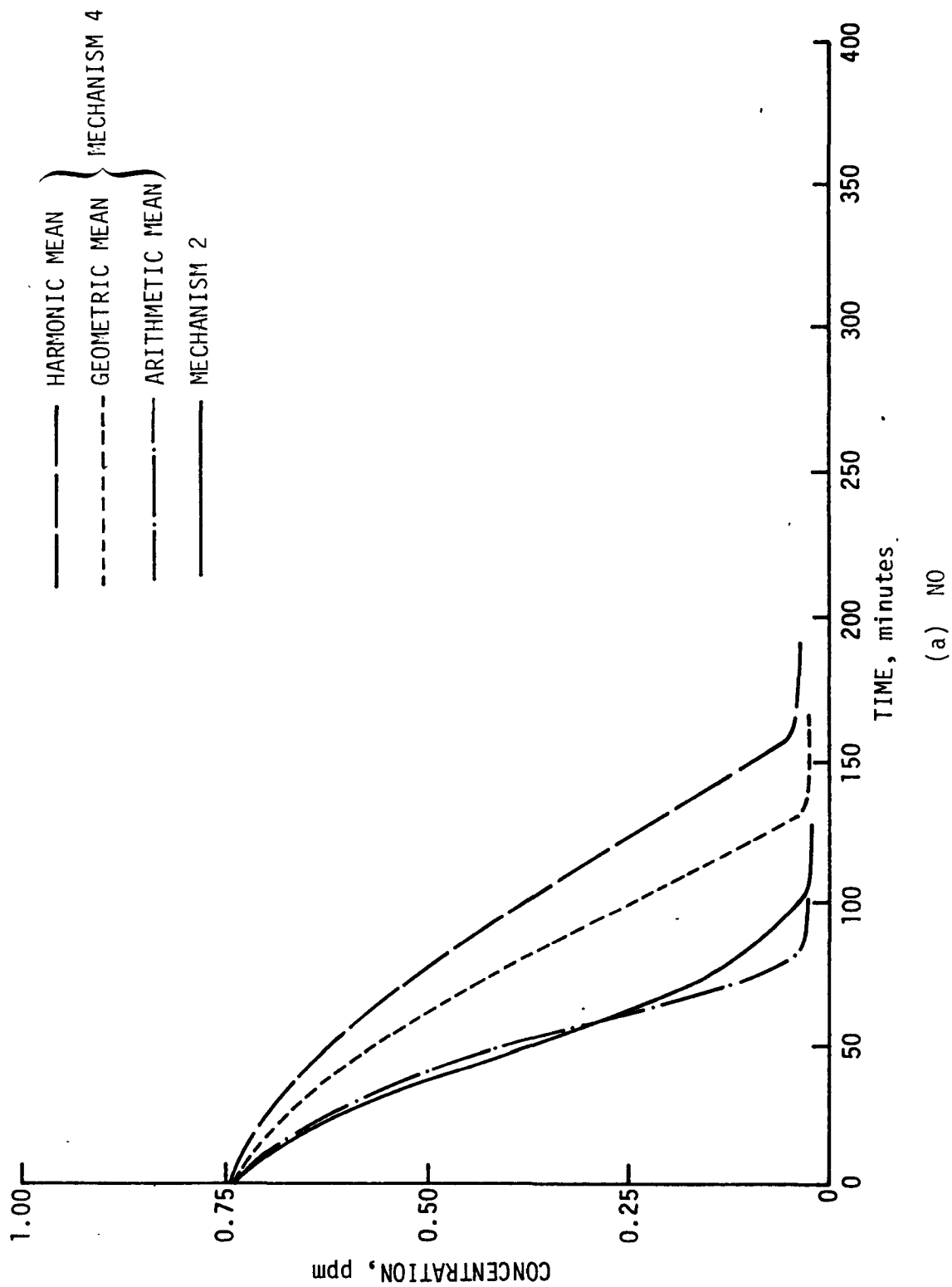
Figure 57. Concentrations of various pollutants in simulations of a multiolefin experiment (EC-150) using Mechanisms 2 and 4

(a) NO
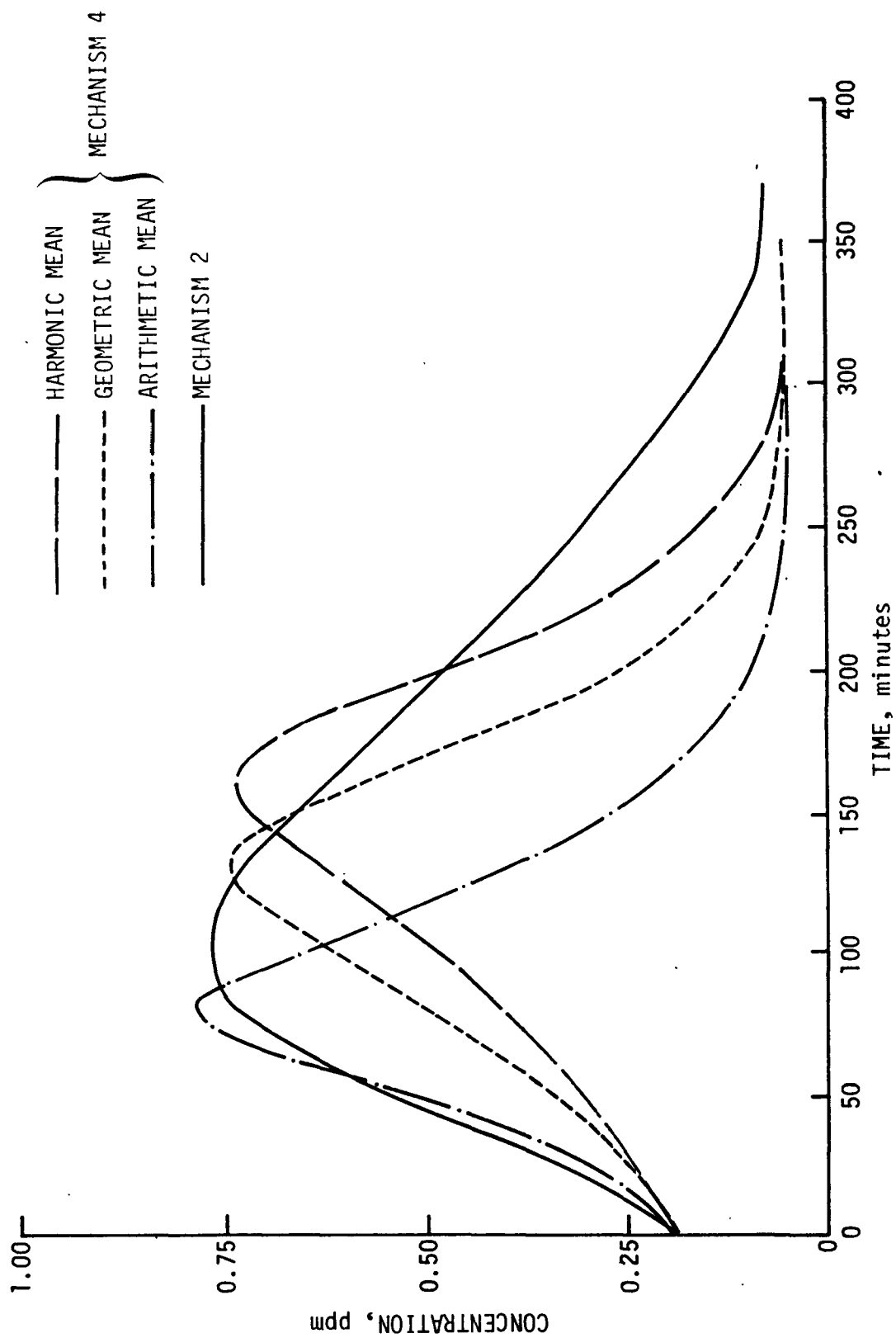
(b) NO$_2$

Figure 57 (Continued)

206

(c) O_3
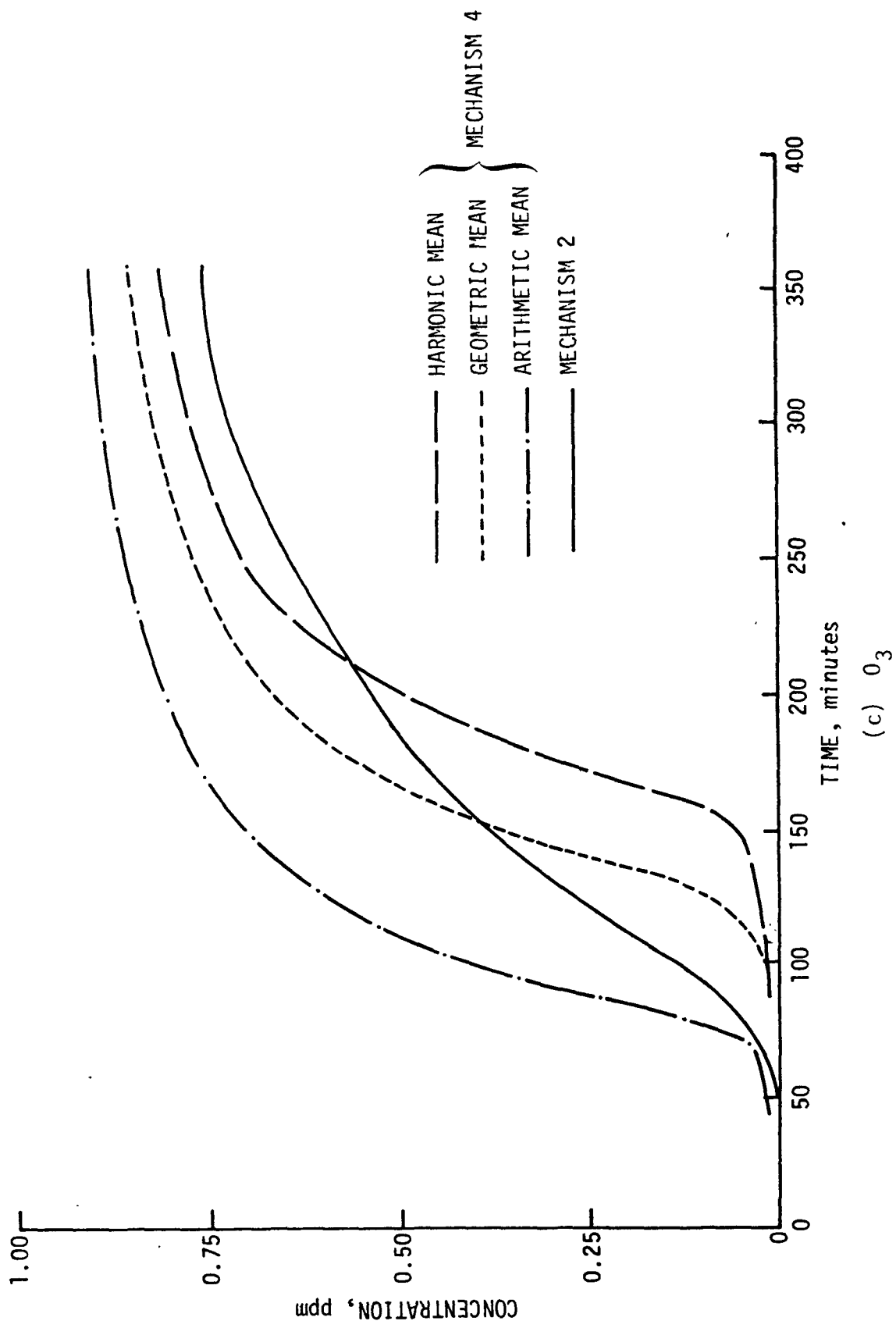
Figure 57 (Concluded)

207

Any time two or more reactants are represented by a single surrogate species with an averaged rate constant some loss in accuracy is unavoidable. In the early stages of any simulation, the more reactive species disappear more rapidly than the less reactive ones, and so the averaged rate constant is too low early in the simulation and too high late in the simulation. Hecht, Liu, and Whitney (1974) showed that a continuously updated average rate constant could be used in a mechanism with condensed primary oxidation reactions to attain greater accuracy. Perhaps the Carbon-Bond Mechanism could be combined with such an averaging scheme. The resulting mechanism should give accuracy commensurate with that of Mechanism 2, yet the number of species treated in the kinetics would be as low as in the standard Carbon-Bond Mechanism. Unfortunately, using such an averaging scheme would require more data, namely, the relative amounts of different molecules of the same chemical type.

In summary, this test suggests that mechanisms slightly more condensed than the CBM can be much less accurate if ethylene is grouped with other olefins and that mechanisms with less condensation are only slightly more accurate, indicating that the CBM represents a desirable compromise between compactness of form and accuracy of prediction.

FORMULATION OF THE NEW VERSION OF THE CARBON-BOND MECHANISM

At the time the original CBM was formulated it represented a condensation of existing explicit mechanisms (primarily for propylene and butane). It was also used to simulate a set of smog chamber experiments with a reasonable degree of success. Knowledge of smog chemistry has expanded to include more molecules, however, and the amount of data from smog chamber experiments has increased. Therefore, we sought to improve the Carbon-Bond Mechanism.

Periodic updating of generalized mechanisms such as the CBM is to be preferred to continuous updating. Changes in one reaction may require compensating changes in other reactions to maintain the overall predictive

accuracy of simulations using the mechanism. Consequently, after a change
the mechanism should be tested with an entire set of smog chamber data
to ensure that no special problems have been created that would create
difficulties in atmospheric applications. The cost of such testing makes
it desirable to test the effects of several changes at once. In addition,
documentation of any changes is necessary to keep all users of the mechan-
ism informed.

The formulation of the new version of the CBM reflects the following
changes to the original CBM:

> Elimination of the peroxyformyl radical (HCO_3^-).

> Updating of the rate constants and the exclusion of HONO
  and HOOH.

> Inclusion of the reactions of intermediate Criegee
  species formed from ozone-olefin reactions.

> Inclusion of new surrogate species representing the
  addition products of OH· to double bonds.

> Inclusion of a new formulation for carbonyl photolysis
  and oxidation.

> Treatment of alkyl radicals in long-chain paraffins.

> Treatment of ethylene as an explicit species.

> Treatment of internal olefins as carbonyls.

> Use of a root-mean-square rate constant for the reactions
  of OH·, O, and O_3 with hydrocarbons.

> Incorporation of a new aromatic chemical reaction scheme.

Each of these changes is discussed individually in the following subsections.
Table 34 lists the current version of the CBM.

Elimination of the Peroxyformyl Radical

At the time of the original formulation of the CBM, our explicit
mechanisms included the peroxyformyl radical (HCO_3^-), which no longer

209

TABLE 34. THE NEW CARBON-BOND MECHANISM

Reaction	Rate constant at 298K* $(ppm^{-1}min^{-1})$	Activation energy (K)
$NO_2 + h\nu \rightarrow NO + O$	Experimental[+]	--
$O + O_2 + M \rightarrow O_3 + M$	2.1×10^{-5} [§]	--
$O_3 + NO \rightarrow NO_2 + O_2$	23.9	1,450
$O_3 + NO_2 \rightarrow NO_3 + O_2$	4.8×10^{-2}	2,450
$O + NO_2 \rightarrow NO + O_2$	1.34×10^4	--
$O_3 + OH \rightarrow HO_2 + O_2$	7.7×10^1	1,000
$O_3 + HO_2 \rightarrow OH + 2O_2$	5.0	1,525
$NO_2 + OH \rightarrow HNO_3$	1.4×10^4	--
$CO + OH \xrightarrow{O_2} HO_2 + CO_2$	4.4×10^2	--
$NO + NO + O_2 \rightarrow 2NO_2$	7.1×10^{-10} [§]	--
$NO_3 + NO \rightarrow 2NO_2$	2.8×10^4	--
$NO_3 + NO_2 + H_2O \rightarrow 2HNO_3$	1.56×10^{-3} [§]	-10,600
$HO_2 + NO \rightarrow NO_2 + OH$	1.2×10^4	--
$HO_2 + HO_2 \rightarrow$	1.5×10^4	--
$PAR + O \rightarrow MEO_2 + OH$	2×10^1	--
$PAR + OH \rightarrow MEO_2$	1.5×10^3	--
$OLE + O \rightarrow MEO_2 + ACO_3 + X$	2.7×10^3	--
$OLE + O \rightarrow CARB$	2.7×10^3	--
$OLE + OH \rightarrow RAO_2$	4.2×10^4	--
$OLE + O_3 \rightarrow CARB + CRIG$	8×10^{-3}	--
$OLE + O_3 \rightarrow CARB + MCRG$	8×10^{-3}	--
$ETH + O \rightarrow MEO_2 + HO_2 + CO$	6×10^2	--
$ETH + O \rightarrow CARB$	6×10^2	--

(Continued)

210

TABLE 34 (Continued)

Reaction	Rate constant at 298K $(ppm^{-1}min^{-1})$	Activation energy (K)
$ETH + OH \rightarrow RBO_2$	1.2×10^4	--
$ETH + O_3 \rightarrow CARB + CRIG$	2.4×10^{-3}	
$ACO_3 + NO \rightarrow NO_2 + MEO_2 + CO_2$	3.8×10^3	--
$RBO_2 + NO \rightarrow NO_2 + 2\ CARB + HO_2$	1.2×10^4	--
$RAO_2 + NO \rightarrow NO_2 + 2\ CARB + HO_2$	1.2×10^4	--
$MEO_2 + NO \rightarrow NO_2 + CARB + MEO_2 + X$	$(1.2 \times 10^4)(A-1)/A^{**}$	--
$MEO_2 + NO \rightarrow NO_2 + CARB + HO_2$	$(1.2 \times 10^4)/A^{**}$	--
$MEO_2 + NO \rightarrow Nitrate$	5×10^2	--
$RBO_2 + O_3 \rightarrow 2\ CARB + HO_2$	5.0	--
$RAO_2 + O_3 \rightarrow 2\ CARB + HO_2$	2×10^2	--
$MEO_2 + O_3 \rightarrow CARB + HO_2$	5.0	--
$CARB + OH \rightarrow \alpha(HO_2 + CO) + (1 - \alpha)(ACO_3 + X)$	$(2.4 - \alpha) \times 10^4$	--
$CARB + h\nu \rightarrow CO$	$\alpha k_f^{*\dagger\dagger}$	--
$CARB + h\nu \rightarrow (1 + \alpha)HO_2 + (1 - \alpha)(MEO_2 + X) + CO$	$\left(\frac{\alpha + 1}{2}\right)k_f^{*\dagger\dagger}$	--
$X + PAR \rightarrow$	1×10^5	--
$ACO_3 + NO_2 \rightarrow PAN$	2×10^3	--
$PAN \rightarrow ACO_3 + NO_2$	$2.8 \times 10^{-2^+}$	12,500
$ACO_3 + HO_2 \rightarrow$	4×10^3	--
$MEO_2 + HO_2 \rightarrow$	4×10^3	--
$CRIG + NO \rightarrow NO_2 + CARB$	1.2×10^4	--
$CRIG + NO_2 \rightarrow NO_3 + CARB$	8×10^3	--
$CRIG + CARB \rightarrow Ozonide$	2×10^3	--
$MCRG + NO \rightarrow NO_2 + CARB$	1.2×10^4	--
$MCRG + NO_2 \rightarrow NO_3 + CARB$	8×10^3	--

TABLE 34 (Concluded)

Reaction	Rate constant at 298K $(ppm^{-1}min^{-1})$	Activation energy (K)
MCRG + CARB → Ozonide	2×10^3	--
CRIG → CO	$6.7 \times 10^{2\dagger}$	--
CRIG → Stable Products	$2.4 \times 10^{2*}$	--
CRIG → 2HO$_2$ + CO	$9 \times 10^{1*}$	--
MCRG → Stable Products	$1.5 \times 10^{2*}$	--
MCRG → MEO$_2$ + OH + CO + X	$3.4 \times 10^{2§}$	--
MCRG → MEO$_2$ + HO$_2$ + X	$4.25 \times 10^{2*}$	--
MCRG → CARB + 2HO$_2$ + X	$8.5 \times 10^{1*}$	--
ARO + OH → Y + HO$_2$	1.5×10^4	--
ARO + OH → Y + OH	9×10^3	--
Y + NO → NO + AERO	1×10^1	--
Y + NO → NO + HCHO + PAR	2×10^1	--
Y + NO$_3$ → HNO$_3$	3.5×10^4	--
Y + O$_3$ → PAR + PAR	5×10^{-1}	--

* The rate constants shown are as used to model eleven experiments at UCR that used mixes of seven hydrocarbons. For that study the default values, α = 0.5 and A = 1.5, were used.

+ Units of min^{-1}.

§ Units of ppm^{-2}min^{-1}.

** A is the average number of RO$_2$-type radicals from a hydrocarbon between attack by OH· and generation of HO$_2$.

++ α is the fraction of total aldehydes that represents formaldehyde and ketones. k_f is the rate constant for the reaction HCHO + hν → 2HO$_2$ + CO.

appears in our explicit chemistry (see Section 5 for further discussion). To account for this change, we introduced a new surrogate species, $ACO_3^\bullet$, which is-a surrogate for $RCO_3^\bullet$ radicals (where R has one or more carbon atoms). $ACO_3^\bullet$, which has two carbon atoms, is formed in the CBM from the reaction of OH· with CARB, which represents only one carbon atom. Thus some correction must be made to preserve carbon mass balance. The correction we used is suggested by a reaction of $RCO_3^\bullet$ in the explicit mechanisms. Recall that in those mechanisms $RCO_3^\bullet$ ($R \geq CH_3$) can react with NO to produce NO_2, CO_2, and $RO_2^\bullet$. The significance of that reaction is that it initiates the oxidation of the carbon atom adjacent to the $CO_3^\bullet$ group in $RCO_3^\bullet$ without any involvement of OH· or O. Thus it corresponds, in the terms used in the CBM, to the conversion of PAR to MEO_2 by a pathway not previously accounted for in the CBM. In the revised Carbon-Bond Mechanism $ACO_3^\bullet$ reacts with NO to produce NO_2, CO_2, and MEO_2 (the surrogate for $RO_2^\bullet$). When this reaction is included in the CBM one PAR must be subtracted to account for the MEO_2 formed (i.e., to maintain carbon mass balance). We accomplished this by means of a fictitious compound X. One X is produced whenever an extra carbon atom appears on the right side of a chemical reaction. This X immediately removes one PAR by means of the reaction PAR + X→ , which is given a very high rate constant. Typically the appearance of X accounts for the oxidation of a single-bonded carbon atom from the PAR pool by pathways other than direct reaction with OH· or O. These other pathways were not accounted for in the original formulation of the CBM.

At present, we do not treat the case of X being produced when no saturated carbon atoms remain (i.e., [PAR] = 0). None of the UCR experiments simulated to date seems to require consideration of this potential problem. During the coming year, we will investigate such possibilities as a competitive reaction for X with the $ACO_3^\bullet$ or the MEO_2 produced at the same time; either reaction would produce $HO_2^\bullet$.

Updating of the Reaction Rate Constants

The reaction rate constants from the original CBM developed by Whitten and Hogo (1977) were updated to those shown in Table 34 as discussed in Sections 4 and 5. One of the new features of the CBM is the inclusion of activation energies to account for variations in temperatures.

On the basis of studies of the effects of HONO chemistry in the explicit mechanisms (see Section 4), we have eliminated HONO chemistry from the CBM. For the smog chamber simulations, we have introduced a species "RX", with a decay constant and concentrations similar to those of the initial HONO used in the explicit mechanism as a source of radicals found initially in the simulations (see Section 4 for further discussion).

Hydrogen peroxide as an explicit chemical species has been eliminated from the CBM on the basis of investigations of the explicit mechanisms showing that the photolysis of hydrogen peroxide plays only a minor role as a radical source. Thus, the only reaction used in the CBM is:

$$HO_2^\bullet + HO_2^\bullet \rightarrow \qquad , \qquad k = 1.5 \times 10^4 \ ppm^{-1}min^{-1} \quad .$$
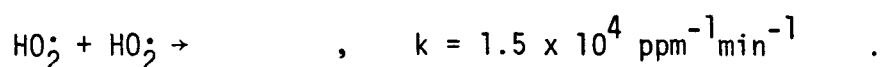
Products of the Ozone-Olefin Reactions

Because Criegee intermediates from the ozone-olefin reaction were added to the explicit mechanisms, we included them in the Carbon-Bond Mechanism. The Criegee intermediates are represented by the symbols CRIG for CH_2O_2 and MCRG for $CH_3CH_2O_2$, the two Criegee intermediates found in the explicit mechanisms. Since the reactions of the Criegee intermediates are the same as those discussed in Section 5, they are not discussed here. As noted in Section 5, the rate and amount of production of radicals from Criegee intermediates is still uncertain. Therefore, the CBM may be further updated as more information concerning the fate of these intermediates becomes known.

Carbonyl Photolysis and Oxidation

A necessary part of the formulation of the Carbon-Bond Mechanism is the condensation of the reactions of aldehydes and ketones into two types of reactions, namely, photolysis and oxidation by hydroxyl radical.

In general, aldehydes larger than formaldehyde appear to photolyze as follows:

$$RCHO + h\nu \rightarrow R'O_2^{\cdot} + HO_2^{\cdot} + CO \qquad k_{78} = \phi k_f \qquad . \qquad (78)$$

The photolysis rate constant ϕk_f is defined as: ϕ is the average quantum yield, and k_f is the photolysis rate constant for formaldehyde producing two radicals. (Note that k_f is the same as FORM→Products, which is defined and discussed in detail in Section 4.) In all computer simulations discussed in the previous sections, a value of 0.5 for ϕ was assigned to all higher aldehyde photolysis reactions. We used k_f to represent the photolysis rate constant for all aldehydes.

In the photolysis of formaldehyde under a typical solar spectrum, two reaction pathways occur at approximately equal rates (see Section 4):

$$HCHO + h\nu \rightarrow H_2 + CO \qquad k_{79} = k_f \qquad , \qquad (79)$$

$$HCHO + h\nu \rightarrow HO_2^{\cdot} + HO_2^{\cdot} + CO \qquad k_{80} = k_f \qquad . \qquad (80)$$
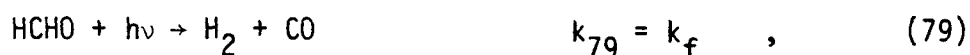
Thus the total photolysis rate for formaldehyde is $2 \times k_f$. For the photolysis of ketones, we assumed that the rate constant is k_f, as was done in the explicit mechansims.

To condense all the aldehydes and carbonyls into one reaction,

$$CARBONYLS + h\nu \rightarrow RO_2^{\cdot} + HO_2^{\cdot} + CO \qquad k_{81} = k \qquad , \qquad (81)$$
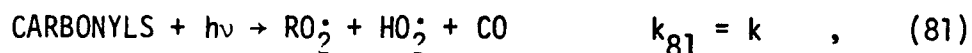
we define a variable α as the fraction of the total aldehydes and ketones that is formaldehyde and ketones:

$$\alpha = \frac{[\text{Formaldehyde}] + [\text{Ketones}]}{[\text{Total Carbonyls}]} \quad ,$$

$$1 - \alpha = \frac{[\text{Higher Aldehdyes}]}{[\text{Total Carbonyls}]} \quad .$$

Defining CARB as the concentration of carbonyls (i.e., the sum of the aldehyde and ketone concentrations), we can write:

$$CARB + h\nu \rightarrow \alpha(H_2 + CO) = \alpha CO + \alpha H_2 \quad , \tag{82a}$$

$$CARB + h\nu \rightarrow \alpha(HO_2^\bullet + HO_2^\bullet + CO) = 2\alpha HO_2^\bullet + \alpha CO \quad , \tag{82b}$$

$$CARB + h\nu \rightarrow (1 - \alpha)(MEO_2 + X + HO_2^\bullet + CO) \quad , \tag{82c}$$
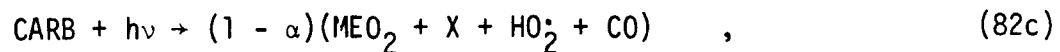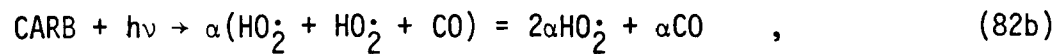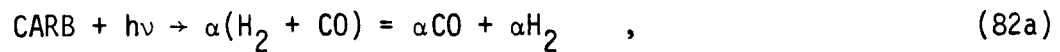
Each of the above reactions represents the photolysis of the aldehydes [Reactions (82a and 82b) represent formaldehyde, and Reaction (82c) represents the higher aldehydes]. The sum of Reactions (82b) and (82c) is:

$$CARB + h\nu \rightarrow (1 + \alpha)HO_2 + (1 - \alpha)(MEO_2 + X) + CO \quad k_{82d} = k \quad . \tag{82d}$$
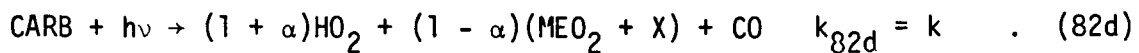
The rate constant for Reaction (82d) is:

$$k = k_{82b} + k_{82c} \quad ,$$

where $k_{82b} = \alpha k_f$ and $k_{82c} = (1 - \alpha)\frac{k_f}{2}$.

Therefore,

$$k = \left(\frac{1 + \alpha}{2}\right) k_f \quad .$$

Thus, we can write Reactions (82a) through (82d) as:

$$CARB + h\nu \rightarrow H_2 + CO \qquad\qquad k_{83} = \alpha k_f \quad , \qquad (83)$$

$$CARB + h\nu \rightarrow (1 + \alpha)HO_2 + (1 - \alpha)(MEO_2 + X) + CO \qquad k_{84} = \left(\frac{\alpha + 1}{2}\right)k_f \quad . \qquad (84)$$
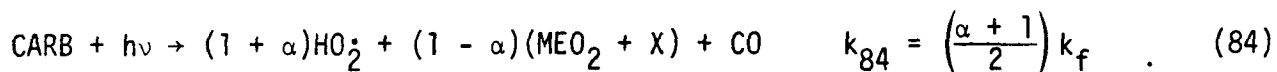
Note that in systems with pure formaldehyde, Reactions (83) and (84) would reduce to Reactions (79) and (80). For systems with higher aldehydes and zero formaldehyde ($\alpha = 0$), Reaction (83) would not occur, and Reaction (84) would reduce to Reaction (78). By grouping ketones and formaldehyde as α, we can simulate the effect of the ketones in our present explicit mechanisms. Reactions (83) and (84) can be further condensed to one equation:

$$CARB + h\nu \rightarrow \frac{(\alpha + 1)^2}{3\alpha + 1} HO_2 \quad ,$$

$$+ \frac{(1 - \alpha^2)}{3\alpha + 1}\left(MEO_2 + X\right) + CO \qquad k_{85} = \left(\frac{3\alpha + 1}{2}\right)k_f \quad .$$
$$(85)$$
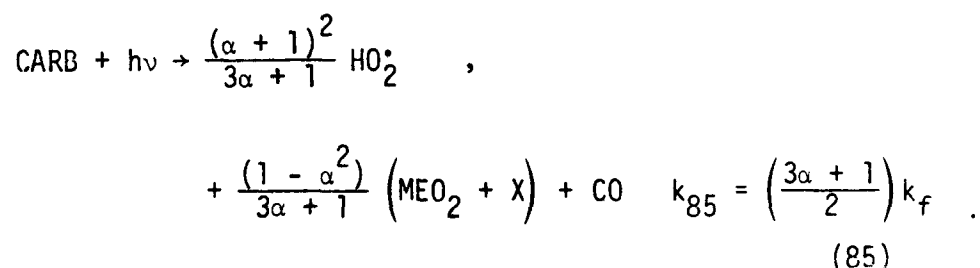
The second major reaction of aldehydes is oxidation by hydroxyl radicals:

$$RCHO + OH\cdot \rightarrow \begin{cases} HO_2 + CO + H_2O & \text{for formaldehyde} \\ \\ ACO_3 + H_2O & \text{for higher aldehydes} \end{cases} \quad .$$
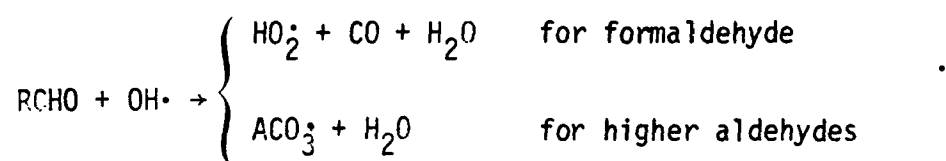
Using our definition of α, we can write the oxidation reaction as one general reaction:

$$CARB + OH\cdot \rightarrow \alpha(HO_2 + CO) + (1 - \alpha)(ACO_3 + X) \qquad k_{86} = (2.4 - \alpha) \times 10^4 \quad . \qquad (86)$$
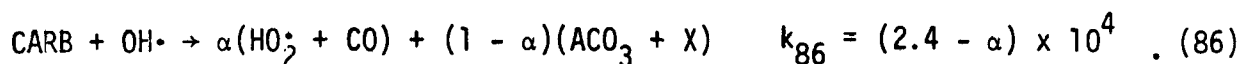
Since α represents both formaldehyde and ketones, we assumed that the carbonyl oxidation reaction (No. 86) approximates the actual ketone oxidation reaction.

Treatment of Alkyl Radicals

In the discussion of alkylperoxy radicals in Section 5, we note the following general reactions:

$$RO_2^• + NO \rightarrow RO• + NO_2 \quad , \tag{87}$$

$$RO_2^• + NO \rightarrow Nitrates \quad , \tag{88}$$

$$RO• + O_2 \rightarrow Aldehyde + HO_2^• \quad , \tag{89}$$

$$RO• \xrightarrow{O_2} HORO_2^• \quad , \tag{90}$$

$$RO• \xrightarrow{O_2} R'O_2• + Aldehyde \quad , \tag{91}$$

$$RO_2^• + HO_2^• \rightarrow Stable Products \quad . \tag{92}$$
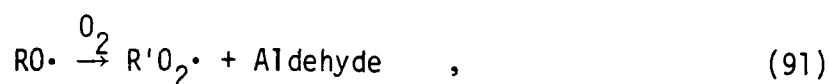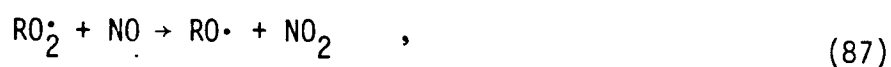
We have condensed these reactions as follows

$$MEO_2 + NO \rightarrow NO_2 + CARB + HO_2^• \quad , \tag{93}$$

$$MEO_2 + NO \rightarrow NO_2 + CARB + (MEO_2 + X) \quad , \tag{94}$$

$$MEO_2 + NO \rightarrow Nitrates \quad , \tag{95}$$

$$MEO_2 + HO_2^• \rightarrow Stable Products \quad . \tag{96}$$
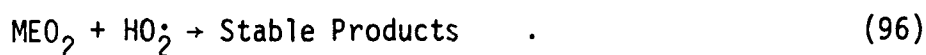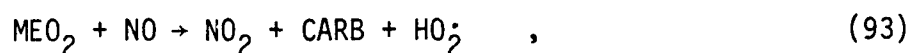
Reactions (90) and (91) occur in systems with carbon chains greater than or equal to four (e.g., butane and 2,3-dimethylbutane). The present

explicit mechanisms show that for butane and 2,3-dimethylbutane, the amount of RO_2^*-type radicals formed per oxidation (via OH· attack) of the initial hydrocarbon is greater than one. Part of this oxidation is due to an isomerization reaction (No. 90). To account for the extra RO_2^*-type radicals formed before HO_2^* is generated, we have defined a new parameter A, which represents the average number of RO_2^*-type radicals formed per initial hydrocarbon oxidized until an HO_2^* is formed. For short-chain hydrocarbons (i.e., carbon number less than four), A = 1.

The 2,3-dimethylbutane molecule predominantly forms a tertiary peroxyalkyl radical after reaction with OH·. That radical can react with NO to produce NO_2 and a tertiary alkoxyl radical, which in turn leads to one more peroxy radical (according to our present explicit mechanism; see Table 21 in Section 5). The HO_2^* radical does not appear until this second peroxy radical has reacted with NO to yield NO_2. Thus, $A \cong 2$ for 2,3-dimethylbutane.

The rate constants for Reaction (93), (94), and (95) are related as follows:

$$k_{93} + k_{94} + k_{95} = 1.2 \times 10^4 \ ppm^{-1}min^{-1} \quad ,$$

$$k_{94} = k_{93} (A - 1) \quad .$$

The relationship between k_{93} and k_{94} is derived from the sum of an infinite geometric series. For 2,3-dimethylbutane, using an A = 2 and ignoring nitrate formation (k_{95} = 0) implies that $k_{94} = k_{93}$. Consequently, half the time MEO_2 would be re-formed when MEO_2 reacts with NO. Therefore, the cycle would be:

$$1 + \frac{1}{2} + \frac{1}{4} + \frac{1}{8} + \ldots = 2 \quad .$$

In computer simulations with detailed mechanisms, we found that alkyl nitrate formation from RO_2^* + NO can be important in long-chain hydrocarbon systems (Darnall et al., 1976a). Thus, we included Reaction (95) in the

Carbon-Bond Mechanism. For simulations of small hydrocarbons, we used a rate constant of 100 ppm^{-1}min^{-1} for Reaction (95). For longer chain hydrocarbons (butane and 2,3-dimethylbutane), we assumed a value of 1000 ppm^{-1}min^{-1}. For mixtures of hydrocarbons, we assumed an intermediate value of 500 ppm^{-1}min^{-1}, which produced nitrate levels in agreement with the UCR measurements.

Treatment of Ethylene Chemistry

Ethylene was grouped with aromatics in the original CBM. Since we have developed a separate scheme for aromatics, we now treat ethylene as a species in its own class. The ethylene chemistry consists of the same reactions as the explicit ethylene mechanism given in Section 5.

Treatment of Internal Olefins as Carbonyls

Detailed investigations of the trans-2-butene experiment have led us to postulate the initial trans-2-butene/NO$_x$ experiments as essentially aldehyde/NO$_x$ experiments. After approximately 60 minutes of an experiment, virtually all of the trans-2-butene has been oxidized. Therefore, for the Carbon-Bond Mechanism, we have assumed all of the initial trans-2-butene to be carbonyls. One trans-2-butene can be represented as two carbonyls.

Two computer simulations with the CBM were performed, one using trans-2-butene as the initial olefin (Figure 58) and the other using trans-2-butene as carbonyls (Figure 59). As shown in these figures, the results of the simulations are essentially the same, except that the NO$_x$ crossover time is late in Figure 59. When trans-2-butene is considered a carbonyl, we lose some radicals associated with the trans-2-butene + O(^{3}P) reaction that are needed initially and possibly some early conversions of NO to NO$_2$ as well. By increasing the initial radical source "RX" slightly, we can shift the NO$_x$ crossover to be more consistent with the observed data and the explicit mechanism simulations. The ozone-olefin reactions do not become important because no trans-2-butene is left when the ozone forms. For mixtures
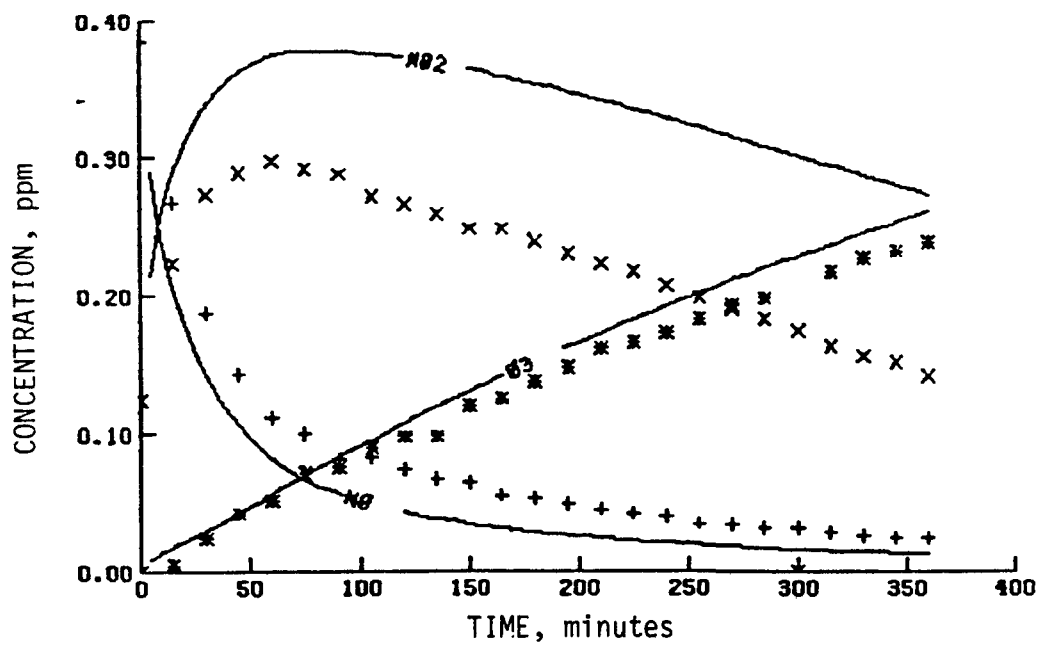
(a) NO_2, NO, and O_3
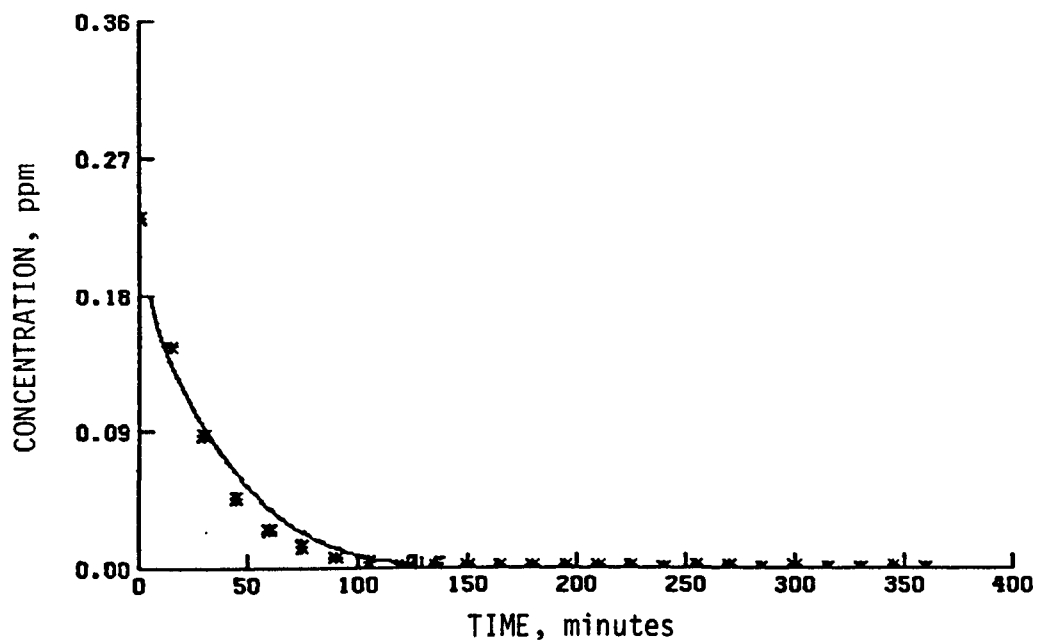
(b) Olefins

Figure 58. Simulation results of a UCR trans-2-butene equipment (EC-146) with the Carbon-Bond Mechanism
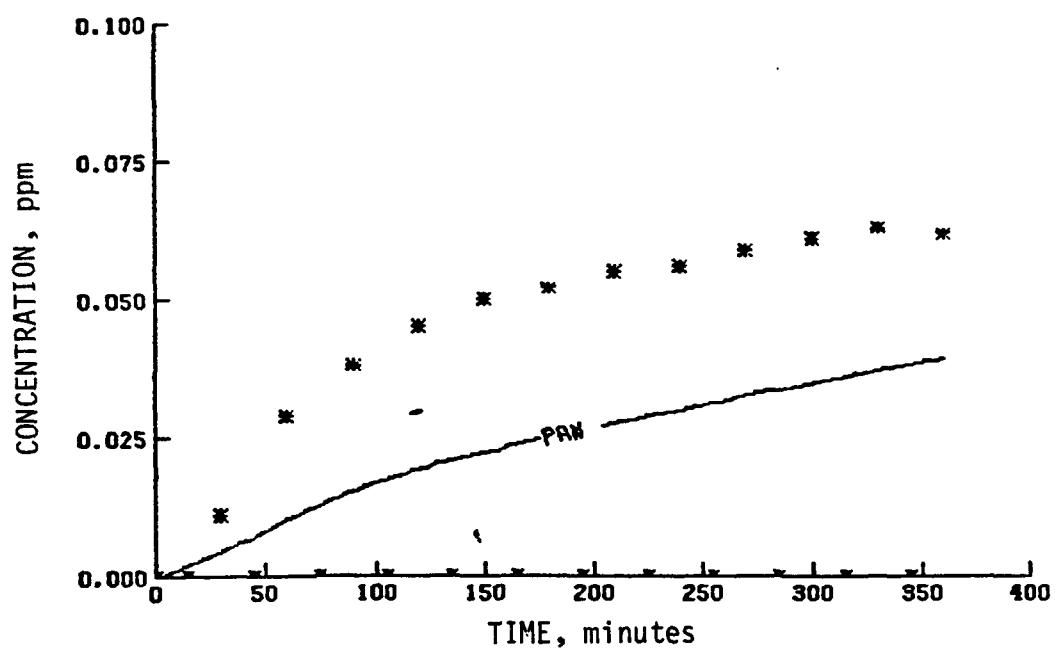
(c) PAN

Figure 58 (Concluded)
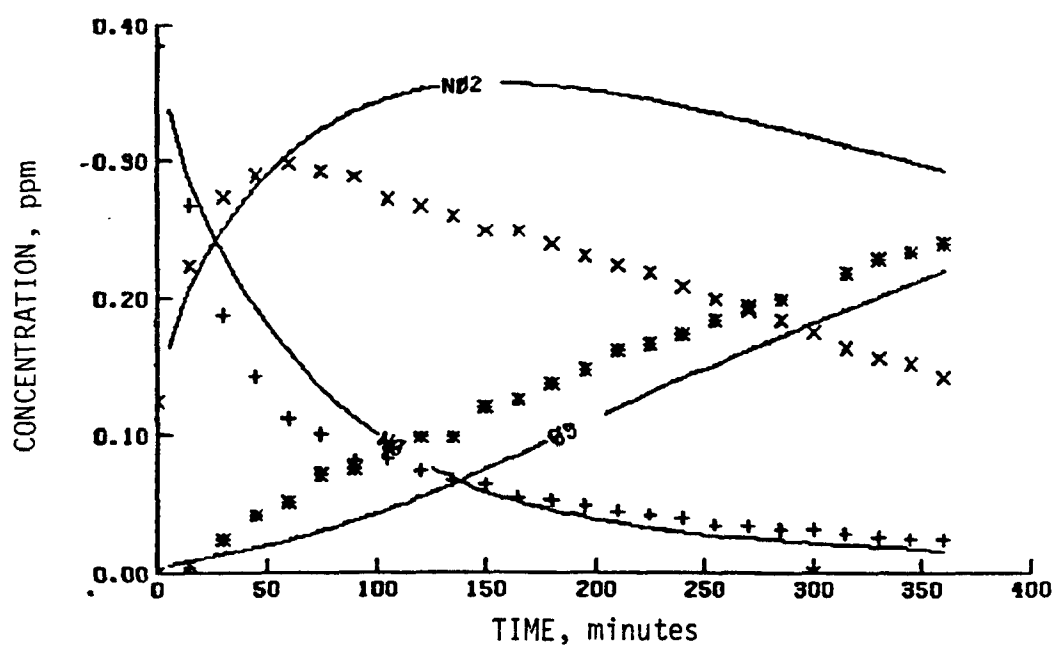
(a) NO_2, NO, and O_3
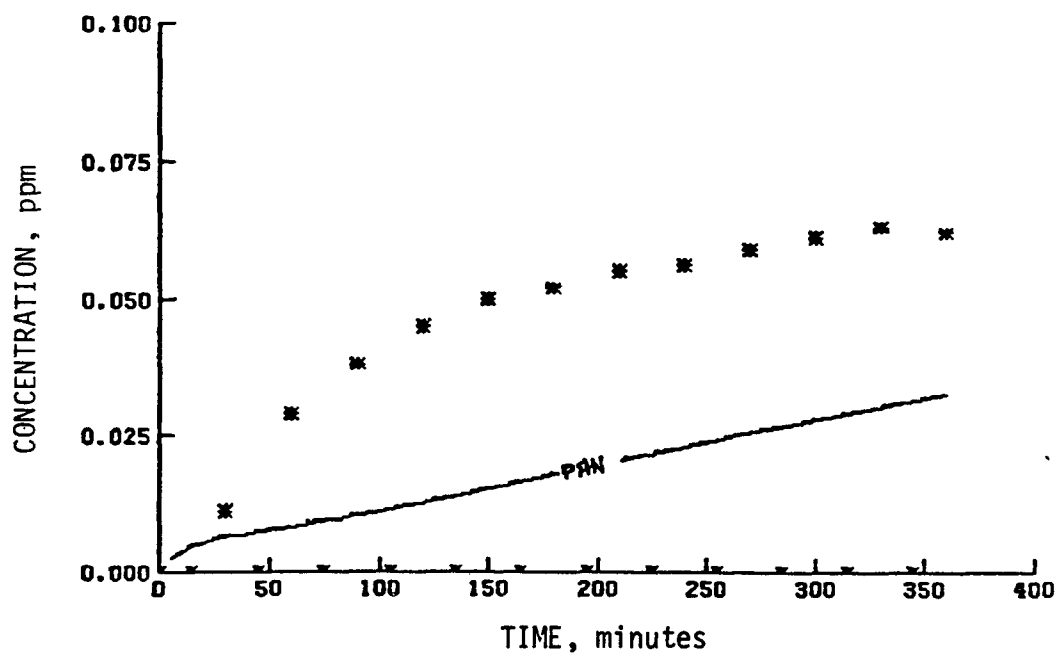
(b) PAN

Figure 59.   Simulation results of a UCR trans-2-butene experiment
(EC-146) with the Carbon-Bond Mechanism (trans-2-
butene assumed to be a carbonyl)

223

containing internal olefins, the approximation of considering these olefins as carbonyls should be even more valid. However, the effect of adding these olefins after ozone is present warrants further testing. For the current version of the CBM, we treated all internal olefins present at the beginning of an experiment as part of the carbonyls.

Rate Constants for the OLE + OH· and PAR + OH· Reactions

Based on the study of the mulitolefin Run EC-150 with the original CBM, we have concluded that the root-mean-square rate constant for OLE + OH· reactions (and OLE + O, OLE + O_3) will produce the best agreement between predictions and observational data for the multihydrocarbon/NO_x systems. A similar but tentative decision has been made for the PAR + OH· (and PAR + O) reactions.

Rate constants for the generalized species in the CBM are not always easily defined. For instance, the single-bonded carbon atoms in a mixture of olefins would be treated in the CBM as PAR. In such cases we used a generalized or default PAR + OH· rate constant of 1500 $ppm^{-1}min^{-1}$, which was derived as discussed below. To simulate pure methane or ethane systems one should lower the PAR + OH· rate constant appropriately.

As discussed by Whitten and Hogo (1977), grouping carbon atoms by bond type normally reduces the range of rate constants to be treated in a mechanism. By Greiner's (1970) formula, several alkanes (C_4 or larger) were calculated to react with OH· at rate constants within about 30 percent of 1300 $ppm^{-1}min^{-1}$ per carbon atom. For the original CBM Whitten and Hogo (1977) therefore suggested 1300 $ppm^{-1}min^{-1}$ as a rate constant for all PAR + OH· reactions. We now suggest 1500 $ppm^{-1}min^{-1}$ as the universal PAR + OH· rate constant. The higher number reflects recent studies of some alkanes, notably butane, that suggest higher rate constants than those calculated from Greiner's formula (see Section 5 on butane chemistry).

224

For the double bond species OLE in the CBM, we generally used the rate constants for the corresponding reactions of propylene unless specific information on the rate constants was available. For example, in a comparison of CBM and explicit mechanism simulations of experiments started with a mixture of four olefins (described earlier), the rate constants and relative concentrations of each olefin were available, and so that information was used in the simulations.

In the explicit olefin mechanisms, we incorporated the reaction of the hydroxyperoxyalkyl radical with ozone. To include this reaction in the CBM, it was necessary to use the surrogate species RAO_2 and RBO_2 for the products of the reactions of hydroxyl radicals with double bonds.

A New Aromatic Chemistry Scheme

Aromatic hydrocarbons are an important component of atmospheric hydro-carbons (typically 20 to 30 percent of the total NMHC). Thus, our need for a mechanism that adequately simulates the fate of the aromatics precludes the option of waiting for an accurate explicit description of the chemistry. Since a validated explicit aromatic mechanism similar in accuracy to those available for propylene and butane does not exist, our efforts to produce a condensed kinetic mechanism for aromatic compounds must be viewed as conjectural.

We analyzed the mechanism proposed by Hendry et al. (1978) as an explicit description of toluene oxidation chemistry. The basic structure of toluene chemistry described by Hendry et al. (1978) is similar to the Carbon-Bond aromatic formulation, though their explicit mechanism is much more complicated. However, their explicit mechanism does not satisfactorily describe ozone formation and limitation. Thus, we are forced to rely on empirical relationships combined with our best speculations as to the true nature of the chemistry involved.

We base our description of the main features of aromatic chemistry on the following information:

> The UCR toluene smog chamber runs--EC-77 through EC-86
  and EC-264 through EC-273.

> The UCR seven-component mix runs--EC-231 through EC-247.

> A simulated diurnal cycle smog chamber experiment con-
  ducted by R. B. Stanfield (private communication, 1978)
  of Exxon Research and Engineering Company involving nine
  components (three aromatics $\approx$ 30 percent of the mix).

The first-approximation mechanism described by Whitten and Hogo (1977)
contained reactions of aromatic hydrocarbons with O_3 and NO_3. These reactions
were given rate constants considerably higher than the true rate of aromatic
reactions with these species so as to represent the reaction of the ring-
opened compounds that form from aromatic oxidation. The species formed from
an opened aromatic ring are expected to behave as a highly unsaturated
diolefin with correspondingly high rates of reaction with O_3 and NO_3.

We have retained, at least temporarily, the convention of treating
aromatic bonds as three double bonds. We assume that the ring in toluene,
like most other hydrocarbons, reacts initially with OH·. We speculate
that the reaction proceeds as follows:

$$\text{Toluene} + \text{OH·} \rightarrow \text{HC}_2^{\cdot} + \text{Cresol} \quad ,$$

$$\text{Cresol} + \text{OH·} \rightarrow \text{HO}_2^{\cdot} + \text{Z} \quad ,$$
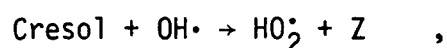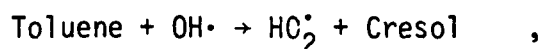
where Z represents (or will lead to the production of) reactive, ring-
opened species. The sum of these reactions is

$$\text{Toluene} + 2\text{OH·} \rightarrow 2\text{HO}_2^{\cdot} + \text{Z} \quad .$$
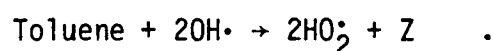
These reactions are represented in the CBM by two reactions involving
ARO (a two-carbon-atom species):

$$\text{ARO} + \text{OH·} \rightarrow \text{HO}_2 + \text{Y} \quad ,$$

$$\text{ARO} + \text{OH·} \rightarrow \text{OH·} + \text{Y} \quad .$$
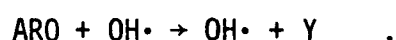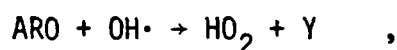
The former reaction is given a rate constant twice as large as the latter so that their sum,

$$3ARO + 2OH\cdot \rightarrow 2HO_2^- + 3Y \quad ,$$
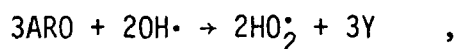
corresponds to the sum of the two reactions discussed above. Hence three AROs represent a toluene molecule. (The methyl group in toluene is treated separately as PAR in the CBM). The three Ys are a surrogate for the unknown, reactive species Z. We treated Y as a species capable of reacting with NO to effect an NO-to-NO_2 conversion, similar to the inter-mediate species X1, X2, X3, and X4 described by Hendry et al. (1978).

$$Y + NO \rightarrow NO_2 + HCHO + PAR \quad .$$
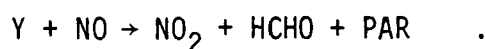
This arrangement provides somewhat greater parametric flexibility in esti-mating the average number of NO-to-NO_2 conversions before the atoms in the aromatic molecule enter the carbonyl pool in the Carbon-Bond Mechanism. Other reactions involving the ring-opened species Y represent an electro-philic addition to a highly unsaturated double bond:

$$Y + O_3 \rightarrow Aldehydes + Organic\ Acids \quad ,$$

$$Y + NO_3 \rightarrow Aldehydes + Nitric\ Acid \quad .$$
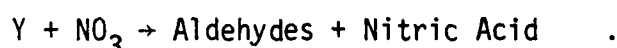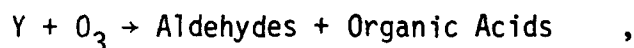
Similar reactions appear to be responsible for the restriction of ozone formation noted in the UCR toluene experiments. Note that the reaction of Y with O_3 is no longer taken to be a radical source, but rather an O_3 sink.

Y reacts in three different ways, and the ratios of the rate constants for the three reactions determine the behavior of the system. Using the averages of the reaction rates for the reactions of O_3 and NO_3 with 2,3-dimethyl-2-butene and 2-methyl-2-butene (Japar and Niki, 1975), we found that the rate constant for the reaction of Y with NO that provided good simulations was quite low--only 20 $ppm^{-1}min^{-1}$.

SIMULATIONS USING THE NEW CBM

The new version of the CBM was used to simulate a series of experiments for which explicit simulations were available. The results of these simulations are presented in the appendix. In each case, the results should be compared with the corresponding simulation using the explicit mechanism. A sample CBM simulation for a four-olefin mix (EC-152) is shown in Figure 60. Table 35 lists initial conditions for the simulations of this series of experiments using the new CBM. Table 36 summarizes the results of most of the simulations. The results of simulations of toluene experiments are not reported because the aromatic oxidation mechanism is in a state of flux. Graphs of simulated and observed pollutant concentrations for all experiments are given in Volume 2.

The derivation of the initial conditions presented in Table 35 is described in detail here to provide some examples in the use of the CBM

> Formaldehyde--The explicit and CBM mechanisms in this case are identical except for the elimination of HONO and H_2O_2 in the CBM. The parameters α and A are set equal to 1.0, although the latter is meaningless for formaldehyde systems because no single-bonded carbon atoms are present.

> Acetaldehyde--The methyl group is considered as a single-bonded species, so the initial PAR and CARB concentrations are each equal to the actual measured acetaldehyde concentration. Since some formaldehyde forms in this system α was set to 0.1 (during the explicit simulations formaldehyde varied from zero to 30 percent of the total aldehyde concentration). The definition of A does not apply to acetaldehyde and so A was set to 1.0. The experiments (EC-253 and EC-254) contained trace quantities of butane in order to monitor the OH· concentration. In the CBM simulation butane was not treated as PAR. Instead, in both the explicit and CBM simulations the reaction BUT + OH· → was added with a rate

228
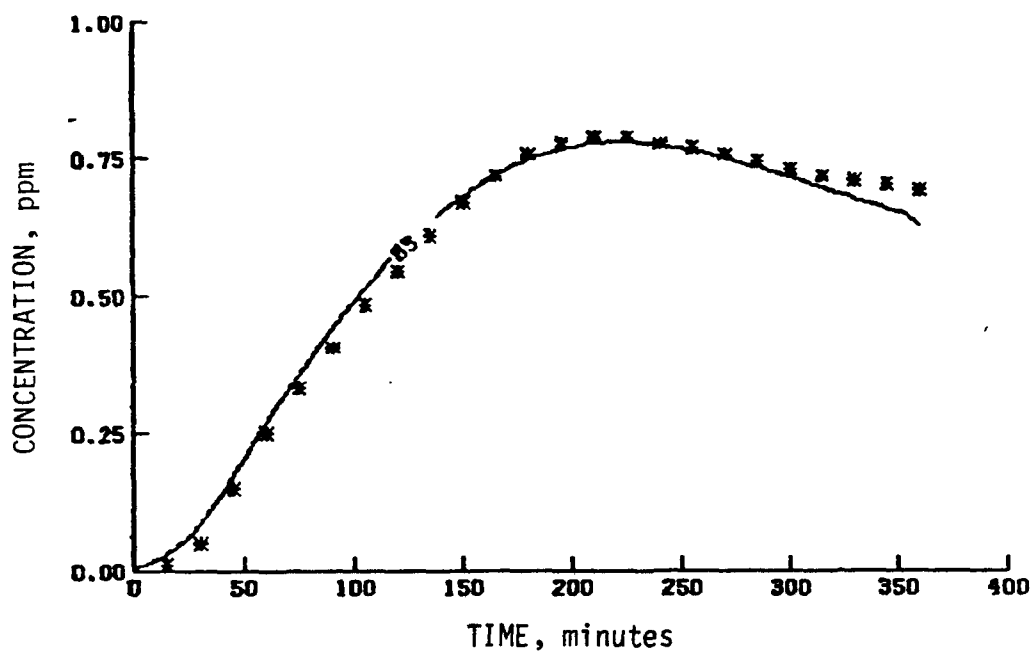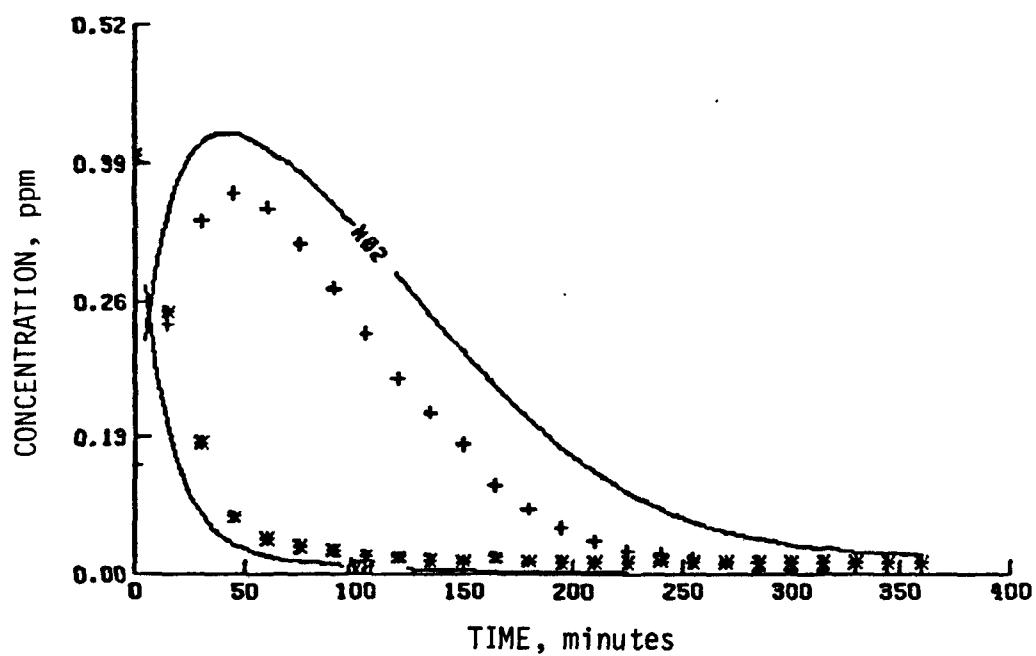
Figure 60. Simulation results of an UCR multiolefin experiment (EC-152) with the Carbon-Bond Mechanism
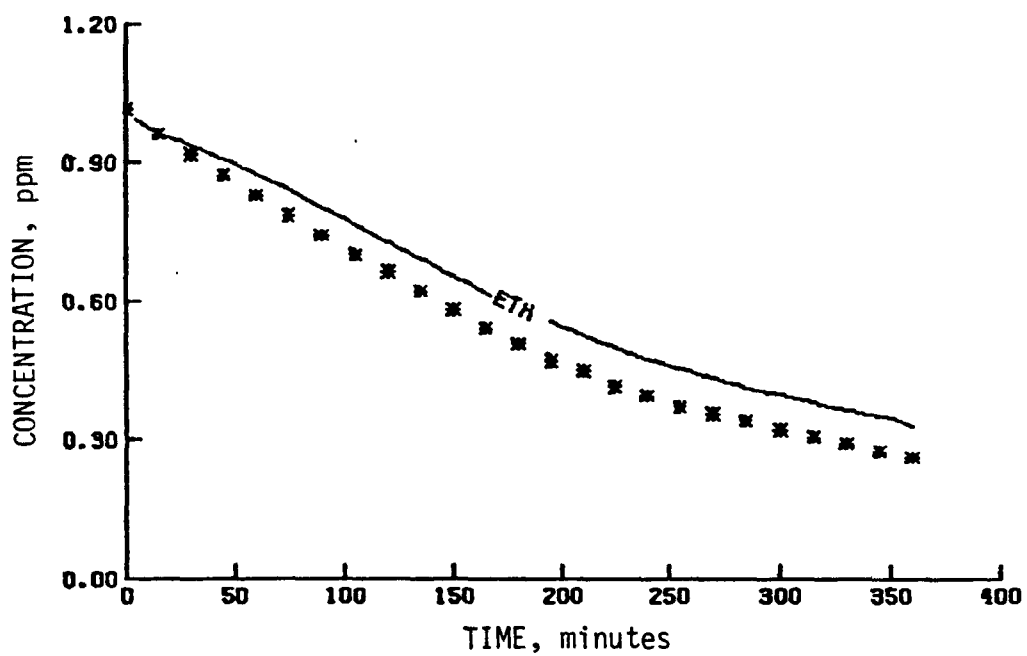
(c) Ethylene
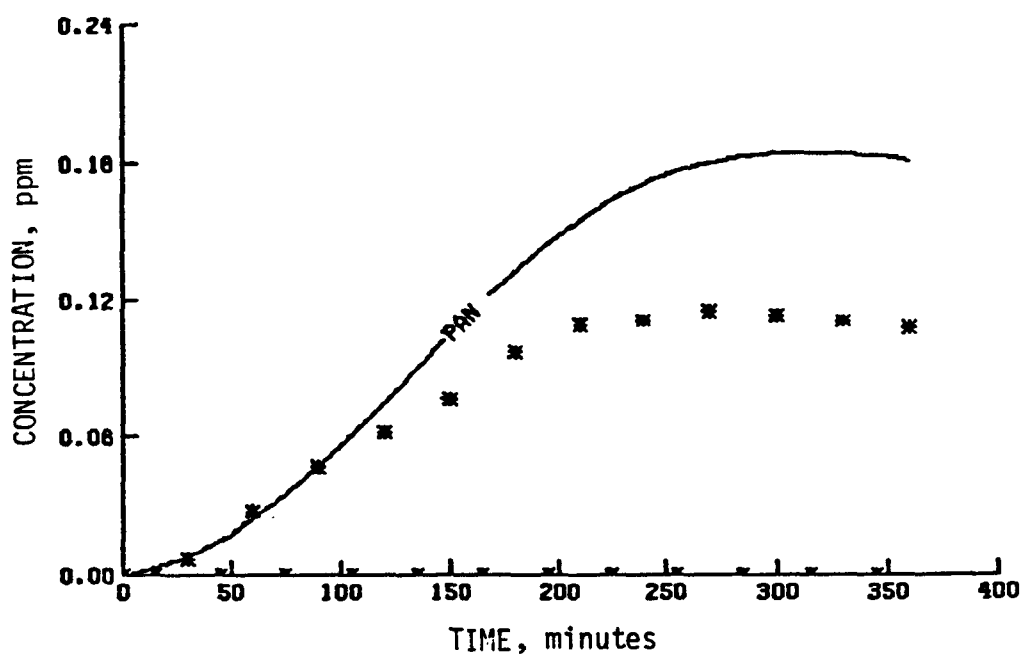
(d) PAN

Figure 60 (Concluded)

TABLE 35. INITIAL CONDITIONS OF THE EXPERIMENTS SIMULATED WITH THE CARBON-BOND MECHANISM

Exp. no.	Hydrocarbon	Initial concentration (ppm)						RX	Photolysis rate constant (min^{-1})		
		NO	NO$_2$	Olefin	Paraffin	Ethylene	Carbonyl		NO$_2$→NO+O	RX+hv	ALD+hv
EC-250	Formaldehyde	0.008	0.0	0.0	0.0	0.0	0.5	0.0	0.3	0.0	6×10^{-4}
EC-251		0.08	0.033	0.0	0.0	0.0	0.55	0.0	0.3	0.0	6×10^{-4}
EC-252		0.392	0.103	0.0	0.0	0.0	0.56	0.0	0.3	0.0	6×10^{-4}
EC-255		0.006	0.0	0.0	0.0	0.0	0.51	0.0	0.3	0.0	6×10^{-4}
EC-253	Acetaldehyde	0.001	0.0	0.0	0.517	0.0	0.517	0.0	0.3	0.0	6×10^{-4}
EC-254		0.085	0.027	0.0	0.508	0.0	0.52	0.0	0.3	0.0	6×10^{-4}
EC-142	Ethylene	0.322	0.158	0.0	0.005	0.92	0.055	0.005	0.33	0.099	1.1×10^{-3}
EC-143		0.39	0.11	0.0	0.0026	1.95	0.0023	0.006	0.33	0.099	1.1×10^{-3}
EC-256		0.52	0.044	0.109	0.11	0.0	0.043	0.002	.3	0.083	6×10^{-4}
EC-276		0.41	0.106	0.51	0.511	0.0	0.017	0.0	0.35	0.1	1.1×10^{-3}
EC-277	Propylene	0.098	0.10	0.564	0.565	0.0	0.006	0.0	0.35	0.1	1.1×10^{-3}
EC-278		0.366	0.128	1.016	1.016	0.0	0.008	0.003	0.35	0.1	1.1×10^{-3}
EC-279		0.73	0.244	1.1	1.1	0.0	0.018	0.0005	0.35	0.1	1.1×10^{-3}
EC-168	Butane	0.327	0.166	0.0	7.68	0.0	0.101	0.02	0.33	0.062	1.1×10^{-3}
EC-178		0.087	0.011	0.0	7.845	0.0	0.001	0.02	0.33	0.0608	1.2×10^{-3}
EC-123	1-Butene	0.401	0.106	0.404	0.809	0.0	0.0012	0.005	0.28	0.07	1.1×10^{-3}
EC-146	Trans-2-butene	0.385	0.124	0.231	0.462	0.0	0.002	0.01	0.33	0.099	8×10^{-4}
EC-146	Trans-2-butene as CARB	0.385	0.124	0.0	0.462	0.0	0.464	0.01	0.33	0.099	8×10^{-4}
EC-169	2,3-Dimethylbutane	0.127	0.064	0.0	4.35	0.0	0.0?	0.005	0.33	0.0917	1.2×10^{-3}
EC-113	Propylene/butane	0.091	0.021	0.41	8.73	0.0	0.0	0.001	0.351	0.092	1×10^{-3}
EC-114		0.794	0.205	0.758	15.44	0.0	0.008	0.009	0.351	0.092	1×10^{-3}
EC-152	Multiolefins	0.398	0.104	0.338	7.66	1.015	0.206	0.007	0.33	0.09	1.2×10^{-3}
EC-153		0.774	0.197	0.515	1.319	1.9	0.389	0.015	0.34	0.09	1.2×10^{-3}

(Continued)

TABLE 35 (Concluded)

Exp. No.	Hydrocarbon	Initial concentration (ppm)								Photolysis rate constant (min⁻¹)		
		NO	NO2	Aromatic	Paraffin	Carbonyl	H2O	HNO2	CO	NO2→NO + O	ALD + hv	HNO2 + hv
EC-77		0.518	0.058	0.828	0.276	0.004	1.6×10^4	5×10^{-3}	1.68	0.16	9×10^{-4}	0.06
EC-78		0.069	0.032	0.69	0.23	0.004	1.6×10^4	3×10^{-3}	2.04	0.16	9×10^{-4}	0.06
EC-79		0.08	0.019	2.928	0.976	0.013	1.8×10^4	3×10^{-4}	2.12	0.16	9×10^{-4}	0.06
EC-80		0.40	0.095	3.06	1.02	0.001	1.86×10^4	7×10^{-3}	2.23	0.16	9×10^{-4}	0.06
EC-81	Toluene	5.88	0.094		1.96	0.002	1.78×10^4	7×10^{-3}	2.03	0.16	9×10^{-4}	0.06
EC-82		0.679	0.337	5.64	1.88	0.003	1.78×10^4	4×10^{-4}	2.13	0.16	9×10^{-4}	0.06
EC-83		1.363	0.664	16.89	5.63	0.017	1.0×10^3	0	2.0	0.16	9×10^{-4}	0.06
EC-84		0.338	0.081	2.904	0.968	0.044	2.93×10^4	1×10^{-3}	1.7	0.16	9×10^{-4}	0.06
EC-85		0.431	0.092	5.76	1.92	0.009	1.7×10^4	3.3×10^{-4}	2.07	0.16	9×10^{-4}	0.06
EC-86		0.407	0.08	3.27	1.09	0.163	1.44×10^4	0	2.13	0.16	9×10^{-4}	0.06

TABLE 36. COMPARISON BETWEEN THE CARBON-BOND MECHANISM AND OBSERVATIONAL DATA

(a) Single Hydrocarbon and Propylene/Butane Experiments

Exp. no.	Hydrocarbon	Maximum [O3] (ppm)*		Difference in O3 maxima (percent)†	Time to maximum [O3] (minutes)§		Difference in times to O3 maxima (percent)†	Maximum [NO2] (ppm)		Difference in NO2 maxima (percent)†	Time to maximum [NO2] (minutes)§		Difference in times to NO2 maxima (percent)†
		Sim.	Meas.		Sim.	Meas.		Sim.	Meas.		Sim.	Meas.	
EC-250		0.2	0.21	-5	>360	>360	--	0.016	0.021	-24	>360	>360	--
EC-251	Formaldehyde	0.26	0.27	-4	150	150	0	0.084	0.077	9	30	30	0
EC-252		0.03	0.019	58	>360	>360	--	0.24	0.24	0	100	100	0
EC-255		0.19	0.19	0	>360	>360	--	0.015	0.017	-12	>360	>360	--
EC-253	Acetaldehyde	0.13	0.12	8	>360	>360	--	0.01	0.009	11	>360	30	--
EC-254		0.28	0.24	17	>360	>360	--	0.08	0.064	25	50	60	-17
EC-142	Ethylene	0.75	0.77	-3	~330	~330	--	0.35	0.30	17	130	100	30
EC-143		0.96	1.07	-10	170	170	0	0.41	0.38	8	70	60	17
EC-256		0.009	0.002	350	>360	>360	--	0.21	0.2	5	>360	>360	--
EC-276		0.49	0.33	49	>360	>360	--	0.39	0.36	8	130	125	4
EC-277	Propylene	0.3	0.30	0	70	100	-30	0.09	0.086	5	30	30	0
EC-278		0.66	0.60	10	130	150	-13	0.41	0.39	5	50	70	-29
EC-279		0.81	0.65	25	300	330	-9	0.77	0.71	8	110	105	5
EC-168	Butane	0.66	0.66	0	590	630	0	0.34	0.3	13	120	50	140
EC-178		0.38	0.38	0	350	360	-3	0.07	0.063	11	80	40	100
EC-123	1-Butene	0.54	0.50	8	330	~330	0	0.40	0.32	25	80	60	33
EC-146	Trans-2-butene	0.24	0.23	4	>360	>360	--	0.37	0.29	28	80	60	33
EC-146	Trans-2-butene as CARB	0.20	0.23	-13	>360	>360	--	0.35	0.29	21	150	60	150
EC-169	2,3-Dimethylbutane	0.50	0.49	2	450	590	-24	0.14	0.11	27	140	105	33
EC-113	Propylene/butane	0.40	0.34	18	90	100	-10	0.092	0.08	15	20	30	-33
EC-114		0.88	0.73	21	290	300	-3	0.79	0.70	13	110	90	22

O_3 maxima: average difference = 10 percent; standard deviation = ±18 percent.
NO_2 maxima: average difference = 10 percent; standard deviation = ±12 percent.

* Maximum one-hour-average concentrations.
† [(Simulated Value - Measured Value) ÷ Measured Value] × 100.
§ Time from beginning of irradiation to beginning of the period during which the maximum one-hour-average concentration occurred.

233

TABLE 36 (Concluded)

(b) Multiolefin and Seven-Hydrocarbon Experiments

Exp. no.	Hydrocarbon	Maximum [O3] (ppm)*		Difference in O3 maxima (percent)†	Time to maximum [O3] (minutes)§		Difference in times to O3 maxima (percent)†	Maximum [NO2] (ppm)		Difference in NO2 maxima (percent)†	Time to maximum [NO2] (minutes)§		Difference in times to NO2 maxima (percent)†
		Sim.	Meas.		Sim.	Meas.		Sim.	Meas.		Sim.	Meas.	
EC-152	Multiolefins	0.77	0.77	0	160	180	-11	0.41	0.35	17	40	45	-11
EC-153		0.96	0.96	0	150	170	-12	0.80	0.71	13	40	40	0
EC-231		0.71	0.60	18	190	180	6	0.4	0.36	11	60	60	0
EC-232		0.38	0.27	41	>360	>360	--	0.36	0.33	9	170	150	20
EC-233		0.34	0.32	6	150	120	25	0.08	0.07	14	30	30	0
EC-237		0.68	0.63	8	220	190	16	0.40	0.37	8	60	60	0
EC-238		0.82	0.68	21	420	420	0	0.73	0.66	11	110	80	38
EC-241	Seven hydrocarbons	0.46	0.35	31	>360	>360	--	0.36	0.33	9	150	120	25
EC-242		0.60	0.66	-9	80	80	0	0.43	0.4	8	20	30	-3
EC-243		0.70	0.70	0	90	90	0	0.42	0.4	5	50	70	-29
EC-245		0.84	0.86	-2	150	150	0	0.81	0.75	8	60	60	0
EC-246		0.66	0.54	22	520	520	0	0.37	0.36	3	190	120	58
EC-247		0.63	0.64	-2	180	180	0	0.4	0.37	8	70	60	17
												50	140

O3 maxima: average difference = 12 percent; standard deviation = ±16 percent.
NO2 maxima: average difference = 9 percent; standard deviation = ±3 percent.

* Maximum one-hour-average concentrations.
† [(Simulated Value - Measured Value) ÷ Measured Value] x 100.
§ Time from beginning of irradiation to beginning of the period during which the maximum one-hour-average concentration occurred.

constant of 4200 ppm^{-1}min^{-1}, and the products of butane
oxidation were ignored. (Butane constituted roughly 1 per-
cent of the initial hydrocarbon.) The default rate constant
for PAR + OH of 1500 ppm^{-1}min^{-1}, discussed earlier in this
section, was used in the CBM simulations.

> Ethylene--As for formaldehyde, the CBM and the explicit mech-
anism are virtually identical. The parameters α and A are
both 1.0. The only real differences in chemistry are a minor
pathway to acetaldehyde production and HONO, H$_2$O$_2$, and O(^{1}D)
chemistry, which appear only in the explicit mechanism. Trace
amounts of acetaldehyde were reported by UCR, which accounts
for the minor initial concentrations of PAR listed in Table 35.

> Propylene--The initial concentrations of PAR and OLE were
set equal to the initial propylene concentration used in
the explicit propylene simulations. Where minor amounts
of initial aldehydes were reported by UCR, small additions
to the initial concentrations of PAR and CARB were made for
the CBM simulations. The parameter α was set at 0.5 and
again A was set to 1.0, since it does not apply.

> Butane--To model butane with the CBM we needed to determine
α and A plus the rate constant for the reaction of alkylperoxy
radicals with nitric oxide to produce nitrates relative to the
total rate constant. The initial PAR concentration was simply
four times the molecular concentration used in the explicit
simulations.

The value of α used was 0.5 because in the explicit simulations
the sum of formaldehyde and ketones was typically about one-
half of the total simulated carbonyl concentration. A is the
average number of RO$_2^\cdot$-type radicals generated following an
OH$\cdot$ oxidation unitl an HO$_2^\cdot$ is formed (counting only the RO$_2^\cdot$

235

reactions with NO which form NO_2). For the butane explicit
mechanism A = 1.32, which is calculated as follows: The initial
OH· attack gives two RO_2^*-type radicals (SCO_2^* and $C_4O_2^*$) in a six-
to-one ratio. SCO_2^* forms a secondary alkoxyl radical (SCO·)
after reaction with NO. One-fourth of the SCO· produces another
RO_2^* (plus acetaldehyde) via decomposition and three-rourths
produces HO_2^* (plus methylethylketone). The average number of
RO_2^*-type radicals from butane by the SCO_2^* pathway is [(1/4) x 2 +
(3/4) x 1 = 1.25]. $C_4O_2^*$ produces C_4O· after reaction with NO.
C_4O· then reacts to produce an RO_2^* via OH· migration and an
HO_2^* (plus butyraldehyde) in a 20-to-7 ratio. The average number
of RO_2^*-type radicals for the $C_4O_2^*$ pathway is 1.74 [(20 x 2 + 7 x 1)/
27 = 1.74]. Since the ratio of SCO_2^* to $C_4O_2^*$ production is six,
the overall average A for butane is 1.32 [(6 x 1.25 + 1 x 1.74)/
7 = 1.32].

Comparison of CBM simulations with the simulations using
the current explicit chemistry is not straightforward.
As discussed in Section 5, the explicit butane mechanism
uses a rather high photolysis rate constant for the major
oxidation product of butane, methylethylketone. Further-
more, one of the products of that photolysis is taken to
be the peroxyacetyl radical. (The CBM equivalent would
be ACO_3, which is not presently a product of carbonyl
photolysis in the CBM.) Besides the higher PAN concentra-
tion that this type of radical provides in the explicit
chemistry, its reaction with NO provides one more NO-to-
NO_2 conversion than an RO_2^*-type radical provides. Hence
there is some extra reactivity in the explicit mechanism
that has no direct counterpart in the CBM at present. As
interim measures, we investigated two possible means of pro-
viding this extra reactivity.

One means is the use of the default PAR + OH· rate constant
($1500 \text{ ppm}^{-1}\text{min}^{-1}$), rather than one-fourth of the actual
butane + OH· rate constant ($4200/4 = 1050 \text{ ppm}^{-1}\text{min}^{-1}$). The
simulations shown in this report use $1500 \text{ ppm}^{-1}\text{min}^{-1}$. It
is partially justified by the formulation of the CBM, in
which single-bonded carbon atoms react independently. In
the explicit chemistry, a four-carbon species reacts to
yield primarily methylethylketone (MEK). The secondary
single bonds in MEK have a rate constant for reaction with
OH· of $4900 \text{ ppm}^{-1}\text{min}^{-1}$. Since the CBM conceptually keeps
these single-bonded carbon atoms in the PAR pool, a rate
constant of $1050 \text{ ppm}^{-1}\text{min}^{-1}$ for all PARs would be too low.

The other means of providing the extra reactivity is the
use of the default value of A (1.5) rather than the value
computed from the explicit mechanism (1.32). With the
default value of A the lower PAR + OH· rate constant, 1050
$\text{ppm}^{-1}\text{min}^{-1}$, is used. This method of providing the extra
reactivity might be justified on the grounds that it does
not require knowledge of an explicit mechanism (which may
be erroneous) and it is certainly straightforward and
simple. However, the good agreement between the simula-
tions with the default value of A and the measurements
may merely be fortuitous.

> 1-Butene--The CBM simulation of this molecule is a simple
extension of the propylene simulations. The OLE + OH·
rate constant was set equal to the value used in the
explicit mechanism for 1-butene ($70,000 \text{ ppm}^{-1}\text{min}^{-1}$). The
α and A values were the same as used for propylene, 0.5
and 1.0. The initial PAR concentration for 1-butene is
twice the molecular concentration because two single-
bonded atoms are contained in the molecule.

> Trans-2-butene--The CBM was applied in two different ways
to the single trans-2-butene experiment (EC-146). The
internal double bond was treated in one case as an olefin
and in the other as two carbonyls. (In the explicit
simulations trans-2-butene reacts rapidly to generate
two molecules of acetaldehyde.) In both cases the two
single-bonded carbons were treated as PAR. In treating
trans-2-butene as an olefin we used the same rate constants
used for 1-butene, except that the rate constants for the
reactions of CLE with O, OH·, and O_3 were set equal to those
used in the explicit trans-2-butene mechanism (28,000, 120,000,
and 0.39 $ppm^{-1}min^{-1}$, respectively). The value of α used in
both cases was 0.2 because in the explicit simulations form-
aldehyde made up from zero to forty percent of the total
carbonyls. The choice of α does not seriously affect the
simulated ozone concentration, but it does affect the PAN
results.

> 2,3-Dimethylbutane--The simulation of EC-169 used an α of 0.5
and an A of 2.0; the derivation of latter value was pre-
sented earlier. Using the default value for α is somewhat
arbitrary because the dominant carbonyl compound produced
in the present explicit mechanism is acetone. Most of the
PAN produced in the explicit simulation stems from acetone
photolysis, but such a pathway does not exist in the present
CBM. The PAR + OH· rate constant used was the default value
of 1500 $ppm^{-1}min^{-1}$, as was used for the butane simulations
just described. An important reaction in the CBM simulation
of 2,3-dimethylbutane is nitrate formation from peroxy
radicals, which was given a rate constant of 1000 $ppm^{-1}min^{-1}$
to match the nitrate production in the explicit simulation.

> Propylene/Butane--In this application of the CBM we combined
the parameters used for propylene and for butane. The initial

concentration for PAR was four times the molecular concentra-
tion of butane plus the molecular concentration of propylene.
Since the PAR + OH· rate constant used in simulations of both
species was 1500 $ppm^{-1}min^{-1}$, the combination presents no problems.
Similarly, 0.5 was used for α in the separate systems and in the
combination. To determine a "proper" value for A seems some-
what complex. However, the introduction of the RAO_2^* radicals
into the new formulation of the CBM to account for the special
addition product of OH· to olefins eliminated a major source
of the surrogate RO_2^* radicals in the original CBM. This change
in chemistry tends to separate the overall olefin chemistry from
the paraffin chemistry with respect to RO_2^*-type radicals. Hence
we chose a value of A equal to 1.25, which is near the value
for butane of 1.32. Similarly, the rate constant for nitrate
production was set at 800 $ppm^{-1}min^{-1}$ (somewhat less than the
value for butane of 1000 $ppm^{-1}min^{-1}$).

> Multiolefins--The initial conditions for the simulations of
four olefins were determined by treating ethylene separately,
trans-2-butene as two carbonyls and two PARs per molecule, and
1-butene and propylene as one OLE and two PARs and one OLE
and one PAR, respectively. Since both 1-butene and propylene
were treated as OLE, the OLE + OH· rate constants used were
the weighted root-mean-square values of 6.2 x 10^4 $ppm^{-1}min^{-1}$
for EC-152 and 6.6 x 10^4 $ppm^{-1}min^{-1}$ for EC-153. The parameters
α and A were set at 0.5 and 1.0. The default value of α was
used because it should be appropriate for mixtures. The value
of A does not matter because no aliphatic chains greater than
two carbon atoms are present. The absence of long aliphatic
chains is also the reason that the rate constant for nitrate
formation from RO_2^* + NO reactions was set to only 100 $ppm^{-1}min^{-1}$.
A CBM simulation of an experiment with a four-olefin mix is
shown in Figure 60.

> Toluene--The aromatics mechanism was in a rapid state of develop-
  ment as this report was written. Therefore the simulations
  of the UCR toluene experiments represent a sampling of current
  progress rather than a final demonstration of the mechanism.
  Slightly different versions of the CBM were used for the toluene
  and the seven-hydrocarbon simulations. The mechanism for the
  latter is shown in Table 34. For toluene the total ARO + OH·
  rate constant was 8000 $ppm^{-1}min^{-1}$, of which 5000 $ppm^{-1}min^{-1}$ then
  reacted to produce $HO_2^·$. The rate constant used for NO + Y →
  NO_2 + 2 x CARB in the toluene simulations was 20 $ppm^{-1}min^{-1}$.
  For the Y + NO_3 reaction the rate constant used was 2.5 x 10^4
  $ppm^{-1}min^{-1}$ with the products being HNO_3 + CARB. For the

  Y + O_3 reaction the rate constant used was 2 $ppm^{-1}min^{-1}$
  with the product being 0.5 x CARB. An additional reaction,
  Y + O → $ACO_3^·$ + MEO_2, was included with a rate constant of
  6.0 x 10^5 $ppm^{-1}min^{-1}$.

  The aromatic mechanism was tested using some toluene data from
  UCR. Rather high photolysis rate constants were required to
  obtain the agreement shown in the appendix (Volume 2). Figure 61
  shows the simulation results for EC-80. Further work on the
  aromatic mechanism is under way to allow similar photolysis rate
  constants to be used for the carbonyls formed from aromatics
  and those formed from olefins and paraffins.

> Seven Hydrocarbon Mixes--Each of the 11 smog chamber experi-
  ments used the same hydrocarbons: ethylene, propylene, trans-
  2-butene, butane, 2,3-dimethylbutane, toluene, and xylene.
  Three basic mixes were used: an intermediate mix intended to
  resemble an urban mix; a mix high in paraffins but low in
  aromatics; and a mix low in paraffins but high in aromatics.
  Tables 37 and 38 summarize the initial conditions used in
  the simulations. In all simulations α and A were set at the
  default values we recommend for hydrocarbon mixes, namely
  0.5 and 1.5. The only rate constant varied over the eleven
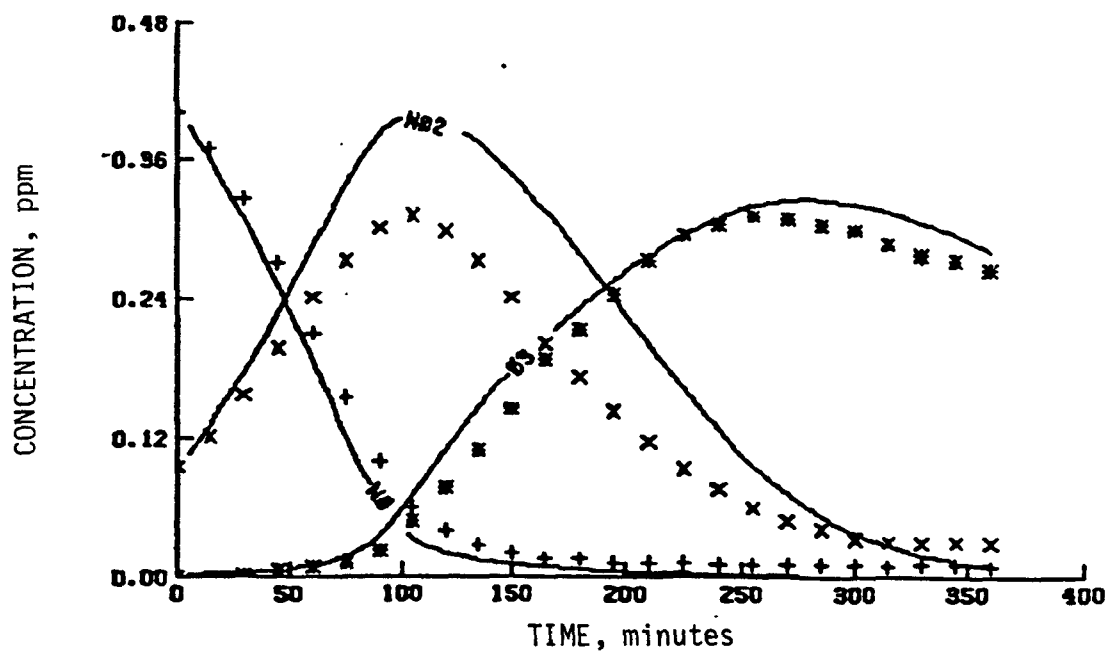
(a) NO_2, NO, and O_3
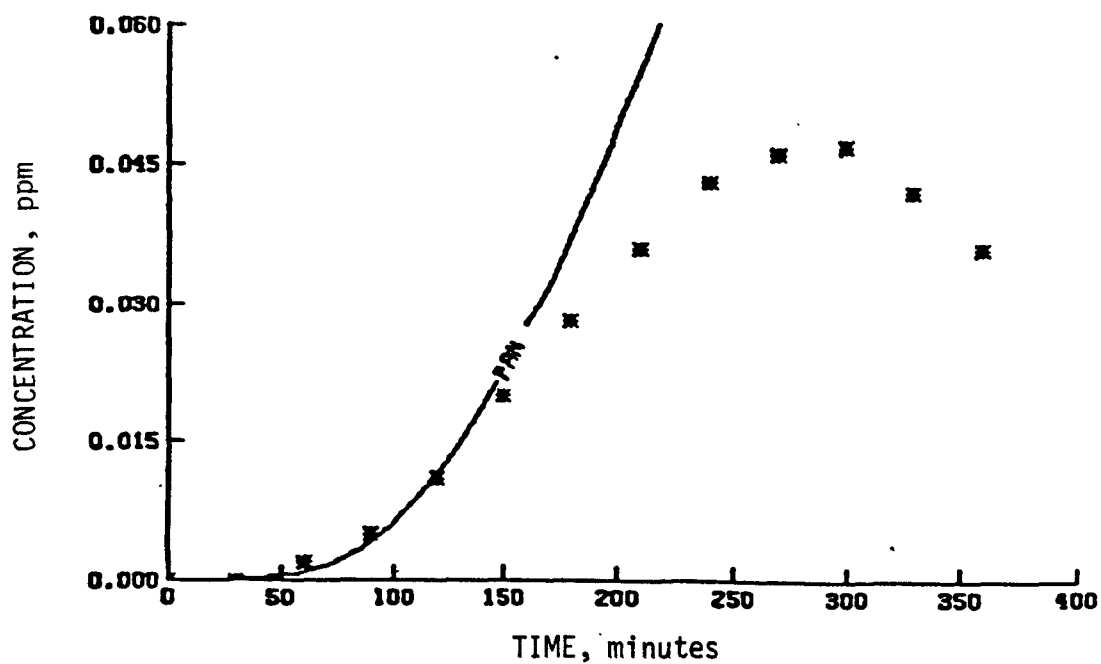
(b) PAN

Figure 61.   Simulation Results of a UCR Toluene Experiment (EC-80)
with the Carbon-Bond Mechanism

241
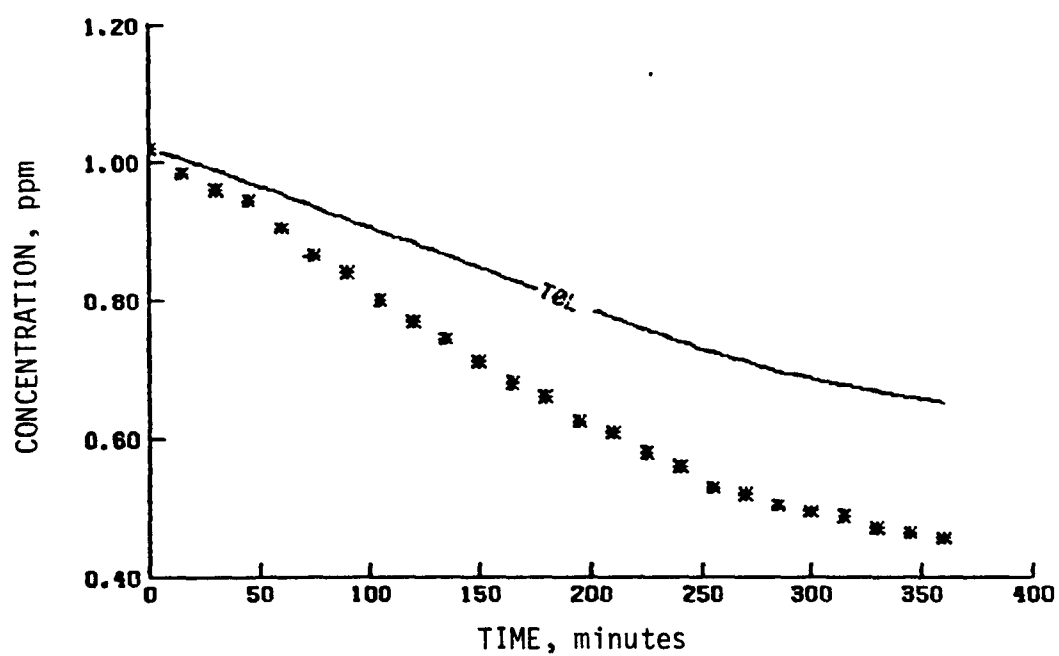
(c) Toluene

Figure 61 (Concluded)

TABLE 37. INITIAL CONDITIONS FOR THE SEVEN-HYDROCARBON/NO$_x$ EXPERIMENTS

Run number	NO	NO$_2$	Initial concentration (ppm)							Initial HC/NO$_x$ (ppmC/ppm)
			Ethylene	Propylene	Butane	t-2-Butene	2,3-Dimethylbutane	Toluene	m-Xylene	
EC-231	0.44	0.052	1.051	0.108	1.13	0.055	0.715	0.121	0.108	26.8
EC-232	0.469	0.024	0.258	0.051	1.102	0.026	0.612	0.032	0.029	18.9
EC-233	0.096	0.007	0.260	0.051	1.085	0.025	0.648	0.034	0.033	92.2
EC-237	0.377	0.106	0.875	0.100	1.025	0.050	0.463	0.086	0.091	21.7
EC-238	0.718	0.234	0.982	0.093	0.966	0.047	0.420	0.083	0.084	10.6
EC-241	0.379	0.110	0.404	0.045	0.464	0.024	0.211	0.04	0.044	10.1
EC-242	0.377	0.125	2.014	0.109	0.558	0.108	0.203	0.306	0.306	25.5
EC-243	0.386	0.114	1.939	0.109	0.568	0.110	0.084	0.155	0.154	19.4
EC-245	0.743	0.259	2.055	0.104	0.534	0.102	0.185	0.321	0.317	13.0
EC-246	0.386	0.122	0.253	0.049	1.058	0.026	0.538	0.023	0.023	16.9
EC-247	0.38	0.125	1.025	0.054	0.273	0.053	0.080	0.145	0.145	12.2

243

TABLE 38. NORMALIZED INITIAL CONDITIONS FOR THE SEVEN-HYDROCARBON/NO$_x$ EXPERIMENTS (ppmC)

Run number	Total HC (ppmC)	Initial conditions (percent of total HC)						Photolysis rate constant (min^{-1})		
		1-Olefins*	Paraffins†	Aromatics§	Ethylene	Carbonyls**	RX††	k$_1$	RX+hν	ALD+hν
EC-231	13.187	1.64	71.02	10.42	15.94	0.98	0.002	0.3	0.087	9 x 10^{-4}
EC-232	9.323	1.10	88.77	3.93	5.53	0.67	0.002	0.3	0.087	9 x 10^{-4}
EC-233	9.5	1.07	88.65	4.23	5.47	0.58	0.005	0.3	0.087	9 x 10^{-4}
EC-237	10.463	1.91	70.25	10.15	16.72	0.97	0.01	0.3	0.087	9 x 10^{-4}
EC-238	10.094	1.84	67.59	9.93	19.45	1.19	0.009	0.3	0.087	9 x 10^{-4}
EC-241	5.141	1.75	67.22	9.80	18.84	2.39	0.001	0.3	0.087	9 x 10^{-4}
EC-242	12.855	1.70	36.51	28.56	31.33	1.90	0.008	0.3	0.087	1.6 x 10^{-3}
EC-243	9.743	2.24	36.65	19.02	39.81	2.28	0.01	0.3	0.087	1.6 x 10^{-3}
EC-245	12.875	1.62	35.02	29.73	31.92	1.71	0.001	0.3	0.087	1.6 x 10^{-3}
EC-246	8.566	1.14	89.11	3.23	5.90	0.62	0.01	0.3	0.087	9 x 10^{-4}
EC-247	6.174	1.74	35.10	28.19	33.20	1.77	0.002	0.3	0.087	1.6 x 10^{-3}

* Propylene only.

† Butane, 2,3-dimethylbutane, and all single-bonded carbon atoms from the olefins, aromatics, and carbonyls.

§ Toluene and m-Xylene.

** All aldehydes and internal olefin (trans-2-butene).

†† In ppm.

experiments was for nitrate formation via the RO_2^* + NO
reaction. For the high paraffin mix (EC-232, EC-233, and
EC-246) a value of 1000 $ppm^{-1}min^{-1}$ was used, but in the other
eight simulations a value of 500 $ppm^{-1}min^{-1}$ was used.

Initial values for the CBM species were determined as follows:
Ethylene was treated as ethylene, OLE was set equal to the
reported molecular propylene concentration, CARB was twice
the reported molecular concentration of trans-2-butene plus
any reported initial carbonyls, and PAR was the sum of four
times the reported butane concentration, six times the
reported 2,3-dimethylbutane concentration, the reported
propylene concentration, twice the trans-2-butane concentra-
tion, the toluene concentration, and twice the xylene concen-
tration. ARO was three times the molecular concentrations
of toluene and xylene. The only rate constant involving the
initial hydrocarbons that had to be determined was for ARO +
OH·, for which a value of 2.4 x 10^4 $ppm^{-1}min^{-1}$ was used.
This value is approximately the weighted root-mean-square
between the rate constants for the reactions of m-xylene
and toluene with OH·. The ARO + OH· reaction, as discussed
above, was assumed to yield HO_2^* approximately two-thirds
of the time.

A photolysis compatibility problem is demonstrated in the
simulations of mixtures containing seven hydrocarbons. As
shown in Table 38, we had to use almost twice the calculated
aldehyde photolysis rate constant for the four high-aromatic
experiments. Figures 62 and 63 show sample simulations of
low aromatic concentrations (EC-233) and high aromatic con-
centrations (EC-245). Table 36 shows the one-hour-average
NO_2 and O_3 maxima.
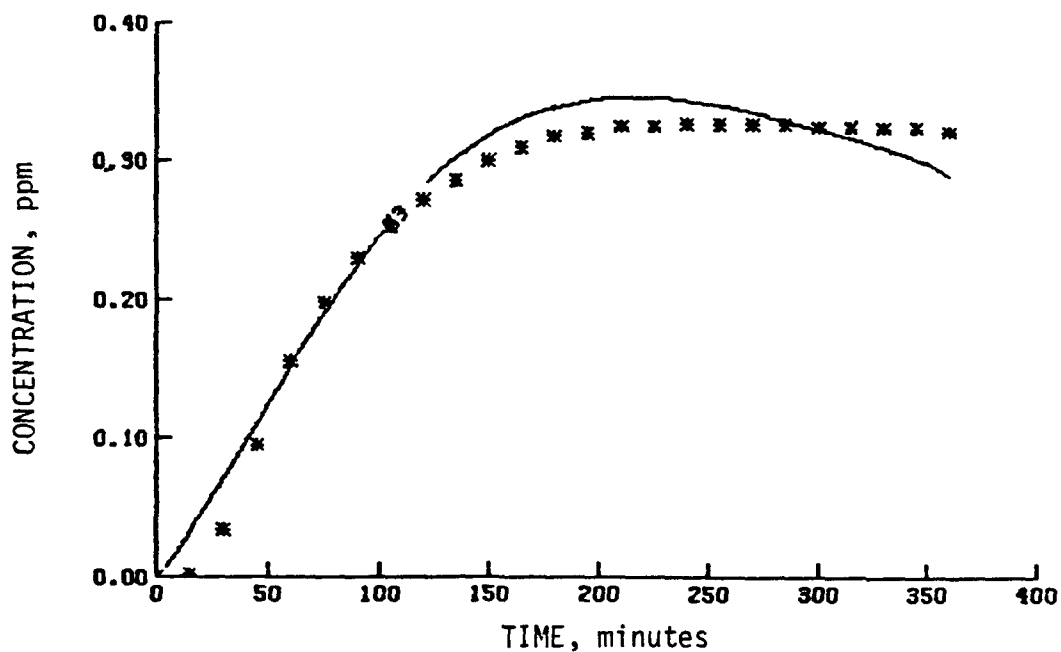
(a) O_3
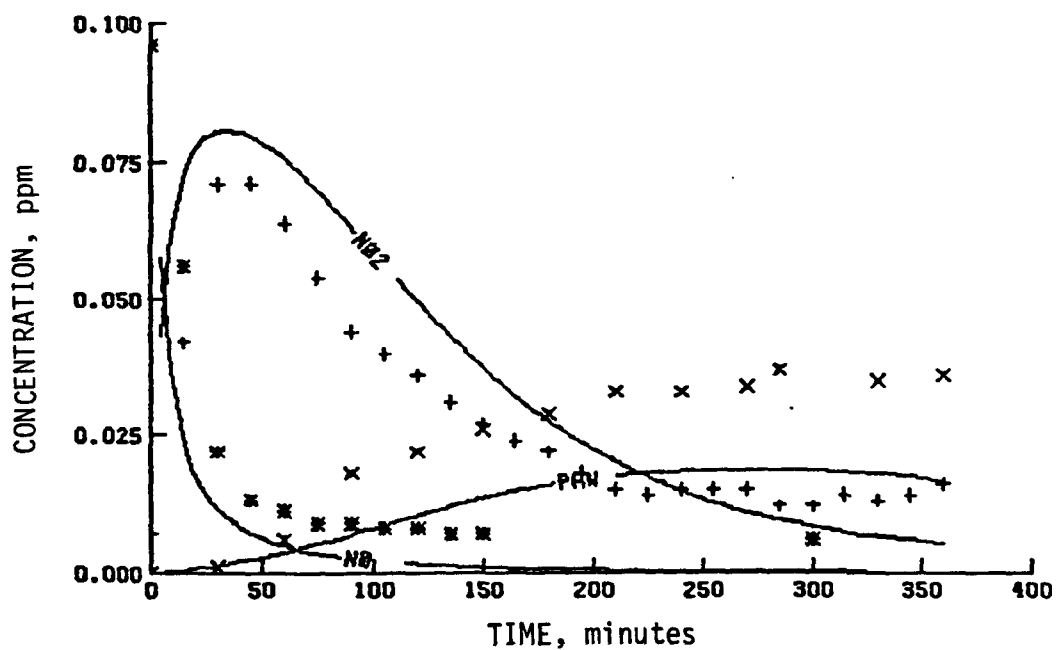
(b) PAN, NO_2, and NO

Figure 62. Simulation results of a UCR seven-hydrocarbon experiment (EC-233) with the Carbon-Bond Mechanism (low aromatic mixture)

246
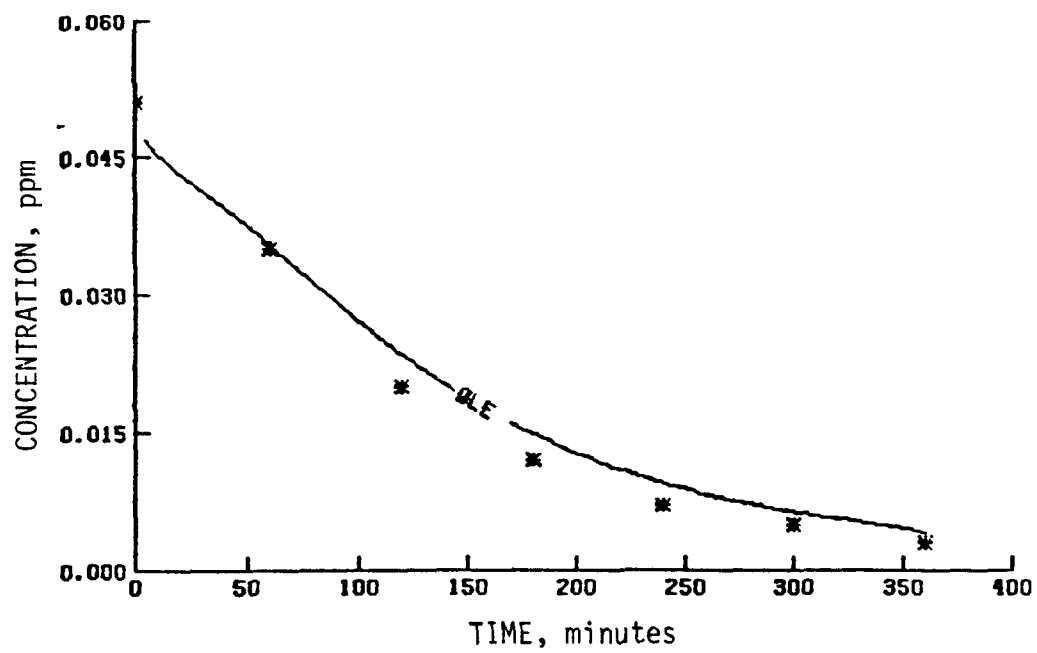
(c) Olefins
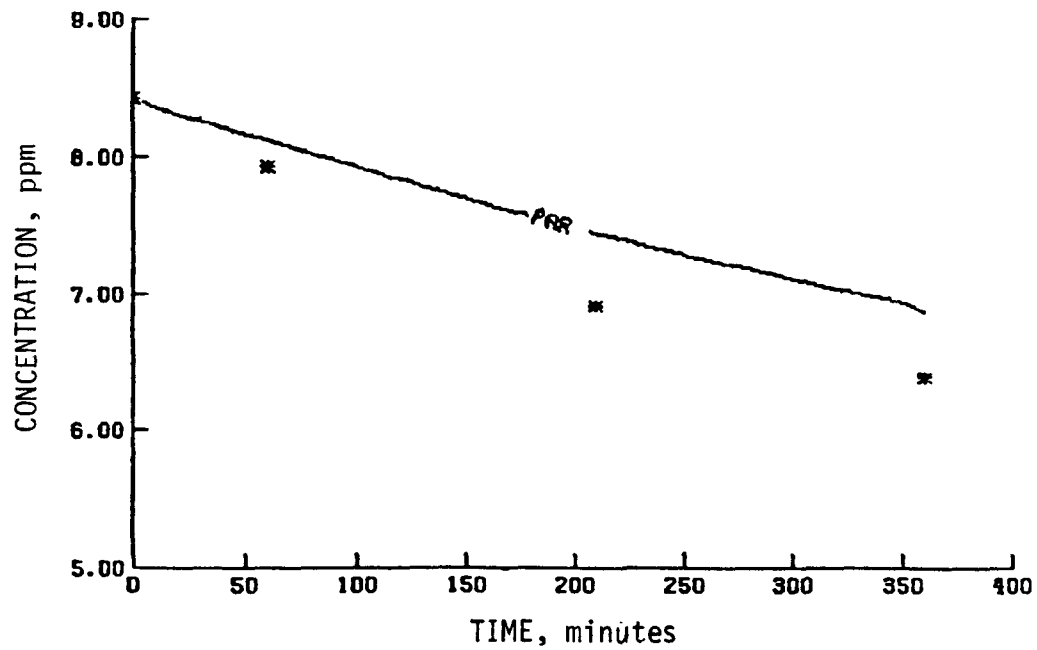
(d) Paraffins

Figure 62 (Continued)
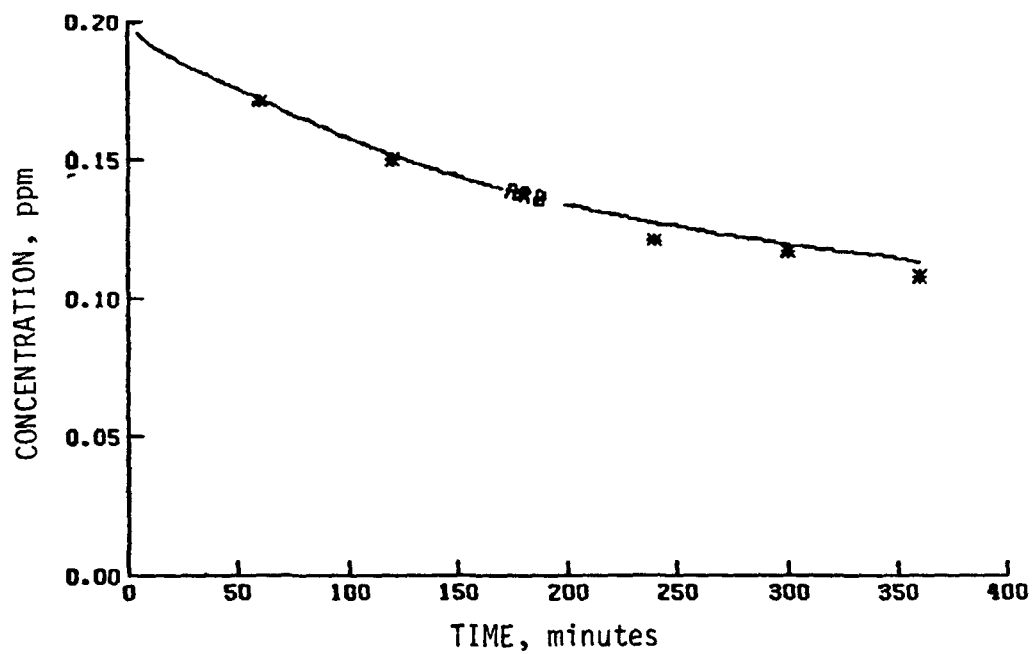
(e) Aromatics
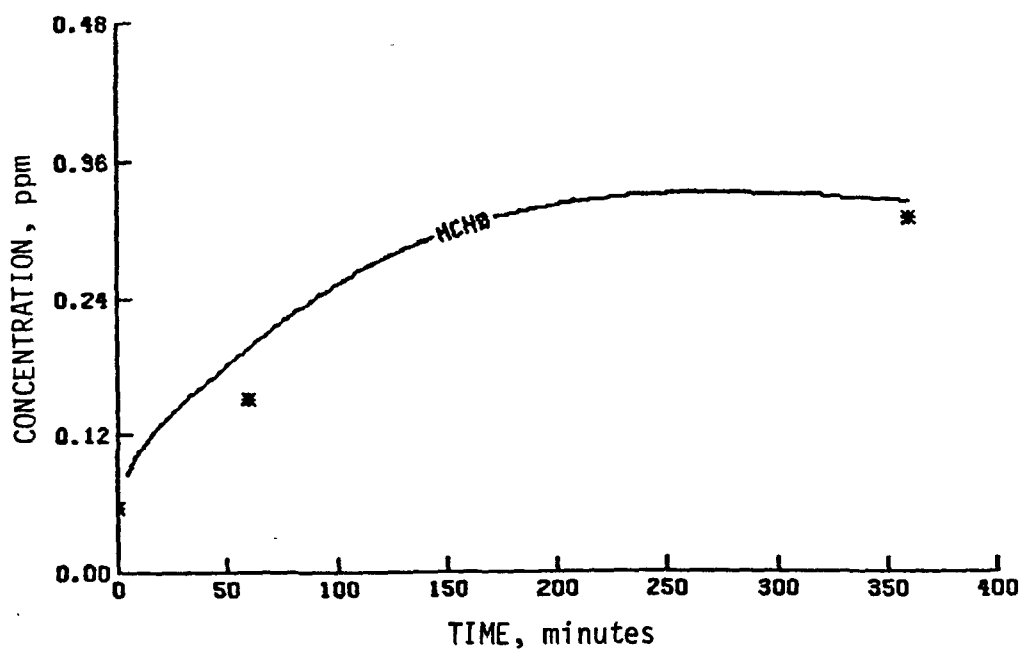
(f) Formaldehyde

Figure 62 (Continued)

248
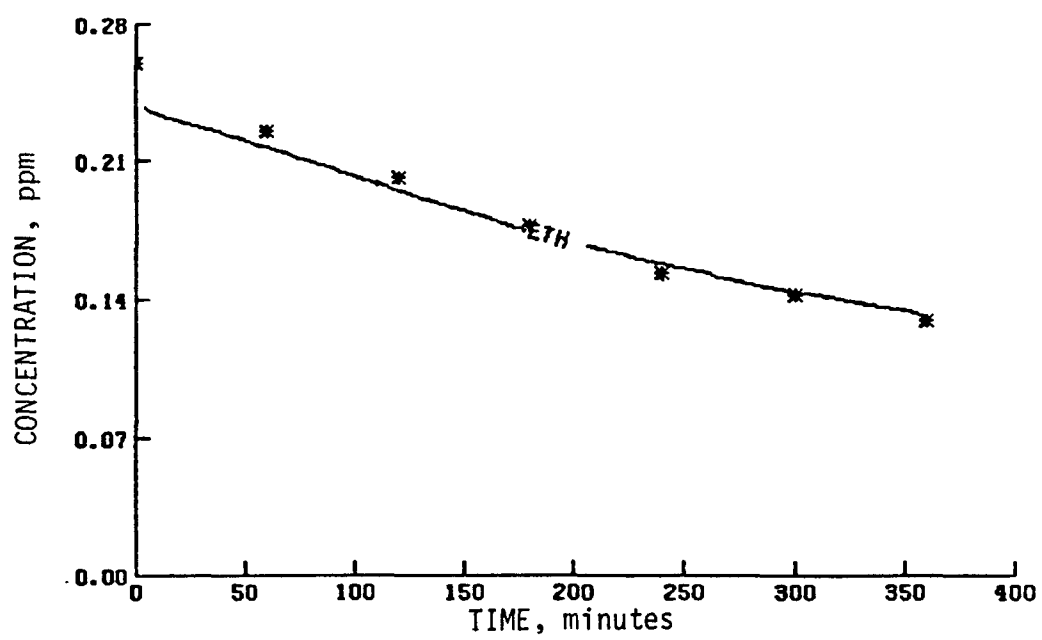
(g) Ethylene

Figure 62 (Concluded)
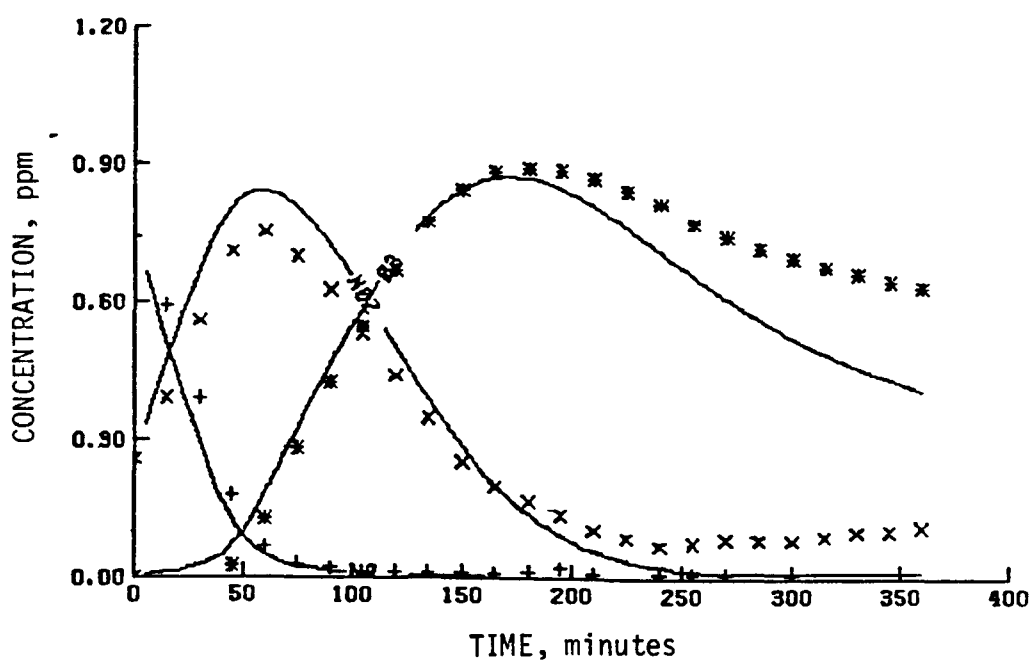
(a) NO_2, NO, and O_3
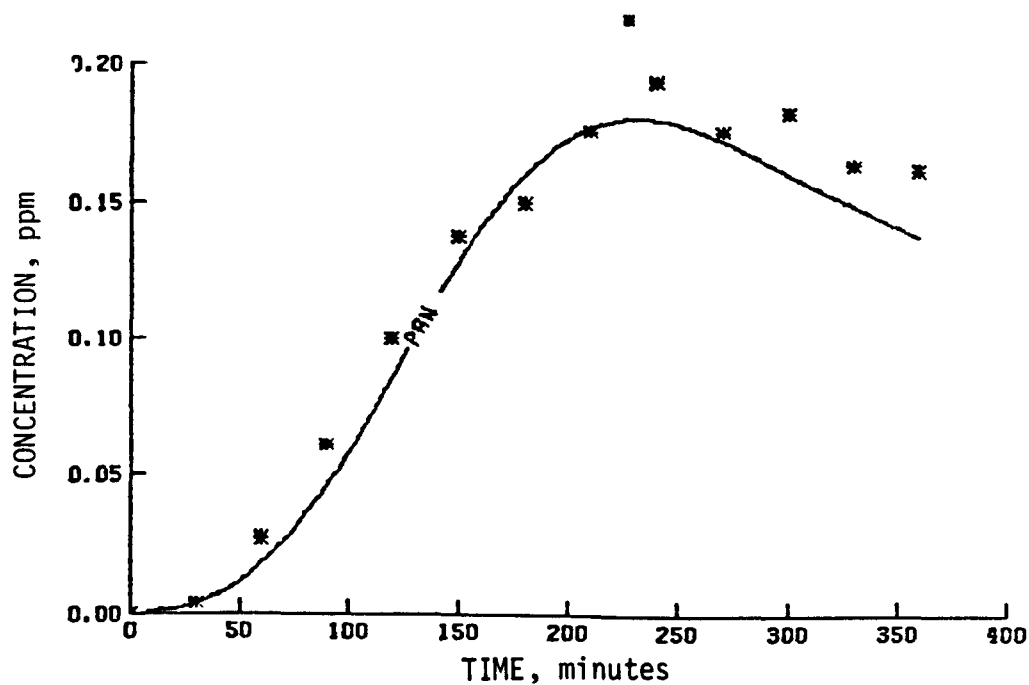
(b) PAN

Figure 63.   Simulation results of a UCR seven-hydrocarbon
experiment (EC-245) with the Carbon-Bond
Mechanism (high aromatic mixture)

250
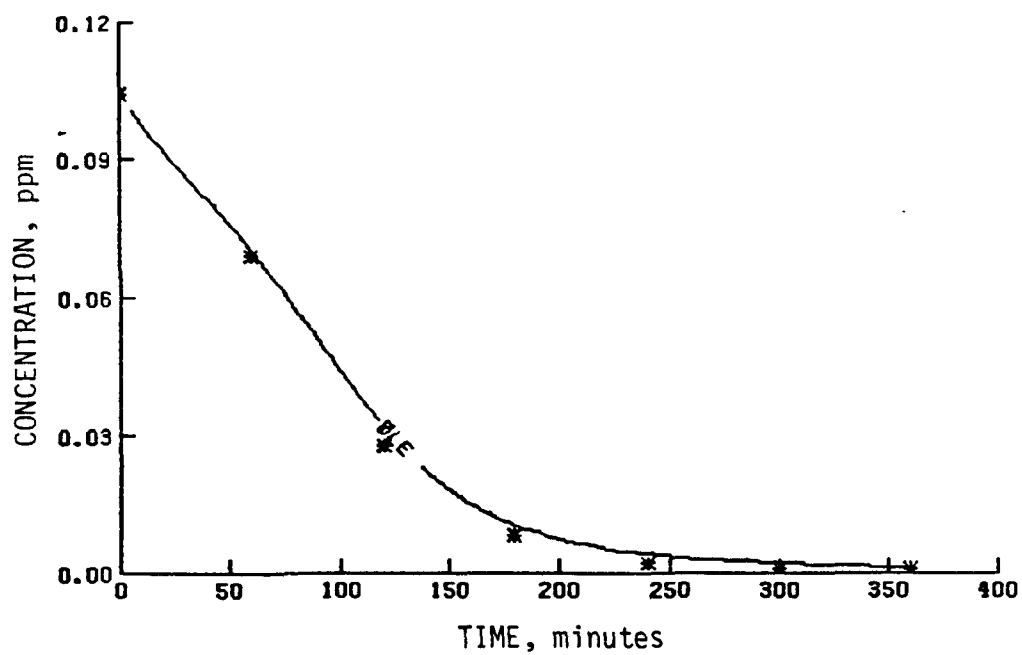
(c) Olefins
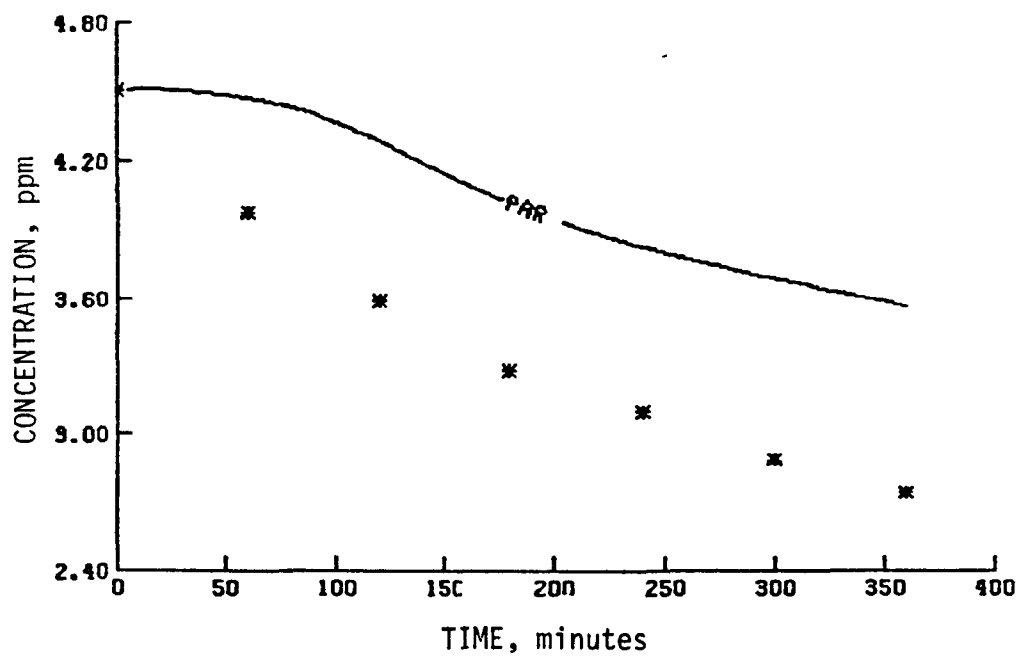
(d) Paraffins

Figure 63 (Continued)
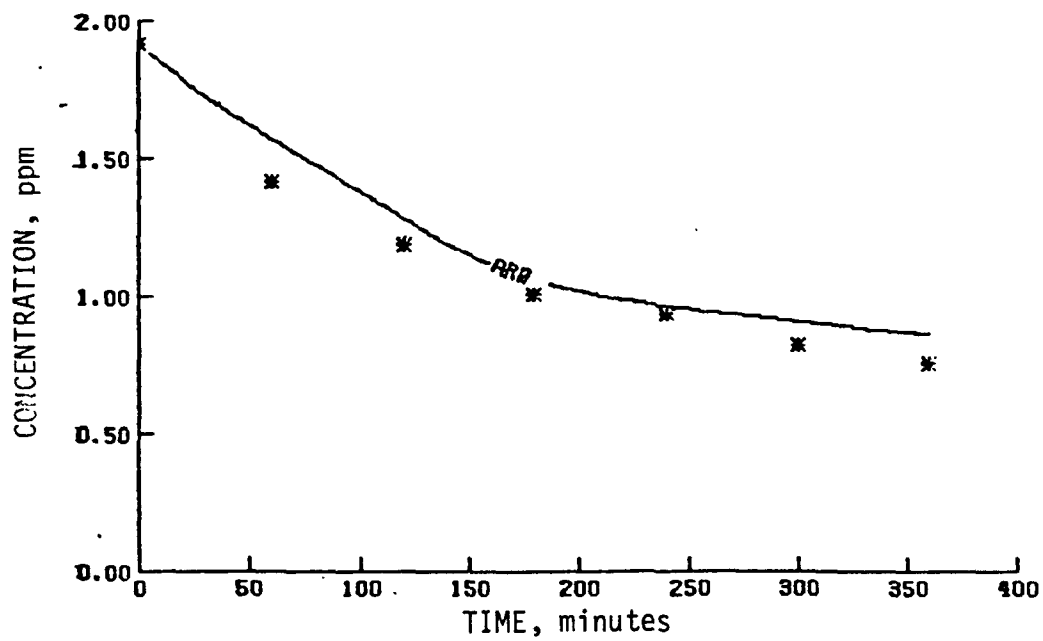
(e) Aromatics
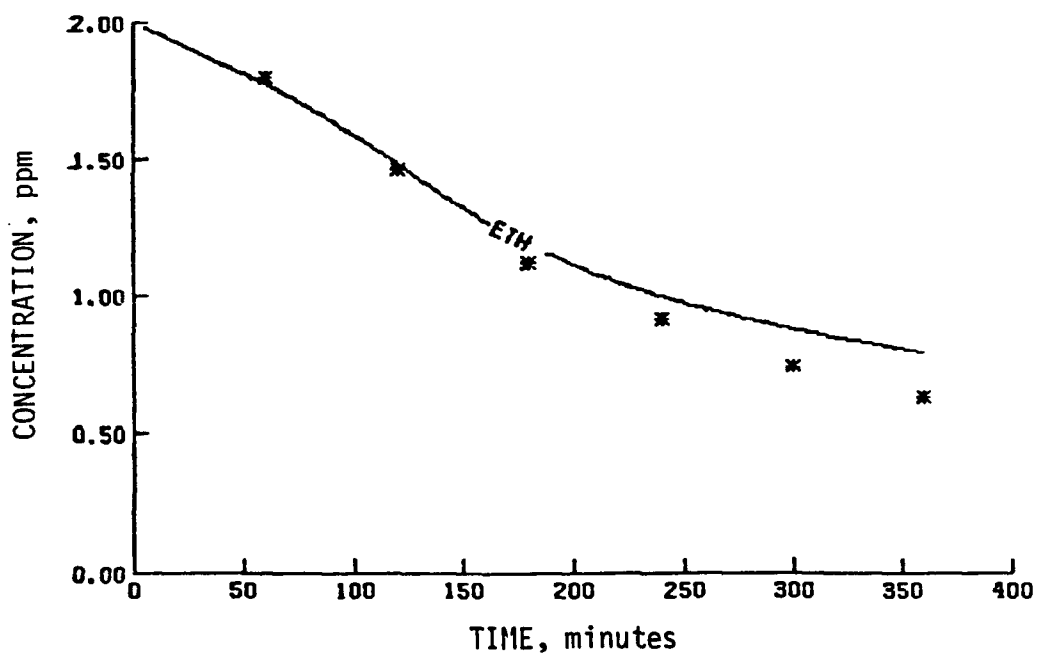
(f) Ethylene

Figure 63 (Continued)
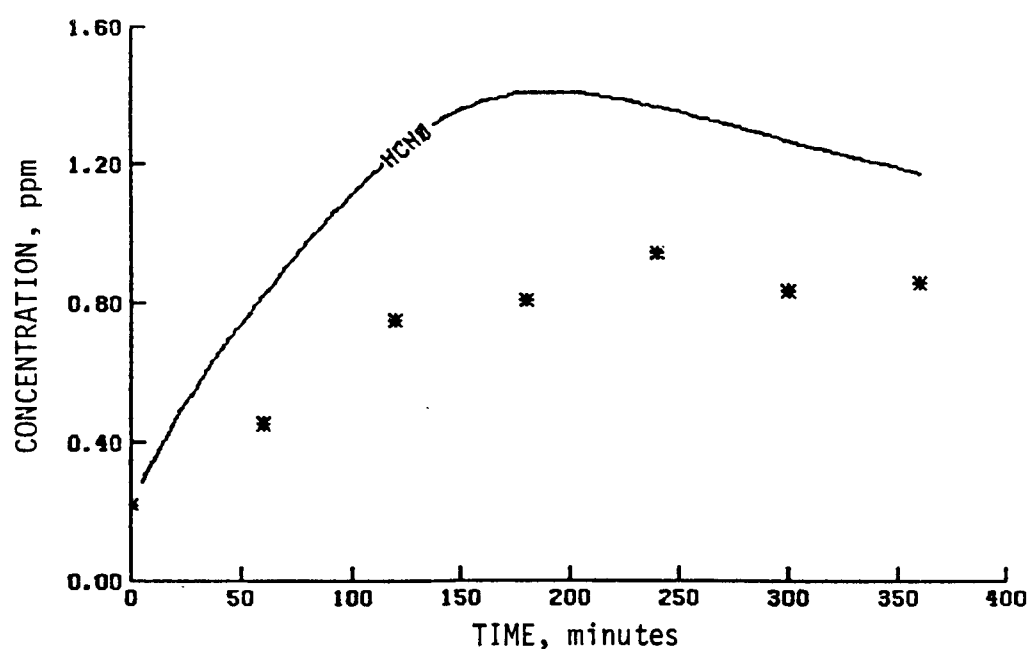
(g) Formaldehyde

Figure 63 (Concluded)

SECTION 7

SIMULATION OF PROPYLENE/NO$_x$ EXPERIMENTS
IN SEVERAL SMOG CHAMBERS

INTRODUCTION

A major part of the current contract calls for studying the simulations of similar propylene/NO$_x$ experiments performed in different smog chambers. The reasons for such a study are twofold:

> To elucidate chamber effects.

> To expand the data base used to validate explicit and generalized kinetic mechanisms.

As defined here, chamber effects include any effect that would produce different results from similar experiments in different smog chambers or from a hypothetical well-mixed air parcel in the open air compared with a smog chamber.

Although the study will continue for another year, the results at this time indicate four areas of chamber effects: analytical, wall, temperature, and lighting. The analytical effects lead to experimental uncertainties rather than to the difference between smog formation in chambers compared with the open atmosphere. Such effects would be common to virtually any comparison of similar experiments performed using different equipment. However, these effects are discussed because the uncertainties in the measurements are often large enough to mask the other differences among smog chambers. Wall effects may be the most commonly considered type of chamber effects. Indeed, one might argue that wall effects constitute the only real difference between a smog chamber and the open atmosphere (at least for small, well-mixed air parcels). However, the preliminary findings of the present study

indicate that wall effects play only a minor role in most smog chamber experiments. Refinement of kinetic mechanisms has greatly reduced the need to hypothesize radical sources or sinks on chamber walls to obtain simulations in agreement with measurements.

The latest mechanisms show a very high sensitivity to spectral distribution (Whitten and Hogo, 1977). Hence, application of these mechanisms to the atmosphere or to various chambers requires a careful assessment of the spectral distribution. Although present kinetic mechanisms are highly sensitive to spectral effects, they do not respond to changes in temperature adequately enough to simulate similar smog chamber experiments performed at different temperatures. A case can still be made that wall effects explain some of the temperature effects. Lowering the wall temperature might condense radicals or aldehydes, thereby slowing smog formation, and raising the temperature might condense fewer radicals or aldehydes. A higher temperature might also cause radical precursors such as aldehydes form previous experiments to "boil off" the walls and to accelerate smog formation.

If chamber effects can be elucidated sufficiently, the expanded data base to be used for developing and validating smog mechanisms will provide a more rational basis for acceptance of generalized mechanisms for modeling the atmosphere. In Section 3 we described the overall mechanism as composed of four stages: inorganics, single-carbon-atom species, higher aldehydes and other partially oxidized hydrocarbons, and initial hydrocarbons--paraffins, olefins, and aromatics. Presumably, the chamber effects would mostly be common to the hierarchical levels below hydrocarbons. Hence, the study of chamber effects for propylene/NO_x experiments should be applicable to smog chamber experiments using other initial hydrocarbons. Of course, hydrocarbon-specific chamber effects may occur; an example is toluene since poor accounting for carbon mass is common to smog chamber experiments using toluene.

DEVELOPMENT OF A DATA BASE

Several factors must be considered in the development of a data base for the chamber effects study:

> Initial pollutant concentration

- $[C_3H_6] \leq 10$ ppmC.
- $[NO_x] \leq 2$ ppm.
- Data from experiments at many different initial concentrations should be supplied if possible.

> Light source

- Type (e.g., blacklights or xenon arc).
- Spectrum (preferably measured--otherwise manufacturer's specifications).
- Intensity in chamber (k_1, k_d, or other photometric measurements, including the most recent measurement reported before each experiment).
- Age of light sources before each experiment (average age and spread in ages for multiple sources).
- Operating temperatures of fluorescent light sources.

> Analytical methods

- Listing of instrumentation used for the actual experiments reported.
- User's estimates of accuracy in the measurements.
- Corrections applied for interferences with measurement methods, if any.
- Documentation of the most recent calibration before each experiment, the calibration method, the number of points on the calibration curve, and the concentration at each calibration point.

> Chamber cleaning and seasoning

- Method of cleaning.
- Deliberate seasoning method, if any.
- Number and general type of experiments since the last cleaning (to evaluate the possible action of the walls as contaminant sources).
- Most recent "light" and "dark" ozone decay data before each experiment.

> Mixing time (should be determined with lights on if possible--otherwise, use mixing data without lights).

> Chemical data (data for all chemical species measured during each experiment, preferably in tabulated form, or else graphical presentations).

> Miscellaneous data (variations during the run when known--otherwise use of chamber operating temperatures, humidity (RH or dewpoint), and dilution rate).

One of the decision factors in the choice of the data base is the availability of the data. Much of the data were reported in graphical form, and chamber characteristics were often obscure. Furthermore, uncertainty ranges were not reported for some of the chamber runs. The following runs were chosen based on availability and the other factors mentioned above:

> UCR-EC (Runs 121, 177).

> UNC (runs performed on 9 August 1975, 5 November 1976, and 8 August 1977).

> Research Triangle Institute (RTI) (runs performed on 11 October 1976).

> Battelle (S-019, S-114, S-115).

> National Air Pollution Control Administration (NAPCA) (156, 164, 172).

> UCR-AGC (runs performed on 24 February 1973 and 5 March 1973).

> CALSPAN (11, 15, 16).

> Lockheed (40, 41, 42, 43).

Of the eight facilities listed above, UCR provided the most detailed discussion of experimental conditions. The 5775-liter UCR chamber is an evacuable cylinder (EC) coated with FEP Teflon 3.66 m long and 1.37 m in diameter. There are quartz windows on each end of the chamber. The surface-to-volume ratio is 0.054 cm^{-1}. The irradiation source is a xenon short arc lamp

that uses 25 kilowatts (Pitts et al., 1977). Two repeated runs (EC-121 and EC-177) were chosen from nine UCR runs with the same initial concentrations because the uncertainty of the reported light intensities seemed to be the lowest for those experiments. (The light source had been replaced just before each of those experiments.) Sampling techniques should be more certain in those runs than in earlier runs, mainly because of the experience gained from previous experiments.

The University of North Carolina and Research Triangle Institute both have outdoor smog chamber facilities. The UNC facility consists of two compartments (red side and blue side), so that two experiments can be performed simultaneously. Each side is an A-shape frame (9.14 m wide, 6.1 m high at the peak, and 12.19 m long) with walls made of FEP Teflon film (Jeffries, Fox, and Kamens, 1975). The volume of the chamber is 3.1×10^5 liters. The surface-to-volume ratio is 0.013 cm^{-1}. Of the alternatives for which detailed data were available, five are propylene/NO_x experiments. One set of experiments, performed on 16 August 1975, had continuous injection of propylene and NO in the blue side of the facility but not the red side. This set of experiments will be investigated in the coming year. For the current study, we chose four experiments (one on 9 August 1975, two on 5 November 1976, and one on 8 August 1977) as part of the data base for the chamber effects study. The use of natural sunlight as the irradiation source increases the need for spectral measurements of the sunlight during the day. Jeffries, Fox, and Kamens (1975) reported an empirical relationship between the NO_2 photolysis rate and the total solar radiation. From the total solar radiation measurements by UNC for the days of the experiments, we were able to estimate the NO_2 photolysis rate constant and all other photolysis rate constants required in the propylene/NO_x kinetic mechanism.

The RTI facility is similar to the UNC facility. RTI has four separate chambers that allow four experiments to be carried out simultaneously. The surface-to-volume ratio for each chamber is 0.019 cm^{-1}. We received data on two sets of four experiments performed at RTI on 6 October and 11 October 1976. These experiments were carried out for 35 hours. The data from

experiments on 6 October 1976 are questionable because a correction factor for the ozone measurements was needed to compensate for insufficient sample flow rates. In the set of experiments performed on 11 October 1976, no ozone was formed in Chamber 1. Therefore, only three experiments could be used as part of the data base for our chamber studies. For the RTI experiments, we assumed the same total solar radiation as for the UNC experiments, since the facilities are located in the same area.

The Battelle chamber is constructed of aluminum and is Teflon-coated (Scofield, Levy, and Miller, 1969). The 18,272-liter smog chamber has a surface-to-volume ratio of 0.026 cm^{-1} and is irradiated with fluorescent blacklights. Data for only three propylene/NO_x experiments were received from Battelle. The reported experimental conditions are detailed enough that we were able to perform simulations of all three experiments, but we had to assume a blacklight spectrum.

The National Air Pollution Control Administration chamber was a 9500-liter chamber made of aluminum with Mylar windows (Korth, 1963). It was irradiated with fluorescent blacklights. Data for six propylene/NO_x experiments performed at NAPCA were available to us. The only intensity spectrum for the light source available to us was reported by Korth, Rose, and Stahman (1964). The propylene/NO_x experiments were performed in 1965, one year later. Thus, the uncertainty in the light spectrum is great.

The 6370-liter UCR all-glass chamber (AGC) is made of Pyrex glass and is similar in size to the evacuable chamber (Pitts et al., 1977). Its surface-to-volume ratio is 0.0324 cm^{-1}. The glass chamber is irradiated with fluorescent blacklights. Two runs from the UCR glass chamber were chosen solely on the basis of data availability. Since the available data were limited, we had to assume a blacklamp spectrum for these experiments based on the reported k_d value.

The smog chamber at CALSPAN is a cylindrical chamber 9.14 m in diameter and 9.14 m high, with a surface-to-volume ratio of 0.0066 cm^{-1}

(Kocmond et al., 1973). The walls of the chamber are coated with a fluoro-epoxy urethane having surface energy and reactivity properties similar to FEP Teflon. The light source consists of 24 lighting modules, each containing two 40-watt sunlamps, eight 85-watt high output blacklamps, and two 215-watt specially produced blacklamps. The measured NO_2 decay rate (k_d) was 0.35 min^{-1}.

Of the seven propylene/NO_x experiments performed at CALSPAN from 21 October 1974 to 3 January 1975, raw data for two experiments (Nos. 15 and 16) were available to us. Initial conditions and concentration versus time plots were reported for Experiments 11 and 14. Only concentration versus time profiles were reported for the other three experiments (Nos. 10, 12, and 13). For the computer simulations, we chose Experiments 15 and 16 because of the detailed data on them. We chose Experiment 11 but not Experiment 14 because a new reactive HC analyzer was used with Experiment 14. We feel that the errors associated with the use of a new instrument may be greater in Experiment 14 than the errors associated with an instrument already used in the earlier Experiment 11.

The 1866-liter hexagonal smog chamber at Lockheed (Jaffe and Last, 1974) is made of six flat side panels with Teflon-coated aluminum frames. The surface-to-volume ratio varies depending on the material used and the initial conditions of the experiments; the surface-to-volume was 0.047 cm^{-1} when Teflon was used. The light source in the Lockheed chamber is a xenon arc lamp with a spectrum reported by Jaffe and Last (1974). Propylene/NO_x experiments under various chamber conditions were performed, including different wall materials, surface-to-volume ratios, and cut spectrum (280 to 350 nm light removed). We chose four experiments (Nos. 40, 41, 42, 43), all performed with Teflon-coated walls and a surface-to-volume ratio of 0.043 cm^{-1}. Both conditions are similar to the UCR evacuable chamber. Two of the Lockheed experiments (Nos. 40 and 41) were performed with a cut spectrum ranging from 350 to over 500 nm. (The full spectrum ranges from

280 nm to over 500 nm.) These experiments provide comparison runs for examining the effects of aldehyde photolysis and ozone photolysis in the propylene kinetic mechanism because both photolysis reactions are significant only in the 280 to 340 nm range.

Thus, the data base for the chamber study consists of at least two to three experiments in each of eight smog chambers. For many of the chambers, data were available only for the two or three experiments chosen. The most important uncertainty in nearly all of these experiments is the spectrum of the light source. Since we did not have light spectra for the Battelle, CALSPAN, RTI, and UCR glass chambers, we assumed representative spectra. Table 39 summarizes the data base for the chamber study.

THEORETICAL ANALYSIS OF PARTICLE FLOW IN THE SMOG CHAMBER

Before performing computer simulations for each of the experiments listed above, we investigated theoretical aspects of particle flow in smog chambers and particle collision frequencies with chamber walls. The purpose of this effort was to develop a deeper understanding of wall effects. After the effects of chamber geometries and stirring procedures are isolated, the way will be cleared for investigating the role of light sources and the chemistry of various reactive intermediates.

We begin by deriving a picture of the transport of materials to the chamber walls, and then we use this description as a first step in assessing the relative importance of wall effects on gas-phase chemical reactions. Ideally, such an assessment would be based on knowledge of an experimentally determined decay constant for each of the i reacting species. Detailed measurements of the transport properties (temperature, concentration, and velocity profiles) would then provide input to some transport description obtained by complete solution of the coupled equations of continuity, motion, and energy for the entire system. In practice, these ideal conditions are compromised in one or both of the following ways:

TABLE 39.   SUMMARY OF DATA BASE FOR CHAMBER EFFECTS STUDY

Chamber	Run no. or date	Initial concentration (ppm)		k_d (min^{-1})	Light source	Chamber material	Surface-to-volume ratio (cm^{-1})	Ozone measuring instrument or method
		Propylene	NO$_x$					
UCR-EC	121	0.483	0.51	0.3*	25 kW solar simulator	Teflon	0.034	Dasibi 1070
	177	0.493	0.463	0.33*	25 kW solar simulator	Teflon	0.034	Dasibi 1070
UNC blue	8/9/76	0.66	0.41	Variable	Sunlight	Teflon	0.013	Chemiluminescent
UNC blue	11/5/76	1.15	0.554	Variable	Sunlight	Teflon	0.013	Chemiluminescent
UNC red	11/5/76	0.43	0.526	Variable	Sunlight	Teflon	0.013	Chemiluminescent
RTI-2	10/11/76	0.786	1.57	Variable	Sunlight	Teflon	0.019	
RTI-3	10/11/76	0.421	0.519	Variable	Sunlight	Teflon	0.019	
RTI-4	10/11/76	0.389	0.468	Variable	Sunlight	Teflon	0.019	
Battelle	S-019	1.52	0.552	0.3*	Blacklight	Aluminum and Teflon	0.026	Chemiluminescent
	S-114	0.95	0.449	0.38*	Blacklight	Aluminum and Teflon	0.026	Chemiluminescent
	S-115	0.97	0.525	0.38*	Blacklight	Aluminum and Teflon	0.026	Chemiluminescent
NAPCA	156	2.06	2.06	0.4	Blacklight	Aluminum and plastic film windows	--	Chemiluminescent
	164	1.85	0.99	0.4	Blacklight	Aluminum and plastic film windows	--	Chemiluminescent
	172	2.04	0.99	0.4	Blacklight	Aluminum and plastic film windows	--	Chemiluminescent
Lockheed	40	3.0	1.5	0.3	Xenon arc	Teflon	0.043	McMillan 1100
	41	3.0	1.5	0.3	Xenon arc	Teflon	0.043	McMillan 1100
	42	3.0	1.5	0.3	Xenon arc	Teflon	0.043	McMillan 1100
	43	3.0	1.5	0.3	Xenon arc	Teflon	0.043	McMillan 1100
CALSPAN	11	1.0	0.59	0.35	Blacklight (mainly)	Fluoroepoxy urethane	0.0066	Chemiluminescent (Bendix 8002)
	15	1.0	0.50	0.35	Blacklight (mainly)	Fluoroepoxy urethane	0.0066	Chemiluminescent (Bendix 8002)
	16	1.0	0.50	0.35	Blacklight (mainly)	Fluoroepoxy urethane	0.0066	Chemiluminescent (Bendix 8002)
UCR-AGC	2/23/73	0.52	0.30	0.35	Blacklight	Glass	0.0324	Dasibi 1003
	3/5/73	0.50	0.255	0.35	Blacklight	Glass	0.0324	Dasibi 1003

* Value of k_1 rather than k_d.

262

> With few exceptions, no data on the concentrations of
  reactive intermediates are available. In particular,
  there is a paucity of information on the decay rates
  of any individual species in unirradiated chambers.
> The transport properties of most chambers are inade-
  quately characterized, especially in terms of temperature
  and velocity profiles, to permit input to a sophis-
  ticated transport description.

In view of the points above, we devised the highly simplified picture
of transport within chambers described below, which has as inputs quantities
that are either already available or easily measurable. The validation of
this picture for the transport of ozone to the walls and the results of
applying it to the eight smog chambers are discussed later.

Reactant Transport Inside Smog Chambers

The objective of the transport description is to relate the observed
concentration c_i of reacting species i to its rate of removal by the cham-
ber walls. The approach consists of assuming the existence of a stagnant
boundary layer of thickness δ at the chamber walls; since the layer is
associated with the convective motion of the air, δ depends on the local
air velocity; and consequently, at a distance of δ or greater from the
wall the velocity component parallel to the wall is assumed to be V_∞,
which is to be determined experimentally or deduced from mixing time
data. Transport to the wall is considered as though the wall were a semi-
infinite flat surface, with the x-direction parallel to the surface. Some
physical grounds exist for this approach (see Figure 64). The solution
for $\delta(x)$ (Bird, Stewart, and Lightfoot, 1960) is:

$$\delta(x) = 4.64 \left(\nu x / V_\infty \right)^{1/2} \quad , \tag{97}$$

where ν is the kinematic viscosity of air (taken as 0.15 cm^2 sec^{-1}).

263

VELOCITY IN X-DIRECTION = V_∞

BOUNDARY LAYER $\delta(X)$

VELOCITY IN X-DIRECTION AT SURFACE = 0
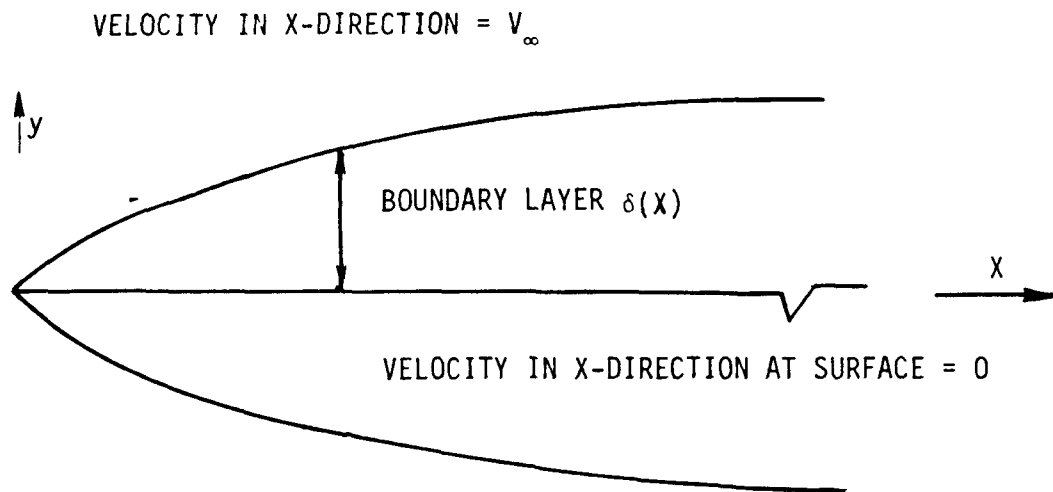
(a) Boundary layer around a thin, semi-infinite flat surface

$V = V_\infty$

BOUNDARY LAYER $\delta(x)$
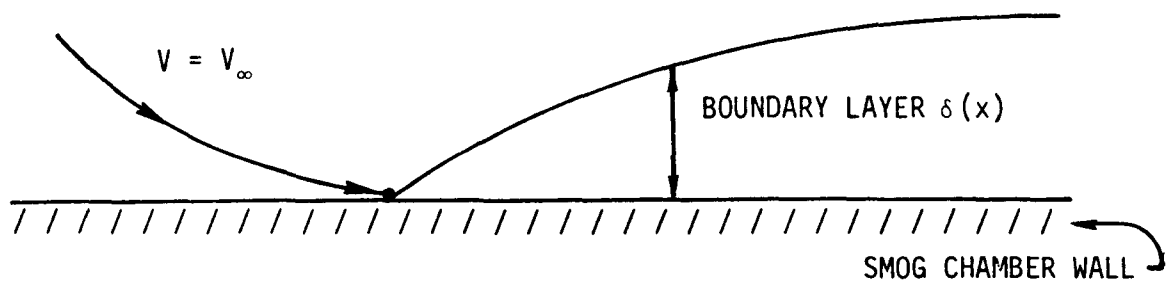
SMOG CHAMBER WALL

(b) Boundary layer caused by circulation of air near the smog chamber wall

Figure 64. Simplified boundary layers

A velocity profile,

$$\frac{V_x}{V_\infty} = \frac{3}{2} \frac{y}{\delta(x)} - \frac{1}{2}\left[\frac{y}{\delta(x)}\right]^3 \quad , \tag{98}$$

where y is the distance above the plate, was assumed in calculating the solution above. Computation of $\delta(x)$ thus reduces to finding an expression for x/V_∞. We chose x to be a characteristic length whose physical significance is shown in Figure 65. We approximate V_∞ by

$$V_\infty \approx x'/t_{mix} \quad , \tag{99}$$

where t_{mix} is the mixing time in the chamber and x' is the length within which mixing is presumed to occur (i.e., the longest dimension of the chamber). We set $x' = x$ (Figure 65), yielding

$$\delta(x) \approx (t_{mix})^{1/2} \quad , \tag{100}$$

where δ is in cm and t_{mix} is in seconds. It is then straightforward to describe the transport and wall reaction of species i by using the coordinate system of Figure 66.
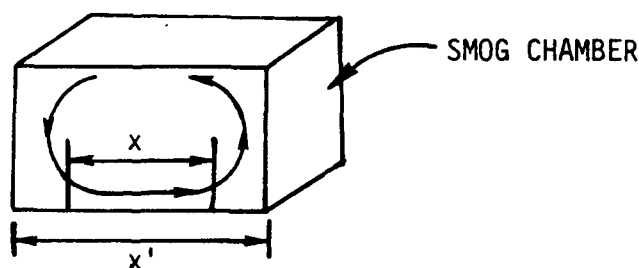
Figure 65.   Characteristic lengths in smog chambers. Arrows represent air circulation from convection or stirring.

$$V = V_\infty \quad \text{-----} \quad c_i = c_1 \quad \text{---------------} \quad z = 0$$

BOUNDARY
LAYER

$$c_i = N_i/K'$$

$$V = 0 \quad \text{_____} \quad z = \delta$$

/ / / / / / / / / / / / / /
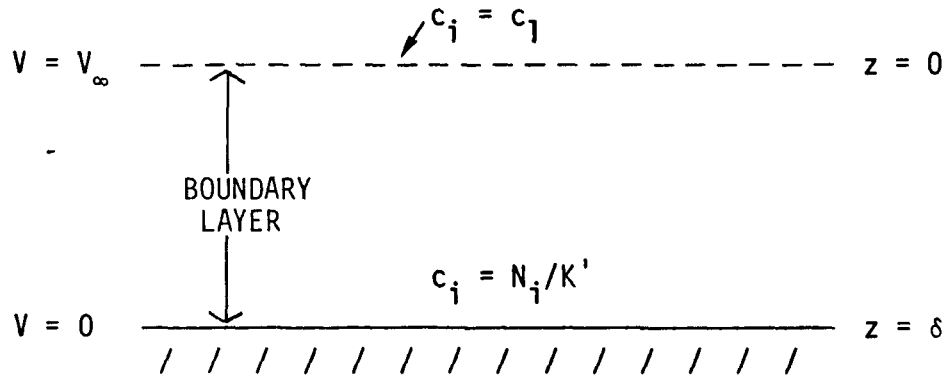
Figure 66.   Transport to the chamber walls

In the discussion below, we adopt the following notation:

N_i = flux of species i in the z-direction, in molecules $cm^{-2}sec^{-1}$,

c = total gas concentration, in molecules cm^{-3},

c_i = local concentration of species i,

c_1 = concentration of species i for $z \le 0$, i.e., bulk concentration,

D = diffusion coefficient of species i in air, in $cm^2 sec^{-1}$,

K_w = rate constant, in sec^{-1}, for bulk concentration change due to wall reaction: $dc_1/dt = -K_w c_1$,

K' = rate constant, in $cm\ sec^{-1}$, for removal of species i in terms of surface flux,

S = chamber surface area,

V = chamber volume.

A mass balance at steady state gives $dN_i/dz = 0$. Differentiating Eq. (100) and applying the boundary conditions $c_i = c_1$ at $z = 0$ and $c_i = N_i/K'$ at $z = \delta$ leads directly to the solution

$$N_i = \frac{\dfrac{cD}{t_{mix}^{1/2}}}{1 + \dfrac{D}{K't_{mix}^{1/2}}} \ell n \left(\frac{1}{1 - \dfrac{c_1}{c}} \right) \cdot \qquad (101)$$

From Eq. (101), for small c_1, we have

$$N_i \approx \frac{\dfrac{Dc_1}{t_{mix}^{1/2}}}{1 + \dfrac{D}{K' t_{mix}^{1/2}}} \quad . \tag{102}$$

If the reaction product is not adsorbed irreversibly but is released as species j (i.e., if $i \xrightarrow{\text{wall}} j$), then $N_i = -N_j$, and Fick's Law becomes

$$N_i = -D\frac{dc_i}{dz} + \frac{c_i}{c}(N_i + N_j) = -D\frac{dc_i}{dz} \quad , \tag{103}$$

which upon integration gives Eq. (102) exactly.

Note that N_i and c_1 are related through the surface-to-volume ratio:

$$-\frac{dc_1}{dt} = K_w c_1 = N_i \left(\frac{S}{V}\right) \quad . \tag{104}$$

Solving for N_i, substituting into Eq. (102), and solving for K' gives

$$K' \approx \frac{\left(\dfrac{D}{t_{mix}^{1/2}}\right)}{\left(\dfrac{D}{t_{mix}^{1/2}}\right)\left(\dfrac{S}{VK_w}\right) - 1} \tag{105}$$

where K' is in cm sec^{-1}. Equation (105) is the desired relation between K' and K_w. Calculation of a few test cases indicates that, for the chambers listed in Table 40, the mixing time effect contributes a correction on the order of 20 percent or less to K'; indeed, for the limiting case where $[D/(t_{mix})^{1/2}] \cdot [S/(VK_w)] \gg 1$, $K_w \approx K'(S/V)$. Clearly, mixing times are most important in relatively quiescent chambers.

TABLE 40. SURFACE-RELATED OZONE DECAY PARAMETERS FOR SELECTED SMOG CHAMBERS

Chamber	Date of run	Material	Surface-to-volume ratio (cm^{-1})	Lights on	k_w (10^6sec^{-1})	K' (10^4cm sec^{-1})	k_m (10^6sec^{-1})	K'$_m$ (10^4cm sec^{-1})
UCR-EC	3-12-74	Teflon	0.034	No	36.4	14.2	--	--
	3-12-74	Teflon	0.034	Yes *	46.6	14.8	--	--
	4-19-74	Teflon	0.034	No	10.1	3.2	--	--
	4-26-74	Teflon	0.034	No	10.3	3.2	--	--
	5-31-74	Teflon	0.034	Yes	46.5	14 ?	--	--
	5-31-74	Teflon	0.034	No	28.4	10.3	--	--
	6-3-74	Teflon	0.034	No	19.6	6.6	--	--
	6-7-74	Teflon	0.034	No	17.0	5.7	--	--
	7-6-76	Teflon	0.034	Yes	33.0	10.3	--	--
	7-6/7-76	Teflon	0.034	No	12.0	3.8	--	--
UNC red	11-4-73[†]	Teflon	0.013	Yes	9.4	7.18	--	--
UNC blue	12-6-73[§]	Teflon	0.013	Yes	11.5	8.80	--	--
	11-4-73[†]	Teflon	0.013	Yes	9.6	7.34	--	--
	12-6-73[§]	Teflon	0.013	Yes	10.0	7.65	--	--
UNC red	11-4/5-73[–]	Teflon	0.013	No	4.0	3.06	--	--
	12-6-73[–]	Teflon	0.013	No	3.1	2.36	--	--
UNC blue	11-4/5-73[–]	Teflon	0.013	No	3.8	2.9	--	--
	12-6-73[∇]	Teflon	0.013	No	2.6	2.0	--	--
RTI 1	8-14-75**	Teflon	0.019	Yes[†††]			--	--
RTI 2	8-14-75**	Teflon	0.019	Yes[†††]			--	--
RTI 3[§§]	8-14-75**	Teflon	0.019	Yes[†††]	19	± 10% 10	--	--
RTI 4	8-14-75**	Teflon	0.019	Yes[†††]			--	--
RTI 1	8-14-75**	Teflon	0.019	No	8.8	4.7	--	--
RTI 2	8-14-75**	Teflon	0.019	No	7.2	3.8	--	--
RTI 3	8-14-75**	Teflon	0.019	No	8.4	4.4	--	--
RTI 4	8-14-75**	Teflon	0.019	No	6.7	3.5	--	--
Battelle	--	Aluminum-Teflon	0.026	No	27	11.0	--	--
	--	Aluminum-Teflon	0.026	Yes	55	21.0	--	--

(continued)

268

TABLE 40 (Concluded)

Chamber	Date of run	Material	Surface-to-volume ratio (cm^{-1})	Lights on	k_w $(10^6 sec^{-1})$	K' $(10^4 cm\ sec^{-1})$	k_m $(10^6 sec^{-1})$	K'_m $(10^4 cm\ sec^{-1})$
Lockheed[$\Delta\Delta$]	--	Pyrex[$\nabla\nabla$]	0.047	No	26	6.2 ***	--	--
"	--	Aluminum	0.090	No	34	3.8	7.2	1.7
"	--	Aluminum	0.136	No	43	3.1	16.0	1.8
"	--	Pyrex	0.090	No	32	3.8	7.2	1.7
"	--	Pyrex	0.136	No	34	2.4	5.3	0.6
"	--	Teflon	0.090	No	39	3.7	6.2	1.4
"	--	Teflon	0.136	No	33	2.9	12.0	1 [c]
"	--	Stainless	0.090	No	72	5.3	34.0	7.9
"	--	Stainless	0.136	No	61	3.7	45.0	5.1
"	--	Pyrex[$\nabla\nabla$]	0.047	Yes	64	14.0	--	--
"	--	Aluminum	0.090	Yes	54	6.0	--	--
"	--	Aluminum	0.136	Yes	55	4.0	--	--
"	--	Pyrex	0.090	Yes	42	4.7	--	--
"	--	Pyrex	0.136	Yes	38	2.8	--	--
"	--	Teflon	0.090	Yes	42	4.8	--	--
"	--	Teflon	0.136	Yes	57	4.3	--	--
"	--	Stainless	0.090	Yes	96	11.0	32.0	7.4
"	--	Stainless	0.136	Yes	115	8.5	51.0	5.8
Mean value[+][+]	--	--	--		37	34.0	77.0	2.7
$100\left(\frac{\sigma}{mean}\right)$[+][-]	--	--	--		34	36.0	89.0	92.0

* 20 kW xenon arc lamp filtered through new Pyrex pane.

+ Run carried out from 1028 to 1404 EST.

[c] Run carried out from 1301 to 1501 EST.

: Run carried out from 2102 to 0500 EST

⊤ Run carried out from 1901 to 2358 EST

** Dates not given. Data were taken from an RTI progress report dated 14 August 1975.

++ Natural sunlight through Teflon walls.

§§ Stirring data indicated V_ω = 800 fps. We used this value and x as the chamber circumference in the expression $\delta = 4.64(\nu x/V_\omega)^{1/2}$ and used that value of δ in Eq. (105).

$\Delta\Delta$ Values for the chamber in the presence of inserts fabricated from the materials shown. .

$\nabla\nabla$ Base chamber (empty): $K_w = K_B$.

*** K' calculated using the relation $K_w = K'(S/V)$.

⁺⁺⁺ Lockheed chamber only.

Validation of the Transport Picture

We calculated first-order light and dark decay constants (K') for ozone based on measured ozone half-lives in the RTI, UCR-EC, UNC, Battelle, and Lockheed chambers. The results of the calculations are presented in Table 40. All the light and dark decay constants for ozone were averaged to generate the statistical information in Table 41.

The main conclusion to be drawn from Table 41 is that standard deviations amongst the chambers in the apparent rate of ozone decay (K_W) are substantially reduced under both light and dark irradiation conditions when individual chamber geometries (surface-to-volume ratios and mixing times) are taken into account by calculating K'.

Materials Effects--The Lockheed Data

The runs in the Lockheed chamber (Jaffe and Last, 1974) provide some opportunity to examine the effects of construction material on the value of K'. Jaffe and Last obtained ozone decay times under both light and dark conditions when samples of different materials were inserted into the chamber shell. An attempt was made to estimate the influence of materials on ozone decay by assuming all decay processes to be independent and first order. If K_B and K_B' are the volume and the surface decay rate constants, respectively, for the base chamber, then one can associate with each construction material the analogous rate constants K_m and K_m', where

$$K_m = K_w - K_B = K_m' \left(\frac{S_m}{V} \right) , \qquad (106)$$

and K_m and K_m' are the volume and surface decay rate constants, respectively, for each of the different materials inserted into the base chamber.

TABLE 41.   INFLUENCE OF CHAMBER GEOMETRY ON THE ESTIMATION OF
SURFACE-RELATED OZONE DESTRUCTION*

Rate constant	Value	Coefficient of deviation[†] (percent)
$10^6 \times K_w$, light	19.6 ± 10.8	55%
$10^4 \times K'$, light	9.6 ± 1.8	18
$10^6 \times K_w$, dark	8.1 ± 5.3	65
$10^4 \times K'$, dark	3.9 ± 1.1	29

* Materials effects are not considered.

† Coefficients of deviation (i.e., standard deviation ÷ mean
value) are expressed as percentages of mean values.

Clearly, the effectiveness of this type of analysis is greatest when
$K_m \gg K_B'$. However, as the data in Table 40 show, the K_m's for the Lock-
heed chamber are generally less than K_B; moreover, the dark decay data
of Table 40 show anomalous values for Pyrex and stainless steel. In the
runs with lower surface-to-volume ratios, ozone was apparently destroyed
more rapidly than in the runs with higher surface-to-volume ratios, which
would imply negative K_m's. In addition, during photolysis, ozone was
removed less rapidly in the presence of material other than Pyrex. Ozone
was removed more rapidly in the presence of stainless steel than in the
presence of Pyrex. As a consequence, it was generally impossible to
associate surface rate constants with different materials during irradia-
tions of ozone in the Lockheed chamber. In the dark, values of K_m' were
in good agreement for Teflon and for aluminum, but not for Pyrex or stain-
less steel. (For a given material, values of K_m' in the light and dark
should be identical.) Thus, from the Lockheed chamber data, the following
conclusions can be drawn:

> The effects of chamber geometry are outweighed by the
effects of different materials. Note that no improve-
ment in the coefficient of deviation resulted when surface
ozone decay rates were expressed in terms of K' rather
than K or in terms of K_m' rather than K_m.

> Surface-related effects for Pyrex and for stainless steel
were possibly dominated by history-dependent phenomena,
in view of the decrease in K' and (for dark reactions)
K_m' with increasing surface-to-volume ratio. For stainless
steel, K_m' was little affected whether the light source was
on or off, suggesting that surface effects may have been
associated more with changes in surface reactivity than
with contamination found on the sample materials.

> Tne apparent lack of dependence of K_m' on area for aluminum
and for Teflon raises the possibility that geometric effects
in chambers constructed of these materials could be part-
ially accounted for by simple corrections for the surface-
to-volume ratios for mixing time.

Wall Reactions of Species Other Than Ozone

Upper limits were estimated for the removal of species other than
ozone at the walls of the UCR chamber* by using the expression:

$$K_{w,i} = \left(D_i / t_{mix}^{1/2} \right) \left(S/V \right) \quad , \quad (107)$$

where $K_{w,i}$ is the rate constant for removal of species i at the wall, D_i
is the diffusion coefficient of species i in air, and the rest of the terms
are as defined earlier. The reliability of these constants depends primarily
on the choice of D_i and t_{mix}; D_i was usually estimated by using Graham's law

---

* The UCR chamber was chosen for simulation only because of our previous
experience with an explicit propylene mechanism tested with smog chamber
data from that facility. No conclusion regarding the actual reactivity
of the UCR chamber walls should be inferred from this study. In fact,
Eq. (107) is based on the assumption of an infinitely reactive surface.

272

and measured diffusion coefficients for gases of similar molecular weight. More refined estimates would have to be based on Lennard-Jones parameters, which might be obtained from viscosity data or critical point data, neither of which seem to be available for reactive intermediates. We believe that the accuracy limits are governed by the uncertainty in the use of $(t_{min})^{1/2}$ as an approximation to the boundary layer thickness. [We point out here that the dimension of the expression $(t_{min})^{1/2}$ is centimeters; strictly speaking the boundary layer thickness δ should be expressed as $\delta = C(t_{min})1/2$, where C is a proportionality constant having a value of unity when δ and t_{min} are expressed in cgs units.]

Table 42 gives the species examined and their rate constants. Figures 67, 68, and 69 show the influence of the reactions that affected the concentrations of O_3, NO_2, and propylene, respectively. Under the initial conditions chosen, wall reactions of OH·, O atoms, NO_3, and RCO_3^- had no effect on the concentrations of the three species examined; all three, however, were sensitive to HONO. The propylene simulations were unaffected by ozone-wall reactions, even though the maximum possible rate of ozone loss to the walls was sufficient to suppress completely the buildup of ozone. We emphasize that the simulations above are valid only for the initial conditions chosen; they should not be extended to other systems.

RESULTS OF THE CHAMBER EFFECTS STUDIES

Much of the work for the eight different chambers listed above was done with the explicit kinetic mechanism for propylene discussed in Section 5 of this report.

Results of the Study of the UCR Experiments

The simulation results of the propylene experiments are discussed earlier (see Section 5). In this section, we summarize some of the conclusions reached from investigation of UCR Runs EC-121 and EC-177.

Although the light source was replaced just before each of these runs, we found that even using a higher than calculated photolysis rate constant

- TABLE 42. MAXIMUM RATE CONSTANTS FOR HYPOTHETICAL WALL REACTIONS IN THE UCR CHAMBER

Species	$K_w(min^{-1})$
$CH_3CH(O_2^{\cdot})CHOH$	0.47
$HO_2^{\cdot}$	1.4
O	2.2
$HONO$	0.71
NO_3	0.54
PAN	0.18
$CH_3O_2^{\cdot}$	1.2
$Ozonide$	0.3
$CH_3C(O)O_2^{\cdot}$	0.84
$OH\cdot$	2.2
O_3	0.62

Figure 67. Maximum influence of wall reactions on ozone concentrations during the NO/propylene irradiations. Curves represent the simulated ozone concentrations when species shown are presumed to react with walls at the maximum rate constants given in Table 42.

275
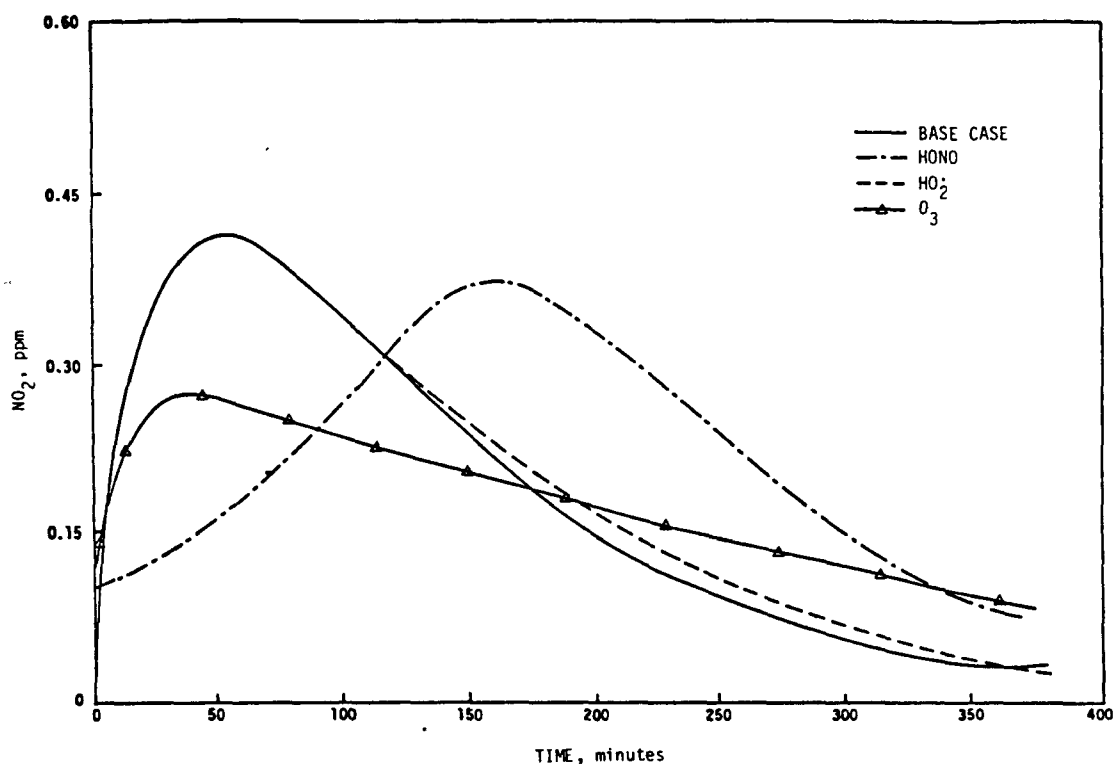
Figure 68. Maximum influence of wall reactions on NO₂ concentrations during the simulated NO/propylene irradiations. An initial HONO concentration of 30 ppb was assumed. Curves represent simulated NO₂ concentrations when species shown are presumed to react with walls at the maximum rate constants given in Table 42.
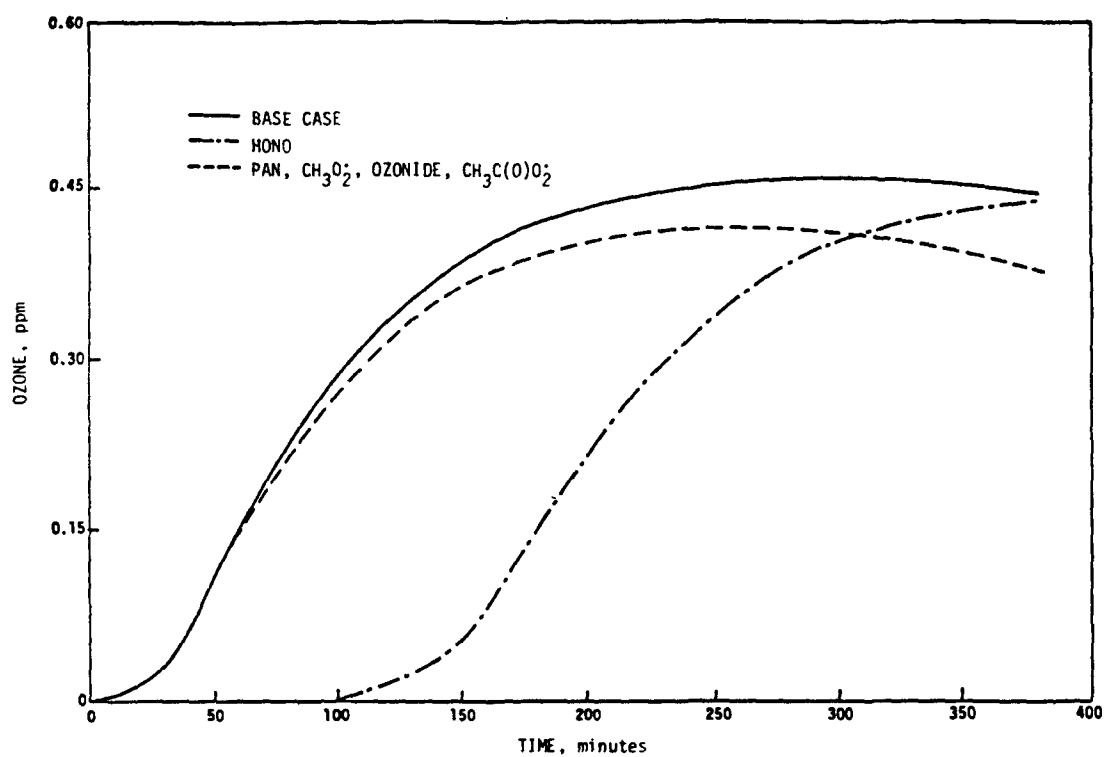
Figure 69. Maximum influence of wall reactions on propylene concentrations during the NO/propylene irradiations. Curves represent the propylene simulated concentrations when species shown are presumed to react with walls at the maximum rate constants given in Table 42.
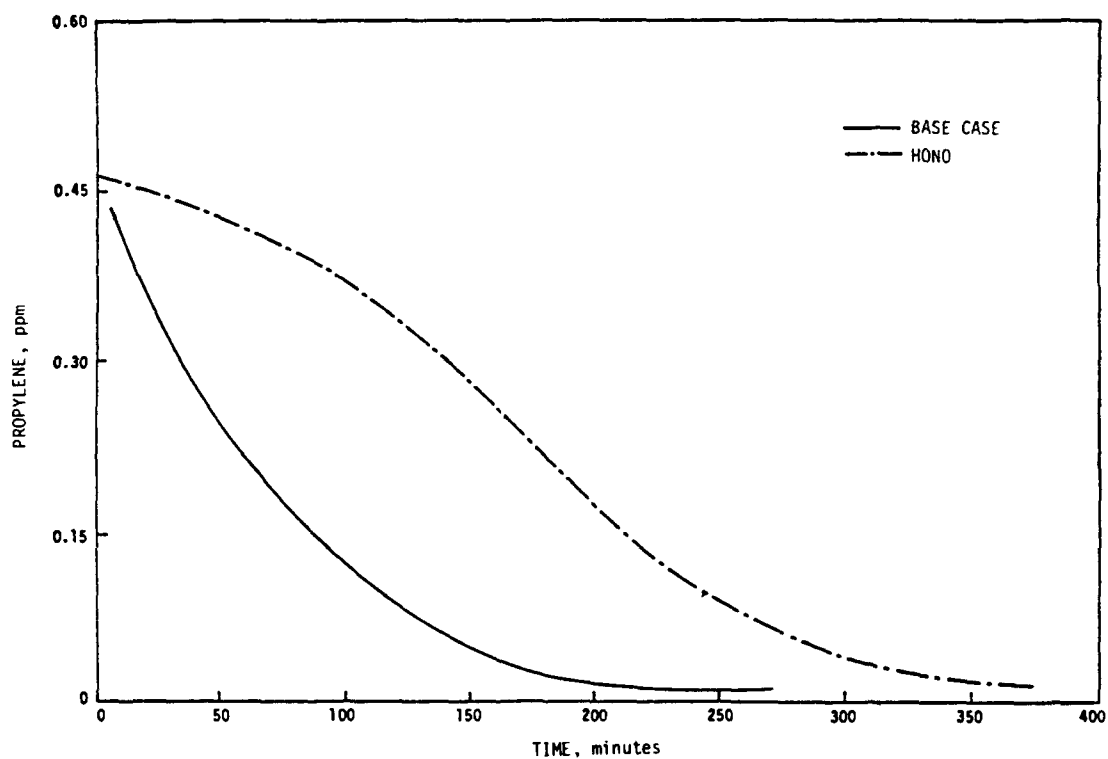
277

we were not able to follow the propylene decay; thus, the ozone behavior was overpredicted. We chose EC-121 and EC-177 for this study because the reported light spectrum should be accurate, and deterioration effects would not have occurred. Yet, there may be some problems in the data documentation because we can simulate the propylene decay much better in other UCR propylene experiments with the same initial conditions. In future studies of the UCR experiments, we will investigate the possible chemical reactions that may affect the propylene decay and the effect of chamber cleaning on some of the UCR experiments. Prior to the EC-121 experiment, the UCR chamber was cleaned by "boiling off" any chemical species that may have adsorbed onto the walls. If the chamber was not "seasoned" after this cleaning period, then ozone or other species may have been affected more in EC-121 than in other UCR experiments.

Results of the Study of the UNC Outdoor Smog Chamber

The second chamber investigated was the outdoor smog chamber at the University of North Carolina. The main differences between this chamber and the UCR evacuable chamber are the natural irradiation and the temperature in the UNC chamber. The physical characteristics and operating conditions of the chamber were discussed by Jeffries, Fox, and Kamens (1975). Of the reactions listed in Table 1 (see Section 4), only two reactions (besides the photolysis reactions) are important in chamber effects studies: (1) $O_3 \rightarrow$ wall and (2) $N_2O_5 + H_2O$. Jeffries, Fox, and Kamens (1975) found that the nighttime O_3 loss rate in the UNC chamber yielded an O_3 half-life between 48 and 70 hours. We estimate the rate constant for the $O_3 \rightarrow$ wall reaction to be approximately 2.2×10^{-4} min^{-1}.

Jeffries, Fox, and Kamens (1975) also reported a rate constant of 5.6×10^{-7} $ppm^{-1}min^{-1}$ for the $N_2O_5 + H_2O$ reaction. This value is a factor of 9 lower than the value of 5×10^{-6} $ppm^{-1}min^{-1}$ used in the UCR chamber simulations described in Section 5. Since effects of the $N_2O_5 + H_2O$ reaction tend to occur after the NO_2 peak and since the UNC NO_2 measurements do not include PAN separately, we were not able to derive a better estimate

of the rate of the N_2O_5 + H_2O reaction in the UNC chamber. We tentatively subtracted the simulated concentration of PAN from the measured NO_2 concentration to obtain an estimate of the actual NO_2 concentration and, hence, the effects of the N_2O_5 + H_2O reaction.

Figure 70 shows a typical solar radiation profile for the UNC experiments. The chamber experiments begin early in the morning (usually before sunrise). The speed of the overall chemistry increases slowly as the sun rises and then begins to decrease in the afternoon as the sun starts to set. In constant-light experiments, the speed also varies as propylene is consumed. Thus, the combination of light-induced acceleration and chemically induced acceleration can test the mechanism in a novel manner. We incorporated a variable radiation and temperature algorithm into our kinetic program using a simple linear interpolation scheme.

The run of 9 August 1975 was affected by clouds, causing "choppiness" in the solar radiation profile. Jeffries, Fox, and Kamens (1976) suggested that the "choppiness" may cause an increase in O_3 production. Their conclusions were based on experiments with the same initial concentrations of hydrocarbons and NO_x performed on two consecutive days: a clear sunny day and a partly cloudy day. More O_3 was measured in the chamber on the partly cloudy day.

We performed three simulations of the 9 August 1975 run varying only the "choppiness" of the solar radiation profile. In these simulations we used the propylene mechanism presented by Whitten and Hogo (1977). Figures 71 and 72 show the solar radiation profiles used. Curve 1 in Figure 71 represents our estimate of the solar radiation profile on a clear day. Curve 2 was estimated by averaging through the peaks in the observed solar radiation profile. Figures 72(a) and 72(b) show solar radiation profiles based on input data every 15 minutes and every 5 minutes. Figure 72(b) is the closest representation of the solar radiation profile presented in Figure 70. Computer simulations with these four profiles show the same results for oxidant formation (Figure 73), except for Curve 1. Thus, our old mechanism does not show any effect due to "choppiness" at 5-minute or 15-minute intervals.

279

SOLAR INTENSITY PROFILE, langleys

HOURS, EDT
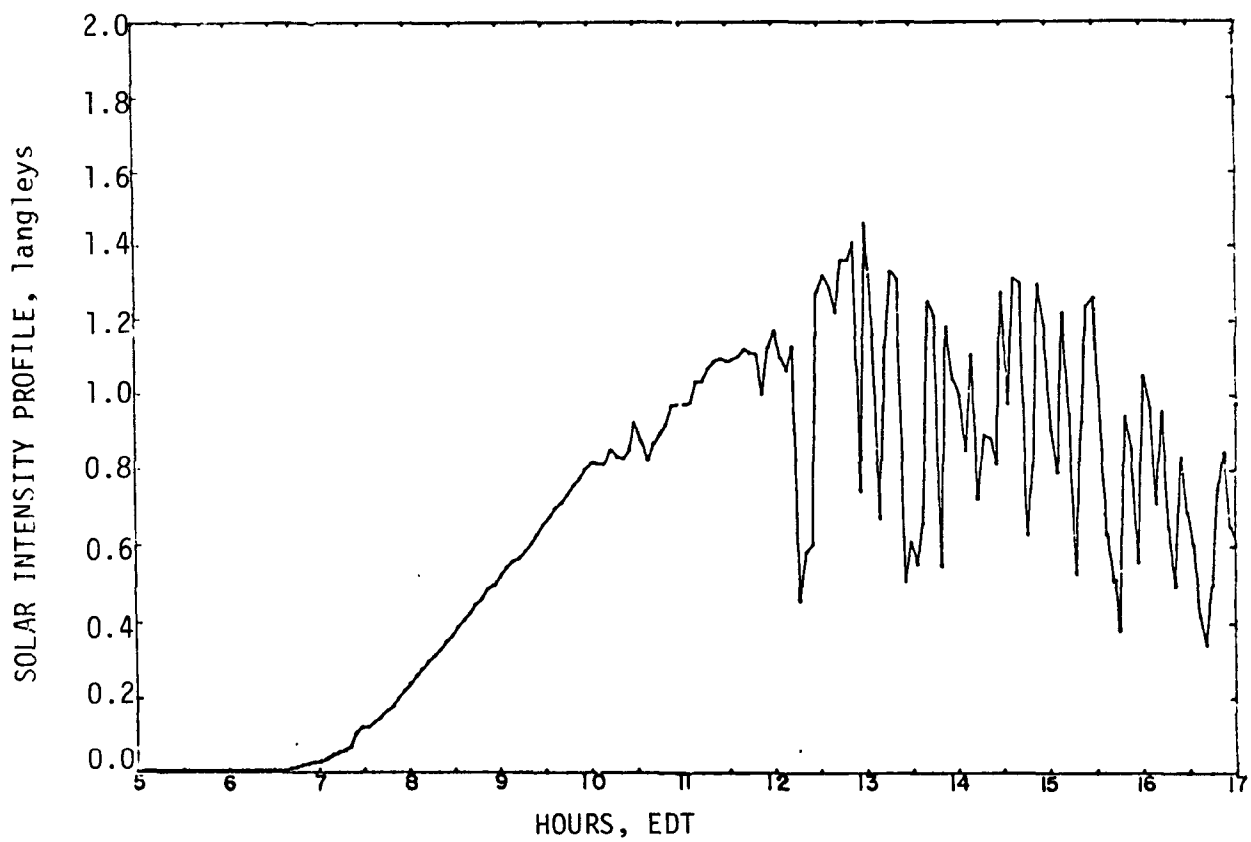
Source: Jeffries (1976).

Figure 70. Observed diurnal variation in solar intensity at the UNC chamber on 9 August 1975

280
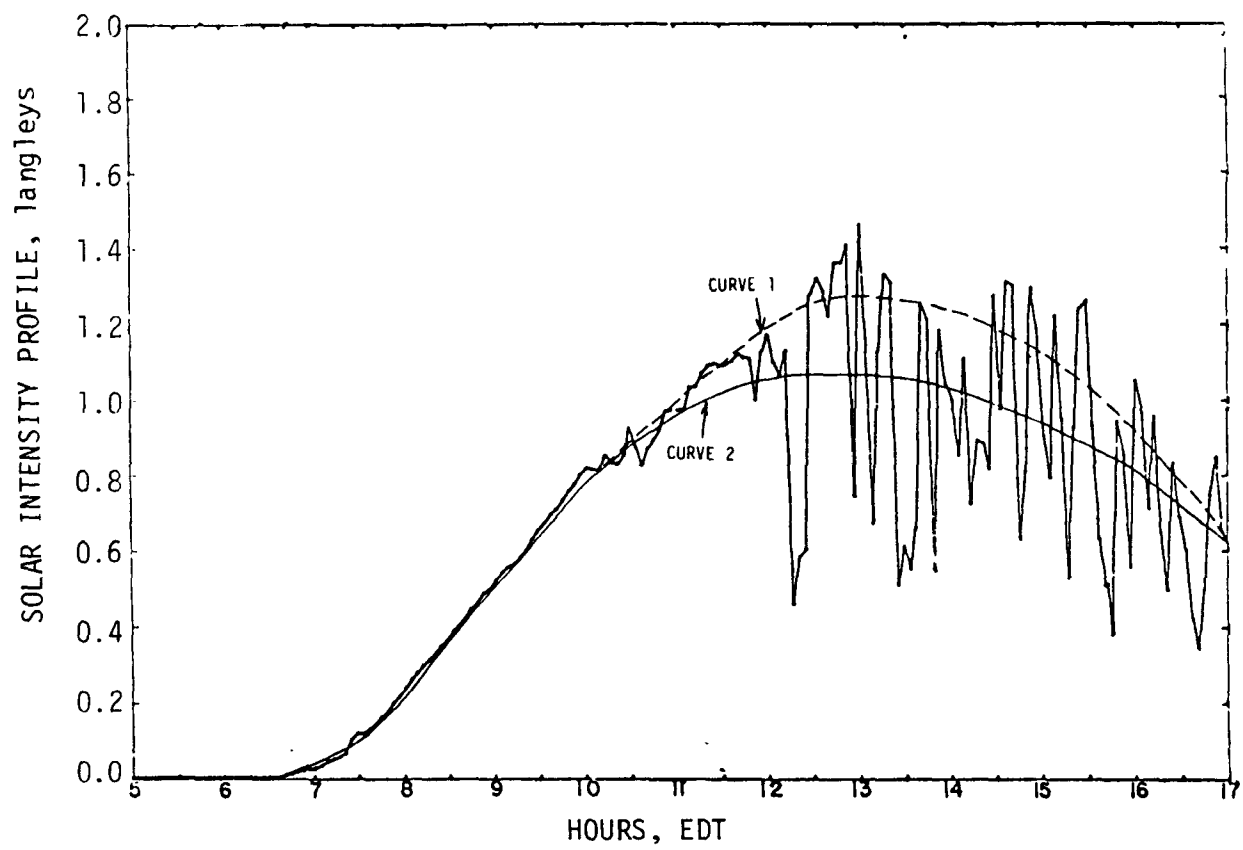
Figure 71. Approximations to the observed solar intensity at UNC
on 9 August 1975

281
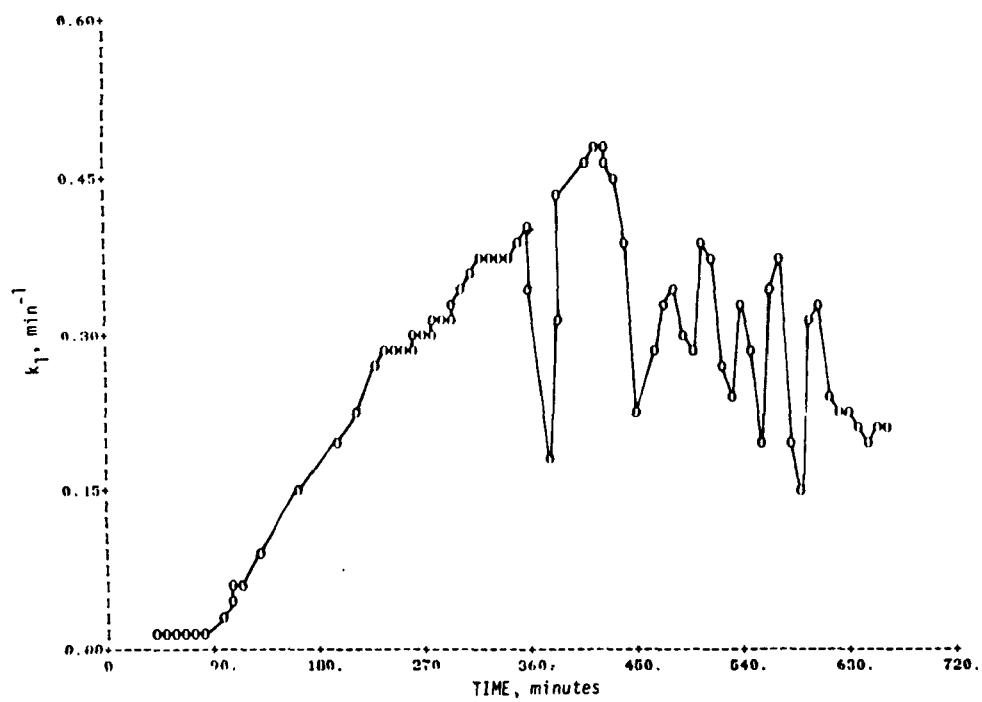
(a) 15-minutes intervals

Figure 72. Calculated diurnal variation of the NO_2 photolysis rate constant (k_1) in the UNC chamber on 9 August 1975

282
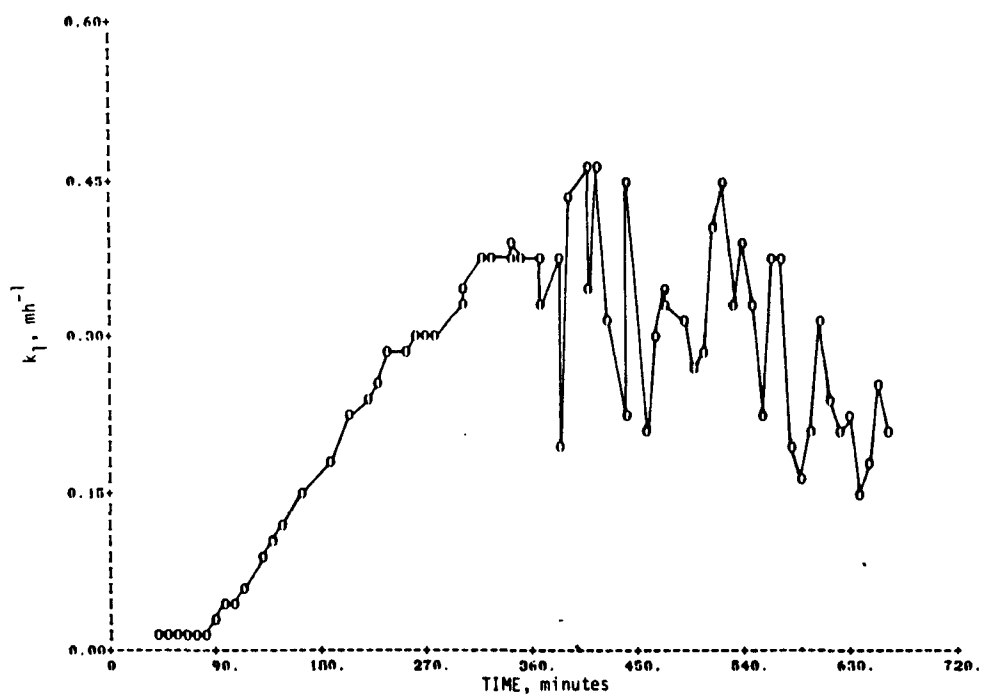
(b) 5-minute intervals

Figure 72 (Concluded)

283

Figure 73. Effect of different NO_2 photolysis rate constants or ozone concentrations in UNC blue chamber experimen' on 9 August 1975. Asterisks indicate ozone measur ments in the chamber.

Temperature, with a diurnal variation similar to that of solar
radiation, may also have a large effect on the overall chemistry. In
our first simulation of the 9 August 1975 run, we varied the tempera-
ture as observed. We then performed the same simulation with a constant
average temperature. The temperature for the 9 August 1975 run averaged
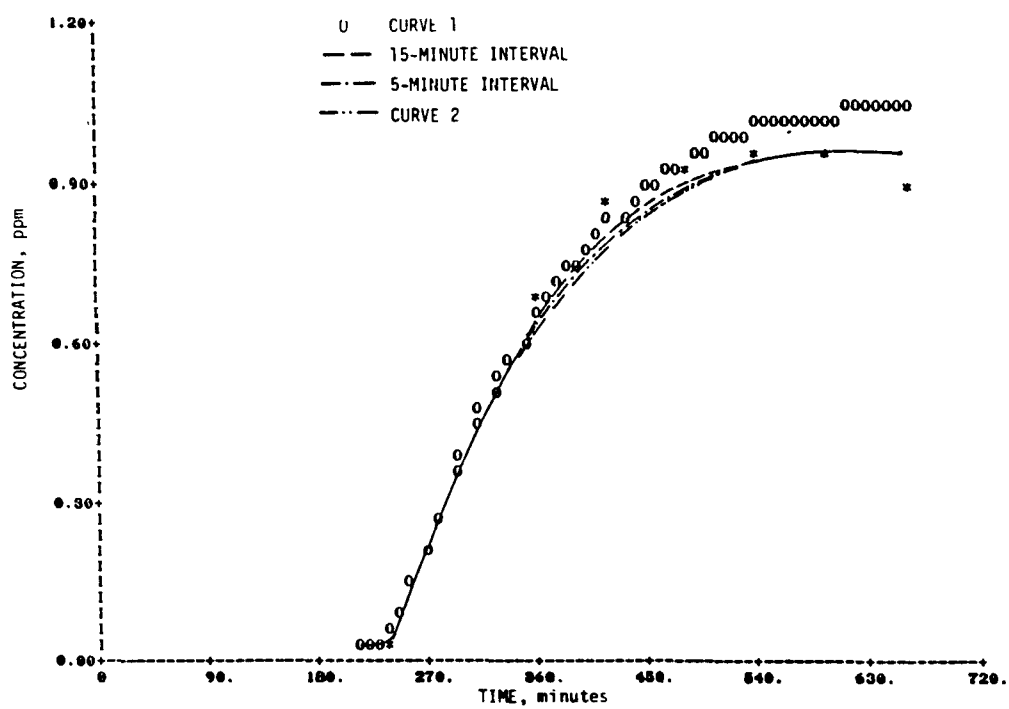over 11 hours is 299K. In both runs, we used the Curve 2 solar radia-
tion profile in Figure 71. Figure 74 shows the O_3 predictions from the
two simulations. As one can see, O_3 is produced at nearly the same rates
during the early parts of the simulations, but not as much O_3 is produced
at the end of the simulation at a constant temperature.
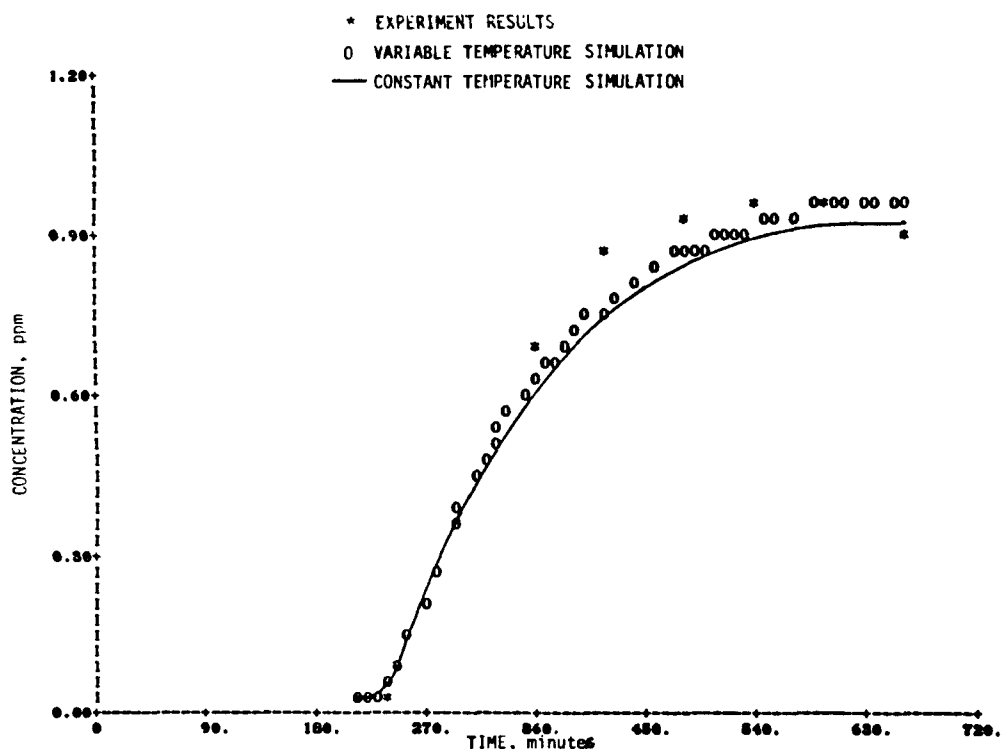

Figure 74.   Effects of different temperature profiles on
              simulated ozone concentrations

The final simulations were performed on four UNC chamber runs (one on
9 August 1975, two simultaneously on 5 November 1976, and one on 8 August
1977) with the propylene mechanism presented in Section 5. The simulation
results are presented in Volume II of this report.

285

An interesting observation is the difference between summer and late fall radiation intensities. During the fall months, the total radiation is lower and the ratio of aldehyde to NO_2 photolysis rate constants is different. It is also known that this ratio is not constant during the course of a day.

In simulations of the 5 November 1976 runs, we had to lower the aldehyde/NO_2 photolysis rate constant ratio by 40 percent to fit the observed data. Two UNC runs with different initial hydrocarbon concentrations were performed simultaneously. We are able to simulate both runs fairly closely up to the O_3 peak (Figures 75 and 76). For the blue chamber run, we could not simulate the O_3 concentrations after the O_3 peak. For the red chamber run, we were not able to simulate NO_x as closely as O_3 and propylene. However, the use of a significantly lower photolysis ratio for these November runs probably accounts more for the colder temperature then than the actual change in the photolysis ratio.

Results of the RTI Chamber Study

The Research Triangle Institute outdoor smog chambers are similar to the UNC chamber and are located in the same area. Therefore, we assumed the same solar radiation profile for RTI as for the UNC chamber. Of the experimental data available, we investigated the propylene/NO_x experiments performed in October 1976 because this set of data appeared to have the least experimental errors in the O_3 values. The rate constants of the $O_3 \rightarrow$ wall reaction and the $N_2O_5 + H_2O$ reaction were changed in the mechanism to 5.1×10^{-4} min^{-1} and 5×10^{-6} $ppm^{-1}min^{-1}$, respectively.

Although RTI performed runs for 35 hours, we simulated only the first 18 hours of each run. The simulation results for Chambers 2, 3, and 4 are presented in Volume II (no O_3 was observed in Chamber 1). As shown by these results, we are able to simulate the data fairly well for the first day, except for Chamber 2 (Figure 77). The NO_2 data shown have been corrected for PAN by subtracting the simulated PAN concentrations from the NO_2 data as was done with the UNC data.
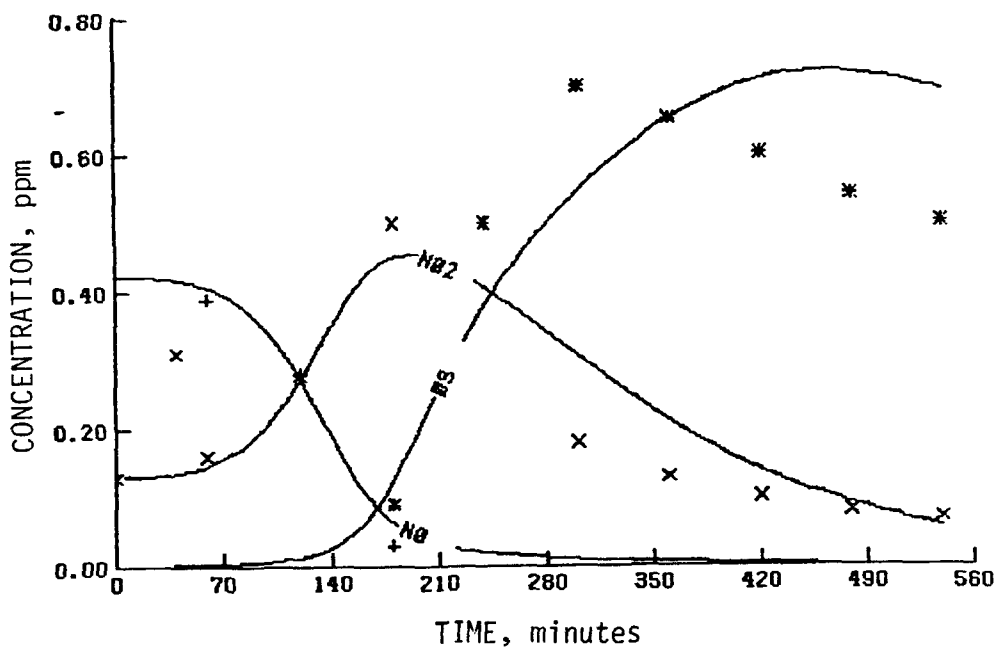
(a) NO_2, NO and O_3
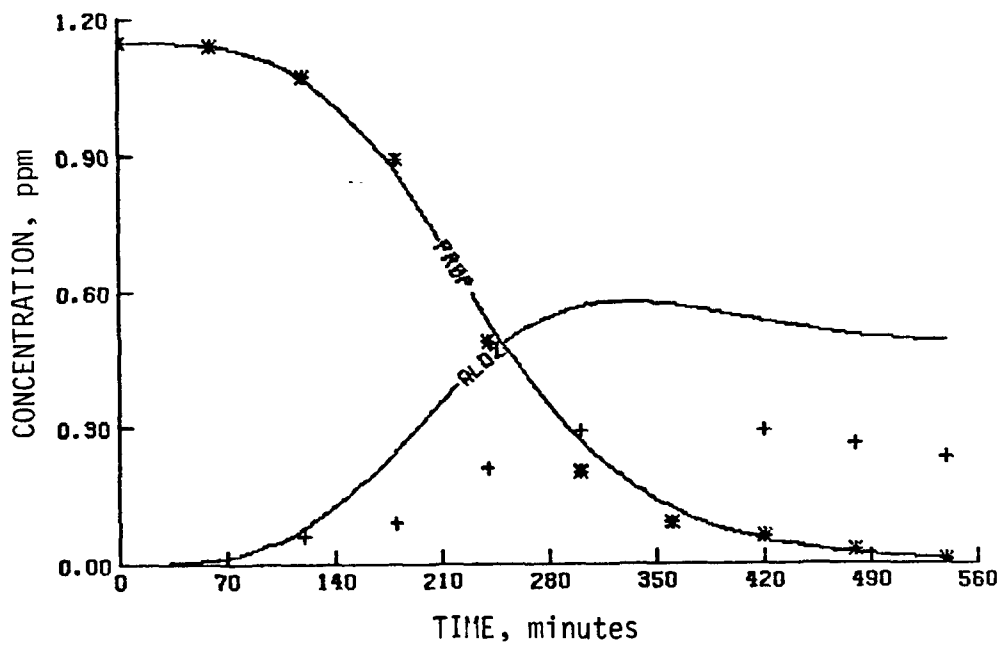
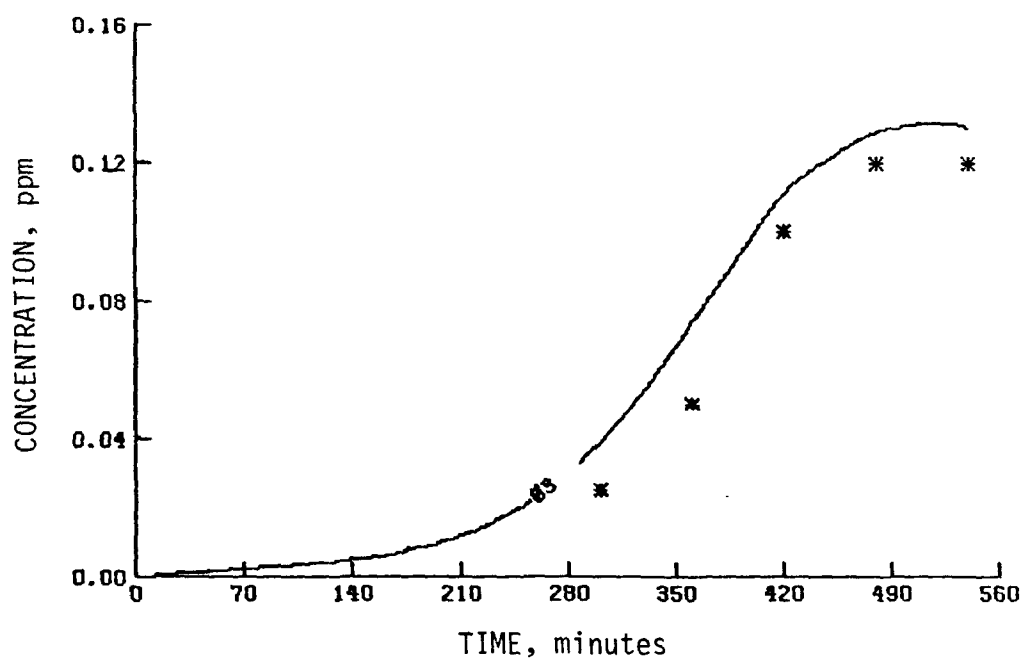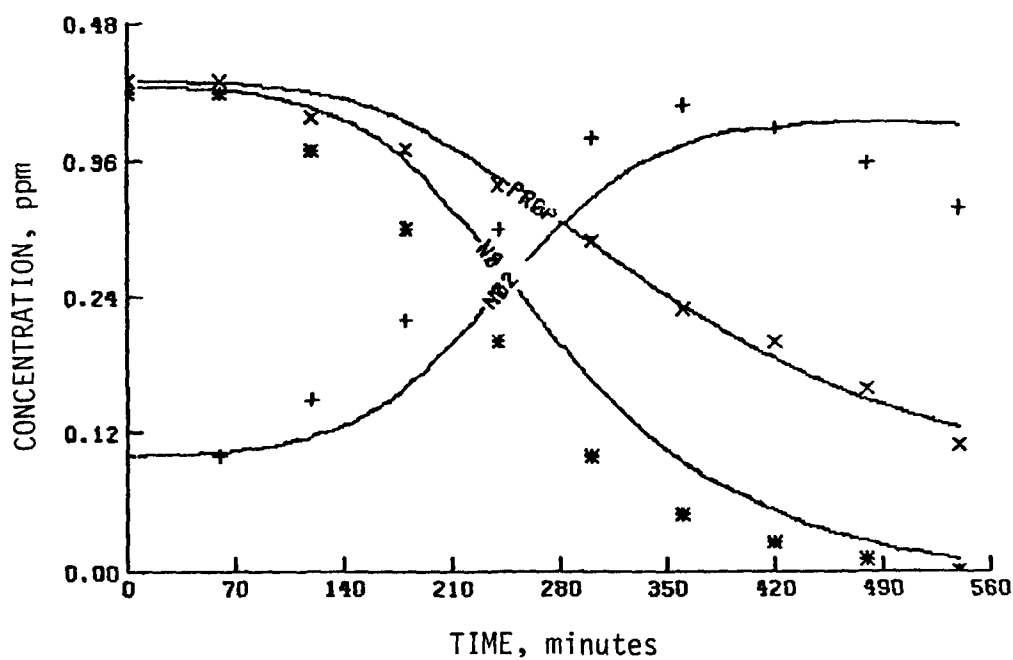

(b) Acetaldehyde and propylene

Figure 75.   Simulation results of a UNC propylene experiment on
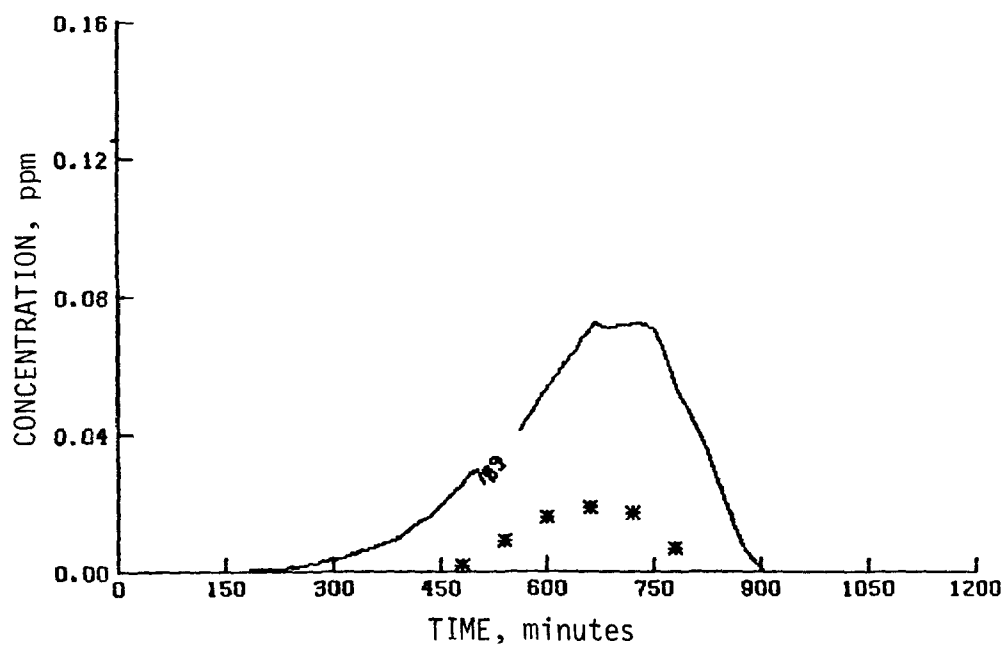5 November 1976 (blue side)
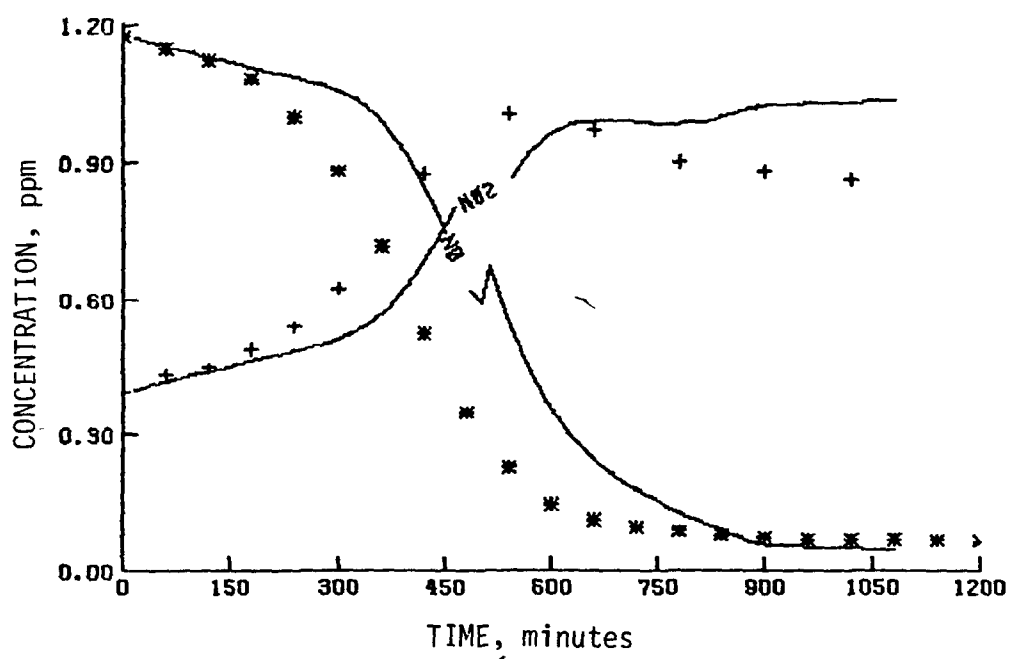
287

(a) O_3

(b) Propylene, NO_2, and NO

Figure 76. Simulation results of a UNC propylene experiment on 5 November 1976 (red side)

(a) O_3

(b) NO_2 and NO

Figure 77. Simulation results of an RTI propylene experiment on 11 October 1976 (chamber 2)

289

The O_3 data reported for Chamber 2 are suspicious. At the NO_2 peak, reported O_3 concentrations are approximately a factor of 10 lower than the amounts predicted by steady-state calculations. The O_3 values reported for Chambers 3 and 4 at the NO_2 peak were low by only a factor of about 3. Our simulated O_3 values are high for Chamber 2 by a factor of 3 but are fairly close for Chamber 3. One aspect of the RTI data that we have not taken into account is the effect the fan has on the species behavior. The fan was turned off in Chamber 3 only. When the fan is left running, we expect a greater wall effect owing to the turbulence caused by the fan. This might account for the overprediction of ozone in the simulation of Chamber 2.

The ozone was also overpredicted in Chamber 4, perhaps also because of the turbulence caused by the fan. Another possible explanation is that the chamber has not been "seasoned" long enough. Simulations with a higher $O_3 \rightarrow$ wall reaction (at 2.5×10^{-3} min^{-1}) resulted in better fits of the ozone concentrations in Chamber 4, but had little effect on the results of Chamber 2. Figure 78 shows the simulation results of this run. Thus, we feel that a longer "seasoning" period may be required for Chamber 4. Note that in Figure 78 the predicted ozone in Chamber 4 decays rapidly after the ozone peak while the observational data remains constant. If the chamber is not well seasoned before the experiment, it becomes a little more seasoned during the experiment. Thus, the $O_3 \rightarrow$ wall reaction rate may decrease with time, and the observed ozone would remain constant.

During the next contract year, we hope to investigate the turbulence effect caused by the fans and the need to have the chamber "seasoned" sufficiently in the RTI experiments.

Results of the Study of the Battelle and NAPCA Chambers

Both the Battelle and NAPCA chambers use constant irradiation sources similar to that in the UCR chamber. Both groups reported values for the NO_2 decay rate. Battelle reported an actual k_1 (NO_2 photolysis rate), which was used in the computer simulations.
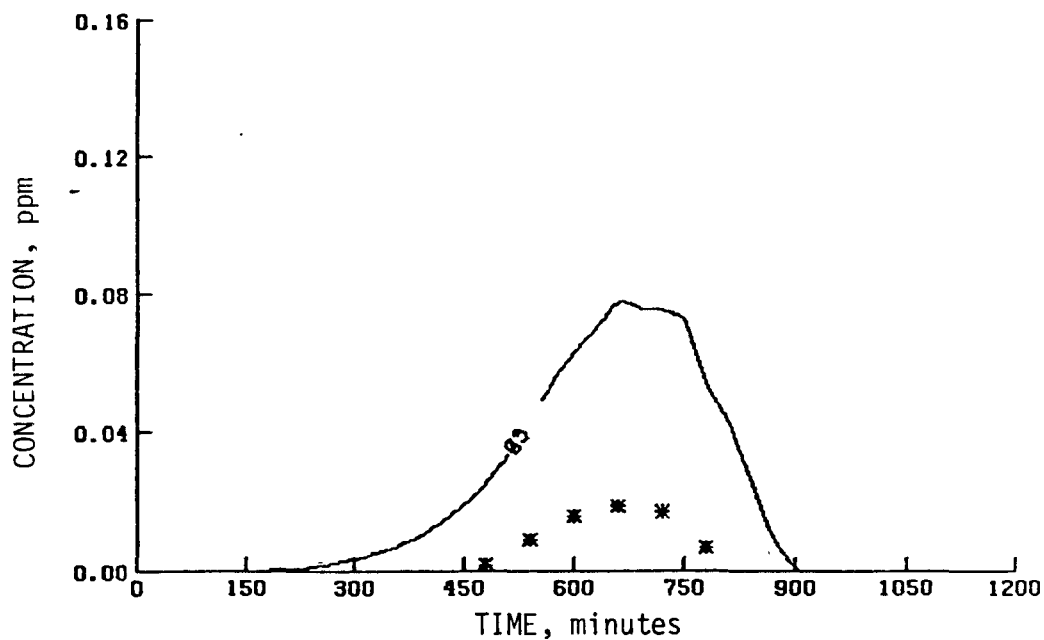
(a) Ozone
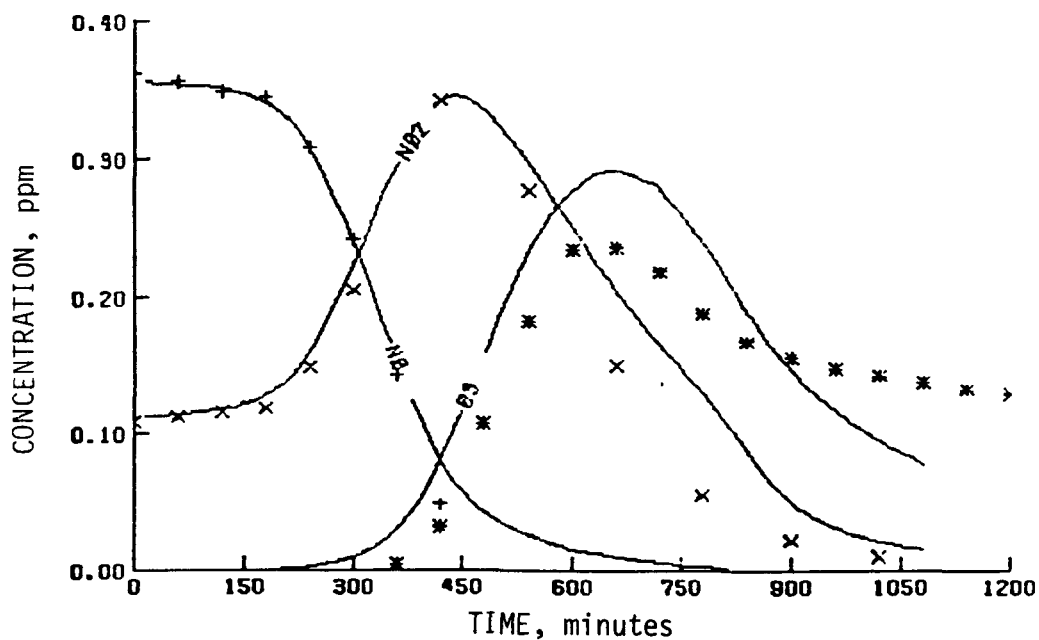
(b) NO_2, NO, and O_3

Figure 78.   Simulation results of the ozone behavior in RTI
Chambers 2 and 4 with the ozone wall reaction
at 2.5 x 10^{-3} $ppm^{-1}min^{-1}$

We investigated three Battelle runs (S-019, S-114, and S-115) performed with blacklight irradiation (k_1 equal to 0.3 min^{-1} for S-019 and 0.16 min^{-1} for S-114). Initial simulations using the blacklight spectral distribution reported for the NAPCA chamber showed high ozone for S-019 but low ozone predictions for Runs S-114 and S-115. However, the fit was improved if the NO_2 photolysis rate constant was raised from 0.16 min^{-1} to 0.2 min^{-1}. [This change of 25 percent is within the estimated limit of 30 percent uncertainty reported by Wu and Niki (1975)]. The simulation results for Battelle Runs S-019, S-114, and S-115 are shown in Volume II.

Of the five propylene/NO_x experiments available to us from NAPCA, we chose three runs with similar operating conditions (Runs 156, 164, and 172). Each run was statically charged and run in Chamber 2. Run 156 was performed at full light intensity, and Runs 164 and 172 were performed at one-third of the full light intensity. The only light intensity spectrum available was reported by Korth, Rose, and Stahman (1964). The k_d value used was 0.4 min^{-1} (Kuntz, Kopczynski, and Bufalini, 1973). From estimates of k_1 from a k_d value due to blacklamps, we estimated the k_1 value for the NAPCA chamber to be approximately 0.27 min^{-1}.

In our initial simulations of NAPCA Runs 156, 164, and 172, the propylene decay rate was too rapid and the NO_2 induction period too short. These simulations are not shown. Because the reported light spectrum was taken in 1963 and the propylene experiments were performed in 1965, we suspect that the light source may have deteriorated. We applied short wavelength attenuation to the reported light spectrum of Korth, Rose, and Stahman, (1974) and calculated a new set of photolysis ratios (Table 43). Simulations with the shifted spectrum produced better fits (see Volume II).

TABLE 43. PHOTOLYSIS RATE CONSTANTS (RELATIVE TO $k_1 = 1$) USED IN COMPUTER SIMULATIONS OF THE NAPCA RUNS*

Reaction	Original rate constant[†]	Attenuated rate constant[§]
$O_3 + h\nu \rightarrow O(^1D)$	0.0257	0.0052
$O_3 + h\nu \rightarrow O(^3P)$	0.034	0.03
$HONO + h\nu \rightarrow NO + OH\cdot$	0.426	0.375
$H_2O_2 + h\nu \rightarrow 2OH\cdot$	0.0037	0.0014
$HCHO + h\nu \xrightarrow{O_2} HO_2 + HCO\cdot$	0.0065	0.0038
$HCHO + h\nu \rightarrow H_2 + CO$	0.0065	0.0038
$CH_3CHO + h\nu \xrightarrow{O_2} CH_3O_2 + HCO\cdot$	0.0065	0.0038
$CH_3CH_2CHO + h\nu \xrightarrow{O_2} CH_3CH_2O_2 + HCO\cdot$	0.007	0.0038

* The light intensity was cut to one-third the full intensity for Runs 164 and 172. Therefore, we lowered the aldehyde photolysis by one-half to simulate this condition.

† Calculated from data reported by Korth, Rose and Stahman (1964).

§ Calculated for the 1965 runs assuming deterioration of short-wavelength intensity of the light source from the 1964 data.
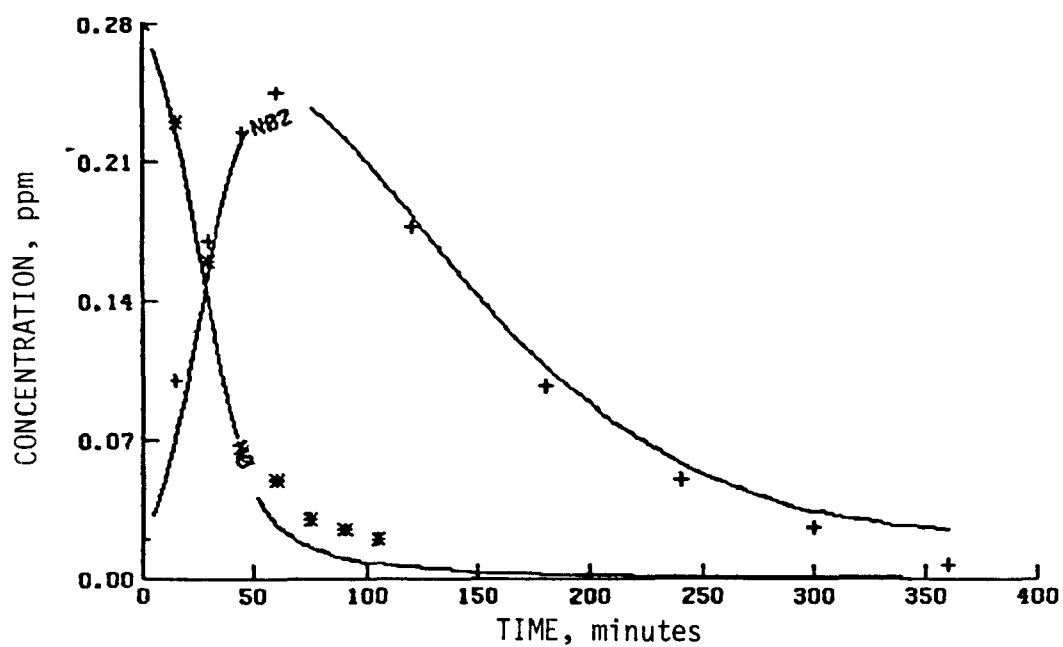
Results of the Study of the UCR Glass Chamber

One of the advantages of using a glass wall smog chamber for hydro-carbon/NO_x experiments may be the low adsorption of NO_x to the glass walls compared with the adsorption by walls constructed of Teflon. We used the rather low value of 8×10^{-7} $ppm^{-1}min^{-1}$ for the $N_2O_5 + H_2O$ reaction rate constant.

We were able to obtain only limited information on two UCR glass experiments performed in 1973. Since the reported k_d for these experiments is 0.35 min^{-1}, we used a value of 0.3 min^{-1} for k_1 in the computer simulations. The simulated predictions of the NO_x, propylene and ozone behavior are shown in Figures 79 and 80. Further investigations using higher alde-hyde photolysis show an effect on the ozone induction period with little effect on the ozone maximum (see Figure 81). Another investigation using a higher k_1 value (0.5 min^{-1}) showed that by raising the NO_2 photolysis rate constant we were able to predict the ozone behavior without affecting the NO_x and propylene predictions (see Figure 82). Although this last set of simulations shows the closest agreement for ozone maxima between simulations and the UCR glass experiments, we are skeptical about the high NO_2 photolysis rate constant used in the simulations.

During the next contract year, we hope to obtain more information concerning these experiments and perhaps to elucidate the apparently high concentrations of ozone found in these experiments.

Results of the Study of the CALSPAN Chamber

For the CALSPAN chamber, we investigated three propylene/NO_x experiments (Runs 11, 15, and 16). Of these, only Run 11 did not contain any hydro-carbon concentration versus time profile. The computer simulations of Runs 11, 15, and 16 are shown in Figures 83, 84, and 85. In the simulations of Runs 15 and 16 (Figures 84 and 85) the propylene decay was simulated, but not the ozone behavior. In the simulations of Run 16 (Figure 85), the simu-lations have a shorter time to NO_x crossover compared with the actual data;
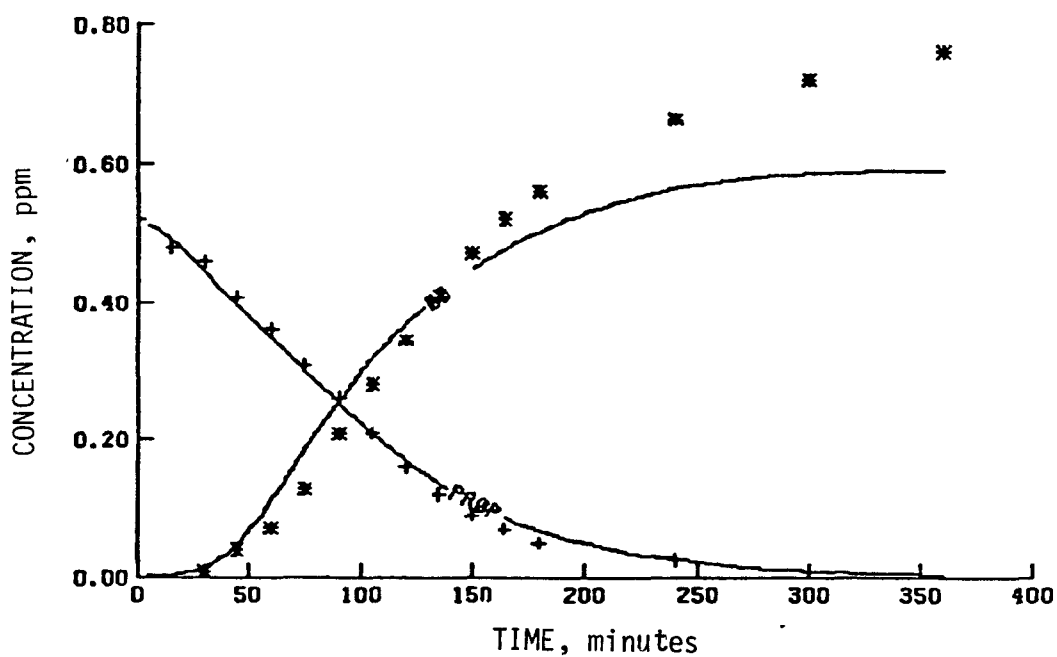
Figure 79. Simulation results of the UCR glass chamber experiment performed on 23 February 1973
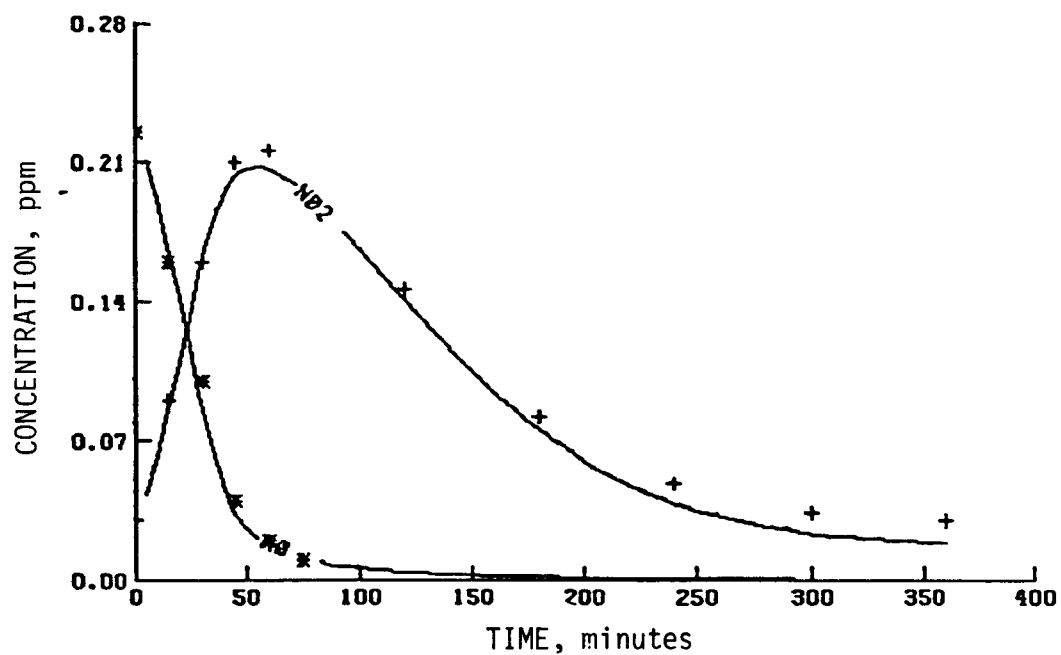
(a) NO_2 and NO
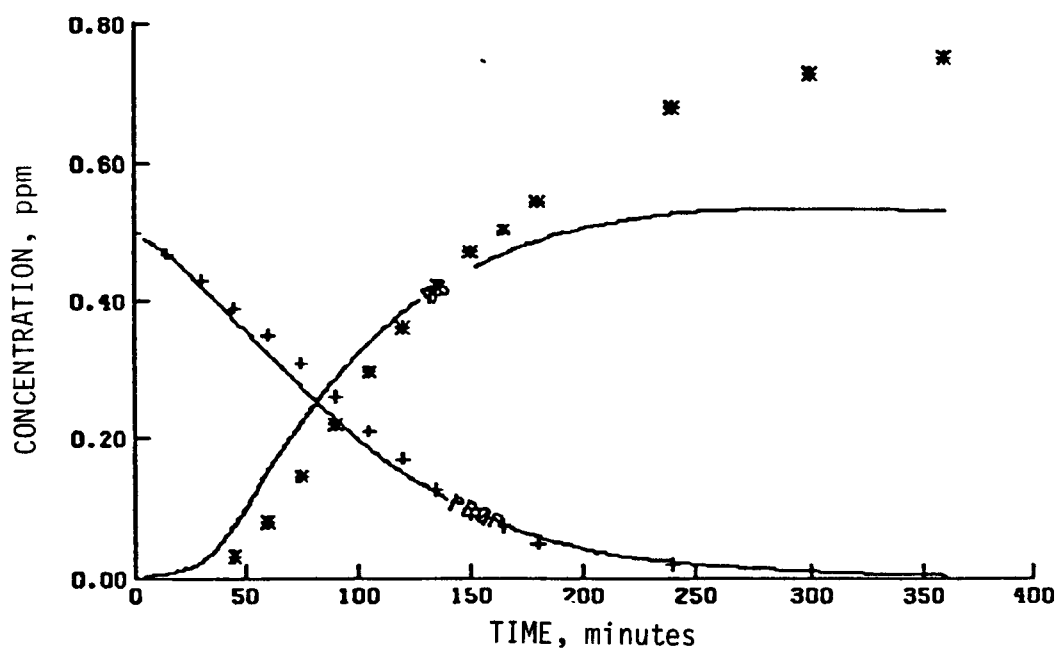
(b) Propylene and O_3

Figure 80.   Simulation results of an UCR glass chamber experiment
performed on 5 March 1973

296
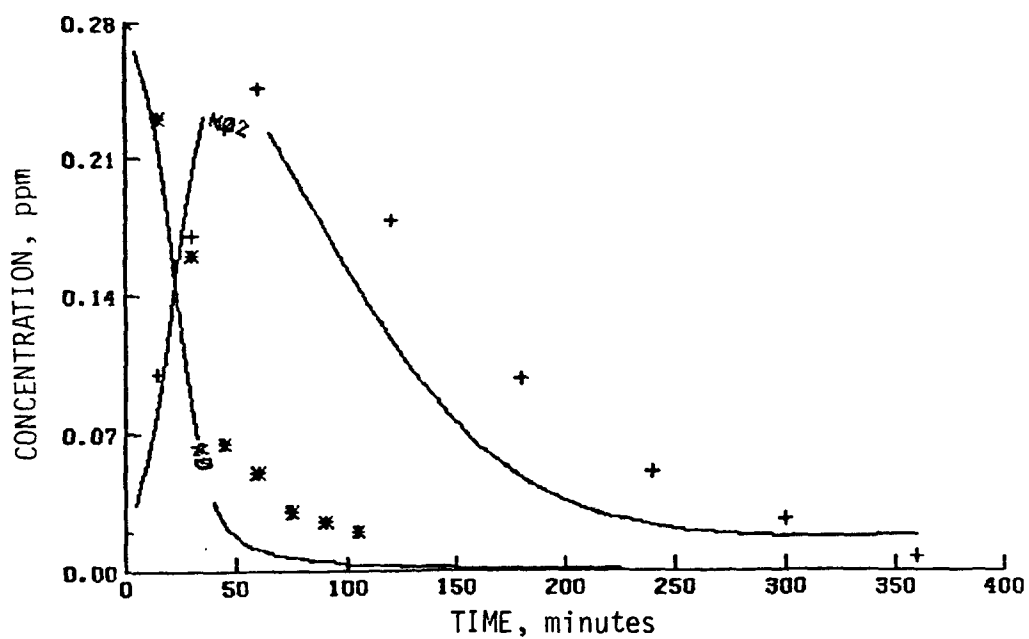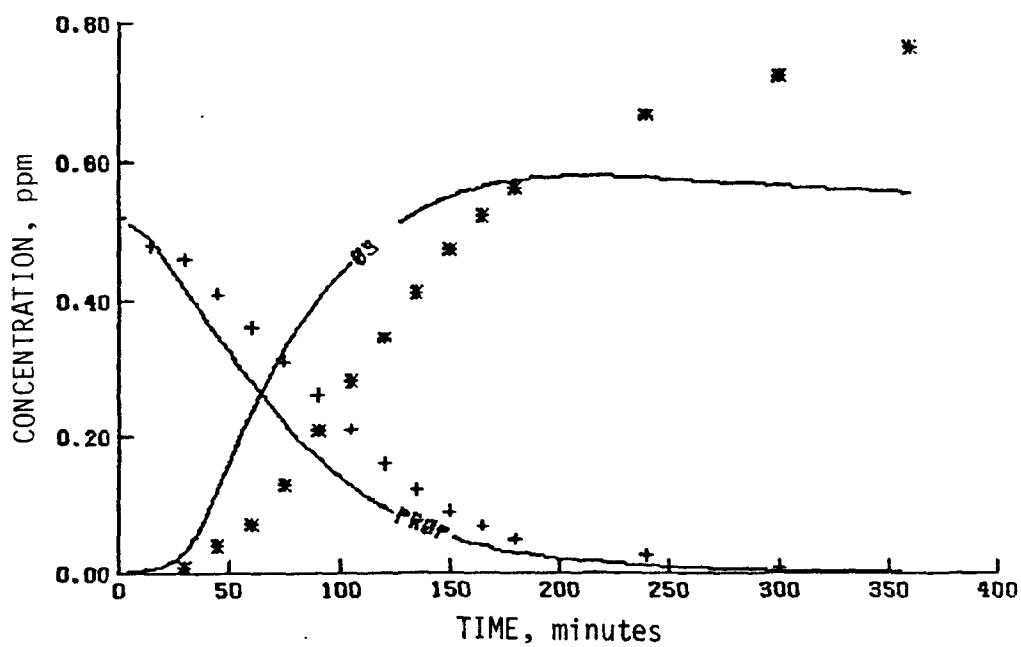
(a) NO$_2$ and NO

(b) Propylene and O$_3$

Figure 81. Simulation results of an UCR glass chamber experiment with the formaldehyde photolysis at 3 x 10^{-3} min^{-1}

297
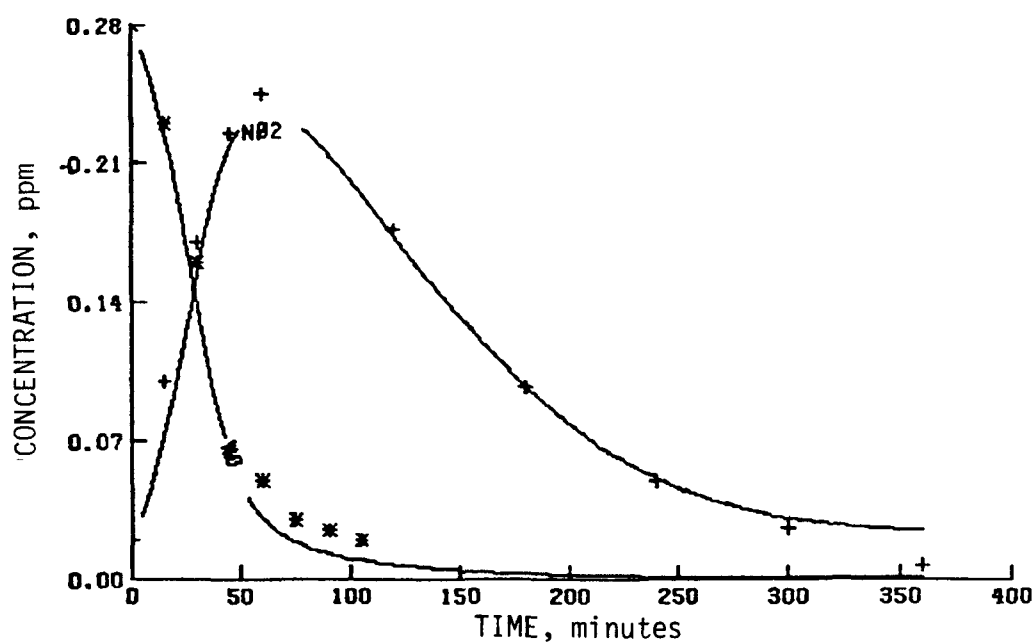
(a) NO_2 and NO
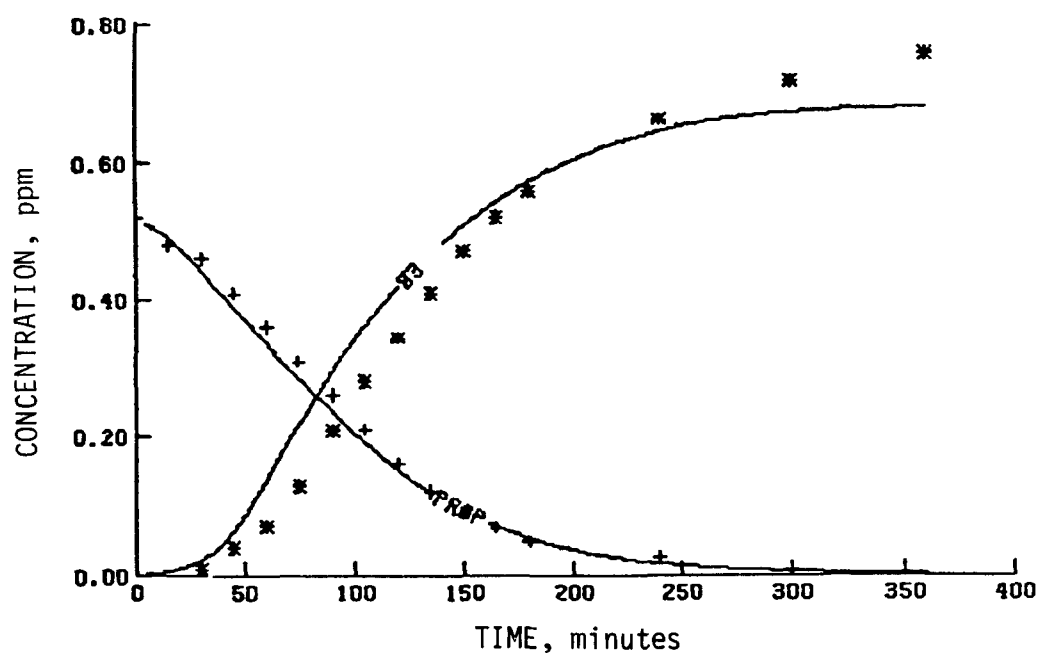
(b) Propylene and O_3

Figure 82. Simulation results of an UCR glass chamber experiment
with the NO_2 photolysis at 0.5 min^{-1}

298
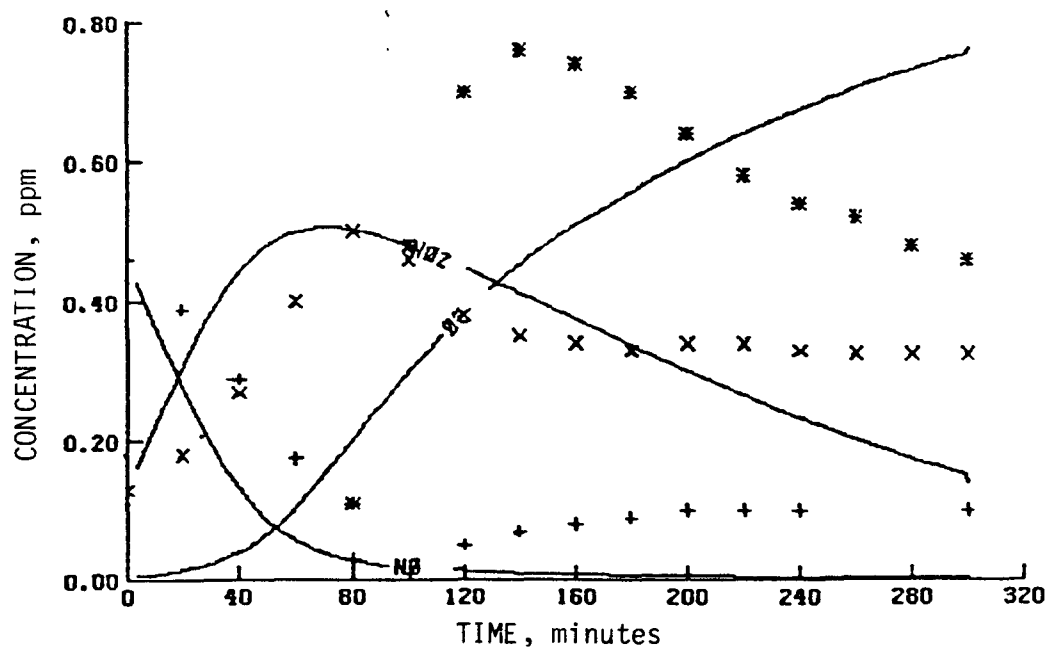
Figure 83. Simulation results of propylene/NO$_x$ Experiment 11
performed in the CALSPAN chamber

299
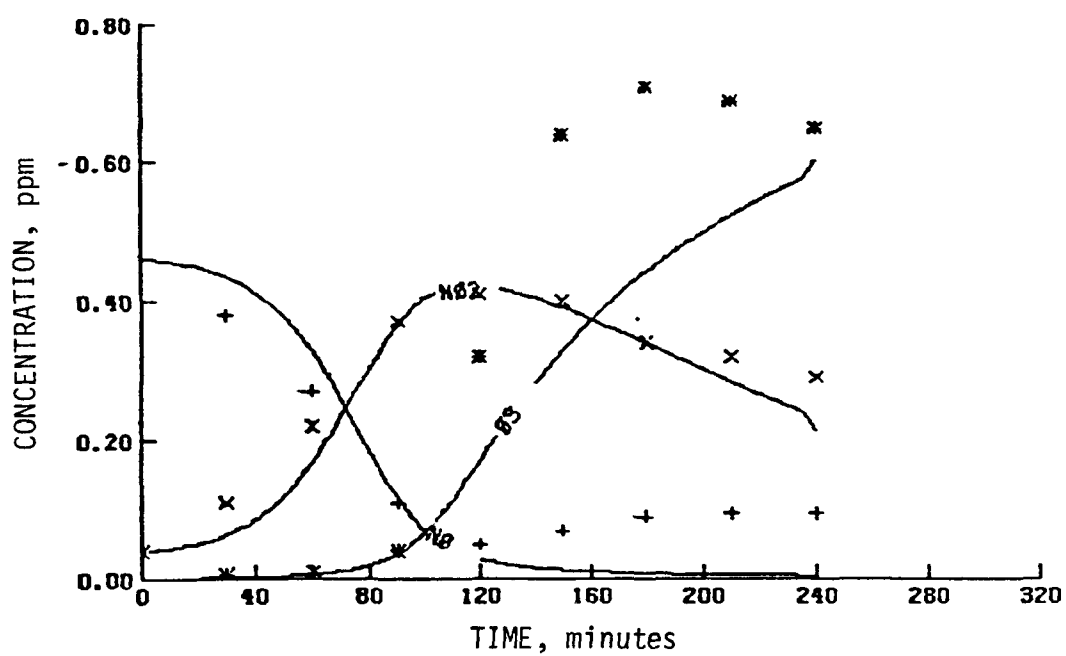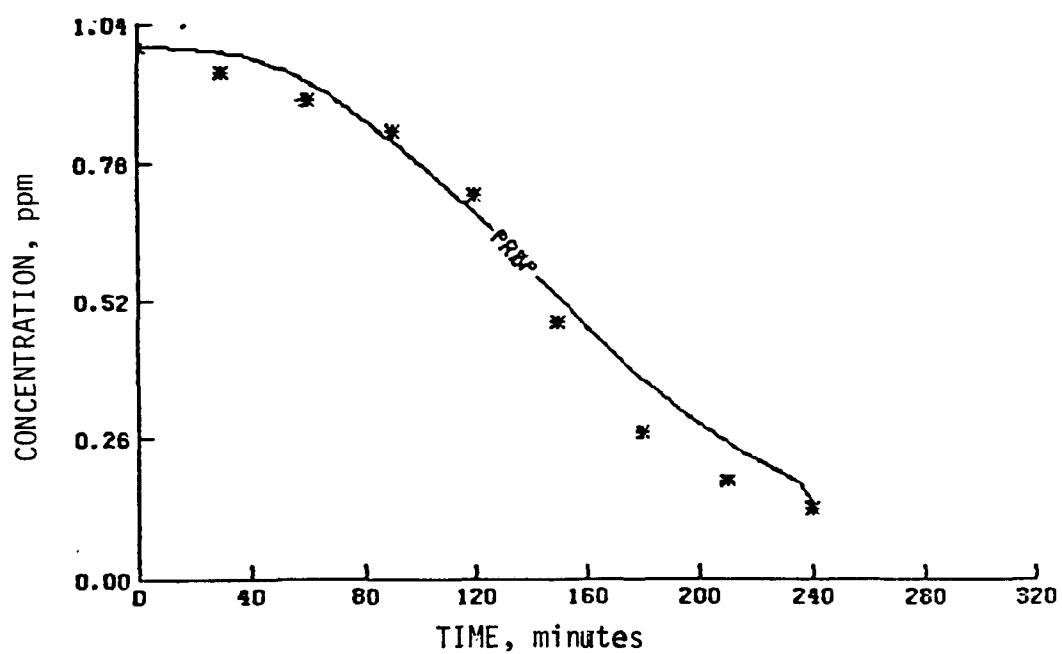
(a) NO_2, NO, and O_3

(b) Propylene

Figure 84. Simulation results of propylene/NO_x Experiment 15 performed in the CALSPAN chamber
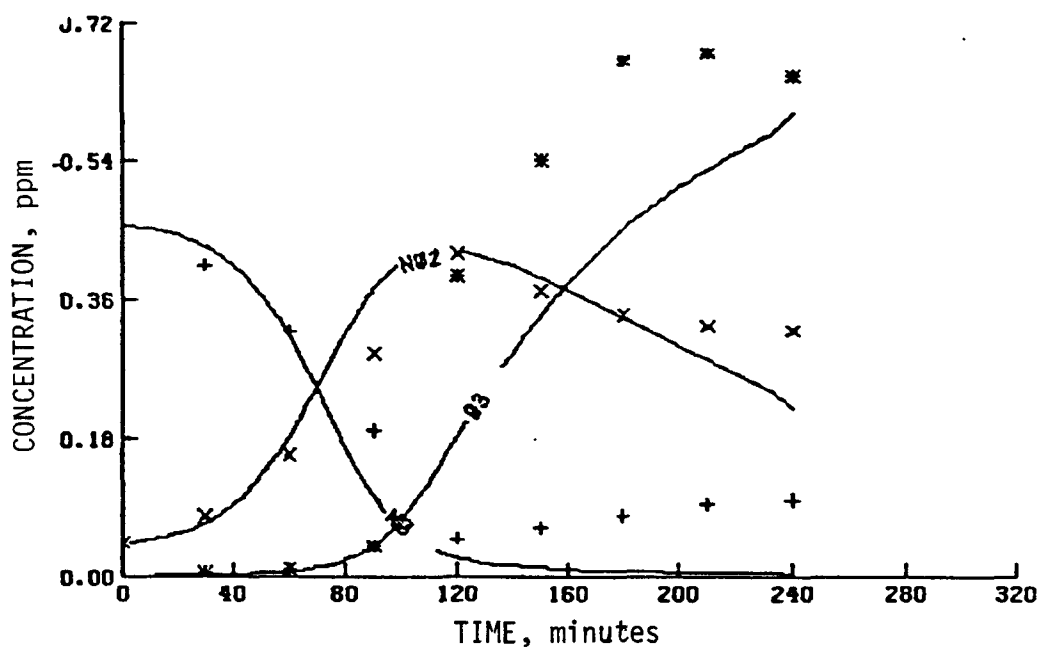
(a) NO_2, NO, and O_3
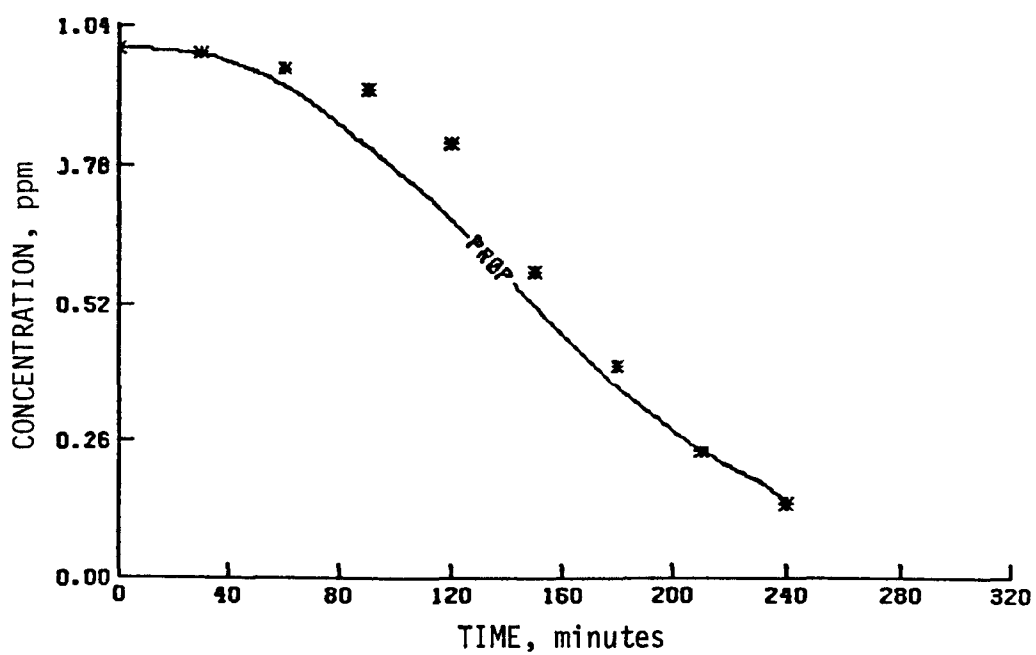
(b) Propylene

Figure 85. Simulation results of propylene/NO_x Experiment 16
performed in the CALSPAN chamber

Using the reported light spectra, we calculate photolysis ratios for both the cut and uncut spectra (Table 44). Jaffe and Last (1974) reported a k_d of 0.3 min^{-1} for both spectra. Wu and Niki (1975) provided the following equation to calculate k_1 from data on the decay of NO_2 in N_2:

$$k_1 = \frac{0.5}{(t_2 - t_1)} \left[1 + \frac{k_4[M]}{k_3} - \frac{k_5[M]}{k_3} \ell n \frac{[NO_2]_1}{[NO_2]_2} \right.$$

$$\left. + \frac{k_5[M]}{k_3} \left(\frac{1}{[NO_2]_2} - \frac{1}{[NO_2]_1} \right) [NO_x]_0 \right] , \qquad (108)$$

where $[NO_2]_1$ and $[NO_2]_2$ are the concentrations of NO_2 at times t_1 and t_2, $[NO_x]_0 = [NO_2] + [NO]$, and k_3, k_4, and k_5 are the rate constants for the reactions of triplet oxygen atoms with NO_2, NO_2+M, and NO, respectively. This equation should be used when $[NO]/[NO_2] \geq 0.5$. Data taken from Jaffe and Last (1974) indicate that $[NO_2]_1 = 0.58$ ppm, $[NO_2]_2 = 0.415$ ppm, $[NO_x] = 1.6$ ppm, $t_1 = 3$ minutes, and $t_2 = 4$ minutes. By eq. (108), these data and the rate constants recommended by Hampson and Garvin (1978) indicate that $k_1 = 0.33$ min^{-1}. Use of the value of 0.33 min^{-1} in the computer simulations resulted in prediction of an early NO_x crossover and fast propylene decay. Simulation results for Runs 40 and 42 are presented in Figures 86 and 87; simulation results for Runs 41 and 43 are presented in Volume II of this report. To help simulate the high amounts of NO_2 in the data, we included a reaction that simulates NO_2 desorption off the walls at a rate of 2×10^{-3} ppm min^{-1}. But even with this rate, we were not able to predict the NO_2 peak concentrations.

In the cut spectrum Run 40 (Figure 86) we could not follow the ozone behavior or the propylene decay. Note in Figure 86 that the propylene decay has two distinctive slopes: It is fairly slow until approximately 200 minutes and then becomes much faster. This period (200 minutes) also marks the point in which the ozone begins to influence the propylene decay. In earlier simulations with the propylene mechanism presented by Whitten

302

TABLE 44. PHOTOLYSIS RATE CONSTANTS (RELATIVE TO k_1 = 1) USED IN SIMULATIONS OF LOCKHEED CHAMBER RUNS

Reaction	Full spectrum	Cut spectrum
$O_3 + h\nu \rightarrow O(^1D)$	0.0064	0
$O_3 + h\nu \rightarrow O(^3P)$	0.0127	0.14
$HONO + h\nu \rightarrow NO + OH\cdot$	0.18	0.18
$H_2O_2 + h\nu \rightarrow 2OH\cdot$	0.001	0.00044
$HCHO + h\nu \xrightarrow{O_2} HO_2 + HCO\cdot$	0.0018	0.00015
$HCHO + h\nu \rightarrow H_2 + CO$	0.0018	0.00015
$CH_3CHO + h\nu \xrightarrow{O_2} CH_3O_2 + HCO\cdot$	0.0018*	0
$CH_3CH_2CHO + h\nu \xrightarrow{O_2} CH_3CH_2O_2 + HCO\cdot$	0.0018*	0

* Quantum yield equals one.

303
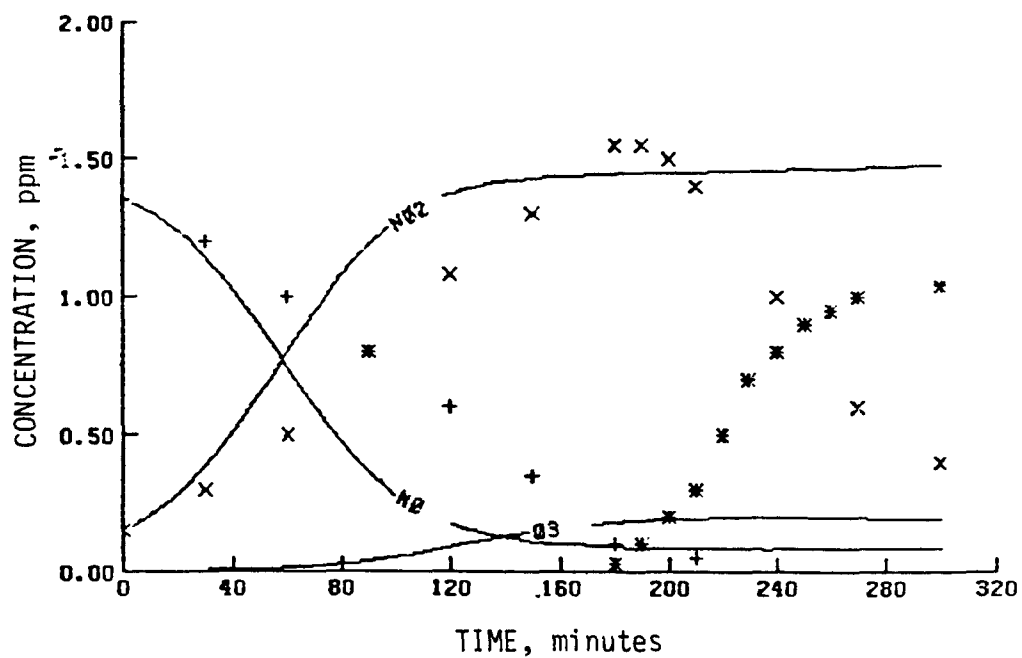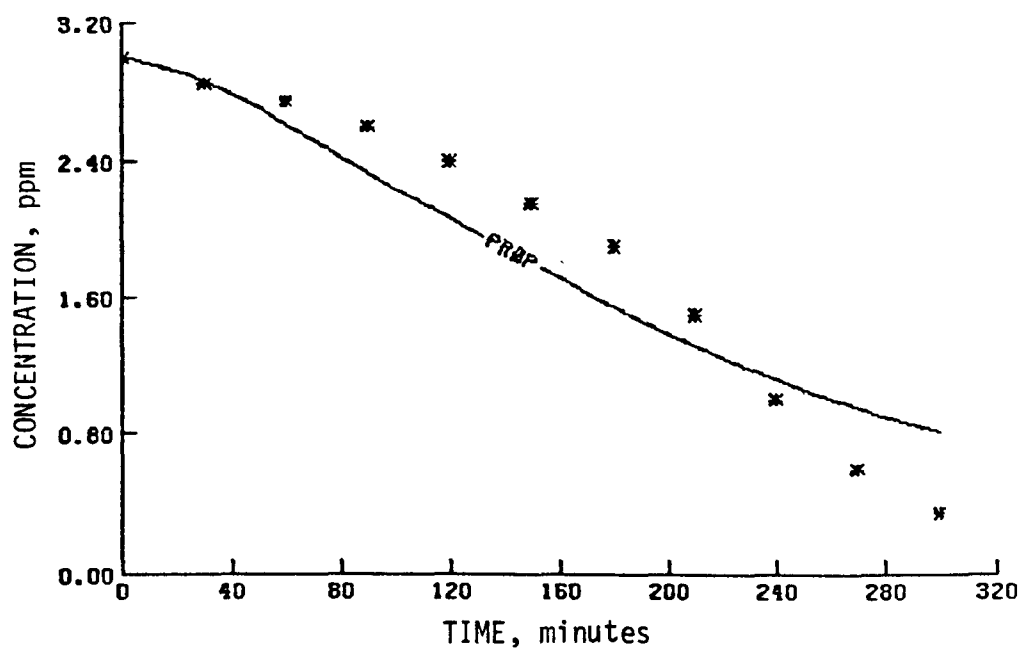
(a) NO_2, NO, and O_3

(b) Propylene

Figure 86.   Simulation results of propylene/NO_x Experiment 40 performed at Lockheed using a cut spectrum

304
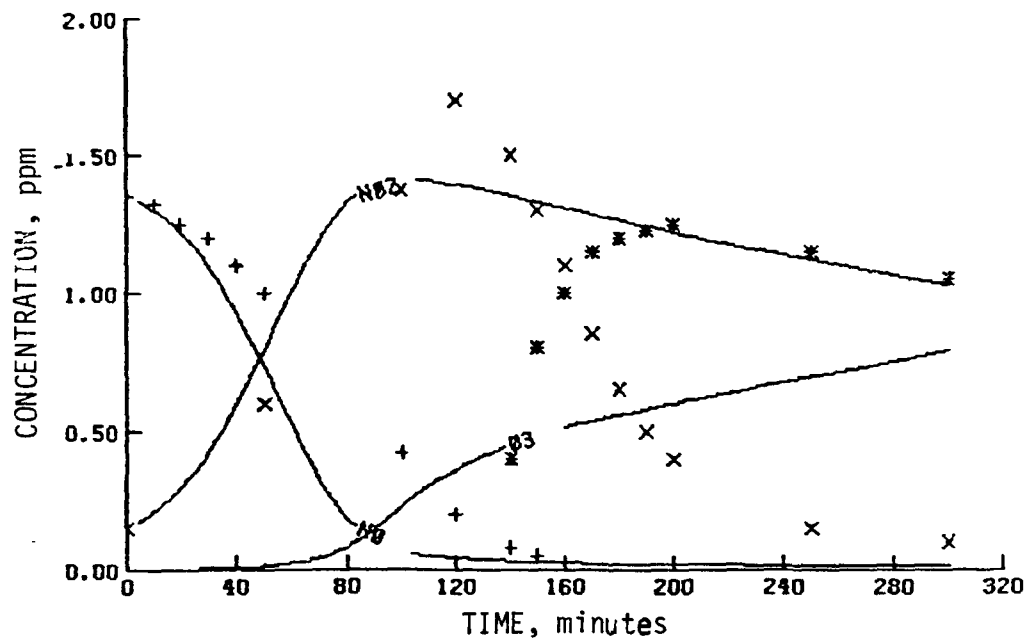
(a) NO_2, NO, and O_3
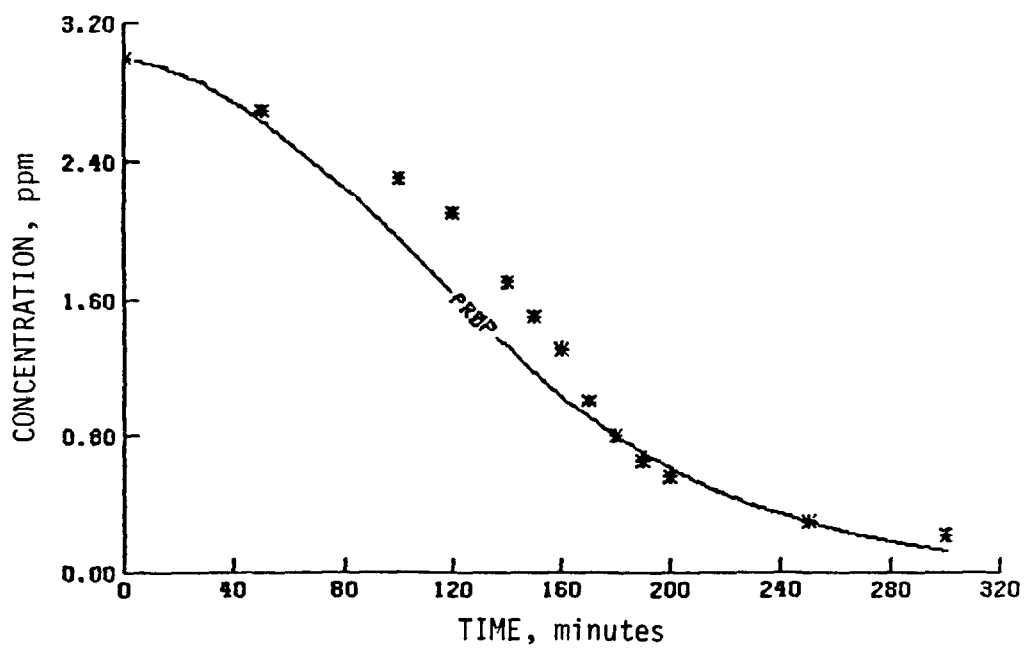
(b) Propylene

Figure 87.   Simulation results of propylene/NO_x Experiment 42
performed at Lockheed using a full spectrum

305

and Hogo (1977), we found that the major source of radicals is the ozone-olefin reaction. Since the present propylene mechanism does not have a high radical yield from the ozone-olefin reaction, the simulations do not follow the propylene decay as well. In future work the ozone-olefin reaction will be investigated further to determine, if possible, the amount of radicals required to simulate the Lockheed experiments. Also we will examine the extent of NO_x desorption from the walls and will investigate other experiments using different materials to see whether or not NO_x desorption occurs extensively.

CONCLUDING REMARKS

Our work to date seems to be leading toward the conclusion that the same basic propylene mechanism is adequate for simulating experiments in most chambers. The most important chamber-specific effects seem to be the overall light intensity and the spectral distribution of the light. Wall effects appear to play a small but important role in the overall chemistry. At this time, the effects from uncertainties in analytical data and light source data seem to be larger than the effects due to the walls.

We have received more propylene/NO_x runs from UNC, which we are currently simulating with the hope of elucidating certain wall effects, such as NO_x and formaldehyde adsorption/desorption in the UNC chamber. For the RTI chamber, we are evaluating the effect of turbulence due to the fan. In the CALSPAN and Lockheed chambers there seem to be strong NO_x desorption effects, since the total NO_x concentration increases in some of these experiments. We plan to estimate what effects NO_x coming off the wall has in all of the chambers.

During the coming year, we also plan to investigate the effect of temperature on the mechanism using the results of a temperature study performed at UCR.

306

REFERENCES

Anderson, G. E., et al. (1977), "Air Quality in the Denver Metropolitan Region 1974-2000," EF77-222, EPA-908/1-77-002, Environmental Protection Agency Region VIII, Denver, Colorado.

Atkinson, R., and R. J. Cvetanovic (1971), "Determination of the Absolute Values of the Rate Constants of the Reactions of $O(^3P)$ Atoms with Alkenes by a Modulation Technique," J. Chem. Phys., Vol. 55, pp. 659-663.

Atkinson, R. and J. N. Pitts, Jr. (1978), J. Chem. Phys., Vol. 68, p. 3581.

Baldwin, A. C., and D. M. Golden (1978), "Application of RRKM Theory Using a Hindered Rotational Gorin Model Transition State to the Reaction $HO_2NO_2 + N_2 \rightleftarrows HO_2 + NO_2 + N_2$," in press.

Barker, J. R., and D. M. Golden (1977), "Measurement of Rate Constants of Importance in Smog," Quarterly Progress Report, SRI International, Menlo Park, California.

Barker, J. R., S. W. Benson, and D. M. Golden (1977), "The Decomposition of Dimethyl Peroxide and the Rate Constant for $CH_3O + O_2 \rightarrow CH_2O + HO_2$," Int. J. Chem. Kinet., Vol. 9, pp. 31-53.

Barker, J. R., et al. (1977), "Measurement of Rate Constants of Importance in Smog," EPA-600/3-77-110, Environmental Protection Agency, Research Triangle Park, North Carolina.

Bird, B., W. E. Stewart, and E. N. Lightfoot (1960), Transport Phenomena (John Wiley & Sons, New York, New York).

Bufalini, J. J., B. W. Gay, Jr., and K. L. Brubaker (1972), "Hydrogen Peroxide Formation from Formaldehyde Photooxidation and Its Presence in Urban Atmospheres," Environ. Sci. Technol., Vol. 6, pp. 816-821.

Calvert, J. G., and J. N. Pitts, Jr. (1966), Photochemistry (John Wiley & Sons, New York, New York).

Carter, W.P.L., et al. (1978), "Computer Modeling of Smog Chamber Data: Progress in Validation of a Detailed Mechanism for the Photooxidation of Propene and n-Butane in Photochemical Smog," Int. J. Chem. Kinet., accepted for publication May 1978.

_____ (1976), "Evidence for Alkoxy Radical Isomerization in C_4-C_6 Alkanes in NO_x-Air Systems," Extended Abstracts, 12th Informal Conference on Photochemistry, National Bureau of Standards, Washington, D.C., pp. N4-1 to N4-5.

Cox, R. A., and R. G. Derwent (1976), "The Ultra-Violet Absorption Spectrum of Gaseous Nitrous Acid," J. Photochem., Vol. 6, pp. 23-34.

_____ (1975), "Kinetics of the Reaction of HO_2 with Nitric Oxide and Nitrogen Dioxide," J. Photochem., Vol. 4, pp. 139-153.

Cox, R. A., and M. J. Roffey (1977), "Thermal Decomposition of Peroxyacetyl-nitrate in the Presence of Nitric Oxide," Environ. Sci. Technol., Vol. 11, pp. 900-906.

Cox, R. A., R. G. Derwent, and P. M. Holt (1976), "Relative Rate Constants for the Reactions of OH Radicals with H_2,CH_4, CO, NO, and HONO at Atmospheric Pressure and 296K," J. Chem. Soc., Farad. Trans., Vol. 72, pp. 2031-2043.

Chan, W. H., et al. (1977), "The Pressure Dependence of the Rate Constant for the Reaction: $HO + CO \rightarrow H + CO_2$," Chem. Phys. Lett., Vol. 45, pp. 240-244.

Darnall, K. R., et al. (1976a), "Importance of RO_2 + NO in Alkyl Nitrate Formation from C_4-C_6 Alkane Photooxidation Under Simulated Atmospheric Conditions," J. Phys. Chem., Vol. 80, pp. 1948-1950.

_____ (1976), "Reactivity Scale for Atmospheric Hydrocarbons Based on Reaction with Hydroxyl Radical," Environ. Sci. Technol., Vol. 10, pp. 692-696.

Davis, D. D. (1976), private communication with Dr. M. Dodge of EPA.

Davis, D. D., et al. (1975), "A Kinetics Study of the Reaction of OH Radicals with Two C_2 Hydrocarbons: $C2H4$ and C_2H_2," J. Chem. Phys., Vol. 63, pp. 1707-1712.

_____ (1972), "Absolute Rate Constants for the Reaction of Atomic Oxygen with Ethylene over the Temperature Range 232 - 500K," J. Chem. Phys., Vol. 56, pp. 4868-4876.

Demerjian, K. L., A. J. Kerr, and J. G. Calvert (1974), "The Mechanism of Photochemical Smog Formation," in Advances in Environmental Science Technology, J. N. Pitts and R. L. Metcalf, eds. (John Wiley & Sons, New York, New York).

Dodge, M. C., and R. R. Arnts (1978), "A New Mechanism for the Reaction of Ozone with Olefins," submitted to Int. J. Chem. Kinet.

Durbin, P. A., T. A. Hecht, and G. Z. Whitten (1975), "Mathematical Modeling of Simulated Photochemical Smog," EPA-650/4-75-026, Systems Applications, Incorporated, San Rafael, California.

Graham, R. (1975), private communication.

Graham, R. A., and H. S. Johnston (1978), "The Photochemistry of NO_3 and the Kinetics of the N_2O_5-O_3 System," J. Phys. Chem., Vol. 82, pp. 254-268.

Hampson, R. F., Jr., and D. Garvin (1978), "Reaction Rate and Photochemical Data for Atmospheric Chemistry-1977," NBS Special Publication 513, National Bureau of Standards, Washington, D.C.

Hecht, T. A., and J. H. Seinfeld (1972), "Development and Validation of a Generalized Mechanism for Photochemical Smog," Environ. Sci. Technol., Vol. 6, pp. 47-57.

Hecht, T. A., M. K. Liu, and D. C. Whitney (1974), "Mathematical Simulation of Smog Chamber Photochemical Experiments," EPA-650/4-74-040, Systems Applications, Incorporated, San Rafael, California.

Hecht, T. A., J. H. Seinfeld, and M. C. Dodge (1974), "Further Development of a Generalized Mechanism for Photochemical Smog," Environ. Sci. Technol., Vol. 8, pp. 327-339.

Hendry, D. G., and R. A. Kenley (1977), "Generation of Peroxy Radicals from Pernitrates (RO_2NO_2). Decomposition of Peracylnitrates," J. Amer. Chem. Soc., Vol. 99, p. 3198.

Hendry, D. G., et al. (1977), "Computer Modeling of Simulated Photochemical Smog," Progress Narrative 8, SRI International, Menlo Park, California.

Herron, G. T., and R. E. Huie (1974), "Rate Constants for the Reactions of Atomic Oxygen (O^3P) with Organic Compounds in the Gas Phase," J. Phys. and Chem. Ref. Data, Vol. 2, pp. 467-518.

Herron, J., and R. E. Huie (1977), "Stopped-Flow Studies of the Mechanisms of Ozone-Alkene Reactions in the Gas Phase. Ethylene," J. Amer. Chem. Soc., Vol. 99, p. 5430.

Howard, C. J. (1977), "Kinetics of the Reaction of HO_2 with NO_2," J. Chem. Phys., Vol. 67, pp. 5258-5263.

_____ (1976), "Rate Constants for the Gas-Phase Reactions of OH Radicals with Ethylene and Halogenated Ethylene Compounds," J. Chem. Phys., Vol. 65, pp. 4771-4777.

Howard, C. J., and K. M. Evenson (1977), "Kinetics of the Reaction of HO_2 with NO_2," Geophys. Res. Lett., Vol. 4, pp. 437-440.

Jaffe, R. J., and K. W. Last (1974), "Study of Factors Affecting Reactions in Environmental Chambers," Report No. LMSC-D406484, Lockheed Missiles and Space Company, Sunnyvale, California.

Japar, S. M., and H. Niki (1975), "The Gas-Phase Reactions of the Nitrate Radical with Olefins," J. Phys. Chem., Vol. 79, pp. 1629-1632.

Japar, S. M., C. H. Wu, and H. Niki (1974), "Rate Constants for the Reaction of Ozone with Olefins in the Gas Phase," J. Phys. Chem., Vol. 78, pp. 2318-2320.

Jeffries, H. (1976), Progress Report to Dr. M. C. Dodge of the EPA from the University of North Carolina, dated November 1976.

Jeffries, H., D. Fox, and R. Kamens (1976), "Outdoor Smog Chamber Studies: Light Effects Relative to Indoor Chambers," Environ. Sci. Technol., Vol. 10, pp. 1006-1011.

_____ (1975), "Outdoor Smog Chamber Studies: Effect of Hydrocarbon Reduction on Nitrogen Dioxide," EPA-650/3-75-011, University of North Carolina, Chapel Hill, North Carolina.

Kaiser, E. W., and C. H. Wu (1977), "A Kinetic Study of the Gas Phase Formation and Decomposition Reactions of Nitrous Acid," J. Phys. Chem., Vol. 81, pp. 1701-1706.

Kajimoto, O., and R. J. Cvetanovic (1976), "Temperature Dependence of $O(^1D)$ Production in the Photolysis of Ozone at 313 nm," Chem. Phys. Lett., Vol. 37, pp. 533-536.

Kocmond, W. C., et al. (1973), "Determination of the Formation Mechanisms and Composition of Photochemical Aerosols," EPA-650/3-73-002, CALSPAN Corporation, Buffalo, New York.

Korth, M. W. (1963), "Dynamic Irradiation Chamber Tests of Automotive Exhaust," Publication No. 999-AP-5, Robert A. Taft Sanitary Engineering Center, U.S. Public Health Service, Cincinnati, Ohio.

Korth, M. W., A. H. Rose, Jr., and R. C. Stahman (1964), "Effects of Hydrocarbon to Oxides of Nitrogen Ratios on Irradiated Auto Exhaust, Part 1," J. Air Poll. Contr. Assoc., Vol. 14, pp. 168-175.

Kuntz, R. L., S. L. Kopczynski, and J. S. Bufalini (1973), "Photochemical Reactivity of Benzaldehyde-NO_x and Benzaldehyde-Hydrocarbon-NO_x Mixtures," Environ. Sci. Technol., Vol. 7, pp. 1119-1123.

Leighton, P. A. (1961), Photochemistry of Air Pollution (Academic Press, New York, New York).

Levine, S. Z., et al. (1977), Chem. Phys. Lett., Vol. 48, p. 528.

Lin, C. L., N. Rohatgi, and W. B. DeMore (1978), "The Absorption Cross Sections of Hydrogen Peroxide," 13th Informal Conference on Photochemistry, Clearwater Beach, Florida.

Lloyd, A. C., et al. (1976), "Relative Rate Constants for Reactions of the Hydroxyl Radical with a Series of Alkanes, Alkenes, and Aromatic Hydrocarbons," J. Phys. Chem., Vol. 80, pp. 789-794.

MacCracken, M. C., and G. D. Sauter, eds. (1975), "Development of an Air Pollution Model for the San Francisco Bay Area," UCRL-51920, Vol. 1, Lawrence Livermore Laboratory, Livermore, California.

Meagher, J. F., and J. Heicklen (1976), "Reaction of HO with C_2H_4," J. Phys. Chem., Vol. 80, pp. 1645-1652.

Moortgat, G. K., et al. (1978), "Wavelength Dependence of Relative and Absolute Quantum Yields in the Near UV-Photolysis of Formaldehyde at 25°C," 13th Informal Conference on Photochemistry, Clearwater, Beach, Florida.

Morris, E. D., Jr., and H. Niki (1973), "Reaction of Dinitrogen Pentoxide with Water," J. Phys. Chem., Vol. 77, pp. 1929-1932.

_____ (1971a), "Mass Spectrometric Study of the Reaction of Hydroxyl Radical with Formaldehyde," J. Chem. Phys., Vol. 55, pp. 1991-1992.

_____ (1971b), "Reactivity of Hydroxyl Radicals with Olefins," J. Phys. Chem., Vol. 75, pp. 3640-3641.

Niki, H., (1978), "Reactions of Olefins with Hydroxyl Radical and with Ozone," presented at EPA/NBS Workshop on Chemical Kinetic Data Needs for Modeling the Lower Troposphere, 15-17 May 1978, Reston, Virginia.

Niki, H., E. Daby, and B. Weinstock (1972), "Mechanisms of Smog Reactions," in Photochemical Smog and Ozone Reactions, Advances in Chemistry Series, R. F. Gould, ed., Vol. 113, pp. 16-57 (American Chemical Society, Washington, D.C.).

_____ (1969), Proc. 12th Combustion Symposium, Poitiers, France, p. 277.

Niki, H. et al. (1977), Chem. Phys. Lett., Vol. 45, p. 564.

Pastrana, A. V., and R. W. Carr, Jr. (1975), "Kinetics of the Reaction of Hydroxyl Radicals with Ethylene, Propylene, 1-Butene, and trans-2-Butene," J. Phys. Chem., Vol. 79, pp. 765-770.

Philen, D. L., R. T. Watson, and D. D. Davis (1977), "A Quantum Yield Determination of $O(^1D)$ Production from Ozone via Laser Flash Photolysis," J. Chem. Phys., Vol. 67, pp. 3316-3321.

Pitts, J. N., Jr., et al. (1977), "Mechanisms of Photochemical Reactions in Urban Air. Volume II. Chamber Studies," EPA-600/3-77-014b, State Air Pollution Research Center, University of California at Riverside, Riverside, California.

Reynolds, S. D. et al., (1974), "Mathematical Modeling of Photochemical Air Pollution--III. Evaluation of the Model," Atmos. Environ., Vol. 8, pp. 563-596.

Scofield, F., A. Levy, and S. E. Miller (1969), "Design and Validation of a Smog Chamber," Scientific Circular No. 79, National Paint, Varnish, and Lacquer Association, Washington, D.C.

Sie, B.K.T., R. Simonaitis, and J. Heicklen (1976), "The Reaction of OH with CO," Inter. J. Chem. Kinet., Vol. 8, pp. 85-98.

Simonaitis, R., and J. I. Heicklen (1974), "Reactions of CH_3O_2 with NO and NO_2," J. Phys. Chem., Vol. 78, pp. 2417-2421.

Spicer, C. W., et al. (1973), "The Reactions of Methylperoxy Radicals with NO and NO_2," J. Amer. Chem. Soc., Vol. 95, p. 13.

Stedman, D. H. (1977), "Large Scale, High Levels of Ambient Ozone in Lower Michigan," First Annual Report to National Science Foundation, Grant No. ATM 76-03793.

Tesche, T. W., and C. S. Burton (1978), "Simulated Impact of Alternative Emissions Control Strategies on Photochemical Oxidants in Los Angeles: Volume I--Preliminary Discussion of Results," EF78-22R, Systems Applications, Incorporated, San Rafael, California.

Tuesday, C. S. (1961), Chemical Reactions in the Lower and Upper Atmosphere, R. D. Cadle, ed., pp. 1-49 (Interscience Publications, New York, New York).

Walter, T. A., J. J. Bufalini, and B. W. Gay, Jr. (1977), "Mechanism for Olefin-Ozone Reactions," Environ. Sci. Technol., Vol. 11, pp. 382-386.

Westenberg, A. A., and N. de Haas (1969), Proc. 12th Combustion Symposium, Poitiers, France, p. 289.

Whitbeck, M. R., et al. (1976), "A Kinetic Study of CH_3O_2 and $(CH_3)_3CO_2$ Radical Reactions by Kinetic Flash Spectroscopy," Extended Abstracts, 12th Informal Conference on Photochemistry, National Bureau of Standards, Washington, D.C., pp. K1-1 to K1-5.

Whitten, G. Z., and M. C. Dodge (1976), "Aldehydes and Photochemical Smog," 171st National Meeting, American Chemical Society, April 1976, New York, New York.

Whitten, G. Z., and H. Hogo (1977), "Mathematical Modeling of Simulated Photochemical Smog," EPA-600/3-77-011, Systems Applications, Incorporated, San Rafael, California.

Whitten, G. Z., and J. P. Meyer (1975), "CHEMK: A Computer Modeling Scheme for Chemical Kinetics," CS75-70R2, Systems Applications, Incorporated, San Rafael, California.

Wilson, W. E., Jr. (1972), "A Critical Review of the Gas-Phase Reaction Kinetics of the Hydroxyl Radical," J. Phys. and Chem. Ref. Data, Vol. 1, pp. 535-573.

Wu, C. H., and H. Niki (1975), "Methods for Measuring NO_2 Photodissociation Rate," Environ. Sci. Technol., Vol. 9, pp. 46-52.

Wu, C. H., S. H. Japar, and H. Niki (1976), "Relative Reactivities of HO-Hydrocarbon Reactions from Smog Reactor Studies," J. Environ. Sci. and Health, Vol. A-11, pp. 191-200.

TECHNICAL REPORT DATA
(Please read Instructions on the reverse before completing)

1 REPORT NO. EPA-600/3-79-001a	2	3. RECIPIENT'S ACCESSION NO.

4. TITLE AND SUBTITLE	5. REPORT DATE
MODELING OF SIMULATED PHOTOCHEMICAL SMOG WITH KINETIC MECHANISMS Volume 1. Interim Report	January 1979
	6. PERFORMING ORGANIZATION CODE

7. AUTHOR(S)	8. PERFORMING ORGANIZATION REPORT NO.
G.Z. Whitten, H. Hogo, M.J. Meldgin, J.P. Killus, and P. J. Bekowies	EF78-121A

9. PERFORMING ORGANIZATION NAME AND ADDRESS	10. PROGRAM ELEMENT NO.
Systems Applications, Incorporated 950 Northgate Drive San Rafael, California 94903	1AA603 AC-19 (FY-78)
	11. CONTRACT/GRANT NO. Contract No. 68-02-2428

12. SPONSORING AGENCY NAME AND ADDRESS	13. TYPE OF REPORT AND PERIOD COVERED
Environmental Sciences Research Laboratory-RTP, NC Office of Research and Development U.S. Environmental Protection Agency Research Triangle Park, N.C. 27711	Interim 7/76-7/78
	14. SPONSORING AGENCY CODE EPA/600/09

15. SUPPLEMENTARY NOTES

Volume 2. Appendix   EPA-600/3-79-001b

16. ABSTRACT

Computer modeling of smog chamber data is discussed in three parts. First, a series of detailed chemical mechanisms were developed to describe the photochemical formation of ozone from nitrogen oxides and the following organic compounds (alone and in various combinations): formaldehyde, acetaldehyde, ethylene, propylene, butane, 1-butene, trans-2-butene, and 2,3-dimethylbutane. Second, a generalized kinetic scheme intended for use in models simulating the formation of ozone in urban atmospheres was refined. The generalized mechanism includes a condensed version of the detailed mechanisms developed in the first part plus a semi-empirical scheme to describe the oxidation of aromatic hydrocarbons. Third, the effects of smog chambers on ozone formation were examined. For this part of the study, similar experiments using nitrogen oxides and propylene in eight different smog chambers were simulated using the detailed propylene mechanism. The main chamber effects identified thus far are apparently due to nitrogen oxides degassing from the walls during experiments and differences between chambers in the spectral distribution of ultraviolet irradiation.

Volume 1 contains all textual material. Volume 2 contains graphs of measured and simulated pollutant concentrations for many smog chamber experiments.

17. KEY WORDS AND DOCUMENT ANALYSIS

a. DESCRIPTORS	b.IDENTIFIERS/OPEN ENDED TERMS	c. COSATI Field/Group
* Air pollution * Reaction kinetics * Photochemical reactions * Test chambers * Mathematical models * Computerized simulation		13B 07D 07E 14B 12A 09B

18. DISTRIBUTION STATEMENT	19. SECURITY CLASS *(This Report)* UNCLASSIFIED	21. NO. OF PAGES 332
RELEASE TO PUBLIC	20. SECURITY CLASS *(This page)* UNCLASSIFIED	22. PRICE

EPA Form 2220-1 (9-73)

If your address is incorrect, please change on the above label
tear off; and return to the above address.
If you do not desire to continue receiving these technical
reports, CHECK HERE ☐, tear off label, and return it to the
above address,

EPA-600/3-79-001a